Polish Academy of Sciences
University of Engineering and Economics in Rzeszów
University of Life Sciences in Lublin
Faculty of Production Engineering

TEKA

COMMISSION OF MOTORIZATION AND ENERGETICS IN AGRICULTURE

AN INTERNATIONAL QUARTERLY JOURNAL ON MOTORIZATION, VEHICLE OPERATION, ENERGY EFFICIENCY AND MECHANICAL ENGINEERING

Vol. 14, No 4

LUBLIN–RZESZÓW 2014

All the articles are available on the webpage: http://www.pan-ol.lublin.pl/wydawnictwa/Teka-Motrol.html

All the scientific articles received positive evaluations by independent reviewers

Linguistic consultant: *Małgorzata Wojcieszuk*
Typeset: *Adam Niezbecki*
Cover design: *Hanna Krasowska-Kołodziej*

Editorial Office address

Polish Academy of Sciences Branch in Lublin
Pałac Czartoryskich, Plac Litewski 2, 20-080 Lublin, Poland
e-mail: eugeniusz.krasowski@up.lublin.pl

Printing

elpil
Artyleryjska Str. 11, 08-110 Siedlce, Poland
e-mail: info@elpil.com.pl

ISSN 1641-7739

Edition 60+16 vol.

Drying Faba Bean Seeds in a Silo with a Vertical Air Circulation System

Janusz Bowszys, Teresa Bowszys***

* Department of Agricultural Process Engineering, University of Warmia and Mazury in Olsztyn, Katedra Inżynierii Systemów, Uniwersytet Warmińsko-Mazurski w Olsztynie
ul. Heweliusza 14,10-718 Olsztyn, e-mail: j.bowszys@uwm.edu.pl
** Department of Agricultural Chemistry and Environmental Protection, University of Warmia and Mazury in Olsztyn, Katedra Chemii Rolnej i Ochrony Środowiska, Uniwersytet Warmińsko-Mazurski w Olsztynie, e-mail: bowter@uwm.edu.pl

Received December 03.2014; accepted December 17.2014

Summary. Legume seeds harvested by combine harvesters in the fall are characterized by a high moisture content. In this study, faba bean seeds were dried at low temperatures in a silo with a vertical air circulation system. Low temperature and long drying time of 90 hours minimized thermal stress in seeds. The objective of the study was to describe the drying process of faba bean seeds in a silo with vertical air flow, slightly heated by a 13.5 kW electric heater. The results of the study have indicated that the amount of air pumped into the silo by a WP-25 fan ranges from 723 $m^3 \cdot Mg^{-1} \cdot h^{-1}$ to 150 $m^3 \cdot Mg^{-1} \cdot h^{-1}$, subject to the degree of silo filling with faba bean seeds. A vertical air circulation system with a ventilation cone facilitates the process of drying faba bean seeds. Faba bean seeds are dried most rapidly along the silo's axis of symmetry, whereas the drying rate is lowest along the silo's outer walls. Seeds are dried faster in the lower part of the silo, therefore, a two-phase drying process is recommended in planes W1, W2 and W3. Seeds dried in the lower part of the silo should be removed upon the achievement of the optimal moisture content for storage. The remaining seeds should be dried in the second stage of the process.

Key words: silos, drying, storage, faba beans.

INTRODUCTION

New low-tannin faba bean varieties with a determinate growth habit, containing a minimal amount of tannins (0.014 mg per g DM), could contribute to the popularity of faba beans grown for fodder, in particular, if imports of genetically modified soybean meals are limited. The faba bean is a legume plant of great environmental significance that plays an important role in crop rotation schemes with a predominance of cereals. Legume seeds harvested by combine harvesters in the fall are characterized by a high moisture content. Intensive drying of faba bean seeds in roof dryers leads to thermal stress, which damages the embryo and causes seeds to develop microcracks [8, 9]. Roof dryers are not suitable for drying crop seeds. Several attempts have been made to dry faba bean seeds at low temperatures in silos with radial or vertical air flow [2, 3, 4]. Low temperature and long drying time of 90 hours minimized thermal stress in seeds [12, 10]. The positive results of experiments where cereal seeds were dried in silos [2] prompted the current attempt to dry faba bean seeds in a silo with a vertical air circulation system. The objective of this study was to describe the drying process of faba bean seeds in a silo with vertical air flow, slightly heated by a 13.5 kW electric heater. The silo's ventilation efficiency and the amount of air supplied to the silo, subject to the height of the seed layer inside the silo, were determined to evaluate the drying process.

MATERIALS AND METHODS

A drying silo with a vertical air circulation system was designed at the former Department of Process Devices (presently the Department of Agricultural Process Engineering) of the University of Warmia and Mazury in Olsztyn. A patent application was submitted to the Polish Patent Office, which issued copyright No. 74982 for the silo [1, 5]. The device was designed for drying and storing cereal grain. A diagram of the silo used in this experiment is presented in Figure 1.

The silo is a steel structure. The cylindrical section with a diameter of 3 m is made of galvanized steel coated with plastic on both sides. Air is pumped into the silo by a fan (7). The ventilation cone (5) with a base diameter of 1.63 m is made of perforated steel with vent openings. The slant height of the cone is parallel to the slant height of the discharge tube. The cone is separated from the discharge tube by a distance of 0.7 m. Research results indicate that the designed ventilation system permits air movement throughout the entire bulk [2]. For the needs of this experiment, inspection openings, marked W1, W2, W3 and

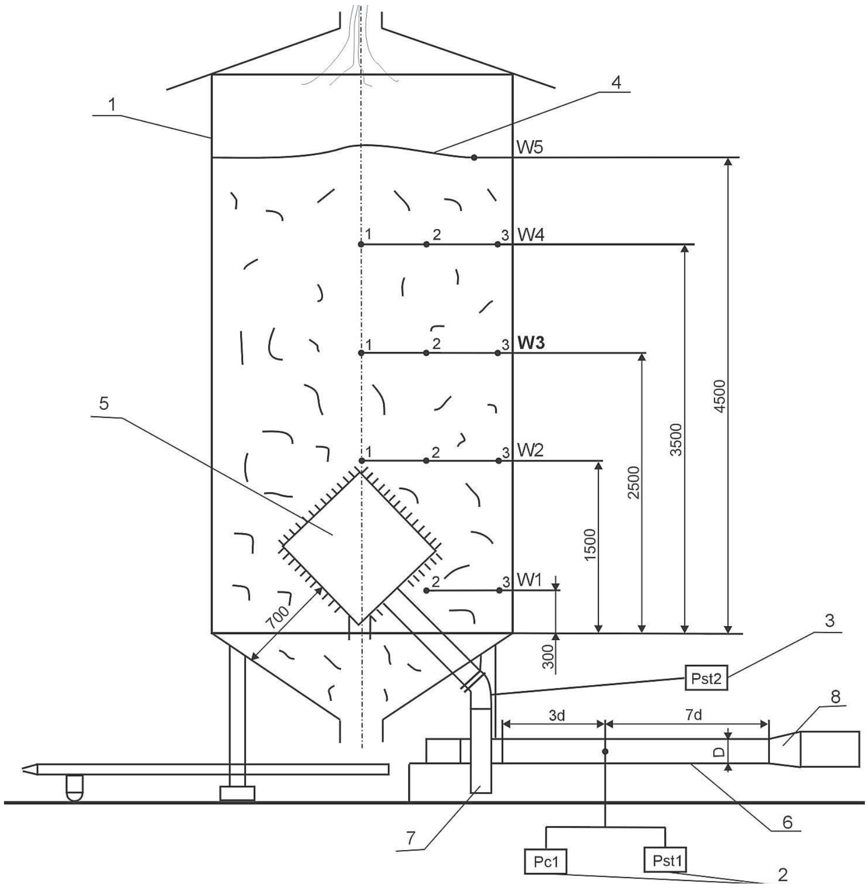

Fig. 1. A diagram of the experimental silo with a vertical air circulation system and a ventilation cone: 1 – silo, 2 – micro pressure gauge for measuring pressure inside the suction pipeline, 3 – pressure gauge, 4 – top surface of the seed layer, 5 – ventilation cone, 6 – suction pipeline, 7 – fan, 8 – electric heater, W_1, W_2, W_3, W_4 – sampling planes (1 – the silo's axis of symmetry, 2 – at mid-radius, 3 – by the wall), W_{31}, W_{32}, W_{33} – sampling points where seed temperature was measured continuously.

W4, were drilled along the silo's four longitudinal planes at the distances given in Figure 1. The silo was equipped with a 13.5 kW heater (8), WP-25 fan and micro gauges (2) for measuring the total pressure and static pressure of pumped air. Pressure was measured to the nearest Pa. Inspection openings were used to collect samples from various locations in the bulk. Total airstream pressure and static pressure were measured to calculate fan efficiency and the amount of air pumped into the silo. The first measurement was performed for an empty silo (H=0), and successive measurements were performed when seeds were added in layers of 0.5 m until the height of the seed bed inside the silo reached 4.5 m. The thickness of the seed layer should not exceed 4.5 m due to the risk of seed damage under the exerted load [11]. The measurements were used to calculate ventilation efficiency and the amount of air supplied to the silo in line with the presented method [2, 3]. Faba bean seeds were harvested from the same field in five batches. Seed purity ranged from 87.52 to 92.12%, with 7.08 to 11.12% content of usable impurities and 0.52 to 1.36% content of non-usable impurities. Total seed weight was determined at 25.4 Mg. Samples for the determination of seed moisture content were collected at various points along four sampling planes: the silo's axis of symmetry (W21, W31, W41), at the distance of 0.75 m from the axis of symmetry (W12, W22, W32, W42) and along the silo wall (W13, W23, W33, W43). The moisture content of seeds was determined by the drying method with the accuracy of 0.01%. Seeds were dried for 90 hours by circulating heated air throughout the silo. The parameters of circulating air are given in Figure 4. Samples for evaluating seed moisture content were collected eight times, approximately every 10 hours. The temperature and moisture content of drying air were determined upon sample collection.

RESULTS

The results of calculations revealed that the total area of vents in the ventilation cone is larger that cross-sectional area of the pipeline connecting the fan with the silo. Therefore, air flow was not throttled inside the silo. Changes in ventilation efficiency as a function of the height of the seed layer are presented in Figure 2. Initially, at H=0, air was pumped by the fan into the silo at a rate of 4270 $m^3 \cdot h^{-1}$. Ventilation efficiency was reduced to 4090 $m^3 \cdot h^{-1}$ when the thickness of the seed layer reached 1 m. Faba bean seeds were added in successive layers of 0.5 m until the height of the seed bed inside the silo reached 4.5 m. The fan was active and pressure was measured every time a new batch of seeds was added to the silo. The results of ventilation efficiency calculations are presented in Figure 2. The curve indicates that fan efficiency reached 3950 $m^3 \cdot h^{-1}$ when the silo was full. This is a constant value at which faba been seeds were dried for 90 hours. The correlation between ventilation efficiency and the height of the seed layer was described by a regression equation (Fig. 2). Changes in the amount of air pumped into the silo as the height of the seed layer increased from 1 to 4.5 m are presented in Figure 3. The seed layer with the height of 1 m was aired at 723 $m^3 \cdot Mg^{-1} \cdot h^{-1}$. When the height of the seed layer increased to 4.5 m, the amount of air pumped into the silo was reduced to 155 $m^3 \cdot Mg^{-1} \cdot h^{-1}$, and the drying process was conducted at this air flow rate for 90 hours. Changes in the amount of air supplied to the silo as the thickness of the seed layer increased from 1 to 4.5 m were described with a regression equation (Fig. 3). Regression equations can be used to calculate ventilation efficiency and the amount of air supplied at any thickness of the seed layer (Figs. 2 and 3). Seed drying inside a silo is determined by ventilation efficiency, air temperature and relative moisture content [2, 4, 6]. In this study, drying air had stable parameters with temperature of 18 to 21° and relative moisture content of 46 to 57%. Changes in air parameters as a function of time are presented in Figure 4.

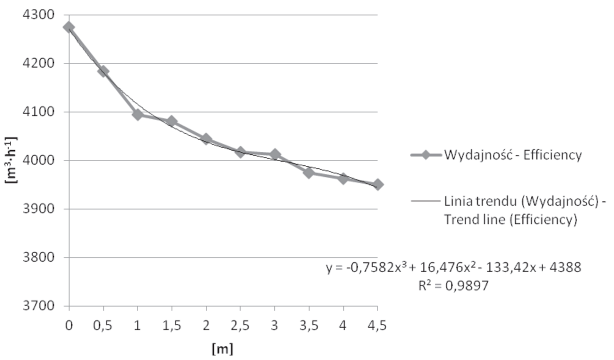

Fig. 2. Changes in ventilation efficiency, subject to the height of the seed layer in the silo.

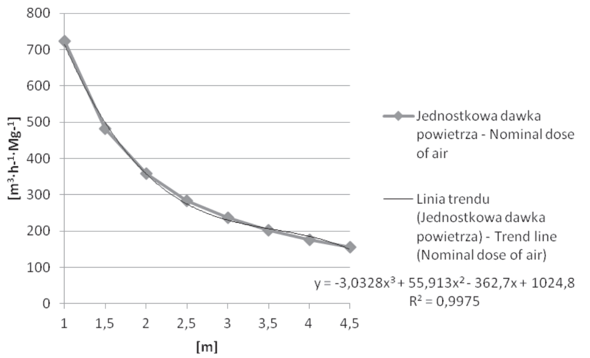

Fig. 3. Changes in the amount of air supplied to faba bean seeds in the silo.

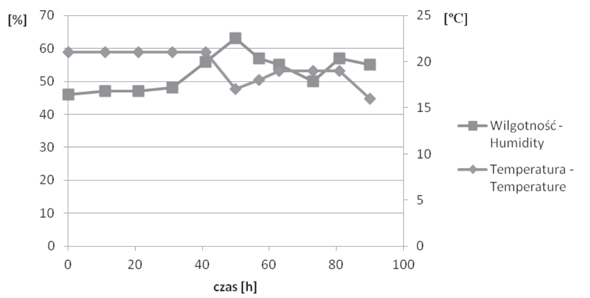

Fig. 4. Temperature and relative moisture content of air as a function of drying time.

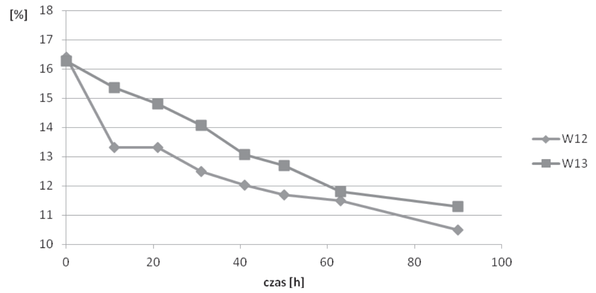

Fig. 5. Actual drying process in the silo in sampling plane W1.

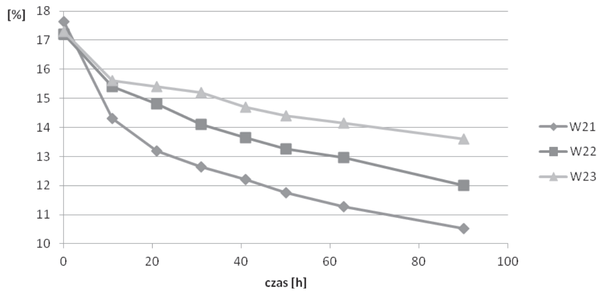

Fig. 6. Actual drying process in the silo in sampling plane W2.

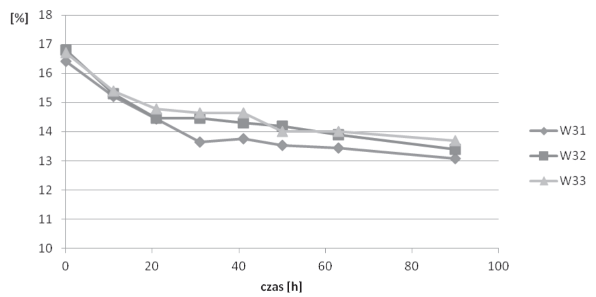

Fig. 7. Actual drying process in the silo in sampling plane W3.

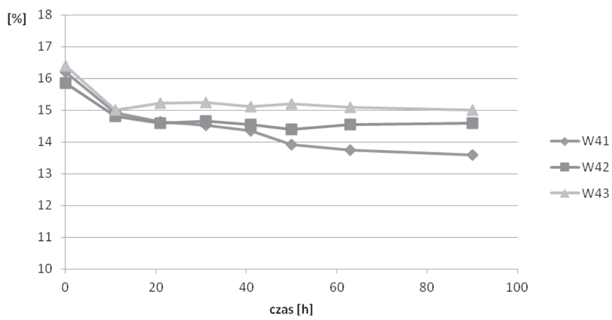

Fig. 8. Actual drying process in the silo in sampling plane W4.

In plane W1, samples were collected at two points, W12 and W13, between the discharge tube and the ventilation cone (Fig. 5). Ventilation efficiency curves indicate that drying in plane W1 proceeded at the highest rate after 90 hours, and relative moisture content was determined at 10.5% and 11.3%, respectively. The drying rate at points W12 and W13 was very high because seeds were dried by air with the lowest moisture content.

The initial moisture content of seeds in plane W2 was 17.5% (Fig. 6). At the end of drying, the highest drop in moisture content to 10.5% was noted along the axis of symmetry, whereas the lowest drop to 13.6% was observed by the silo wall. The above results can be attributed to increased air flow resistance due to seed segregation along the silo wall [2, 7].

The drying process was most stable in plane W3, and changes in air moisture content were similar at all points. The drying process was slowest in plane W4 (Fig. 8). After 90 hours of drying, moisture content was determined at 13.6% in point W41, 14.6% in W42 and 15% in W43. Air passing through the thickest seed layer is more moist than at the beginning of the process (planes W1 and W2). Ventilation curves indicate that seeds were dried most rapidly along the silo's axis of symmetry. The seed bulk was characterized by the highest porosity along the axis of symmetry, which minimized air flow resistance inside the silo [2].

CONCLUSIONS

1. The amount of air supplied to the silo by the WP-25 fan ranges from 723 $m^3 \cdot Mg^{-1} \cdot h^{-1}$ to 150 $m^3 \cdot Mg^{-1} \cdot h^{-1}$, subject to the degree of silo filling with faba bean seeds.
2. A vertical air circulation system with a ventilation cone facilitates the process of drying faba bean seeds.
3. Faba bean seeds are dried most rapidly along the axis of symmetry, whereas the drying rate is lowest by the silo's outer wall.
4. Faba beans are dried faster in the lower part of the silo, therefore, a two-phase drying process is recommended in planes W1, W2 and W3. Seeds dried in the lower part of the silo should be removed upon the achievement of the optimal moisture content for storage. The remaining seeds should be dried in the second stage of the process.

REFERENCES

1. **Bowszys J. 2003.** Rozkład temperatur w masie ziarna pszenicy przechowywanej w metalowych silosach zbożowych. Proceedings of the National Agricultural University of Ukraine, "Mechanization of Agricultural Production", Kyiv, 14:173-179
2. **Bowszys J. 2006.** Doskonalenie technologii suszenia i przechowywania w cylindrycznych silosach zbożowych. Zeszyt 302. Wydział Inżynierii Produkcji AR Lublin.
3. **Bowszys J. 2013.** Wpływ grubości warstwy nasion składowanych w silosach z pionowym układem wietrzenia na parametry przepływu powietrza. MOTROL Motoryzacja i Energetyka Rolnictwa vol 15, No1.11-14
4. **Bowszys J., Bowszys T. 2013.** Przebieg procesu suszenia oraz zmiany jakości nasion bobiku w silosie z promieniowym układem wietrzenia (cz. I). MOTROL Motoryzacja i Energetyka Rolnictwa vol 15, No1.15-18.
5. Bowszys J., Cydzik R. Silos zbożowy do dosuszania ziarna nr patentu 74982.
6. **Bowszys J., Grabowski J., Tomczykowski J. 2004.** Temperatures in seed mass stored in a metallic immediatelyt after harvest. Techn. Sc. 7/2004.
7. **Bowszys J., Tomczykowski J. 2007.** Self-segregation of maize kernels during gravitational discharge from a silo. TEKA Kom. Mot. Power Ind. Agricult. VII. 38-43.
8. **Figiel A. Konieczna M. 2001.** Fizyczne i biologiczne wskaźniki podatności nasion bobiku na uszkodzenia w procesie suszenia i nawilżania. Acta Agrophysica 46: 55-62.
9. **Grzesiuk S., Górecki R. 1994.** Fizjologia plonów. Wprowadzenie do przechowalnictwa. Wyd. ART. Olsztyn.
10. **Kusińska E. 2006.** An influence of outer energy on moisture content distribution in grains stoned in a model silo. TEKA Kom. Mot. Power Ind. Agricult. VI. 75-84.
11. **Nadulski R., Kusińska E., Guz T., Kobus Z. 2012.** Wpływ wilgotności ziarniaków i nacisku pionowego na ich energię i zdolność kiełkowania. Inżynieria Rolnicza, 2(137):221-229.
12. **Szwed G., Kusińska E. 2005.** Zmiana cech geometrycznych ziarniaków pszenicy w wyniku niekorzystnych warunków przechowywania. MOTROL Motoryzacja i Energetyka Rolnictwa 7, 196-207.

PROCESS SUSZENIA NASION BOBIKU W SILOSIE Z PIONOWYM PRZEPŁYWEM POWIETRZA

Streszczenie. Nasiona roślin strączkowych zebrine przy użyciu kombajnu jesienią charakteryzują się wysoką zawartością wilgoci. W tym badaniu, nasiona bobiku suszono w niskich temperaturach w silosie z pionowym przepływem powietrza. Niska temperatura i długi czas suszenia wynoszący 90 godzin zminimalizowały stres cieplny w nasionach. Celem badania było opisanie procesu suszenia nasion bobiku w silosie z pionowym przepływem powietrza, lekko ogrzewanym przez 13,5 kW grzejnik elektryczny Wyniki tego badania wskazują, że ilość powietrza pompowanego do silosu przez wentylator WP-25 wynosi od 723 $m^3 \cdot Mg^{-1} \cdot h^{-1}$ do 150 $m^3 \cdot Mg^{-1} \cdot h^{-1}$, zależnie od stopnia wypełnienia silosu nasionami bobiku. Pionowy obieg powietrza ze stożkiem wentylacyjnym ułatwia proces suszenia nasion bobiku. Bobik suszy się najszybciej wzdłuż osi symetrii silosu, natomiast szybkość suszenia jest najniższa wzdłuż zewnętrznych ścian silosu. Nasiona suszą sie szybciej w dolnej części silosu, zatem zaleca się dwufazowy proces suszenia w płaszczyznach W1, W2 i W3.

Nasiona suszone w dolnej części silosu należy usuwać po osiągnięciu optymalnej zawartości wilgoci w celu przechowywania. Pozostałe nasiona powinny być suszone w drugim etapie procesu.

Słowa kluczowe: silosy, suszenie, przechowywanie, bobik.

Application of Generalized Method of Lines for Solving the Problems of Thick Plates Thermoelasticity
Part I. Construction of resolving equations

Valery Chybiryakov, Anatoly Stankevich, Dmitry Levkivskiy, Vladimir Melnychuk

Kyiv National University of Construction and Architecture
Povitroflotskyy Prosp., 31, Kyiv, Ukraine, 03680, e-mail: dmitriylev88@gmail.com

Received December 07.2014; accepted December 17.2014

Summary. The authors proposed a new version of lowering dimensionality in the application of the method of lines. The basic idea is lowering the dimensionality of input equations per the spatial coordinate by projection method, including the Bubnov-Galerkin method.

Key words: metod of lines, Bubnov-Galerkin-Petrov thermoelasticity method, thick plates, structural mechanics.

INTRODUCTION

The authors proposed a new version of lowering dimensionality in the application of the method of lines. It is greatly expanding the capabilities of method of lines. The proposed generalized method of lines may be used for calculating the plates of variable thickness, and also problems of dynamics. The basic idea of generalized method of lines is lowering the dimensionality of input equations per the spatial coordinate by projection method. The projection method includes the Bubnov-Galerkin method, generalized by Petrov [4].

PURPOSE OF WORK

One of the most effective methods of solving multidimensional problems of structural mechanics is the combination approach. In this approach a problem is solved in two stages:

1) decreasing the dimension of the input equations by one or two coordinates;
2) the reduced problem is solved analytically or numerically.

Traditionally in structural mechanics, lowering dimensionality of input equations is based on certain hypotheses. Accordingly, the first stage of the method was excluded in a separate research: theory of rods, plates and, shells. Applied hypotheses were strong enough but less accurate. It lead to creation of various theories of plates and shells.

Currently, lowering dimensionality is performed using mathematical methods (for example, the theory of shells I.N.Vekua [1]). With the next solution of reduced equations, lowering the dimension creates a combined method for solving problems of mathematical physics. Such methods include Vlasov-Kantorovich's method. These combined methods are alternative, compared to the general numerical methods such as finite element method, finite difference and variation-difference method.

Mathematical methods of lowering dimensionality are associated with the geometrical characteristics of the considered objects. It greatly restricts the geometry of the problems, for which it is possible to use the combined methods. However, limiting the complexity of the geometry allows the application of very efficient numerical methods. It increases the accuracy and stability of numerical calculation. It also significantly reduces computer time using.

One of the known methods of lowering dimensionality input equations is the "method of lines". In this method, the finite difference method is used for one of the two coordinates. This method will be effective, if the input equations are systems of ordinary differential equations. In the case of constant coefficients in these equations, it is possible to use analytical solution of system of equations (Vinokurov [2], Shkelov L.T. [3]). In this regard, the method of lines is used for the solution of static problems for plates and shells of constant thickness.

The authors proposed a new version of lowering dimensionality in the application of the method of lines. It is greatly expanding the capabilities of method of lines. The proposed generalized method of lines may be used for calculating the plates of variable thickness, and also problems of dynamics. The basic idea of generalized method of lines is lowering the dimensionality of input equations per the spatial coordinate by projection method. The projection method includes the Bubnov-Galerkin method, generalized by Petrov [4].

In the case of thick plates with constant thickness for equations of plate deformations per thickness, locally basic restricted discrete linear functions are chosen (Fig. 1.).

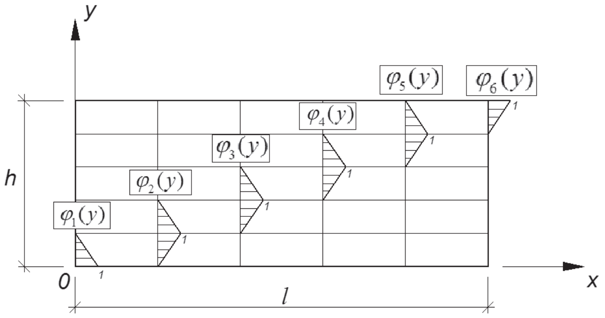

Fig. 1. Basis functions

As in the traditional version of the method of lines, a cross-section of the plate is divided into inflict n lines (including two boundary lines) with an equal range Δ. However, in order to reduce dimensionality, we do not use method of finite differences, but the generalized method of Bubnov-Galerkin-Petrov. By coordinate y the unknown functions $f(x,y)$ is approximated in this manner:

$$f(x,y) \approx f^i(x) \cdot \varphi_i(y) \tag{1}$$

The constructed algorithm of lowering dimensionality formally resembles algebraic transformations of tensor calculus. In this connection, the generalized method of lines essentially tensor symbols and relevant rules are used. For example, by repeated indexes is assumed summation. Resolving equations according to Bubnov-Galerkin method, after substituting approximate ratios of the form (1) are scalar multiplied in Hilbert space for basic functions $\varphi_i(y)$.

It should be noted that in Bubnov-Galerkin method, the basis functions must satisfy the homogeneous boundary conditions per coordinate y. These basis functions do not satisfy such conditions. However, according to the generalization of Petrov [4] it is enough that these functions satisfy natural boundary conditions. It should be noted that in the construction of reduced equations for intensive unknowns (displacement in the theory of elasticity) and extensive unknowns (stresses) transformation of corresponding components is performed differently. Herewith we get two basic matrices – G and B, which are recorded in an index form as: $g_{ij} = (\varphi_i, \varphi_j)$, $b_{ij} = (\varphi_i, \frac{d\varphi_j}{dy})$. This is the scalar product of two functions:

$$(\varphi_i, \varphi_j) = \int_0^h \varphi_i(y) \cdot \varphi_j(y) \cdot dy\,. \tag{2}$$

Conversion of components with derivative y of the function n -type displacement and stresses-type functions is formed in different ways. This is the use of lowering dimension of a plane problem using the theory of elasticity (3, 4).

The peculiarity of this functional basis is that this basis is not orthogonal, and thus there exist two types of index values, f^i and f_i. These magnitudes are different by rules of conversion at transition on another basis. Contravariant magnitudes denoted by upper index and covariant magnitudes – lower index. Accordingly, $\{g_{ij}\}$ – two indexes magnitude is twice covariant metric tensor and the inverse matrix $\{g_{ij}\}^{-1} = \{g^{ij}\}$ is twice contravariant metric tensor. Metric tensor provides a transition from covariant to contravariant components and vice versa:

$$f_i = g_{ij} \cdot f^j\,,\; f^i = g^{ij} \cdot f_j\,. \tag{5}$$

The scalar product in this case is the integral of multiplication functional factors. Therefore in mathematics covariant and contravariant function magnitudes have an identified name. Because the covariant magnitudes appear in the decomposition by basis (fig. 1), they are called coefficients. Covariant magnitudes appear as a scalar product of the basis elements:

$$f(x,\, y) = (f(x,\, y), \varphi_i(y)) = \int_0^h f(x,\, y) \cdot \varphi_i(y) dy\,,$$

they are called – moments.

Therefore, reduced equations can be written in four ways:

– In moments, if displacement and stresses in the moments;
– In coefficients, if all unknowns are written in coefficients;
– Two versions of combined record: displacement in the moments, stresses in the coefficients or displacement in coefficient, stresses in the moments.

$$\begin{aligned}(\frac{\partial u(x,y)}{\partial y}, \varphi_i(y)) &= \int_0^h \frac{\partial u(x,y)}{\partial y} \cdot \varphi_i(y) dy = \int_0^h \frac{\partial (u^j(x)\varphi_j(y))}{\partial y} \cdot \varphi_i(y) dy = \\ &= u^j(x) \int_0^h \varphi_i(y) \varphi_j'(y) dy = b_{ij} u^j(x),\end{aligned} \tag{3}$$

$$\begin{aligned}&(\frac{\partial \sigma_x(x,y)}{\partial y}, \varphi_i(y)) = \int_0^h \frac{\partial \sigma_x(x,y)}{\partial y} \cdot \varphi_i(y) dy = \sigma_x(x,y)\varphi_i(y)\Big|_0^h - \int_0^h \sigma_x(x,y) \cdot \varphi_i'(y) dy = \\ &(\sigma_x(x,h) \cdot \varphi_n(h) - \sigma_x(x,0) \cdot \varphi_1(0)) - \int_0^h \sigma_x{}^j(x) \cdot \varphi_j(y) \cdot \varphi_i'(y) dy = \\ &(\sigma_x(x,h) \cdot \varphi_n(h) - \sigma_x(x,0) \cdot \varphi_1(0)) - b_{ji} \sigma_x{}^j(x)\end{aligned} \tag{4}$$

After formulating the constructing equations, we need to formulate the reduced boundary value and initial – boundary value problem in index form.

The described technique can be applied to solve the problem of thermal stresses in a rod of rectangular cross-section (Fig. 2.), which occupies a three-dimensional region: $[0 \le x \le l] \times [0 \le y \le h_y] \times [0 \le z \le h_z]$.

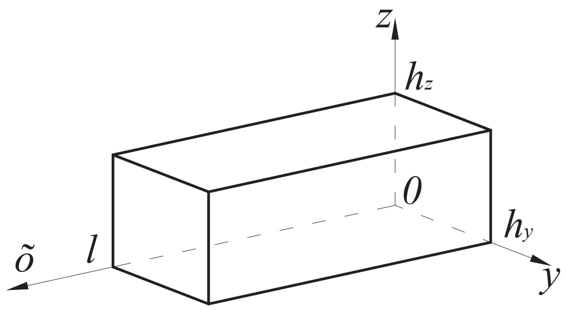

Fig. 2. Beam of rectangular cross section

The problem of thermal stresses is considered within limits of an important partition of the theory of elasticity – thermoelasticity [5, 6]. In this problem we consider two physical fields – thermal and mechanical.

Thermal field in solids is described by the thermal conductivity equation. In the most general form, thermal field depends not only on three spatial coordinates but also on time coordinates. The corresponding problem in determining of the component of thermal field is described by the equations of non-stationary thermal conductivity. Components depend on the time coordinate. As a system of differential equations in partial derivatives of the first order in the spatial and time coordinates, these equations are written in the form:

$$\begin{cases} \rho c \dfrac{\partial T}{\partial t} = \dfrac{\partial q_x}{\partial x} + \dfrac{\partial q_y}{\partial y} + \dfrac{\partial q_z}{\partial z} + Q \\ q_x = -\lambda_T \dfrac{\partial T}{\partial x} \\ q_y = -\lambda_T \dfrac{\partial T}{\partial y} \\ q_z = -\lambda_T \dfrac{\partial T}{\partial z} \end{cases}, \qquad (6)$$

where $T = T(x, y, z)$ – temperature function, q_x, q_y, q_z – components of the heat flux $\vec{q}(x, y, z)$, ρ – density of the material, c – specific heat, λ_T – coefficient of thermal conductivity. Q – the quantity of heat generated by internal heat sources.

To ensure unity of solution of the system (6) we need to specify the initial and boundary conditions. The initial conditions are in the form:

$t = 0$, $T(x, y, z) = T_0(x, y, z)$,

where:

$T_0(x, y, z)$ – temperature distribution throughout the volume of the body at the initial time.

The boundary conditions of the problem will be set as conditions of convective heat transfer.

when $x = 0$:

$$q_x(0, y, z, t) = \alpha_{xT}^0 (T_{xC}^0 - T_x^0) - q_{xC}(0, y, z, t),$$

when: $x = l$,

$$q_x(l, y, z, t) = \alpha_{xT}^l (T_x^l - T_{xC}^l) + q_{xC}(l, y, z, t). \qquad (7)$$

The temperatures and heat flows of external environment from the side of relevant part of boundary surface of beam are marked as “C”:

when: $y = 0$,

$$q_y(x,0,z,t) = -\alpha_{yT}^0 (T_y(x,0,z,t) - T_{yC}(x,0,z,t)) - q_{yC}(x,0,z,t),$$

when: $y = h_y$, (8)

$$q_y(x,h_y,z,t) = \alpha_{yT}^{h_y} (T_y(x,h_y,z,t) - T_{yC}(x,h_y,z,t)) + q_{yC}(x,h_y,z,t),$$

when: $z = 0$,

$$q_z(x,y,0,t) = -\alpha_{zT}^0 (T_z(x,y,0,t) - T_{zC}(x,y,0,t)) - q_{zC}(x,y,0,t),$$

when $z = h_z$: (9)

$$q_z(x,y,h_z,t) = \alpha_{zT}^{h_z} (T_z(x,y,h_z,t) - T_{zC}(x,y,h_z,t)) + q_{zC}(x,y,h_z,t).$$

In the next numerical calculations, such form of boundary conditions allows to take into account the relevant part of surface boundary conditions of first order $\alpha_T \to \infty$ and second order $\alpha_T \to 0$.

Changing temperature of solid body in time practically does not cause dynamic effects. Therefore, mechanical fields (displacement, stress and strain fields) are stationary and are described by static equations.

These equations are written as equations in partial derivatives of first order:

$$\frac{\partial \sigma_x}{\partial x} = -\frac{\partial \tau_{xy}}{\partial y} - \frac{\partial \tau_{xz}}{\partial z} - X, \qquad (10)$$

$$\frac{\partial \tau_{xy}}{\partial x} = -\frac{\partial \sigma_y}{\partial y} - \frac{\partial \tau_{yz}}{\partial z} - Y, \qquad (11)$$

$$\frac{\partial \tau_{xz}}{\partial x} = -\frac{\partial \tau_{yz}}{\partial y} - \frac{\partial \sigma_z}{\partial z} - Z, \qquad (12)$$

$$\frac{\partial u^*}{\partial x} = \frac{\mu}{(\lambda + 2\mu)} \sigma_x - \frac{\lambda}{(\lambda + 2\mu)} \frac{\partial v^*}{\partial y} - \frac{\lambda}{(\lambda + 2\mu)} \frac{\partial w^*}{\partial z} + \frac{(3\lambda + 2\mu)}{(\lambda + 2\mu)} \alpha_T (T - T_0), \qquad (13)$$

$$\frac{\partial v^*}{\partial x} = \tau_{xy} - \frac{\partial u^*}{\partial y}, \qquad (14)$$

$$\frac{\partial w^*}{\partial x} = \tau_{xz} - \frac{\partial u^*}{\partial z}. \qquad (15)$$

The equations can be separately considered:

$$\sigma_y = \frac{\lambda}{\mu}\frac{\partial u^*}{\partial x} + \frac{(\lambda+2\mu)}{\mu}\frac{\partial v^*}{\partial y} + \frac{\lambda}{\mu}\frac{\partial w^*}{\partial z} - \frac{(3\lambda+2\mu)}{\mu}\alpha_T(T-T_0), \quad (16)$$

$$\sigma_z = \frac{\lambda}{\mu}\frac{\partial u^*}{\partial x} + \frac{\lambda}{\mu}\frac{\partial v^*}{\partial y} + \frac{(\lambda+2\mu)}{\mu}\frac{\partial w^*}{\partial z} - \frac{(3\lambda+2\mu)}{\mu}\alpha_T(T-T_0), \quad (17)$$

$$\tau_{yz} = \left(\frac{\partial w^*}{\partial y} + \frac{\partial v^*}{\partial z}\right), \quad (18)$$

where: $f^* = \mu \cdot f$.

Boundary conditions of stress-strain state in general are written by the analogy of work [7] (19)-(24).

For construction of the boundary conditions (19)-(24) we write the sum of projections of all power factors that act on the boundary contour, on corresponding axis. In (Fig. 3.) on the plane $x0y$, the magnitudes which act on area $x=0$ are shown.

The first index —signifies the number of the axis which is perpendicular to the area. The second index shows the direction of displacement or stress.

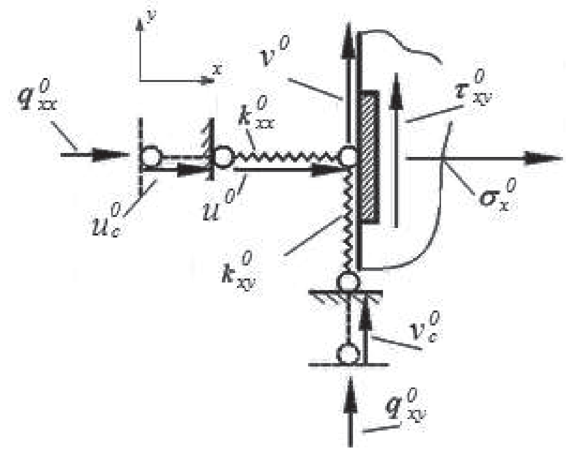

Fig. 3. Modeling of the boundary conditions

u_c, v_c — displacement of points of the external environment,
u, v — horizontal and vertical displacement of points of object,
q_{xx}, q_{xy} — external load on object,
σ_x, τ_{xy} — normal and tangential (shear) stresses along the contour inside the object,
k_{xx}, k_{xy} — spring stiffness.

when: $x=0$,

$$\frac{1}{\sqrt{1+(k^0_{xx})^2}}\sigma^0_x - \frac{k^0_{xx}}{\sqrt{1+(k^0_{xx})^2}}u^0 + \frac{1}{\sqrt{1+(k^0_{xx})^2}}q^0_{xx} + \frac{k^0_{xx}}{\sqrt{1+(k^0_{xx})^2}}u^0_c = 0, \quad (19)$$

$$\frac{1}{\sqrt{1+(k^0_{xy})^2}}\tau^0_{xy} - \frac{k^0_{xy}}{\sqrt{1+(k^0_{xy})^2}}v^0 + \frac{1}{\sqrt{1+(k^0_{xy})^2}}q^0_{xy} + \frac{k^0_{xy}}{\sqrt{1+(k^0_{xy})^2}}v^0_c = 0, \quad (20)$$

$$\frac{1}{\sqrt{1+(k^0_{xz})^2}}\tau^0_{xz} - \frac{k^0_{xz}}{\sqrt{1+(k^0_{xz})^2}}w^0 + \frac{1}{\sqrt{1+(k^0_{xz})^2}}q^0_{xz} + \frac{k^0_{xz}}{\sqrt{1+(k^0_{xz})^2}}w^0_c = 0, \quad (21)$$

when: $x=l$,

$$-\frac{1}{\sqrt{1+(k^l_{xx})^2}}\sigma^l_x - \frac{k^l_{xx}}{\sqrt{1+(k^l_{xx})^2}}u^l + \frac{1}{\sqrt{1+(k^l_{xx})^2}}q^l_{xx} + \frac{k^l_{xx}}{\sqrt{1+(k^l_{xx})^2}}u^l_c = 0, \quad (22)$$

$$-\frac{1}{\sqrt{1+(k^l_{xy})^2}}\tau^l_{xy} - \frac{k^l_{xy}}{\sqrt{1+(k^l_{xy})^2}}v^l + \frac{1}{\sqrt{1+(k^l_{xy})^2}}q^l_{xy} + \frac{k^l_{xy}}{\sqrt{1+(k^l_{xy})^2}}v^l_c = 0, \quad (23)$$

$$-\frac{1}{\sqrt{1+(k^l_{xz})^2}}\tau^l_{xz} - \frac{k^l_{xz}}{\sqrt{1+(k^l_{xz})^2}}w^l + \frac{1}{\sqrt{1+(k^l_{xz})^2}}q^l_{xz} + \frac{k^l_{xz}}{\sqrt{1+(k^l_{xz})^2}}w^l_c = 0. \quad (24)$$

where: $f^0 = f(0,y,z)$, $\quad f^l = f(l,y,z)$.

By changing stiffness we can specify any standard conditions of interaction of the object with the external environment.

For equations (6)-(24) the procedure of lowering dimension is performed by coordinates y, z. At first — reduction by y. Basic functions are applied $\{\varphi_i = \varphi_i(y)\}$, $i = 1,...,n$, where the following rules are taken into account:

$$f(x,y,z,t) = f^i(x,z,t) \cdot \varphi_i(y),$$

$$(f(x,y,z,t), \varphi_i(y)) = \int_0^{h_y} f(x,y,z,t) \cdot \varphi_i(y)dy =$$

$$= f_i(x,z,t);$$

$$\left(\frac{\partial f(x,y,z,t)}{\partial x}, \varphi_i(y)\right) = \int_0^{h_y} \frac{\partial f(x,y,z,t)}{\partial x} \varphi_i(y)dy =$$

$$\frac{\partial}{\partial x}\int_0^{h_y} f(x,y,z,t) \cdot \varphi_i(y)dy = \frac{\partial}{\partial x} f_i(x,z,t).$$

Where f is a factor of stress, then

$$\left(\frac{\partial f(x,y,z,t)}{\partial y}, \varphi_i(y)\right) = \int_0^{h_y} \frac{\partial f(x,y,z,t)}{\partial y} \varphi_i(y)dy =$$

$$= f(x,y,z,t)\varphi_i(y)\Big|_{y=0}^{y=h_y} - \int_0^{h_y} f(x,y,z,t)\varphi_i'(y)dy =$$

$$= f(x,h_y,z,t)\varphi_i(h_y) - f(x,0,z,t)\varphi_i(0) -$$

$$-\int_0^{h_y} f^j(x,z,t)\varphi_j(y)\varphi_i'(y)dy =$$

$$= f^i(x,h_y,z,t)\delta_{i\cdot}^{\cdot n} - f^i(x,0,z,t)\delta_{i\cdot}^{\cdot 1} -$$

$$-b_{ji}g^{j\alpha} f_\alpha(x,z,t).$$

When: f is a factor of temperature and displacement (T,u,v,w), then:

$$\left(\frac{\partial f(x,y,z,t)}{\partial y}, \varphi_i(y)\right) = \int_0^{h_y} \frac{\partial f(x,y,z,t)}{\partial y} \varphi_i(y)dy =$$

$$= \int_0^{h_y} \frac{\partial (f^j(x,z,t)\varphi_j(y))}{\partial y} \varphi_i(y)dy =$$

$$= \int_0^{h_y} \varphi_i(y)\varphi_j'(y) f^j(x,z,t)dy = b_{ij}g^{j\alpha} f_\alpha(x,z,t).$$

The first equation of system (6) is multiplied as a scalar by $\{\varphi_i = \varphi_i(y)\}$ where $i = 1,...,n$, and than integrated by coordinate y:

$$\begin{gathered}
((\frac{\partial q_x}{\partial x} + \frac{\partial q_y}{\partial y} + \frac{\partial q_z}{\partial z} - \rho c\frac{\partial T}{\partial t} + Q(x,y,z,t)) = 0, \varphi_i(y)), \\
\frac{\partial q_{xi}}{\partial x} + \delta_{\cdot i}^{n\cdot} \cdot q_y{}^i(x,z,t) - \delta_{\cdot i}^{1\cdot} \cdot q_y{}^i(x,z,t) - \\
-b_{ji}g^{j\alpha} q_{y\alpha}(x,z,t) + \frac{\partial q_{zi}}{\partial z} - \rho c\frac{\partial T_i}{\partial t} + Q_i(x,z,t) = 0.
\end{gathered} \tag{25}$$

In the next step we perform the reduction by z of equation (20):

$$\begin{gathered}
(\frac{\partial q_{xi}}{\partial x} + \delta_{\cdot i}^{n\cdot} \cdot q_y{}^i(x,z,t) - \delta_{\cdot i}^{1\cdot} \cdot q_y{}^i(x,z,t) - \\
b_{ji}g^{j\alpha} q_{y\alpha}(x,z,t) + \frac{\partial q_{zi}}{\partial z} - \rho c\frac{\partial T_i}{\partial t} + \\
+Q_i(x,z,t) = 0, \varphi_k(z)), \\
\frac{\partial q_{xik}}{\partial x} + \left[\delta_{\cdot i}^{n\cdot} \cdot q_{y\cdot k}^{\,i\cdot}(x,t) - \delta_{\cdot i}^{1\cdot} \cdot q_{y\cdot k}^{\,i\cdot}(x,t)\right] - \\
-b_{ji}g^{j\alpha} q_{y\alpha k}(x,t) + \left[\delta_{\cdot k}^{m\cdot} \cdot q_{zi\cdot}^{\,\cdot k}(x,t) - \delta_{\cdot k}^{1\cdot} \cdot q_{zi\cdot}^{\,\cdot k}(x,t)\right] - \\
b_{pk}g^{ps} q_{zis}(x,t) - \rho c\frac{\partial T_{ik}}{\partial t} + Q_{ik}(x,t) = 0,
\end{gathered} \tag{26}$$

$$\text{Here } \left[\delta_{\cdot i}^{n\cdot} \cdot q_{y\cdot k}^{\,i\cdot} - \delta_{\cdot i}^{1\cdot} \cdot q_{y\cdot k}^{\,i\cdot}\right] = \begin{bmatrix} -q_{y\cdot k}^{\,1\cdot} \\ 0 \\ \vdots \\ 0 \\ q_{y\cdot k}^{\,n\cdot} \end{bmatrix},$$

$$\left[\delta_{\cdot k}^{m\cdot} \cdot q_{zi\cdot}^{\,\cdot k} - \delta_{\cdot k}^{1\cdot} \cdot q_{zi\cdot}^{\,\cdot k}\right] = \begin{bmatrix} -q_{zi\cdot}^{\,\cdot 1} \\ 0 \\ \vdots \\ 0 \\ q_{zi\cdot}^{\,\cdot m} \end{bmatrix},$$

n – number of lines along the axis y, m - number of lines along the axis z.

Indexes $i, j, \alpha, \beta, \gamma$ - are related to reduction by coordinate y; indexes $k, p, s, \phi, \varepsilon$ - reduction by coordinate z.

Taking into account the boundary conditions (8)-(9):

$$\left[\delta_{\cdot i}^{n\cdot}\cdot q_{y\cdot k}^{\;i\cdot}-\delta_{\cdot i}^{1\cdot}\cdot q_{y\cdot k}^{\;i\cdot}\right]=\begin{bmatrix}\alpha_{yT}^{0}\cdot T_{y\cdot k}^{1\cdot}\\0\\\vdots\\0\\\alpha_{yT}^{h_y}\cdot T_{y\cdot k}^{n\cdot}\end{bmatrix}-\begin{bmatrix}\alpha_{yT}^{0}\cdot T_{yC\cdot k}^{\;1\cdot}\\0\\\vdots\\0\\\alpha_{yT}^{h_y}\cdot T_{yC\cdot k}^{\;n\cdot}\end{bmatrix}+\begin{bmatrix}q_{yC\cdot k}^{\;1\cdot}\\0\\\vdots\\0\\-q_{yC\cdot k}^{\;n\cdot}\end{bmatrix}$$

$$\left[\delta_{i\cdot}^{\cdot m}\cdot q_{zi\cdot}^{\;\cdot k}-\delta_{i\cdot}^{\cdot 1}\cdot q_{zi\cdot}^{\;\cdot k}\right]=\begin{bmatrix}\alpha_{zT}^{0}\cdot T_{zi\cdot}^{\cdot 1}\\0\\\vdots\\0\\\alpha_{yT}^{h_z}\cdot T_{zi\cdot}^{\cdot m}\end{bmatrix}-\begin{bmatrix}\alpha_{yT}^{0}\cdot T_{zCi\cdot}^{\;\cdot 1}\\0\\\vdots\\0\\\alpha_{yT}^{h_z}\cdot T_{zCi\cdot}^{\;\cdot m}\end{bmatrix}+\begin{bmatrix}q_{zCi\cdot}^{\;\cdot 1}\\0\\\vdots\\0\\-q_{zCi\cdot}^{\;\cdot m}\end{bmatrix}$$

The substitution:

$$\begin{bmatrix}\alpha_{yT}^{0}\cdot T_{y\cdot k}^{1\cdot}\\0\\\vdots\\0\\\alpha_{yT}^{h_y}\cdot T_{y\cdot k}^{n\cdot}\end{bmatrix}=T\alpha_{y\cdot k}^{\;i\cdot},\quad\begin{bmatrix}\alpha_{yT}^{0}\cdot T_{yC\cdot k}^{\;1\cdot}\\0\\\vdots\\0\\\alpha_{yT}^{h_y}\cdot T_{yC\cdot k}^{\;n\cdot}\end{bmatrix}=TC_{y\cdot k}^{\;i\cdot},\quad\begin{bmatrix}q_{yC\cdot k}^{\;1\cdot}\\0\\\vdots\\0\\-q_{yC\cdot k}^{\;n\cdot}\end{bmatrix}=q_{yC\cdot k}^{\;i\cdot},\tag{27}$$

$$\begin{bmatrix}\alpha_{zT}^{0}\cdot T_{zi\cdot}^{\cdot 1}\\0\\\vdots\\0\\\alpha_{zT}^{h_z}\cdot T_{zi\cdot}^{\cdot m}\end{bmatrix}=T\alpha_{zi\cdot}^{\;\cdot k},\quad\begin{bmatrix}\alpha_{zT}^{0}\cdot T_{zCi\cdot}^{\;\cdot 1}\\0\\\vdots\\0\\\alpha_{zT}^{h_z}\cdot T_{zCi\cdot}^{\;\cdot m}\end{bmatrix}=TC_{zi\cdot}^{\;\cdot k},\quad\begin{bmatrix}q_{zCi\cdot}^{\;\cdot 1}\\0\\\vdots\\0\\-q_{zCi\cdot}^{\;\cdot m}\end{bmatrix}=q_{zCi\cdot}^{\;\cdot k}.\tag{28}$$

Taking into account the boundary conditions (27)-(28) in equation (20):

$$\begin{aligned}&(\frac{\partial q_{xik}}{\partial x}+\left[g^{i\alpha}\cdot T\alpha_{y\alpha k}-g_{k\varepsilon}TC_{y}^{\;i\varepsilon}+g^{i\alpha}\cdot q_{yC\alpha k}\right]-\\&-b_{ji}g^{j\alpha}q_{y\alpha k}+\\&\left[g^{k\varepsilon}\cdot T\alpha_{zi\varepsilon}-g_{i\alpha}TC_{z}^{\;\alpha k}+g^{k\varepsilon}\cdot q_{yCi\varepsilon}\right]-\\&-b_{pk}g^{ps}q_{zis}-\rho c\frac{\partial T_{ik}}{\partial t}+Q_{ik}=0\end{aligned}\tag{29}$$

Similarly, the reduction of remaining equations of system (6) is done:

$$q_{xik}=-\lambda_{T}\frac{\partial T_{ik}}{\partial x},\tag{30}$$

$$q_{yik}=-\lambda_{T}b_{ij}g^{j\alpha}T_{\alpha k}(x,t),\tag{31}$$

$$q_{zik}=-\lambda_{T}b_{kp}g^{ps}T_{is}(x,t).\tag{32}$$

Substituting (30)-(32) in (29), equation (33) is formed:

$$\begin{aligned}&-\lambda_{T}\frac{\partial^{2}T_{ik}}{\partial x^{2}}+\left[g^{i\alpha}\cdot T\alpha_{y\alpha k}-g_{k\varepsilon}TC_{y}^{\;i\varepsilon}+g^{i\alpha}\cdot q_{yC\alpha k}\right]+\\&+\lambda_{T}b_{ji}g^{j\alpha}b_{\alpha\beta}g^{\beta\gamma}T_{\gamma k}+\\&\left[g^{k\varepsilon}\cdot T\alpha_{zi\varepsilon}-g_{i\alpha}TC_{z}^{\;\alpha k}+g^{k\varepsilon}\cdot q_{yCi\varepsilon}\right]+\\&+\lambda_{T}b_{pk}g^{ps}b_{s\phi}g^{\phi\varepsilon}T_{i\varepsilon}-\rho c\frac{\partial T_{ik}}{\partial t}+Q_{ik}=0\end{aligned}\tag{33}$$

The reduced initial conditions will look like $T_{ik}(x,0)=T_{0ik}(x)$.

The next step is the reduction of equations of system (10)-(14) In this system, the process of reduction expressions are substituted for $\sigma_y,\sigma_z,\tau_{yz}$ (16)-(18), using the above mentioned operations:

$$\frac{du^*_{ik}}{dx}=\frac{\mu}{(\lambda+2\mu)}\sigma_{xik}-\frac{\lambda}{(\lambda+2\mu)}b_{ij}g^{j\alpha}v^*_{\alpha k}-\frac{\lambda}{(\lambda+2\mu)}b_{kp}g^{ps}w^*_{is}+\frac{(3\lambda+2\mu)}{(\lambda+2\mu)}\alpha_T(T_{ik}-T_{0ik}), \quad (34)$$

$$\frac{dv^*_{ik}}{dx}=\tau_{xyik}-b_{ij}g^{j\alpha}u^*_{\alpha k}, \quad (35)$$

$$\frac{dw^*_{ik}}{dx}=\tau_{xzik}-b_{kp}g^{ps}u^*_{is}, \quad (36)$$

$$\frac{d\sigma_{xik}}{dx}=-b_{ji}g^{j\alpha}\tau_{xy\alpha k}+b_{pk}g^{ps}\tau_{xzis}-\left[\delta^{n\cdot}_{\cdot i}\tau_{xy\cdot k}^{\ \ i\cdot}-\delta^{1\cdot}_{\cdot i}\tau_{xy\cdot k}^{\ \ i\cdot}\right]-\left[\delta^{m\cdot}_{\cdot k}\tau_{xy\, i\cdot}^{\ \ \cdot k}-\delta^{1\cdot}_{\cdot k}\tau_{xy\, i\cdot}^{\ \ \cdot k}\right]-X_{ik}, \quad (37)$$

$$\begin{aligned}\frac{d\tau_{xyik}}{dx}&=\frac{\lambda}{\lambda+2\mu}b_{ji}g^{j\alpha}\sigma_{x\alpha k}+\frac{4(\lambda+\mu)}{\lambda+2\mu}b_{ji}g^{j\alpha}b_{\alpha\beta}g^{\beta\gamma}v^*_{x\gamma k}+\\&+\frac{2\lambda}{\lambda+2\mu}\left[b_{ji}g^{j\alpha}\right]\cdot\left[b_{kp}g^{ps}\right]w^*_{\alpha s}-\frac{2(3\lambda+2\mu)}{\lambda+2\mu}b_{ji}g^{j\alpha}\alpha_T(T_{\alpha k}-T_{0\alpha k})+\\&+b_{pk}g^{ps}b_{s\phi}g^{\phi\varepsilon}v^*_{i\varepsilon}+\left[b_{pk}g^{ps}\right]\cdot\left[b_{ij}g^{j\alpha}\right]w^*_{\alpha s}-\left[\delta^{n\cdot}_{\cdot i}\sigma_{y\cdot k}^{\ \ i\cdot}-\delta^{1\cdot}_{\cdot i}\sigma_{y\cdot k}^{\ \ i\cdot}\right]-\left[\delta^{m\cdot}_{\cdot k}\tau_{xz\,i\cdot}^{\ \ \cdot k}-\delta^{1\cdot}_{\cdot k}\tau_{xz\,i\cdot}^{\ \ \cdot k}\right]-Y_{ik},\end{aligned} \quad (38)$$

$$\begin{aligned}\frac{d\tau_{xzik}}{dx}&=\frac{\lambda}{\lambda+\mu}b_{pk}g^{ps}\sigma_{xis}+\frac{4(\lambda+\mu)}{\lambda+2\mu}b_{pk}g^{ps}b_{s\phi}g^{\phi\varepsilon}w^*_{xi\varepsilon}+\frac{2\lambda}{\lambda+2\mu}\left[b_{pk}g^{ps}\right]\cdot\left[b_{ij}g^{j\alpha}\right]v^*_{\alpha s}-\\&-\frac{2(3\lambda+2\mu)}{\lambda+2\mu}\alpha_T b_{pk}g^{ps}(T_{is}-T_{0is})+\left[b_{ji}g^{j\alpha}\right]\cdot\left[b_{kp}g^{ps}\right]v^*_{\alpha\varepsilon}+b_{ji}g^{j\alpha}b_{\alpha\beta}g^{\beta\gamma}w^*_{\gamma k}-\\&-\left[\delta^{n\cdot}_{\cdot i}\tau_{yz\cdot k}^{\ \ i\cdot}-\delta^{1\cdot}_{\cdot i}\tau_{yz\cdot k}^{\ \ i\cdot}\right]-\left[\delta^{m\cdot}_{\cdot k}\sigma_{z\,i\cdot}^{\ \cdot k}-\delta^{1\cdot}_{\cdot k}\sigma_{z\,i\cdot}^{\ \cdot k}\right]-Z_{ik}\end{aligned} \quad (39)$$

The reduced boundary conditions of stress-strain state will look like:

$$\begin{aligned}&\frac{\mu}{\sqrt{1+(k^0_{xx})^2}}\sigma^0_{xik}-\frac{k^0_{xx}}{\sqrt{1+(k^0_{xx})^2}}u^{*0}_{ik}+\frac{\mu}{\sqrt{1+(k^{*0}_{xx})^2}}q^0_{xxik}+\frac{k^0_{xx}}{\sqrt{1+(k^0_{xx})^2}}u^{*0}_{cik}=0,\\&\frac{\mu}{\sqrt{1+(k^0_{xy})^2}}\tau^0_{xyik}-\frac{k^0_{xy}}{\sqrt{1+(k^0_{xy})^2}}v^{*0}_{ik}+\frac{\mu}{\sqrt{1+(k^0_{xy})^2}}q^0_{xyik}+\frac{k^0_{xy}}{\sqrt{1+(k^0_{xy})^2}}v^{*0}_{cik}=0,\\&\frac{\mu}{\sqrt{1+(k^0_{xz})^2}}\tau^0_{xzik}-\frac{k^0_{xz}}{\sqrt{1+(k^0_{xz})^2}}w^{*0}_{ik}+\frac{\mu}{\sqrt{1+(k^0_{xz})^2}}q^0_{xzik}+\frac{k^0_{xz}}{\sqrt{1+(k^0_{xz})^2}}w^{*0}_{cik}=0,\\&-\frac{\mu}{\sqrt{1+(k^l_{xx})^2}}\sigma^l_{xik}-\frac{k^l_{xx}}{\sqrt{1+(k^l_{xx})^2}}u^{*l}_{ik}+\frac{\mu}{\sqrt{1+(k^l_{xx})^2}}q^l_{xxik}+\frac{k^l_{xx}}{\sqrt{1+(k^l_{xx})^2}}u^{*l}_{cik}=0,\\&-\frac{\mu}{\sqrt{1+(k^l_{xy})^2}}\tau^l_{xyik}-\frac{k^l_{xy}}{\sqrt{1+(k^l_{xy})^2}}v^{*l}_{ik}+\frac{\mu}{\sqrt{1+(k^l_{xy})^2}}q^l_{xyik}+\frac{k^l_{xy}}{\sqrt{1+(k^l_{xy})^2}}v^{*l}_{cik}=0,\\&-\frac{\mu}{\sqrt{1+(k^l_{xz})^2}}\tau^l_{xzik}-\frac{k^l_{xz}}{\sqrt{1+(k^l_{xz})^2}}w^{*l}_{ik}+\frac{\mu}{\sqrt{1+(k^l_{xz})^2}}q^l_{xzik}+\frac{k^l_{xz}}{\sqrt{1+(k^l_{xz})^2}}w^{*l}_{cik}=0.\end{aligned} \quad (40)$$

The next step – the problem numerically is simulated using the method of discrete orthogonalization by S.K.Hodunov [8]. Differential equations in partial derivatives are solved using the method of Runge-Kutta-Merson. This problem is programmed by the Fortran programming language. Depending on the geometry and initial-boundary conditions; temperature, displacement and stress are determined at certain points of the construction.

CONCLUSIONS

The suggested modification of the method of lines significantly increases the accuracy of calculation. The problem of setting boundary function is solved and this allows the solution of problem of dynamics and thermoelasticity.

REFERENCES

1. **Vekua I.N., 1982.** Some common methods of constructing different versions of the theory of shells. M .: Science. Home Editorial physical and mathematical literature, 288 p. (in Russian).
2. **Vinokurov L.P., 1956.** Direct methods for solving spatial and contact problems for arrays and foundations. Kharkiv. Publ Kharkov. Univ, 279 p. (in Russian).
3. **Shkelёv L.T., Stankevich A.N., Poshivach D.V., 2004.** Application of the method of lines for the determination of the stress and strain states of the spatial and plate structural elements: Monograph. – K .: KNUCA, 2004. -136 p. (in Russian).
4. **Mikhlin S.M., 1957.** Variational methods in mathematical physics // State-ing because of technical and theoretical l-ry: M – 476 p. (in Russian).
5. **Kovalenko A.D., 1970.** Fundamentals of thermoelasticity, Naukova Dumka, – 308. (in Russian).
6. **Kovalenko A.D.,1975.** Thermoelasticity. Textbook. To .: Vishcha School, – 215 p. (in Russian).
7. **Stankevich A.M., Chibiryakov V.K., Skele L.T., 2010.** The method of lines in prostoroviy zadachi teoriї pruzhnosti // Naukova-tehnichny zbirnik "Opir materialiv i teoriya sporud" – Preview Issue №87, – p.109 – 117. (in Ukrainian).
8. **Godunov S.K**., **1961**. On the numerical solution of boundary value problems for systems of linear ordinary differential equations // Advances Mathematical Sciences. – v.16 – No.3. – P.171 – 174. (in Russian).

ПРИМЕНЕНИЕ ОБОБЩЕННОГО МЕТОДА ПРЯМЫХ К ЗАДАЧАМ ТЕРМОУПРУГОСТИ ТОЛСТЫХ ПЛИТ. СООБЩЕНИЕ 1. ПОСТРОЕНИЕ РАЗРЕШАЮЩИХ УРАВНЕНИЙ

Аннотация. Авторами данной работы предложен новый вариант понижения размерности методом прямых, что существенно расширило его возможности. Обобщенный метод прямых применим для плит переменной толщины, а также в задачах динамики. Основная идея состоит в понижении размерности по пространственной координате с помощью проекционного метода (к проекционному методу относится метод Бубнова – Галеркина, обобщенный Г. И. Петровым [4]). В работе методика понижения размерности используется для редукции уравнений термоупругости.

Ключевые слова: метод прямых, метод Бубнова-Галёркина-Петрова, термоупругость, толстые пластины, строительная механика.

Assessment of The Mechanical Properties of Fresh Soil-grown Cucumber Fruits

Józef Gorzelany, Natalia Matłok, Dagmara Migut

Department of Food and Agriculture Production Engineering of the University of Rzeszów

Received December 01.2014; accepted December 17.2014

Summary. The handling, storage, and transportation of fresh cucumbers affect the water content in the fruit, and consequently its firmness and the quality of final products. This concerns the raw material intended for both direct consumption and processing. The water losses resulting from too long storage substantially affect the final parameters of the product. The aim of this study was the determination of water content impact on the selected mechanical properties of fresh cucumbers, analysis of cucumber section image and assessment of peel and flesh resistance in fresh fruits of the tested cucumber varieties to mechanical damages caused at the process of their puncturing with a 5mm-diameter punch.

Key words: soil-grown cucumbers, mechanical properties, puncture force of peel and tissue, water content.

INTRODUCTION

Cucumber (Cucumis sativus L.) belongs to annual plants of high temperature and soil requirements. It represents pumpkin vegetables of Cucurbitales order. Their distinguished varieties are those for sowing in soil and those for cultivation under covers [6].

The production of soil-grown cucumbers regularly increases due to their high popularity and a wide range of cucumber fruit use. In 2013 the crop was 280,000 tons, and it was close to that of 2012. In comparison with the average production in the period 2006-2011 the production of soil-grown vegetables in 2013 was lower by 4.5 % [4].

Apart from the mass consumption of cucumbers in the form of fresh fruit, a great part of the total crop is used as a popular processing product used for the production of pickled and conserved cucumbers, gherkins, and pickles. Cucumber fruit intended for processing should have small seed chamber, appropriate chemical composition, sugar content above 2 %, resistance to the forming and presence of voids, high yield in the production at industrial scale, and high resistance to pests. Besides, it is important that cucumber fruit is of uniform shape and appropriate, regular and equal colour [11].

Biological materials in general are subjected to various both static and dynamic loads which are connected with the harvest, handling, trans-ship, transport, sorting and storage. As the result of these technological processes, cucumber fruit undergoes mechanical damages manifesting themselves with both external and internal disturbances of their tissue cell structure [5]. Mechanical damages make the commercial value of the raw material lower so they reduce its processing value. Besides, they contribute to the softening of the cucumber by damaging its peel, which is a specific protection barrier supporting the cohesiveness of the raw material. The process of cucumber softening favours the formation of next damages and the development of putrefactive bacteria [1, 3]. The way in which fresh cucumbers are handled, stored, and transported affect the content of water in the fruit, as well as its firmness and the quality of the final products. This concerns the raw material intended for direct consumption as well as for processing. The losses of water content significantly affect the final parameters of the product and the mechanical properties of the raw material.

The investigation of mechanical properties is the basic measurement instrument of the texture and elasticity of the tested biological material [8]. It includes a series of mechanical tests where compressive, shearing, and tensile forces are used [10]. The deformation rate depends on the value of the used force, rate of the tested material forming, shape and size of the investigated sample as well as such factors as the plant variety, maturity/ripeness degree, raw fibre content, water content and the material's specific density [2, 7, 9].

METHODS AND MEASURING APPARATUS

Two size fractions (the 1st one 3.5 to 5.5 cm, and the 2nd one 6 – 8 cm) of five varieties of soil-grown cucumber were investigated: Polan F_1, Śremski F_1, Śremianin F_1 and two cucumber genotypes as reference (standards) material. The samples of the soil-grown cucumber were taken from three farms engaged in the production of vegetables in the village of Ciszyca (Świętokrzyskie Province), and the station of Krakowska Hodowla i Nasiennictwo Ogrodnicze "POLAN" *(Cracow Plant Breeding and Seed Production "POLAN")* with their seat in Kraków (Raciborowice testing grounds).

The water content measurement in fresh cucumbers was conducted in the first stage of drying at the temperature of 70^0 C for 6 hrs by means of laboratory incubator, and then in the second stage of the drying up of the samples in the temperature of 140^0 C with the use of scale incubator. The tests for the content of water were performed on the samples cut out in three places i.e. at the leaf stalk base, in the middle and in the bottom part of the cucumber fruit for two selected fruit fractions.

The investigation of the mechanical properties in the process of the puncturing of the peel and flesh of fresh and pickled cucumbers were performed by means of Zwick / Roell machine for strength testing with the use of the punch of the diameter of Ø 5 mm. The measurement was performed in three places, i.e. at the leaf stalk base, in the middle and in the bottom part of the cucumber fruit.

The tests were conducted on the whole fruits of soil-grown cucumber with 15 repetitions for each of the three measurement places. The measurement was conducted separately for each size fraction. After every measurement series the average force required to puncture cucumber peel and flesh, their deformation, and the energy of puncture was measured.

RESULTS OF THE INVESTIGATION

The average content of water in the fresh cucumber fruits of the investigated varieties was within the range of 94.1% up to 95.6 %. The highest water content was found in the fruit of the Polan variety, the 2nd fraction size, and it amounted to 95.3 %, regardless from which place the sample was taken. The 44 genotype of the 1st size fraction was featured by the lowest water content in the fruit. The lowest value was found at the fruit stalk base of the variety referred to above and it amounted to 93.9 %. From among the tested varieties the highest content of water was found in the Polan variety for both the size fractions. Analyzing the investigation place, the differences in the average water content were insignificant. The highest average water content was observed at the fruit stalk and it amounted to 94.9 %. The average water content in the fresh fruit of soil-grown cucumber was 94.8 %.

The average water content levels in the fresh fruits of the investigated varieties of soil-grown cucumbers are presented in Table 1.

Table 1. The average water content of the analyzed varieties of fresh cucumbers

Variety and fraction	Water content [%]			
	Fruit stalk	Fruit centre	Fruit end	Average
Polan, 1st fraction	95.0	95.2	94.9	95.0
Polan, 2nd fraction	95.6	95.5	95.6	95.6
Average	**95.3**	**95.4**	**95.3**	**95.3**
Śremianin, 1st fraction	94.9	94.7	94.6	94.7
Śremianin, 2nd fraction	95.3	95.3	95.3	95.3
Average	**95.1**	**95.0**	**95.0**	**95.0**
Śremski, 1st fraction	95.2	94.8	94.8	94.9
Śremski, 2nd fraction	95.0	94.8	94.7	94.8
Average	**95.1**	**94.8**	**94.8**	**94.9**
44 genotype, 1st fraction	93.9	94.2	94.2	94.1
44 genotype, 2nd fraction	95.0	94.9	94.3	94.7
Average	**94.5**	**94.6**	**94.3**	**94.4**
54 genotype, 1st fraction	94.2	94.5	94.8	94.5
54 genotype, 2nd fraction	94.7	94.5	94.4	94.5
AVERAGE TOTAL	**94.9**	**94.8**	**94.8**	**94.8**

ANALYSIS OF THE SECTION IMAGE OF THE FRESH FRUITS OF SELECTED CUCUMBER VARIETIES

The average sizes of the seed chamber surface areas and the area of the flesh in the middle part of the investigated varieties of fresh cucumber fruits for two size fractions are presented in Table 2. On the basis of the obtained results it was explicitly found out that the 1st fraction of the Śremianin variety was characterized by the highest percentage share of the seed zone: 55.2 %. The lowest percentage share of the seed zone was found out for the 2nd fraction of the Polan variety, and it amounted to 41.2 %. For the 1st fraction of the 54 genotype, the section surface area was within the range of 129.9 mm², whereas for the 44 genotype it was up to 217.3 mm², and for the 2nd fraction of the 54 genotype, the section surface area was from 252.4 mm² to 354.5 mm² for the Polan variety.

Table 2. Surface areas of the seed chambers and flesh in the middle part of the investigated varieties of cucumber fresh fruits for the two size fractions.

Variety	Fraction	Cucumber section surface area [mm²]	Seed chamber surface area		Flesh surface area	
			[mm²]	[%]	[mm²]	[%]
Polan	1st	424.9	202.1	47.6	222.8	52.4
Polan	2nd	861.1	354.5	41.2	506.6	58.8
Śremianin	1st	345.6	190.9	55.2	154.7	44.8
Śremianin	2nd	703.9	333.6	47.4	370.3	52.6
Śremski	1st	314.6	135.0	42.9	179.6	57.1
Śremski	2nd	663.5	325.5	49.1	338.0	50.9
Genotype 44	1st	395.1	217.3	55.0	177.8	45.0
Genotype 44	2nd	583.3	296.0	50.7	287.3	49.3
Genotype 54	1st	243.2	129.9	53.4	113.3	46.6
Genotype 54	2nd	488.0	252.4	51.7	235.6	48.3

ASSESSMENT OF THE FORCE REQUIRED TO PUNCTURE THE PEEL AND FLESH OF FRESH CUCUMBERS

The force F [N] required to puncture the peel and flesh of fresh cucumbers and their deformation L [mm] depends on the fruit size, variety, the place of puncturing and the water content in the investigated material. In Fig. 1 the average force required to puncture the peel and flesh of the fresh fruits of the investigated cucumber varieties in three places, i.e. at the leaf stalk base, in both the middle and the bottom part of the cucumber fruit is presented.

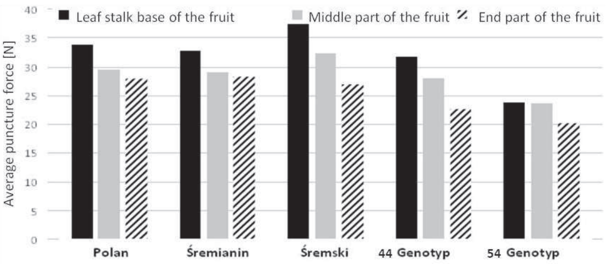

Fig. 1 Average force required to puncture the peel and flesh of the fresh fruits of the selected varieties of cucumbers with the punch of the diameter of 5 mm in three puncture places

For the analyzed varieties the highest force required to puncture the peel and flesh of cucumber was observed at the base of the leaf stalk, and the lowest one at the bottom part of the fruit. The highest forces F[N] required to puncture the peel and flesh were found out for the cucumbers of the Śremski variety, whereas the lowest resistance to puncture was observed for the 54 genotype. The obtained results of the resistance to puncture justify the fact that this genotype has been marked out by Polan company as the standard of the worst technology properties for pickling.

In Fig. 2 the lines of the puncture force trend for the peel and flesh of the selected varieties of fresh cucumber fruits versus their deformation for three measuring places are presented. The differentiated average values of the forces required to puncture the peel and flesh of fresh cucumbers versus their deformation for the analyzed varieties were observed. The curve of the relation of the peel and flesh puncture force in the function of their deformation is described by the quadratic function of second degree: $y = ax^2 + bx + c$.

On the basis of the obtained and presented results (Fig. 2) a very strong relation between the force of the puncture of peel and flesh and the deformation occurring in the process of the puncturing with a punch at the base of the leaf stalk was found out. The determination coefficients were $R^2 = 0.98$ and $R^2 = 0.91$ for the 1st fraction (small cucumbers) and 2nd fraction (big cucumbers), respectively. For the middle and the end part of the fresh fruits of selected cucumber varieties the observed relations between the peel and flesh puncture force and the deformation were smaller and differentiated. The determination coefficients were:

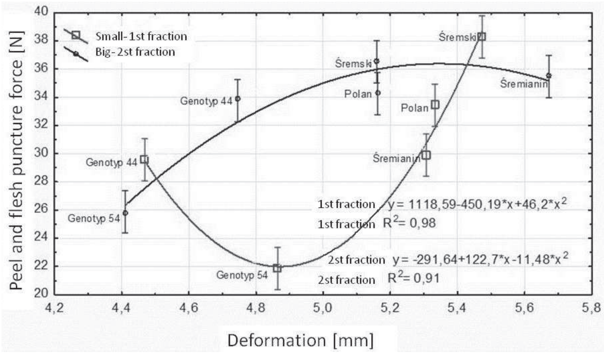

Fruit leaf stalk base

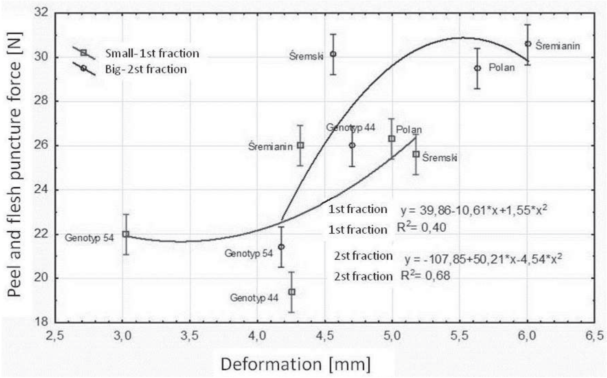

Middle part of the fruit

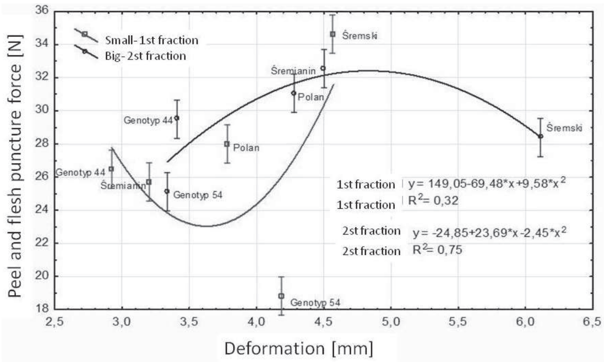

End part of the fruit

Fig. 2. Lines of the trend of the average force F [N] required to puncture the peel and flesh of the fresh cucumbers of selected varieties with the punch of the diameter of 5 mm versus their deformation L [mm] in three puncture places.

The middle part of cucumber fruit: 1st fraction – $R^2 = 0.32$.
2nd fraction – $R^2 = 0.75$.
The end part of cucumber fruit: 1st fraction – $R^2 = 0.40$.
2nd fraction – $R^2 = 0.68$.

The average deformation L [mm] values until the fresh cucumber fruits were punctured had been within the range from 3.9 mm up to 7.1 mm. The biggest deformation was observed for the Polan variety, the 1st size fraction, and it amounted to 7.05 mm, whereas the smallest one – in the 44 genotype, also for the 1st size fraction, and it was 3.88 mm.

The average puncture energy rate for peel and flesh as well as the peel and flesh breaking stress for the analyzed fresh cucumber varieties versus their size fraction is presented in Table 3.

Table 3. Average rate of the puncture energy for the cucumber peel and flesh and the breaking stresses

Variety and fraction	Energy W [J]	Breaking stress [MPa]
Polan, 1st fraction	76,5	1,57
Polan, 2nd fraction	89,3	1,69
Śremianin, 1st fraction	64,6	1,46
Śremianin, 2nd fraction	94,3	1,76
Śremski, 1st fraction	87,3	1,76
Śremski, 2nd fraction	89,8	1,70
Genotyp 44, 1st fraction	54,0	1,35
Genotyp 44, 2nd fraction	71,4	1,59
Genotyp 54, 1st fraction	48,2	1,12
Genotyp 54, 2nd fraction	52,7	1,29
Average – 1st fraction	**66,1**	**1,45**
Average – 2nd fraction	**79,5**	**1,61**

Based on the obtained results it was found out that the average breaking stress values were 1.45 MPa and 1.61 MPa for the 1st and 2nd size fraction, respectively. The average values of the energy needed to puncture the peel and flesh for the analysed 1st and 2nd fractions were 66.1 J and 79.5 J, respectively. The highest energy needed to puncture the peel and flesh of the analysed fresh cucumber fruits was observed for the Śremianin variety, the 2nd fraction, and the smallest one for the 54 genotype – the 1st size fraction. Those values were 94.3 J and 48.2 J, respectively. The lowest breaking stress was observed for the 54 genotype, the 1st fraction – it amounted to 1.12 MPa, whereas the highest ones – for the Śremianin variety, the 2nd size fraction, and the Śremski variety, the 1st fraction – went up to 1.76 MPa.

CONCLUSIONS

1. The average content of water for the analyzed cucumber varieties was slightly differentiated and it was in the range from 94.1 % for the 44 genotype, the 1st fraction, to 95.6 % for the Polan variety, the 2nd fraction.
2. In the middle part of the cucumber fresh fruits of the tested varieties the highest percentage share of the seed zone was observed for the Śremianin variety, the 1st size fraction, and the lowest one for the Polan variety, the 2nd fraction, and they amounted to 55.2 % and 41.2 %, respectively.
3. The average force F [N] needed to puncture the peel and flesh of the analyzed varieties of fresh cucumber fruits was within the range of 20.9 – 32.9 N, and the highest resistance to puncturing was shown by the Śremianin variety, whereas the 54 genotype showed the lowest one.
4. The average rates of deformation L [mm] to the moment when the peel and flesh were punctured had been within the range of 3.8 up to 7.1 mm.
5. The average energy W [J] required to puncture the peel and flesh of the fresh cucumbers of the tested varieties and the breaking stress σ [MPa] were: the 1st and the 2nd size fraction – 66.1 J and 79.5 J, respectively, and the 1st and the 2nd size fraction – 1045 MPa and 1,61 MPa, respectively.

REFERENCES

1. **Bargel H., Neinhuis C., 2005:** Tomato fruit growth and ripening as related to the biomechanical properties of fruit skin and isolated cuticle. Journal of Experimental Botany. 56(413), 1049-1060.
2. **Bohdziewicz J., Czachor G., 2010:** Wpływ obciążenia na przebieg odkształcenia warzyw o kształcie kulistym. Inżynieria Rolnicza 1(119), 85-91.
3. **Ciupak A., Gładyszewska B., 2010:** Właściwości mechaniczne skórki owoców pomidora w różnych temperaturach przechowywania. Acta Agrophysica. 15(1), 45-54.
4. Główny Urząd Statystyczny: Wynikowy szacunek produkcji głównych ziemiopłodów rolnych i ogrodniczych w 2013 roku. Informacja sygnalna.
5. Dynamiczne metody pomiaru własności mechanicznych owoców i warzyw. Acta Agrophysica. 8(1), 69-82.
6. **Brickell, C. D.; Alexander, C.; David, J. C.; Hetterscheid, W. L. A.; Leslie, A. C.; Malecot, V.; XiaoBai Jin; Cubey, J. J., 2009:** International Society for Horticultural Science. International code of nomenclature for cultivated plants.
7. **Jakubczyk E., Lewicki P.P., 2003:** Właściwości mechaniczne tkanki jabłka w odniesieniu do jej struktury. Acta Agrophysica. 2(3), 549-557.
8. **Jakubczyk E., Uziak D., 2005:** Charakterystyka instrumentalnych metod badania właściwości mechanicznych wybranych owoców i warzyw. Inżynieria Rolnicza. 11 (71), 181-189.
9. **Marzec A., Pasik S., 2008:** Wpływ metody suszenia na właściwości mechaniczne i akustyczne suszy marchwiowych. Inżynieria Rolnicza 1(99), 291-296.
10. **Szczęśniak A. S., 2002:** Texture is a sensory property. Food Quality and Preference. 13, 215-225.
11. **Wrzodak A., Korzeniowski M., 2012:** Jakość sensoryczna ogórków kwaszonych z owoców traktowanych fungicydami w uprawie polowej. Nowości Warzywnicze. 54-55, 5-13.

OCENA WYBRANYCH WŁAŚCIWOŚCI MECHANICZNYCH ŚWIEŻYCH OWOCÓW OGÓRKA GRUNTOWEGO

Streszczenie. Sposób postępowania, przechowywania i transportu świeżych ogórków ma wpływ na zawartość wody w owocu w konsekwencji na jego jędrność i jakość produktów finalnych. Dotyczy to surowca przeznaczonego bezpośrednio do spożycia, jak również do przetwórstwa. Ubytki wody wynikające ze zbyt długiego przechowywania mają istotny wpływ na parametry końcowe produktu. Celem pracy było określenie wpływu zawartości wody na wybrane cechy mechaniczne świeżych ogórków, analiza obrazu przekroju oraz ocena odporności skórki i miąższu świeżych owoców badanych odmian ogórków na uszkodzenia mechaniczne powstałe w procesie przebicia stemplem o średnicy 5mm.

Słowa kluczowe: ogórki gruntowe, właściwości mechaniczne, siła przebicia skórki i tkanki, zawartość wody

TEKA. COMMISSION OF MOTORIZATION AND ENERGETICS IN AGRICULTURE – 2014, Vol. 14, No. 4, 19–22

Quality of Dill Pickled Cucumbers Depending on The Variety And Chemical Composition of Pickle Brine

Józef Gorzelany[1], Natalia Matłok[1], Dagmara Migut[1], Tomasz Cebulak[2]

[1]Department of Food and Agriculture Production Engineering of the University of Rzeszów
[2]Department of Technology and Assessment of Plant Products

Received December 11.2014; accepted December 19.2014

Summary. Dill pickled cucumbers is the product obtained from fresh cucumbers with the addition of taste-aromatic seasonings poured with a water solution of table salt and subjected to lactic acid fermentation. There are many kinds of pickling technology, and many types of pickle brines. This is the reason our work was aimed at the qualitative assessment of dill pickled cucumbers depending on the pickle brine chemical composition. On the basis of organoleptic assessment, a diversified sensory quality assessment of the tested dill pickled cucumbers was carried out depending on pickle brine chemical composition.

Key words: dill pickled cucumbers, pickle brines, organoleptic assessment

INTRODUCTION

Dill pickled cucumbers are very popular in our country and they win over larger and larger group of connoisseurs and customers from abroad. Apart from the characteristic taste they have many pro-health properties, and that is why they are often recommended by dieticians as an item of a well-balanced diet [1]. The lactic acid formed by the fermentation process and contained in silages lowers the pH values in intestines and by this it favours the proliferation of the intestinal flora. The endogenic strains of lactic acid bacteria, when present in a ready product, contribute to the formation of the characteristic taste of ensilaged products [7]. Dill pickled cucumbers contain also vitamin C and the B-group vitamins.

The quality of the final product is significantly affected by both the cucumber variety and the components of the pickle brine used. An appropriate selection of raw materials and their share in the ready pickle brine allow obtaining an optimum taste-smell effect. The important aspect is the use of water of appropriate quality conforming to the requirements for drinking water and its hardness, which may be increased by adding calcium carbonate. The pickle brine is a water based solution of table salt enriched with natural taste-aromatic additives, the most common of which are dill and horseradish. They create a characteristic, strong aroma of dill pickled cucumbers [2].

Sodium chloride added to the brine enables an initial selection of microorganisms and faster growth of lactic acid mesophilic bacteria such as *L. paracasei, L. casei, L. plantarum, L. rhamnosus* [4, 10].

Addition of probiotic starter cultures to the pickle brine allows to obtain a high-quality product due to their antagonistic reactions to detrimental moulds or yeasts, The essential hazard arising during spontaneous fermentation process is the risk of infection by *Geotrichum candidum* or *Picha manshurica* yeasts which by raising the environmental pH due to the oxidation of organic acids enable the development of putrefactive bacteria [3].

Salt, as a component of pickle brine reduces the osmotic pressure and by this the brine gets enriched in nutritional components and becomes an appropriate environment for the development of the fermentation microflora. Diffusion processes proceed slowly, and that it is why the fermentation in the anaerobic environment is a lengthy process [8]. Sensory assessment carried out by predisposed tasters, i.e. those without changes in the felt taste and disorders such as the so called taste daltonism manifesting itself as a lack of sense of taste and feeling no differences between the four basic tastes, in appropriate concentration is an important element while introducing the product to the market as well as during laboratory tests aimed at the improvement of technological processes. Changes in taste perception may be caused by too low content of zinc in the human organism, which can be often observed in people on vegetarian diets [5, 6].

Sensory assessment, apart from physical-chemical one, is a supplementary method of the assessment of product quality. Such assessments provide information on the reaction of the senses to the consumption of a product [9].

MATERIAL AND METHODOLOGY

The tested material were the fruits of three varieties of soil-grown cucumbers (Polan F_1, Śremski F_1 and Śremianin F_1) and the genotype 44 subjected to the pickling process. The cucumbers of the selected varieties were pickled in large glass jars with the pickle brines of three different chemical compositions. The genotype 44 singled out by the Krakowska Stacja Hodowli i Nasiennictwa „Polan” *(Cracow Plant Breeding and Seed Production “POLAN”)* as a standard of the variety non-predisposed to pickling was subjected to this process in one type of pickle brine in order to confirm its worthlessness to the technological process in question. Until an intensive fermentation started, the jars were stored in the room temperature, and after that they were transferred to a room with the temperature of 5^0 C. The chemical composition of pickle brines is presented in Table 1.

The tests included the organoleptic assessment of the quality features, such as general appearance, colour, consistency, taste, and smell. The organoleptic assessment was carried out by the score method (5 point method) consisting in the determination of the quality levels of individual quality features (determinants) by means of numerical values, and expressing the total quality of the

Table 1. Chemical composition of the pickle brines used for the pickling of the tested varieties of soil-grown cucumbers.

PICKLE BRINE CHEMICAL COMPOSITION					
A		B		C	
Component	**Addition for 100 kg of cucumbers (%)**	**Component**	**Addition for 100 kg of cucumbers (%)**	**Component**	**Addition for 100 kg of cucumbers (%)**
Water solution of NaCl	4-10	Water solution of NaCl	3	Water solution of NaCl	4
Fresh dill	2.5	Fresh dill	2.5	Fresh dill	2.5
Horseradish root	0.2	Horseradish root	0.2	Horseradish root	0.2
Mustard	0.04	Garlic	0.15	Garlic	0.15
Garlic	0.15	Mustard	0.04	Mustard	0.04
Currant leaves	0.05	Bay leaves Oak tree leaves	0.01 0.05	Bay leaves	0.01
Bay leaves	0.01	Bay leaves	0.06	Bay leaves	0.06
Green marjoram	0.02	Whole grain dark pepper	0.04	Probiotic EM	0.04

Table 2. Card of the assessment by score method for tested dill pickled cucumbers

QUALITY FEATURES OF DILL PICKLED CUCUMBERS						
Quality determinant	**Weightiness coefficients**	**Scale of score points**				
		5 points	**4 points**	**3 points**	**2 points**	**1 point**
Consistency	0.3	very hard, crispy, no void cavities inside	medium hard, no void cavities inside	soft, with small void cavities inside	soft, significant void cavities inside	very soft, large void cavities inside
Taste	0.4	very salty, very sour, typical for dill pickled cucumbers	salty, sour	medium salty and sour	too salty and sour, too little-salty and too little	oversalted, too sour, no perceptible taste of salt non-sour
Smell	0.2	intense, aromatic, typical for dill pickled cucumbers with perceptible smell of herbs and other additives	medium perceptible with medium aroma of additives and herbs	hardly perceptible with faint aroma of additives and herbs	slightly perceptible with no perceptible aroma of additives and herbs	not perceptible, musty
Colour	0.1	very good, full-dark green colouring, typical for dill pickled cucumbers	good, close to typical for dill pickled cucumbers, lighter spots along the whole length	with not numerous discolouration spots at the ends	with well visible large brown, dark brown or white spots at the ends	brown, dark brown or white indicating rooting
General appearance	0.2	very good, typical for dill pickled cucumbers	good, close to typical for dill pickled cucumbers	medium, minimally differing from typical for dill pickled cucumbers	minimal indications of rooting and getting mouldy	mouldy, spoiled

product being assessed on the basis on those values. The score assessment was based on the comparison of the quality of subsequent product features with the quality definitions specified in the score assessment card (Table 2) and writing the obtained data down into a special report form. The obtained data were multiplied by appropriate weightiness coefficients of quality determinants of the final product. The participants in the procedure of dill pickled cucumbers assessment were 10 employees of the University of Rzeszów, having appropriate sensory sensitivity. The organoleptic assessment of dill pickled cucumbers was carried out in the Laboratory of Organoleptic Assessment of Products of the Faculty of Biology and Agriculture at the University of Rzeszów.

To determine the possible usefulness for the processing of the analyzed varieties of cucumbers some photographs of the cross-sections of soil-grown cucumbers were taken during the pickling process. The pictures were taken in three places: at the leaf stalk base, in the central and in the end part of the cucumber fruit. The pictures were taken for two size fractions: I-fraction, i.e. small fruits, II-fraction. i.e. large fruits. The views of the surfaces of the cross-sections were obtained by the view scanning method by scanning slices cut off from the eatable part of the fruits of the analysed varieties.

RESULTS OF TESTS AND DISCUSSION

Fig. 1 presents the results of the assessment of individual quality futures (general appearance, consistency, taste, colour, and smell) of the fruits of the tested varieties of soil-grown cucumbers dill pickled in three pickle brines of different chemical composition. Irrespective of the cucumber variety and the brine chemical composition, the assigned tasters assessed the general appearance of dill pickled cucumbers as the highest (appraisal arithmetic mean was 4.2), and the taste as the lowest (arithmetic mean 3.5). The arithmetic mean values for the consistency, smell, and colour of the tested dill pickled cucumbers were 4.1, 3.6, and 4.1 – respectively. The highest score, amounting to 4.8, was given by the assessing persons to the general appearance of the cucumbers of the Śremianin F_1 variety pickled in the pickle brine A, whereas the lowest score was obtained by the consistency of the cucumbers of the Śremski F_1 variety pickled in the brine B.

The organoleptic assessment of dill pickled cucumbers was conditioned by both the cucumber variety and the pickle brine chemical composition. The highest score, in the scale of 0 to 5, was given to the fruits of soil-grown cucumber of the Śremski F_1 variety pickled in the brine B. The lowest one, only 3.6 points, was obtained by the cucumbers of the Polan F_1 variety pickled in the brine B. During the organoleptic assessment of the cucumber fruits singled out by the Krakowska Stacja Hodowli i Nasiennictwa „Polan", i.e. the genotype 44, as the variety useless for the dill pickling process, this variety obtained average score 2.67 points. The results of the organoleptic assessment of the dill pickled cucumbers versus the variety and the chemical composition of pickle brine are presented in Fig. 1.

The lowest score, irrespectively of the pickle brine chemical composition, was obtained by the Śremski F_1 variety (4.81 points), whereas the lowest one (4.42 points) was given to the Polan F_1 variety. On the basis of the results of the organoleptic assessment of dill pickled soil-grown cucumber it can be stated that from among the tested varieties the most useful for dill pickling variety is the Śremski F_1, while the least useful one is the Polan F_1. The results of the usefulness of the tested cucumber varieties for dill pickling are presented in Fig. 2.

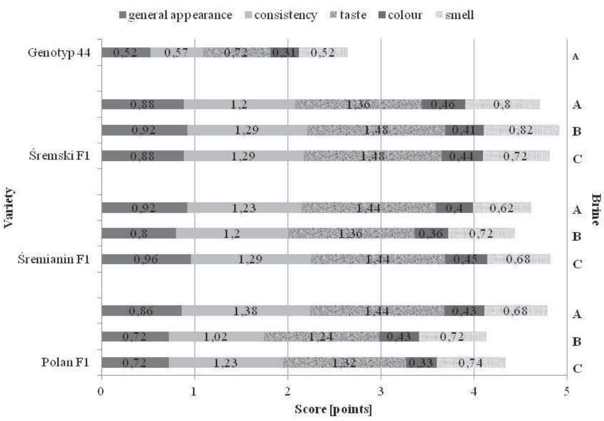

Fig. 1. Assessment of the tested quality features of dill pickled cucumbers as the function of variety and chemical composition of pickle brine.

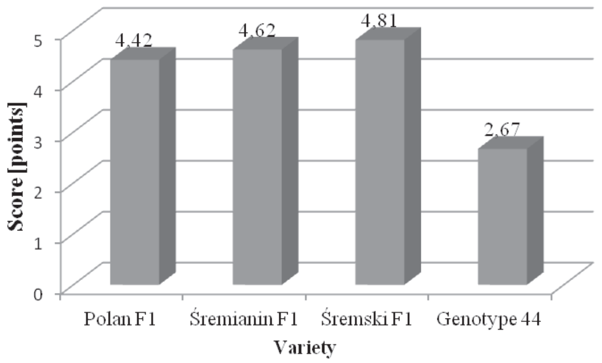

Fig. 2. Mean scores of the tested quality features of dill pickled soil-grown cucumbers with regard to their usefulness for dill pickling.

Regardless of the variety of soil-grown cucumbers, the best score was given to the cucumbers subjected to pickling in the pickle brine C. The mean value for all the tested varieties in this brine was 4.7 points. The lowest score, 4.5 points, obtained the cucumbers pickled in the brine B, and the cucumbers pickled in the brine A were given 4.65 points. On the basis of the obtained results it was found out that, regarding chemical composition, the C brine is the most suitable for pickling cucumbers, whereas the B brine – the least suitable. The results of the assessment of pickle brines of three different chemical compositions with regard to their usefulness for pickling are presented in Fig. 3 below.

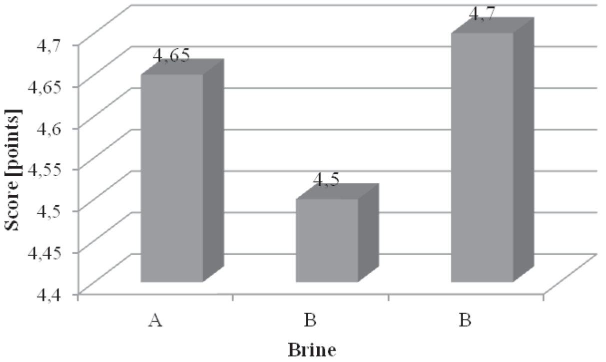

Fig. 3. Mean values of the assessment of brines of different chemical composition with regard to their usefulness for pickling cucumbers.

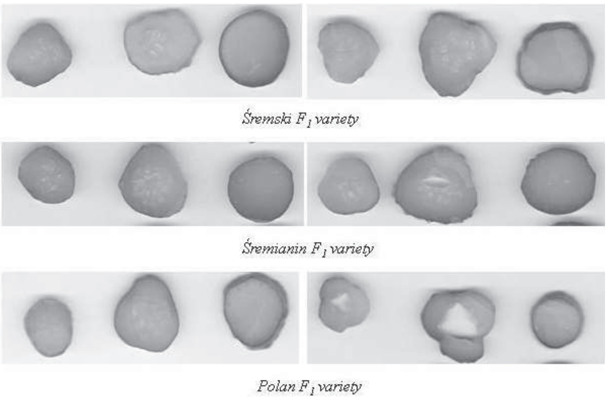

Fig. 4. Cross-sections of the tested varieties of dill pickled soil – grown cucumber

The examples of the views of the cross-sections of cucumbers of the tested varieties on the 30th day of pickling process are shown in Fig. 4. When analysing the view of the cross-sections of the tested pickled cucumber fruits, the largest air spaces were found for the Polan F_1 variety, which consequently affected the general sensory assessment of the final product (results of the carried out organoleptic assessment).

CONCLUSIONS

1. The quality of the final product obtained through the process of dill pickling of soil-grown cucumbers is conditioned by both the variety and the chemical composition of the pickle brine.
2. From among the varieties of soil-grown cucumbers being tested, the Śremski F1 variety proved to be the most useful for pickling, and the least useful was the Polan F_1. Regardless of the chemical composition of the brine used in the pickling process, the cucumbers of the varieties referred to above obtained the following organoleptic assessment scores: Śremski F_1 – 4,81 points, Polan F_1- 4,42 points.
3. Based on the organoleptic assessment it was found out that the pickle brines of the chemical composition C and A are the most useful for dill pickling of the analyzed varieties of soil-grown cucumber fruits.

REFERENCES

1. **Caplice E., Fitzgerald G., 1999:** Food fermentation: role of microorganisms in food production and preservation. Int. J. Food Microbiol. 50/1999, 131–149.
2. **Chabłowska B., Piasecka- Jóźwiak K., Rozmierska J., Szkudzińska-Rzeszowiak E., 2012:** Initiated lactic acid fermentation of cucumbers from organic farm by application of selected starter cultures of lactic acid bacteria. J. Res. Appl .Agric. Eng., 3/2012, 31–36.
3. **Franco W., Perez-Diaz I., Johanningsmeier S., McFeeters R., 2012:** Characteristic of spoilage-associated econdary cucumber fermentation. Appl.Environ. Microbiol., 78(4)/2012, 1273-1284.
4. **Gajewska J., Błaszczyk M., 2012:** Probiotyczne bakterie fermentacji mlekowej (LAB). Post. Microbiol. 51/1/2012, 55–65.
5. **Galiński G., Gawęcki J., Anioła J., 2009.:** Effect of sensorily varied foodstuffs on sensory specific satiety in young adults depending on their sex – a short report. Pol. J. Food Nutr. Sci., 59 (1)/2009, 87–90.
6. **Galiński G., Walkowiak J., Wójciak R. W., Gawęcki J., Krejpciol Z., 2011:** Stan wysycenia organizmu cynkiem a wrażliwość smakowa i występowanie zjawiska sytości sensorycznie specyficznej u młodych wegetarian. Bromat. Chem. Toksykol. XLIV, 3/2011, 556–560.
7. **Hansen E., 2002:** Commercial bacterial starter cultures for femented foods of the future. Int. J. Food Microbiol. 78/2002, 119–131.
8. **Piasecka-Jóźwiak K, Chabłowska B., Rozmieska J., 2013:** Zastosowanie bakterii fermentacji mlekowej jako kultur starterowych w kiszeniu warzyw. Przemysł fermentacyjny i owocowo-warzywny. 1/2013, 10–12.
9. **Wrzodak A., Korzeniowski M., 2012:** Jakość sensoryczna ogórków kwaszonych traktowanych fungicydami w uprawie polowej. Now. Warz. 54-55/2012, 5–13.
10. **Zaręba D., Ziarno M., 2011:** Alternatywne probiotyczne napoje warzywne i owocowe. Bromat. Chem. Toksykol. XLIV, 2/2011, 160–168.

JAKOŚĆ OGÓRKÓW KWASZONYCH W ZALEŻNOŚCI OD ODMIANY I SKŁADU CHEMICZNEGO ZALEWY

Streszczenie. Ogórki kwaszone to produkt otrzymany ze świeżych ogórków z dodatkiem przypraw smakowo- aromatycznych, zalanych roztworem soli kuchennej i poddanych procesowi fermentacji mlekowej. Istnieje bardzo duża liczba technologii kwaszenia, a także rodzajów zalew. Dlatego też celem pracy była ocena jakościowa ogórków kwaszonych w zależności od składu chemicznego zalewy. Na podstawie przeprowadzonej oceny organoleptycznej stwierdzono zróżnicowaną jakość sensoryczną badanych odmian ogórków kwaszonych w zależności od odmiany i składu zalewy.

Słowa kluczowe: ogórki kwaszone, zalewy, ocena organoleptyczna.

TEKA. COMMISSION OF MOTORIZATION AND ENERGETICS IN AGRICULTURE – 2014, Vol. 14, No. 4, 23–30

Research on the Frost Resistance of Concretes Modified with Fly Ash

Jacek Halbiniak, Bogdan Langier

Department of Technology of Building Processes and Materials
Czestochowa University of Technology, Faculty of Civil Engineering
Akademicka 3, 42-200 Częstochowa, halbiniak@wp.pl;langier@op.pl

Received December 04.2014; accepted December 17.2014

Summary. The paper presents the influence of adding fly ashes and air-entraining admixture on the frost resistance of concrete tested by the direct method and on the characteristics of air pores. The frost resistance test was done for 150 freeze-thaw cycles. The porosity structure of concrete composites was tested by means of a device for automatic image analysis that uses the computer program Lucia Concrete. The analysis involved control concrete and concrete with the addition of fly ash – half the maximum permissible quantity – that was air-entrained with various doses of air-entraining admixture.

Key words: concrete, fly ashes, air pores characteristics, frost resistance.

INTRODUCION

Concrete durability is a set of designed properties that the material retains for the longest possible usage period of the engineering construction. The basic factor that determines the usefulness of concrete for a construction is its compressive strength. However, there are other factors that influence concrete durability in a construction besides its strength, like for example proper selection of ingredients and their appropriate quality, proper moulding, curing and processing, the influence of corrosive environments, as well as cement slurry microstructure and the structure of the aggregate-cement slurry transitory layer [5, 7. 9, 11, 12, 15, 16].

Concrete is a composite whose features can be shaped by additives: micro-fillers and admixtures. They make it possible to obtain concretes with special properties, but to obtain high frost resistance of concretes with a large quantity of additives a proper air-entrainment is necessary [10, 19].

The norm PN-EN 206-1 introduces concrete exposure classes from XF1 to XF4 dependent on the influence of frost on concrete. The XF1 class includes concretes (vertical elements) that are moderately saturated with water, without anti-icing agents. Vertical concrete elements exposed to weather conditions and anti-icing agents should be made with the XF2 class concrete. Horizontal concrete elements , highly saturated with water without anti-icing agents, exposed to frost should be made with the XF3 class concrete. Concrete surfaces of roads and bridges, exposed to high saturation with water and anti-icing with chemical agents should be made with the XF4 class concrete. The XF2, XF3 and XF4 concretes require air-entrainment of the concrete mix. Concretes that belong to the above-mentioned exposure classes should meet the following requirements, presented in Table 1.

The content of air in road surface concretes presented in the Polish catalogue [8] depends on the maximal diameter of aggregate grains. The values are shown in Table 2.

According to German requirements, the minimal content of air in road surface concretes should be: 4% for concretes without plasticizers and 5% for concretes with plasticizers, according to [20].

According to French requirements, the minimal amount of air in surface concretes should be 3%, and the -maximal – 6%, according to [1].

Air-entraining admixtures are used to form microscopic air bubbles with a diameter of approximately 50μm. The air bubbles are distributed in the cement slurry and they break the continuity of capillaries, which leads to higher resistance of concrete to freeze-thaw cycles. When water in saturated concrete turns from a liquid state to a solid state, its volume increases and the ice squeezes into empty air bubbles. Air-entraining makes concrete more frost resistant and the concrete mixture becomes more workable.

Air-entraining admixtures change the structure of the cement slurry from micro-capillary to micro-porous (Fig. 1). The admixture has a foaming effect and forms enclosed air bubbles with the diameter of approximately 20-50μm, which are evenly distributed. As the concrete hardens, the surface of the air bubbles undergoes mineralization and becomes the phase of the hardened concrete. They break the capillary network and reduce the rise of water [2,6].

Table 1. Concrete mix composition requirements according to PN-EN 206-1

Hazard type	Exposure class	Minimal quantity of cement [kg/m³]	Maximal W/C ratio	Minimal strength class of concrete
Aggression caused by freezing and thawing	XF1	300	0.55	C30/37
	XF2	300	0.55	C25/30
	XF3	320	0.50	C30/37
	XF4	340	0.45	C30/37

Table 2. Required content of air in the concrete mix, according to [8]

Maximal diameter of aggregate grains [mm]	Content of air in the concrete mix [%]			
	Without a plasticizing admixture		With a plasticizing admixture	
	Average	Minimal	Average	Minimal
Up to 8	5.5	5.0	6.5	6.0
Up to 16	4.5	4.0	5.5	5.0
Up to 31.5	4.0	3.5	5.0	4.5

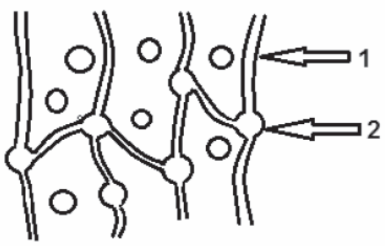

Fig. 1. The distribution of air bubbles in concrete: 1 – capillaries, 2 – micro-pores

Adding air-entraining admixtures to the concrete mix can also have unwanted effects. It leads to higher porosity of concrete and lower strength [3,4].

Jamroży [6] claims that the compression strength of concrete can be raised after air-entraining if the cement content is below 250kg/m³. If the [cement content is over 250kg/m³, concrete strength is lowered by about 4% for every additional 1% of air. According to Rusin [17], for concretes with the W/C ratio of 0.45÷0.72, the average drop of strength can be even 5% for 1% of additional air in the mix after air-entraining.

Air-entraining the concrete mix does not guarantee full frost-thaw resistance of the concrete. What is important in air-entraining the concrete mix is the distribution of air pores in hardened concrete and the distance between them. A large distance between the spots where ice is formed and the nearest void leads to higher hydraulic pressure. Small distances between pores are the effect of excessive air-entraining of the concrete mix, which leads to a large drop of compression strength. What determines the proper air-entraining of the concrete mix is the spacing factor L of pores in concrete. The factor determines the average largest distance from a random spot in the cement slurry (in the concrete) to the nearest air pore.

The norms PN-EN 206-1 and PN-EN 480-11 do not determine the porosity structure of hardened concrete. It is universally assumed that in order to obtain frost resistant concrete, the proper spacing factor should be $L \leq 0.20$mm and the content of micropores with the diameter smaller than 300 µm (class 18): $A_{300}>1{,}5\%$. Concretes with $L\leq 0{,}18$ mm and $A_{300}>1{,}8\%$ are considered to guarantee a very high level of frost resistance. However, some authors claim that the evaluation of frost resistance of fly ash concretes based on the values L and A_{300} are of little use because of air pores in the grains of ash [13, 14, 17, 18].

Concrete durability is also determined by proper moulding, maintenance and processing of the concrete composite [7, 9].

THE RESEARCH ON CONCRETES

The research program aimed at determining the influence of fly ashes and an air-entraining admixture on the quantity and quality parameters of concrete and the characteristics of the concrete mix. The base concrete (marked as "0-0") was made from: natural aggregate with grain size up to 16mm and the sand point – 33%; cement CEM I 42,5R and plasticizing admixture based on policarboxylates.

Table 3. Composition of the tested series of concretes

Ingredient [kg/m³]	Series of tested concretes							
	0-0	0-2	0-5	0-8	1-0	1-2	1-5	1-8
Cement	386	386	386	386	362.1	362.1	362.1	362.1
Water	193	193	193	193	193	193	193	193
Aggregate	1845	1845	1845	1845	1823	1823	1823	1823
Plasticizer	6.95	6.95	6.95	6.95	6.95	6.95	6.95	6.95
Fly ash	-	-	-	-	63.7	63.7	63.7	63.7
Air-entraining admixture	-	0.772	1.93	3.088	-	0.772	1.93	3.088

The modifications of the base version consisted in adding an air-entraining admixture in the amount of 0.2% (0-2 series), 0.5% (0-5 series) and 0.8% (0-8 series) in relation to the mass of cement.

Next, the base series was modified by adding half the maximum permissible quantity of fly ash (1-0 series). Then, an air-entraining admixture was added to fly ash concrete in the amounts corresponding to the control series.

This resulted in concrete series marked as 1-2, 1-5 , 1-8. Table 3 presents the composition of all 8 tested series of concrete mixes and concretes.

All concretes were tested for: air content in the concrete mix, consistency by the concrete slump method, compressive strength after 28 days of curing, saturation, depth of water penetration, and resistance to 150 freeze-thaw cycles. The porosity structure of selected concrete series was tested by determining: the total amount of air in hardened concrete A, the spacing factor F, the micro-pores content A_{300}, and the distribution of air pores. The tests were done with cubical samples with an edge of 150mm, that were demoulded 24 hours after they had been made, and then they were kept for 27 days in water at the temperature of 20°C.

THE RESULTS OF TESTS FOR CONSISTENCY AND AIR CONTENT

The tested concrete mixes were mixed in a paddle concrete mixer for 70 seconds and then the following was determined: consistency by the concrete slump method in accordance with PN-EN 12350-2, and air content by the pressure method according to PN-EN 12350-7.

The results are presented in Table 4.

The result of the slump test for the control series concrete mix 0-0 was 50mm (S2 consistency class) and air content test showed the amount of 2.35%. As the amount of the air-entraining admixture was raised, the liquidity of concrete mixes also grew together the air content. Concrete mixes without fly ash and with maximal quantity of the air-entraining admixture (0.8% of the cement mass) had the air content of 4.3%. At the same time this concrete mix has the highest level of liquidity and its consistency class was marked as S3.

The presence of fly ash (series 1) influenced consistency, the liquidity was considerably higher. The measured amount of air in fly ash mixes was also higher with the same amount of the air-entraining admixture.

Adding fly ash to concrete instead of cement raised the air content by 6.4%. With the addition of the air-entraining admixture in the amount of 0.2 and 0.5% the observed increase of the tested characteristics was by about 17% in fly ash mixes. The greatest difference in air content was noticed for the air-entraining admixture in the amount of 0.8%. The air content in the fly ash mix was higher by 55.8%.

THE RESULTS OF TESTS FOR COMPRESSIVE STRENGTH AND THE PENETRATION DEPTH OF PRESSURIZED WATER

The compressive strength test was done after 28 days of curing the samples in laboratory conditions. The saturation test was done on the basis of the PN-88/B-06250 norm. The results are presented in Table 5.

The series 0-0 control concrete had the average compressive strength f_{cm}=54.1 MPa. The test results classified the control series to the C40/50 strength class. Using fly ash as a cement substitute resulted in the drop of compressive strength by 4.4%. This changed the concrete strength class to C35/45.

The modification of the tested concretes by using an air-entraining admixture lowered the average values of compressive strength. The greatest drop was noted in the series where the amount of added air-entraining admixture was 0.8% of the cement mass (0-8 and 1-8 series). This resulted in classifying both the series to a still lower strength class C30/37.

Figure 2 presents the comparison of average compressive strength of concretes with and without fly ash.

The average compressive strength of the concrete containing half the maximal permissible amount of fly ash was lower in every tested sample. The largest strength drop caused by the use of fly ash was noticed in the series without an air-entraining admixture (4.7%) and with the largest amount of the air-entraining admixture (5.6%).

Figure 3 presents compressive strength drop together with the increasing amount of the air-entraining admixture.

Table 4. Concrete mix test results

Characteristics of concrete mixes	Series of tested concretes							
	0-0	*0-2*	*0-5*	*0-8*	*1-0*	*1-2*	*1-5*	*1-8*
Slump test [mm]	50	80	90	100	150	175	185	200
Consistency class	S2	S2	S2	S3	S3	S4	S4	S4
Air content	2.35	2.8	3.5	4.3	2.5	3.3	4.1	6.7

Table 5. Average values of compressive strength, and the penetration depth of pressurized water, of concreted modified with fly ash and air entraining admixture.

Characteristics of concretes	Series of tested concretes							
	0-0	*0-2*	*0-5*	*0-8*	*1-0*	*1-2*	*1-5*	*1-8*
Compressive strength f_{cm} [MPa]	54.1	50.1	49.0	48.2	51.7	49.4	47.6	45.5
Strength class	C40/50	C35/45	C35/45	C30/37	C35/45	C35/45	C30/37	C30/37
Depth of water penetration [mm]	70	75	82	98	90	90	75	80

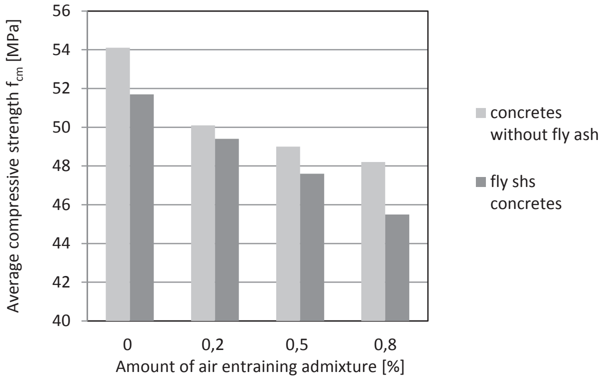

Fig. 2. The influence of an air-entraining admixture on compressive strength

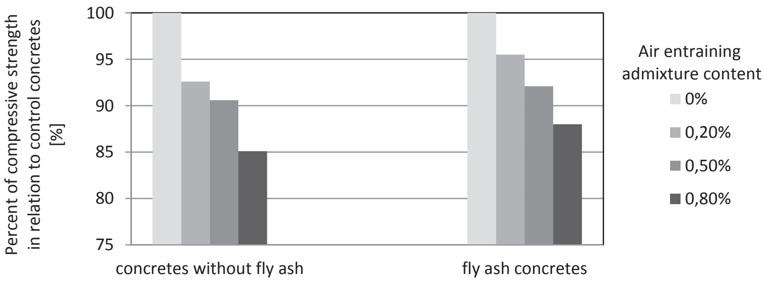

Fig. 3. The influence of the amount of the air-entraining admixture on the compressive strength percentage of concretes with and without fly ash

Adding an air-entraining admixture resulted in lower strength of the tested concretes. The amount of the air-entraining admixture equal to 0.2% of the cement mass resulted in lowering the average compressive strength to 50.1MPa (Table 5). The increase in the amount of the air-entraining admixture causes lowering the compressive strength, which dropped to 48.2 with the maximal amount of the admixture. A similar result was observed in fly ash concrete. The compressive strength dropped from 51.7MPa in the series without the admixture to 45.5MPa in the series with the maximal amount of the air-entraining admixture.

The water penetration test was done in accordance with the PN-EN 12390-8 norm. The results are presented in figure 4.

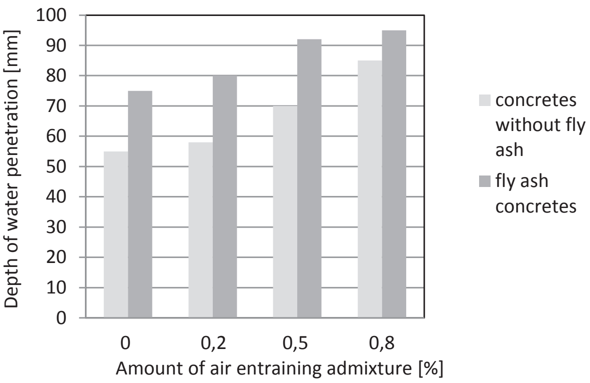

Fig. 4. The influence of the amount of the air-entraining admixture on the penetration depth by pressurized water in concretes with and without fly ash

The use of fly ash as a cement substitute caused an increase in the depth of water penetration in concretes both with and without the air-entraining admixture. Similarly, the amount of the air-entraining admixture increased together with the depth of water penetration.

THE RESULTS OF THE FROST RESISTANCE TEST (150 CYCLES)

The norm PN-EN206-1 does not mention any method for determining the frost-thaw resistance of concretes. However, the concretes that belong to the XF2 and XF4 exposure classes must contain an air-entraining admixture. At present, all concretes exposed to frost-thaw cycles are tested for frost resistance according to the PN-88/B-06250 norm.

The tested series of concrete underwent 150 freeze-thaw cycles. The results are presented in Table 6.

None of the tested series had any mass loss after 150 cycles. The compressive strength drop for the control concrete 0-0 was 32.0%. According to the PN-88/B-06250 norm, maximal strength drop cannot exceed 20%. The concrete series without fly ash: the control one 0-0 and the one with minimal amount of the air-entraining admixture 0-2 didn't have frost resistance after 150 freeze-thaw cycles. Fly ash concretes (1-0) and the ones with minimal amount of the air-entraining admixture (1-2) didn't have frost resistance after 150 freeze-thaw cycles either.

The remaining series of tested concretes with the amount of the air-entraining admixture of 0.5% and 0.8% had the frost resistance F150.

THE RESULTS OF TESTS CONCERNING THE CHARACTERISTICS OF AIR PORES IN HARDENED CONCRETE

The air pores characteristics tests were done in accordance with the research procedure described in the PN-EN480-11 norm. The test was done with the use of an automatic system for analysing the image of air pores in concrete (Fig. 5), and the computer program Lucia Concrete. For all tested concrete series, the following parameters determining concrete structure were obtained: the total amount of air in concrete A, the spacing factor F, the micro-pore content A_{300} (class 18), the distribution of chords in particular size classes of pores.

The obtained results are presented in Table 7.

All the series had the spacing factor L < 0.20mm, which is recommended to obtain frost resistance of concrete.

Figure 6 presents the cumulated air content in particular pore classes for concretes without fly ash, dependent on the amount of the air-entraining admixture.

Figure 7 presents cumulated air content in particular pore classed for fly ash concretes, dependent on the amount of the air-entraining admixture.

Fly ash concretes had considerably higher cumulated air content than concretes without fly ash. The obtained

Table 6. Compressive strength drop and mass loss after 150 freeze-thaw cycles

Characteristics of concretes	Series of tested concretes							
	0-0	*0-2*	*0-5*	*0-8*	*1-0*	*1-2*	*1-5*	*1-8*
Compressive strength drop after 150 freeze-thaw cycles [%]	32.0	25.1	12.4	6.6	26.9	23.4	8.1	8.0
Mass loss [%]	0	0	0	0	0	0	0	0
Frost resistance F150	NO	NO	YES	YES	NO	NO	YES	YES

Table 7. The results of tests concerning the characteristics of air pores

Characteristics of air pores	Series of tested concretes							
	0-0	*0-2*	*0-5*	*0-8*	*1-0*	*1-2*	*1-5*	*1-8*
Total air content in concrete A [%]	3.3	5.6	8.9	7.9	8.5	10.0	17.6	20.8
Spacing factor L [mm]	0.179	0.194	0.135	0.159	0.134	0.114	0.106	0.091
Micro-pore content A_{300} [%]	2.1	2.1	4.2	3.8	4.6	6.0	9.1	11.2

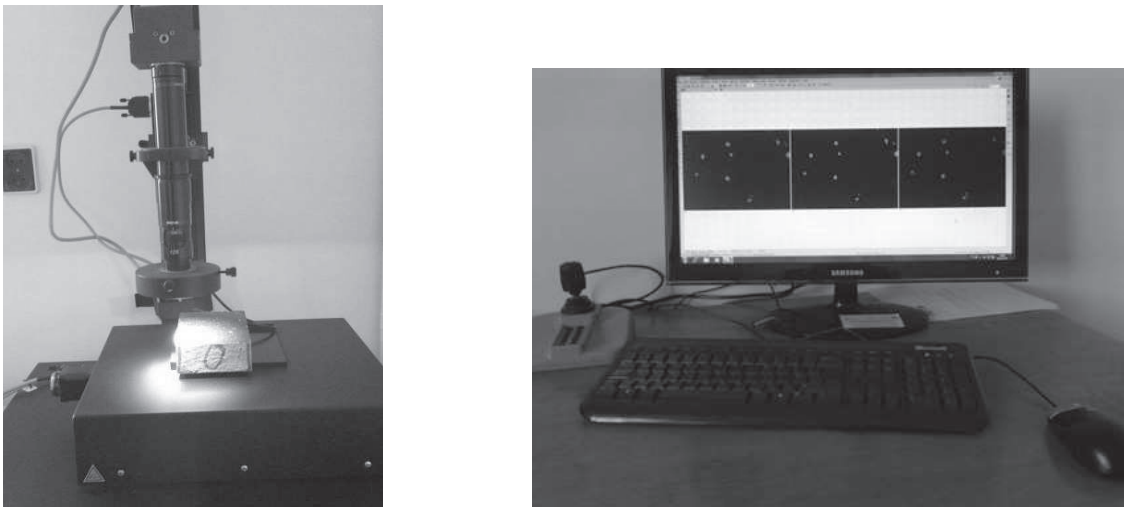

Fig. 5. A workstation for testing the pore structure in hardened concrete

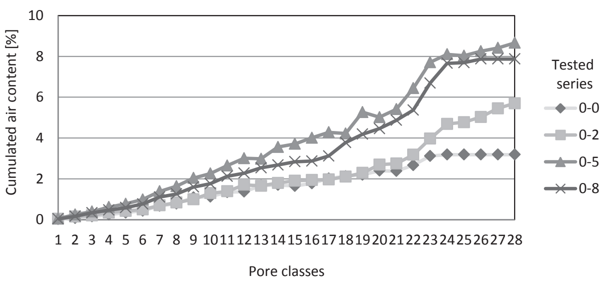

Fig. 6. The influence of an air-entraining admixture on cumulated air content in concretes without fly ash, dependent on the pore class

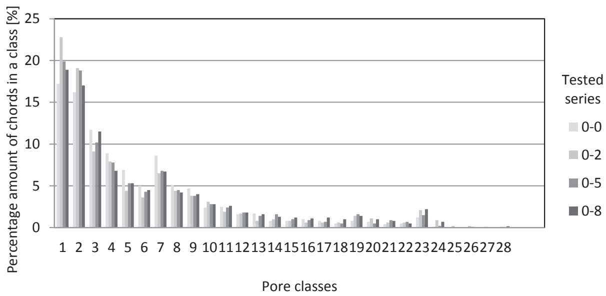

Fig. 8. A histogram of air pores distribution in concretes without fly ash

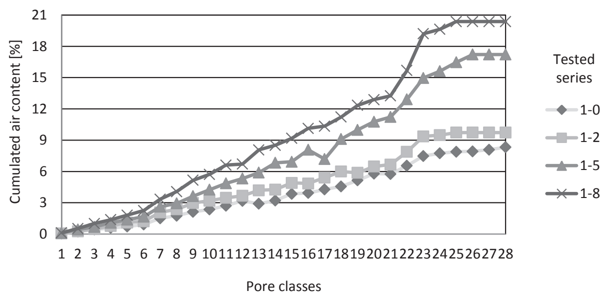

Fig. 7. The influence of an air-entraining admixture on cumulated air content in fly ash concretes, dependent on the pore class

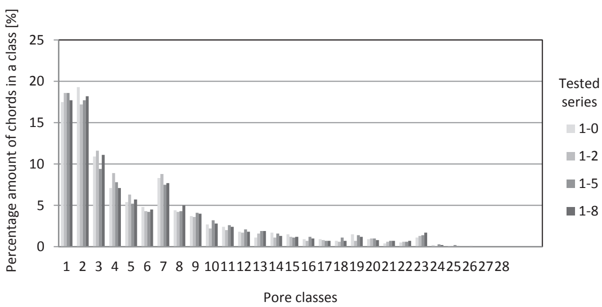

Fig. 9. A histogram of air pores distribution in fly ash concretes

values of the total pore content in hardened concrete (A) are quite clearly higher than the air content obtained in the pressure method tests of concrete mixes. Particularly large differences were noticed in fly ash concretes. This confirms the opinions expressed in [13, 14, 17, 18] that fly ash can increase the A parameter.

Figures 8 and 9 present histograms of the percentage distribution of air pores in all size classes.

The content of micro-pores A_{300} obtained in the test ranged from 2.1% in the series 0-0 and 0-2 to 11.2% in the series 1-8 (Table 7). All the tested series had the factor A_{300}, required for concrete frost resistance, with the value above the minimal 1.8%.

It is commonly assumed that in order to obtain frost resistant concrete, the proper spacing factor should be $L \leq 0.20$mm and the content of micro-pores with the diameter smaller than 300 μm (class 18): $A_{300}>1,5\%$. Concretes with $L\leq 0,18$ mm and $A_{300}>1,8\%$ are considered to guarantee a very high level of frost resistance.

In a direct frost resistance test, despite having obtained proper parameters in the porosity structure test, in the series 0-0, 0-2, 1-0, 1-2 there were no concretes that could be included in the F150 frost resistance class.

CONCLUSIONS

The paper presents the results of research on the characteristics of air pores, compressive strength, the depth of penetration by pressurized water, and frost resistance after 150 cycles in concretes modified by fly ash and an air entraining admixture.

The research that was carried out has led to the following conclusions:

– fly ash raises the effectiveness of air-entraining the concrete mix and it helps to increase air content,
– an air-entraining admixture improves frost resistance of concrete, increases the liquidity of the concrete mix and improves its workability,
– air-entraining admixtures result in a considerable drop of compressive strength, up to 20% in comparison with concrete without the admixture. It can lead to lowering the strength class of concrete by even 2 degrees,
– additional air in the concrete mix can also lead to increasing the depth of water penetration, which is rarely mentioned by the admixture manufacturers. Therefore, the composition of concrete must be corrected at the designing stage,
– the characteristics of air pores distribution is an effective tool to estimate the frost resistance of concrete composites.

REFERENCES

1. **Chaussées en béton, 2000:** Guide technique, LCPC, SETRA.
2. **Czarnecki L., 2003:** Domieszki do betonu – możliwości i ograniczenia, Polski Cement – Budownictwo, Technologie, Architektura, numer specjalny.
3. **Halbiniak J., 2010:** Optymalizacja stosunku cementowo-wodnego w napowietrzanych mieszankach betonowych. W: Zwiększenie efektywności procesów budowlanych i przemysłowych. Pod red. Marleny Rajczyk Rozdział w monografii Wyd. Pol. Częstochowskiej.
4. **Halbiniak J., Pietrzak A., 2007:** Beton napowietrzany, Drogownictwo, Miesięcznik Naukowo – Techniczny Stowarzyszenia Inżynierów i techników Komunikacji.
5. **Halbiniak J., 2004:** Warstwa przejściowa kruszywo – zaczyn cementowy w kompozytach betonowych, Zwiększenie efektywności procesów przemysłowych i budowlanych, Wyd. Pol. Częstochowskiej, Częstochowa.
6. **Jamroży Z., 2005:** Beton i jego technologie, Wydawnictwo Naukowe PWN, Warszawa.
7. **Kalisty M., Małaszkiewicz D., 2010:** Metody badania mrozoodporności betonów. Ocena mrozoodporności betonu z cementem hutniczym, Budownictwo i Inżynieria Środowiska, 1, 293-300.
8. Katalog typowych konstrukcji nawierzchni sztywnych, 2001**:** GDDP, Warszawa.
9. **Kurdowski W., Szeląg H., Bochenek A., 2013:** Czynniki wpływające na odporność betonu na działanie mrozu, XXVI Konferencja Naukowo-Techniczna Awarie budowlane, 851-856.
10. **Łaźniewska-Piekarczyk B., 2012:** The influence of selected new generation admixtures on the workability, air-voids parameters and Frost-resistance of self-compacting concrete, Construction and Building Materials 31, 310-319.
11. **Małolepszy J**., **2000:** Wybrane zagadnienia z trwałości betonów, Beton na progu nowego milenium, Kraków.
12. **Neville A.M**., **2012: Właściwości betonu, Polski Cement, Kraków**.
13. **Nowak – Michta A**., **2008:** Identyfikacja porowatości napowietrzonych betonów z dodatkiem popiołu lotnego, Dni betonu.
14. **Powers T.C., 1945:** A working hypothesis for further studies of frost resistance. Journal of the American Concrete Institute, 16(4).
15. **Rajczyk J., Halbiniak J**., **2012:** Influence of Microsilicss and Air Entraining Additives on Particular Features of Concrete Composite. W: Proceedings of 4th International Conference on Contemporary Problems in Architecture and Construction. Sustainable Building Industry of the Future. September 24-27, 2012, Wyd. Pol. Częstochowskiej.
16. **Rajczyk J., Halbiniak J., Langier B.**, **2012:** Technologia kompozytów betonowych w laboratorium i w praktyce, Wyd. Pol. Częstochowskiej, Częstochowa.
17. **Rusin Z**., **2002:** Technologia betonów mrozoodpornych, Polski Cement, Kraków.
18. **Wawrzeńczyk J, Molendowska A**., **2011:** Struktura porów, a mrozoodporność betonów napowietrzonych za pomocą mikrosfer, Cement Wapno Beton, nr 5.
19. **Wawrzeńczyk J., Molendowska A.**, **2014:** Mrozoodporność betonów napowietrzonych za pomocą mikrosfer polimerowych, Dni Betonu.

20. **ZTV Beton – StB01, 2001:** Zusätzliche Technische Vertagsbedingungen und Richtlinien fűr den Bau von Fahrbahndecken aud Beton.

BADANIA TRWAŁOŚCI MROZOWEJ BETONÓW MODYFIKOWANYCH DODATKIEM POPIOŁU LOTNEGO

Streszczenie. W pracy przedstawiono wpływ dodatku popiołów lotnych i domieszki napowietrzającej na mrozoodporność betonu badaną metodą bezpośrednią oraz charakterystykę porów powietrznych. Badanie mrozoodporności przeprowadzono dla 150 cykli zamrożeń i rozmrożeń. Dla betonów wykonano badanie struktury porowatości kompozytów betonowych, które przeprowadzono przy użyciu urządzenia do automatycznej analizy obrazu z wykorzystaniem programu komputerowego Lucia Concrete. Analizie poddano beton kontrolny oraz beton z dodatkiem popiołu lotnego w ilości połowy maksymalnej dopuszczalnej normowo ilości, napowietrzane różnymi dawkami domieszki napowietrzającej.

Słowa kluczowe: beton, popioły lotne, charakterystyka porów powietrznych, mrozoodporność.

Assessment of Monthly Mean Total Ozone Distribution Changes With Regard to Atlantic Ocean Surface Temperatures Variations

Alexander Holoptsev[1], Alexander Bolshikh[1], Valeriya Bekirova[2], Mariya Nikiforova[2]

[1]Sevastopol Maritime Academy
Rybakov Str., 5A, Sevastopol, Crimea, 299014; e-mail: kholoptsev@mail.ru
[2]Sevastopol National Technical University
Universitetskaya Str., 33, Sevastopol, Crimea, 299053; e-mail: maha.ukraine@gmail.com

Received December 03.2014; accepted December 17.2014

Summary: Taking into account monthly average surface temperatures changes of Atlantic water areas, which have a strong influence on monthly mean total ozone distribution above Poland, allows to imply their effective modeling and forecasting for several years. Prediction errors are at the maximum in June and rise as the forecast period increases. Nevertheless, when forecast is made for 1 – 2 years, their levels (modulo) do not exceed absolute error of total ozone measurements instrumentally based on the most exact of existing devices – Dobson spectrophotometer.
Key words: variability of total ozone distribution over Poland, surface temperatures, significant ocean areas, modeling, forecasting, statistical relationship, interaction of the troposphere and stratosphere.

INTRODUCTION

Variability of total ozone content (TOC) distribution in the atmosphere influences changes of UV solar radiation fluxes, which take part in creating tropospheric and surface ozone, growth of all land plants, animals and microorganisms, and affect human health as well. Therefore, improvement of the techniques of its monitoring is a topical problem of physical geography, meteorology and ecology.

Nowadays, since January 1979, variability and distribution of daily mean and monthly mean TOC have been researched by the means of global monitoring system. TOC values for different regions of the Planet which are not in the area of a pole night are measured by spectrophotometers TOMS (till 2013) and OMI. (2013 – present day) Such data go to the World ozone and ultraviolet data centre (Toronto), and are presented in the Internet for free access. Possibilities of these tools and data processing procedures provide resolution of 25 Dobson units (DU) with spatial grid 1.5°x1.5° [1].

Ground based TOC measuring stations are located in different cities; the most accurate device in use here is Dobson spectrophotometer, with measurement error around 5 DU. This allows to study the process peculiarities in more detail. Nevertheless, developing alternative monitoring techniques of TOC variability is of a great interest.

It has been established that changes of ozone depleting substances fluxes, entering different atmosphere segments, is one of the essential factors, causing TOC distribution changes in terrestrial atmosphere [2]. Such species of technogenic and natural origin are formed on ground surface and can be delivered by air streams to stratosphere, where mainly ozone is located. Within troposphere their transport is carried out by streams, which arise at various convectional and synoptic processes [3]. The mechanisms that allow such substances to enter stratosphere are not yet known with assurance. According to H.P. Pogosyan [4], the main role here is played by advection of tropospheric air through tropopause breakdowns, which are located above subtropical jet streams. Nevertheless, this mechanism does not explain how exactly such substances, which have gotten to the lower stratosphere, are distributed in steadily stratified upper layers, where ozone destruction occurs.

E.A. Zhadin [5] suggested, that the essential role in this process is carried out by planetary and gravity waves, which arise as a result of various interactions of atmosphere and the Earth's surface. They also can be generated by movement of cyclones and anticyclones, interaction of jet streams and orographic or pressure irregularities [6,7]. Being nonlinear and large-scale, such waves break at some distance from the source, as their wave profile transforms while spreading [8]. This results in turbulent rising air currents, which can transfer air to any heights in stratosphere.

An important role in generating pressure irregularities is played by exposure of the atmosphere to heat and water vapor fluxes which arise from the World ocean surface. Hence, a relation between surface temperature changes of some water areas and TOC over many world regions can exist.

The adequacy of such assumptions has been confirmed by many researchers [9]. This suggests a possibility of using surface temperature measurement results of some World ocean areas in the monitoring of TOC variations over the majority of the planet regions.

The Atlantic Ocean is the biggest and warmest part of the world oceans. This suggests a possibility of existence of such regions within it, whose surface temperature changes influence the ozonosphere state over Poland.

The occurrence was established of significant statistic relationships on coinciding time periods between TOC changes in the majority of atmosphere and surface temperature variations of many Atlantic water areas. On average, connections between these processes are weaker when the temporary shift between them grows [10].

Observations of surface temperature changes for the majority of Atlantic Ocean areas have been made for over 100 years. Their results in time series form are presented in the Internet. The data present the values of monthly mean anomalies calculated as an average of a segment, limited by parallels and meridians differing on 5° [11].

The disposition of water areas, influencing TOC distribution variations over one or other world region the most, (which we will further call 'significant'), is not clearly understood. It does not allow to use connections between the mentioned processes in modeling and forecasting TOC changes over such regions.

On this basis, the object of the research was monthly mean TOC distribution changes over Poland and monthly mean surface temperatures of various Atlantic Ocean areas.

The subject of the research was elaboration of monthly mean TOC distribution changes monitoring with regard to surface temperatures variations of the Atlantic Ocean significant areas on the example of Poland.

The purpose of the work was to identify the Atlantic Ocean significant areas, modeling accuracy assessment and TOC distribution variations forecasting over Poland.

To attain these ends the following tasks were solved:

1. Identification of Atlantic Ocean areas, whose monthly mean surface temperature inter-annual changes significantly influence (in coinciding time periods) monthly mean TOC variations over the majority of Poland's regions.
2. Identification of interannual TOC changes predictive models over the Poland's territory.
3. Developing TOC distribution changes forecasts over the Poland's territory and their adequacy assessment.

METHODOLOGY AND DATA

One of the most universal mathematical modeling methods of stochastic processes is a multiple regression method [12]. It is also applied for their prediction if the factors, considered as arguments, are connected with the studied process. Proving existence of stochastic connections between such natural process as TOC changes over Poland and other natural processes is really hard, in many cases – impossible. It is much easier to establish an existence of statistical connection between them.

The application of factors, connected statistically with the studied process, as factors in multiple regression model, does not guarantee its practicality in the forecasting tasks. But the possibility is the higher, the stronger the statistical connections considered in modeling are. Hence, the application of this method in developing forecasting techniques of studied process was accepted as admissible.

The mentioned technique included two stages.

At the first stage the first task was solved with the use of correlation analysis. Among all the Atlantic Ocean areas (5x5°) the ones were identified whose surface temperature inter-annual changes were significantly correlated with TOC in one or other atmosphere segment (1x1°) over Poland's territory. As a quantity measure of connection between the studied processes a pair correlation coefficient was used. The latter, with due regard to freedom degrees of corresponding time series, was accepted significant when exceeding 99% by Student's t-test. Further, among such water areas the significant ones were established. Their temperature changes were significantly connected with TOC variations at coinciding time periods in not less than 75% of atmosphere segments over the studied territory.

At the second stage the models' monthly mean TOC inter-annual changes , corresponding to each atmosphere segment over Poland, were identified.

Linear multiple regression was used as a predictive model:

$$\mathrm{Y}(t) = c_0 + c_1 x_1(t) + c_2 x_2(t) + \ldots + c_N x_N(t), \qquad (1)$$

here: c_i – constants, which were chosen so that the sum of deviation squares $z(t) = Y(t) - y(t)$ for all the time periods t was minimal;

$y(t)$ – time series for each predictable process during the 1979–2008 period;

$Y(t)$ – its model;

$x_i(t)$ – state in a time moment t of some process, which is significantly statistically connected with $y(t)$.

As model arguments (1) the time series of monthly mean surface temperatures of significant world oceans areas were used. They correspond to the 1979 – 2008 period in some time moments t coinciding with the studied processes.

Forecasting was made for 2009 and 2010, since there are results of satellite TOC monitoring for these years over Poland so their comparison can be made.

It was suggested that the number of model arguments (1) was equal to the number of significant areas – N. Time series for each of them contained M members ($M = 2N$). Then model coefficients (1) were calculated as components of ($N+1$)-vector $\underline{\tilde{N}}$, which is a solution to vector-matrix equation:

$$\underline{B} = A * \underline{C}, \qquad (2)$$

where:

$\underline{\tilde{N}} - N+1$-vector

$$B = \begin{Bmatrix} \sum_{i=1}^{M} y_i \\ \sum_{i=1}^{M} y_i x_{i,1} \\ \ldots \\ \sum_{i=1}^{M} y_i x_{i,N} \end{Bmatrix},$$

A – matrix $(N+1)\times(N+1)$

$$A=\begin{Bmatrix} M & \sum_{i=1}^{M} x_{i,1} & \sum_{i=1}^{M} x_{i,2} & \dots & \sum_{i=1}^{M} x_{i,N} \\ \sum_{i=1}^{M} x_{i,1} & \sum_{i=1}^{M} x_{i,1}x_{i,1} & \sum_{i=1}^{M} x_{i,2}x_{i,1} & \dots & \sum_{i=1}^{M} x_{i,N}x_{i,1} \\ \sum_{i=1}^{M} x_{i,2} & \sum_{i=1}^{M} x_{i,1}x_{i,2} & \sum_{i=1}^{M} x_{i,2}x_{i,2} & \dots & \sum_{i=1}^{M} x_{i,N}x_{i,2} \\ \dots & \dots & \dots & \dots & \dots \\ \sum_{i=1}^{M} x_{i,N} & \sum_{i=1}^{M} x_{i,1}x_{i,N} & \sum_{i=1}^{M} x_{i,2}x_{i,N} & \dots & \sum_{i=1}^{M} x_{i,N}x_{i,N} \end{Bmatrix}$$

The mentioned solution would look like:

$$\underline{C} = A^{-1} * \underline{B}, \quad (3)$$

here: A^{-1} is an inverse matrix to A. Vector $\underline{C}$ was identified for each considered Poland's region. The forecasting was made by substitution in equation (1) time series of arguments, corresponding to 2009 and 2010 yy. TOC values were calculated for each month and each Poland's region. For each of them prediction accuracy was estimated.

As data time series of monthly mean surface temperatures, anomalies of all the Atlantic Ocean areas (5x5°) were used. They were obtained from [11]. In doing so, only time series with no gaps during 1979 – 2010 were used. As ozone variability data, time series were taken of monthly mean TOC values over each Earth surface square 1°x1°, limited by parallels 55°N and 49°N and meridians 14°E and 24°E, received from [1]. Such atmosphere segment completely covers the whole Poland's territory and some regions of Germany, Ukraine and Belarus.

RESULTS AND DISCUSSION

With the use of the mentioned technique, significant areas of Atlantic Ocean for all the months were identified. The smallest amount of such regions (15) occurred in June. Coordinates of the established significant areas of Atlantic Ocean are tabulated in Table 1.

Locations of such regions are presented in Figure 1.

As is seen from Table 1 and Figure 1, the mentioned regions are located in the area where a strong interaction of Gulf Stream and Labrador Current is found. So, here the most contrastive pressure gradients are observed. Their interplay with jet streams makes the last ones vertically oscillate. This arises planetary and gravitation waves, tropopause breakdown and allows ozone depleting species enter the stratosphere.

When solving the second task for each month, the TOC changes models (1) were identified for all the considered atmosphere segments.

With the use of these models, TOC values were predicted for various parts of Poland in June 2009 and 2010. These forecasts, as well as the fact values of TOC over various regions of Poland in June 2009 are tabulated in Table 2.

Table 1. Coordinates of the regions' centers of Atlantic Ocean, which were significant in modeling TOC changes above Poland in June

# №	latitude (°)	longitude (°)	# №	latitude (°)	longitude (°)	# №	latitude (°)	longitude (°)
1	57.5N	42.5W	6	52.5N	42.5W	11	37.5N	42.5E
2	57.5N	37.5W	7	42.5N	47.5W	12	37.5N	37.5W
3	52.5N	57.5W	8	42.5N	42.5W	13	32.5N	67.5W
4	52.5N	52.5W	9	37.5N	52.5W	14	32.5N	37.5E
5	52.5N	47.5W	10	37.5N	47.5W	15	27.5N	72.5W

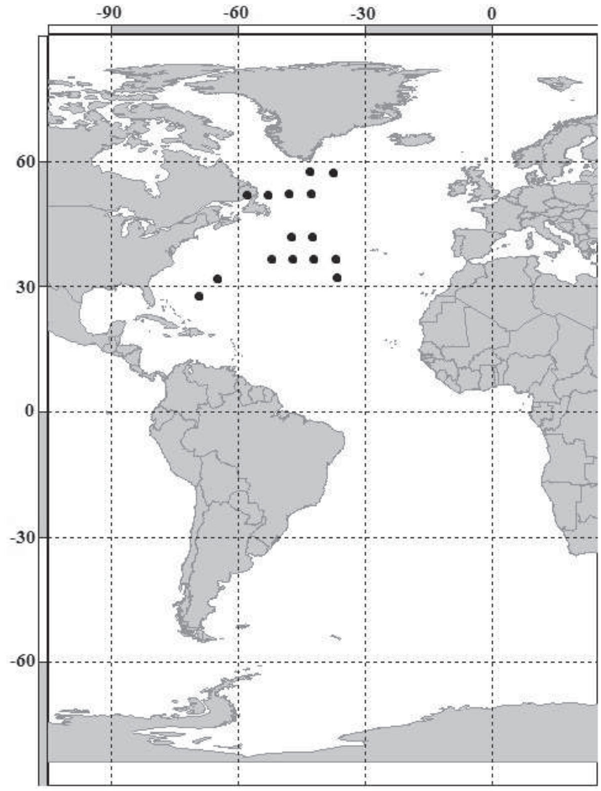

Fig. 1. Location of the regions' centers of Atlantic Ocean, whose surface temperature changes were significant in modeling TOC changes above Poland in June

Table 2. Fact and forecasted TOC values over the Poland regions in June 2009

Fact	14°E	16°E	18°E	20°E	22°E	24°E
55°N	355.3	354.7	354.6	353.7	354.7	355.2
53°N	350.9	350.9	351.7	351.5	351.6	352.1
51°N	348.8	348.9	350.2	349.8	350.5	349.8
49°N	349.9	350.3	350.9	350.8	350.2	349.7
Outlook						
55°N	352.6	351.8	348.8	346.8	345.9	346.0
53°N	352.5	352.2	350.6	350.0	340.0	348.5
51°N	350.9	349.5	350.0	351.8	350.6	350.7
49°N	350.9	350.6	350.9	352.3	351.9	351.8
Forecast error						
55°N	2.7	2.9	5.8	6.8	8.9	9.1
53°N	-1.6	-1.3	1.0	1.5	1.6	3.5
51°N	-2.1	-0.5	0.2	-2.0	-0.1	-0.9
49°N	-1.1	-0.3	-0.1	-1.4	-1.7	-2.0

As is seen from Table 2, the maximum forecast errors (9.1 DU) correspond to Poland region with center coordinates 55°N, 24°E. Average error value over the whole Poland territory for a one-year forecast measures 1.44 DU, which is less than TOC measurement error, obtained on Dobson spectrophotometer.

Related comparisons for 2010 have shown, that prediction mean error, made for 2 years, measures 4.6 DU. If the forecast for 2010 is made with the use of model (1), factor changes in 1980 – 2009 period (i.e. the forecast for one year), mean error value measures 2.64 DU. In other months the amount of significant Atlantic Ocean areas is greater, and the TOC forecasts mistakes over Poland are fewer.

A)

B)

C)

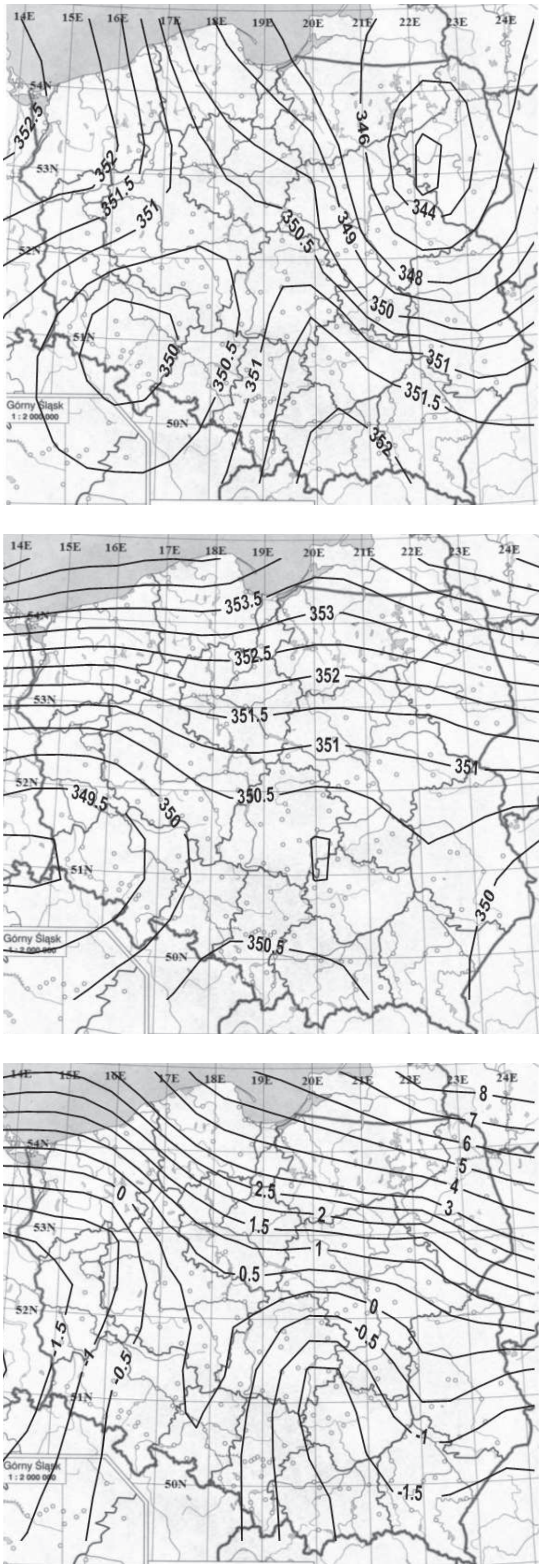

Pic. 2. Distribution over Poland territory of forecasted (A) and fact (B) TOC values in June 2009, and prediction errors (C)

CONCLUSIONS

1. There are Atlantic Ocean areas whose surface temperature inter-annual changes significantly influence the TOC variations over Poland in coinciding time periods. It supports the adequacy of hypothesis about wave nature of the distribution mechanism in the stratosphere of ozone depleting substances.
2. Prediction errors of TOC distribution changes over Poland are maximal in June and increase when forecast is made on greater time shifts. Nevertheless, when forecast is made for 1 – 2 years, their levels (modulo) do not exceed absolute error of total ozone measurements instrumentally based on the most exact of existing devices – Dobson spectrophotometer. This reinforces application efficiency of predicting technique in the studied forecasting process.

REFERENCES

1. World ozone and ultraviolet data center: http://www.woudc.org
2. **Alexandrov, E.L., Y.A. Izrael,I.L. Karol, A.H. Hrgian, 1992.** Ozonic shield of the Earth and its changes. S. Petersburg, Gidrometeoizdat, 286.
3. **Chkolny, E.P., 1997.** Physics of the atmosphere. Odessa, 698.
4. **Poghosyan H. P., 1972.** General circulation of the atmosphere. Leningrad.
5. **Jadin, E.A., 2004.** Influence of interannual temperature variations of the surface of the ocean circulation of the atmosphere and the ozone layer. The dissertation for scientific degree of the doctor of physical and mathematical Sciences. Dolgoprudny, Moscow Institute of physics, 211.
6. **Holton, J. R., P.H. Haynes and M.E. McIntyre, 1995.** Stratosphere troposphere exchange. Rev. Geophys., 403-440.
7. **Salby M.L., 1996.** Fundamentals of Atmospheric Physics. New York, Academic Press, 560.
8. **Lighthill, M.J., 1970.** Nonlinear theory of wave propagation. Moscow, "World", 230.
9. **Mohanakumar, K., 2011.** Interaction of the stratosphere and troposphere. Translation from English P.U. Lukyanova, edited by G.V. Alexeev. Moscow, FIZMATLIT, 451.

10. **Holoptsev, A.V., 2013.** The geographic position of the waters of the Pacific ocean as a factor of significant influence of changes of surface temperature on the state of the ozone layer. The Karazin Kharkiv national University, "Man and environment. The problem of neo-ecology trend", №3-4, 60-68.
11. Overview of current ocean reanalyses. reanalyses.org/ocean.
12. **Draper, N., H, Smith, 2007.** Applied regression analysis. Multiple regression. Moscow, "Dialectic", 912.

OCENA ZMIAN MIESIĘCZNEJ ŚREDNIEJ CAŁKOWITEJ DYSTRYBUCJI OZONOWEJ W ASPEKCIE WAHAŃ TEMPERATURY WÓD POWIERZCHNIOWYCH OCEANU ATLANTYCKIEGO

Streszczenie: Biorąc pod uwagę średnie miesięczne zmiany temperatury powierzchni w wodach Atlantyku, które mają silny wpływ na miesięczną średnią całkowitej dystrybucji ozonowej nad Polską, można sugerować ich skuteczne modelowanie i prognozowanie przez kilka lat. Błędy przewidywania są najwyższe w czerwcu i rosną wraz ze wzrostem okresu prognozowania. Niemniej jednak, gdy prognoza jest robiona na 1–2 lata ich poziom (modulo) nie przekracza błędu absolutnego sumy pomiarów ozonu w oparciu o najbardziej dokładne z istniejących urządzeń – spektrofotometr Dobsona.

Słowa kluczowe: zmienność całkowitego rozkładu ozonu nad Polską, temperatury powierzchniowe, znaczące obszary oceaniczne, modelowanie, prognozowanie, statystyczny związek, interakcja troposfery i stratosfery.

Dynamic Viscosity of Water and Milk Suspensions of Extruded Corn Porridge

Magdalena Klimek, Leszek Mościcki, Agnieszka Wójtowicz, Tomasz Oniszczuk, Maciej Combrzyński, Marcin Mitrus

Department of Food Process Engineering, Lublin University of Life Sciences
Doświadczalna 44, 20-236 Lublin, Poland

Received December 01.2014; accepted December 17.2014

Abstract: The purpose of this study was to determine the effect of temperature and the content of extruded corn porridge on the dynamic viscosity of water and milk suspensions. Extrusion-cooking process was carried out using a single extrusion-cooker TS-45. During the measurements it was noted that the viscosity of the suspensions was affected by the kind of liquid used, the temperature of the suspension and the content of porridge in the mixture. The highest viscosity was found in a 20% milky suspension tested at 20ºC.
Key words: extruded, extrusion-cooking, corn porridge, suspensions, viscosity, food

INTRODUCTION

Current trends show an increase in consumption of convenience food, which does not require a long time to prepare. Nowadays the consumers attach more and more importance to healthy eating, which is a challenge for manufacturers of functional foods for direct consumption. Innovations used in food processing, i.e. extrusion-cooking, micronization, expanding and combining plant additives call for the replacement of popular snacks with a new type of healthy products [7, 23, 28, 33].

Extrusion-cooking is processing of vegetable raw materials under high pressure and high temperature, which causes significant changes in their physical and chemical properties. During processing the material is mixed, compacted, compressed, melted and plasticized in the final extruder zone. Baro-thermal treatment can be performed in conditions of up to 200ºC and pressures up to 20 MPa. Extrusion-cooking technology is used in the food industry for the production of various types of food products such as snacks, instant cereal baby food, breakfast cereals, texturized vegetable protein, crisp bread, etc. [8, 13, 14, 17, 26].

Corn grits is one of the most popular material used in the production of extrusion-cooked food [10, 20]. Processing in appropriate conditions allows to obtain a new type of products different in relevant properties, texture, appearance and quality of health [5, 33, 34]. Qualitatively better products are derived from harder maize, which is caused by the higher amylose content in composition [4]. Corn products and dishes are hypoallergenic and gluten-free. Due to the different composition of protein compared to other cereals, corn products are recommended for people suffering from celiac disease. [5, 10, 31, 32].

MATERIALS AND METHODS

The main raw material used in our experimental study was commercial corn grits (Vegetus, Lubartów, Poland) with a moisture content of 13% d.m.. Extrusion was carried out in a single screw extrusion-cooker TS-45 (ZMCh Metalchem, Gliwice, Poland) using a single die of 3 mm diameter. Thermal treatment was at 130-135°C at the constant screw rotation – 120 rpm. The obtained corn extrudates were grounded in a laboratory mill type LMN10 (TestChem, Radlin) to the particle size of 1 mm [15, 19].

Moisture was determined by a drying chamber method, in accordance to standard – PN-A-888034 [1, 22, 29].

Water and milk suspensions of 10 and 20% share of extrudates were studied.

Samples were mixed for 10 minutes to obtain a uniform consistency. The values of dynamic viscosity were measured at two temperatures: 20ºC and 40ºC. Measurements were registered six-times.

Samples with hot distilled water and milk were prepared as follows: a weighed sample of the extrudate was mixed water or milk at a temperature of 85°C. Every single sample was mixed for 10 min, then cooled to 40°C, at which measurement was taken. The measurements carried out at 20°C did not require additional heating.

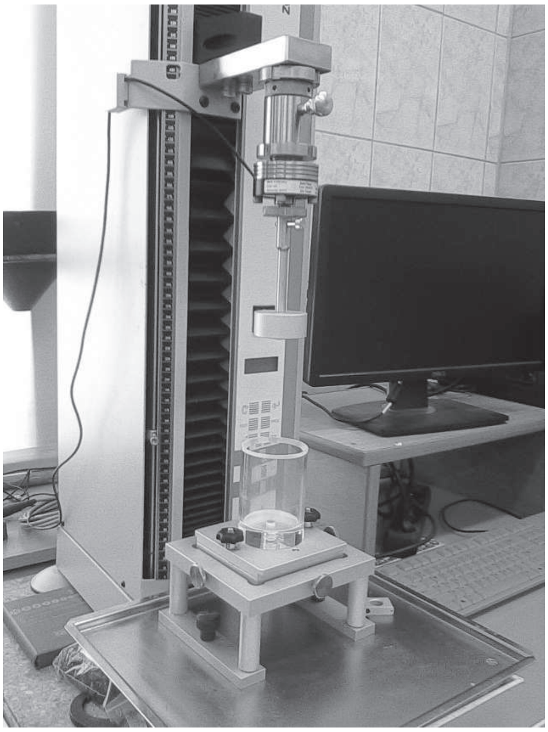

Fig. 1. Testing Machine Zwick type of BDO-FB0.5TH with mounted "back-extrusion" snap

Changes in viscosity of suspensions were measured using a universal testing machine Zwick / Roell BDO-FB0.5TH (Zwick GmbH & Co., Germany) (Fig. 1) equipped with a back extrusion snap. During measurements were used: a chamber of 60 mm height and internal diameter of 50 mm, and a plunger of 46 mm diameter and a height of 20 mm.

Resistance force was recorded during movement of the piston through the slurry in two measuring cycles: down and up, which was converted to the value of the coefficient of viscosity. Profiles of the dynamic viscosity, average decrease in shear strength, and the standard distance were recorded. The test Xpert 10v11 was used for the proper measurements procedure [2, 3, 6, 12, 16, 25].

RESULTS AND DISCUSSION

The moisture content of the extruded corn porridge has a great importance during storage, for maintaining the sensory qualities as well as the microbiological safety [22]. Taking all these aspects into account we can say that our products were very safe, their moisture content was less than 8% at average.

Dynamic viscosity of water suspensions made from the extruded corn porridge significantly changed with increasing its percentage share. The increase of the extrudate in the suspension resulted in higher values. Viscosity of water suspension at 20°C reached 0.54 Pa·s at the concentration of 10%. At the double concentration – 20% the obtained value was 18.15 Pa·s. Heating of the suspension up to 40°C resulted in the lowering of viscosity index, which varied from 0.33 Pa·s at 10% concentration for corn porridge to 12.40 Pa·s at 20% concentration for corn grits (see Fig. 2).

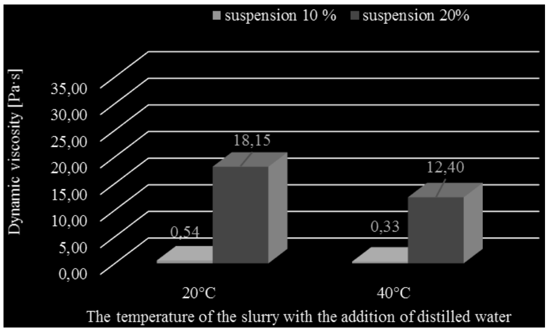

Fig. 2. Effect of corn grits and temperature on the viscosity of aqueous solutions of corn grits

Fig. 3 shows the viscosity of milk suspension at 20ºC and 40ºC, respectively. During the measurements it was found out that milky suspension was characterized by higher levels of dynamic viscosity compared to the water solutions. For example the viscosity of the milk suspension containing 10% extruded corn was almost twice as high as that of the water suspension and amounted up to 1.03 Pa·s at 20⁰C.

Also in that case we can say that the temperature of the suspensions played an important role. Higher temperature decreased the viscosity value. The highest viscosity value (30.26 Pa·s) was obtained for 20% milk suspension at 20°C. For the same suspension at 40ºC the dynamic viscosity was 18.91 Pa·s.

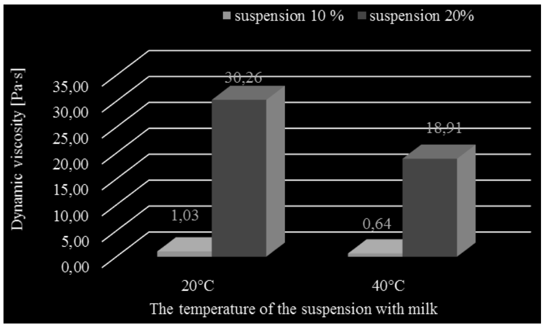

Fig. 3. Viscosity of corn grits – milk suspension

CONCLUSIONS

1. The study confirmed the possibility of using extrusion-cooking technology in the production of safe instant corn porridge. The average moisture content of the extruded products was 7.42%.
2. Increased temperature decreased the dynamic viscosity of the suspensions. The highest dynamic viscosity was measured for the milky suspension at 20°C.
3. Increasing amount of the extruded corn porridge in the mixture resulted in the increasing of the dynamic viscosity of the suspension.

REFERENCES

1. **ASAE Standard: ASAE S269.3, 1989:** Wafers, pellet and crumbles – definitions and methods for determining density, durability and moisture content.

2. **Bhattacharya S., Sudha M.L., Rahim A., 1999:** Pasting characteristics of an extruded blend of potato and wheat flours. Journal of Food Engineering., 40, 107-111
3. **Chaunier L., Valle G.D., Lourdin D., 2007:** Relationships between texture, mechanical properties and structure of cornflakes. Food Research International., 40, 493-503
4. **Czerwińska D., 2011:** Przetwory z kukurydzy – rodzaje, charakterystyka, wykorzystanie. PrzeglądZbożowo – Młynarski. 01, 09-11
5. **Gondek E., Jakubczyk E., Wieczorek B., 2013:** Właściwości fizyczne bezglutenowego pieczywa chrupkiego. Zeszyty Problemowe Postępów Nauk Rolniczych., 574, 29-38
6. **Gujral H.S., Sodhi N.S., 2002:** Back extrusion properties of wheat porridge (Dalia). Journal of Food Engineering 52, 53-56
7. **Guy R.**, 2001: Extrusion Cooking. Technologies and Applications. CRC Press Inc. Boca Raton, FL. USA
8. **Harper J.M., 1981:** Extrusion of Foods vol. I i II. CRC Press. Inc. Floryda USA 1981.
9. **Jurga R.**, 2011: Przetwory z kukurydzy uzyskane metodą ekstruzji. Przegląd Zbożowo-Młynarski., 02, 7-9
10. **Jurga R., 2012:** Przetwórstwo kukurydzy – możliwości wykorzystania. Przegląd Zbożowo-Młynarski., 09, 34-38
11. **Kunachowicz H., Przygoda B., 2008:** Wzbogacać żywność czy nie wzbogacać? Przemysł Spożywczy., 8, 86-87
12. **Lee S-Y., Luna-Guzman I., Chang S., Barrett D.M., Guinard J-X., 1999:** Relating descriptive analysis and instrumental texture data of processed diced tomatoes. Food Quality and Preference. 10, 447-455.
13. **Mercier C., Linko P., Harper J.M., 1998:** Extrusion cooking, St. Paul, American Association of Cereal Chemists, Inc
14. **Mitrus M., Oniszczuk T., Mościcki M., 2011:** Changes of specific mechanical energy during extrusion-cooking of potato starch. TEKA Kom. Mot. I Energ. Roln. – OL PAN., 11c, 200-207
15. **Mitrus M., Wójtowicz A., 2011:** Extrusion-cooking of wheat starch. TEKA Kom. Mot. I Energ. Roln. – OL PAN, 11c, 2008-2015
16. **Mouquet C., Salvignol B., Hoan N.V., Monvois J., Treche S., 2003:**Abitity of a "very low-cost extruder" to produce instant infant flours at a small scale in Vietnam. Food Chemistry., 82, 249-255
17. **Mościcki L., Mitrus M., Wójtowicz A., 2007:** Technika ekstruzji w przemyśle rolno-spożywczym. Warszawa. PWRiL
18. **Mościcki L., 2013:** Ekstruzja w przetwórstwie rolno-spożywczym. Cz. II. Surowce stosowane w produkcji wyrobów ekstrudowanych. Przegląd Zbożowo – Młynarski., 02, 6-8
19. **Mościcki L., Mitrus M., Wójtowicz A., Oniszczuk T., Rejak A., Janssen L., 2012:** Application of extrusion-cooking for processing of thermoplastic starch (TPS), Food Research International, Vol. 47, , pp 291-299.
20. **Naz S., Siddigi R., Sheikh H., Sayeed S.A., 2005:** Deterioration of olive, corn and soybean oils due to air, light, heat and deep-frying. Food Res. Internat., 38, 2, 127-134
21. **Oniszczuk T., Wójtowicz A., Mitrus M., Mościcki L., Combrzyński M., Rejak A., Gładyszewska B., 2012:** Biodegradation of TPS mouldings enriched with natural fillers, TekaCommision of Motorization and Energetics in Agriculture, Polish Academy of Sciences Branch in Lublin, vol. 123, No 1, pp. 175-180
22. **PN-A-888034: 1998**. Chrupki. Metodybadań
23. **Ramirez-Jimenz A., Guerra-Hernandez E., Garcia-Villanowa B., 2003:** Evolution of non-enzymatic browning during storage of infant rice cereal. Food Chemistry., 83, 219-225
24. **Rzedzicki Z., Zarzycki P., 2006:** Wpływ ekstruzji na skład frakcji błonnika pokarmowego ekstrudatów z udziałem owsa nagonasiennego. Biuletyn Instysutu Hodowli i Aklimatyzacji Roślin., 239, 281-293
25. **Sciarini L.S., Ribotta P.D., Leon A.E., Perez G.T., 2010:** Influence of Gluten-free Flours and their Mixtures on Batter Properties and Bread Quality. Food Bioprocess Technol., 3, 577-585
26. **Singh S., Gamlath S., Wakeling L., 2007:** Nutritional aspects of food extrusion: a review, International Journal of Food Science & Technology, 42, 916-929
27. **Waszkiewicz – Robak B., Świderski F., 2007:**Nutraceutyki dodatki prozdrowotne i bioaktywne składniki żywności. Przemysł Spożywczy., 63, 09, 38-40
28. **Wójtowicz A., 2007:** Ocena wybranych cech jakościowych ekstrudowanych zbożowych kaszek błyskawicznych. Żywność. Nauka. Technologia. Jakość., 4, 53, 46-54
29. **Wójtowicz A.**, 2008: Influenfe of legumes addition on proceeding of extrusion-cooking proces of precooded pasta. TEKA Kom. Mot. Energ. Roln. – OL PAN., 8a, 209-216
30. **Wójtowicz A.**, Pasterniak E., Juśko S., Hodara K., Kozłowicz K., 2012: Wybrane cechy jakościowe chrupek kukurydzianych z dodatkiem odtłuszczonych nasion lnu. Acta Sci. Pol., TechnicaAgraria 11, 3-4, 25-33
31. **Wójtowicz A.**, 2011: Influence of Extrusion-Cooking Process Parameters on Selected Mechanical Properties of Precooked Maize Pasta Products. TEKA Kom. Mot. I Energ. Roln. – OL PAN., 11, 430-440
32. **Wójtowicz A.**, 2011: Influence of Extrusion-Cooking Process Parameters on Selected Physical and Textural Properties of Precooked Maize Pasta Products. TEKA Kom. Mot. I Energ. Roln. – OL PAN., 11, 441-449
33. **Wójtowicz A.**, Pasterniak E., Juśko S., Hodara K., Kozłowicz K., 2012: Wybrane cechy jakościowe chrupek kukurydzianych z dodatkiem odtłuszczonych nasion lnyu. Acta Sci. Pol., TechnicaAgraria 11(3-4) , 25-33
34. **Zarzycki P.**, Rzecki Z., 2009: Wpływ dodatku komponentów wysokobiałkowych na właściwości fizyczne ekstrudatów kukurydziano-owsianych. Acta Agrophys. 13, 1, 281-291

WYZNACZANIE LEPKOŚCI ZAWIESIN Z UDZIAŁEM EKSTRUDOWANEJ KASZKI KUKURYDZIANEJ

Streszczenie: Celem badania było określenie wpływu temperatury oraz udziału ekstrudowanej kaszki kukurydzianej na zmiany jej wodnych i mlecznych roztworów. Ekstruzję prowadzono używając jednoślimakowego ekstrudera TS 45. W czasie pomiarów odnotowano, że lepkość zawiesin zależała od obróbki termicznej, rodzaju cieczy oraz udziału procentowego kaszki. Najwyższe wartości lepkości miała mleczna zawiesina kaszki o 20% udziale przetrzymywana w temperaturze 20°C.

Słowa kluczowe: ekstruzja, ekstrudowana kaszka kukurydziana, zawiesina, lepkość dynamiczna

The Note on Application of Logistic Model in Agriculture Research

Andrzej Kornacki

Department of Applied Mathematics and Computer Science University of Life Sciences in Lublin
Akademicka 12, 20-950 Lublin, e-mail: Andrzej.Kornacki@up.lublin.pl

Received December 10.2014; accepted December 19.2014

Summary. In the study an example was presented when the application of the coefficient of determination R^2, a commonly used goodness of fit measure of the model to the empirical results leads to wrong conclusions. It is an example of a logistic model. Theoretical considerations were applied to the model describing the germination of seeds which underwent laser biostimulation prior to sowing. Moreover, the origin of problems that appears in the described situation was explained.
Key words: logistic model, coefficient of determination R^2, laser biostimulation prior to sowing.

INTRODUCTION

Describing processes by mathematical models is a problem of interest to a number of researchers in various areas of science. However, the model shape also requires the verification of its correctness based on empirical data. The measure of the goodness of fit of the model to empirical data that is often used is the coefficient of determination R^2 [2,4,6,7]. This coefficient for characteristic y is defined as [8,10]:

$$R^2 = 1 - \frac{SSE}{SST}, \tag{1}$$

where:
$SST = \sum_{i=1}^{n} (y_i - \bar{y})^2$ is total sum of square for given feature,
$SSE = \sum_{i=1}^{n} (y_i - f_i)^2$ is error sum of square.

and
y_i – denotes empirical data,
f_i – denotes the values of a function describing the model.

Coefficient R^2 works perfectly in case of linear models and some nonlinear ones which are brought to linear models using the relevant transformations (i.e. nonlinear internal linear models [1]). It takes on the values from the range <0,1>. Values close to 1 prove the goodness of fit of the model (or regression function) to experimental data whereas those close to 0 indicate poor fit. Moreover, value R^2 determines which part of variability of the experimental results is explained by the model (or regression function).

However, in case of some nonlinear models, value R^2 can be negative. In such a case the application of this coefficient is incorrect.

THE OBJECTIVE AND SCOPE OF STUDY

The objective of the study was to demonstrate that the coefficient of determination R^2 for some nonlinear models can take on negative values. This study describes such a case regarding a logistic model. Theoretical considerations were applied to the model describing the germination process of seeds that underwent laser biostimulation prior to sowing. Moreover, it was explained why the use of a coefficient of determination is incorrect in this situation.

MATERIAL AND METHODS

At the Department of Physics of the University of Life Sciences in Lublin the research was conducted aiming at the determination of the germination process of tomato seeds and the impact of the laser biostimulation of the sowable material on this process [3]. In the research the seeds of Promyk variety were used. In laser biostimulation the adjustable doses of energy method were used assuming the dose equal to 4.5 mJ. For comparative reasons a control sample of seeds (non- biostimulated) was taken. The test group was represented by 700 seeds sown on Petri plates with tissue paper lining, in 7 samples 100 seeds per sample. The plates were placed in an electrostatic furnace, ensuring temperature stabilisation with the accuracy to $\pm 1^0$C. The seeds germinated without access of light. Every few hours the germinating seeds were counted. The seed was considered germinated if it formed a germ which was at least 2 mm long. During the experiment the constant moisture content of the tissue paper was maintained by dosing distilled water.

MATHEMATICAL MODEL OF THE GERMINATION PROCESS OF TOMATO SEEDS

The germination process of tomato seeds undergoing laser biostimulation before sowing can be described by means of a mathematical model which is expressed by means of the logistic function [3] in the form of:

$$n(t) = \frac{n_k}{1 + (n_k - 1)e^{-\alpha_p n_k (t - t_0)}}, \qquad (2)$$

where:
n_k – final number of germinated seeds,
n(t) – number of seeds germinated after given time t,
α_p – coefficient of germination speed [1/h]
t_0 – time germination of the first seeds sown [h]

Values α_p and t_0 are determined on an experimental basis.

In a general case the logistic curve can be described by a formula with three parameters

$$f(t) = \frac{A}{1 + Be^{Ct}}. \qquad (3)$$

RESULTS AND DISCUSSION

Using formula (2) the number of germinated seeds n(t) was calculated and then the sums of squares SST and SSE and, finally, from formula (1) the value of the coefficient of determination R^2. The results for germinated seeds of Promyk variety tomatoes which underwent laser biostimulation with 4.5 mJ dose at temperature 15^0C are presented in Table 1.

Table 1. The values of sums of squares and the coefficient of determination R^2 for germinated seeds of Promyk variety tomatoes stimulated with the dose of 4.5 mJ at temperature 15^0C.

SST	25554,54
SSE	35549,37
R^2	-0,90

Similar results for germinated seeds of Promyk variety tomatoes which underwent laser biostimulation with the dose of 4.5 mJ at temperature 20^0C, the control sample (non-biostimulated seeds) at temperature 25^0C and the samples of biostimulated seeds at temperature 30^0C are presented in Tables 2 and 3 as well as Table 4.

As Tables 1-4 show, in the considered cases, the coefficient of determination takes on negative values. In such a situation it does not have any interpretation at all and consequently it cannot be used as a measure of goodness of fit of the model to empirical data. Let us demonstrate the source of the existing situation.

Table 2. The values of sums of squares and the coefficient of determination R^2 for germinated seeds of Promyk variety tomatoes stimulated with the dose of 4.5 mJ at temperature 20^0C.

SST	1512,90
SSE	2076,50
R^2	-0,37

Table 3. The values of sums of squares and the coefficient of determination R2 for nonstimulated germinated seeds of Promyk variety tomatoes at temperature 250C.

SST	691,21
SSE	959,55
R2	-0,39

Table 4. The values of sums of squares and the coefficient of determination R2 for germinated seeds of Promyk variety tomatoes stimulated with the dose of 4.5 mJ at temperature 300C.

SST	392,57
SSE	26,199,30
R2	-65,74

It is demonstrated [9,5] that in the linear regression model some basic identity takes place.

$$\sum_{i=1}^{n}(y_i - \hat{y})^2 = \sum_{i=1}^{n}(y_i - f_i)^2 + \sum_{i=1}^{n}(f_i - \bar{y})^2 \;\; so \quad SST = SSE + SSR, \qquad (4)$$

where
$$SSR = \sum_{i=1}^{n}(f_i - \bar{y})^2, \qquad (5)$$

denotes regression sum of square.

The proof of the identity (4) is based on the linearity of the regression model and the evaluation of its coefficients using the least square method. Consequently, identity (4) is true for linear models with coefficients evaluated using the least square method. The range of value of coefficient R^2 <0,1> results in an obvious way from identity (4). The logistic model is an example of a **non-linear model** for which identity (4) does not occur. It is proved by the sums of squares in Tables 1-4. It is this particular fact that is the source of negative values of the coefficient of determination.

CONCLUSIONS

To sum up the considerations contained in the study, the following conclusions can be formulated:

1. Coefficient of determination R^2 is a very good measure of goodness of fit of **linear** models and some nonlinear but **internal linear** ones to empirical data.
2. It is not recommended that the coefficient of determination R^2 be used as a goodness of fit criterion for a logistic model.

REFERENCES

1. **Dobosz M., 2001:** Computer aided statistical analysis of test results Akademicka Oficyna Wydawnicza Exit. Warszawa.[in Polish],
2. **Białobrzeski I., Myhan R., Cydzik R., 2005:** Effective water diffusion coefficient in Faba bean seeds during

drying. Part II Analysis of estimation errors. Electronic Journal of Polish Agricultural Universities Vol 8 Issue 2, http://www.ejpau.media.pl//volume8/issue2/art-29.html,
3. **Gładyszewska B., 1998:** Evaluation of the impact of pre-laser bio-stimulation of seeds of tomatoes on the process of germination. The doctoral dissertation. Uniwersytet Przyrodniczy w Lublinie.[In Polish],
4. **Molenda M. Lukaszuk J., Horabik J., 2005:** Airflow resistance of wheat as affected by grain density and moisture content. Electronic Journal of Polish Agricultural Universities Vol 8 Issue 4. http://www.ejpau.media.pl/volume8/issue 4/art-67.html,
5. **Królczyk J., Matuszek D., Tukiendorf M., 2010:** Modelling of quantity changes in a multicomponent granular mixture during mixing. Electronic Journal of Polish Agricultural Universities Vol 13 Issue 1. http://www.ejpau.media.pl/articles/volume13/issue1/art-11.pdf,
6. **Oniszczuk T., Mościcki L., 2011:** Efect of fillers addition on SME of extrusion-cooking of thermoplastic wheat starch. Teka Kom.Mot.Energ.Roln.-OL PAN, 11, 245-251.
7. **Oniszczuk T., Mościcki L., 2011:** Production of biodegradable packaging materials by extrusion-cooking Teka Kom.Mot.Energ.Roln.-OL PAN, 11, 252-260.
8. **Ryan T.P. 1997:** Modern regression methods. John Wiley & Sons, New York.
9. **Seber G.A.F., 1977:** Linear regression analysis. John Wiley & Sons, New York,
10. **Seber G.A.F., Wild C.J. 1989:** Nonlinear regression, John Wiley & Sons New York.

NOTA O ZASTOSOWANIU MODELU LOGISTYCZNEGO W BADANIACH ROLNICZYCH

Streszczenie. W pracy opisano przykład, kiedy użycie współczynnika determinacji R2, powszechnie stosowanej miary dobroci dopasowania modelu do wyników eksperymentu prowadzi do niewłaściwych wniosków. Jest to przypadek modelu logistycznego. Rozważania teoretyczne zastosowano do modelu opisującego proces kiełkowania nasion poddanych przedsiewnej laserowej biostymulacji. Ponadto, wyjaśniono co jest źródłem problemów pojawiających się w opisanej sytuacji.

Słowa kluczowe: model logistyczny, współczynnik determinacji R2, przedsiewna biostymulacja nasion.

TEKA. COMMISSION OF MOTORIZATION AND ENERGETICS IN AGRICULTURE – 2014, Vol. 14, No. 4, 45–52

An Analysis of Pressure Distribution in Water and Water Emulsion In a Front Gap of a Hydrostatic Bearing

Konrad Kowalski, Tadeusz Zloto

Institute of Mechanical Technologies, Czestochowa University of Technology
Al. Armii Krajowej 21, 42-201 Czestochowa, konrad@itm.pcz.czest.pl, zlotot@o2.pl

Received December 05.2014; accepted December 18.2014

Summary. The paper presents pressure distributions for water and water emulsion in a variable-height gap of a hydrostatic thrust bearing with a rotating upper wall. On the basis of the Navier-Stokes equations and the continuity equation a formula is established for obtaining pressure in the gap. The paper also analyses the influence of geometrical parameters and exploitation conditions on the distribution of circumferential pressure around the smallest height of the gap.
Key words: pressure distribution, variable-height gap, hydrostatic thrust bearing, water, water emulsion.

INTRODUCTION

The problem of gap flow concerns a number of hydraulic devices and machines in which contact parts are separated by liquid-filled gaps of very small height. For gap flow of working liquids the Reynolds number is small and the flow is laminar [13, 26].

There are gaps of various shapes and dimensions. Since each gap in a hydraulic system is a source of loss [5, 6, 13, 21], it is important to examine phenomena that occur in them [14]. Losses are essentially dependent on the gap height: the greater the gap height the smaller the mechanical losses and the greater the volumetric losses [22].

Hydrostatic bearings are applied in popular hydrostatic drive systems [3, 4, 10, 16, 18, 19, 20]. In the case of axial pumps with a flat swash plate, a front gap can be found between slipper and swash plate and between cylinder block and valve. The smallest gap height between the slipper and swash plate is much greater than that between the cylinder block and valve plate [2]. The working liquid used in a hydraulic system is of crucial importance, too. The liquid is responsible for transferring large forces and torques of the system's elements. Selecting a working liquid has therefore economic and often environmental consequences.

Over the centuries, the discipline of fluid mechanics, including broadly conceived hydraulics, was developed by a number of prominent scientists, such as Thales of Miletus, Aristotle, Ktesibios, Archimedes, Da Vinci, Stevin, Torricelli, Pascal, Boyle, Newton, Bernoulli, Euler, Armstrong or Bramah [27]. In 1795, Bramah designed, patented and constructed the first hydraulic water press [11]. It was however observed that water as working liquid caused corrosion of metal elements and at the beginning of the 20th century American scientists Harvey Williams and Reynolds Janney came up with the idea of using mineral oil instead of water. They were the first to construct a hydrostatic piston axial gear with a swing swash plate [14]. This invention marks the beginning of the rapid development of oil hydraulics, which continues until today.

In hydraulic systems various liquids are used as working agents (Fig. 1). At present the one most frequently used is mineral oil [7, 23]. In places under the risk of fire, such as mines, non-flammable liquids are used.

The liquids applied are not perfect. With the multitude of industrial applications, it is necessary to search for liquids meeting the requirements as closely as possible.

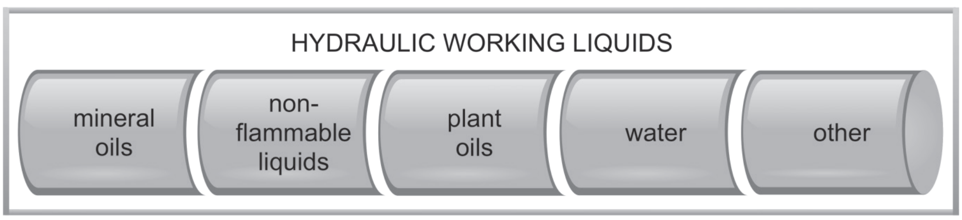

Fig. 1. Working liquids used in hydraulic drives

Because of that, studies are conducted on the application of plant oils in hydraulic systems. New opportunities seem to be offered by what is known as intelligent fluids, including electro-rheological and magneto-rheological fluids.

Besides, in the recent years there has been a revival of interest in water. Its applicability as a working agent in hydraulic systems is expected to rise due to the fact that it is environment-friendly and much cheaper than the other liquids currently used [11, 12, 17]. Following intensive research on water hydraulics [12], many producers and suppliers offer parts for modern water systems.

OBJECTIVES OF THE STUDY

The present study aims to examine the influence of exploitation parameters and dimensions on pressure distributions in the area surrounding the smallest height of the front gap in a hydrostatic thrust bearing with water and with a water emulsion. The study assumes an analytic model of pressure distribution in a front gap of the hydrostatic thrust bearing with a rotating upper wall.

A MODEL BASED ON THE NAVIER-STOKES EQUATIONS AND THE CONTINUITY EQUATION OF LIQUID PRESSURE DISTRIBUTION IN A FRONT GAP OF A HYDROSTATIC BEARING

Pressure distribution in the front gap of a hydrostatic thrust bearing (Fig. 2) can be best described analytically by means of a system of equations consisting of the Navier-Stokes equation and the continuity equation represented in a cylindrical system of coordinates r, φ, z [8, 15, 25]. A fluid element ABCDEFGH of dimensions dr, $rd\varphi$, dz is presented in Fig 3.

To solve the system of equations (1- 4) analytically, it is necessary to adopt the following simplifying assumptions:

- The gap is of micrometre high and is completely filled with incompressible liquid of constant viscosity;
- Surfaces are rigid;
- Liquid flow is laminar, uniform, steady and isothermal;
- Tangent stress is Newtonian;
- Liquid particles directly adjacent to the rotating wall surface have the same velocity as the rotating wall;
- Inertia is negligible.

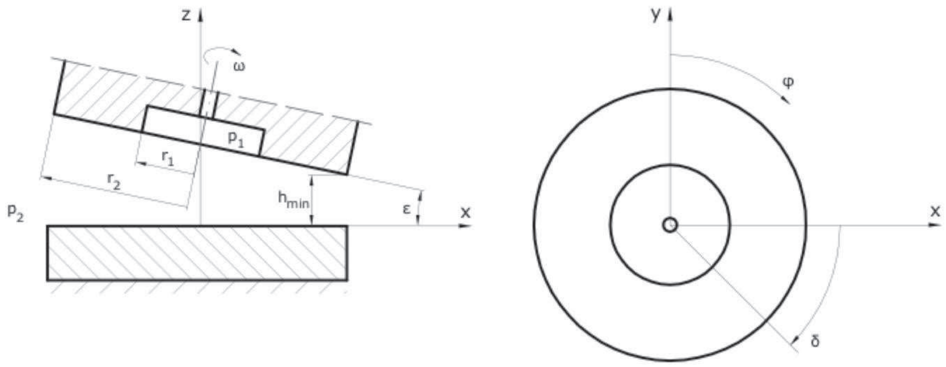

Fig. 2. Front gap of a hydrostatic thrust bearing [25]

The base system of equations is [8, 15, 25]:

$$\begin{cases}
\dfrac{\partial v_r}{\partial t}+v_r\dfrac{\partial v_r}{\partial r}+\dfrac{v_\varphi}{r}\dfrac{\partial v_r}{\partial \varphi}+v_z\dfrac{\partial v_r}{\partial z}-\dfrac{v_\varphi^2}{r}= \\
=F_r+\nu\left(\dfrac{\partial^2 v_r}{\partial r^2}+\dfrac{1}{r}\dfrac{\partial v_r}{\partial r}+\dfrac{1}{r^2}\dfrac{\partial^2 v_r}{\partial \varphi^2}+\dfrac{\partial^2 v_r}{\partial z^2}-\dfrac{v_r}{r^2}-\dfrac{2}{r^2}\dfrac{\partial v_\varphi}{\partial \varphi}\right)-\dfrac{1}{\rho}\dfrac{\partial p}{\partial r}, & (1) \\
\dfrac{\partial v_\varphi}{\partial t}+v_r\dfrac{\partial v_\varphi}{\partial r}+\dfrac{v_\varphi}{r}\dfrac{\partial v_\varphi}{\partial \varphi}+v_z\dfrac{\partial v_\varphi}{\partial z}+\dfrac{2v_r v_\varphi}{r}= \\
=F_\varphi+\nu\left(\dfrac{\partial^2 v_\varphi}{\partial r^2}+\dfrac{1}{r}\dfrac{\partial v_\varphi}{\partial r}+\dfrac{1}{r^2}\dfrac{\partial^2 v_\varphi}{\partial \varphi^2}+\dfrac{\partial^2 v_\varphi}{\partial z^2}+\dfrac{2}{r^2}\dfrac{\partial v_r}{\partial \varphi}-\dfrac{v_\varphi}{r^2}\right)-\dfrac{1}{\rho r}\dfrac{\partial p}{\partial \varphi}, & (2) \\
\dfrac{\partial v_z}{\partial t}+v_r\dfrac{\partial v_z}{\partial r}+\dfrac{v_\varphi}{r}\dfrac{\partial v_z}{\partial \varphi}+v_z\dfrac{\partial v_z}{\partial z}= \\
=F_z+\nu\left(\dfrac{\partial^2 v_z}{\partial r^2}+\dfrac{1}{r}\dfrac{\partial v_z}{\partial r}+\dfrac{1}{r^2}\dfrac{\partial^2 v_z}{\partial \varphi^2}+\dfrac{\partial^2 v_z}{\partial z^2}\right)-\dfrac{1}{\rho}\dfrac{\partial p}{\partial z}, & (3) \\
\dfrac{\partial v_r}{\partial r}+\dfrac{1}{r}\dfrac{\partial v_\varphi}{\partial \varphi}+\dfrac{\partial v_z}{\partial z}+\dfrac{v_r}{r}=0. & (4)
\end{cases}$$

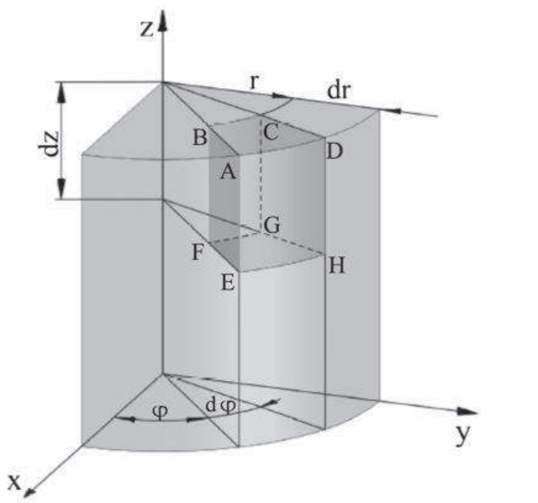

Fig. 3. A fluid element in a cylindrical coordinate system [1]

Besides, if $v_r = v_r(r, z)$ and $v_z = 0$, equations (1 - 4) become:

$$\begin{cases} 0=\nu\dfrac{\partial^2 v_r}{\partial_z^2}-\dfrac{1}{\rho}\dfrac{\partial p}{\partial r}, & (5) \\ 0=\dfrac{\partial^2 v_\varphi}{\partial_z^2}, & (6) \\ 0=\dfrac{\partial p}{\partial z}, & (7) \\ 0=\dfrac{\partial v_r}{\partial r}+\dfrac{1}{r}\dfrac{\partial v_\varphi}{\partial_\varphi}+\dfrac{v_r}{r}. & (8) \end{cases}$$

Equation (5) can be transformed and represented as:

$$\frac{\partial^2 v_r}{\partial_z^2}=\frac{1}{\nu\rho}\frac{\partial p}{\partial r}. \qquad (9)$$

To obtain the velocity v_r, it is necessary to integrate equation (9) twice with respect to the variable z. Then, the result is:

$$v_r=\frac{1}{2\nu\rho}\frac{\partial p}{\partial r}z^2+C_1 z+C_2. \qquad (10)$$

The integration constants C_1 and C_2 were obtained for the boundary conditions presented in Table 1.

Table 1. Boundary conditions for computing the integration constants C_1 and C_2

	No.	*Variable z*	*Velocity* v_r
Boundary conditions	*1.*	$z = 0$	$v_r = 0$
	2.	$z = h$	$v_r = 0$

Then, it follows:

$$C_1=-\frac{1}{2\nu\rho}\frac{\partial p}{\partial r}h, \qquad (11)$$

$$C_2=0, \qquad (12)$$

and after substituting (11) and (12) into equation (10):

$$v_r=\frac{1}{2\nu\rho}\frac{\partial p}{\partial r}(z^2-hz). \qquad (13)$$

After integrating equation (6) twice with respect to the variable z, the velocity v_φ was obtained:

$$v_\varphi=C_3 z+C_4. \qquad (14)$$

The boundary conditions used for computing the integration constants C_3 and C_4 are presented in Table 2.

Table 2. Boundary conditions for computing the integration constants C_3 and C_4

	No.	*Variable z*	*Velocity* v_φ
Boundary conditions	*1.*	$z = 0$	$v_\varphi = 0$
	2.	$z = h$	$v_\varphi = \omega r$

Hence:

$$C_3=\frac{\omega r}{h}, \qquad (15)$$

$$C_4=0, \qquad (16)$$

and after substituting (15) and (16) into equation (14):

$$v_\varphi=\frac{\omega r}{h}z. \qquad (17)$$

When (14) and (17) are substituted into (8):

$$0=\frac{1}{2\nu\rho}\frac{\partial^2 p}{\partial r^2}(z^2-hz)-\omega z\frac{1}{h^2}\frac{dh}{d\varphi}+\frac{1}{2\nu\rho r}\frac{\partial p}{\partial r}(z^2-hz). \qquad (18)$$

Integrating equation (18) with respect to the variable z in the interval from 0 to h and performing some transformations yields:

$$\frac{\partial}{\partial r}\left(r\frac{\partial p}{\partial r}\right)=-6\nu\rho\omega r\frac{1}{h^3}\frac{dh}{d\varphi}. \qquad (19)$$

To obtain a formula describing the pressure p in a front gap, it is necessary to integrate equation (19) twice with respect to the variable r. This leads to:

$$p=-\frac{3}{2}\nu\rho\omega r^2\frac{1}{h^3}\frac{dh}{d\varphi}+C_5\ln r+C_6. \qquad (20)$$

The integration constants C_5 and C_6 were computed for the boundary conditions specified in Table 3.

Table 3. Boundary conditions for computing integration constants C_5 and C_6

	No.	*Radius r*	*Pressure* p
Boundary conditions	*1.*	$r = r_1$	$p = p_1$
	2.	$r = r_2$	$p = 0$

Hence:

$$C_5=\frac{3}{2}\nu\rho\omega\frac{1}{\ln\frac{r_2}{r_1}}\frac{1}{h^3}\frac{dh}{d\varphi}(r_2^{\,2}-r_1^{\,2})-\frac{p_1}{\ln\frac{r_2}{r_1}}. \tag{21}$$

$$C_6=\frac{3}{2}\nu\rho\omega r_2^{\,2}\frac{1}{h^3}\frac{dh}{d\varphi}-\frac{3}{2}\nu\rho\omega\frac{\ln r_2}{\ln\frac{r_2}{r_1}}\frac{1}{h^3}\frac{dh}{d\varphi}(r_2^{\,2}-r_1^{\,2})+\frac{p_1\ln r_2}{\ln\frac{r_2}{r_1}}. \tag{22}$$

Substituting integration constants (21, 22) into equation (20) ultimately leads to

$$p=\frac{3}{2}\nu\rho\omega\frac{1}{\ln\frac{r_2}{r_1}}\frac{1}{h^3}\frac{dh}{d\varphi}\left[(r_2^{\,2}-r^2)\ln\frac{r_2}{r_1}-(r_2^{\,2}-r_1^{\,2})\ln\frac{r_2}{r}\right]+p_1\frac{\ln\frac{r_2}{r}}{\ln\frac{r_2}{r_1}}. \tag{23}$$

RESULTS OF SIMULATIONS OF PRESSURE DISTRIBUTION IN THE FRONT GAP OF A HYDROSTATIC BEARING – AN ANALYSIS

Pressure was calculated in the front gap of a hydrostatic thrust bearing with water and with water emulsion AQUACENT LT 68. The basic physical parameters of these working liquids are presented in Table 4.

Table 4. Parameters of the working liquids

Parameter	Unit	Liquid	
		water	*water emulsion*
density	kg/m^3	988,1	930
kinematic viscosity	mm^2/s	0,548	68
water contents	%	100	41

The following input data were assumed in the computational model:

- Compression pressure p_1 = 20 Mpa,
- The smallest front gap height $h_{min} = 0.6\cdot10^{-6}$ m in the hydrostatic thrust bearing,
- Inclination angle of the upper wall with respect to the lower one $\varepsilon = 0.02°$,
- Angular velocity of the upper wall ω = 150 rad/s,
- Ratio of the external radius to the internal radius of the hydrostatic bearing $r_2/r_1 = 3$.

The height h of the front gap was obtained from the following formula [24]:

$$h=-r\sin\varphi\cos\delta\tan\varepsilon-r\cos\varphi\sin\delta\tan\varepsilon+r_2\tan\varepsilon+h_{min}, \tag{24}$$

where:

r	any radius within the plane of the point u consideration,
φ	current rotation angle,
δ	angle measured with respect to the horizontal a for this angle the height of the front gap is smallest (in the xy plane).

In variable-height gaps there are two zones near the point of the smallest height: the confusor zone and the diffuser zone. In the confusor zone the gap height decreases along the gap and overpressure occurs. In the diffuser zone, on the other hand, the gap height increases along the gap and negative pressure occurs, which is partly limited by the cavitation phenomenon [9]. An example of pressure distribution for water and the radius r = 0.011 [m] near the smallest height point in a hydrostatic bearing is presented in Fig. 4.

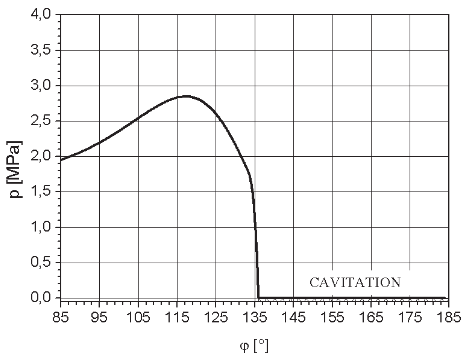

Fig. 4. Circumferential pressure distribution of water near the smallest-height point at the radius r = 0.011 m

A key parameter affecting the pressure of working liquids in a front gap is the kinematic viscosity factor. This can be seen very clearly in Fig. 5, where the values of the circumferential pressure in the hydrostatic bearing front gap are presented for water (ν=0.548 mm^2/s, ρ=988.1 kg/m^3) and for water emulsion AQUACENT LT 68 (ν=68 mm^2/s, ρ=930 kg/m^3), i.e. for working liquids which differ significantly with respect to kinematic viscosity. It can be observed that the values of the circumferential pressure increase as the viscosity of the working liquid increases.

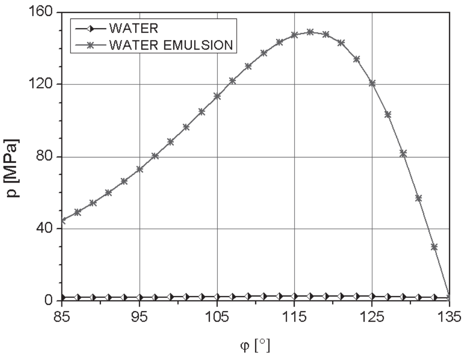

Fig. 5. Circumferential pressure distribution of water and water emulsion near the smallest-height point at the radius r = 0.011 m

In the interest of readability, in the graphs presented below different scales are used on the vertical axis for water and for water emulsion.

Fig. 6 presents circumferential pressure of water (Fig. 6a) and of water emulsion (Fig. 6b) in a confusor-shaped gap of the hydrostatic bearing for various minimal gap heights. The overpressure peaks occurring in the gap are the greater, the smaller the gap is.

Fig. 7 presents circumferential pressure of water (Fig. 7a) and water emulsion (Fig. 7b) in a front gap of the hydrostatic thrust bearing depending on the angle ε of the upper wall inclination. The pressure drops in the gap with increase in the angle ε.

Fig. 8 presents circumferential pressure of water (Fig. 8a) in a front gap of the hydrostatic thrust bearing and of water emulsion (Fig. 8b) depending on the angular velocity of the bearing upper wall. Here the pressure increases with increase in the angular velocity of the upper wall.

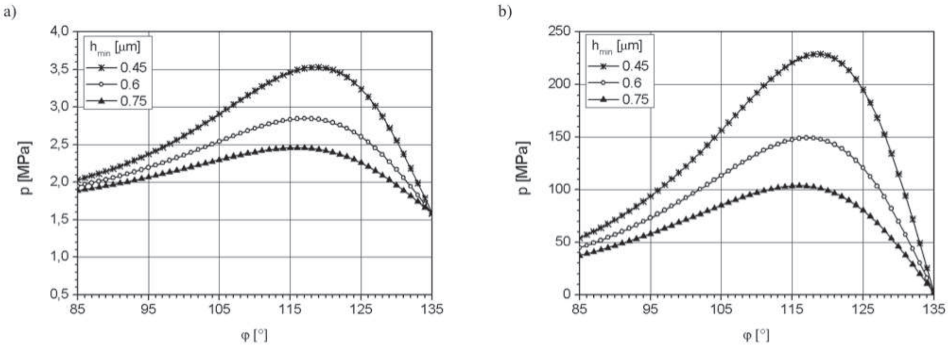

Fig. 6. Circumferential pressure distributions at the radius r = 0.011 m in a front gap for various values of the smallest gap height h_{min} for a) water, b) water emulsion

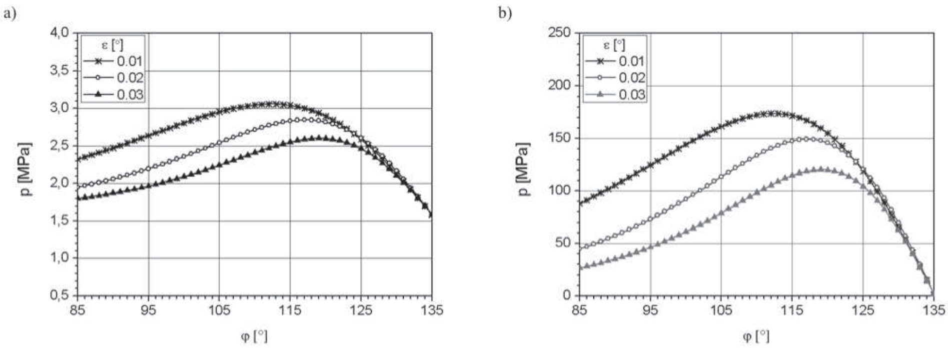

Fig. 7. Circumferential pressure distributions at the radius r = 0.011 m in a front gap for various values of the upper wall inclination angle ε for a) water, b) water emulsion

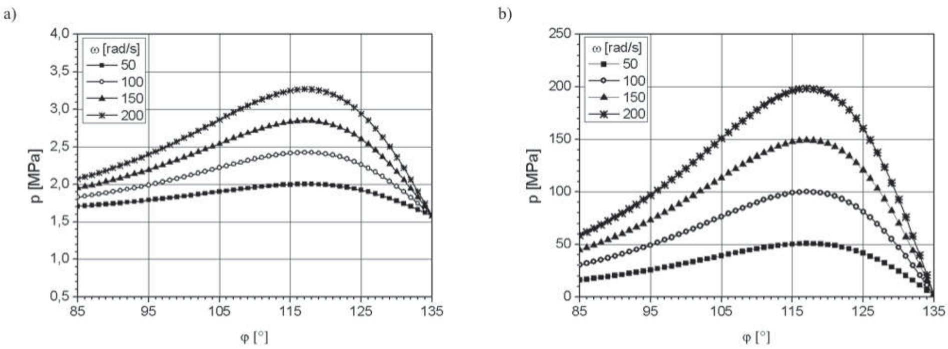

Fig. 8. Circumferential pressure distributions at the radius r = 0.011 m in a front gap for various values of the angular velocity ω of the upper wall for a) water, b) water emulsion

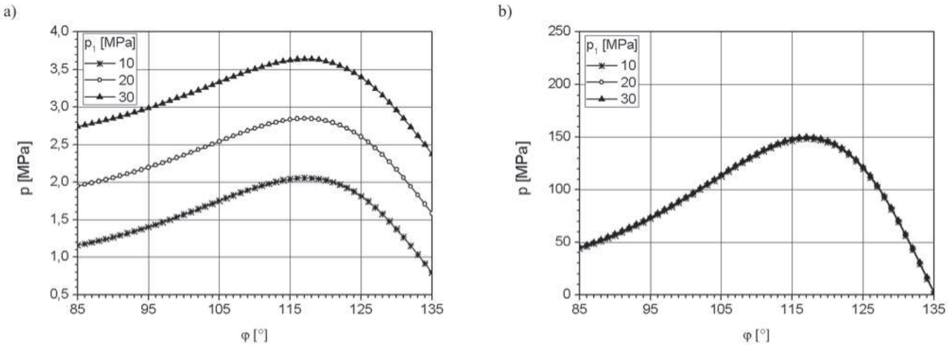

Fig. 9. Circumferential pressure distributions at the radius r = 0.011 m in a front gap for various values of the feeding pressure p_1 of the hydrostatic bearing for a) water, b) water emulsion

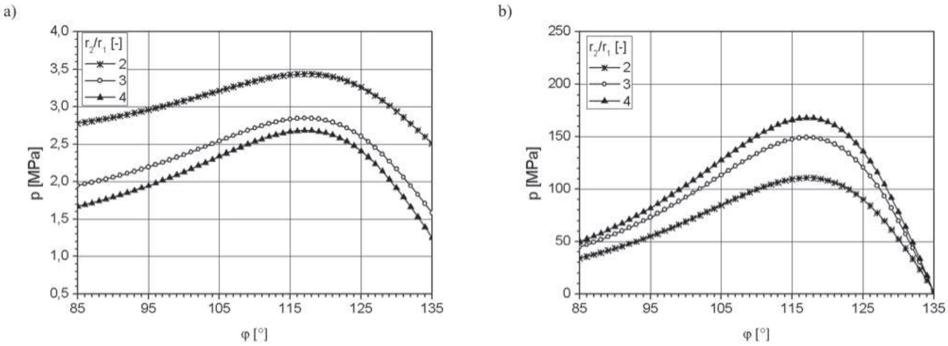

Fig. 10. Circumferential pressure distributions at the radius r = 0.011 m in a front gap for various dimensions of the hydrostatic bearing for: a) water, b) water emulsion

In the case of hydrostatic bearing with water as working liquid, the circumferential pressure in a front gap is significantly affected by the feeding pressure of the bearing. As the feeding pressure grows, the circumferential pressure grows, too (Fig. 9 a). For water emulsion, however, the influence of the feeding pressure is negligible (Fig. 9 b).

The value of the circumferential pressure depends also to a large extent on the dimensions of the hydrostatic bearing. Fig. 10 presents the circumferential pressure of water (Fig. 10a) and of water emulsion (Fig. 10b) in a front gap depending on the ratio of the external radius to the internal radius of the bearing. More specifically, in this study the external radius r_2 was assumed to be constant and only the internal radius r_1 varied to alter the size of the feeding chamber. For water, as the radius of the feeding chamber increases (so that the ratio r_2/r_1 decreases), the pressure grows in the gap. For water emulsion the opposite occurs: the greater the ratio r_2/r_1, the greater the value of the pressure in the gap.

CONCLUSIONS

The analyses presented above lead to the following conclusions:

1. The computational model adopted in the study is suitable for determining liquid pressure distribution in a front gap of a hydrostatic bearing with a rotating upper wall.
2. In the confusor zone near the smallest-height point the circumferential pressure increases. Its value depends on the dimensions and exploitation parameters of the bearing.
3. The pressure is higher for water emulsion than for water due to higher viscosity of the former.
4. In the confusor zone of the front gap there is an additional relief of the bearing caused by pressure increase.

REFERENCES

1. **Czetwertyński E., 1958:** Hydraulika i hydromechanika. PWN, Warszawa.
2. **Exner H. i in., Kempf H. (opracowanie i redakcja), Mecner W. (tłumaczenie) 2007:** Hydraulika. Podstawy, elementy konstrukcyjne i podzespoły. Vademecum hydrauliki, Tom 1, Wydanie 3 poprawione. Bosch Rexroth Sp. z o.o., Polska.
3. **Greczanik T., Stryczek J. 2005:** The concept of the bus fluid power system of the mining machine. Polska Akademia Nauk, Teka Komisji Motoryzacji i Energetyki Rolnictwa, Tom V, 72-79, Lublin.
4. **Hama T., Kurisu K., Matsushima K., Fujimoto H., Takuda H. 2009:** Outflow Characteristics of a Pressure Medium during Sheet Hydroforming, ISIJ International, Vol. 49, Nr. 2, 239-246.

5. **Ivantysyn J., Ivantysynova M. 2001:** Hydrostatic Pumps and Motors. Academia Books International, New Delhi.
6. **Ivantysynova M. 2008:** Innovations in pump design – What are future directions? Symposium on Fluid Power, JFPS, 59-64, Toyama.
7. **Klarecki K. 2012:** Eksploatacja układów hydraulicznych – oleje hydrauliczne. Utrzymanie Ruchu, Wydawnictwo Elamed, Nr 3, 6-8, Katowice.
8. **Kondakow L. A. 1975:** Uszczelnienia układów hydraulicznych. WNT, Warszawa.
9. **Kunze T., Brunner H. 1996:** Vibroakustische und optische Untersuchung der Kavitation bei Axialkolbenmaschinen. Ölhydraulik und Pneumatik, Nr 8, 542-546.
10. **Lasaar R. 2000:** The Influence of the Microscopic and Macroscopic Gap Geometry on the Energy Dissipation in the Lubricating Gaps of Displacement Machines. Proc. Of 1-st FPNI-PhD Symposium, Hamburg.
11. **Lim G.H., Chua P.S.K, He Y.B. 2003:** Modern water hydraulics – the new energy-transmission technology in fluid power. Applied Energy, Vol. 76, 239-246.
12. **Majdič F., Pezdirnik J., Kalin M. 2011:** Experimental validation of the lifetime performance of a proportional 4/3 hydraulic valve operating in water. Tribology International, Vol. 44, 2013-2021.
13. **Nikitin G.A. 1982:** Szczielewyje i łabiryntnyje uplotnienia gidroagregatow. Maszinostrojenie, Moskwa.
14. **Osiecki A. 2004:** Hydrostatyczny napęd maszyn. WNT, Warszawa.
15. **Osipow A. F. 1966:** Objemnyje gidrowliczieskie masziny. Maszinostrojenie, Moskwa.
16. **Osman T.A., Dorid M., Safar Z.S., Mokhtar M.O.A. 1996:** Experimental assessment of hydrostatic thrust bearing performance. Tribology International, Vol. 29, Nr 3, 233-239.
17. **Rokala M., Calonius O., Koskinen Kari T., Pietola M. 2008:** Study of lubrication conditions in slipper-swashplate contact in water hydraulic axial piston pump test rig. Proceedings of the 7th JFPS International Symposium on Fluid Power, TOYAMA 2008, 91-94.
18. **Ryzhakov A., Nikolenko I., Dreszer K. 2009:** Selection of discretely adjustable pump parameters for hydraulic drives of mobile equipment. Polska Akademia Nauk, Teka Komisji Motoryzacji i Energetyki Rolnictwa, Tom IX, 267-276, Lublin.
19. **Sasaki T., Mori H., Hirai A. 1959:** Theoretical Study of Hydrostatic Thrust Bearings. Bulletin of JSME, Vol. 2, Nr 5, 75-79.
20. **Sharma Satish C., Jain S.C., Bharuka D.K. 2002:** Influence of recess shape on the performance of a capillary compensated circular thrust pad hydrostatic bearing. Tribology International, Vol. 35, 347-356.
21. **Slanina F., Spałek J. 2007:** Analiza wpływu rodzaju cieczy roboczej pracującej w układzie hydraulicznycm na temperaturę i straty mocy. Szybkobieżne Pojazdy Gąsiennicowe Vol. 22, Nr 1, 99-104
22. **Stryczek S. 1984:** Napęd hydrostatyczny. Elementy i układy. WNT, Warszawa.
23. **Watton J. 2009:** Fundamentals of Fluid Power Control. Cambridge University Press, New York.
24. **Zloto T. 2009:** Modelling the pressure distribution in oil film in the variable height gap between the valve plate and cylinder block in the Arial piston pump. Polska Akademia Nauk, Teka Komisji Motoryzacji i Energetyki Rolnictwa, Vol. V, Nr 11, 418-430, Lublin.
25. **Zloto T., Kowalski K. 2012:** Pressure distributions in oil film in the front gap of a hydrostatic thrust bearing. Polish Academy of Sciences Branch in Lublin. Teka Commission of Motorization and Energetics in Agriculture, Vol. 12, Nr 2, 257-261, Lublin.
26. **Zloto T., Kowalski K. 2013:** Oil leaks intensity in variable-height gaps. Polish Academy of Sciences Branch in Lublin. Teka Commission of Motorization and Energetics in Agriculture, Vol. 13, Nr 2, 113-118, Lublin.
27. www.tiefenbach-waterhydraulics.com/waterhydraulics/historyofwaterhydraulics.html [dostęp: 22.07.2014]

ANALIZA ROZKŁADÓW CIŚNIENIA WODY I EMULSJI WODNEJ W SZCZELINIE CZOŁOWEJ ŁOŻYSKA HYDROSTATYCZNEGO

Streszczenie. W opracowaniu przedstawiono rozkłady ciśnienia wody i wybranej emulsji wodnej w szczelinie klinowej łożyska hydrostatycznego wzdłużnego z wirującą górną ścianką. W oparciu o równania Naviera-Stokesa i równanie ciągłości, określono zależność na wartości ciśnienia występującego w szczelinie. W pracy analizowano wpływ parametrów geometryczno-eksploatacyjnych łożyska hydrostatycznego wzdłużnego na rozkłady ciśnienia obwodowego w otoczeniu najmniejszej wysokości szczeliny.

Słowa kluczowe: rozkłady ciśnienia, szczelina klinowa, łożysko hydrostatyczne wzdłużne, woda, emulsja wodna.

Exploitation and Repair of Hydraulic Cylinders Used in Mobile Machinery

Konrad Kowalski, Tadeusz Zloto

Institute of Mechanical Technologies, Czestochowa University of Technology
Al. Armii Krajowej 21, 42-201 Czestochowa, konrad@itm.pcz.czest.pl, zlotot@o2.pl

Received December 05.2014; accepted December 18.2014

Summary. Hydraulic cylinders are commonly applied in mobile machinery. They are prone to mechanical damage and wear due to atmospheric conditions. The paper presents selected issues related to the exploitation and repair of hydraulic cylinders. On the basis of practical experience, it offers an algorithm of actions to be undertaken in case of damage of a hydraulic cylinder.
Key words: hydraulic cylinder, exploitation, repair, seals, mobile hydraulics machinery.

INTRODUCTION

Reliable and flawless operation of machines and devices depends on many factors, such as their technological advancement, conditions and type of operation, age, as well as frequency of overhauls and maintenance [9]. A number of hydraulic systems include hydraulic cylinders, whose function is to transform the energy of pressure into mechanical energy. A typical hydraulic cylinder performs a back-and-forth linear movement of a limited stroke [3, 7]. Hydraulic cylinders have numerous applications in industry [11, 12] and in mobile machines [2, 10], such as excavators, loaders, backhoe loaders, dump cars, extension arms, cranes, tractors, refuse collection trucks, harvesters, and others (Fig. 1). Hydraulic cylinders are, however, prone to breakdowns [4], especially those used in harsh and changeable working conditions.

OBJECTIVES OF THE STUDY

The aim of this paper is to offer some practical remarks concerning the exploitation of hydraulic cylinders with pistons and to present an algorithm of actions related to the repair of hydraulic cylinders used in mobile machinery.

TYPES AND CAUSES OF BREAKDOWNS OF HYDRAULIC CYLINDERS

One of the most frequently encountered problems in the exploitation of hydraulic cylinders is the loss of tightness, causing leaks outside and inside the cylinder [3]. The worn or damaged seals do not protect the interior of the cylinder from being contaminated by dirt, which increases the risk of a breakdown. It is thus of crucial importance to use appropriate wiper seals, with a wiper ring being in direct contact with the piston rod in order to collect all dirt accumulating on it as well as to collect dirt from the air. Because of that, it is necessary to take into account the required contact between the wiper seal and the piston rod. In order to ensure that the cylinder is leakage-tight inside, it is necessary to apply appropriate piston and piston rod seals, depending on the cylinder type (unidirectional or bidirectional).

Hydraulic cylinders are operated in various external conditions. The part which is especially prone to breakdowns is the piston rod, which is directly exposed to atmospheric factors, such as water, snow, changing temperature and to dirt, particles and soot [15] as well as to mechanical factors. When a long break in the cylinder operation is planned, the piston rod should be protected from the above mentioned factors [11]. Additionally, it has to be kept in mind that hydraulic cylinders are not suitable for transferring lateral loads [1, 11].

Hydraulic cylinders available on the market have their strength parameters calculated with a certain safety margin. In some cases, however, it is advisable to check the piston rod against buckling, especially in the case of hydraulic cylinders with long strokes. The critical load level above which the piston rod undergoes buckling is obtained from Euler's formula [7]:

Fig. 1. Hydraulic cylinders in mobile machinery

$$F_{kr} = \frac{\pi^2 EJ}{l_s^2}\ , \tag{1}$$

where:

E – Young module of the piston rod material (for steel $E=2.1 \cdot 10^5$ N/mm²),

J – moment of inertia for the piston rod cross-section,

l_s – free buckling length.

Assuming the safety coefficient as n=3.5 [8], the maximal force F that can be transferred by the piston rod is:

$$F = \frac{F_{kr}}{n}\ . \tag{2}$$

Typical breakdowns of hydraulic cylinders are presented in Fig. 2.

Damaged parts of hydraulic cylinders are those that have cracks, cavities, deformations, seizures, and may be corroded to various extent.

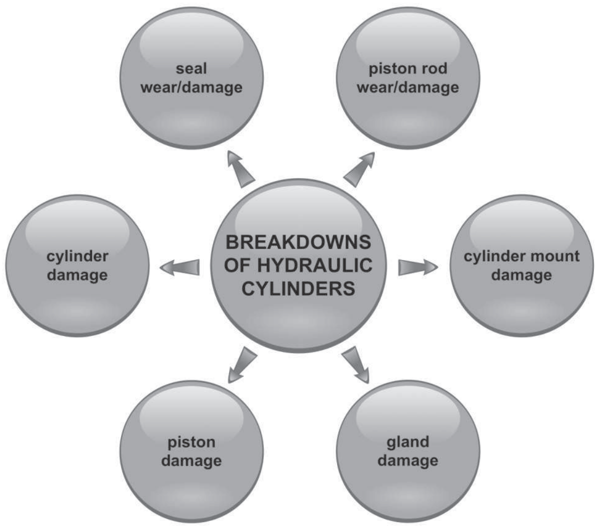

Fig. 2. Possible types of breakdowns of hydraulic cylinders

SEALS IN HYDRAULIC CYLINDERS

A number of types of seals are applied in hydraulic cylinders. They include wiper seals, piston seals, piston rod seals, gland seals and static seals. Examples of typical seals in hydraulic cylinders are presented in Fig. 3.

The main purpose of using seals is to ensure leak tightness inside the cylinder and to protect it from external dirt (wipers). Besides, selecting the shape, material, and tightness of seals affects the magnitude of friction loss between the piston and the cylinder barrel and between the piston rod and the gland. If the seals are inappropriately chosen or mounted, the energy loss can be significant (up to 25%) [7]. When the loss is kept at the minimum level, the total efficiency of a hydraulic cylinder can be at the level of 78÷99% [7].

The most popular static seals are O-rings, with V-rings and X-rings following closely. Among dynamic seals (for pistons and piston rods), the most popular are pack seals (chevron rings, including highly wear-resistant rubber-fabric seals), seals with anti-extrusion rings as well as seals with wear rings and support rings.

When selecting the right seals, one has to take into account the kind of working liquid (mineral oil, non-flammable liquids) so that it is neutral towards the seal material. Besides, the seal has to be suitable for the operating pressure and temperature [12].

Seals come in different cross-section and can be made of different materials [5, 12, 13, 14, 15], such as polyurethane (TPU, H-PU, G-PU, S-PU), fluorine rubber (FPM), silicone MVQ (methyl vinyl silicone rubber) and ethylene propylene diene rubber (EPDM). Most often, however, the material is nitrile rubber – NBR (acrylonitrile- butadiene rubber). Besides, seals can contain components made of other materials to enhance their performance and applicability conditions (e.g. POM, PE-UHMW, PTFE+40% bronze).

Apart from that, wear bands are used in hydraulic cylinders to keep the piston and piston rod precisely along the cylinder axis and to prevent contact between the metallic surfaces of the piston and cylinder [3, 13, 14]. Wear bands are made of polyoxymethylene plastomeres (POM), characterized by very low grinding ability and self-lubrication [14].

REPAIR AND RENOVATION OF HYDRAULIC CYLINDERS

Fig. 4 presents a block diagram of repairs of hydraulic cylinders. The user of the cylinder, referred to as “customer”, notices a breakdown and commissions the repair to a specialised service. The servicing company accepts the commission and undertakes repair as agreed with the customer. After the hydraulic cylinder is transported to the service, it is registered and prepared for repair. At this stage the customer should be notified about the predicted duration of repair.

MEASUREMENTS AND DIAGNOSIS OF THE TECHNICAL CONDITION

When the hydraulic cylinder is disassembled, its parts and seals have to be diagnosed. It is recommended that all measurements and tests should be performed twice, by two different service workers. On the basis of the test results, the technical condition of the hydraulic cylinder can be assessed on the basis of the following criteria:

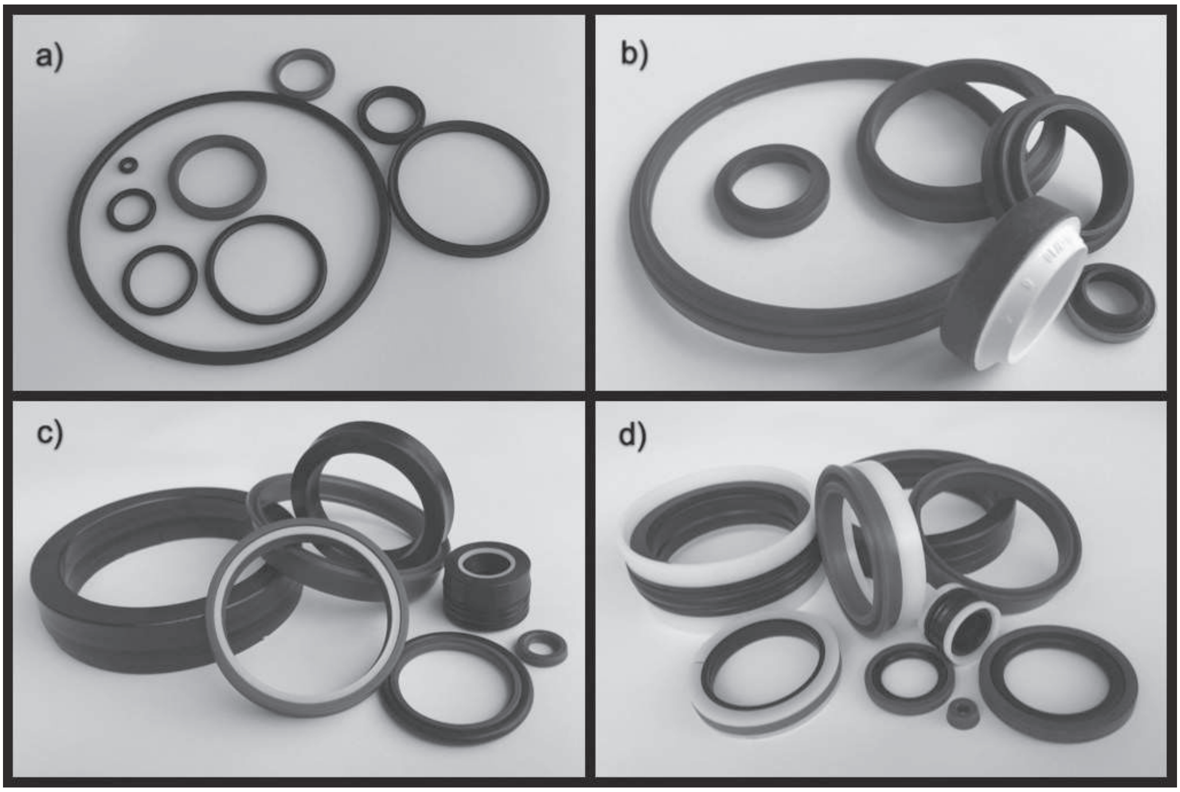

Fig. 3. Seals applied in hydraulic cylinders a) static seals, b) wiper seals, c) piston rod seals, d) piston seals

– Whether it is feasible to repair the hydraulic cylinder depends on economic and technological considerations.
– Components made of cast iron or steel casting may have cracks, which makes them unsuitable for repair [6].
– Hydraulic cylinders displaying high degree of wear or damage, with such symptoms as seizing, deep corrosion, deep cracks, deformations, cavities, etc. are considered not suitable for repair. An exception can be made for untypical designs, in which case the repair cost will be lower than the cost of producing a replacement cylinder. For instance, in the case of cast hydraulic cylinders with extensive damages, a solution preferred to producing a new cylinder on economic and technological grounds will be bushing [6].
– Repair is the optimum solution for hydraulic cylinders with low degree of damage (scratches, small traces of corrosion).
– Highly damaged piston rods are typically replaced by new ones.
– The final decision on whether a hydraulic cylinder is suitable for repair or not is taken by qualified personnel on the basis of technical and economic considerations.

If a customer requests to be consulted after the hydraulic cylinder is diagnosed, they should be informed about the technical condition and recommendations concerning the repair. With the customer's acceptance, the servicing company can undertake work.

REPAIR OF A HYDRAULIC CYLINDER

The first step is to remove dirt from all surfaces. The hydraulic cylinder is rinsed with a cleaning agent at a special stand, with a container to collect the used agent. The cleaning agent is petroleum ether, which is sprayed with an airbrush. Then, the hydraulic cylinder is wiped with a soft, white cotton cloth. It is essential that the cloth must not leave any fibres on the cylinder. After that, the parts should be moved to the place allocated for the repair. Then, depending on the diagnosis, the piston and/or piston rod can undergo grinding, chromium plating, and polishing. Similarly, the cylinder surface can be subject to chromium plating and honing. The next stage is making grooves for wear bands and processing the collar, if necessary. After that, appropriate seals and wear bands have to be selected.

ASSEMBLY

After the repair is complete, and the seals and wear bands are chosen, the hydraulic cylinder is to be reassembled from its parts. It is essential that no dirt or other contaminants get into the cylinder. The piston, piston rod, and cylinder have to be lubricated with a thin film of hydraulic oil. Seals are mounted by means of special pliers (Fig. 5) with smooth surfaces. Still, special care has to be taken not to damage the seals or scratch the sealed surfaces. A layer of metal-bond-

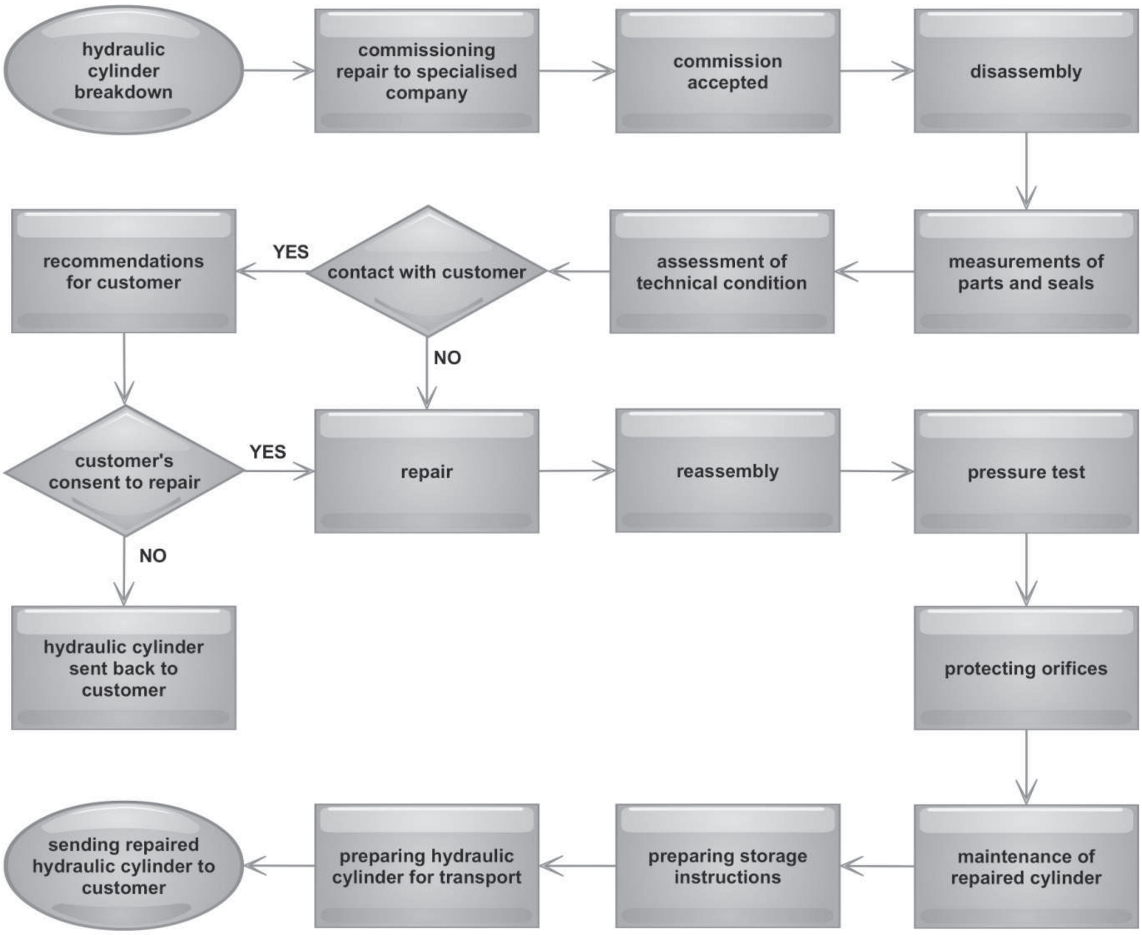

Fig. 4. Algorithm for repair of a hydraulic cylinder by a specialised company

ing glue (e.g. Loctite 243) is then applied on the piston rod-piston screw joint. Depending on the construction, a layer of retainer (e.g.Loctite 638) should be applied on co-axial joints. The piton has to be screwed on the piston rod and the joint is to be protected with a lock-nut. Then, the piston-piton rod couple is inserted in the cylinder. After the assembly, a pressure test should be performed with great care. Optionally, the external surface can be coated with paint to improve its appearance.

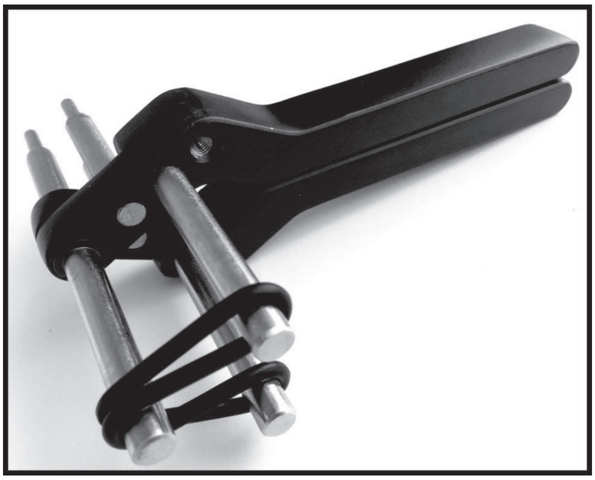

Fig. 5. Pliers for mounting seals

TRANSPORTING THE REPAIRED CYLINDER

If the hydraulic cylinder passes the pressure test, the orifices have to be protected by plugs and the hydraulic cylinder can be prepared for transport. It is necessary to provide a packaging that protects it from damage during transport. Together with a repaired hydraulic cylinder, the customer should also be provided with instructions for storing the hydraulic cylinder.

When the customer does not intend to use the repaired hydraulic cylinder within a short period of time, it is advisable to protect it from corrosion by filling it with hydraulic oil and by covering the piston rod with a thick grease.

CONCLUSIONS

The algorithms of actions to be undertaken in case of hydraulic cylinder breakdowns and repairs is universal and can be applied for any hydraulic cylinder, including those applied in industry (e.g. in hydraulic presses).

If the operating temperature of the hydraulic cylinder is high, the effect of temperature on the working liquid and on other parts, especially rubber seals, has to be taken into account.

The parts that are worn or damaged should be repaired, if possible. If not, such parts must be replaced by new ones.

Whenever a hydraulic cylinder undergoes repair, all seals must be replaced by new ones.

Rubber seals mounted in a hydraulic cylinder can work for years, whereas seals stored in inventories have to be used within a limited period of time, typically up to two years. otherwise rubber hardens and loses its sealing properties.

With appropriate machines and practical experience at one's disposal, it is possible to repair hydraulic cylinders without hiring a professional help. This is feasible, however, when the repair involves a minor issue, such as replacing seals. In the case of major overhauls and repairs, it is much more advisable to hire a specialised company.

REFERENCES

1. **Cundiff J.S. 2002:** Fluid Power Circuits and Controls. Fundamentals and Applications. CRC Press, Boca Raton.
2. **Greczanik** T., **Stryczek** J. **2005:** The concept of the bus fluid power system of the mining machine. Polska Akademia Nauk, Teka Komisji Motoryzacji i Energetyki Rolnictwa; V, 7279, Lublin.
3. **Kotnis G. 2008:** Budowa i eksploatacja układów hydraulicznych w maszynach. Wydawnictwo KaBe, Krosno.
4. **Król R, Zimroz R, Stolarczyk Ł. 2009:** Analiza awaryjności układów hydraulicznych samojezdnych maszyn roboczych stosowanych w KGHM Polska Miedź S.A.. Prace Naukowe Instytutu Górnictwa Politechniki Wrocławskiej. Studia i materiały; 128(36): 127139.
5. **Lipski J. 1981:** Napędy i sterowania hydrauliczne. Wydawnictwa Komunikacji i Łączności, Warszawa.
6. **Okularczyk W. 2009:** Regeneracja siłowników pneumatycznych. Hydraulika i Pneumatyka; 6: 2325.
7. **Osiecki A. 2004:** Hydrostatyczny napęd maszyn. Wydawnictwa Naukowo-Techniczne, Warszawa.
8. **Rabie M.G. 2009:** Fluid Power Engineering. McGraw--Hill, New York.
9. **Rusin A., Wojaczek A. 2007:** Selection of Maintenance Range for Power Machines and Equipment in Consideration of Risk. Eksploatacja i Niezawodnosc – Maintenance and Reliability; 3(35): 4043.
10. **Ryzhakov** A., **Nikolenko I., Dreszer K. 2009:** Selection of discretely adjustable pump parameters for hydraulic drives of mobile equipment. Polska Akademia Nauk, Teka Komisji Motoryzacji i Energetyki Rolnictwa, Tom IX, 267276, Lublin.
11. **Żabicki D. 2012:** Dobór i eksploatacja siłowników hydraulicznych. Utrzymanie ruchu; 3: 3032.
12. **Żabicki D. 2014:** Uszczelnienia. Inżynieria i Utrzymanie Ruchu Zakładów Przemysłowych; http://www.utrzymanieruchu.pl/menu-gorne/artykul/article/uszczelnienia/ [access: 28.08.2014]
13. http://www.hennlich.pl/uploads/Katalog_Uszczelnienia_2014.pdf [access: 28.08.2014]
14. http://www.hydro.com.pl/res/doc/56_537479b579778_Katalog_uszczelnie___-_2013.pdf [access: 28.08.2014]
15. http://www.skf.com/binary/21-161853/12393_2-EN---Hydraulic-seals.pdf [access: 28.08.2014]

EKSPLOATACJA I REGENERACJA SIŁOWNIKÓW HYDRAULICZNYCH W MOBILNYCH MASZYNACH ROBOCZYCH

Streszczenie. Siłowniki hydrauliczne są powszechnie stosowane w maszynach hydrauliki mobilnej. Ze względu na pracę w zmiennych warunkach, narażone są one na uszkodzenia mechaniczne oraz działanie czynników atmosferycznych. W pracy przedstawiono aspekty związane z ich użytkowaniem oraz regeneracją. W oparciu o praktyczne doświadczenia przedstawiono algorytm postępowania z uszkodzonymi siłownikami hydraulicznymi.

Słowa kluczowe: siłownik hydrauliczny, eksploatacja, regeneracja, uszczelnienia, hydraulika mobilna, maszyna robocza.

TEKA. COMMISSION OF MOTORIZATION AND ENERGETICS IN AGRICULTURE – 2014, Vol. 14, No. 4, 59–64

Application of the Computation Procedure in Bayesian Network in Estimation of Total Cost of Natural Stone Elements Production

Andrzej Kusz, Jacek Skwarcz, Mateusz Gryczan

Department of Technology Fundamentals, University of Life Sciences,
ul. Doświadczalna 50A, 20-280 Lublin, Poland, e-mail: andrzej.kusz@up.lublin.pl

Received December 01.2014; accepted December 17.2014

Summary. In the course of data collection and processing, an essential role is played by computation processes which can be performed automatically. Moreover, these processes should naturally allow for uncertainties. The article presents such a process realized with the aid of Bayes network technique. The model enables the user to monitor the total production cost of elements which are made of natural granite stone. Inference mechanisms built into the system make it possible to retrieve the information necessary for a rational production management. The basis for estimation is an approach based on a probability distribution defined over a set of values of decision variables representing parameters of the production process. It has been shown how to carry out a simulation research in a range of situations where inference mechanisms are applied.

Key words: production process, natural stone, granite, computation processes, production costs, Bayesian networks.

INTRODUCTION

Granite machining process consists of many operations affecting the overall course of the process as well as the final effect. Each operation is an integral part of the entire process, having an impact on the other stages of the process, or it is determined by them. It is not possible to determine causal links without the knowledge of proper complete course of the process [12]. Structural non-homogeneity, high variability of process parameters burdened with randomness, justify treating the process components as random variables and a probabilistic model as a natural way of representing them.

The necessity of taking uncertainty present in the process into consideration, makes Bayesian network a useful system of knowledge representation, when it is needed to clearly encode an uncertainty factor and understanding issue in terms of nondeterministic cause-effect relations. These network capabilities can be employed in creating production process predictability.

The possibility of automation of data collection process, as well as of data processing, is an essential aspect [5, 6, 9] whereas the computation processes are performed automatically basing on advanced cognitive modelling systems. The process stages and the states of objects used in specific processes are known within the accuracy of probability distribution. Cognitive modelling can be based on Bayesian network technique.

An important computation process in technical systems engineering, which needs to be embedded in the system, is the possibility of monitoring production costs. It is a multidimensional process, which refers to entire systems, their components (subsystems), and finally, specific groups and machine types. Production cost optimization forms the groundwork for effective technical systems utilization. Entire production cost estimation, based on the information obtained from database, allows comparing the technology of a particular production process to other production technologies. Computational procedures are based on a deterministic approach including financial ratio methods.

An alternative approach is the approach based on Bayesian network. Such an approach is justified by the uncertainty factor which is integrally related to production process. The essence of the offered approach is that each cost component and the factors which determine its size are represented by random variables.

Bayesian network has many applications where it is needed to explicitly encode uncertainty coefficient and reasoning in terms of nondeterministic causal link relations [13, 14, 23, 24]. They are therefore a useful tool to model uncertainties in production processes [17, 18, 19, 20], predictability of technical objects behavior [2, 3], computer-aided decision making processes [14, 20], and to express reliability knowledge both in terms of practical approach [4, 8, 15] as well as for theoretical analyses purposes [1, 25].

Another field of application of the Bayesian network is the problem of complex flowchart management [16, 22].

The aim of this study is to present a conceptualization method of computation process realizing a problem in Bayesian network language, by illustrating it with an example of estimation of the total cost of natural stone (granite) elements machining process. An assumption has been made during designing the model, according to which the process components are represented as random variables. Bayesialab program was used in building the model. This environment has built-in inference mechanisms allowing the model to operate as a prognostic and explanatory system.

MODEL CONCEPTION AND STRUCTURE

Natural stone machining process modelling is based on the analysis of the granite features which are important in terms of modelling, and the machining process elements which influence different costs, as well as operating-supervising time. Factors which influence the cost and operating-supervising time have been presented as variables and their values implemented in Bayesialab environment [10]. The variables are represented by nodes and their labels correspond to the process component represented by a specific node. It has been assumed that variables values can be continuous within a given range or they can be of a discrete type. Cause-effect relations are represented by arcs. They reflect relations which take place in the modelled process. Subsequently, a priori probability distributions have been assigned over the range of variable values, defining distribution type and its values.

Nodes can be divided into certain groups representing different aspects of the modelled process. All model elements have values and probability distributions assigned to them and basing on those, values of other variables are determined by arithmetic operations or logical operators.

A layer describing the features of the workpiece is distinguished in the network. Variables representing density, thickness and length of machined material (granite), as well as machining quality belong to this layer. The machined material density is an essential variable in natural stone machining process. It depends on the percentage of each mineral which the natural stone is composed of. The main minerals which granite consists of are: orthoclase, plagioclase, quartz, biotite and a whole series of other minerals in trace amounts. Granite density has an impact on unitary cutting tool consumption cost and feed rate. In the model, density is represented by a discrete random variable, which can have three values: low, average and high. Low density is within the interval from 2400 kg/m^3 up to max. 2600 kg/m^3, e.g. Kashmir White granite, whose density is 2470 kg/m^3. The average density begins from above 2600 kg/m^3 up to 2800 kg/m^3. This interval contains most granite, including: Impala 2710kg/m^3, Strzegom 2630kg/m^3, Vanga 2635kg/m^3. The high density category ranges from 2800 kg/m^3 up to 3000kg/m^3. This density group consists of the following granites: Azul Platino 2820 kg/m^3, New Impal Red 2820 kg/m^3, Star Galaxy 2830 kg/m^3. These intervals include almost all granite densities.

Thickness of the machined granite workpiece is another continuous variable which was considered in the model. The workpiece thickness is based on a client's own taste, as well as on assembly and design capabilities. It was assumed that this variable ranges from 50 mm to 100 mm.

The variable length of the workpiece represents the sum of its side lengths. This variable is used to estimate the cycle time of machining the workpiece surface. It is a continuous variable and it can have values from 500 mm to 620 mm.

The quality of the machining process is a variable which represents a client's expectations concerning the final product quality. Machining parametres and required number of cycles are determined by defining a quality class. It is assumed in the model, that the variable representing quality is a discrete variable and it can take three different values: high, average and economic. The cutting disc feed rate is chosen according to the required quality. Slow cutting disc feed decreases labour consumption during the process of polishing.

The workpiece surface is a continuous-type variable and its values are found as the product of length and thickness variables. This variable can take values from the interval from 0,2 m^2 (minimal value) to 0,62 m^2 (maximal value). The value of this variable impacts on intensity of cutting tool consumption. The machined surface, after polishing, must undergo preservation and gloss finish treatment.

Feed rate is determined by the quality required, as well as by density of the workpiece. Its precise value is found using a logical formula. It was assumed that the values of the variable have normal distributions, an expected value of distribution corresponds to a particular rate and standard deviation is 0,001. Feed rate is a variable which determines cycle time.

Another process parameter is the number of cycles. It depends on the declared quality and it is 26 cycles for economic quality, 27 for average quality and 28 in case of high quality.

Water consumption in machining process is evaluated in the model as the product of unitary water consumption per minute related to the machining time. It was assumed that the variable of unitary water consumption per minute is a continuous variable and it ranges from 10-12 l/min.

Other variables enable estimation of operation time and their costs. They are continuous variables which represent: unitary machining cycle time, workpiece machining time, cutting tool exchange time and worker's work time. Unitary machining cycle time equals a complete cycle time of polishing machine operation. A workpiece machining time is estimated on the basis of information represented by nodes: workpiece length, cutting disc feed rate. In this manner, we obtain probability distributions over a set of estimated possible machining time values. Extending machining time has a significant impact on the final cost, since workload, water and electricity consumption increase.

Cutting tool exchange time is a variable whose values depend on the worker's experience, abilities, manual and motor coordination skills. In the model, this time is represented by a continuous variable of 20-25 min. A worker's worktime is a variable evaluated by the sum of a workpiece machining time and the time required for cutting tools exchange. This variable can range from 35 to 345 minutes.

The last group of variables considered in the model, are the variables which represent costs. Costs represent quantitative expenditure corresponding to the realization of a specific version of stone machining process. They include: unitary cutting tool consumption cost, preservation and gloss finish cost, as well as evaluated consumption costs of cutting tools, finishing elements, water, energy, utilities and labour. The range of each variable was either assigned or evaluated, according to possible versions of the process and current prices.

The final variable in the model is a continuous variable representing the total cost of machining a single workpiece. The total cost is evaluated as the sum of values of three nodes: finishing elements cost, utilities cost and labour cost. The node shows probability distribution over a set of cost values which can be reached during the machining process of natural stone.

A graphical form of the conceptualization presented above, and at the same time, the structure of a network allowing for the estimation of a single workpiece machining cost in Bayesian network technique, has been shown in the Fig. 1. The variables used in computations, representing machined pieces features, machining parameters, times and all constituent costs are represented by equally named variables in the network. Probability distributions over sets of the variables considered in the model are illustrated in a graphical form in the Fig. 2.

ESTIMATION OF TOTAL GRANITE ELEMENTS PRODUCTION COST

For the purpose of verification of the model, a computation concerning machining process of natural granite stone elements has been carried out. Inference mechanisms, typical in Bayesian networks, were applied in the verification.

The standard mechanism of the network working (prediction of the consequences of decisions) provides the process total cost according to the workpiece features, quality requirements and operator's competence.

In the analyzed problem, it has been assumed that the variables: the workpiece length –of 0.536*10 m, machining quality – average, cutting tool exchange time of 20.5 min, wage rate according to category equals 0.225 zł. per minute, the number of cycles is 27, and unitary water consumption has been fixed at 10.75 litres per min. The total cost has been evaluated for the workpiece thickness of 0.065m and various density values: low (A), average (B), high (C). Computation results as probability distribution over a set of total cost values have been presented in the Fig. 3.

The above calculations were repeated, assuming the workpiece thickness to equal 0,85 m. Calculations results are presented in the Fig. 4. In the first case (thickness of 0.65 m), the lowest total cost 48,893 was obtained for the low density of the workpiece, and the highest for the high density, and amounts to 164,317 zł. It should be noted that in case of low density with probability of 0,71, a possible outcome of costs can range from 39,7 to 62.9 zł. Whereas, in case of high density, the total cost can take values from intervals: 132.6-155.8, 155.8-179.2, 179.2-202.3 zł. practically, with equal probability (0.23, 0.29, 0.21, respectively). For average workpiece density the total cost is 106,228 zł.

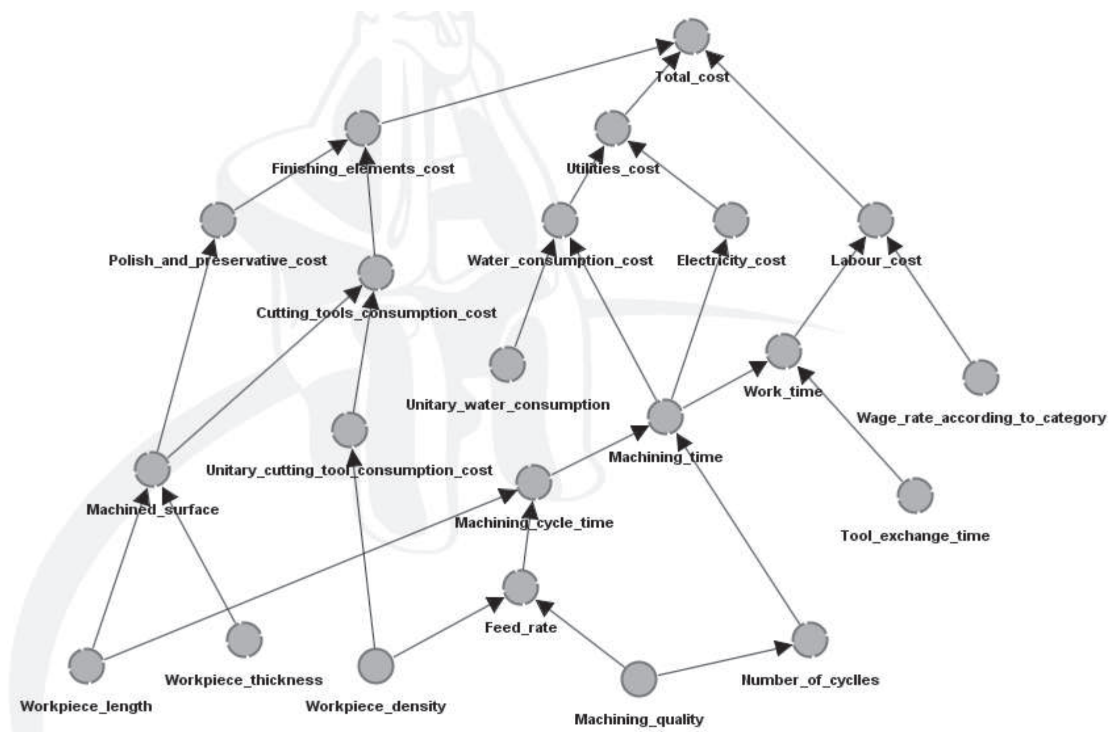

Fig. 1. Network structure used for estimation of natural stone machining process cost

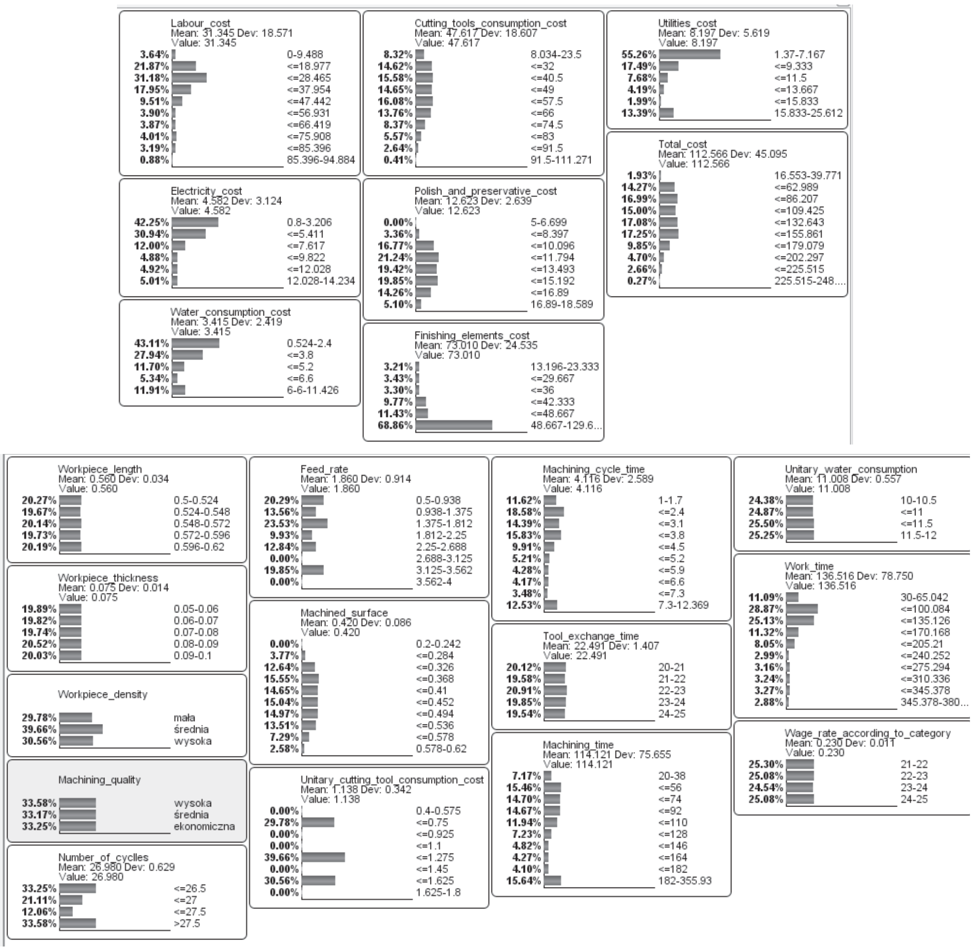

Fig. 2. Probability distributions over random variable values

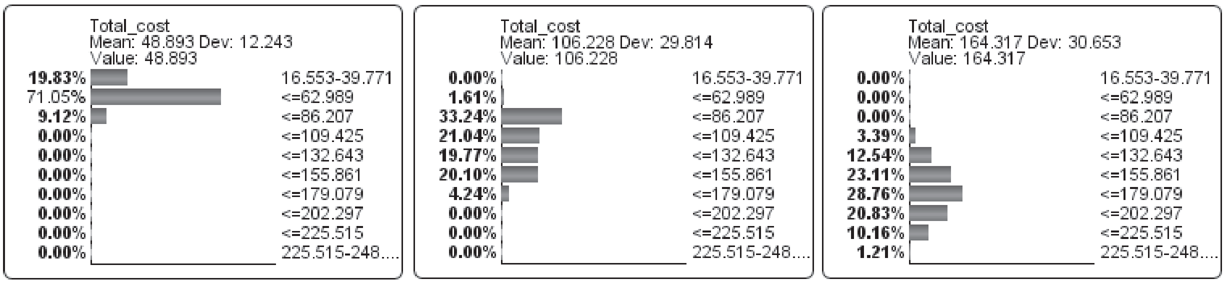

A B C

Fig. 3. Total cost (thickness 0,065) depending on the density of the machined stone

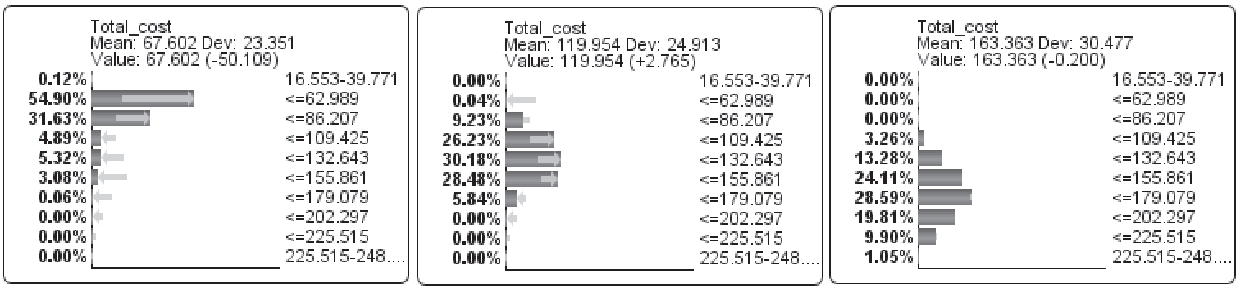

A B C

Fig. 4. Total cost (thickness 0,065) depending on the density of machined stone

For the variable ‘workpiece thickness’ at the value of 0.85, the total cost obtained was 67.602 for low density, 119.95 for the average and 163.36 for the high. In this case, the knowledge of probability distribution allows for estimating the chance of getting a desired value of the total cost.

The diagnostic inference mechanism available in the network is useful in a situation when we want to determine conditions that must be satisfied in order to achieve the assumed level of the total cost. Fig. 5 shows points which correspond to constant total costs (K_1 = 144.252 and K_2 = 74.598) depending on thickness and length of the workpiece.

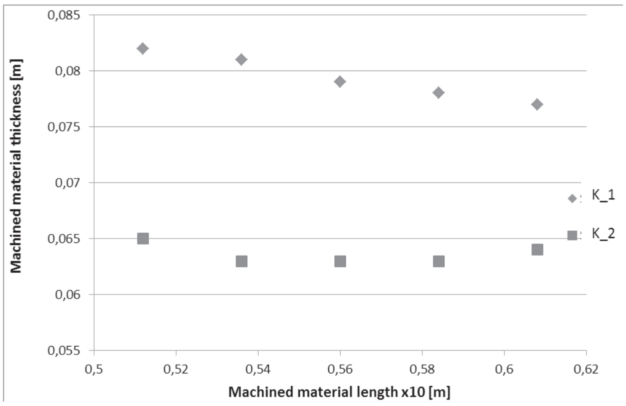

Fig. 5. Points corresponding to constant total costs of machining process depending on thickness and length of the workpiece

The working scheme of the model shown above can be applied to estimation of other cost components. Information possible to obtain by simulation experiments is of a great practical importance and can be used in the natural stone element production management.

CONCLUSIONS

The procedure of estimating the total cost of natural stone machining, which is implemented in Bayesian network, is an example of a computation process which can be entirely automated by virtue of embedded inference mechanisms. The convenience of input data which can be formed arbitrarily basing on available resources and predicted production conditions, account for its significant importance at the stage of design, planning, monitoring and analysis of production process with reference to natural stone elements in specific condition of realization.

Prognostic inference allows for analysing all possible versions depending on model input variables. A set of acceptable solutions can be determined, accurate to probability distribution. For expected values of the terminal variable (in this case, for total production cost), hypothetico-deductive inference (temporal backward projection) facilitates, with an accuracy of probability distribution, determination of requirements regarding variables representing each cost component and variables describing features of the workpiece, as well as machining process parameters.

Machine learning mechanisms which are available in the system [11] facilitate adaptability of the model, both in terms of topology (adjusting the model to object types) as well as in determination of a priori probability distributions.

REFERENCES

1. **Barlow RE.** Using influence diagrams.1988. In: Clarotti CA, Lindley DV, editors. Accelerated life testing and experts’ opinions in reliability, 145-57.
2. **Bartnik G., Kalbarczyk G. and Marciniak A. W.2011.** Application of the operational reliability model to the risk analysis in medical device production. Teka, Vol. XIC,366-370.
3. **Bartnik G., Kusz A. and Marciniak A. 2006.** Dynamiczne sieci bayesowskie w modelowaniu procesu eksploatacji obiektów technicznych. Inżynieria Wiedzy i Systemy Ekspertowe, Oficyna Wydawnicza Politechniki Wrocławskiej, t. II, 201-208.
4. **Bartnik G. and Marciniak A. W. 2011.** Operational reliability model of the production line. Teka, Vol. XIC, 361-365.
5. **Berners-Lee T., Karger D.R., Stein L.A., Swick R.R., Weitzner D.J.** Proposal: Semantic Web Development Retrieved from W3C 2000.
6. **Berners-Lee, Hendler J., Lassila O. 2001.** The Semantic Web. Scientific American.
7. **Chmielecki A. 2004.** Konceptualne podstawy kognitywistyki – krytyka i propozycje własne. Szczecin: VII Zjazd Filozoficzny.
8. **Chun Su, Ye-qun Fu. 2014.** Reliability Assessment for Wind Turbines Considering the Influence of Wind Speed Using Bayesian Network. Eksploatacja i Niezawodnosc – Maintenance and Reliability, 16 (1), 1–8.
9. **Cost S., Finin T., Joshi A. 2002**.A Case Study in the Semantic Web and DAML+OIL. IEEE Intelligent Systems.
10. Dokumentacja programu BayesiaLab. http://www.bayesia.com, 10.06.2014.
11. **Doguc O. and Ramirez-Marquez J.E. 2009.** A generic method for estimating system reliability using Bayesian networks. Reliability Engineering and System Safety, 94, 542-550.
12. **Halpern J., Y. 2005.** Reasoning about uncertainty. The MIT Press Cambridge, Massachusetts, London.
13. **Hołaj H., Kusz A., Maksym P., Marciniak A. W. 2011.** Modelowanie problemów decyzyjnych w integrowanym systemie produkcji rolniczej. Inżynieria Rolnicza, 6 (131), 53-60.
14. **Kocira S., Kuboń M. 2011.** The operating costs machines and general type of farming. Roczniki Naukowe Stowarzyszenia Ekonomistów Rolnictwa i Agrobiznesu SERiA, Tom XIII, Zeszyt 6, 103-107.
15. **Kusz A., Maksym P., Marciniak A. W. 2011.** Bayesian networks as knowledge representation system in domain of reliability engineering. Teka, Vol. XIC, 173-180.
16. **Kusz A., Maksym P., Skwarcz, J. Grudziński J. 2013.** The representation of actions in probabilistic networks. Teka, Vol. XII, 41-47.

17. **Kusz A., Marciniak A.W. 2010.** Modelowanie niezawodności złożonych systemów bioagrotechnicznych. Inżynieria Rolnicza, 5 (114), 147-154.
18. **Maksym P. 2011.** Podstawowe zasady modelowania procesu produkcji rolniczej. Inżynieria rolnicza, 1 (126), 155-162.
19. **Maksym P., Marciniak A. W., Kostecki R. 2006.** Zastosowanie sieci bayesowskich do modelowania rolniczego procesu produkcyjnego. Inżynieria Rolnicza, 12 (87), 321-330.
20. **Maksym P., Marciniak A. W., Kusz A. 2011.** Modelowanie syntezy działań ochronnych w rolniczym procesie produkcyjnym. Inżynieria Rolnicza, 4 (129), 213-220.
21. **Marciniak A. 2005.** Projektowanie systemu reprezentacji wiedzy o rolniczym procesie produkcyjnym. Rozprawy naukowe Akademii Rolniczej w Lublinie, Wydział Inżynierii Produkcji, zeszyt 298.
22. **Oniśko A., Marek J. Druzdzel M. J., Wasyluk H. 2001.** Learning Bayesian network parameters from small data sets: Application of noisy-or gates. International Journal of Approximate Reasoning, 27(2), 165-182.
23. **Pearl J. 1986.** Fusion, Propagation, and Structuring in Belief Networks. Artificial Intelligence, 29(3), 241-288.
24. **Pearl J. 1988.** Probabilistic Reasoning in Intelligent Systems: Network of Plausible Inference. Morgan Kaufmann.
25. **Tchangani A.P. 2001.** Reliability analysis using Bayesian networks. Stud. Inform. Control, 10(3), 181-188.

ZASTOSOWANIE PROCEDURY OBLICZNIWEJ W SIECI BAYESOWSKIEJ DO WYZNACZANIA KOSZTÓW CAŁKOWITYCH PRODUKCJI ELEMENTÓW Z KAMIENIA NATURALNEGO

Streszczenie: W Proces gromadzenie danych oraz ich przetwarzania istotna rolę odgrywają procesy obliczeniowe, które mogą być realizowane automatycznie a ponadto w naturalny sposób powinny umożliwiać uwzględnienie niepewności. W artykule przedstawiono przykład takiego procesu realizowanego w technologii sieci bayesowskich. Model umożliwia monitorowanie kosztów całkowitych produkcji elementów wykonanych z kamienia naturalnego granitu. Wbudowane w system mechanizmy wnioskowania pozwalają wydobywać informacje niezbędne do racjonalnego zarządzania produkcją Podstawą oceny jest podejście oparte o rozkład prawdopodobieństwa określony nad zbiorem wartości zmiennych decyzyjnych reprezentujących parametry procesu produkcyjnego. Pokazano w jaki sposób wykorzystując mechanizmy wnioskowania można prowadzić symulacyjne badania różnych wariantów sytuacyjnych.

Słowa kluczowe: proces produkcji, kamień naturalny, granit, procesy obliczeniowe, koszty produkcji, sieci bayerowskie.

TEKA. COMMISSION OF MOTORIZATION AND ENERGETICS IN AGRICULTURE – 2014, Vol. 14, No. 4, 65–70

The Analysis of Oil Balance in Crank Bearing

Khachatur Kyureghyan[1], Wiesław Piekarski[2]

[1]Department of Applied Mathematics and Computer Science, University of Life Sciences
20-950 Lublin, Akademicka 13, e-mail: chaczik@wp.pl
[2]Department of Energy and Transportation, University of Life Sciences
20-959 Lublin, Poniatowskiego 1, e-mail: wieslaw.piekarski@up.lublin.pl

Received December 09.2014; accepted December 19.2014

Summary. The paper presents an analytical calculation of the balance of oil flowing through the dynamically loaded main and crank bearing. Theoretical considerations are based on solving the Reynolds equation (analytical distribution of oil pressure in the cross slide bearing) with boundary conditions that characterize the working conditions in the bearings used in motors s-4002/4003 (agricultural tractors).The quantitative and volumetric evaluations of lubricant fluid flowing through the bearing are presented adequately to the construction of a diagnostic signal, which allows for a dynamic comparative analysis carried out for the model bearings, the new ones as well as the ones with a particular classification of wear.

Key words: hydrodynamic lubrication, cross slide bearing, Reynolds equation, diagnostic analysis, diagnostic signal parameters.

Physical values:

h - thickness of the wedge [*mm*],
ε - relative bearing eccentricity [-],
c - bearing clearance [*mm*],
η - coefficient of dynamic oil viscosity [$Pa \cdot s$],
V - peripheral speed of crankshaft [*m/s*],
e - eccentricity [*mm*],
$P(x,z)$ - oil pressure inside bearing [*Pa*],
x,z – coordinat variables, $x \in \langle 0, 2\pi R \rangle$, $z \in \left\langle -\frac{L}{2}, \frac{L}{2} \right\rangle$ [*mm*],
L – the width of the pan [*mm*],
p_w, p_0 - supply pressure ambient pressure [*Pa*],
p_z - supply pressure [*Pa*],
a - cord diameter [*mm*],
Q - oil intensity passing through the crank bearing [dm^3/min],
Q_1, Q_2 - partial intensity[dm^3/min],
S_0, S_{gr} - values for Q_1, Q_2 from experiment[dm^3/min],
$h_0 = \min_{x \in \langle 0, 2\pi R \rangle} h(x)$ - the minimum thickness of oil wedge [*mm*],
$c_{dot} = c_0$ - clearance after getting proper association (at optimal operation after 100mth) [*mm*],
c_{gr} - critical value of clearance [*mm*],
D_p - coefficent of dynamic passing [-],
d_p - experimenthal value of D_p determined as a parametr of the diagnostic signal

Mathematical solutions

$\Delta[f]_a^b = f(a) - f(b)$ - operator różnicowy,
$f_K = \sum_{k=1}^{K} f_k$ - suming operator, $k, K \in \mathbf{N}$,
$[f]$ - część całkowita wyrażenia f,
C_1, C_{11}, C_{1K} - Reynolds equation constants determined by boundary conditions

INTRODUCTION

The parameters of diagnostic signals defining the course of change in the tightness of slide bearings are a very important factor in assessing the technical state of engines examined in this study on the example of farm tractors. It should be noted that in the lubrication subsystem the main slide bearings and the crank ones of the crankshaft determine the technical condition of the engine, and its ability to perform useful functions. Increased clearances in the bearings make the lubricant oil flow freely through the gaps between the pivots and the cups, which in turn is manifested by an increase in oil flow and pressure drop in the engine lubrication system.

In diagnostic considerations, the evaluation of work behavior of a dynamically loaded slide bearing is based on the simplified model of a standard cross slide bearing and is based mostly on the minimum thickness of oil gap and the value of the maximum pressure and maximum temperature of the oil film.

However, as noted by several authors [1,2,4,7,16], in diagnostic tests, particularly in predicting the technical state of emergency crank system operation, application of a single-parameter diagnostic signal based solely on the measurement of relative drop in oil pressure at selected points of the bearing, is not sufficient to assess the degree of bearing wear. [16,17] presented a multivariate statistical analysis (curvilinear regression model for the associated random variables) of the diagnostic signal based on measurements of four parameters, where the measurement of the relative pressure drop and loss of lubricant in the bearings were considered as associated variables. The purpose of this study is to analyze the theoretical value of the diagnostic signal parameter described by an analytical balance of oil in the cross slide bearing.

In diagnostic studies of changes in oil flow through the crankshaft bearing and at the constant supply pressure in static conditions, the oil flow rate depends mainly on the size of oil gap. And according to the relation:

$$h = L_t(1-\varepsilon\cos\theta),$$

the gap value depends on oil bearing clearance (L_t) and relative bearing eccentricity (ε), in further considerations we use a simplified designation:

$$L_t = c\,.$$

Determination of this value in the experimental way is based on measurements of diagnostic parameters, the commonest of which are oil pressure or relative drop of oil pressure in the lubrication subsystem (bearing seal). By way of contrast, the theoretical determination of the oil gap is based on the equations of hydrodynamics for a viscous substance.

MATHEMATICAL MODEL OF BEARING AND ASSUMPTIONS

Assessment of work of dynamically loaded crank bearing is one of the most important tasks of the crank subsystem diagnostics in internal combustion engines. In this paper, theoretical considerations and the resulting mathematical calculations are shown on the basis of a cross slide bearing model, characterizing the operating parameters of crank bearing in S-4002/4003 type of internal combustion engines. In the process of exploitation, the growing bearing clearance values cause an increase in the impact of oil flowing from the bearing, causing a decrease in tightness of the bearings.

The balance of oil flowing through a dynamically loaded crank bearings can be determined analytically using a pressure distribution which is the solution of the Reynolds equation:

$$\frac{\partial}{\partial x}\left(\frac{h^3}{\eta}\frac{\partial P}{\partial x}\right)+\frac{\partial}{\partial z}\left(\frac{h^3}{\eta}\frac{\partial P}{\partial z}\right)=6V\frac{\partial h}{\partial x}\,. \tag{1}$$

After considering the constant coefficient of dynamic oil viscosity ($\eta = const$) as well as the following simplified expressions for the functions describing the thickness of the wedge and the bearing wear [5,9,14,18]:

$$h = h(x) = c\left(1-\varepsilon\cos {x}/{R}\right), \tag{2}$$

$$\frac{3}{h(x)}\frac{\partial h(x)}{\partial x} = \frac{3e\sin {x}/{R}}{Rc\left(1-\varepsilon\cos {x}/{R}\right)}, \tag{3}$$

equation (1) can be written as:

$$P''_{xx}(x,z)+P''_{zz}(x,z)+\frac{3e\sin {x}/{R}}{Rc\left(1-\varepsilon\cos {x}/{R}\right)}P'_x(x,z)-\frac{6\eta e\sin {x}/{R}}{Rc^3\left(1-\varepsilon\cos {x}/{R}\right)^3}V=0 \tag{4}$$

with the boundary conditions:

$$P = p_0 \ \text{for}\ z=\pm\frac{L}{2}, \tag{5}$$

$$P = p_w(x)\ \text{for}\ z=0, \tag{6}$$

$$\left(\frac{\partial P(x,z)}{\partial z}\right)_W = -\frac{3\pi a^4(p_z-p_w)}{4c^3\eta L\left(1-\varepsilon\cos {x}/{R}\right)^3}, \tag{7}$$

for $z=0$

where:

p_0 - the ambient pressure [Pa],

p_z - supply pressure [Pa],

p_w - oil pressure at the inlet to the placenta [Pa],

a - cord diameter [mm],

L - the width of the pan [mm].

According to [5,12,14], the analytical distribution in the bearing oil pressure as the solution of equation (4) can be written as follows:

$$P(x,z)=p_0+C_1\left(z-\frac{L}{2}\right)+\left[\frac{1-\varepsilon\cos {x}/{R}}{1+\varepsilon}\right]^{-\frac{3e}{\varepsilon}}\cdot$$
$$\cdot\sum_{K=1}^{\infty}C_{1K}\left(e^{Kz}-e^{K(L-z)}\right)\left[\Phi_{RK}\left({x}/{R}\right)+\Psi_{RKV}^{-2}\left({x}/{R}\right)\right], \tag{8}$$

where

$$\Phi_{RK}\left({x}/{R}\right)=-\frac{\sin^2 {x}/{R}}{4}\left(\frac{1-\cos {x}/{R}}{2}\right)^{-\left(R^2K^2+1\right)}, \tag{9}$$

$$\Psi_{RKV}\left({x}/{R}\right)=\left(\frac{2\pi RK}{nV}\right)^2\sum_{i=1}^{\left[R^2K^2\right]}\left[\left(\frac{R^2K^2V}{i}\right)\frac{1}{i}\left(\frac{1-\cos {x}/{R}}{2}\right)-\right.$$
$$\left.-\ln\left(\frac{1-\cos {x}/{R}}{1+\cos {x}/{R}}\right)^i-\left(\frac{1-\varepsilon\sqrt{V}\cos {x}/{R}}{\pi\left(1+e\sqrt{V}\right)}\right)^{-\frac{3e}{\varepsilon}}\right], \tag{10}$$

$$C_1=\frac{\Delta_L}{1+\frac{L}{2}\Delta_L}\left(p_z-p_0\right), \tag{11}$$

$$C_{11} = \frac{3\Delta_L \Gamma_L (p_z - p_0)}{(1+\varepsilon)^{\frac{3e}{\varepsilon}} \left[1 + \frac{1+\varepsilon}{1-\varepsilon}\left(\Phi(0) + \Psi^{-2}(0)\right) - \left(\frac{1+\varepsilon}{1-\varepsilon}\right)^{\frac{3e}{\varepsilon}} \left(\Phi\left(\pi/2\right) + \Psi^{-2}\left(\pi/2\right)\right)\right]}, \tag{12}$$

$$\Delta_L = \frac{15\pi a^4}{2c^3 \eta L}, \tag{13}$$

$$\Gamma_L = \frac{1-\varepsilon^2}{1+3\varepsilon}\Delta_L\left(e^L - 1\right). \tag{14}$$

ANALYTICAL BALANCE OF OIL

Analytical determination of the amount of oil flowing through bearing is based on the solution of equation (4), i.e. function P (x, z) describing the distribution of pressure in the crank bearing [9,18]. The value of the intensity of Q passing through the crank bearing can be represented as two partial streams Q_1,Q_2, where $\mathbf{Q_1}$ is part of the stream flow caused by the rotation of the crankshaft, while Q_2 is part of a stream of pressurized forced power Q_2. By virtue of the above considerations, the dependencies representing the partial streams of flowing oil can be written as follows:

$$Q_1 = Q_{1,x=0} - Q_{1,x=R\pi} = \frac{1}{6\eta}\int_{-L/2}^{L/2} h^3 \Delta\left[\frac{\partial P}{\partial x}\right]_0^{R\pi} dz = $$
$$= \frac{1}{6\eta}\int_{-L/2}^{L/2} h^3\left[\frac{\partial P}{\partial x}\right]_{x=0} dz - \frac{1}{6\eta}\int_{-L/2}^{L/2} h^3\left[\frac{\partial P}{\partial x}\right]_{x=R\pi} dz, \tag{15}$$

$$Q_2 = Q_{2,z=0} - Q_{2,z=\pm\frac{L}{2}} = \frac{1}{6\eta}\int_0^{2\pi} h^3 \Delta\left[\frac{\partial P}{\partial z}\right]_0^{\pm\frac{L}{2}} dx = $$
$$= \frac{1}{6\eta}\int_0^{2\pi} h^3\left[\frac{\partial P}{\partial z}\right]_{z=0} dx - \frac{1}{6\eta}\int_0^{2\pi} h^3\left[\frac{\partial P}{\partial z}\right]_{z=\pm\frac{L}{2}} dx, \tag{16}$$

where:

$$Q_{1,x=0} = \frac{c^3 C_{1K}\left(1-\exp\{KL\}\right)}{6\eta RK}(1-\varepsilon)^3\left(\frac{1+\varepsilon}{1-\varepsilon}\right)^{\frac{3e}{\varepsilon}}, \tag{17}$$

$$Q_{1,x=R\pi} = \frac{c^3 C_{1K}\left(1-\exp\{KL\}\right)}{48\eta RK}(1+\varepsilon)^3, \tag{18}$$

$$Q_{2,z=0} = \frac{c^3 K\pi\left(1+\exp\{KL\}\right)}{6\eta}\left[2C_1 + \frac{C_{1K}(6e+\varepsilon)}{3e+2\varepsilon}(1-\varepsilon)^{\frac{3e}{\varepsilon}}\right], \tag{19}$$

$$Q_{2,z=\pm\frac{L}{2}} = \frac{c^3 K\pi \exp\{KL\}}{3\eta}\left\{2C_1 + \frac{C_{1K}(6e+\varepsilon)}{3e+2\varepsilon}(1-\varepsilon)^{\frac{3e}{\varepsilon}}\right\}. \tag{20}$$

The relationships (17) - (20) omitted elements of the order o(ε^3) and used the following indications:

$$C_1 = -\frac{\Delta_L}{1+\frac{L}{2}\Delta_L}(p_z - p_0), \tag{21}$$

$$C_{1K} = \sum_{k=1}^{K} C_{1k} = \sum_{k=1}^{K}\left(p_0 - C_1\frac{L}{2} + \left[\frac{1-\varepsilon}{1+\varepsilon}\right]^{-\frac{3e}{\varepsilon}} \frac{\Delta_L}{\pi C_1\left(1-\frac{KL}{4}\right)}\right), \tag{22}$$

where:

$$K = 1,2,\ldots,\left[\left(\frac{R}{e}\right)^2 - 1\right]. \tag{23}$$

Due to (17) - (20), oil streams Q_1, Q_2 can be written as follows:

$$Q_1 = \frac{c^3 C_{1K}\left(1-\exp\{KL\}\right)}{6\eta RK}\left[(1-\varepsilon)^3\left(\frac{1+\varepsilon}{1-\varepsilon}\right)^{\frac{3e}{\varepsilon}} - \left(\frac{1+\varepsilon}{2}\right)^3\right], \tag{24}$$

$$Q_2 = \frac{K\pi\left(1-\exp\{KL\}\right)}{6\eta}\left[2C_1 + \frac{C_{1K}(6e+\varepsilon)}{3e+2\varepsilon}(1-\varepsilon)^{\frac{3e}{\varepsilon}}\right]. \tag{25}$$

Finally, by equation (15), (16), the balance of oil flowing through the crank bearing can be written as the following relationship:

$$Q = Q_1 + Q_2 = \frac{c^3\left(1-\exp\{KL\}\right)}{6\eta}\left[2C_1 + C_{1K}\left(\frac{\Omega_1}{RK} + K\pi\Omega_2\right)\right], \tag{26}$$

where:

$$\Omega_1 = (1-\varepsilon)^3\left(\frac{1+\varepsilon}{1-\varepsilon}\right)^{\frac{3e}{\varepsilon}} - \left(\frac{1+\varepsilon}{2}\right)^3, \tag{27}$$

$$\Omega_2 = \frac{6e+\varepsilon}{3e+2\varepsilon}(1-\varepsilon)^{\frac{3e}{\varepsilon}}. \tag{28}$$

PERFORMANCE ANALYSIS OF DIAGNOSTIC SIGNAL

In the crank bearings of the engine type S-4002/4003 (agricultural tractors C-355, 360), the maximum value of bearing clearance is characterized by accelerated wear of crank mechanism (the boundary condition of the bearing crank is 0.2 mm), which can be derived from the average dependence given by Kozłowiecki and Przustka [10] as well as Thum [18, 19]:

$$C_{gr} = \frac{C_{dot}^2}{4h_0}, \tag{29}$$

using the classical formula Vogelpohl:

$$C_{dot} = 0.92\cdot 10^{-3}\sqrt[4]{V}, \tag{30}$$

where:

C_{dot} - clearance after getting proper association (at optimal operation after 100mth)

h_0 - the minimum thickness of oil wedge,
V - the peripheral speed of crankshaft.

In the boundary conditions of dynamically loaded crank bearing's operation, the diagnostic signal parameters describing the relative decline in the oil pressure inside the bearing and its flow through the bearing score significantly higher values than when working under optimal conditions, which points to accelerated wear of the crank. Piekarski [16] applied the model to assess the value of diagnostic signal parameters based on measurements of the relative pressure drop and oil flow dynamics at the measurement narrowing. As an indicator of the dynamics, the following value describing oil flow through the bearing was accepted:

$$d_p = \frac{S_{gr} - S_0}{S_0}, \tag{31}$$

Analytical interpretation of the above relation, using the average value of clearance limit (at the speed of the shaft 1200 $\min^{-1}$)

$$C_{gr} = 2{,}3 \cdot 10^{-3} \sqrt{V} = 1{,}42 \cdot C_0$$

can be obtained by equation (26) as follows:

$$D_p == \left(\frac{c_{gr}}{c_0}\right)^3 \cdot \frac{2C_1 + C_{1K}\left(\dfrac{\Omega_{1gr}}{RK} + K\pi\Omega_{2gr}\right)}{2C_1 + C_{1K}\left(\dfrac{\Omega_{10}}{RK} + K\pi\Omega_{20}\right)} - 1 =$$
$$= 2{,}86 \cdot \frac{\Phi_{gr}}{\Phi_0} - 1, \tag{32}$$

where:
Ω_{i0} - quantity calculated from solutions (27), (28) for $c = c_0$, *i=1;2,*
Ω_{igr} - quantity calculated from solutions (27), (28) for $c = c_{gr}$, *i=1;2,*

$$\Phi_0 = 2C_{10} + C_{1K}\left(\frac{\Omega_{10}}{RK} + K\pi\Omega_{20}\right),$$

$$\Phi_{gr} = 2C_{1gr} + C_{1K}\left(\frac{\Omega_{1gr}}{RK} + K\pi\Omega_{2gr}\right),$$

$$K = \begin{cases} 1 & for\ c = c_0 \\ 2 & for\ c \in (c_0, c_{gr}) \\ 3 & for\ c = c_{gr} \end{cases} .$$

In diagnostic tests, the dynamic of determined signal changes should be as high as possible. It is assumed that the determined change induced by an increase in consumption occurring in the crank subsystem is the relative increase in oil pressure drop, which is treated as a diagnostic signal.

CONCLUSIONS

Knowledge of the dynamics of steam friction (pivot - cup) in a crank system, expressed by escalation of clearance between its elements, allows to determine the probability of reliable operation of the considered friction pair. A proper technical maintenance of the engine operation is necessary, provided the information is available on its properties.

This information can be known only by the changes of bearing clearance and course changes in the dynamics of the diagnostic signal.

The terms of co-operation of the functional subsystem crank pivot - cup decide on the reliable operation of the engine. The worsening conditions for cooperation of these subsystems as a result of processes of consumption lead to premature engine wear, and even more to significant increase in fuel and oil consumption and increased difficulty in starting.

Requirements for operational progress are becoming more frequently recognized and formulated. It has been noted that the effectiveness of the management of technical objects in many cases reduces the high operating expenses, which may even get higher than expenses associated with designing and manufacturing. The high operating expenses can be reduced by improving the quality of technical objects, as well as conditions of their use and handling. For this purpose, the pursuit is necessary of rational, science-based exploitation of technical objects.

REFERENCES

1. **Bałuciński J., Stępiński J., 1993:** Wykorzystanie metod oceny stanu technicznego silników przy kwalifikowaniu ich do naprawy. Techn. Moto., 11, 48-52.
2. **Będkowski L., 1981:** Elementy ogólnej teorii diagnostyki technicznej. Biul. WAT, 3.
3. **Cislikowski B., Pedryc N., 2009:** Koncepcja nadzoru nad maszynami przez computer pokładowy ciągnika w czasie rzeczywistym z wykorzystaniem magistrali informatycznej LIN. Inżynieria Rolnicza 9(118), 29-33
4. **Das S., Guha S.K., Chattopadhyay A.K., 2005:** Linear stability analisis od hydrodynamic journal bearings under micropolar lubrication. Trybology International,38, 31-35
5. **Hebda M., Wachal A., 1980:** Trybologia, WNT, Warszawa.
6. **Juściński S., Piekarski W., 2008:** Zarządzanie logistyczne autoryzowanym serwisem ciągników i maszyn rolniczych. Eksploatacja i Niezawodność – Maintenance and Reliability, 2, 25-33
7. **Mienann G., 1980:** Mashinenelemente. Springer Verlag, Berlin.
8. **Niewczas A., 1991:** Zastosowanie pomiarów przedmuchów spalin do prognozowania trwałości silników spalinowych. Krajowa Konf. Naukowo – Techniczna Kiekrz, 67, 53-62.
9. **Kozłowiecki H., 1974:** Łożyska tłokowych silników spalinowych. WKiL, Warszawa.
10. **Kozłowiecki H., Przustek J., 1975:** Współczesne metody obliczania parametrów pracy łożysk mechanizmu korbowego silników spalinowych. Silniki Spalinowe, 2, 62-69.
11. **Krasowski P., 2006:** Zmiana ciśnienia w poprzecznym łożysku ślizgowym przy laminarnym niestacjonarnym

smarowaniu. Zeszyty Naukowe Akademii Morskiej w Szczecinie,10(82): 287-298.
12. **Kurowski W., 1978:** Systemy diagnostyczne urządzeń mechanicznych. DUM, Ossolineum.
13. **Kyureghyan Kh., 2002:** Theoretical calculation of size on an oil slit in a transverse sliping bering, Mathematical Methods in Agriculture,11, 388-393
14. **Kyureghyan Kh., Kornacki A., Piekarski W., 2006:** Analityczna zależność do wyznaczania ciśnienia w hydrostatycznym łożysku poprzecznym ślizgowym, Inżynieria Rolnicza, 6(98).
15. **Kyureghyan Kh., Piekarski W., 2008:** Analisis of detetermining pressure distribution in crank bearing, Eksploatacja i Niezawodność – Maintenance and Reliability, 4(40),19-24.
16. **Piekarski W., 1993:** Prognozowanie trwałości par trących się na przykładzie łożysk wału korbowego silnika S – 312C. Zeszyty Naukowe AR Szczecin,85, 372-386.
17. **Piekarski W. i inni., 1988:** Diagnostyka pojazdów rolniczych Wyd. AR, Lublin, 77
18. **Thum H.:** Über den Verlauf des Schmierfilmdruckes in dynamisch beanspruchten Gleitlagern. Wiss. Z. Techn. Hochsch. Magdeburg, 5.99.
19. **Thum H., 1985:** Zur Bestimmung der Verschleiss-bedingungen Lebensdauer von Wälzlagern bei verschie-denen Überlebenwahrscheinlichkeiten. Schimrungs-technik,16, 101-112.
20. **Vogelpohl G., 1969:** Über die Ursachen der Unzu-reichenden Bewertung von Schemierungsfragen im Vorigen fahrundert. Schmiertechnik, 5.

ANALIZA BILANSU OLEJU W ŁOŻYSKU KORBOWYM

Streszczenie: Praca przedstawia analityczną kalkulację bilansu oleju przepływającego przez dynamicznie obciążone łożysko główne i korbowe. Teoretyczne rozważania bazują na rozwiązaniu równania Reynoldsa (analityczny rozkład ciśnienia oleju w łożysku poprzecznym ślizgowym) o warunkach brzegowych charakteryzujących warunki pracy w/w łożysk zastosowanych w silnikach S-4002/4003 (ciągniki rolnicze). Ilościowo-objętościową ocenę cieczy smarującej przepływającej przez łożysko przedstawiono adekwatnie do teoretycznej wartości sygnału diagnostycznego co pozwala na dynamiczną analizę porównawczą przeprowadzoną dla wzorcowych, nowych, jak również dla łożysk o ustalonej klasyfikacji stopnia zużycia.
Słowa kluczowe: smarowanie hydrodynamiczne, łożysko poprzeczne ślizgowe, równanie Reynoldsa, analiza diagnostyczna, parametry sygnału diagnostycznego.

TEKA. COMMISSION OF MOTORIZATION AND ENERGETICS IN AGRICULTURE – 2014, Vol. 14, No. 4, 71–80

The Development of New Technologies for Processing and Disposal of the Oil Containing Wastes Enterprises of Railway Infrastructure

Anna Leshchyns'ka, Yuliya Zelen'ko, Marina Bezovs'ka, Michael Sandowski

Dnipropetrovsk National University of Railway Transport Named after Academician V. Lazaryan
Academician Lazaryan st., 2, Dniepropetrovsk, Ukraine, 49010
e-mail: anna.leshchynskaya@gmail.com, j.zelenko@mail.ru

Received December 11.2014; accepted December 19.2014

Summary. In article traditional methods of utilization and renewal of the fulfilled cooling lubricants and waste compressor oils of separate brands are considered. In developing the scheme of recovery of operating quality of the oil containing wastes for the purpose of forming and calculating the process flow diagram suggested, the process optimization, namely temperature, reagent amount, and time of its contact with oil was conducted. The new technologies with use of surface-active substances are offered.
Key words: waste compressor oils, cooling lubricants (coolants), surface-active substances, environmental safety, utilization.

INTRODUCTION

The creation and development of high-efficient technologies subject to demands on resource and energy conservation as well as environmental safety are prerequisites for the production development at the present stage.

The railway infrastructure is one of the largest consumers of valuable material resources such as petroleum, because the environmental safety of the railways is one of the priorities [25, 26].

MATERIALS AND METHODS

To reduce the negative impact of railway transport in all parts of the biosphere during regular operation, the degree of its impact should be constantly monitored and regulated. Analysis of the annual activities of the railway under-takings suggests that more than 40% of water consumed is discharged into surface water reservoirs in the form of wastewater contaminated with oil products, salts of heavy metals, synthetic surface active substances, etc.; over 50 tons of harmful substances are emitted into the atmosphere from stationary sources, only about 30% of them are recaptured and detoxified; more than 65 tons of waste are formed as a result of industrial activity; railway facilities in Ukraine occupy approximately 263 hectares withdrawn from agricultural sector [24].

Large part of emissions (about 85%) is produced by fuel combustion during operation of diesel mainline and shunting rolling stock, refrigerated trains.

The quality of wastewater of the railway undertakings varies widely. Water pollution by industrial wastewaters creates a potential threat to public health, restricts the use of water reservoirs for household, drinking, cultural and domestic purposes, causes great damage to fisheries and agriculture [25, 26].

The sources of wastes in railway transport are all its subdivisions. Major transport companies, which include, in particular, locomotive, railcar depots, railway stations, railway machinery repair plants and bases supporting them, tend to form and accumulate processing wastes, oil-contaminated ones being the most common of them (Table 1).

Table 1. Processing wastes of railway undertakings

Type of waste	Technological process that forms wastes	Waste volume per annum
Oil sludge	Purification of wastewaters	up to 200 thous. t
Washing machinery sludge	Washing of bearings, bearing boxes, four-wheel trucks and carriage bodies of rolling stock, various details before repair works	up to 2000 m³
Galvanic sludge	Purification of washing waters of galvanic sections	up to 20 t
Dry-cleaning machinery subsidence	Work wear cleaning	500-1600 m³
Scavenge oils	Cleaning of bearing boxes before repair, scavenge oil change	5-7 thous. T
Scavenge diesel oils	Scavenge diesel oils change during rolling stock maintenance and repair	Over 1 thous. T

Type of waste	Technological process that forms wastes	Waste volume per annum
Contaminated soil	Cleaning of industrial sites, midpoint pump station, sleeper impregnation plant, railside territories of depots, plants etc.	up to 1 mln. T
Cross-sleepers	Replacement of used cross-sleepers during repair works	1-1,2 mln. pcs.
Fluorescent lamps	Replacement of defective lamps in administrative premises and workshops of the undertakings	up to 40-50 thous. pcs.
Mechani-cal-rubber wastes	Replacement of brake shoes during repair works, of battery jars and other rubber pieces	500-700 t

Amount of managed waste of all grades is negligible, due to the general economic trend of decline in production, which in turn is a condition for reducing the volume of financing environmental measures aimed at increasing the level of waste utilization not only in railway transport, but also in all industries in Ukraine.

Storage and disposal of waste in railway transport, as in other industries, do not often meet sanitary requirements, leading to contamination of groundwater, soil and atmosphere.

The most effective approach to minimizing the negative environmental impact is to develop eco-protection technologies based on the monitoring data, which allows for taking into account the peculiarities of the objects.

At the railway undertakings oil-contaminated and oily waste (waste oils, cooling lubricants, contaminated soils, grease, technology sludge (petroleum slime), etc.) constitute a significant part of the total volume of all wastes. This follows, for example, from the analysis of the dynamics of the formation of different types of waste that were formed at the undertakings of different railway departments.

In particular, the major contributors to the formation of such waste are the undertakings of locomotive department, so, Fig. 1 presents the data on the formation of all types of waste at the undertakings of that department of the Prydniprovska railway in 2010 [6].

Fig. 1 clearly shows that in general for the undertakings of the railway locomotive department it is scavenge oils that constitute the main group of waste; process sludge comes third after accumulator batteries.

According to the public management policy in the field of waste treatment, all processing waste for which the methods for recycling and rational use in the national economy are developed, are to be used as secondary raw material and should not be transported to landfills.

Disposal of exhausted petroleum and oil-containing wastes is an important scientific-and-technical challenge because they are classified as hazardous waste, which adversely affect all objects of the environment – air, soil and water. For instance, water pollution by petroleum products is 20% of the total man-made contamination [20].

In most developed countries the relevant laws, environmental standards and economic conditions regulate the collection and disposal of exhausted oils. Increased attention to meeting these laws is stipulated by large amounts of waste oils, high environmental risk they lead to and also the valuable properties of oils as hydrocarbon-containing raw [9]. A well-adjusted mechanism of recycling waste oils provides the return them to production or consumption sector as secondary products or intermediates, which provides real saving the resources in oil importing countries [15].

For example, in Germany more than 0.5 million tons of the exhausted oils is collected annually, while in the U.S.A. – ca. 5 million tons. Despite the stabilization of production and use of lubricants at the level of 40-43 million tons per year, in the coming years, according to experts' forecasts, the steady amount growth in the collection of waste oils is expected. This is due to the improvement of the legal and economic mechanisms of managing the turnover of commodity and waste oils, the development of technologies for collecting and recycling the latter, strengthening the state and public control over the handling of hazardous wastes and other factors [7].

Experts estimate that today the global production volume of lubricating oils of different brands is about 38.5 mln. tons per year. An insignificant part thereof (10-20%) is irrevocably lost in the course of use due to evaporation, spills, burn-out and leak-offs. Their bigger part (80-90%) is gradually contaminated by various metal, mineral and organic impurities, is thermally decomposed through interaction

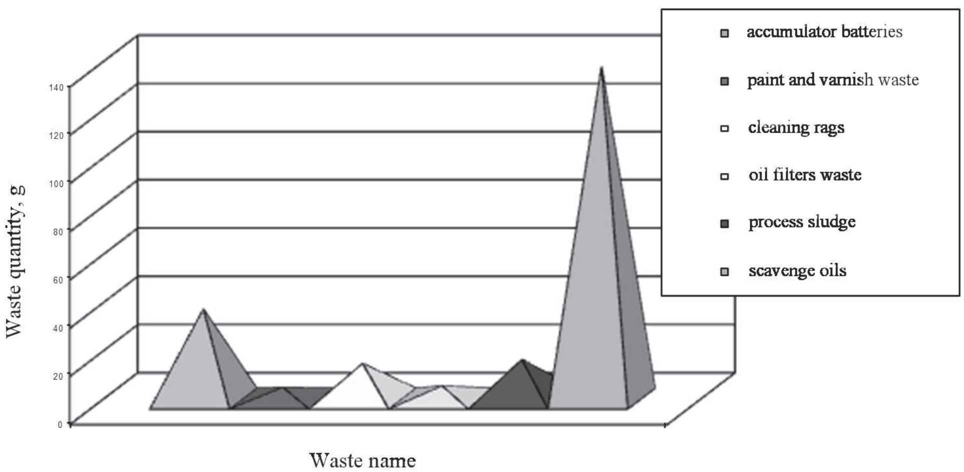

Fig. 1. Formation of waste at the undertakings of locomotive department of the Prydniprovska railway in 2010, t/year

with hot parts of the equipment, oxidized by atmospheric oxygen, exposed to such environmental factors as pressure, electric field and natural lighting. As a result, scavenge oil completely changes its properties and turns into very thick, ooze-like black or dark-brown substance, thick mixture of various kinds of liquids with addition of solids – metal oxides, wear debris.

Regeneration of waste oils for railway companies is virtually non-existent, except for certain physical methods (settling and centrifugation), which do not ensure the full effect [5].

At present, waste oils are often used without regeneration as heating and boiler fuel directly at railway enterprises or transferred for further use or regeneration to other businesses that leads to significant repeated economic expenses [24]. E.g., the regeneration of waste oils is often conducted in petroleum refineries by a full technological scheme. It is a well-known fact that with proper organization of process the cost of recovered oils is less by 40-70% than the cost of the fresh oil at almost the same quality [18].

In the operation, physical and chemical properties of oils vary but experiments have shown that in the main the group chemical composition of the oil varies slightly [19]. Products of physicochemical transformations of oils as well as harmful impurities, which get from outside and make the oil unfit for further work, are only a small part of their total mass and by means of using special processing methods they can be removed. After removal of contaminants, the original properties of oils are recovered therefore they can be re-used in a mixture with fresh oils [3].

A joint processing in a mixture with petroleum at oil refineries and their target processing with obtaining the grease components (regeneration) are the main areas of processing the exhausted oils.

Generally, regeneration methods are divided into: physical, chemical, physical and chemical, biological and complex. Here is a schematic diagram of a comparative analysis of scavenge oil disposal/recycling technologies (Fig. 2) [18].

To physical belong such methods that provide for removal of only mechanical impurities, i.e, dust, sand, metal particles, water, tarry, asphaltum-like substances and carbon blacks, as well as fuel, without affecting the chemical base of oils to be refined. These include sedimentation, filtration, separation, flushing with water; also, if necessary, light fractions recovery is carried out.

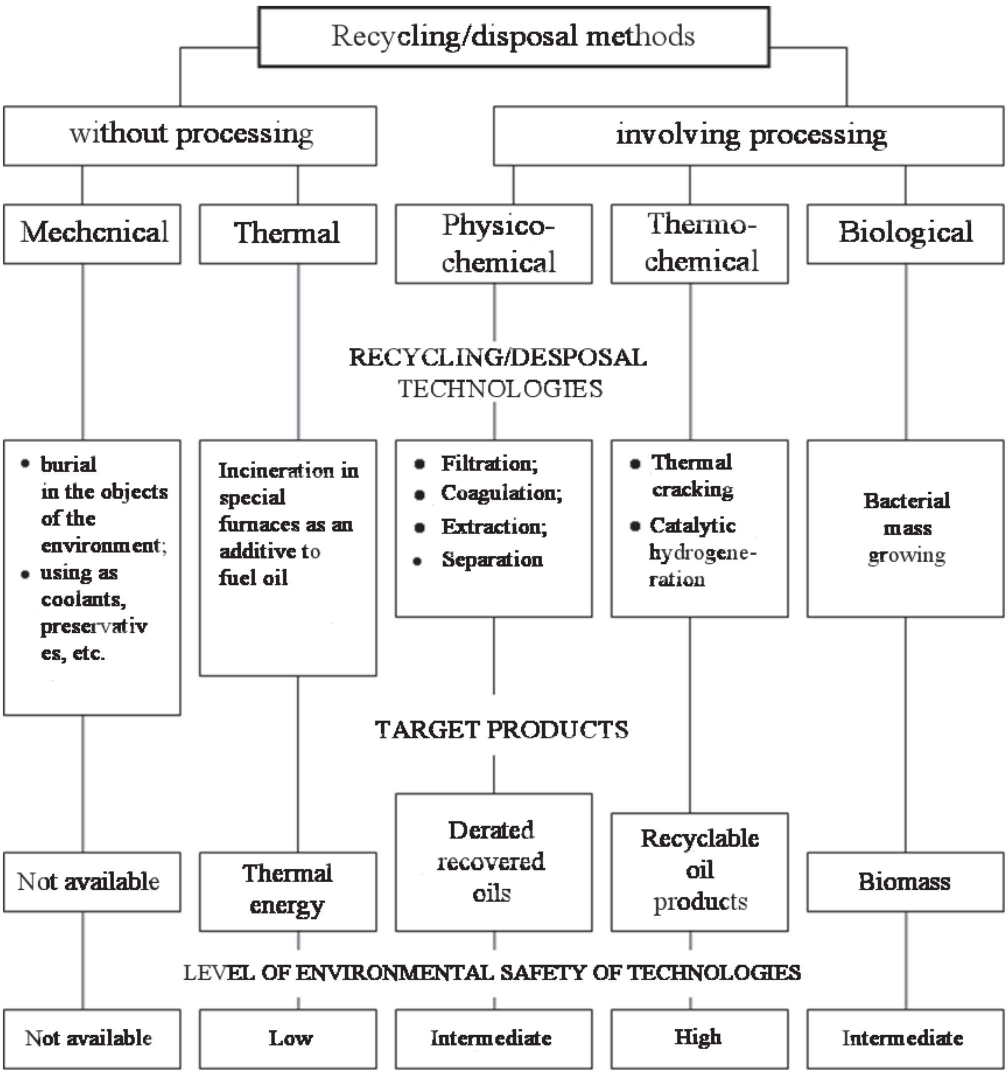

Fig. 2. Diagram of scavenge oil disposal/recycling technologies

Sedimentation is the first and mandatory operation of the regeneration process. Mechanical impurities and water, suspended in the oil, sediment at the oil still standby for 2-18 hours depending on the heating temperature and the height of the liquid column. Sedimentation is based on the principle of particle settling by gravity. The greater the particles' sedimentation rate (from Stokes equation), the bigger their size and specific gravity, and the lower the fluid viscosity [2, 9].

Separation allows for deeper purification of scavenged oil. This is a centrifugation process when products, affected by centrifugal effort, are separated according to their density: the heaviest contaminating impurities are pushed to the walls of the container, forming an annular layer of sediments; the next annular layer is made up of water that is released, and the third one located near the axis of rotation is refined oil.

Filtration is a process of separation of heterogeneous systems through porous walls that block some phases of these systems and let through others. These processes include separation of suspensions into pure liquid and wet sediment, such as separation of mechanical impurities or bleaching clay from oil. Filtering is one of the most efficient methods of regeneration, because it can be used directly in the operation, when the lubrication systems of engines and tools include tailor-made filters.

The disadvantage of this method is low cleaning efficiency due to the fact that contaminant particulates as small as 1 micron pass through the pores of the filters. Additionally, filtration only removes mechanical impurities and has no effect on the processes that lead to changes in the physical and chemical properties of the oil, and therefore requires further processing with chemical reagents [19, 15].

In addition to the above-mentioned methods, which refer to the list of physical ones, one should also note thermal methods that allow for getting the heat, but constitute additional challenges due to the installation of expensive equipment and auxiliary machinery for cleaning the combustion products [8].

Physical and chemical methods include coagulation and adsorption. During the coagulation the particles of colloidal system coalesce and grow to form loose aggregates, thereby exacerbating sedimentation of contaminants. Adsorbents take in and retain on its surface a significant amount of asphalt pitch, acidic compounds, ethers and other products of aging.

For recovery of oils that are not filtered different detergents and surfactants are used as coagulants [2, 19].

The disadvantages of the method are the difficulties in finding coagulants and conditions under which the coagulation process is successful (temperature, necessity and intensity of mixing).

An important condition for adsorption purification is the intensity and time of contact of oil with an adsorbent which is usually achieved by two methods. In the first method an adsorbent is fed into the oil with vigorous stirring of 1000...1400 rpm, which lasts for at least half an hour; then the used adsorbent is separated by sedimentation. The second method is a filtration through a layer of coarse adsorbent [18].

A common disadvantage of the adsorption method is the need for removal of waste adsorbents and sludge, which will no longer be recycled, but simply thrown away, which leads to contamination of the environment. In addition, some adsorbents due to insufficiently high mechanical properties (strength, resistance to abrasion) degrade filter performance, generally complicating the cleaning process.

Quite often chemical methods of regeneration are used. Sulfuric acid, alkaline sodium silicate solutions are used more often than others, but there is a more effective method of chemical treatment , which provides for the use of different selective solvents and their mixtures (phenol, propane, mixtures of phenol with propane) used for treatment of residual oil that belonged to irreversibly lost ones.

The disadvantage of the use of sulfuric acid is the presence of residual acid and sulpha compounds that adversely affect the physical and chemical properties of oil and increase its corrosion activity. Also formed is acidic sludge, which is difficult to dispose. Removal of acidic compounds requires a significant investment of time and money and is accompanied by a loss of up to 50% of oil. Also to get a neutral reaction, alkaline agents should be added to the oil.

Insufficient degree of scavenge oil purification by alkaline treatment method is associated with the presence in many oils of different types of additives that significantly impair coagulation and flocculation functions of alkaline agents. Therefore, for successful regeneration one should choose specific conditions for each type of oil [3, 13].

In practice, for better effect the combined methods best suited to provide high-quality cleaning and recovery of waste oils are applied.

RESULTS, DISCUSSION

At the railway businesses the personnel applies compressor oil of mark CS-19 as all-seasonal lubricant for friction units of compressors of diesels and diesel trains [23].

In the operation, chemical engineering laboratories at each depot investigate oil on suitability for further use, comparing the results of analyzes with scrap indices [2, 23] (numeric values of quality parameters when the lubricants lose their functional properties). When sampling for rejection on the results of laboratory analysis, the full replacement of oils in compressors is conducted.

The analysis of current technologies and schemes of regeneration of waste oils led to drawing the conclusion that the physical-and-chemical methods are the most promising [4, 12], in particular the use of different types of advanced surface-active substances (surfactants).

In the operation, chemical engineering laboratories at each depot investigate oil on suitability for further use, comparing the results of analyzes with scrap indices (numeric values of quality parameters when the lubricants lose their functional properties). When sampling for rejection on the results of laboratory analysis, the full replacement of oils in compressors is conducted.

The analysis of current technologies and schemes of regeneration of waste oils led to drawing the conclusion that the physical-and-chemical methods are the most promising, in particular the use of different types of advanced surface-active substances (surfactants).

We conducted the laboratory studies to recover the properties of waste compressor oils with a wide range of surface-active substances (surfactants). Specifically, some quantity of surfactants tested, among which ethyl oxide sodium lauryl sulfate (Emal 270d) gave the best result.

In developing the scheme of recovery of operating quality of waste compressor oils for the purpose of forming and calculating the process flow diagram suggested, the process optimization, namely temperature, reagent amount, and time of its contact with oil was conducted.

In Fig. 3, the result is presented as the quality recovery scheme for a waste compressor oil CS-19, developed and proposed for railway usage.

The obtained results of verification of key operational indices of waste compressor oil and comparison of them to the indices of refined oil and rejection parameters are given in Table 2.

Table 2. Comparison of key parameters of the fulfilled and cleared oil with rejection indicators

Physico-chemical properties	Rejection index	Rejected oil	Parameter value after cleaning
Contamination, τ cm^{-1}	1300	181	27.24
Flash point in open crucible, °C	Below 180	179	191
Viscosity at 100 °C, mm²/s	Below 15	14.50	15.30
Alkaline number, mg KOH/g	≤ 0.35	0.72	0.75
Water percentage, %	≥ 0.03	Traces (<0.03)	Traces (<0.02)

As the above table shows, the main operating indices of purified oil exceeded the rejection indices, i.e. it is possible to draw the conclusion that the use of this technology gives a positive result.

Yield of purified product with using this scheme is about 91.3%, while for treatment it was 86.7%.

The analysis of the dynamics of formation (Table 3) of the oil-contaminated waste at the Prydneprovska railway shows that 6–9 tons of the process sludge are annually formed at the undertakings of various departments. If you look at percentages, you can see that they take up a significant share (about 40%) of the total volume of the passenger department waste [5, 16].

In appearance processing waste represented by process sludge are brown mass, having crumby structure. Often process sludge refers to the third class of hazard and are moderately hazardous.

Oil sludge of the operating units of the railways are accumulated in wastewater of the undertakings after washing of cars, locomotives and their parts, that is why most of them are formed in the railcar and passenger car de-pots of the railways, as it is here where washing of the rolling stock during repair works is made.

One of the most common ways of disposing oil sludge is a thermal method, such as incineration. However, process sludges are limited combustible substances, for this reason their incineration can be performed only by using additional quantities of fuel. For example, for railway undertakings it is offered to incinerate them when mixed with solid fuel in the furnaces of stationary steam engines located in the territory of the depot. The ash that remains after burning is recommended to check for the presence of heavy metals [5, 6].

Table 3. Analysis of the formation of oil-contaminated waste at the Prydniprovska rail-way, t/year

No.	Type of waste	Department or division								
		locomotive	car service	public facilities	Railway tracks	electrification	water supply	freight commercial	passenger	Total
1	Used oil filters	68,55	0,08	-	5,16	0,19	-	0,08	-	73,64
2	Scavenge engine oils	223,46	7,60	-	35,38	3,01	1,99	0,90	56,92	329,26
3	Oil sludge	76,63	-	-	-	-	-	-	-	76,63
4	Oily rags	25,45	13,04	-	2,23	1,51	-	2,05	0,11	44,40
5	Wastewater residual oils	191,61	-	-	-	-	-	-	-	191,61
6	Oil-contaminated soil	1,30	-	-	5786,5					5787,8

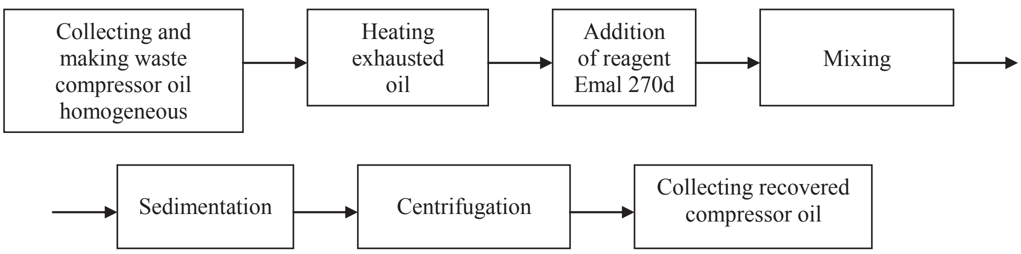

Fig. 3. Recovery scheme for waste compressor oil

However, these technologies are low-production, energy and financially costly because of the high price of boilers, besides, one has to install additional expensive equipment to purify atmospheric emissions; they do not allow the complete recycling and disposal of oil sludge and do not ensure the environmental safety.

When choosing a technology of process sludge disposal, one should take into account the frequency of formation of these wastes, their limited amount, significant consumption of additional fuel to support the combustion process. Therefore, to account for these characteristics of the railway sludge, we offer to apply much cheaper mechanical methods. For example, to install in the depots decanters of different design depending on the overall composition of the sludge and composition of each of its major components: hydrocarbon-bearing particles, water and mechanical impurities [15, 16].

Decanters provide for oil product incineration in standard containers, the possibility of waste disposal directly at the place of their formation at a special site of any depot. Singled out should be a better quality of incineration compared to open burning, high explosive hazard rate as a result of combustion chamber blow-down.

As railway oil sludges are sufficiently watered, being the wastes of rolling stock washing, they do not need to be further diluted with water to reduce the percentage of mechanical impurities. It is recommended to use decanters with a screw that is covered with special protection, such as ceramics or tungsten carbide.

Such measures are caused by the presence in process sludges of so-called "hard" mechanical impurities (sand, forge slag, metal chips and so on), which can cause premature wear of the working parts of the equipment. Additionally, to prevent ingress of large mechanical impurities into decanter, it is advisable to in-stall strainer screens of various fineness of treatment or vibratory separators.

The effectiveness of the decanter depends on the parameters of raw materials, such as their homogeneity and temperature. The first parameter will allow the decanter to run in continuous operation and eliminate the constant human control over the parameters of its operation; indeed, it takes minimum 15 minutes for the employee who services the decanter to set it for the necessary parameters. Another parameter provides the necessary viscosity of the material and is usually 80-90ºC; higher temperatures can lead to overheating of the device. Typically, this heating is carried out directly in the repository for the oil sludge (by heating intermediate containers) or "on the go" with special heat exchangers, when oil sludge is heated while passing through them.

Below in Fig. 4 shown is the general scheme of sludge processing using a centrifuge-decanter and heat exchanger.

Practical research shows that for optimum separation of three phases of process sludges required are different types of flocculants for each case. Depending on the type of the equipment used for the treatment of oil sludge (centrifuges, filter presses, vacuum filters) selected is the most appropriate type of reagent to be used in further processing.

From the experience of using cationic flocculants, most effectively they influence organic compounds, while anionic ones are more suitable for inorganic substances. Due to the diversity of the structure and properties of sludges, the selection of effective flocculants in each case should be made with prior laboratory and industrial tests.

For example, widely known are such flocculants as FT-410, PT-506, Zetag-89 flocculants, industrial polyacrylamide (PAA) and others. Thus, water-based cationic flocculant Zetag-89 manufactured by Swiss company Ciba Specialty Chemicals is used in the oil-refinery industry in the process of oil sludge dehydration at the consumption rate of 2 kg per ton of dry residue.

Known are the results of studies into the opportunity of sludge treatment in the presence of Zetag-89 and Praestol 853 flocculants and polyacrylamide at the consumption rate of 10 grams per one ton of sludge. The results showed that at low consumption of the flocculant one can clearly separate mechanical impurities from oil products. The content of oil products in the lower layer-sediment, when using Zetag-89 and Praestol 853 flocculants, was 6-10%, and in the sediment without flocculants – 18% [16].

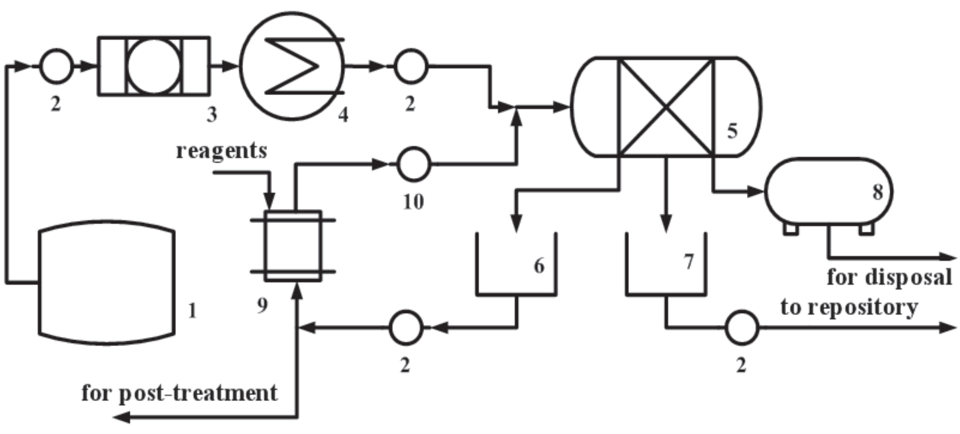

Fig. 4. Schematic diagram of the reagent sludge processing using a decanter and a heat exchanger: 1 – the oil sludge storage tank; 2 – the pumps; 3 – the coarse filter; 4 – the heat exchanger; 5 – the decanter-centrifuge; 6 – the container for collecting water; 7 – the container for collecting centrate (hydrocarbons); 8 – the container for collecting sediment; 9 – the container for preparation of rea-gents; 10 – the dosing pump for feeding reagents

To get rid of wasted mechanical impurities, several options are usually offered: their disposal at the landfill; burning; gradual decomposition using biologically active sorbents at the specially prepared sites.

Under the conditions of the depot it would be reasonable to make gradual accumulation and exportation of wastes to the landfill for disposal.

The water that remains after oil sludge treatment is fed for the post-treatment and subsequently can be used, as already mentioned above, for preparing solution of reagents and included in the production cycle of the enterprise as technical water or the discharged into water bodies.

As reagents recommended for use as flocculants are surfactants (Synthanol and Neonol).

Significant contribution to the human pressure on the environment make metalworking shop of numerous companies, such as machine-building and rail companies (wagon, locomotive depots etc.) [1].

Intensification of processes of metal mechanical treatment, implementing high-performance equipment, automated processes, extensive use of structural materials lead to the fact that metal cutting becomes impossible without the use of efficient cooling lubricants (coolants).

Coolants are a water emulsion of mineral oil stabilized by surfactants and various organic additives aimed at preventing the premature emulsion aging. In the process of use, the coolant loses its technological properties and needs to be replaced with fresh one. An exhausted cooling lubricant (coolant) refers to hazard class 3 [10, 21].

During the use of coolants, they are prone to contamination with:

– smallest mechanical particles (impurities) emitted from the oxidized metal layer, sludge after pickling and products of metal wear during pickling and cold rolling;
– free (non-emulsified) oils extracted from the emulsion as a result of separation;
– oils falling into an emulsion system as a result of leakage from the mechanical and hydraulic components and other metal treatment equipment and so on [14].

The waste coolant (emulsion) is a special type of sewage water that is very dangerous for the environment, since it contains a large number of stable emulsified petroleum products and heavy metals. In this regard, a complex of measures for neutralization of waste coolant is necessary [11, 17].

The spent coolant is subject to obligatory rendering safe from the most toxic components. Existing methods of neutralizing the emulsions of the kind of coolant-containing sewage water can be divided into three main groups:

– thermal;
– physicochemical;
– biological.

However, none of these groups alone can meet the modern requirements concerning the quality of water after its purification and the amount of waste materials generated. The use of common chemical and physicochemical methods leads to secondary contamination due to the formation of various wastes. Most methods of neutralization of coolant-containing wastewater are either economically inefficient or environmentally unacceptable [21]. Therefore, the problem of neutralization of coolants remains urgent.

Local cleaning the wastewater of various compositions, eliminating or reducing the total quantity of discharges of exhausted process liquids due to their regeneration, and reuse of purified sewage waters in closed systems of water turnover and technical water supply in companies can be considered as the most appropriate ways to reduce the harmful effects of contaminated sewage waters of metalworking shops of various industries on the aquatic environment. Repeated use of waste water does not require their deep purification, it is even enough to remove only those substances, which have a negative impact on the quality of products to be manufactured, and to set their MPC values in the water under usage [11, 22].

We conducted research in the field of rendering safe and neutralization of exhausted cooling lubricants, including “Emulsol SVK” using different types of surface-active substances (surfactants). E.g., surfactants such as asparal F, cocamidopropylbetain, oxyethylated monoalkylphenylic acid (neonol AF 9-12), ethoxylated sodium lauryl sulfate (Emal 270d), cocamidopropylaminoxide SAO (Yevroksid SRO), stearox, Syntanol ALM-10, sulphonol (pasta of mark “technical”) were first tested. To intensify the process of sediment loss, the possibility of using an acidic agent such as alkyl benzene sulfuric acids (ABSA) was investigated. As a research result, the combination of neonol AF 9-12 and ABSA led to the best result.

In Fig. 5, the result is presented as scheme for neutralization of waste cooling lubricants developed and proposed for railway usage.

The use of the technology suggested provides the following indices: the degree of purification is 71.4%, the yield of purified water is 95.3%, the yield of oil and petroleum products is 1.7%.

The oil and petroleum products obtained can be offered as commodities to various petroleum refineries, and companies producing concrete constructions, asphalt.

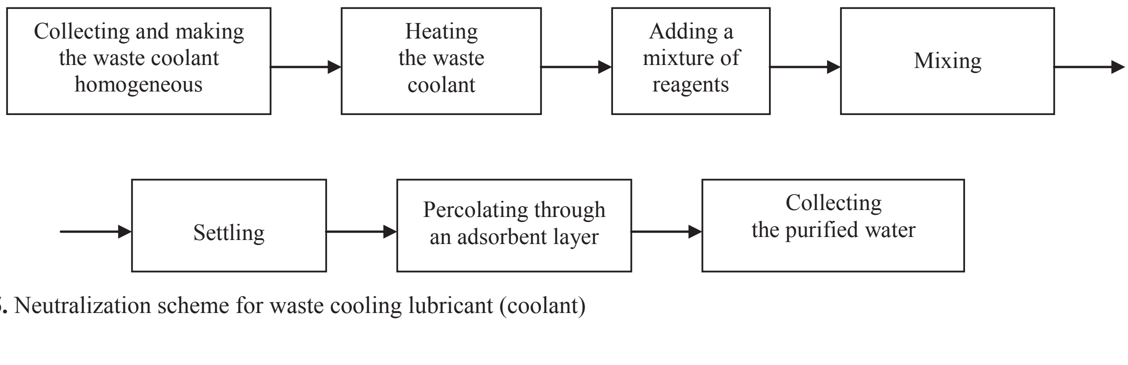

Fig. 5. Neutralization scheme for waste cooling lubricant (coolant)

The water purified can be used in industrial turnover for internal consumption or for the preparation of new cooling lubricant or while maintaining the sanitary requirements it can be dropped into urban sewer network and even into the water basins.

The water after regeneration of the adsorbent can be used for washing a railway rolling stock.

The given technology can be applied in metalworking shops of railway enterprises, machine-building, metallurgical and other industries, where coolant-containing drainage is a part of wastewater complex generated. One of the most promising examples of using this technology for recycling a waste coolant is its introduction at local purification stations of locomotive and wagon depots, as well as railway stations of complex neutralization.

CONCLUTIONS

1. The scheme for a waste compressor oil CS-19 developed and proposed for railway usage. Yield of purified product with using this scheme is about 91.3%, while for treatment it was 86.7%.
2. The proposed scheme sludge processing using centrifuge-decanter and heat exchanger.
3. The scheme for neutralization of waste cooling lubricants that proposed for introduction at local treatment plants and locomotive depots, as well as comprehensive utilization railway stations.
4. The technology for neutralization of waste cooling lubricants ensures a double effect: the environmental effect (owing to minimizing the amount of waste belonging to the IIIrd class of danger, and rational use of water resources) and the economic impact (due to reusing the water in the circulating system of water supply as well as oil and petroleum products).

REFERENCES

1. **Anserov Yu.M., Durnev V.D., 1989:** Engineering and environmental protection, Leningrad, Mashinostroenie, 224.
2. **Bannov P.G., 2005:** Principles of analysis and standard methods for quality control of oil products Moscow, TsNIITEneftehim, 792.
3. **Bezovska M.S., Zelenko Yu.V., 2012:** New eco-model himmotolohichni treatment of waste oils railways, National scientific and technical journal «Questions of chemistry and chemical technology», Dnepropetrovsk «New ideology», №1, 145-148.
4. **Bezovska M.S., Zelenko Yu.V., YarishkIna L.O., 2009:** Waste oils: formation, storage, regeneration, Scientific journal «Railway Transport of Ukraine», Kiev, Vid-vo DNDTs UZ, №6, 33-35.
5. **Bezovska M.S., Zelenko Yu.V., YarishkIna L.O., Babenko O.B., 2008:** Utilization of oil sludge and oil generated in the structural units of railways, Scientific journal «Railway Transport of Ukraine», Kiev, Vid-vo DNDTs UZ, №1, 36-38.
6. **Bezovska M.S., Zelenko Yu.V., YarishkIna L.O., Shevchenko L.V., 2011:** Development of a common scheme of regeneration of waste oils railways, Vestnik HNTU, №1 (40), 43-47.
7. **Boychenko S.V., Ivanov S.V., Burlaka V.G., 2005:** Motor fuels and oils for a modern technique: Monograph, Kiev, NAU, 216.
8. **Chayka O.H., 2012:** Prevention of Environmental Pollution spent motor oil, Abstract for the degree of candidate. Sc. Sciences, Sumy: SumDU, 21.
9. **Evdokimov A.Yu., Fuks I.G., Shabalina T.N., Bagdasarov L.N., 2000:** Lubricating materials and problems of ecology, Moscow, GUP Izd-vo Neft i gaz RGU nefti i gaza im. I.M. Gubkina, 424.
10. **Koganovskiy A.M. and others, 1989:** Purification of waste water and industrial, Moscow, Himiya, 288.
11. **Kostyuk V.I., Karnauh G.S., 1990:** Waste water treatment engineering companies, Kiev, Tehnika, 120.
12. **Leshchynskaya A.L., Zelen'ko Y.V., Bezovskaya M.S., 2012:** Technology of restoration of the fulfilled compressor oils of the railway enterprises, Zbirnik naukovih prats DonIZT, №31, 198-201.
13. **Leshchynskaya A.L., Zelen'ko Y.V., Bezovskaya M.S., 2013:** The use of surfactants to recover waste oils, National scientific and technical journal "Questions of chemistry and chemical technology", Dnepropetrovsk "New ideology", №3, 181-184.
14. **Leshchynskaya A.L., Zelen'ko Yu. V., Sandowski M., 2013:** Development of resource-saving technologies of utilization of the fulfilled lubricant cooling fluids, Scientific journal «Railway Transport of Ukraine», Kiev, Vid-vo DNDTs UZ, №3-4.
15. **Nikulin F.E., 1990:** Recycling and treatment of industrial waste, Leningrad, Sudostroenie, 232.
16. **Plahotnik V.N., Yaryishkina L.A., Sirakov V.I. and others, 2001:** Environmental activities at the railway transport of Ukraine: problems and solutions, Kiev, Transport Ukrainyi, 244.
17. **Proskuryakov V.A., Shmidt L.I., 1997:** Wastewater treatment in the chemical industry, Moscow, Himiya, 464.
18. **Shashkin Y.I., Bray I.V., 1990:** The regeneration of waste oilsб Moscow,Himiya, 304.
19. **Shkolnikov V.M., 1999:** Fuels, lubricating materials, technical liquids. Assortment and application. Reference book, Moscow, Tehinform, 596.
20. **Smetanin V.I., 2003:** Protecting the environment from waste production and consumption: a training manual, Moscow, Koloss, 230.
21. **Smirnov D.N., Genkin V.E., 1989:** Cleaning of effluents is in the processes of treatment of metals, Moscow, Metallurgiya, 224.
22. **Sultan Ramazanov, Anna Voronova, 2014:** Economic-mathematical modeling of rational water use and minimization engineering enterprise's negative impact on the environment// TEKA Commission of Motor.

and Energ. in agriculture. – Lublin – Lugansk. – 2014, Vol. 14.

23. **TsT–0060: Instructions for use of lubricants for traction rolling stock of railways of Ukraine, 2003**, Kiev, Standart, 51.
24. **Zelenko Yu.V., 2010:** Scientific bases of ecological safety of technology of transporting and use of oil products on a railway transport: Monograph, Dn-vsk, Vid-vo Makovetskiy, 192.
25. **Zerkalov D.V., 1998:** Economy of oil products, Kiev, TOV „MIzhnar. fIn. agentsIya", 197.
26. **Zerkalov D.V., 1998:** Ecologization of energy consumption, Kiev, TOV „Mizhnar. fin. agentsiya", 273.

РАЗРАБОТКА НОВЕЙШИХ ТЕХНОЛОГИЙ ПЕРЕРАБОТКИ И УТИЛИЗАЦИИ НЕФТЕСОДЕРЖАЩИХ ОТХОДОВ ПРЕДПРИЯТИЙ ЖЕЛЕЗНОДОРОЖНОЙ ИНФРАСТРУКТУРЫ

Аннотация. В статье рассмотрены традиционные методы утилизации и регенерации отработанных смазочно-охлаждающих жидкостей и компрессорных масел. При разработке схем регенерации нефтесодержащих отходов с целью формирования и расчета предложенных технологических схем была проведена оптимизация технологического процесса, а именно температуры, количества реагента и времени контакта. Предложены новые технологии с использованием поверхностно-активных веществ.

Ключевые слова: отработанные компрессорные масла, смазочно-охлаждающие жидкости, поверхностно-активные вещества, экологическая безопасность, утилизация.

TEKA. COMMISSION OF MOTORIZATION AND ENERGETICS IN AGRICULTURE – 2014, Vol. 14, No. 4, 81–86

Strength Properties of Horse Bean Seeds (*Vicia faba L. var. minor*)

Rafał Nadulski[1], Jacek Skwarcz[2], Grzegorz Łysiak[3], Ryszard Kulig[3]

[1]Department of Food Engineering and Machines,
[3]Department of Equipment Operation and Maintenance in the Food Industry University of Life Sciences,
Doświadczalna 44, 20-280 Lublin, Poland, e-mail: rafal.nadulski@up.lublin.pl
[2]Department of Technology Fundamentals, University of Life Sciences,
ul. Doświadczalna 50A, 20-280 Lublin, Poland

Received December 02.2014; accepted December 17.2014

Summary. The research results of the seed strength properties concerning three horse bean varieties are presented here. The investigation was carried out under quasistatic conditions by means of the apparatus Instron 4302. Individual horse bean seeds were placed with their cotyledons parallel to the apparatus base and loaded with plate, slat or penetrator. The maximum force values and corresponding to them deformation values capable of transporting a seed to the destruction moment have been read off from the obtained force-deformation characteristics. In the course of investigations, it was found out that the hardness features depended to a great extent on a given variety. It has been stated additionally that the increase of seeds moisture content causes a considerable decrease of their hardness.
Key words: horse bean, variety, strength properties.

INTRODUCTION

In Poland, where animal feeding is In 80% based on imported soya grits, the crucial problem is finding the alternating source of protein in animal feeding [10]. Oil industry products (rapeseed oil cake and press cake) as well as seeds of leguminous plants (e.g. lupine, horse bean and pea) are the domestic products which can replace soya bean having comparable protein content [9]. Horse bean seeds containing from 26% to 32% of the protein constitute a good component for the production of the feed mixture [11]. The protein from horse bean seeds is characterized by the high biological value and the wide usefulness for feeding. The interest in horse bean (*Vicia faba SPP. minor*) cultivation as a valuable feeding has developed in Poland and other countries with similar climate conditions [17].

The physical properties of seeds are to be known for design and improve of relevant machines and facilities for harvesting, storing, handling and processing [2, 5, 12, 13, 16]. A wide survey of literature shows small number of publications in the research work concerning horse bean seeds (*Vicia faba L. var. minor*) hardness. The investigations on this subject have been carried out only by few researches [4, 6, 7, 14, 18]. Only few papers deal with investigations of mechanical properties of (*Vicia faba L. var. major*) [1, 8]. Taking into consideration the fact that the knowledge of horse bean seeds hardness is indispensable in working out technological processes and preservation of machines necessary in their processing and allows to characterize the quality of material, and therefore it is well motivated to carry out the research work whose results aim at establishing the characteristics of horse bean seeds (*Vicia faba L. var. minor*). In measuring seed resistance loading by means of penetrators with different endings /in the shape of cylinder, cone, or semicircle/ has been used. Taking into account fact that in processing seed material into feed there is a wide use of a beater in which a working element differs in its shape from loading elements used in resistance measurements, it has been decided to carry out such investigations using a loading slat with blunt edge – an element similar in its shape to beater. The seed of loading plays an important role in all investigations concerning seed resistance that aim at reflecting the conditions approximating these in real life, while to carry out any investigations under such conditions is very difficult therefore measurements presented here have been carried out under quasistatic loading conditions.

The goal of this research work has been to determine hardness features of horse bean seeds having different moisture content under quasistatic loading of seeds with plate, slat and penetrator. Additionally, the results obtained enabled to comparison of the values of seed resistance measured by three different methods.

MATERIAL AND METHODS

The research work has been carried out on horse bean seeds of Dębek, Nadwiślański and Jasny varieties. In order to establish the influence of seeds moisture content and size on the investigated hardness features, the input material was humidified into eight moisture content levels in the range from 10 *%* to 24 *%* every ca 2 *%,* and then it was divided according to thickness. The seeds moisture contents were determined using the oven-drying method. Selected fraction of seeds with thickness from 7.0 to 8.0 mm was used for the compression experiments. For each moisture, 30 repetitions were done. The measurements of hardness features have been carried out by means of Instron 4302 apparatus equipped with head with a loading range 0-1.0 kN. Individual seeds have been placed with their cotyledons parallel to the lower stationary plate, and then, they were loaded by means of a disc, cutting slat 1 mm thick or a penetrator with a cylinder end with diameter 1,0 mm thick. Loading elements have been moving in all cases with a constant speed v = 10 mm·min^{-1} according to the standard proposition presented by Frączek et al [3]. The loading force operated along the seed thickness. The measurements have been carried out to the seed destruction moment i. e. splitting, cutting, or puncturing of seed coat. After that, they ended. The force curve as deformation functions were recorded. Then, the values of deformation forces for the seeds loaded with plate F_n, slat F_c or penetrator F_p were read from the obtained graphs together with the relative deformation values (e_n, e_c, e_p) corresponding to these forces. The deformation work for seeds loaded with plate (W_n), slat (W_c) and penetrator (W_p)was determined as the area below the curve in the force – deformation relation [15].

Statistical analysis of the data was performed with Statistica software (Statistica 6.1, StatSoft Inc., Tulsa, OK, USA) using analysis of variance for factorial designs. The significance of differences between mean values was determined using Fisher's exact test at a level of $p < 0.05$. The investigation parameters have been made to depend on moisture content and the obtained relations have been described by means of regression equation.

RESULT AND DISCUSSION

In Table 1 the minimal and maximum force values obtained by means of different methods of horse bean seed loading has been presented. The highest hardness value of seeds loaded by plate, slat and penetrator is characteristic of dry horse bean seed of Jasny variety. The lowest hardness value of seeds loaded by plate, slat and penetrator is characteristic of dry horse bean seed of Dąbek variety.

Table 1. Deformation force *F* values for horse bean seeds loaded by plate, slat and penetrator

Variety	Moisture content, %	Extreme value of forces F, N		
		plate loading	slat loading	penetrator loading
Dębek	10.1-23.9	156.1-445.2	48.2-199,1	20.4-212.2
Nadwiślański	10.4-23.8	148.2-554.3	53.4-279.9	26.2-342.4
Jasny	10.2-23.9	188.2-665.4	94.2-295.3	31.1-408.9

The greatest difference of force values occur in the case of horse bean seeds of Nadwiślański i Jasny variety loaded by penetrator. In this case maximum forces are nearly 13 times higher than the minimum ones. Much smaller differences between the maximum and minimum forces were observed in case of seeds loaded with a plate.

The changes of the values of deformation forces depending on seed moisture content were shown in Fig. 1, 2 and 3. The increase of seed moisture content causes a considerable decrease of their hardness.

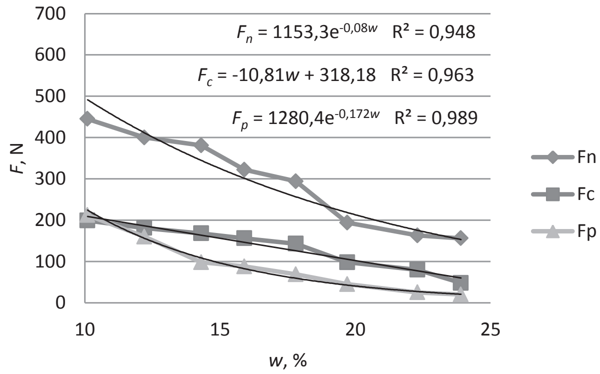

Fig. 1. The influence of moisture content (%) on deformation force for horse bean seed variety Dębek loaded by plate (F_n), penetrator (F_p) and slat (F_c)

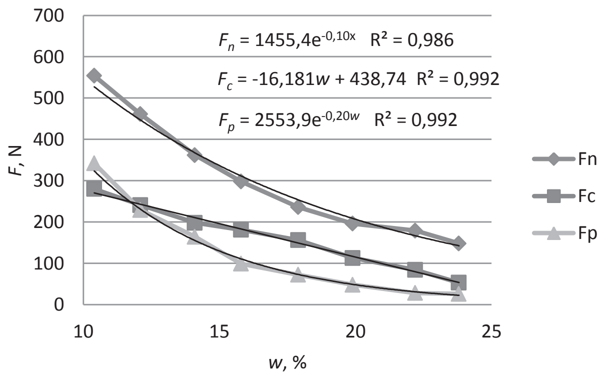

Fig. 2. The influence of moisture content (%) on deformation force for horse bean seed variety Nadwiślański loaded by plate (F_n), penetrator (F_p) and slat (F_c)

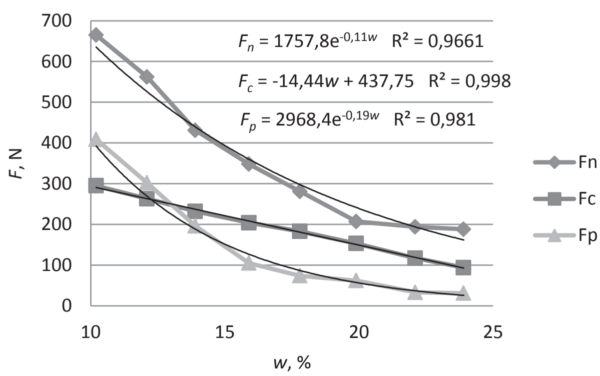

Fig. 3. The influence of moisture content (%) on deformation force for horse bean seed variety Jasny loaded by plate (F_n), penetrator (F_p) and slat (F_c)

In Table 2 the relative deformation values corresponding to the deformation force values obtained by seed loaded with plate, slat and penetrator have been presented. It has been stated that deformation values depend moisture content and horse bean variety. The highest deformation values in all loading cases have been obtained for horse bean seeds with about 24 % moisture content of Jasny variety.

Table 2. Relative deformation *e* values for horse bean seeds loaded by plate, slat and penetrator

Variety	Moisture content, %	Min-max value of relative deformation *e*, %		
		plate loading	slat loading	penetrator loading
Dębek	10.1-23.9	4.9-26.4	5.1-22.9	4.8-14.2
Nadwiślański	10.4-23.8	5.6-25.6	6.8-24.1	5.2-14.4
Jasny	10.2-23.9	5.2-25.6	6.9-26.9	6.8-17.2

For all the varieties, the increase of seed moisture content causes the increase of deformation values and the maximal values are 3-5 times higher than minimal. The lowest values of the relative deformation were obtained for seeds loaded with the penetrator. The changes of the values of relative deformation depending on seed moisture content were shown in Fig. 4, 5 and 6. In each case the increase in moisture content of seeds causes the increase in the relative deformation values.

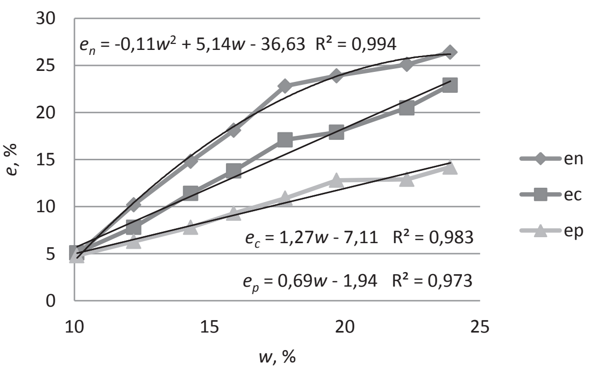

Fig. 4. The influence of moisture content (%) on relative deformation *e* for horse bean seed variety Dębek loaded by plate (e_n), slat (e_c) and penetrator (e_p)

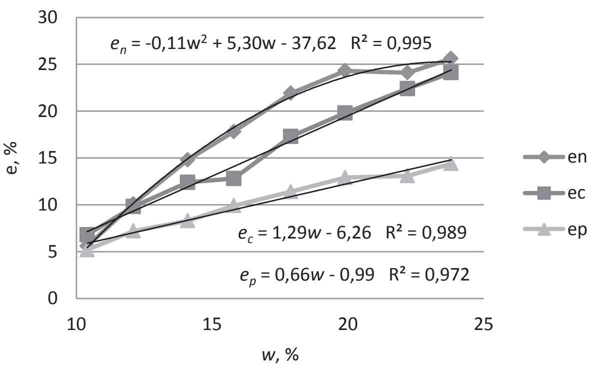

Fig. 5. The influence of moisture content (%) on relative deformation *e* for horse bean seed variety Nadwiślański loaded by plate (e_n), slat (e_c) and penetrator (e_p)

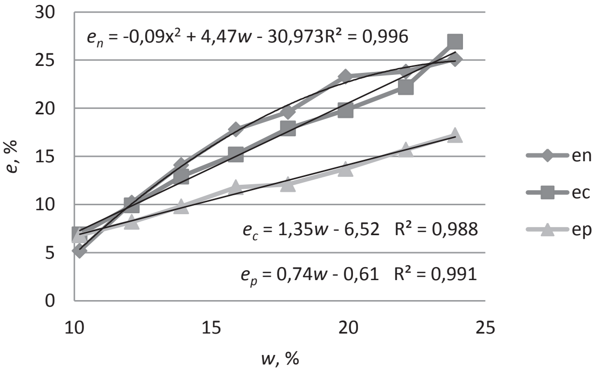

Fig. 6. The influence of moisture content (%) on relative deformation *e* for horse bean seed variety Jasny loaded by plate (e_n), slat (e_c) and penetrator (e_p)

In Table 3 the work of deformation values obtained by seed loaded with plate, slat and penetrator have been presented. It has been stated that the work of deformation values depend on moisture content of seeds and horse bean variety. The biggest differences between the minimum and maximum values of the deformation work were observed in case of the penetrometric test.

Table 3. Work of deformation *W* values for horse bean seeds loaded by plate, slat and penetrator

Variety	Moisture content, %	Min-max value of work of deformation *W*, J		
		plate loading	slat loading	penetrator loading
Dębek	10.1-23.9	0.053-0.221	0.211-0.681	0.007-0.051
Nadwiślański	10.4-23.8	0.112-0.292	0.212-0.821	0.024-0.084
Jasny	10.2-23.9	0.093-0.231	0.223-0.912	0.022-0.141

The changes of the values of relative deformation depending on the seed moisture content were shown in Fig. 7, 8 and 9. In case of seeds loaded with plate and slat the value of deformation work gradually increases with the increase in moisture content of seeds and after reaching the maximum it slightly decreases. In case of the penetrometric test the increase in seed moisture causes the constant gradual decrease in work deformation value.

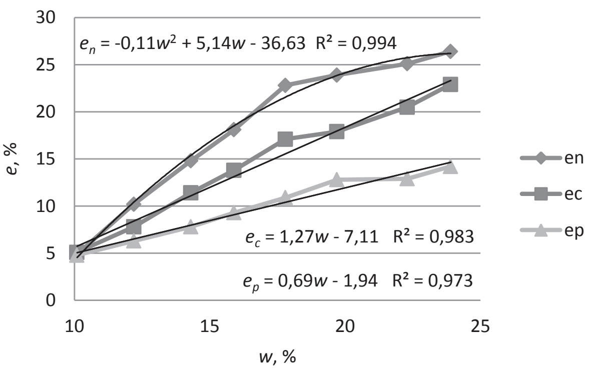

Fig. 7. The influence of moisture content (%) on the work of deformation for horse bean seed variety Dębek loaded by plate (W_n), penetrator (W_p) and slat (W_c)

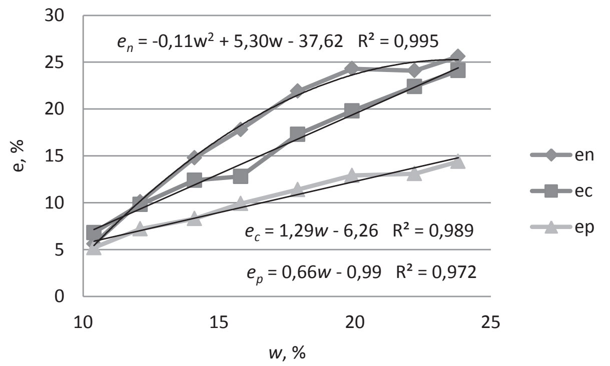

Fig. 8. The influence of moisture content (%) on the work of deformation for horse bean seed variety Nadwiślański loaded by plate (W_n), penetrator (W_p) and slat (W_c)

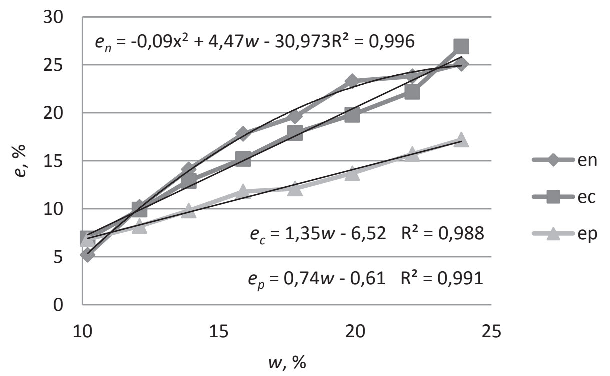

Fig. 9. The influence of moisture content (%) on the work of deformation for horse bean seed variety Jasny loaded by plate (W_n), penetrator (W_p) and slat (W_c)

The carried out analysis shows that using only one test in seed strength tests may not be enough. It is essential especially in case of the measurement of deformation work of loaded seeds. Different relationship between deformation work and seed moisture is observed depending on the test. In case of deformation strength and relative deformation, however, different scope and dynamics of the change with the increase in seed moisture depending on the used strength test was noticed.

CONCLUSIONS

The carried out investigations concerning hardness allow to formulate the following conclusions:

1. Deformation force, relative deformation and work of deformation depend on horse bean variety.
2. In the case of the all used tests the increase of seeds moisture content causes a considerable change of their strength properties.
3. The increase in seed moisture causes the significant decrease in the value of deformation strength. The dependence between the deformation strength and seed moisture was described by exponential equations in case of loading the seeds with the plate and penetrator and by linear equations in case of seeds loaded with the slat.
4. The increase in seed moisture causes the significant increase in relative deformation value. The dependence between the relative deformation and seed moisture was described with the linear equation in case of seeds loaded with the slat and penetrator and with quadratic equations in case of loading the seeds with the slat.
5. In case of seed loaded with the plate and slate the increase in seed moisture causes the gradual increase in deformation work and after reaching the maximum the decrease in its value. In case of the penetrometric test increase of seeds moisture content causes a considerable decrease of deformation force. The dependence between the deformation work and seed moisture was described by quadratic equations in case of seed loaded with the plate and slat and by exponential equations in case of penetrometric test.
6. The choice of strength test influences the scope and dynamics of changes of seed resistance for mechanical loading. Thus, to describe fully the changes of seed resistance for mechanical loading it is advisable to use the results obtained in different strength tests.

REFERENCES

1. **Altunta E., Yıldız M. 2007.** Effect of moisture content on some physical and mechanical properties of faba bean (*Vicia faba L.*) grains. Journal of Food Engineering 78, 174–183.
2. **Dziki D., Cacak-Pietrzak G., Biernacka B., Jończyk K., Różyło R., Gładyszewska B. 2012.** The grinding energy as an indicator of wheat milling value. TEKA Commission of Motorization and Energetics in Agriculture, Vol. 12(1), 29-33.
3. **Frączek J., Kaczorowski J., Ślipek Z., Horabik J., Molenda M. 2003.** Standarization of methods for the measurement of the physico-chemical properties of plant granular materials (in Polish). Acta Agrophysica, 92.
4. **Gorzelany, J., Puchalski, C. 1994.** The effect of loading-force direction and magnitude on mechanical damage to horse bean seeds. Zemědělska Technika, 40(2), 105-112.
5. **Grochowicz J., Andrejko D. 2006.** Effect of the moisture content on energy consumption at grinding of lupine seeds. TEKA Commission of Motorization and Energetics in Agriculture, Vol. 6, 22-28.
6. **Grochowicz J., Nadulski R. 1984.** The Influence Humidity and Horse Bean Size on Their Strength Characteristics. Conference materials VII Golloąuium Gate – PAN, Agricultural University, Godollo, Hungary.
7. **Grochowicz J., Nadulski R. 1985.** The Mechanical Properties of Some Leguminous Plant Seeds. Conference materials. 3rd International Conference CIGR, "Physical Properties of Agricultural Materials", Praga, Czechoslovakia, 289-292.
8. **Hacıseferogulları H., Gezer I., Bahtiyarca Y., Menge H.O. 2003.** Determination of some chemical and physical properties of Sakız faba bean (*Vicia faba L. Var. major*). Journal of Food Engineering, 60, 475–479.
9. **Hanczanowska E., Księżak J. 2012.** Krajowe źródła białkowych pasz roślinnych jako zamienniki śruty sojo-

wej GMO w żywieniu świń (in Polish). Roczniki Nauk Zootechniki, 39(2), 171–187.

10. **Jerzak M.A., Czerwińska-Kayzer D., Florek J., Śmiglak-Krajewska M. 2012.** Determinanty produkcji roślin strączkowych jako alternatywnego źródła białka – w ramach nowego obszaru polityki rolnej w Polsce (in Polish). Roczniki Nauk Rolniczych, Seria G, t. 99, z. 1, 113-120.
11. **Kulig B., Pisulewska P., Sajdak A. 2007.** Wpływ ilości wysiewu na plonowanie oraz wielkość powierzchni asymilacyjnej wybranych odmian bobiku (in Polish). Zeszyty Problemowe Postępów Nauk Rolniczych, z. 522, 263-270.
12. **Kuźniar P., Jarecki W., Bobrecka-Jamro D. 2013.** Właściwości mechaniczne nasion wybranych roślin strączkowych a ich masa i grubość. Inżynieria Rolnicza. 4(1470), 171-178.
13. **Laskowski J., Skonecki S. 2006.** Wpływ wielkości komory i masy materiału na zagęszczanie nasion bobiku. Inżynieria Rolnicza, 3 (78), 225-232.
14. **Łysiak G., Laskowski J. 2004.** Investigation of mechanical properties of faba bean for grinding behavior prediction. Acta Agrophysica, 4(3), 753-762.
15. **Mohsenin N. N. 1986.** Physical Properties of Plant and Animal Materials: Structure, Physical Characteristics, and Mechanical. 2nd Edn, Gordon and Breach. New York, USA.
16. **Nadulski R., Kusińska E., Kobus Z., Guz T. 2012.** Effect of selected factors on grain mass creep test under simulated load conditions. TEKA Commission of Motorization and Energetics in Agriculture, Vol. 12(1), 159-162.
17. **Prusiński J. 2007.** Postęp biologiczny w hodowli i uprawie grochu siewnego i bobiku. Fragmenta Agronomica, 4(96), 113-119.
18. **Sosnowski, S. 1991.** Determining of the influence of the direction of loading forces on mechanical damage of bean seeds. Zeszyty Problemowe Postępów Nauk Rolniczych, 389, 176-183.

WŁAŚCIWOŚCI WYTRZYMAŁOŚCIOWE NASION BOBIKU (*VICIA FABA L. VAR. MINOR*)

Streszczenie. W pracy przedstawiono wyniki dotyczące badań właściwości wytrzymałościowych nasion trzech odmian bobiku. Badania przeprowadzono w warunkach obciążeń quasistatycznych przy użyciu maszyny wytrzymałościowej Intron 43002. Nasiona umieszczano liścieniami równolegle do podstawy urządzenia a następnie obciążano przy pomocy płyty, noża i penetratora. Z wykresu siła-przemieszczenie wyznaczono maksymalną siłę prowadzącą do zniszczenia nasiona, odpowiadającą jej przemieszczenie i pracę deformacji. Wykazano, że wytrzymałość nasion istotnie zależy od odmiany. Stwierdzono, że wzrost wilgotności nasion powoduje wyraźny spadek ich wytrzymałości mechanicznej.

Słowa kluczowe: bobik, odmiana, właściwości wytrzymałościowe.

TEKA. COMMISSION OF MOTORIZATION AND ENERGETICS IN AGRICULTURE – 2014, Vol. 14, No. 4, 87–92

Comparative Analysis of The Variability of Daily Electric Power Loads

Krzysztof Nęcka, Małgorzata Trojanowska

Department of Power Engineering and Agricultural Processes Automation, Agricultural University of Cracow
Balicka Str. 116B, 30-149 Cracow, Poland
e-mail: krzysztof.necka@ur.krakow.pl; malgorzata.trojanowska@ur.krakow.pl

Received December 02.2014; accepted December 17.2014

Summary. This publication analyses the variability of loads in rural medium and low voltage distribution networks compared to the variability of energy demand in the national power grid. Values of standard indicators used to characterise power demand, such as load factors and balancing factors, have been identified and compared. This analysis was carried out based on data recorded at 6 main supply stations and 37 15/0.4 kV transformer stations.
Key words: power grid, distribution networks, load variability.

INTRODUCTION

One of the important problems of power system engineering is to optimise the time curves of electrical loads, which practically boils down to balancing them and reducing peak power. This is why it is so important to correctly analyse power demand curves. In order to characterise their variability, various measures (functions and coefficients) are used, whose examples can be found in the literature of the subject [2, 3, 4, 7, 8, 9, 11, 12, 13, 14]. The majority of these measures come from classical methods of analysing power system loads [1, 6, 10]. These make it possible to characterise loads during 24 hours, a week, a month and a year, at various supply voltages, caused by individual consumers, groups of consumers or all consumers in total. The total of loads of all consumers constitutes the load on the national power grid ("national grid"). In practice, it is not only analyses of the curves themselves that are important, but also their comparisons.

This publication presents the results of a comparative analysis of the variability of loads in rural medium (MV) and low voltage (LV) distribution networks compared to the variability of energy demand in the national power grid. Since it is only the variability of load over 24 hours that is significant for power system management, this publication is limited to analysing the 24h variability of power demand, which has been described using standard indicators characterising electrical power loads.

MATERIALS AND METHODS

This analysis is based on the results of power measurements taken at the main supply stations on the medium voltage side and in MV/LV transformer-distribution stations on the low voltage side. In total, research work covered 6 main supply stations over at least 1 year and 37 MV/LV stations. Figures on national grid loads were taken from *Monthly reports on the operation of the National Power Grid and the Balancing Mechanism.*

RESULTS

For the purpose of this comparative analysis, reduced load graphs were drawn, with mainly relative indicators used to characterise load curves. The reference value was either peak load P_s and indicators thus calculated are referred to as load factors m, or the average load P_{sr}, with balancing factors l being calculated. Detailed definitions of load and balancing factors can be found, *inter alia*, in the collective publication [1971] and in Góra's publication [1975].

The 24h variability of loads is most frequently presented graphically, usually as a calendar graph. The comparison of individual power values to the peak power produces the reduced graph of loads. These were the graphs plotted for the analysed systems. Internal analyses confirmed other authors' observations that the 24h curve of power consumption is mainly driven by the rhythm and intensity of human activities and the season of the year (Fig. 1). Consequently, when presenting the variability of power demand, averaged profiles of loads contrasted with the annual peak power P_{sr} were presented separately for different seasons, split into business days and holidays (Fig. 2-3). Figures 2a and 3a present graphs of national grid loads in the form of averaged load curves for 9 years, thus significantly reducing the random factor. The remaining illustrations are 24h schedules of loads on systems supplying rural consumers. A characteristic feature of these curves is the smooth, low load during the morning peak starting around 6 a.m. regardless of the season and type of day, and a general lack of an afternoon trough. Changes in the shape of load curves are mainly caused by the changing length of the day, influencing the time at which the evening peak load materialises. In winter, the evening peak starts around 4 p.m., but in summer as late as at 7 p.m. and lasts almost till 11 p.m. The season also influences the level of power demand, which is much greater in winter than in summer.

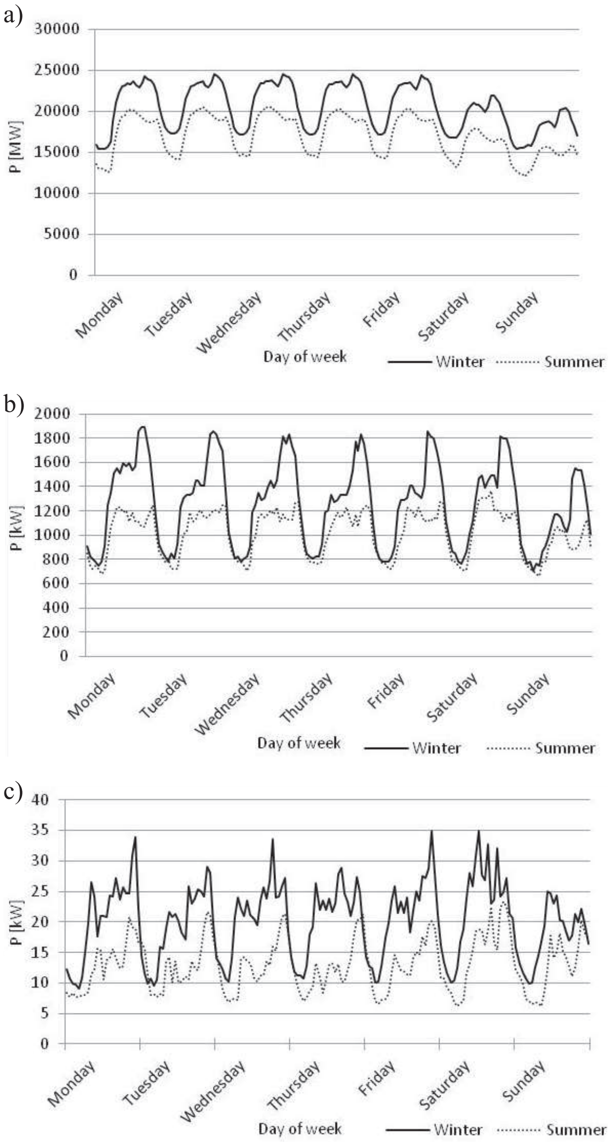

Fig. 1. Example curves of the power demand variability in selected periods of the year: a) national grid, b) MV, c) LV

To characterise loads over 24 hours, mean values of daily load and balancing factors were determined for the analysed systems. In particular, the following were calculated [1, 6, 12]:

– average load factor:

$$m = \frac{P_{sr}}{P_s} \quad , \tag{1}$$

– base load factor:

$$m_o = \frac{P_o}{P_s} \, , \tag{2}$$

– balancing factor of the base load:

$$l_o = \frac{P_o}{P_{sr}} \quad , \tag{3}$$

where: P_o, P_{sr}, P_s represent the base (lowest), mean and peak power, respectively.

Mean values of these indicators for business days and holidays, split by season, are presented in Table 1, while their values for a selected winter and summer week for exemplary transformer-distribution stations and the national grid are shown in Figure 4.

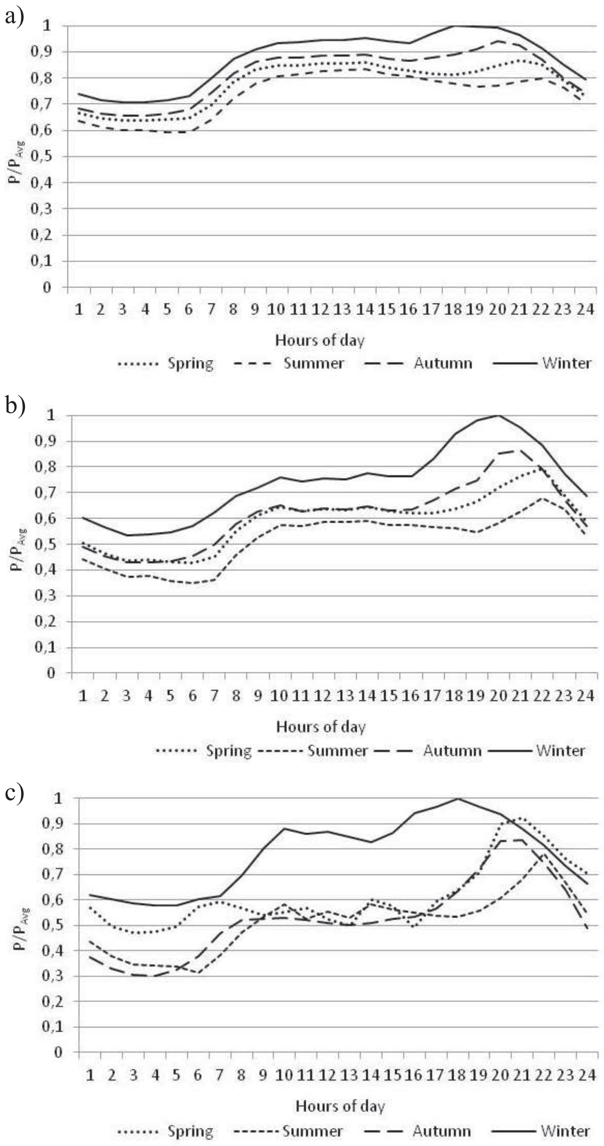

Fig. 2. Averaged load profiles during a business 24h period: a) national grid, b) MV, c) LV

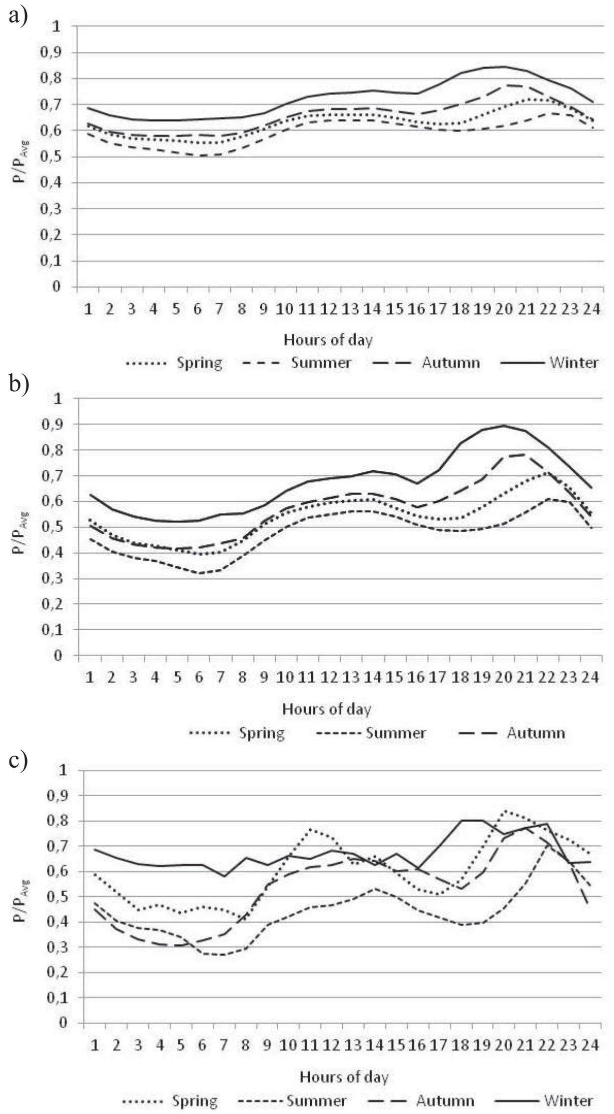

Fig. 3. Averaged load profiles for a 24h holiday period: a) national grid, b) MV, c) LV

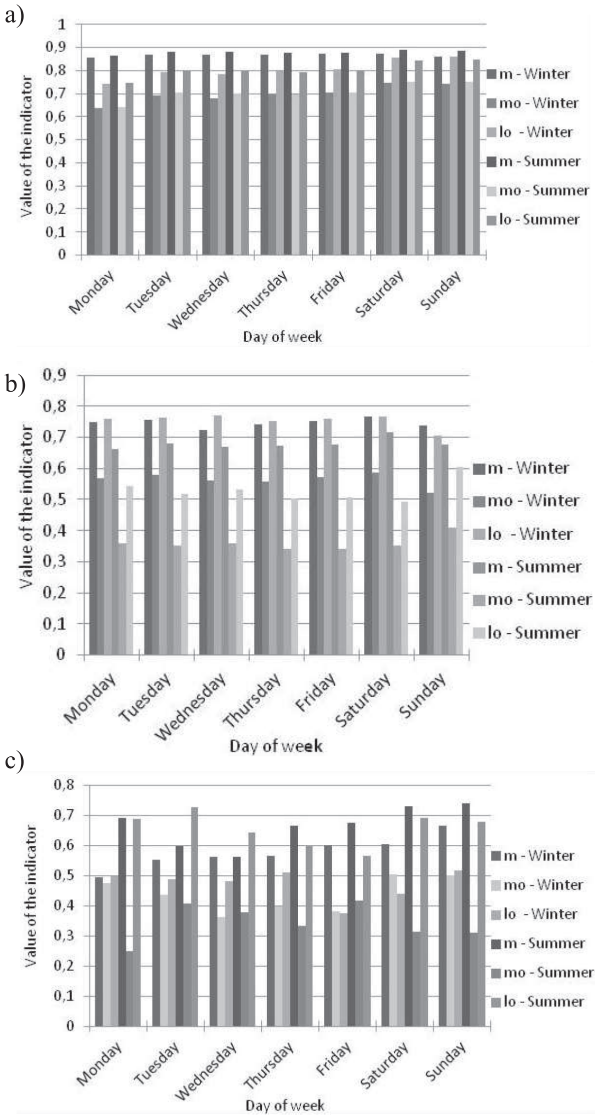

Fig. 4. Daily load and balancing factor values in a selected winter and summer week for the national power grid and for exemplary transformer-distribution stations: a) national grid, b) MV, c) LV

Table 1. Mean values of daily load and balancing factors

Period		National Grid			MV			LV		
		m	m_o	l_o	m	m_o	l_o	m	m_o	l_o
Business day	spring	0,88	0,70	0,80	0,70	0,46	0,65	0,50	0,19	0,34
	summer	0,87	0,69	0,78	0,69	0,40	0,58	0,65	0,37	0,55
	autumn	0,85	0,66	0,77	0,68	0,46	0,67	0,57	0,29	0,48
	winter	0,86	0,68	0,78	0,75	0,54	0,72	0,63	0,35	0,54
Holiday	spring	0,86	0,74	0,86	0,72	0,49	0,67	0,54	0,20	0,32
	summer	0,89	0,74	0,83	0,71	0,43	0,60	0,66	0,39	0,58
	autumn	0,84	0,72	0,85	0,68	0,46	0,68	0,62	0,31	0,48
	winter	0,86	0,73	0,85	0,75	0,56	0,74	0,67	0,43	0,62
average		0,87	0,72	0,82	0,73	0,49	0,68	0,60	0,31	0,48
coefficient of variation [%]		2,3	6,7	5,6	7,1	13,7	9,4	20,3	55,6	42,7

The lowest values of the analysed indicators, and their greatest variabilities, characterise the curves of power demand recorded on the low voltage of a MV/LV transformer station and confirm a significant inequality of power demand. The m_o indicator is best suited for assessing the load inequality. Its lowest values for 24h loads caused by consumers supplied at low voltage are observed in the spring, on Mondays, Saturdays and Sundays. Load inequality assessed by the value of m_o on medium voltage is, on average, one third lower than on the low voltage, and approx. one third greater than in the national grid.

The indicator most frequently used for analysing the variability of loads in Poland and abroad is the average load factor *m* [5]. It is also used to classify consumer load schedules and predict the electrical capacity and energy demand. Figures 5 and 6 show the values of this indicator for individual days of the week and individual months of the year.

As graphs for the entire power grid and medium voltage grids show, neither the season of the year nor the type of day influences the average values of the *m* indicator. The impact of the season is observable only for the low voltage grid, in which the mean value of *m* changed in the studied period from 0.46 in November to 0.68 in July.

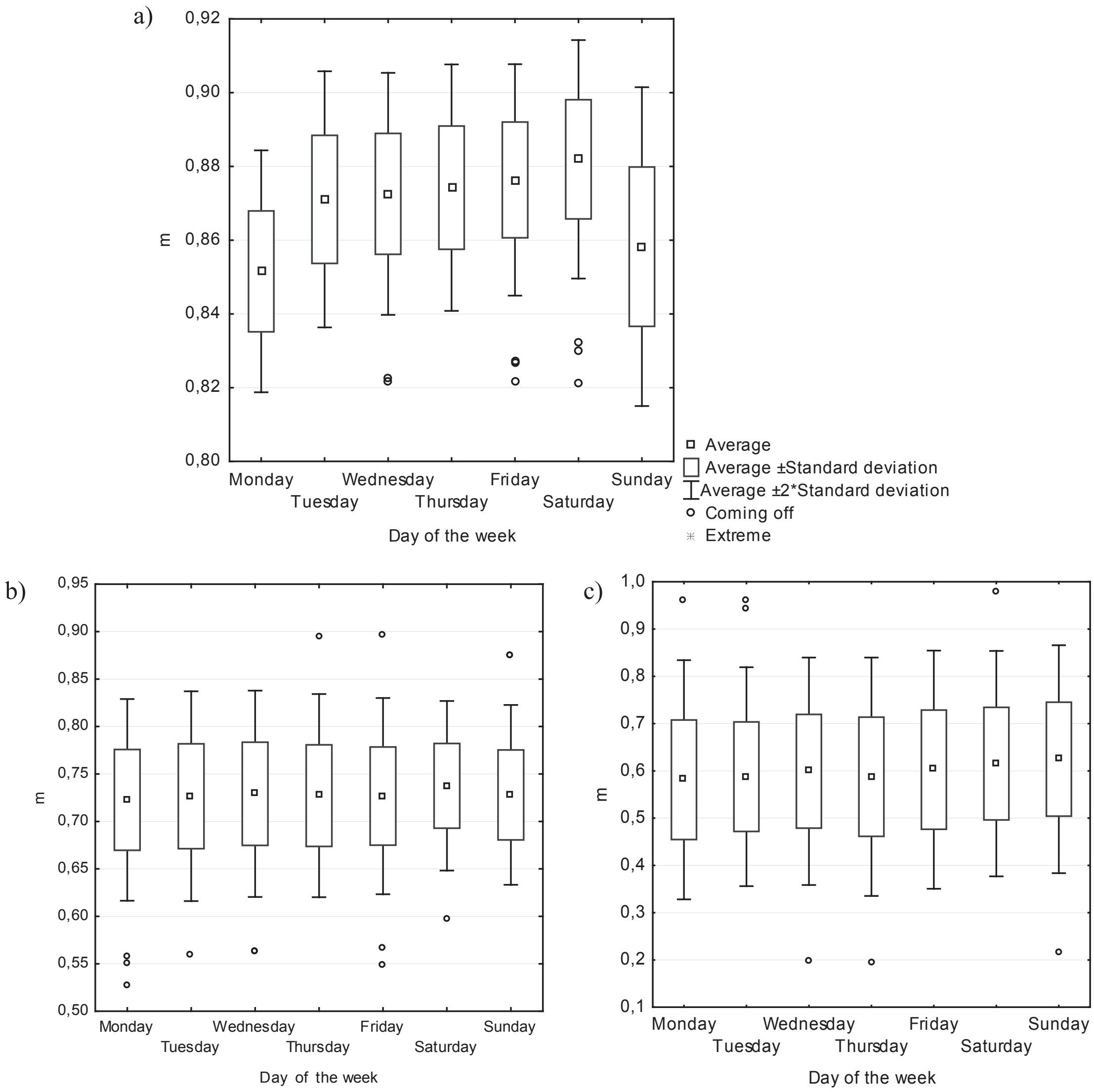

Fig. 5. Weekly variability of the *m* indicator: a) national grid, b) MV, c) LV

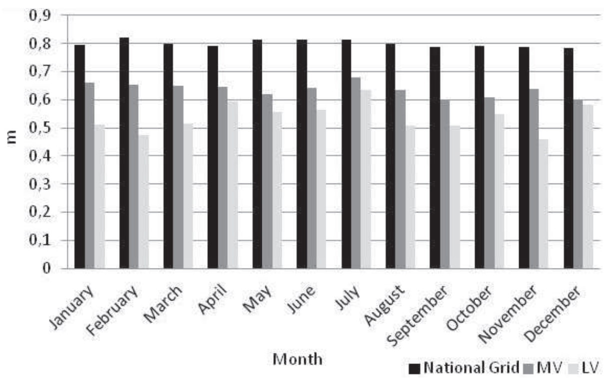

Fig. 6. Monthly variability of the *m* indicator

The greatest inequality is noted in loads of consumers recorded on low voltage. Their variability is significant regardless of the type of day and the season. The variability of rural consumer loads recorded at main supply stations is 30% lower on average.

Characterising the variability of electrical power loads using indicators such as load and balancing factors makes the comparative analysis easier and can be used by distribution companies when defining typical load schedules of consumers and modelling the demand for electrical power and energy.

CONCLUSIONS

Daily schedules of rural consumer loads recorded on the low and medium voltage are characterised by a low load during the morning peak, which is good for the national grid, but the evening peak load in rural areas coincides with the peak load on the entire power grid.

REFERENCES

1. Analiza i prognoza obciążeń elektroenergetycznych. Praca zbiorowa. 1971. WN-T Warszawa.
2. **Bieliński W. 1998:** Typowe wykresy obciążeń elektroenergetycznych wybranych odbiorców. Materiały V Konferencji Naukowo – Technicznej „Rynek energii elektrycznej REE'98". Nałęczów. 307–314.

3. **Chojnacki A. Ł. 2009.** Analiza dobowej, tygodniowej i rocznej zmienności obciążeń elektroenergetycznych w sieciach wiejskich oraz miejskich. Przegląd Elektrotechniczny 6, 9–12.
4. **Dudek G. 2004.** Wybrane metody analizy szeregów czasowych obciążeń elektroenergetycznych. Materiały VII Konferencji Naukowej *Prognozowanie w elektroenergetyce*. Częstochowa, 116–125.
5. **Ferreira A.M.S., Cavalcante C.A., FontesC.H., Marambio J. 1012.** A New proposal of typification of load profiles to support the decision-making in the sector of electric energy distribution. Internacional Industrial Conference on Engineering and Operations Management. 9–12 July 2012 Guimarães Portugalia, ID 18.1–ID18.7,
6. **Góra S. 1975.** Gospodarka elektroenergetyczna w przemyśle. PWN Warszawa.
7. **Derecka M., Bieliński W. 2002.** Nowe charakterystyki zmienności mocy pobieranej przez odbiorców. Materiały VI Konferencji Naukowej *Prognozowanie w elektroenergetyce PE'2002*. Częstochowa, 39–47.
8. **Kaźmierczak. A., Chojnacki A. Ł. 2011.** Analiza dobowej i tygodniowej zmienności obciążeń mocą czynną i bierną elektroenergetycznych sieci dystrybucyjnych SN, miejskich oraz terenowych. Energetyka 1, 29–37.
9. **Nęcka K. 2007.** Analiza szeregów czasowych obciążeń elektroenergetycznych na obszarach wiejskich. Inżynieria Rolnicza 2, 145–151.
10. Prognozowanie w elektroenergetyce. Zagadnienia wybrane. (red. I. Dobrzańska). 2002. Wydawnictwo Politechniki Częstochowskiej, Częstochowa.
11. **Trojanowska M. 2003.** Wyznaczenie obciążeń wiejskich sieci niskiego napięcia. Inżynieria Rolnicza 3. 359–365.
12. **Trojanowska M. 2010.** Analiza zapotrzebowania na moc i energię elektryczną w zakładzie mleczarskim. Journal of Research and Applications in Agricultural Engineering 55(2), 113–116.
13. **Trojanowska M., Nęcka K. 2009.** Determination of typical electric power loads for rural end users. TEKA Komisji Motoryzacji i Energetyki Rolnictwa Vol. IX, 357–363.
14. **Zalewski W. 2010.** Statystyczna analiza zmienności obciążeń w sieciach rozdzielczych. Economy and Management 4, 206–213.

ANALIZA PORÓWNAWCZA ZMIENNOŚCI DOBOWYCH OBCIĄŻEŃ ELEKTROENERGETYCZNYCH

Streszczenie. Przedstawiono analizę zmienności obciążeń w wiejskich sieciach dystrybucyjnych średniego i niskiego napięcia na tle zmienności zapotrzebowania na energię w krajowym systemie elektroenergetycznym. Wyznaczono i porównano wartości standardowych wskaźników wykorzystywanych do charakteryzowania zapotrzebowania na moc, takich jak stopnie obciążenia i stopnie wyrównania. Analiza została przeprowadzona w oparciu o dane zarejestrowane w 6 głównych punktach zasilających i w 37 stacjach transformatorowych 15/0,4 kV.

Słowa kluczowe: system elektroenergetyczny, sieci dystrybucyjne, zmienność obciążeń

TEKA. COMMISSION OF MOTORIZATION AND ENERGETICS IN AGRICULTURE – 2014, Vol. 14, No. 4, 93–98

Short-Term Forecasting of Natural Gas Demand by Rural Consumers Using Regression Models

Krzysztof Nęcka, Małgorzata Trojanowska

Department of Power Engineering and Agricultural Processes Automation, Agricultural University of Cracow
Balicka Str. 116B, 30-149 Kraków, Poland
e-mail: krzysztof.necka@ur.krakow.pl; malgorzata.trojanowska@ur.krakow.pl

Received December 02.2014; accepted December 17.2014

Summary. The study used various kinds of multiple regression models (standard and non-parametric) to predict the daily demand for natural gas by rural consumers. The construction of forecasting models was performed in the workspace of *STATISTICA Data Miner*, using the data mining technique. The analysis of forecast errors showed that all models applied in the study i.e. standard regression models, neural networks, regression trees, models based on the *MARS*, *SVM* and *k-Nearest Neighbours* methods generate good-quality forecasts, while artificial neural networks turned out to be the most effective method.
Key words: short-term forecasts, multiple regression, data mining.

INTRODUCTION

For natural gas companies, like for other enterprises in the energy sector, the forecasting of demand for energy carriers is one of the basic activities required by the management of these businesses, and the quality of forecasts directly affects the energy security of consumers as well as the profits of these enterprises. In natural gas companies, forecasts of demand for natural gas are prepared for various time horizons.

The short-term forecast of demand for gas includes hourly and daily forecasts for a maximum of seven days in advance. These activities facilitate the operational management of an enterprise, and, in particular, serve to plan daily purchases of gas.

Medium-term forecasts are daily and monthly with a time horizon of between one week and a year. These are used for planning purchases of gas in longer periods, and for planning gas transmission operations.

Long-term forecasts are annual predictions with the perspective of a forecast of between 5 to 10 years. These are used by gas companies in the long-term planning of gas purchases, and for planning the development of gas infrastructure.

Under the progressing liberalization of the natural gas market, short-term forecasts are becoming increasingly important. In recent years, an increasing number of studies have emerged, aimed at improving the quality of this type of forecast. The short-term prediction of demand for natural gas uses both traditional methods and methods based on artificial intelligence, as well as combined methods [14, 15, 17].

Traditional forecasting methods can be divided into those which use linear [6, 9, 11, 12, 13, 16] and non-linear models (logistic model, exponential model, Gompertz model, and the like) [4, 12] or models of auto-regression and means (*ARIMAX*, *SARIMAX*, recursive autoregression models *RARX*) [3, 9, 10, 11, 18]. In recent years, there has been an increase in the number of published studies which use neural networks [2, 5, 7, 8, 10, 16, 18, 20], recursive neural networks [11], fuzzy neural networks [1], and neural networks optimized by using genetic algorithm [19] to forecast the daily consumption of natural gas.

Among Polish publications in this field, most studies deal with long-term forecasts of the demand for gas. Publications dealing with short-term forecasts are few [6, 7].

The objective of this study was to use various types of regression models to predict the daily demand for natural gas by rural consumers, and to carry out comparisons in this area.

MATERIALS AND METHODS

The consumer demand for natural gas depends on a number of factors. For this reason, multiple regression models are very suitable for such forecasts. The regression function can be given not only in the form of a mathematical formula, but also as an algorithm. In the study, the construction of forecasting models was performed using standard linear regression models, but also using algorithms in the form of neural networks, regression trees, as well as applying *MARS*, *SVM* and *k-Nearest Neighbours* methods.

The construction of the models was carried out in the workspace of *STATISTICA Data Miner*, using data mining methodologies. Developing models was preceded by a correlation analysis aimed at finding the factors of greatest effect on the daily usage of natural gas by rural consumers.

The calculations and analyses were carried out on the basis of hourly measurements of gas usage by consumers from rural areas of southwestern Poland, who are supplied by a low-pressure network via a selected gas pressure reduction station. Data from the 2008–2011 period was used. Data from 2008-2010 was used as a training set, whereas data from 2011- was used as a testing set. The quality of the models was evaluated on the basis of values for ex-post forecast errors, using the following formula:

$$\omega_1 = \frac{\left|G_t - G_t^p\right|}{G_t} \cdot 100, \qquad (1)$$

$$\omega_2 = \frac{1}{n} \cdot \sum_{t=1}^{n} \frac{\left|G_t - G_t^p\right|}{G_t} \cdot 100, \qquad (2)$$

$$\omega_3 = \frac{\sum_{t=1}^{n} \left|G_t - G_t^p\right|}{G_c} \cdot 100, \qquad (3)$$

where:
G_t – actual daily consumption of gas,
G_t^p – forecast of daily gas consumption,
G_c – actual consumption of gas during *n* days of observation.

RESULTS

Among other forecasts, natural gas enterprises in Poland are obliged to make forecasts of daily gas consumption one day in advance. A day of consumption is defined as 24 hrs from 6AM to 6AM the next day.

The course of hourly and daily natural gas consumption by rural consumers within the study period is presented in Figs 1 and 2.

Meteorological and time factors were considered among the factors affecting gas consumption. The meteorological factors taken into account included: temperature (daily – mean, maximum, minimum), humidity (daily – mean, maximum, minimum), wind velocity (daily – mean), wind direction (daily – mean), pressure (daily – mean), with these values taken with delay to the day of analyzed gas consumption.

Time factors include the correlation between the values for daily gas consumption with the values of the variable delayed with the time and the day of the week. A total of 144 variables were considered in the correlation analysis.

It was found that the greatest effect on the value of daily gas consumption by rural consumers was exerted by this value delayed by one day, the mean temperature of the previous day, and the day of the week. In further statistical analyses, these values were adopted as the variables explaining the daily demand for natural gas.

In order to develop prediction models which permit finding the daily demand for natural gas, a project was created in the graphic environment of *Statistica 10 Data Miner* (Fig. 3). Among other elements, the nodes were placed there to permit drawing forecasts based on: *Neural Networks (NN*), *Classification and Regression Trees (CART*), *Multivariate Adaptive Regression Splines (MARS)*, *Support Vector Machine (SVM*), *k Nearest Neighbours (k-NN*), as well as standard *Multiple Regression (MR*).

Standard multiple regression requires meeting many assumptions pertaining to sample size, explained and explaining variables, residuals of the model, although in data mining these assumptions are tested less restrictively than in traditional statistics. The other procedures used in this study are non-parametric procedures which do not require meeting any initial assumptions.

Among the latter procedures, the oldest and best described is the method of artificial neural networks. It has been dynamically developing for several decades and it is now regarded as a very refined modelling technique, capable of mapping very complex relationships.

Classification and Regression Trees are other advanced prediction tools of *Data Mining*. The tree is a graphical model created as a result of the recurrent division of a set of observations into *n* of disjoint subsets. In most general terms, the objective of the analysis with the applied *CART* algorithm is to find the set of logical conditions for division, of the *if-so,* leading to the unambiguous classification of objects.

The *MARS* method can be regarded as an extension of regression trees and multiple regression. The *Multivariate Adaptive Regression Splines* algorithm utilises the method of the recurrent division of trait space in the nodes of basic functions to construct the regression model in the form of spline curves. The relationship between variables is modelled with the use of a set of basic coefficients and functions generated on the basis of data. The *SVM* method is the next one implemented in the *Statistica* software, which serves to solve regression and classification problems. It consists of constructing non-linear decision borders, separating areas in the space of predictors, corresponding to different values of the dependent variable.

K Nearest Neighbours is a method where instead of matching the model, similar objects are sought. The basis of the method is an intuitive conviction that similar objects will fall into the same class. The predictions of the *k-NN* method are determined on the basis of *k* objects from the training set which are most similar to the object for which the value of the dependent variable is determined.

Mean errors were calculated for the training set (Table 1) and testing set (Table 2) for forecasts found with the use of particular methods. The most accurate method turned out to be the neural networks, whereas the standard regression was the least accurate.

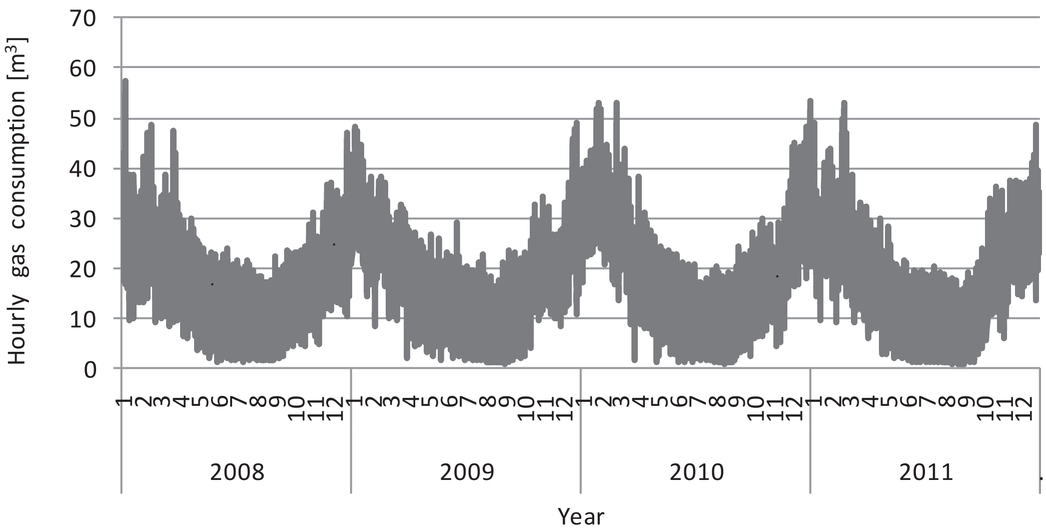

Fig. 1. Hourly natural gas consumption

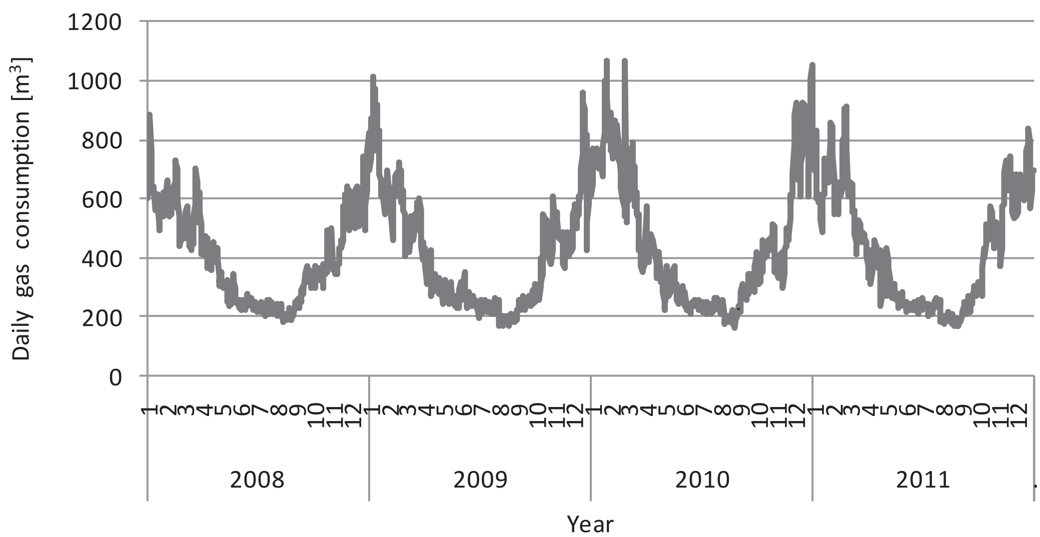

Fig. 2. Daily natural gas consumption

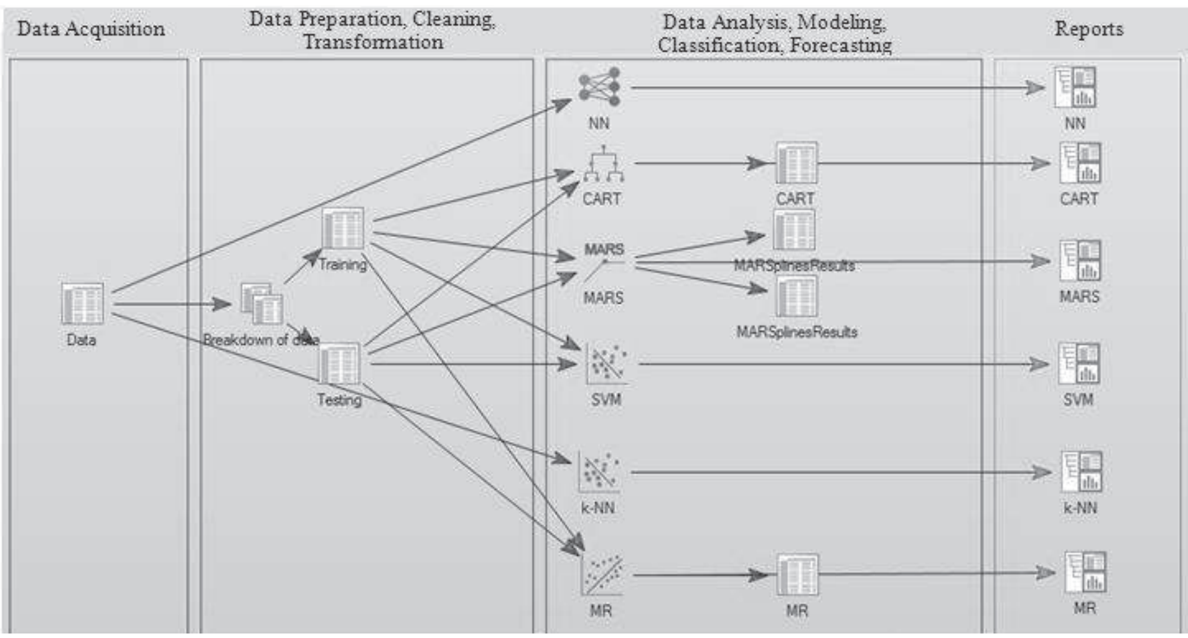

Fig. 3. View of models constructed in the workspace of *Data Miner*

Table 1. Forecast errors found for training set

Model / Error	*NN*	*CART*	*MARS*	*SVM*	*k–NN*	*MR*
ω_2 [%]	5.44	6.88	6.39	6.81	5.54	7.39
ω_3 [%]	5.52	6.62	6.27	6.44	5.26	6.98

Table 2. Forecast errors found for testing set

Model / Error	*NN*	*CART*	*MARS*	*SVM*	*k–NN*	*MR*
ω_2 [%]	5.39	6.05	6.25	6.25	6.38	6.78
ω_3 [%]	5.39	5.64	5.97	5.96	5.97	6.30

For the purpose of analyzing daily gas consumption forecasts, the distribution functions of relative errors w_1 were determined and their courses for the testing set are presented in Fig.4. As shown in the figure, irrespective of the method used, the proportion of smallest errors is similar (11-14%). Greater differences between the w_1 frequencies of occurrence for the studied models were seen when this proportion increased. In the *k–NN* model, the proportion of errors amounting to less than 10% was 70% of observations whereas for the *NN* model it was 83%. The advantage of the *NN* model over the other models is also visible in the proportion of highest observed errors. They did not exceed 20% in as many as 99% of the observations.

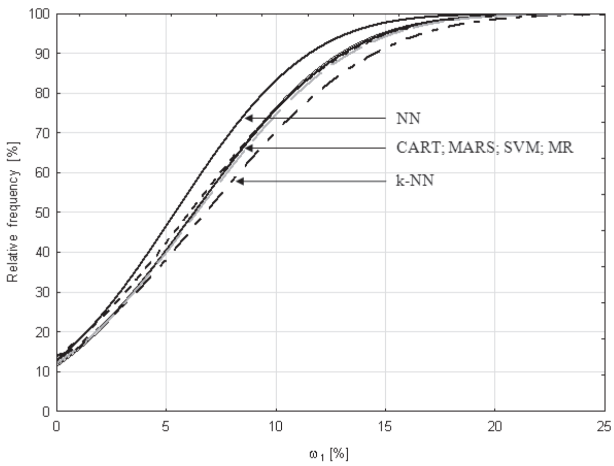

Fig. 4. Empirical distribution functions of w_1 forecast errors

CONCLUSIONS

The greatest effect on the value of daily gas consumption by rural consumers was exerted by this value delayed by one day, mean temperature of the previous day, and the day of the week.

In view of the requirements of the quality of short-term forecasts posed by gas enterprises, the forecasts determined on the basis of multiple regression models, both standard and non-parametric i.e. *NN, CART, MARS, SVM,* and *k–NN* can be considered admissible ($5.44\% \leq w_2 \leq 7.39\%$) and accurate ($5.39\% \leq w_2 \leq 6.78\%$).

The analysis of forecast errors proved that the most effective methods are the neural networks, whereas the greatest errors in forecasts are generated in standard regression.

REFERENCES

1. **Azadeh A., Asadzadeh S.M., Ghanbari A. 2010:** An adaptive network-based fuzzy inference system for short-term natural gas demand estimation: Uncertain and complex environments. Energy Policy 38, 1529-1536.
2. **Azari A.; Shariaty-Niassar M., Alborzi M. 2012:** Short-term and medium-term gas demand load forecasting by neural networks. Iranian Journal of Chemistry and Chemical Engineering 31(4), 77-84.
3. **Brabec M., Konar O., Pelikan E., Maly M. 2008:** A nonlinear mixed effects model for the prediction of natural gas consumption by individual customers. International Journal of Forecasting 24, 659-678.
4. **Brabec M., Konar O., Maly M., Pelikan E., Vondracek J. 2008:** A statistical model for natural gas standardized load profiles. J Roy Statist. Soc. Series C: Applied Statistics 58(1), 123-139.
5. **Chen Q., She Y., Xu X. 2013:** Combination model for short-term load forecasting. The Open Automation and Control Systems Journal 5, 124-132.
6. **Dittman P., Szabela-Pasierbińska E. 2007:** Short-term sales forecasts in management of natural gas distributing works. Management 11(1), 147-154.
7. **Kelner J.M. 2003:** Prognozowanie krótkoterminowe poborów gazu z sieci przesyłowych metodą sztucznych sieci neuronowych. Gaz, Woda i Technika Sanitarna 6, 196-204.
8. **Kizilaslan R., Karlik B.2008:** Comparison neural networks models for short term forecasting of natural gas consumption in Istanbul. In: Applications of digital information and web technologies, ICADIWT 2008, 4-6 August 2008, 448-453.
9. **Potocnik P., Govekar E. 2010:** Practical results of forecasting for the natural gas market. http://www.intechopen.com/books/natural-gas/practical-results-of-forecasting-for-the-natural-gas market.
10. **Potocnik P., Govekar E., Grabec I. 2007:** Short-term natural gas consumption forecasting. In: Proceedings of the 16th IASTED International Conference on Applied Simulation and Modelling – ASM 2007, 353-357.
11. **Potocnik P., Soldo B., Simunovic G., Saric T., Jeromen A., Govekar E. 2014:** Comparison of static and adaptive models for short-term residential natural gas forecasting in Croatia. Applied Energy 129, 94-103.
12. **Sabo K., Scitovski R., Vazler I., Zekic-Susac M. 2011:** Mathematical models of natural gas consumption. Energy Conversion and Management 52, 1721-1727.
13. **Simunek M., Pelikan E. 2008:** Temperatures data preprocessing for short-term gas consumption forecast. In: IEEE International Symposium on Industrial Electronics; 1192-1196.
14. **Smith P., Husejn S. 1996:** Forecasting short term regional gas demand using an expert system. Expert Systems with Applications 10(2), 265-273.

15. **Soldo B. 2012:** Forecasting natural gas consumption. Applied Energy 92, 26-37.
16. **Soldo B., Potocnik P., Simunovic G., Saric T., Govekar E. 2014:** Improving the residential natural gas consumption forecasting models by using solar radiation. Energy and Buildings 69, 498-506.
17. **Suganthi L., Anand A. Samuelb A.A. 2012:** Energy models for demand forecasting-A review. Renewable and Sustainable Energy Reviews 16, 1223-1240.
18. **Taspınar F., Celebi N., Tutkun N. 2013:** Forecasting of daily natural gas consumption on regional basis in Turkey using various computational methods. Energy and Buildings 56, 23- 31.
19. **Yu F., Xu X. 2014:** A short-term load forecasting model of natural gas based on optimized genetic algorithm and improved BP neural network. Applied Energy 134, 102-113.
20. **Zhou H., Su G., Li G. 2011:** Forecasting daily gas load with OIHF-Elman Neural Network. Procedia Computer Science 5, 754-758.

PROGNOZOWANIE KRÓTKOOKRESOWE ZAPOTRZEBOWANIA ODBIORCÓW WIEJSKICH NA GAZ ZIEMNY Z WYKORZYSTANIEM MODELI REGRESYJNYCH

Streszczenie. W pracy wykorzystano różnego rodzaju modele regresji wielorakiej (standardowe i nieparametryczne) do predykcji dobowego zapotrzebowania odbiorców wiejskich na gaz ziemny. Budowę modeli predykcyjnych przeprowadzono w przestrzeni roboczej *STATISTICA Data Miner*, przy użyciu metod *data mining*. Analiza błędów prognoz wykazała, że wszystkie zastosowane w pracy modele tj. standardowej regresji, sieci neuronowych, drzew regresyjnych, oparte na metodzie *MARS*, wektorów nośnych oraz k–najbliższych sąsiadów generują prognozy dobrej jakości, przy czym metodą najbardziej efektywną okazały się sztuczne sieci neuronowe.

Słowa kluczowe: prognozy krótkookresowe, regresja wieloraka, data mining.

TEKA. COMMISSION OF MOTORIZATION AND ENERGETICS IN AGRICULTURE – 2014, Vol. 14, No. 4, 99–104

Evaluation of Physical Properties in Briquettes Made from Selected Plant Materials

Ignacy Niedziółka[1], Wojciech Tanaś[1], Mariusz Szymanek[1], Beata Zaklika[1], Józef Kowalczuk[2], Jarosław Tatarczak[2], Janusz Zarajczyk[2]

[1]Department of Agricultural Machines,
[2]Department of Horticultural and Forestry Machines,
University of Life Sciences, 28 Głęboka Street, 20-612 Lublin

Received December 12.2014; accepted December 19.2014

Summary. The purpose of this study was to evaluate the physical properties of briquettes made from selected plant raw materials. The research was carried out on three kinds of raw materials, i.e. wheat straw, maize stover and Sida stalks. It was found out that the plant materials used for the production of briquettes were characterized by low moisture and high calorific value and they could well undergo a process of compaction. Also, the produced briquettes were characterized by favourable properties concerning the studied parameters, i.e. length, mass, proper density and bulk density. The best results for the studied properties were obtained for the briquettes made from maize stover, and slightly worse for the briquettes made from wheat straw and Sida stalks.

Key words: plant biomass, briquetting, physical properties of briquettes.

INTRODUCTION

Energy from fossil fuel resources has been getting more and more expensive due to their depleting reserves. More and more attention has been paid to the problems of environmental protection. These phenomena have been encouraging research into alternative energy sources, among others, biomass. The greatest hopes are connected with the biomass of plant origin and this group includes the straw of cereals and other crops [Borkowska 2006, Denisiuk 2007, Grzybek 2012, Niedziółka et al. 2006, Stolarski 2008].

Virtually any type of straw from cereal, oilseed rape and buckwheat can be used for energy purposes. Due to their properties, the most often used straw is that of rye, wheat, rape and buckwheat. It is assumed that "straw" is ripe or dried plant stalks, having a high dry matter content of up to 85%, and the capacity of water and gas absorption. As a waste product it has a wide range of applications in crop production, horticulture, construction and energy. Despite the different applications of straw in agriculture it should be noted that there still remains a considerable potential of this material which has not found any rational use. Its use as an energy source has become the solution to this situation [Dreszer et al. 2003, Fiszer 2008, Kołodziej and Matyka 2012, Niedziółka and Szymanek 2010, Zarajczyk 2013].

To enhance plant biomass use for energy production, efforts have been made to improve its physical properties [Wu et al. 2011]. Lowering the moisture allows for long-term storage, while increasing the concentration of mass and energy per unit volume makes the transport, storage and dispensing easier. These favourable characteristics can be achieved by concentration of biomass in the form of briquettes, thus gaining a fuel which is competitive with conventional ones [Komorowicz et al. 2009, Lewandowski and Ryms 2013, Niedziółka 2014, Szymanek and Kachel-Jakubowska 2010].

Biomass briquetting means the increasing of energy density and improving the milling properties of the raw material. The most commonly used briquetting presses are the piston, screw and cylindrical ones. They can be used as separate devices or within an in-line process for the manufacture of compact fuel. Construction of the line is dependent on the volume of production, properties of the raw material used and specific requirements for the obtained product [Hejft 2013, Frączek 2010, Kallyan and Morey 2009]. Therefore, the production process may be more or less complicated, depending on the initial parameters of the processed materials as well as their final destination.

The aim of this study was to evaluate the physical properties of briquettes made of selected plant raw materials.

MATERIALS AND METHODS

Wheat straw, maize stover and Sida stalks were used for the production of briquettes. The relative moisture of raw materials was determined by the weight-drier method according to the PN-EN 15414-3: 2011 standard. Measurement of moisture content in the raw materials was performed in triplicate and determined by the formula (1):

$$W = \frac{m_o - m_1}{m_o} \cdot 100, \tag{1}$$

where:
W – humidity of the tested material (%),
m_o – mass of the sample before drying (g),
m_1 – mass of the sample after drying (g).

The net calorific value was calculated based on the gross calorific value determined using a calorimeter KL-12 Mn, in accordance with PN-EN 14918: 2010. The briquetting plant materials were pulverized using a chopper drum substation and universal hammer mill, powered by electric motors with the capacity of, respectively, 7.5 and 4.5 kW. The device used for the compaction process of the shredded plant materials was the hydraulic piston briquetting machine Junior of the POR DETA company, Poland.

After the production of briquettes their geometrical characteristics were determined: diameter and length using calipers (with accuracy of ± 0.1 mm) and mass using a laboratory scale WPT 6.3 (with accuracy of ± 0.1 g). Bulk density of the pellets was determined by freely dropping them into the measuring cylinder with the volume of 50 (dm³), in accordance with PN-EN 15103: 2010. After filling the cylinder and removing the excess strip, all the briquettes were weighed on the scales WPE 200 with accuracy of ± 0.1 g. Bulk density value was calculated as the quotient of the difference in mass of the cylinder with and without fuel pellets and the cylinder's volume, according to the formula (2):

$$\rho = \frac{m_L - m_O}{V}, \tag{2}$$

where:
ρ – bulk density of pellets (kg·m⁻³),
m_L – mass of cylinder with pellets (g),
m_O – mass of the empty cylinder (g),
V – cylinder's volume (dm³).

Photo 1 shows the tested plant materials after their shredding.

Photo 2 shows the hydraulic piston briquetting machine JUNIOR used to produce briquettes.

Photo. 2. The hydraulic piston briquetting machine JUNIOR

Table 1 presents the technical and operational parameters of the hydraulic piston briquetting machine JUNIOR.

Table 1. The technical and operational parameters of the hydraulic piston briquetting machine JUNIOR

Specification	Measurement unit	Data
Type of briquetting device	-	JUNIOR
Diameter of pellets	mm	50
Maximum length of briquettes	mm	60
Briquetting performance	kg·h⁻¹	50
Electric motor power	kW	7.5
Maximum working pressure	MPa	15.0
Oil tank capacity	dm³	110
Briquetting device dimensions (length x width x height)	mm	1600×1100×1500
Briquetting device weight	kg	680

a) b) c)

Photo 1. The tested plant materials after shredding: a) wheat straw, b) maize stover, c) Sida stalks

Photo 3 shows the briquettes made from the tested plant materials.

Photo 3. Briquettes produced from the tested plant raw materials: a) wheat straw, b) maize stover, c) Sida stalks

RESULTS

Figure 1 shows the average moisture content of plant materials used for the production of briquettes. The lowest moisture was recorded for wheat straw (11.9%) and the highest for maize stover (14.3%). The statistical analysis showed that significant differences occurred in the moisture of all the tested materials.

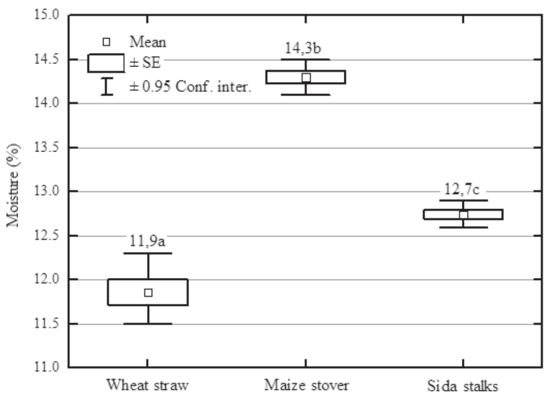

Fig. 1. Average moisture of the compacted plant raw materials

Figure 2 shows the average calorific value of the plant materials used in the manufacture of briquettes. The lowest calorific value occurred for wheat straw (16.9 MJ·kg^{-1}), slightly higher values were recorded for Sida stalks (17.1 MJ·kg^{-1}) and the highest for maize stover (17.6 MJ·kg^{-1}). The analysis showed no statistically significant differences in the calorific value of all the compacted materials.

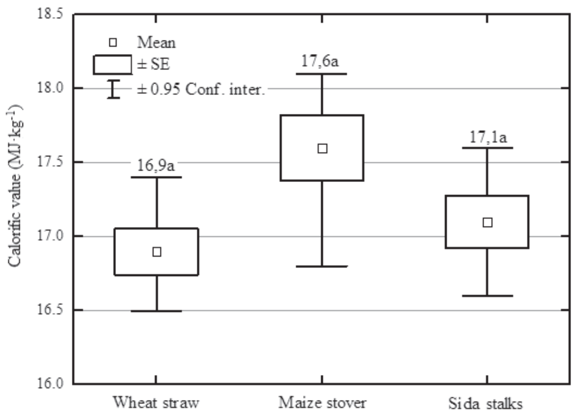

Fig. 2. Average calorific value of compacted plant materials

Figure 3 shows the results of measurements of the length of briquettes made of various plant materials. The shortest briquettes were obtained from wheat straw (38.9 mm), while the longest from Sida stalks (50.2 mm). The analysis of the results showed that statistically significant differences occurred between the length of briquettes produced from wheat straw and maize stover, and the length of briquettes made from Sida stalks. There were no statistically significant differences in the length of briquettes from wheat straw and maize stover.

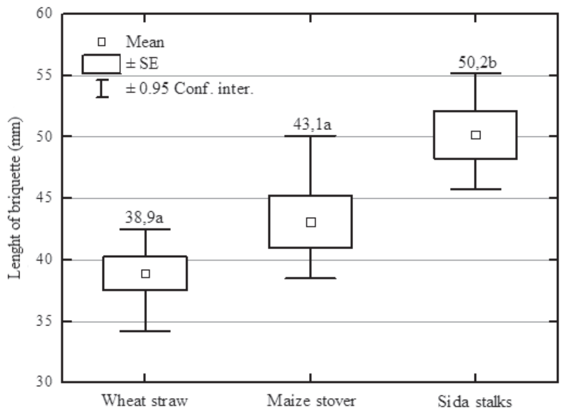

Fig. 3. Average length of briquettes made from plant materials

Figure 4 shows the results of measuring the mass of pellets made from the tested materials. The lowest average mass characterized the briquettes from wheat straw (47.9 g), slightly higher briquette mass was found for Sida stalks (52.4 g) and the highest for maize stover (61.8 g). The statistical analysis indicated that significant differences occurred between the mass of briquettes made from wheat straw or Sida stalks and that of the briquettes made from maize stover. In contrast, no statistically significant differences occurred between the mass of wheat straw and Sida stalks briquettes.

Figure 5 shows the density of briquettes depending on the type of plant raw materials used. The lowest proper density characterized the briquettes from Sida stalks (959.5 kg·m^{-3}) and the highest the briquettes from maize stover (1105.3 kg·m^{-3}). Based on the statistical analysis, it was found out that significant differences occurred between the proper density of briquettes produced from wheat straw or Sida stalks and the proper density of briquettes from maize

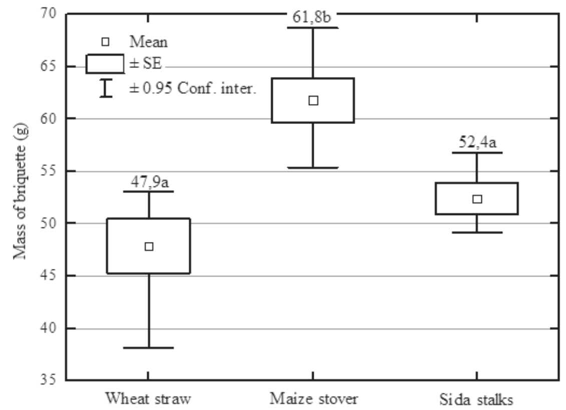

Fig. 4. Average mass of briquettes made from plant materials

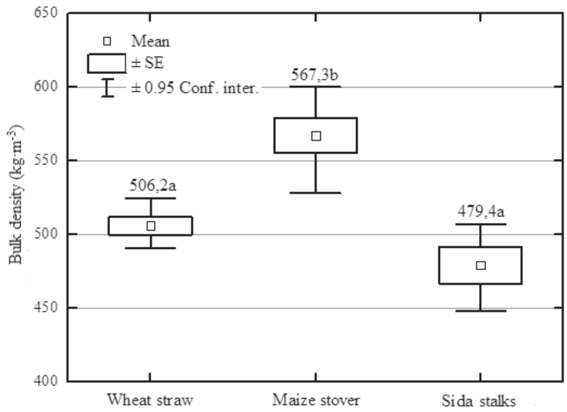

Fig. 6. Average bulk density of briquettes produced from plant materials

stover. However, no statistically significant differences were found in the density of the pellets produced from wheat straw and Sida stalks.

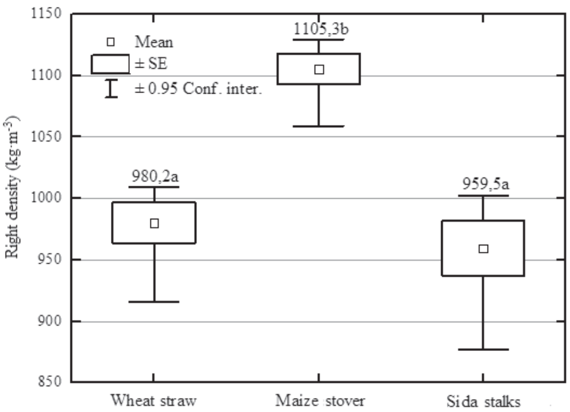

Fig. 5. Average density of briquettes produced from plant materials

The results of measurements of the average bulk density depending on the kind of raw materials used are shown in Figure 6. The lowest bulk density characterized the briquettes produced from Sida stalks (479.4 kg·m^{-3}), and the highest those produced from maize stover (567.3 kg·m^{-3}). Based on the statistical analysis it was found out that significant differences occurred between the bulk density of briquettes made from wheat straw or Sida stalks and the bulk density of briquettes made of maize stover. There were no statistically significant differences in the bulk density of briquettes made from wheat straw and Sida stalks.

CONCLUSIONS

The results of research and statistical analysis allow for the following conclusions:

1. The tested plant materials used for the production of briquettes were characterized by low moisture and high calorific value and were vulnerable for the process of compaction. Also, the produced briquettes were characterized by favourable parameters of the studied properties, i.e. length, mass proper density and bulk density.
2. Among the compacted materials, the lowest moisture (11.9%) and heating value (16.9 MJ·kg^{-1}) was found out for the wheat straw, and the highest for the maize stover, (14.3%) and (17.6 MJ·kg^{-1}), respectively.
3. After the analysis of the results of measurements of length and mass of the produced briquettes it was found out that the shortest briquettes were obtained from wheat straw (38.9 mm), and the longest from Sida stalks (50.2 mm). In contrast, the lowest mass was recorded for the briquettes made from wheat straw (47.9 g), whereas the highest for the briquettes produced from maize stover (61.8 g).
4. Based on the analysis, the lowest values of proper and bulk density were found out for the pellets produced from Sida stalks – (959.5 and 479.4 kg·m^{-3}), respectively, and the highest values for the briquettes manufactured from maize stover – (1105.3 and 567.3 kg·m^{-3}), respectively.

REFERENCES

1. **Borkowska H., 2006:** Pelety ze ślazowca pensylwańskiego na tle normy DIN 51731. Czysta Energia, 6, 22-23.
2. **Denisiuk W., 2007:** Brykiety/pelety ze słomy w energetyce. Inżynieria Rolnicza, 9(97), 41-47.
3. **Dreszer K., Michałek R., Roszkowski A., 2003:** Energia odnawialna – możliwości jej pozyskiwania i wykorzystania w rolnictwie. Ed. PTIR, Krakow–Lublin–Warsaw.
4. **Fiszer A., 2008:** Badania porównawcze współczynnika trwałości brykietów ze słomy. Journal of Research and Applications in Agricultural Engineering, 53(3), 69-71.
5. **Frączek J. (ed.), 2010:** Przetwarzanie biomasy na cele energetyczne. Ed. PTIR, Kraków, ISBN 978-83-917053-9-1.
6. **Grzybek A. (ed.), 2012:** Słoma – wykorzystanie w energetyce cieplnej. Ed. ITP Falenty, ISBN 978-83-62416-48-6.
7. **Hejft R., 2013:** Innowacyjność w granulowaniu biomasy. Czysta Energia, 6(130), 32-34.
8. **Kallyan N., Morey R.V., 2009:** Factors affecting strength and durability of densified biomass products. Biomass and Bioenergy, 33, 337-359.

9. **Kołodziej B., Matyka M. (ed.), 2012:** Odnawialne źródła energii. Rolnicze surowce energetyczne. PWRiL Sp. z o.o. Poznań, ISBN 978-83-09-01139-2.
10. **Komorowicz M., Wróblewska H., Pawłowski J., 2009:** Skład chemiczny i właściwości energetyczne biomasy z wybranych surowców odnawialnych. Ochrona Środowiska i Zasobów Naturalnych, 40, 402-410.
11. **Lewandowski W. M., Ryms M., 2013:** Biopaliwa. Proekologiczne odnawialne źródła energii. WNT Warszawa, ISBN 978-83-63623-73-9.
12. **Niedziółka I., (ed.), 2014:** Technika produkcji brykietów z biomasy roślinnej. Tow. Wyd. Nauk. LIBROPOLIS, ISBN 978-83-63761-38-7.
13. **Niedziółka I., Szymanek M., 2010:** An estimation of physical properties of briquettes produced from plant biomass. Teka Komisji Motoryzacji i Energetyki Rolnictwa, X, 301-307.
14. **Niedziółka I., Szymanek M., Zuchniarz A., 2006:** Energetic evaluation of postharvest corn mass for heating purposes. Teka Komisji Motoryzacji i Energetyki Rolnictwa, VI(6A), 145-150.
15. PN-EN 15414-3: 2011 – Oznaczanie zawartości wilgoci metodą suszarkową – Część 3: Wilgoć w ogólnej próbce analitycznej.
16. PN-EN 14918: 2010 – Biopaliwa stałe – Oznaczanie wartości opałowej.
17. PN-EN 15103: 2010 – Biopaliwa stałe – Oznaczanie gęstości nasypowej.
18. **Stolarski M., Szczukowski S., Tworkowski J., 2008:** Biopaliwa z biomasy wieloletnich roślin energetycznych. Energetyka, 1(643), 77-80.
19. **Szymanek M., Kachel-Jakubowska M., 2010:** Estimation and analysis of chosen factors of the influence on quality and energy consumption at the processing of plant materials for energy purposes. Teka Komisji Motoryzacji i Energetyki Rolnictwa,10, 454-463.
20. **Wu M.R., Schott D.L., Lodewijks G., 2011:** Physical properties of solid biomass. Biomass and Bioenergy, 35, 2093-2105.
21. **Zarajczyk J., 2013:** Uwarunkowania techniczne i technologiczne produkcji peletu z biomasy roślinnej na cele energetyczne. Inżynieria Rolnicza, Monografie i rozprawy, 1(142), T. 2, ss. 81.

OCENA WŁAŚCIWOŚCI FIZYCZNYCH BRYKIETÓW WYKONANYCH Z WYBRANYCH MATERIAŁÓW ROŚLINNYCH

Streszczenie. Celem tego badania była ocena właściwości fizycznych brykietów wykonanych z wybranych surowców roślinnych. Badania przeprowadzono na trzech rodzajach surowców: słomie pszennej, słomie kukurydzianej i łodygach ślazowca pensylwańskiego. Stwierdzono, że materiały roślinne stosowane do wytwarzania brykietów charakteryzuje niska wilgotność i wysoka wartość opałowa i mogą one z powodzeniem być poddawane procesowi zagęszczania. Ponadto, wyprodukowane brykiety charakteryzowały się korzystnymi właściwościami w zakresie badanych parametrów, czyli długości, masy, gęstości właściwej i gęstości nasypowej. Najlepsze wyniki dla badanych właściwości uzyskano dla brykietów ze słomy z kukurydzy, a nieco gorsze dla brykietów ze słomy pszennej i łodyg ślazowca pensylwańskiego.

Słowa kluczowe: biomasa roślin, brykietowanie, właściwości fizyczne brykietów.

TEKA. COMMISSION OF MOTORIZATION AND ENERGETICS IN AGRICULTURE – 2014, Vol. 14, No. 4, 105–112

Increase of Reverse Water Supply Systems Effectiveness in Production of Construction Materials

Ilya Nikolenko, Ervin Karimov

Crimean Federal V.I. Vernadsky University
181, Kievskaya Street, Simferopol, Crimea, e-mail: nikoshi@mail.ru

Received December 02.2014; accepted December 17.2014

Summary. In the article the questions of modeling of hydrodynamic filtering in systems of reverse water supply in production of construction materials are considered. The scheme of experimental installation is provided for realization of pilot research of the hydrodynamic filter and also the technique of pilot researches is given. The plan of three-factorial experiment of GDF of PCM wastewaters is developed, researches are conducted and the regression equation characterizing the removal process of the suspended materials is received. Dependences for calculation of the residual content of the suspended materials depending on initial concentration of impurities, the ratio of a useful and slime expense on the filter and the consumption of the processed fluid are established. It is established that in the production of construction materials the installation of reverse water supply systems with application of hydrodynamic filtering allows using effectively its advantages and providing more rational use of energy and natural resources.

Key words: Productions of construction materials, industrial wastewaters, reverse water supply, hydrodynamic filtering, concentration, expense, residual concentration of impurity, refinement effectiveness

INTRODUCTION

Water in industrial production is essential for ensuring primary and secondary technological processes, as well as fire-fighting, domestic and drinking needs of enterprises. The quantity and quality of technical water which is necessary in any production is defined by the scale and nature of its technological processes. Properties of utilized water, cost of water supply systems and water disposals substantially define quality and prime cost of products and also conditions of the rational use of natural resources. Reserve for water resources saving at any production is the use of circulating water supply where much depends on the technology of wastewaters refinement. With the installation of recycling systems for industrial water supply there are additional reserves on consumption of fresh water and reduction of wastewaters into reservoirs. Industrial wastewaters refinement represents an important technological and methodical problem in developing effective ways for recycling refined water in industrial processes.

Fluids' refinement from various types of impurities that they contain is a widespread problem. It is constantly faced not only in communal services and on the domestic level but also in all the branches of industrial production [1, 2, 3]. In technological processes of production, processing and also the production of construction materials (PCM) large volumes of water are used which become soiled generally by mineral insoluble impurity. For the majority of PCM, in the technological processes water is the main working medium. The use of polluted water to any extent is exposed to refine with its subsequent dumping in water objects or in reverse schemes with the subsequent application in technological process. Requirements quality of industrial wastewaters refinement at their outlet in reservoirs and also at the subsequent application causes broad use of various refinement methods and technologies. While choosing a method of impurities refinement not only their structure in wastewaters is considered but also requirements which have to satisfy waters refinement: when disposing in a reservoir, and at a reuse of the refined wastewaters in production - those requirements which are necessary for realization of actual technological processes.

The current situation is characterized by increasing attention of society to questions of power and resource saving that is directly connected with quality and an expense used in technological water processes [4,5]. The condition of the surrounding water medium, the developed level of understanding of environmental problems demand restriction of unjustified expenses of water resources and industrial wastes disposing in natural reservoirs. Despite the increased scientific and technical capabilities, the problem of water surface protection and in particular sanitary protection of water objects from impurity remains valid and still demands the effective decisions [6, 7]. The choice of optimized technological schemes of industrial water supply refinement is a complex challenge that is caused by a variety of the water impurities and great demands made of refinement quality. The techno-economic rating of the ways of water preparation has a great significance for the preparation of industrial water from industrial wastewaters or insuring conditions of the disposal refinement wastewaters of reservoirs. Reverse systems of industrial water supply usually have got economic advantage.

The solution of this problem for PCM in many cases is connected with the organization of the closed water supply cycles. This task cannot be solved successfully without effective refinement of the circulating reverse water from impurities.

ANALYSIS OF PUBLICATIONS

In PCM water is used both as the main and the secondary technological process. Conventionally, these waters can be divided into the following groups [8,9].

Technological waters are working medium in technological processes. These technological processes include: water concentration of nonmetallic minerals, hydro-mining, hydro-transport, hydro-washing. These waters are heavily polluted and require refinement.

Cooling waters are formed during cooling the equipment, machines and devices which are used in the main technological process. These waters generally have the so-called pollution "temperature". Therefore, they are called conditionally clean. They need only cooling and can be reused in processes.

Washing and de-dusting waters are formed as a washing result of aggregates, machines and equipment and also for dust control on PCM. These waters are heavily polluted and need to be cleaned. All industrial engineering wastewaters in their use and discharge into water bodies generally require refinement.

A large number of various impurities in the IW industrial wastewaters is determined by numerous methods, techniques and technological scheme used while refining them. Ways of industrial wastewaters refinement of insoluble impurities are divided into three groups: mechanical refinement – separation of impurities while going through the passage media; physical refinement – separation of impurities when fluid stays in force fields; combined refinement – separation of impurities from fluid at a joint mechanical and physical refinement. Mechanical refinement of fluid is divided into the following types: surface, volume and mixed. The last type combines features of the two first types. Defecation and clarification of the polluted water in PCM is based on particles on sedimentation of impurities with a higher density than the density of water at its moving with low speed. Such water refinement is made in tank clarifications or settlers of various designs. Tank clarifications are constructed as one, two and multiple-stage ones and for keeping water long-term. Effectiveness of clarification in ponds reaches 50 … 62% but during winter period their operation is poorer . Ponds need to be cleaned regularly, they occupy a big surface area and pollute the environment. The effectiveness of horizontal settles refinement with the regulating perforated baffle plates reaches 39 … 49%, with the system of dispersed water abstraction surface - 62 … 69%, and for settlers with thin layer elements from inclined baffle plates 47 … 70%.

For IW wastewaters refinement from suspended materials hydrocyclone machines are used in which the centrifugal force effecting on particles with a higher density than that of water is used. They successfully replace settlers having a number of advantages: they occupy small space, have high extent of refinement up to 70%, high efficiency, have no moving elements, their operation can be completely automated.

In most cases filtering is used for integrated wastewater treatment of IW after all the preliminary treatment methods. It can be surface filtering through filter baffle plates or volume through grained loading. In case of additional reactant treatment of wastewaters, treatment of IW with coagulant and flocculant on the score of suspended particles agglomeration and other alterations solid particles emission during filtering improves. Reduction of pressure drop on filtering element, increase of refinement precision of power fluid, its preservation from blinding and therefore self-regeneration support can be provided under conditions which will pass the particles through units of surface filtering element the size of which is much lesser than "in light" units size. These conditions are created on hydrodynamic filters.

Hydrodynamic Filtering (HF) is one of the modern effective methods of fluid refinement from impurities. Fluid refinement of HF is based on the hydrodynamic theory of Z.L Finkelstein about the movement of impurity particles in a fluid flow near the filtering element. In this theory it is accepted that the filtering element (FE) represents the plate covered with regularly located holes (units) of a certain size [10, 11].

In case of the standard refinement scheme of the polluted fluid flow it goes perpendicularly to the FE plane. Only those particles whose linear size is lesser that the size of filtering unit do not linger on it. Particles of the bigger size cumulate from the incident flux and gradually "clog" FE openings. Therefore during the work of FE in a flux of the polluted fluid its capacity decreases, drop of pressure on it increases and finally it becomes soiled and loses working capacity. FE is considered clogged if the created pressure losses on it overrun allowable maximum provided by its design. After that it is necessary to transfer the clogged filter to an initial state by replacement or effective flushing which is defined by type of the filter and nature of the detained substances in it. Running time of the filter between two consecutive flashings is called a filtering cycle.

To restore the FE is subject to flush with a pure water backwash, replacement or regeneration. To increase contaminant capability of FE and its service lifetime it is necessary to increase its surface and volume considerably. Therefore such way of fluid refinement is far from perfect in terms of technical and economic indicators as for the period of refinement or FE replacement it is necessary to provide additional, reserve FE, its periodic operation without refinement.

At HF the polluted fluid flow goes parallel to the FE plane. Thus, hydrodynamic features of system are such that through filter units together with fluid penetrate only those particles, which linear size in 3…10 times less than unit size. Big particles are washed away from FE surface by a fluid flow. Therefore, FE of such kind are never clogged with particles of the bigger size. Big particles moving in a fluid flow are removed from FE units and provide its continuous cleaning. The filtering systems with such kind of FE without replacement work from 7 to 10 years without technical servicing and repair.

The purpose of the work consists in studying the possibilities of HF installation in PCM of reverse water supply to increase its effectiveness in the way of energy and natural resource saving in the process of refinement industrial water from impurities.

STATEMENT OF THE PROBLEM

The theory of hydrodynamic refinement is based on consideration of the particle movement located in the polluted zone in an opening zone [12,13]. We will consider the HF scheme in pic.1. The complex movement of pollution particles relatively to FE can be presented as a sum of two movements: longitudinal and transverse. Particles which are in the fluid layers closest to FE surface have maximum likelihood to get into an opening. The basis of HF theory is a model of particle movement relatively to FF with the certain ratio of longitudinal and transverse velocity. If the angle of slope tangent to particle trajectory $\alpha = arctg\left(\frac{\bar{v}_o}{\bar{v}_m}\right)$ is greater than the diagonal section of the unit in the longitudinal plane, the particle of pollution has an ability to pass in a unit space. Restriction of polluted particle detention in units is represented as the speed ratio:

$$\frac{d}{2c} > \frac{v_o}{v_m}. \tag{1}$$

Therefore, depending on the trajectory angle α, dimension ratio of particle diameter d and diameter of the unit opening $2c$. the particle can pass in the space under FE under the action of a cross flux or be displaced by a longitudinal flux along FE.

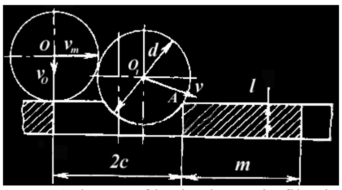

Fig. 1. Scheme of hydrodynamic filtering
c – unit radius; m – the minimum distance between cells; d – particle diameter; v_m– longitudinal flux velocity v_0 – cross flux velocity; v – absolute velocity of particle balance center; l – FE material thickness

For engineering practice development calculation a set of assumptions was accepted, which not significantly change the nature of hydrodynamic filtering process [14, 15]:

– Fluid is incompressible, homogeneous and isothermal;
– Particles are globule and homogeneous;
– Thickness influence of walls and interaction of moving particles on velocity distribution isn't considered;
– Inertia of particles in a longitudinal flux isn't considered;
– Openings in FE are accepter round.

We will use the principle of superposition. We will consider a vector of absolute participle velocity v as a vector sum of flux velocities v_0 through a large number of openings in FE and speed of a longitudinal flux v_m. As a pressure losses of a flux pressure moving lengthways FE are insignificant it is possible to consider sizes of volume expenses through separate openings equal. Summarizing these speed components in a certain point of space we receive sizes of longitudinal and transverse velocities under the influence of pressure drop on FE. For determination of the maximum particle diameter which can pass through FE opening we will consider a critical case. Thee particle with diameter d and center of gravity in a point O is placed on the pic.1.

For calculation we accept the following parameters: Q – supply of the polluted fluid on FE; Q_1 – part of supply which is refined; Δp - pressure drop which is allowed from operation conditions on FE.

We will determine the parameter of a cross flux:

$$q = \frac{Q_1}{kF}, \tag{2}$$

where:
$k = \frac{\pi \cdot c^2}{(2c+m)^2}$, coefficient of flow section, F – FE square

$$q = \frac{Q(2c+m)^2}{F\pi \cdot c^2}. \tag{3}$$

At the set velocity v_0 of cross flux from (2) we define necessary FE square

$$F = \frac{q}{v_0 \cdot \pi \cdot c^2}. \tag{4}$$

We determine the velocity of a longitudinal flux from the condition:

$$Q_2 = Q - Q_1, \tag{5}$$

where:
Q_2 – flow rate of the impure fluid leaving FE

From constructive reasons we choose FE length L on which we find FE width:

$$B = \frac{F}{L}.$$

Considering FE cylindrical its diameter:

$$D_{кр} = \frac{B}{\pi}, \tag{6}$$

The area of a crack between FE and the filter body at the end of a longitudinal flux:

$$S_k = \frac{(Q - Q_1)}{\upsilon_m}. \tag{7}$$

At the beginning of a flux:

$$S_н = \frac{Q}{\upsilon_m}. \tag{8}$$

For realization of this condition diameters of conical part of the body:

$$D_н = \left[\frac{Q}{4\pi\upsilon_m} + \frac{Q^2(2c+m)^4}{\pi^2 q^2 l^2}\right]^{0.5}, \tag{9}$$

$$D_k = \left[\frac{Q - Q_1}{4\pi\upsilon_m} + \frac{Q^2(2c+m)^4}{\pi^2 q^2 l^2}\right]^{0,5}. \tag{8}$$

Thus, at a given supply the certain geometrical parameters of the FE and body are defined speeds of a longitudinal and cross flux on which specifies the fineness of filtration.

If the velocity of a longitudinal flux is accepted by a constant gap section, it corresponds to the assumption of the turbulent mode of the flux movement along FE. The acceptability of such assumption can be proved only by existence of local flux resistance on an entrance to the filter, which is rather small in FE length, in comparison with diameter of rather high longitudinal fluxes.

At the set geometrical parameters and fluid viscosity the mode movement depends only on flux rate. Therefore, at a certain expenses of the polluted fluid on FE it is possible to provide the laminar flow movement. In case of a laminar flow in a ring crack of velocities in a gap are distributed under the parabolic law. We will determine gap size over FE at the beginning of the filter:

$$h_н = \frac{(D_н - D_{cp})}{2}, \tag{10}$$

In the end of the filter:

$$h_k = \frac{(D_k - D_{cp})}{2}. \tag{11}$$

From a condition of average velocities equality on section along FE:

$$\upsilon_{m.cp} = \frac{4Q}{\pi(D_н^2 - D_ф^2)} = \frac{Q_2}{S}. \tag{12}$$

Therefore, velocity on height ring gap is distributed on dependence:

$$\upsilon_m = \frac{6z(h-z)}{h^2}\upsilon_{m.cp}. \tag{13}$$

Thus, despite the preservations average longitudinal velocity constant along the filter length the local velocity in the gap from the surface of FE depends on the ring gap height. The received velocity υ_m for necessary filtration degree in this case won't be equal to average and therefore, it is impossible directly to determine Q_2

At laminar flows it is necessary to write down:

$$d = 2c\frac{\sum\upsilon_0 + \frac{\rho g d^2}{36\mu}}{\sum\upsilon_m + \frac{6z(h-z)}{h^2}\frac{Q_2}{S}}. \tag{14}$$

Critical diameter of a particle after substitutions and transformations is defined in the following manner:

$$d^3\frac{3}{2h^2} - d^2\left(\frac{c\rho g}{18\mu} + 3h\right) - d\upsilon_0 + 2c\upsilon_m = 0 \cdot \tag{15}$$

The last formula can be solved in final coefficients with Cardano's method however it is much simpler to find its value, which is approached on the available ECM algorithms. Further calculations don't undergo changes.

METHOD OF THE EXPERIMENT

Experimental installation, which scheme diagram is shown on pic.2 is developed for physical modeling of process of PCM wastewater refinement from impurities with application of HDF. Installation consists of three capacities: with initial water 1, with cleared 2 and capacities for polluted water storage 3, the drainage pump 4, the hydrodynamic filter 9 – the FKD1.1-60 type, flowmeters 8, manometers 7, and the regulating fittings 6 and the bypass line 5. Water is supplied by drainage pump 4 through, a flowmeter 8, the manometer 7, the cock 6 in the hydrodynamic filter 9 where the flow is divided into two components: the cleared water which is flushed via the pipeline with a flowmeter 8 and the manometer 7 in capacity 2 and the slime flowing to capacity 3. The consumption of the initial polluted water varies the degree of closing of the valve 6 on the supply pipe 6. Other expense through the bypass line 5 merges in the tank 1.

Based on the analysis of wastewater for experimental studies of refinement installation process of partial flow hydrodynamic filter which is intended for refinement of various fluids from insoluble impurity at supply of the polluted liquid to 70 l/min is provided. For creating a longitudinal flux 15 ... 20% of the fluid in circulation, bypassing the refined flow. The process of HDF was modeled on artificial wastewaters. Knowing wastewaters impurity of PCM, which comes to clean, water for experiment is modeled. As the polluting substance the selected tests of slime from slime pit which operate on PCM are applied.

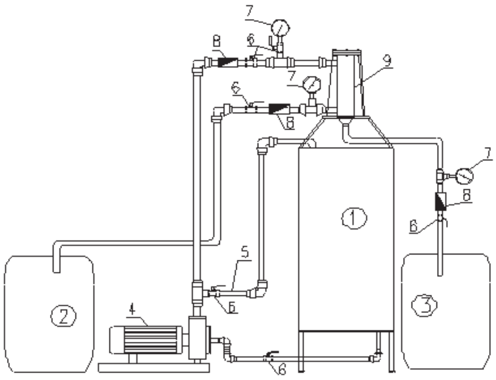

Fig. 2. Scheme of experimental installation

The composition of production wastewaters of Sharkhinsk pits (Alushta,Crimea) which are formed by washing crushed stone is presented in Table 1. The increased image of impurities containing in wastewaters from crushed stone after washing has been received by a micro-photo method is shown in pic. 3. In this fact of data fractional structure of impurities for the FKD1.1-60 filter as FE the metal gauze with a size of units of 40 x 40 microns was accepted therefore the expected fineness of the detained firm mineral particles will make 15 … 20 microns.

Table 1. Fractional composition of slimes in the total remains

Size of fraction, mm	Total mass content, %
1,25…0,63	0,03
0,63…0,315	0,15
0,315…0,15	1,34
0,15…0,08	5,78
0,08…0,05	20,59
0,05…0,01	54,39
0,01…0,005	6,80
0,005…0,002	3,78
0,002…0,001	3,29
<0,001	3,87

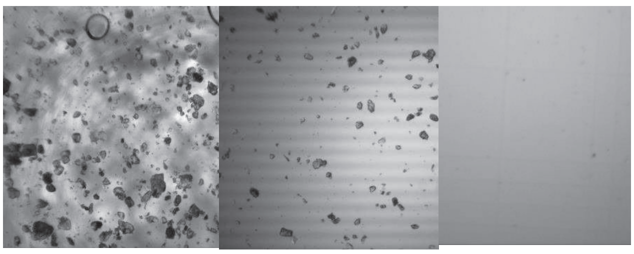

a b c

Fig. 3. Micro-photos of wastewaters impurities received from crushed stone washing:
a, – before refinement; b – after slime stage for 1 min.;
c – after HDF

For receiving artificial wastewater slime is previously dried up to the constant weight in a drying cabinet. Then slime is crushed for the purpose of receiving homogeneous mass and elimination from slime lumps. For HDF parameters process research the kinetics of sedimentation of the suspended materials of artificial wastewaters is previously studied. For this purpose dependence graphic of optical density on weighed substances concentration are under construction. The graphic is under construction according to indications of optical density of the tests which are selected after 1st minute of sedimentation as during this period large particles are drop out and they will not influence on the process of HDF. We will determine the HDF parameters by the actual concentration of impurities. For its determination we use samples of the impure water on PCM slime tests with concentration 1 … 4 g/l, after 1 minute desilting. Then tests which are run through specially prepared paper filters are selected. Further filters are dried up in a drying cabinet. The actual concentration of polluted PCV of artificial wastewater is determined by a difference of mass of the dry filter before filtration and the dry filter with the suspended materials after filtration carried to the volume of the filtered test.

Tests of artificial wastewaters are being prepared and their light transmittance on the photo-colorimeter is checked. Because of a high turbidity of tests in the accepted range of high concentration more than 1 g/l, the selected tests are diluted several times. On the received values the dependence graphic of optical density on the actual concentration of the suspended materials on which the HDF parameters are estimated is under construction.

KEY FINDINGS

The analysis of HDF process allowed allocating three major factors which influence on refinement effectiveness: initial concentration of the suspended materials; a consumption of in-taking wastewater which is regulated by a throttle on filter entrance; a ratio of a useful and slime expense on the filter which are provided with adjustment of a throttle on the bypass line. The method of rotatable design of experiment which allows receiving more exact mathematical description of a surface response in comparison with orthogonal central composite planning was applied to processing of experimental data on HDF [16, 17]. It is reached thanks to increase in number of experiences in the center of the plan and a special size choice of a star shoulder *a*. The main characteristic of a matrix of rotatable design of three-factorial experiment is provided in table 2.

At rotatable central composite design for coefficients calculation of regression and the corresponding estimates of dispersion constants are defined:

$$A = \frac{1}{2B[(n+2)B - n]}, \qquad (16)$$

$$B = \frac{nN}{(n+2)(N - N_0)}, \qquad (17)$$

Table 2. The characteristic of rotatable central composite design for three-factorial HDF researches

Number of factors	Number of factorial design experiences	Number of experiences in star points	Number of experiences in plan centre	Total number of experiences	α
3	8	6	6	20	1,414

Table 3. Actual experimental conditions

Number of factors	n	3	Value of factors at plan code values				
Name of variation factors	Designation of variation factors	Variation interval	1,68	-1	0	1	1,68
Initial conc. of suspended materials	X1	0,5	2,16	2,5	3	3,5	3,84
Consumption of in-taking water, l/min	X2	15	19,8	30	45	60	70,2
Ratio of useful and slime expense	X3	0,3	0,996	1,2	1,5	1,8	2,004

$$C = \frac{N}{N - N_0}\ , \tag{18}$$

where: n - number of factors; N - total number of rotatable central composite design experiences; N_0 - number of experiences in the plane center.

For three-factorial experiment of a constant for coefficients calculation of regression and the corresponding estimates of dispersions; $A = 0{,}45$; $B = 0{,}86$; $C = 1{,}43$.

Based on the results of preliminary experiment ranges and points in vicinities which the plan of three-factorial experiment is determined:

X1 – initial concentration of the weighed substances, 2 … 4 g/l.

X2 – supply of wastewater on the filter, 20 … 70 l/min.

X3 – a ratio of a useful and slime expense on the filter, 1 … 2 K.

The actual conditions for the accepted rotatable central composite design of experiment are presented in table 3 in the form of values of factors and intervals of their variation.

As a result of carrying out according to the chosen plan of experimental studies the subsequent processing of its results the equation of refinement effectiveness regression of HDF as residual concentration functions of rather accepted factors is received:

$$\begin{aligned} Y = {} & 0{,}35204 - 0{,}21373x_1 + 0{,}02754x_2 - 0{,}19582x_3 - \\ & 0{,}00616x_{12} - 0{,}12063x_{13} - 0{,}01778x_{23} + 0{,}08286x_1^2 + \\ & 0{,}00006x_2^2 + 0{,}30484x_3^2 + 0{,}00508x_{123}\ . \end{aligned} \tag{19}$$

We will execute validity check of the received regression equation by Fischer's criterion. For the equation (18) calculated value of Fischer's criterion made $F_p = 5{,}01$. Tabular value of Fischer's criterion at confidence coefficient P_∂=0,95 - $[F]$=5,05 [18, 19]. The validity check $F_p \le [F]$ is satisfied therefore, the regression equation (18) adequately describes a surface response for the considered HDF process. The analysis of the received regression equation allows drawing a conclusion on existence of the actual values of factors which provide optimum conditions of wastewaters refinement from impurities.

The regression equation (18) characterizes the removal process of the suspended materials on the hydrodynamic filter and allows estimating influence of three considered factors on residual concentration of impurity, and also describes a surface response. For evaluation of refinement effectiveness of HDF we will enter function of the following type:

$$Z\% = \frac{x_1 - Y}{x_1} \cdot 100\%\ . \tag{20}$$

The calculation results of HDF refinement effectiveness from the considered factors are given in pic. 3.

From the analysis of the received results obtained application of HDF for the accepted size of units of FE and fractional composition of slimes can provide refinement effectiveness to 88%. Taking into account fractional composition of slimes in size of the total remains (tab. 1) the maintenance of particles less than 10 microns in size contains in tests of artificial wastewaters to 18%, and particles less than 5 microns - to 11%. Therefore, in this range of the sizes of impurity particles the accepted parameters of operating process of HDF provide their full removal according to the size of FE units.

Change of a ratio of a useful and slime expense on the filter in the range $1 \le x_3 \le 2$ significantly influences on refinement effectiveness. With increase in the relation of a useful and slime expense on the filter the residual concentration almost depends less on the size of wastewaters supply on the filter and is defined by generally initial concentration of impurities. On the contrary at reduction of this residual concentration relation almost depends less from initial concentration of impurities but generally defined by the size of wastewaters supply on the filter.

For finding the residual concentration in the refined wastewaters after HDF for other values of the considered parameters on pic. 3 the calculation is carried out on dependence:

$$Y = x_1 \cdot \left(1 - \frac{Z}{100}\right).$$

Thus, the HDF parameters which can form a basis for development of modern technological graphics of reverse water supply of PCM are experimentally established. The residual concentration of the suspended materials received after HDF is sufficient to reuse refined wastewaters in PCM and to reuse separated impurities. Installation in PCM the systems of reverse water supply with application

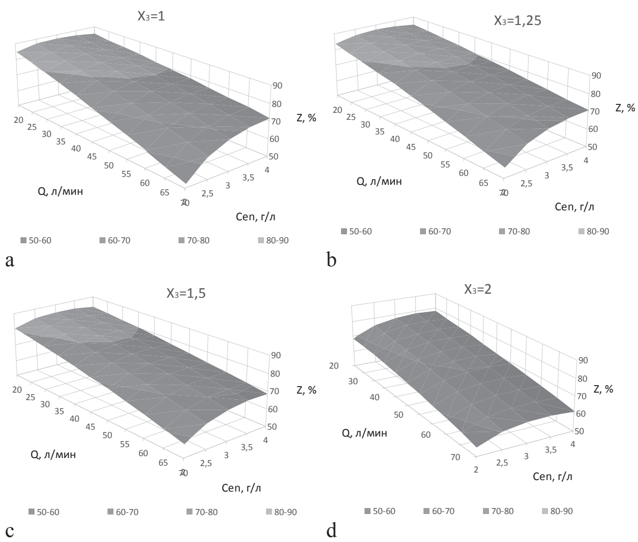

Fig. 3. Dependence of refinement effectiveness of HDF from initial concentration of the suspended materials and from wastewater supply on the filter at various values of a useful and slime expense ratios on the filter: : a - $x_3 = 1{,}0$; b - $x_3 = 1{,}25$; c - $x_3 = 1{,}5$; d- $x_3 = 2{,}0$

Thus, the HDF parameters which can form a basis for development of modern technological graphics of reverse water supply of PCM are experimentally established. The residual concentration of the suspended materials received after HDF is sufficient to reuse refined wastewaters in PCM and to reuse separated impurities. Installation in PCM the systems of reverse water supply with application of HDF allow using effectively their advantages that provide more rational use of energy and natural resources.

CONCLUSIONS

Hydrodynamic filters are intermediate between micro-filters and hydro-clones. At observance of necessary speeds of a flow fineness of the detained particles hydrodynamic filters will be 3 times less, than micro-filters, at the identical sizes of units of grids which will be established in them.

Fineness of the detained particles in the hydrodynamic filter is smaller than fineness of the particles detained in a hydro-clone at identical velocity of a flow. Thus it should be noted that micro-filters and hydro-clones at installation in working conditions have showed good technical and economic indicators. Hydrodynamic filters are deprived of micro-filters shortcomings - they do not demand flushing, and are deprived of hydro-clones shortcomings – they don't have increased mechanical wear. It provides high technical and economic rates at HDF installation in systems of industrial wastewaters refinement.

In practice of water conditioning and purification, wastewaters refinement it is necessary to delete particles of the suspended materials with the sizes from 0,1 microns to 1 mm. The existing grids that are commercially available have the minimum unit size of 40x40 microns therefore the expected fineness of the detained firm mineral particles will make 15 … 20 microns. Such subtlety of refinement is quite acceptable at preliminary stages of mechanical water and wastewaters refinement, and it is sufficient for a number of reverse systems of the industrial enterprises for refinement of technological wastewaters for technical needs. HDF need to be considered as a preliminary stage of mechanical refinement for firm mineral particles removal more than 20 microns in size.

The plan of three-factorial experiment of HDF wastewaters of PCM is developed, researches are conducted and the regression equation characterizing the process of the suspended materials removal is received. Dependences are established which help to calculate the residual content of the suspended material depending on initial concentration of impurity, a ratio of a useful and slime expense on the filter and a consumption of the processed fluid on the hydrodynamic filter. As a result of experimental studies on the simulated composition of PCM wastewaters the regression equation of refinement effectiveness which characterizes the removal process of suspended materials on the hydrodynamic filter is established and allows estimating influence of three considered factors on residual impurity concentration.

HDF provide high extent of refinement at wastewaters refinement of PCM technological capabilities which allows using them effectively in systems of reverse water supply of such industry.

REFERENCES

1. **Sokolov L.I., 1997.** Resursosberegayushchiye tekhnologii v sistemakh vodnogo khozyaystva promyshlennykh predpriyatiy/L.I.Sokolov – M.: ASV. – 256.
2. **Alferova L.A., Nachayev A.P., 1984.** Zamknutyye sistemy vodnogo khozyaystva promyshlennykh predpriyatiy, kompleksov i rayonov./ L.A. Alferova i dr. - M.: Stroyizdat. - 286.
3. **Koganovskiy A.M., 1983.** Ochistka i ispol'zovaniye stochnykh vod v promyshlennom vodosnabzhenii. M.: Khimiya. - 328.
4. **Gromov B. V., Laskorin B. N., 1985.** Problemy razvitiya bezotkhodnykh proizvodstv. - M.: Stroyizdat. – 256.
5. **Zhukov A. I., Mongayt I. L., Rodziller I. D., 1977.** Metody ochistki proizvodstvennykh stochnykh vod/A.I Zhukov i dr. - M.: Stroyizdat. - 204.
6. **Nikolenko I., Saliev Ye., 2012.** The feasibility report on maintainability of the water supply and sewerage system// MOTROL. – Vol. 14, №5. – 119 - 124.
7. **Saliev E., 2009.** Ecologological and Economic Problems of Power Saving up Technologies' Introduction in Ukraine// MOTROL. - № 11B, 104 – 110.
8. **Bazhenov YU.M., Alimov L.A., Voronina V.V., Treskeva N.V., 2005.** Proyektirovaniye predpriyatiy po proizvodstvu stroitel'nykh materialov i izdeliy./ YU. M. Bazhenov i dr. – M.: ASV. - 472.
9. **Bogdanov V.S., Borshchevskiy A.A., Il'in A.S., 2000.** Tekhnologicheskiye kompleksy i linii dlya proizvodstva stroitel'nykh materialov i izdeliy./ V.S. Bogdanov i dr. M.: Stroyizdat. – 198.

10. **Nikolenko I.V., Skidan V.V., 2011.** Perspektivy primeneniya gidrodinamicheskikh fil'trov dlya obespecheniya ratsional'nogo ispol'zovaniya prirodnykh resursov (pri proizvodstve stroitel'nykh materialov)/I. V. Nikolenko // Uchenyye zapiski Krymskogo inzhenerno-pedagogicheskogo un-ta. – Vol. № 27. Tekhn. nauki. – Simferopol'.: NITS KIPU. – 111 – 117.
11. **Mochalin Ye. V., Khalatov A. A., 2010.** Gidrodinamika zakruchennogo potoka v rotatsionnykh fil'trakh. /Ye.V. Mochalin, A.A. Khalatov/ Institut tekhnicheskoy teplofiziki NAN Ukrainy. – K. - 428.
12. **Finkel'shteyn Z. L., 1986.** Primeneniye i ochistka rabochikh zhidkostey dlya gornykh mashin./ Z. L. Finkel'shteyn. - M.: Nedra. – 232.
13. **Finkel'shteyn Z. L., 1979.** Raschet gidrodinamicheskikh fil'trov/ Z. L. Finkel'shteyn // Pnevmatika i gidravlika. Privody i sistemy upravleniya. – Vyp. 7. – M. – 232 – 240.
14. **Bojko N., Finkelstejn Z., Yamkovaya M., 2008.** Filter for cleaning with running magnetic field// MOTROL. - №10 A, 31 – 36.
15. **Z. Finkelstein, Z. Vasilechko, M. Asadi, 2012.** New posibilities for improving reliability of hydraulic equipment with the help of hydrodynamic cleaning// MOTROL. - №14-1, 11 – 15.
16. **Sautin S. N., 1975.** Planirovaniye eksperimenta v khimii i khimicheskoy tekhnologii. - L.: Khimiya. - 386.
17. **Adler YU. N., Markova Ye. V., Granovskiy YU.V., 1973.** Planirovaniye eksperimenta pri poiske optimal'nykh usloviy./ YU. N. Adler i dr. - M.: Nauka. – 348.
18. **Ruzinov L. P., 1972.** Staticheskiye metody optimizatsii khimicheskikh protsessov. - M.: Khimiya. – 364.
19. **Tikhomirov V. B., 1970.** Planirovaniye i analiz eksperimenta. - M.: Legkaya industriya. - 180.

WZROST EFEKTYWNOŚCI SYSTEMÓW DOSTARCZANIA WODY ODWROTNEJ W PRODUKCJI MATERIAŁÓW BUDOWLANYCH

Streszczenie. W artykule rozważane są zagadnienia modelowania filtrowania hydrodynamicznego w systemach dostarczania wody odwrotnej w produkcji materiałów budowlanych. Przedstawiono schemat instalacji doświadczalnej do realizacji badań pilotażowych filtra hydrodynamicznego oraz omówiono techniki tych badań. Opracowano plan trójczynnikowego eksperymentu GDF ścieków PCM, prowadzone są badania i otrzymano równanie regresji charakteryzujące proces usuwania zawieszonych materiałów. Ustalono zależności obliczania resztkowej zawartości zawieszonych materiałów według początkowego stężenia zanieczyszczeń, stosunek użyteczności i kosztu szlamu na filtrze oraz zużycie przetwarzanego płynu. Bezsporne jest, że w produkcji materiałów budowlanych montaż systemów zaopatrzenia w wodę odwrotną z zastosowaniem filtrowania hydrodynamicznego pozwala skutecznie wykorzystywać jego zalety i zapewnić bardziej racjonalne korzystanie z energii i zasobów naturalnych.
Słowa kluczowe: Produkcja materiałów budowlanych, ścieki przemysłowe, dostarczanie wody odwrotnej, filtrowanie hydrodynamicze, stężenie, koszt, resztkowe stężenie zanieczyszczeń, skuteczność oczyszczania.

TEKA. COMMISSION OF MOTORIZATION AND ENERGETICS IN AGRICULTURE – 2014, Vol. 14, No. 4, 113–118

Research on Properties of Bitumen Modified with Polymers Used for Asphalt Concrete Pavement on Bridges

Arthur Onischenko, Mykolay Kuzminets, Sergey Aksenov

National Transport University, Ukraine, Kyiv, str. Suvorova 1,
e-mail: Artur_onish@bigmir.net, Vectra16i@i.ua, Kabysik@bigmir.net

Received December 01.2014; accepted December 17.2014

Summary. There are given the investigation results of bitumen modified with the polymer (SBR) latex Butonal NS 104 depending on temperature, time and the modifying agent amount, taking into account the manufacturing company BASF recommendations. The carried out research has shown the possibility to produce bituminous polymer on the polymer latex Butonal NS basis that meets the Ukraine technological normative requirements. On the conducted investigations basis there have been established the rational parameters of bituminous polymer binding agent production process thus allowing for the determination of the requirements for the polymer latex Butonal NS 104 application under domestic production conditions.

Key words: paving bitumen, polymer latex Butonal NS, bituminous polymer preparation process, binding agent properties.

INTRODUCTION

In road-building industry bitumen modification with polymers is one of the most effective ways to extend service life of the road-building materials produced on the organic binding agents [1-10].

The most effective and recognized are the styrene-butadiene-based polymers [3-8]. Among the polymers of this type the polymer latexes of the Butonal NS 104 series (BASF production, USA) advantageously differ due to their properties [9-10].

Taking into consideration the fact that domestic paving bitumens differ from those used in the USA, a necessity emerged to study influence of such modifying agents on the properties of the paving bitumens used in Ukraine. Cationic latex Butonal NS 198 became one of the first modifying latexes used in Ukraine. On the basis of previous investigations performed by the Derzhdor research institute and KNARU research teams the effect was determined of the polymer latex Butonal NS 198 on the paving bitumen properties [5, 14]. The laboratory test results confirmed the enhancement of the binding agent physical-mechanical properties depending on the polymer amount. This research allowed to apply the Butanol NS 198 polymer at the following highways and bridges construction: Kyiv, Kyiv – Odessa (km 217 – 236, km 247 – 236, km 247 – 252); Kharkov – Simferopol (km 536 – km 538); Kyiv – Chop (km 331 – km 335), and the other objects (Fig. 1).

Fig. 1. South bridge across the Dnieper in Kiev

Recently one more type of polymer latex appeared in Ukraine – Butonal NS 104 designed to enhance the paving bitumens modifying efficiency. However, it is obvious that to achieve the maximum benefit of the polymer use and to study its influence on the bitumen physical-mechanical properties the preparation process rational parameters should be determined taking into account operating conditions. In this paper the influence is investigated of the modified with polymer latex Butonal NS 104 bitumen preparation parameters on the paving bitumen properties. The experimental investigation was conducted to determine the following:

- rational polymer consumption for bitumen modification;
- influence of the bituminous polymer preparation temperature and time on its main characteristics;

– influence of the preparation temperature and time on the bituminous polymer homogeneity.

To perform this work the sample preparation procedures were developed. The experiments were carrying out using samples of bitumen with the polymer latex Butonal NS 104 provided by the BASF representatives – “International chemical production, Ltd.”. The research was performed in the Prof. G.K. Sunya laboratory “Transport Construction Materials and Designs” of the Road Building Materials and Chemistry Department at the National Transport University.

PROCEDURE OF THE BITUMINOUS POLYMER PREPARATION BEFORE TESTING

To determine the influence of the polymer latex Butonal NS 104 on the bituminous polymer’s physical-mechanical properties, during these investigations the petroleum paving bitumen 90/130 was used as one of the most common in Ukraine. The polymer latex was added to this bitumen to determine its amount and other process-dependent parameters which are relevant to production of the bituminous polymer according to domestic requirements.

Output paving bitumen 90/130 had the following output data (Table 1).

Bituminous polymer samples were prepared containing 2%, 4% and 6% of the Butonal NS 104. Temperature during preparation varied from 160 ºC to 200 ºC. The bituminous polymers’ preparation duration varied from 1 to 8 hours. Such extended range of the modifying parameters is used also to determine their limit values under the operating conditions.

Table 1. The output data of paving bitumen 90/130

Parameters description	Unit	UNSt 4044 requirements to petroleum paving bitumen 90/130	Parameter value
Needle penetration depth at 25 ºC	0,1 mm	91 to 130	97
Softening temperature according to R&B	ºC	47 to 53	49,0
Stretchability (shortness) at temperature of 25 ºC	cm	minimum 55	82,6
Properties change after heating: residual penetration softening temperature change	% ˚C	minimum 60 maximum 6	95 2
Fragility temperature	˚C	maximum -10	-22
Flash temperature	˚C	minimum 240	240
Adhesion	%	-	90

To modify bitumen binding agent, a blade mixer installation was developed, (Fig. 2) which allowed for performing the process with the specified technological modes.

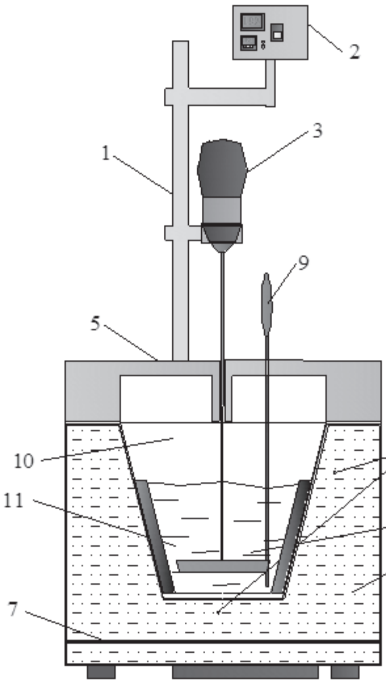

Fig. 2. Laboratory blade mixer (side-view)
1 – tripod, *2* – control unit, *3* – electric motor, *4* – blade agitator, *5* – oil thermostat *6* – oil tank *7* – electric tensor, *8* – thermocouple in the oil thermostat, *9* – thermocouple for modified bitumen, *10* – metal container according to DSTU 3277, *11* – bitumen binder.

LABORATORY RESEARCH RESULTS

The tests on the output bitumen as well as bitumen modified with polymer were carried out according to applicable regulations [9-15]. The output and modified bitumen test results are shown in Fig. 3-5.

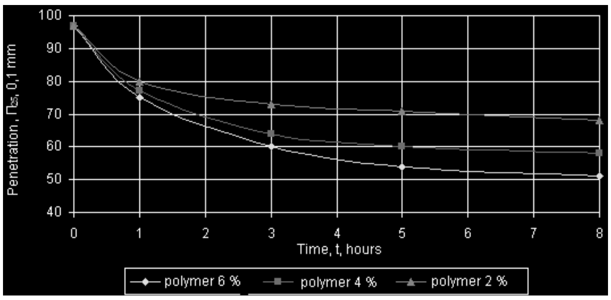

Fig. 3. Bituminous polymer penetration dependence (at 25 ºC) upon the preparation time at various polymer amounts

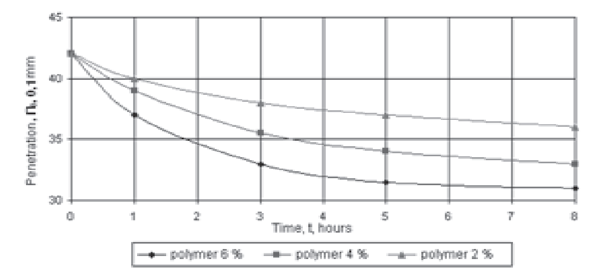

Fig. 4. Bituminous polymer penetration dependence (at 0 ºC) upon the preparation time at various polymer amounts

On the basis of these results the conclusion can be made that to establish the bituminous polymer viscosity factor it is sufficient to modify the binding agent during three hours and after this time period it is possible to determine its grade. While analyzing the bituminous polymer viscosity change in case of the preparation temperature change from 160 ˚C to 200 ˚C it is seen that at its increase the viscosity value increases, too (Fig. 5).

As it may be seen, at the preparation temperature of 160 ˚C with 2 % of polymer the observed viscosity reduction (Π_{25}) equals 16 %, with 4 % of polymer – 18 %, with 6 % of polymer – 20 %. At the temperature of 180 ˚C with 2 % of polymer the observed viscosity reduction equals 25 %, with 4 % of polymer – 34 %, with 6 % of polymer – 37 %; and at the temperature of 200 ˚C – respectively 28 %, 38 % and 48 %. On the basis of such results it is possible to assume that while preparing the bituminous polymer at the temperature of 160 ˚C, the modifying process did not take place completely, which corresponds to BASF recommendations (the recommended range is 170-180 ˚C).

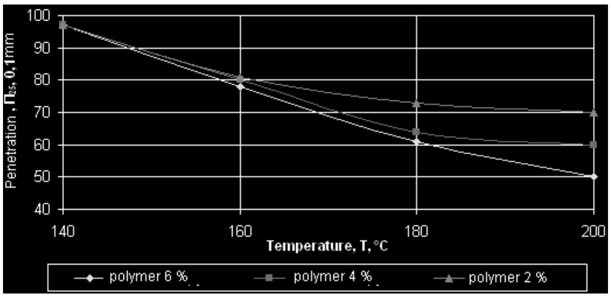

Fig. 5. Bituminous polymer penetration dependence (at 25 ˚C) upon the preparation temperature at various polymer amounts

Decrease of the penetration value of the bituminous polymer prepared at temperatures of 180 ˚C and 200 ˚C is virtually the same, however it can also be assumed that under such conditions simultaneously with the binding agent modifying process the intensive processes of its deterioration occurs. It is important also to note that at the preparation temperature increase and especially at polymer amount increase (up to 6 %) the bituminous polymer may transfer to a more viscose state. This feature of the produced bituminous polymer should be taken into consideration during preparation, placement and consolidation of polymer road concrete mix.

The results of determination of the bituminous polymer softening temperature dependence upon the preparation temperature and time showed its changeable character (Fig. 6, 7) similar to the penetration changeability.

In case of 2 % polymer concentration, already after the first hour of bituminous polymer bending agent preparation (Fig. 6) the heat resistance value increased by 5 ˚C and remained virtually constant at its further maturing in the reactor (Fig. 6).

In case of 4 % polymer concentration the main increase in the heat resistance value took place during the first hour of bituminous polymer bending agent preparation and corresponded to 10 ˚C. After 8 hours of the bituminous polymer bending agent preparation this increase was equal to 14 ˚C.

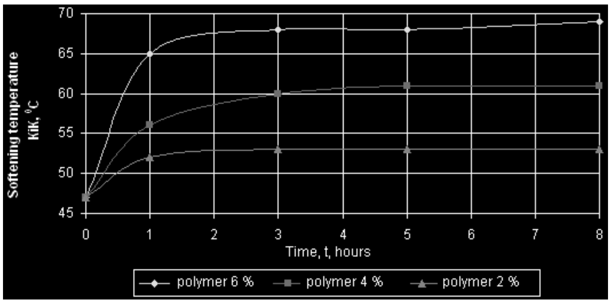

Fig. 6. Bituminous polymer softening temperature dependence upon the preparation time at various polymer amounts

In case of 6 % polymer concentration these parameters were equal to 15 ˚C and 21 ˚C. It is necessary to note that the bituminous polymer bending agent was prepared at the temperature of 180 ˚C according to BASF recommendations. In case of the bituminous polymer bending agent preparation at the temperature reduction from 200 ˚C to 160 ˚C (Fig. 7) the softening temperature value respectively increased by 1 ˚C and decreased by 3-5 ˚C.

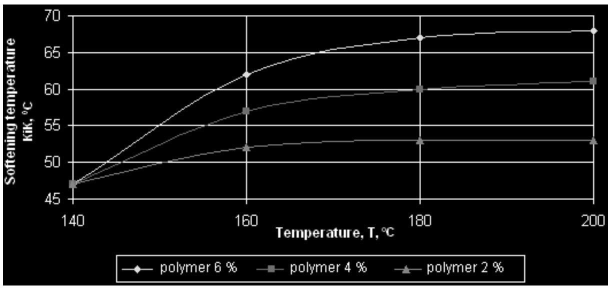

Fig. 7. Bituminous polymer softening temperature dependence upon the preparation temperature at various polymer amounts

It confirms the previous assumption that the bituminous polymer bending agent preparation temperature of 160 ˚C is insufficient for quick polymer integration to get the homogeneous mixture, and the heat resistance slow increase at the preparation temperature of 200 ˚C ensures that the deterioration processes do not develop.

To examine the possible bituminous polymer bending agent deterioration at too high temperatures, the bituminous polymer bending agent elasticity change in a range of the temperatures and preparation time periods was measured. The following results were obtained:

The elasticity occurrence even at the small amount of polymer and modifying time (at 2 %, after 1 hour of preparation (Fig. 8) confirms the possibility of the bituminous polymer bending agent elastic properties considerable enhancement.

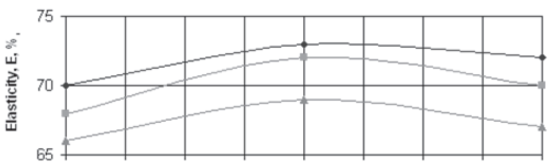

Fig. 8. Bituminous polymer elasticity dependence upon the preparation temperature at various polymer amounts

In case of 2 % polymer concentration after the first hour of preparation the elasticity factor was equal to 62%, after 3 hours – 69 %, and it remained constant at the maximum time of the bituminous polymer bending agent – 8 hours. Similar increase of the elasticity factor was found at modifying 4 % of polymer respectively by 66 % and 73 %, and at 6 % of polymer – 67 % and 73 %. Thus the polymer amount increase even up to 6 % virtually did not influence the increase of the elasticity factor which is also sufficiently high at a smaller amount of the polymer.

It is especially important to note that the elasticity value at the high temperatures of the bituminous polymer bending agent preparation remained virtually invariable (Fig. 9) as compared with the preparation at low temperatures. These results confirm the previous statements concerning the new binding agent deterioration resistance.

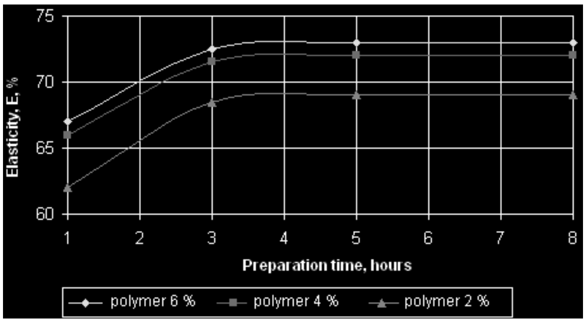

Fig. 9. Bituminous polymer elasticity dependence upon the preparation time at various polymer amounts

The bituminous polymer bending agent important parameters which characterize its processability, usability in production conditions, and also determine the produced binding agent quality, are the bituminous polymer bending agent properties changes after heating and disintegration during storage. Therefore, in this work, investigations were conducted and the results obtained which confirmed the very slight change of such properties at given modifying temperatures.

It may be seen that the bituminous polymer bending agent heat resistance factor change after heating at various polymer amounts and time of its modifying is very slight. After the first hour of modifying at preparation temperature of 180 ˚C this parameter was higher by 2-4 ˚C as compared to the output bituminous polymer bending agent, which is explained by the non-modified bending agent, while after 3 hours of modifying this parameter did not exceed 3 ˚C (Fig. 10), i.e. it met the applicable requirements.

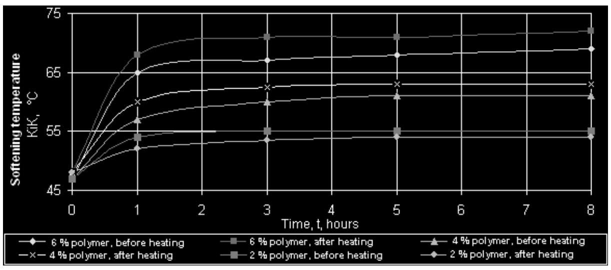

Fig. 10. Bituminous polymer softening temperature change dependence upon the preparation time at various polymer amounts

At lowering the bituminous polymer bending agent preparation temperature to 160 ˚C this parameter remained the same, and at the temperature increase up to 200 ˚C its maximum value was 5 ˚C (Fig. 11), which also met the requirements [8-11].

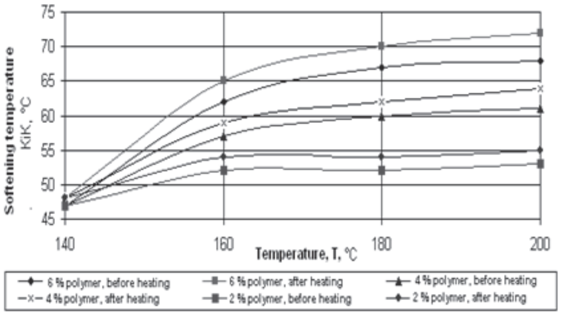

Fig. 11. Bituminous polymer softening temperature change dependence upon the preparation temperature at various polymer amounts

Dependence of the bituminous polymer bending agent disintegration factor during storage (according to penetration factor) on the polymer amount, the preparation time and temperature showed its slight change during modifying both at low temperatures and at high ones (5-7 degrees of penetration) (Fig. 12, 13).

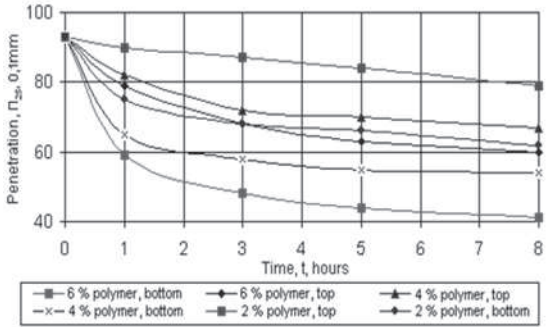

Fig. 12. Bituminous polymer disintegration during storage (according to penetration factor) dependence upon the preparation time at various polymer amounts

Although this parameter is not rated the obtained results show the sufficient homogeneity of produced binding agent after modifying. Dependence of the bituminous polymer bending agent disintegration factor during storage (according to softening temperature) upon the polymer amount and its preparation time showed slight change of this parameter that additionally confirmed the obtained bituminous polymer bending agent homogeneity as well as the ability to be processed. However, it is necessary to note that at the polymer amount increase, the disintegration factor value increases too, although remaining within the allowable limits.

At the polymer concentration of 2 % the KiK factor difference depending on the preparation time varied from 1 to 4 ˚C, while at the polymer concentration of 6% this difference was equal to 3-5˚C (Fig. 14, 15).

Such results are observed in the entire range of the bituminous polymer bending agent preparation temperature change.

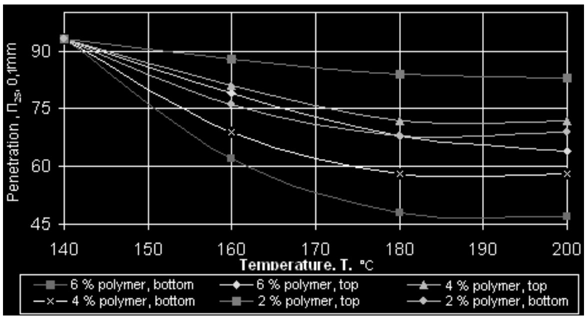

Fig. 13. Bituminous polymer disintegration during storage (according to penetration factor) dependence upon the preparation temperature at various polymer amounts

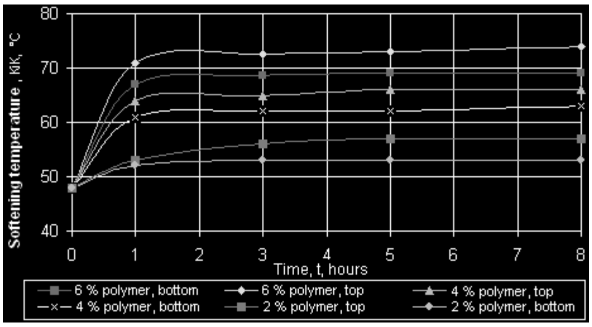

Fig. 14. Bituminous polymer disintegration during storage (according to softening temperature) dependence upon the preparation time at various polymer amounts

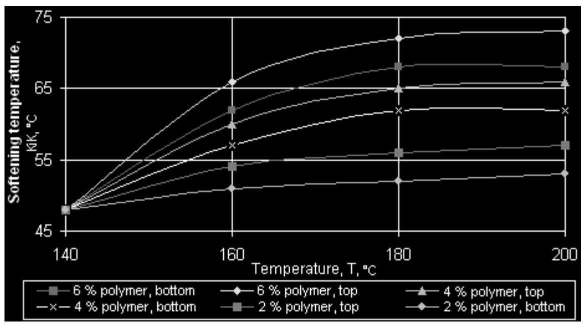

Fig. 15. Bituminous polymer disintegration during storage (according to softening temperature) dependence upon the preparation temperature at various polymer amounts

CONCLUSIONS

1. The bituminous polymer bending agent on the basis of the Butanol NS 104 polymer latex in compliance with all standard parameters meets the requirements to bitumen modified with polymers.
2. The bituminous polymer bending agent physical-mechanical properties change in the wide limits (by 50-100 %) depending on the polymer amount and the preparation process parameters shows the possibility of its properties active regulation under the particular operating conditions.
3. The bituminous polymer bending agent properties resistance and stability under the high process temperatures influence shows the possibility of its sufficiently long-term storage under the production conditions with the original properties retained.
4. Short time of this bituminous polymer bending agent preparation (on average 2-3 hours) allows for the saving of the considerable energy resources and advantageously distinguishes it from the bituminous polymer bending agents produced with the other modifiers. .
5. The Butanol NS 104 polymer latex rational amount for modifying the bitumen of this grade constitutes 2-3 %, the preparation time is within the limits of 2-3 hours, and the optimal preparation temperature is close to 170-180 ˚C.

REFERENCES

1. **SOU 42.1- 37641918 – 100:2013.** “Bitumen, modified using laboratory blade mixer. Methods for process control modifications.
2. **Zolotarev** V.A**., 2009.** Polymer modified bitumen and asfalt polimer cements // Dorozhnaia tehnika. 88-95.
3. **Zolotarev** V.A**., 2003.** Properties of bitumen, SBS polymer-modified type // Avtoshlyahovik of Ukraine. – Issue 3. -Kyiv. 29-31.
4. **King G.N., Radovskii B.S., 2004**. Properties of polymer bitumen binders in the U.S. and methods of testing // Scientific and Technical Information Kit. Novosti v dorozhnom dele – Issue 6.-Moscow. 1-28
5. **King G.N., Radovskii B.S., 2004**. Materials and technology company Koch Materials for the construction and repair of road surfaces// Scientific and Technical Information Kit. Novosti v dorozhnom dele – Issue 6.-Moscow. 28-62
6. **Hochman L. M., 2004.** Complex organic binders based on block copolymers SBS type. – Moscow: “Ekoninform” JSC – 510.
7. **Kirichek Y.A., Dem’yanenko V.V., Suhorebryy O.A., 2008.** Experimental study of the properties of modified bitumen used in road construction // Bulletin of Prydniprovska State Academy of Construction and Architecture. – Dnepropetrovsk: PSABA, -№ 6-7. 14-17.
8. **Onishchenko A.M., 2008.** Improving durability of asphalt layers by the use of polymer latexes. Theses Candidate of sciences 05.22.11. Kyiv, 229.
9. **DSTU B V.2.7-135: 2007** “Bitumen modified with polymers. Specifications “ Zolotarev V.A., Mozgovoy V.V., Zhdanyuk V.K., and other.
10. **DSTU 4044-2001** “Bitumen road viscous. Specifications“
11. **Basov G., Kireev A., Kireeva M., 2010** “Improvement of the ultrasonic diagnosing of axes of the wheeled pairs of rolling stock of railways” // Lublin, Poland, TEKA, XA... 21-28
12. **Druz O., Gitnaya S., 2011** “Choice of the economical method of welding at making of steel constructions” // Lublin, Poland TEKA, XIA... 45-56
13. **Kravchenko A., Sakno O., 2011** “Tire life adjustment on the coefficients of operational and road conditions” // Lublin, Poland, TEKA, XIA... 121-129
14. **Sumorek A., Buczaj M., 2012** “New elements in vehicle communication “media oriented systems transport” protocol» // Lublin, Poland, TEKA, XII_1... 275-281

15. **Kulig R., Skonecki S., Łysiak G., Laskowski J., Rudy S., Krzykowski A., Nadulski R., 2013** "The effect of pressure on the compaction parameters of oakwood sawdust enhanced with a binder" // Lublin, Poland, TEKA, XIII_1... 83-89
16. **Korop G., 2013 "**Development of structure and the concept of functioning the modernized logistic system of service industrial enterprise by railway" // Lublin, Poland, TEKA, XIII_4... 99-107

ИССЛЕДОВАНИЕ СВОЙСТВ БИТУМОВ МОДИФИЦИРОВАНЫХ ПОЛИМЕРОМ ДЛЯ ИСПОЛЬЗОВАНИЯ АСФАЛЬТОБЕТОННЫХ ПОКРЫТИЙ НА МОСТАХ

Аннотация. В работе приведены результаты исследования битума, модифицированного полимерным латексом типа СБР Butonal NS 104, в зависимости от температуры, времени и количества модификатора, с учетом производственных рекомендаций компании BASF. Проведенные исследования показали возможность производства модифицированного битума латексом Butonal NS 104, который соответстует технологическим и нормативным требованиям стандартов Украины. На основе результатов исследований были установлены рациональные параметры модификации битумного вяжущего полимерным латексной Butonal NS 104 в производственных условиях.

Ключевые слова: дорожный битум, полимерный латекс Butonal NS, процесс подготовки битума модифицированного полимером, связывающие свойства битума.

Characteristics of Selected Rheological Properties of Water Suspensions of Maize TPS Biocomposites

Tomasz Oniszczuk, Agnieszka Wójtowicz, Leszek Mościcki, Andrzej Rejak, Maciej Combrzyński

Department of Food Process Engineering, Lublin University of Life Sciences
Doświadczalna 44, 20-236 Lublin, Poland e-mail: tomasz.oniszczuk@up.lublin.pl

Received December 07.2014; accepted December 18.2014

Summary. The research covered the aqueous solutions of maize thermoplastic starch (TPS). The thermoplastic starch granules were produced from mixtures of maize starch, glycerol and an additive of fillers in the form of natural fibres. In the study, a modified single-screw extrusion-cooker TS 45 was used with L/D=16 and L/D=18 with an extra cooling of the end part of the barrel. The research focused on the effect of the extruder screw speed, the plasticizing system and the type of filler used for apparent viscosity of pulverized granules of maize starch. During the measurements, the top values of apparent viscosity were reported for the maize TPS containing an addition of cellulose fibre extruded with the plasticizing system L/D=16.

Key words: viscosity, thermoplastic starch, extrusion, biocomposites.

INTRODUCTION

The recent decades have seen a growing application of plastics in all the areas of human activity. Today, it is difficult to imagine life without plastics in packaging, toys, cars, medical products, etc. However, besides the unquestionable benefits, there are also some negative consequences of their ubiquity. The method of processing and disposal of different types of plastic after their life cycle has a tremendous impact on the natural environment, including human health [9, 12, 13, 18]. It has been asserted that some chemical compounds used in plastics processing for the production of food packaging (biosphenol A – BPA) can affect the human endocrine system and are ranked among cancer-causing substances. The U.S. companies representing the plastics industry decided to withdraw BPA from the process of manufacturing packaging for food storage, and the U.S. government declared amendments to the relevant law on food safety that are expected to eliminate any products containing BPA that are likely to be detrimental to consumers until tests prove the non-carcinogenic effect of BPA on humans [5, 8]. There are many more examples of similar concerns. Therefore, the general public puts more and more attention to the growing problem of plastics and their recycling.

In order to protect the environment, and above all, protect human health, developed countries undertake research into the manufacture of environmentally friendly polymers. The primary focus is on natural materials, including those made of different types of starch. Biopolymers are obtained after mixing starch with a plasticizer (often glycerol) so as to allow the liquefaction of the material at a temperature lower than the decomposition temperature of the starch. Such starch is referred to as thermoplastic starch (TPS) and is regarded as a biodegradable biopolymer [1, 2, 5, 7]. Biodegradable polymers, like petroleum polymers, must meet certain requirements in terms of physical properties. Biopolymer production is done on the machines and equipment used for the production of synthetic polymers. These materials can be an option in the plastics market offering [3, 10, 17, 19].

The aim of the study was to determine the viscosity of thermoplastic maize starch water solutions with an addition of natural fibre of different origin, depending on the production parameters.

MATERIALS AND METHODS

The basic raw material used in the study was maize starch of the type MERIZET 100 produced by Segezha, Ireland. Also, flax fibre was used from a Polish producer, cellulose fibre Vivapur type 102 JRS from a German producer and ground pine bark. The basic characteristics of the ground bark, cellulose fibre and flax fibre are given in Table 1.

Table 1. Basic characteristics of cellulose fibre, flax fibre and bark.

	Cellulose fibre	Flax fibre	Ground pine bark
Feature	Determination results		
Particle size [m]	$50 \cdot 10^{-6} – 160 \cdot 10^{-6}$	$3 \cdot 10^{-3} – 5 \cdot 10^{-3}$	$50 \cdot 10^{-6} – 180 \cdot 10^{-6}$
Bulk density [kg/m^3]	280–330	1500	120–250
Humidity [%]	3–5	5–7	5–8

From among a considerable group of auxiliary substances used as plasticizers and additives improving the quality of obtained material, the study used technical glycerol of 99% purity in the amount of 20% of dry mass of starch [16].

PREPARATION OF TPS MIXTURES

Starch with 16% of moisture content, cellulose fibres, flax fibres, ground bark and glycerol were used to prepare material mixtures. The glycerol accounted TPS for 20% of the mixture weight, and the proportion of fibres was 10, 20 and 30%. Samples were mixed using a laboratory mixer ribbon. Through repeated trials, the effective mixing time was established at 20 minutes. After mixing, the samples were left in sealed plastic bags for 24 hours to homogenize. Immediately before extrusion, the samples were mixed again for 10 minutes to obtain a loose and powdered structure of the mixture.

EXTRUSION

TPS biocomposite granules were made by a single-screw extrusion-cooker equipped with two kinds of plasticizer systems with the screw length/diameter ratio of L/D=16/1 and L/D=18/1 (Photo 1). A steel die was used with a hole of 3 mm in diameter. Granules were produced at the extruder screw speed of 60, 80 and 100 rpm. The extrusion parameters were set in the temperature range 60-110°C and maintained by appropriately adjusting the flow intensity of the cooling liquid. The extruder was equipped with a material feeder, a plasticizing system made up of the screw linked to the drive and housing, a preheating device and a cooling system [8, 11, 14, 15].

MEASUREMENT OF APPARENT VISCOSITY

A Zwick testing machine was used in the study equipped with a back extrusion chamber. The obtained extrudate was ground in a laboratory mill to the grain size below 0.8 mm. From the ground extrudateand distilled water at 20°C, 10% suspensions were prepared by continuous mixing. The viscosity measurement of the suspensions was carried out after 10 minutes of mixing. The measurements were made in the back extrusion chamber, 60 mm in height and 50 mm of inner diameter, using a plunger with a diameter of 46

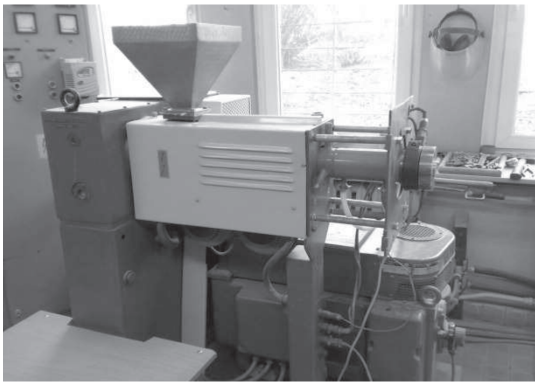

Photo 1. Single-screw extruder TS-45 made by Z. M. Ch. Metalchem in Gliwice, Poland.

mm and a height of 20 mm with a conical bottom surface. The following settings were used in the study: 0.5 kN head force, 2 mm measuring gap, the total test length 60 mm, head speed 50 mm/min^{-1}. During the study, the resistance force of the suspension was recorded during the movement of the plunger in one bottom-up measurement cycle, which was next converted into the apparent viscosity coefficient. The measurements were made using the testXpert 10v11 program. There were five replications, the final result being the arithmetic mean of the measurements [4, 6].

RESULTS

The use of the back extrusion chamber allowed the examination of the apparent viscosity of fine thermoplastic starch granules and of the degree of bonding of the fillers: cellulose fibre, flax fibre and ground bark. These parameters are crucial in determining the processing properties of thermoplastic starch. The addition of natural fillers in the form of granules is intended to stabilize the shape and improve the performance of rigid forms of packaging.

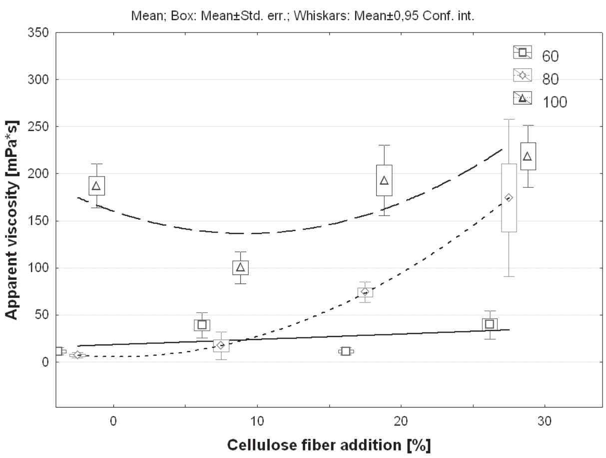

Fig. 1. The influence of cellulose fibres and the extruder screw speed on the apparent viscosity of maize starch solutions (extruder plasticizing system of L/D=16).

Fig. 1 shows the dependence of the viscosity of aqueous solutions of thermoplastic maize starch upon the applied screw speed of the L/D=16 version extruder and upon the content of cellulose fibre in the mixture. It was observed that the viscosity of the solution increased along with the increasing extruder screw speed and a higher addition of cellulose fibre. This dependency is corroborated through the positive values of the slope coefficients of polynomial trend lines for all the applied screw speeds (Table 2). Also, the most significant differences were indicated between the means ($p < 0.05$).

The highest viscosity values were obtained for granulated material produced at the extruder screw speed of 100 rpm^{-1}. This testifies to a good bond between the fibres and biopolymer matrix.

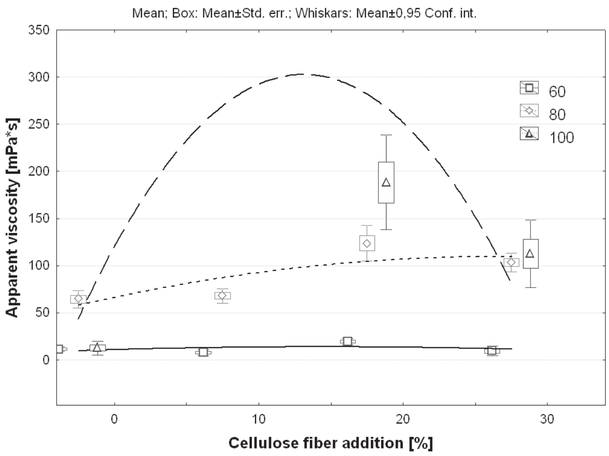

Fig. 2. The influence of cellulose fibres and the extruder screw speed on the apparent viscosity of maize starch solutions (extruder plasticizing system of L/D=18).

The solution of the granulated material obtained using the plasticizing system of the extruder with L/D=18 demonstrated lower apparent viscosity values compared with the results obtained for the shorter version. A similar trend was observed: viscosity increased along with the increasing extruder screw speed and a higher addition of the filler. Also in this case, significant differences were reported between the means (Table 2).

An additive of flax fibre caused a slight increase in the viscosity of solutions (Fig. 3). The highest viscosity values were obtained for granulated maize starch produced at the extruder screw speed of 100 rpm^{-1}. Along with the rising content of flax fibre in all the tested materials, viscosity increased only slightly. The addition of 30% of flax fibres caused a decrease in the viscosity of solutions, which demonstrates a weak bond between the flax fibres and the biopolymer matrix.

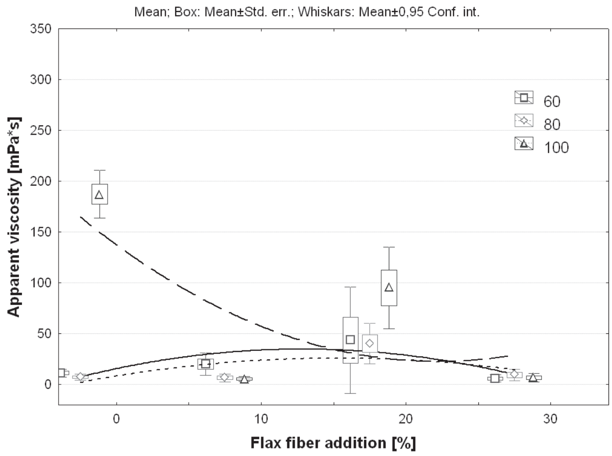

Fig. 3. The influence of flex fibres and the extruder screw speed on the apparent viscosity of maize starch solutions (extruder plasticizing system of L/D=16).

During the examination of the solution of extrudates produced on the longer version of the plasticizing system,

Table 2. The results of the statistical analysis of viscosity of aqueous solutions of thermoplastic starch depending on the additives used.

Additive	L/D version	Screw rotation [rpm^{-1}]	Polynomial regression equation	F test values (3,23)	P value
Cellulose fibre	16	60	$y_{60} = 0.001x^2 + 0.545x + 18.360$	12.599	0.00001
		80	$y_{80} = 0.226x^2 - 0.070x + 5.488$	17.099	0.0000008
		100	$y_{100} = 0.282x^2 - 5.185x + 160.265$	17.048	0.0000009
	18	60	$y_{60} = -0.014x^2 + 0.420x + 10.906$	9.807	0.00010
		80	$y_{80} = -0.06x^2 + 3.220x + 66.557$	28.842	0.000000003
		100	$y_{100} = -1.065x^2 + 27.89x + 120.263$	61.304	0.0000
Flax fibre	16	60	$y_{60} = -0.116x^2 + 2.973x + 15.788$	2.029	0.1295
		80	$y_{80} = -0.075x^2 + 2.301x + 8.523$	12.355	0.00002
		100	$y_{100} = 0.233x^2 - 10.350x + 137.523$	72.707	0.0000
	18	60	$y_{60} = -0.261x^2 + 7.562x + 45.621$	0.932	0.4363
		80	$y_{80} = -0.007x^2 + 0.538x + 77.042$	0.395	0.7567
		100	$y_{100} = -0.029x^2 + 3.914x + 17.891$	1.941	0.1428
Ground pine bark	16	60	$y_{60} = -0.043x^2 + 1.290x + 11.446$	10.963	0.00004
		80	$y_{80} = 0.056x^2 + 0.973x + 12.322$	29.406	0.000000003
		100	$y_{100} = 0.509x^2 - 15.957x + 139.557$	39.170	0.0000
	18	60	$y_{60} = -0.092x^2 + 2.648x + 12.712$	14.284	0.000004
		80	$y_{80} = -0.162x^2 + 3.482x + 57.042$	24.721	0.00000002
		100	$y_{100} = -0.392x^2 + 10.101x + 34.344$	40.680	0.0000

some problems emerged with maintaining the homogeneity of solutions which began to delaminate. Friction rose in the places of fibre settlement, hence the considerable differences in the the viscosity of solutions, which is visible in Fig. 4, showing the results of measurements of the viscosity of solutions of biopolymers obtained by using the extruder plasticizing system of L/D=18. There were no significant differences reported between the means for these granules ($p>0.05$) (Table 2).

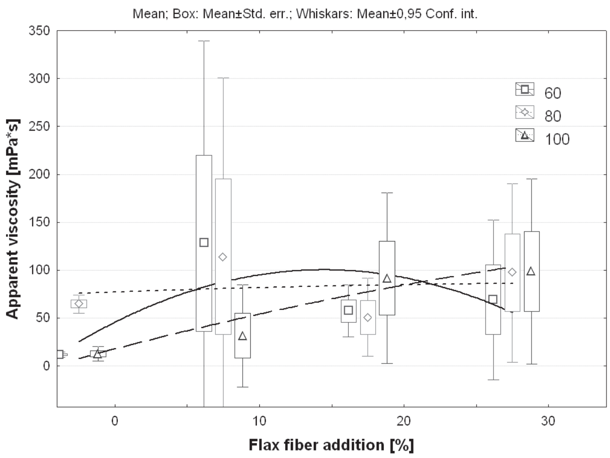

Fig. 4. The influence of flex fibres and the extruder screw speed on the apparent viscosity of maize starch solutions (extruder plasticizing system of L/D=18).

Another type of thermoplastic starch biocomposites subjected to analysis were maize starch granules with the addition of ground bark. Fig. 5 and 6 show the measurement results of the apparent viscosity depending on the version of the plasticizing system used. The viscosity values of the thermoplastic starch solutions with the addition of ground bark were lower than the viscosity of TPS solutions with the cellulose fibre content. During the study, as in the case of flax fibre solutions, the suspensions were delaminated.

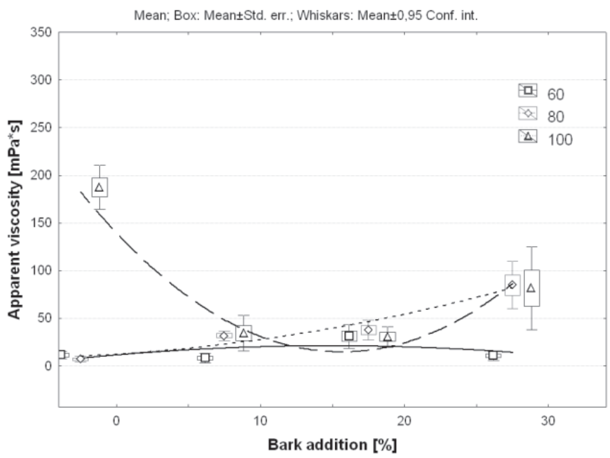

Fig. 5. The influence of ground bark and the extruder screw speed on the apparent viscosity of maize starch solutions (extruder plasticizing system of L/D=16).

The addition of 30% of ground bark to maize starch granules (extruder plasticizing system of L/D=16) contributed to the dispersion of the apparent viscosity values, which was caused by resistance occurring during the study. TPS granule solutions containing ground bark obtained by using the plasticizing system of the extruder with L/D=18 showed higher apparent viscosity values (Fig. 6). The top values were recorded for the addition of 20% of ground bark to the thermoplastic starch extruded at the screw speed of 80 rpm^{-1} (120 mPas).

The lowest viscosity values were demonstrated by the mixtures of maize starch and glycerol containing a 30% addition of ground bark in the whole range of extruder screw speeds.

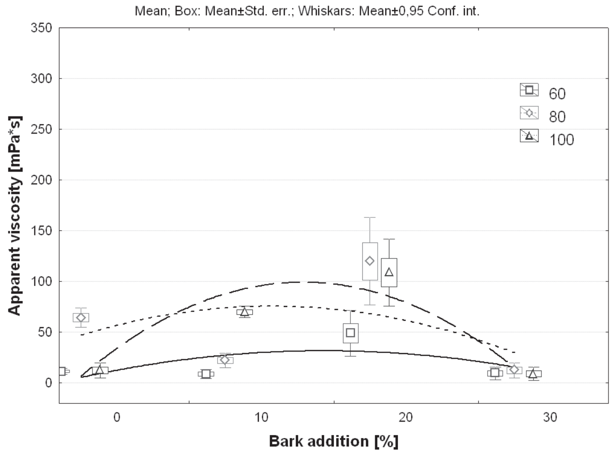

Fig. 6. The influence of ground bark and the extruder screw speed on the apparent viscosity of maize starch solutions (extruder plasticizing system of L/D=18).

CONCLUSIONS

- It was observed that the apparent viscosity of the solutions of thermoplastic maize starch was determined by the rotational speed of the extruder used for the production of the granulated matter.
- The highest apparent viscosity values were reported for solutions of maize TPS with the addition of cellulose fibre.
- The aqueous solutions of granules obtained with the extruder plasticizing system at L/D=16/1 showed higher apparent viscosity values.
- The addition of fillers such as natural fibres increased viscosity in the majority of examined aqueous solutions of extruded maize starch.

REFERENCES

1. **Averous L., Moro L., Dole P., Fringant C., 2000:** Properties of thermoplastic blends: starch – polycaprolactone, Polymer,41, 4157.
2. **Bledzki A.K., Gassan J., 1999:** Composites reinforced with cellulose based fibres, Prog. Polymer Science, 24, 221.
3. **Dyadychev V., Pugacheva H., Kildeychik A., 2010:** Co-injection molding as one of the most popular injection molding Technologies for manufacture of polymeric

details from secondary raw materials, TEKA Commision of motorization and Power Industry in Agriculture, PAN, Volume Xc, 57-62.

4. **Gujral H.S., Sodhi N.S., 2002:** Back extrusion properties of wheat porridge *(Dalia)*. Journal of Food Engineering 52, 53-56.
5. **Janssen L.P.B.M., Moscicki L. (Eds) 2008:** Thermoplastic Starch, Wiley-VCH Verlag GmbH & Co. KGaA, Weinheim, 1-29.
6. **Lee S-Y., Luna-Guzman I., Chang S., Barrett D.M., Guinard J-X., 1999:**Relating descriptive analysis and instrumental texture data of processed diced tomatoes. Food Quality and Preference. 10, 447-455.
7. **Mitrus M., 2006:** Investigations of thermoplastic starch extrusion cooking process stability, TEKA Commission of motorization and Power Industry in Agriculture PAN, Volume VIa, 138-144.
8. **Mitrus M., Oniszczuk T., 2007:** Wpływ obróbki ciśnieniowo – termicznej na właściwości mechaniczne skrobi termoplastycznej, Właściwości geometryczne, mechaniczne i strukturalne surowców i produktów spożywczych, Wyd. Nauk. FRNA, Lublin, 149-150.
9. **Mościcki L. (Ed) 2011:** Extrusion-Cooking Techniques, Wiley-VCH Verlag GmbH & Co. KGaA, Weinheim, 177-188.
10. **Mościcki L., Mitrus M., Wójtowicz A., 2007:** Technika ekstruzji w przemyśle rolno – spożywczym, PWRiL, Warszawa.
11. **Mościcki L., Mitrus M., Wójtowicz A., Oniszczuk T., Rejak A., Janssen L., 2012:** Application of extrusion-cooking for processing of thermoplastic starch (TPS), Food Research International, Vol. 47, , pp 291-299.
12. **Oniszczuk T., Pilawka R.,2013:** Wpływ dodatku włókien celulozowych na wytrzymałość termiczną skrobi termoplastycznej, Przemysł Chemiczny, 2, 265-269,
13. **Oniszczuk T., Pilawka R., Oniszczuk A., 2013:** Wpływ dodatku mielonej kory sosnowej na wytrzymałość termiczną skrobi termoplastycznej, Przemysł Chemiczny, 8, 1554-1557.
14. **Oniszczuk T., Wójtowicz A., Mitrus M., Mościcki L., Combrzyński M., Rejak A., Gładyszewska B., 2012:** Influence of proces conditions and fillers addition on extrusion-cooking efficiency and SME of thermoplastic potato starch, Teka Commision of Motorization and Energetics in Agriculture, Polish Academy of Sciences Branch in Lublin, vol. 123, No 1, pp. 181-184,
15. **Oniszczuk T., Wójtowicz A., Mitrus M., Mościcki L., Combrzyński M., Rejak A., Gładyszewska B., 2012:** Biodegradation of TPS mouldings enriched with natural fillers, Teka Commision of Motorization and Energetics in Agriculture, Polish Academy of Sciences Branch in Lublin, vol. 123, No 1, pp. 175-180,
16. **Sobczak P., 2006:** Sorbitol addition on extrusion process, TEKA Commission of Motorization and Power Industry in Agriculture PAN, Volume VIa, 163-169.
17. **Thomas D.J., Atwell W.A., 1997:** Starch Analysis Methods. In: Starches. Eagan Press, St. Paul, Minnesota, 13-18.
18. **Żakowska H., 2003:** Opakowania biodegradowalne, Centralny Ośrodek Badawczo-Rozwojowy Opakowań, Warszawa, 20-65.
19. **Zhang Y.R., Wang X.L., Zhao G.M., Wang Y.Z., 2013:** Influence of oxidized starch on the properties of thermoplastic starch. Carbohydrate Polymers 96, 358– 364.

CHARAKTERYSTYKA WYBRANYCH CECH REOLOGICZNYCH WODNYCH ROZTWORÓW KUKURYDZIANYCH BIOKOMPOZYTÓW TPS

Streszczenie. Badaniom poddano wodne roztwory granulatów kukurydzianej skrobi termoplastycznej (TPS). Granulaty skrobi termoplastycznej zostały wyprodukowane z mieszanek skrobi kukurydzianej, gliceryny oraz dodatku wypełniaczy w postaci włókien naturalnych. W badaniach zastosowano zmodyfikowany ekstruder jednoślimakowy TS 45 o L/D=16 i L/D=18 z dodatkowym chłodzeniem końcowej części cylindra urządzenia. Badano wpływ prędkości obrotowej ślimaka ekstrudera, zastosowanego układu plastyfikującego oraz rodzaju stosowanego wypełniacza na lepkość pozorną rozdrobnionych granulatów skrobi kukurydzianej.Podczas pomiarów zaobserwowano, że najwyższe wartości lepkości pozornej występowały w przypadku granulatów skrobi kukurydzianej zawierających dodatek włókien celulozowych ekstrudowanych przy zastosowaniu układu plastyfikującego o L/D=16.

Słowa kluczowe: lepkość, skrobia termoplastyczna, ekstruzja, biokompozyty.

This research work has been supported by the funds for science for the years 2010-2013 as a research project NN313275738.

TEKA. COMMISSION OF MOTORIZATION AND ENERGETICS IN AGRICULTURE – 2014, Vol. 14, No. 4, 125–130

Characteristics of Selected Rheological Properties of Water Suspensions of Potato TPS Biocomposites

Tomasz Oniszczuk, Agnieszka Wójtowicz, Leszek Mościcki, Andrzej Rejak, Maciej Combrzyński, Marcin Mitrus

Department of Food Process Engineering, Lublin University of Life Sciences
Doświadczalna 44, 20-236 Lublin, Poland e-mail: tomasz.oniszczuk@up.lublin.pl

Received December 07.2014; accepted December 18.2014

Summary. The research covered the aqueous solutions of granules of potato thermoplastic starch (TPS). The thermoplastic starch granules were produced from mixtures of potato starch, glycerol and an additive of fillers in the form of natural fibres. In the study, two configurations of the plasticizing system were used (L/D=16 and L/D=18) in a modified single-screw extrusion-cooker TS-45 with an extra cooling of the end part of the cylinder. The research focused on the effect of the extruder screw speed and the volume and types of used fillers on the apparent viscosity of pulverized granules of thermoplastic starch. During the measurements, it was observed that the apparent viscosity of extruded potato starch was influenced by the type of the plasticizing system installed in the extruder used for the production of TPS granules. The highest viscosity was reported for the solutions of potato TPS with the addition of flax fibre.

Key words: extruder, fibre, viscosity, thermoplastic starch, extrusion, biocomposites.

INTRODUCTION

The development of procedures for the mass production of biodegradable materials has recently been an area of extensive research, both academic and commercial. This is attributed to the growing scarcity of crude oil resources and to the fact that petroleum-based materials are non-biodegradable [22, 24]. Polymeric biodegradable materials can be divided into two main groups, depending on the source of raw materials for their production: the polymers produced by the traditional chemical synthesis of natural monomers and the polymers produced by microorganisms or modified bacteria, the so-called biopolymers. A practical alternative replacing the polymers based on petroleum are materials produced with the use of starch and belonging to the latter group. Also, the mixing of this natural component with synthetic polymers is an option. Such mixtures are not biodegradable, still, they reveal a lower carbon emission compared with the corresponding petroleum-based plastic and are less expensive to make [2].

Starch is the most important polysaccharide in plants serving as a reserve and accumulated in the form of grains. Particularly starch-rich are the grains of cereals, potato and manioc tubers, as well as maize cobs. Starch hydrolyses only to α-D-glucose but it is not a chemically uniform compound; in fact, it consists of two fractions: unbranched amylose and branched amylopectin [2]. The main advantages of starch are: biodegradability, broad availability, relatively low cost and ease of chemical modification [1, 6, 19, 21].

Pure and dried starch differs materially from synthetic polymers [6, 23]. It should not be regarded as a thermoplastic material since its glass transition temperature (Tg) is significantly higher than the decomposition temperature.

In recent decades, an extrusion-cooked modified starch has appeared on the market. The addition of plasticizers in the process of extrusion results in the lowering of the glass transition temperature of starch below its decomposition temperature and transforms it into thermoplastic starch (TPS) which lends itself to easy processing [12, 13, 16]. Plasticizers are mostly substances of low molecular weight which can be easily embedded into the polymer matrix in order to destroy the hydrogen inter and intra molecular bonds that occur in starch. This, in the end, leads to the improved strength and heat treatment conditions of starch-based materials [1, 18, 20, 21]. The most commonly used plasticizers are glycerol and water [17].

As auxiliary additives that enhance the mechanical and physical properties of natural polymers, various types of fillers can be used such as natural fibre (hemp, flax, jute, coconut, cellulose, cotton) or wood waste [3, 9, 10, 11].

The aim of the study was to examine the apparent viscosity of water suspensions of pulverized granules of potato thermoplastic starch extruded at several configuration settings of the plasticizing system and to determine the impact of the type and quantity of additives on the viscosity of 10%-solutions.

MATERIALS AND METHODS

The main raw material used in the research was potato starch of the type Superior Standard-F (supplied by „Pepees" S.A., KrochmalniaŁomża). As an auxiliary substance acting as plasticizer, technical glycerol was used of 99% purity in an amount of 20% of starch weight.

As additives of natural origin acting as fillers, cellulose fibre (Vivapur type 102, JRS, Germany), flax fibre and pine bark (Poland) were used after being ground on a laboratory mill LMN-10 TestChemRadlin).

Potato starch with a moisture content of 16% and glycerol were used to prepare TPS raw material mixtures to which cellulose fibre, flax fibre and ground bark were added in the amount of 10, 20 and 30% of the mixture weight. So prepared raw material was mixed by means of a laboratory ribbon mixer for 20 minutes. After mixing, the material was left in sealed plastic bags for 24 hours to homogenize the whole mass of the sample. Directly before extrusion, the material was mixed again for 10 minutes in order to loosen the mass before extrusion.

PRODUCTION OF GRANULES

Potato starch granules with the addition of natural plant fillers were extruded in the temperature range 60-110ºC and moulded through a die with a single hole of a diameter of 3 mm. In the process, a modified version of the single screw extrusion-cooker TS-45 was used (ZMCh Metalchem, Gliwice, Poland). The modification involved the application of two types of a plasticizing system with the screw/diameter ratio of L/D=16/1 and L/D=18/1, equipped with a temperature control system and the cooling of the end part of the cylinder. Granules were produced at a variable extruder screw rotation, namely 60, 80 and 100 rpm. The obtained granules were ground before tests in the laboratory mill LMN-10 (TestChem, Radlin) to the particle size of 0.8 mm and stored in dry environment until measurements [5, 8, 14, 15].

MEASUREMENT OF APPARENT VISCOSITY

To measure apparent viscosity, 10%-solutions were prepared of ground granules and distilled water of 20°C. Prepared suspensions were mixed for 10 minutes and subjected to a viscosity testing cycle. A back extrusion component was mounted on the testing machine Zwick/Roell BDO-FB0.5TH, equipped with a 0.5 kN force head (Fig. 1). The chamber parameters were as follows: cylinder height – 60 mm, inner diameter – 50 mm, plunger diameter – 46 mm, plunger height – 20 mm, the plunger having a conical bottom surface. During the test, the head speed was set to 50 mm•min^{-1}, the measuring gap was 2 mm, and the total test length was 60 mm.

During the test, the value of the apparent viscosity coefficient was determined based on the recorded resistance force of the suspension during the movement of the plunger in one bottom-up measurement cycle; the force was next converted into apparent viscosity in the testXpert 10v11

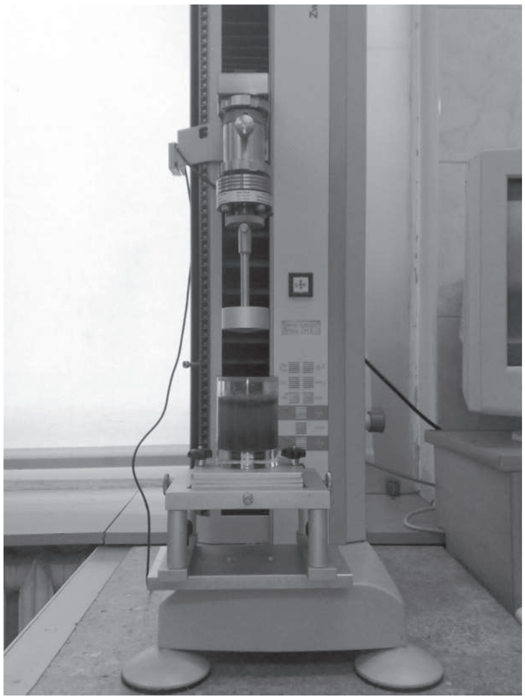

Photo 1. Testing machine Zwick BDO-FB0.5TH with mounted back extrusion component to measure viscosity

program. There were five replications, the final result being the arithmetic mean of the measurements [4, 7].

RESULTS

The apparent viscosity of aqueous solutions of potato thermoplastic starch with the addition of cellulose fibre extruded in a plasticizing system configuration of L/D=16 increased along with the increasing extruder screw speed (Fig. 1). The increase in the content of cellulose fibre in the mixture of raw materials caused higher viscosities of potato starch solutions and significant ($p<0.05$) differences between the means (Table 1).

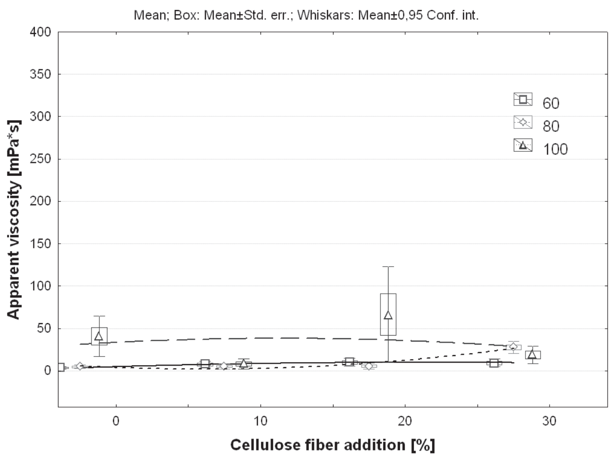

Fig. 1. The influence of the addition of cellulose fibre and the extruder screw speed on the apparent viscosity of potato starch solutions (extruder plasticizing system of L/D=16).

Fig. 2 illustrates the results of measurements of apparent viscosity of 10% aqueous solutions of granules with the addition of cellulose fibre. The use of extended plasticizing system of L/D=18 and a variable extruder screw speed during the production of potato starch granules with the addition of 30% of cellulose fibre in the recipe did not entail any significant changes in the viscosity of thermoplastic starch solutions.

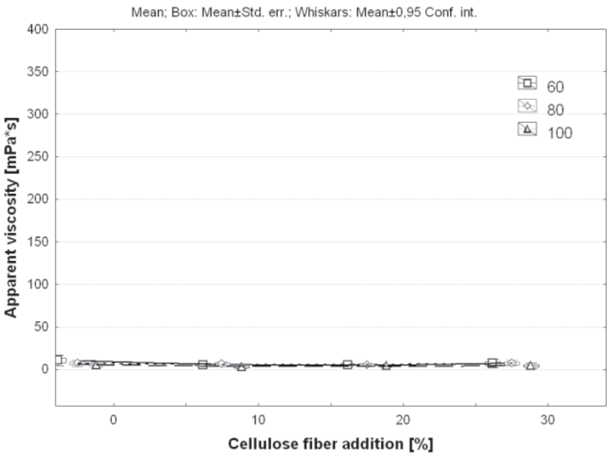

Fig. 2. The influence of the addition of cellulose fibre and the extruder screw speed on the apparent viscosity of potato starch solutions (extruder plasticizing system of L/D=18).

A very low viscosity of the examined solutions may indicate insufficient pressure and thermal treatment in the cooling conditions and with the application of the extended plasticizing system, which prevented the granules with the addition of cellulose fibre to obtain a stable structure.

Fig. 3 and 4 show the effect of the addition of flax fibre and the extruder screw speed on the apparent viscosity of aqueous solutions of TPS extruded in different configurations of the plasticizing system. The aqueous solutions of TPS granules obtained with the extruder plasticizing system at L/D=16/1 displayed higher viscosity values.

Both the increase of the screw speed during the production of granulates and the higher content of natural flax fibre significantly improved the viscosity values (Table 1). The highest apparent viscosity values were reported for TPS solutions containing 30% of flax fibre. However, in this case, the higher screw speed during extrusion resulted in the lower values of the tested parameter (Fig. 3).

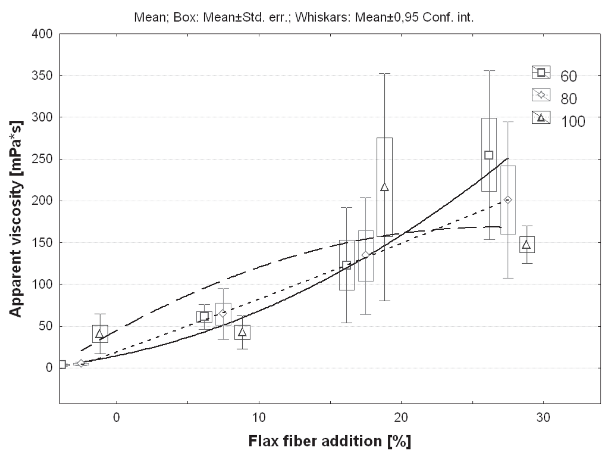

Fig. 3. The influence of flex fibres and the extruder screw speed on the apparent viscosity of potato starch solutions (extruder plasticizing system of L/D=16).

A similar trend was observed for the extended plasticizing system, namely along with the increasing content of flax fibre, the apparent viscosity of aqueous solutions of granules rose; yet, the measured viscosity values were slightly lower.

Such considerable differences in viscosity measurements were caused by problems occurring during the measurement. During the measurement, the solution began to delaminate, which significantly affected its viscosity. This, in turn, demonstrates an uneven internal structure of potato starch

Table 1. The results of the statistical analysis of viscosity of aqueous solutions of thermoplastic potato starch depending on the additives used.

Additive	L/D version	Screw rotation [rpm^{-1}]	Polynomial regression equation	F test values (3,23)	P value
Cellulose fibre	16	60	$y_{60} = -0.011x^2+0.494x+4.612$	3.094	0.0407
		80	$y_{80} = 0.053x^2-0.641x+3.712$	35.581	0.0000
		100	$y_{100} = -0.037x^2+0.837x+33.352$	3.606	0.0238
	18	60	$y_{60} = 0.018x^2-0.539x+8.695$	1.837	0.1603
		80	$y_{80} = 0.007x^2-0.173x+6.647$	0.507	0.6804
		100	$y_{100} = 0.008x^2-0.237x+4.903$	1.103	0.3623
Flax fibre	16	60	$y_{60} = 0.186x^2+3.523x+14.372$	16.214	0.000001
		80	$y_{80} = 0.018x^2+6.151x+19.198$	10.551	0.00006
		100	$y_{100} = -0.177x^2+9.365x+44.631$	7.815	0.0005
	18	60	$y_{60} = 0.421x^2-5.174x+6.922$	3.889	0.0178
		80	$y_{80} = -0.057x^2+2.909x+9.933$	2.277	0.0985
		100	$y_{100} = 8.0556E\text{-}5x^2+2.559x+7.989$	3.089	0.0409
Ground pine bark	16	60	$y_{60} = -0.287x^2+8.724x+19.972$	13.053	0.000010
		80	$y_{80} = -0.638x^2+16.426x+61.465$	52.863	0.0000
		100	$y_{100} = -0.233x^2+7.359x+59.625$	9.576	0.0001
	18	60	$y_{60} = -0.005x^2+0.243x+8.908$	4.906	0.0065
		80	$y_{80} = 0.006x^2+0.090x+7.207$	1.835	0.1607
		100	$y_{100} = 0.003x^2+0.118x+6.449$	2.991	0.0454

biocomposites and a weak bond between flax fibres and the starch matrix in the conditions of intense cooling and with the application of the extended plasticizing system.

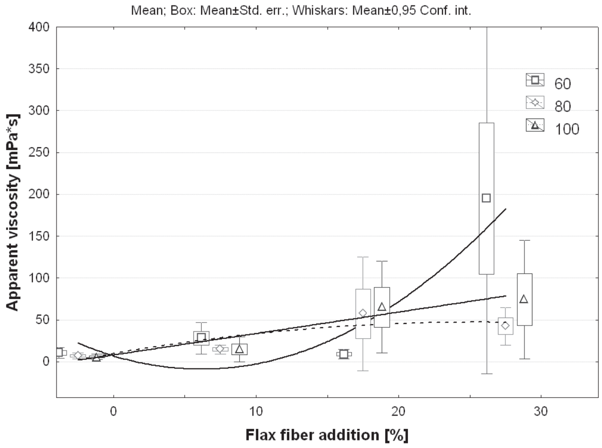

Fig. 4. The influence of flex fibres and the extruder screw speed on the apparent viscosity of potato starch solutions (extruder plasticizing system of L/D=18).

The addition of ground bark to the potato TPS potato starch resulted in higher apparent viscosity of its aqueous solutions than in the case of granules without this added content. The lowest viscosity was reported in TPS solutions that contained no filler (Fig. 5). The highest value of the apparent viscosity was obtained while testing granules with a 10% addition of ground bark. Raising the bark content to 30% in the whole range of applied extruder screw speeds had a significant influence ($p<0.05$) one the decline in the apparent viscosity of TPS solutions, as shown by the negative values of the slope coefficients of the lines of the trend expressed by a square polynomial (Table 1).

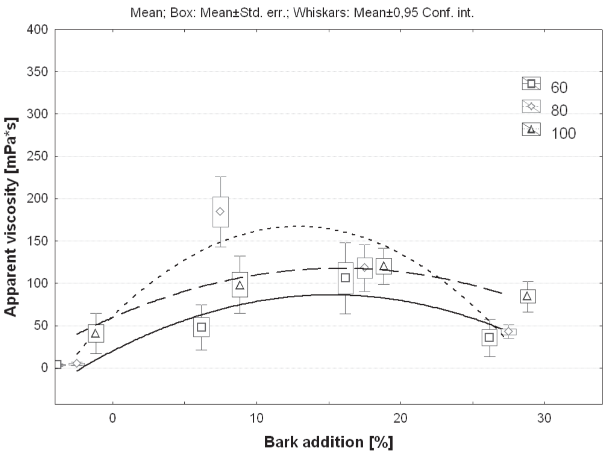

Fig. 5. The influence of ground bark addition and the extruder screw speed on the apparent viscosity of potato starch solutions (extruder plasticizing system of L/D=16).

No explicit effect was observed of the applied screw speeds during extrusion; still, the lowest screw speed resulted in the lowest viscosity of granulate solutions produced in the proposed conditions with the shorter version of the plasticizing system. The viscosity of solutions of potato TPS granules produced with the L/D=18 plasticizing system with the addition of ground bark changed only slightly. The higher filler content and the extruder screw speed did not have a noteworthy effect on the value of apparent viscosity in this case. The results indicate only a loose bond between bark and potato starch in the granulated structure, which translates into the low viscosity of prepared aqueous solutions.

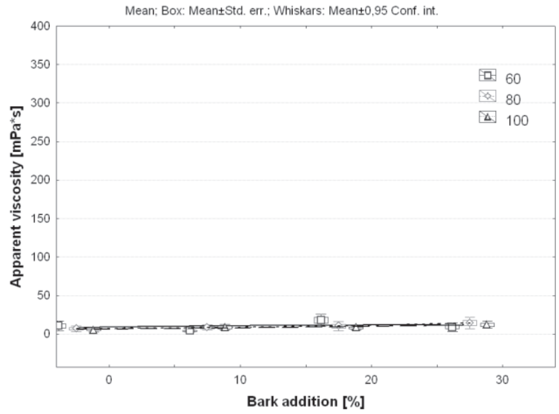

Fig. 6. The influence of ground bark addition and the extruder screw speed on the apparent viscosity of potato starch solutions (extruder plasticizing system of L/D=18).

CONCLUSIONS

- The highest apparent viscosity values were reported for solutions of TPS with the addition of flax fibre.
- The apparent viscosity of the solutions was determined by the rotational speed of the extruder used for the production of the TPS granulated matter.
- The aqueous solutions of TPS granules obtained with the L/D=16 extruder plasticizing system displayed higher apparent viscosity values.
- The addition of fillers such as natural fibres increased viscosity in the majority of examined aqueous solutions of TPS.

REFERENCES

1. **Bledzki A.K., Gassan J., 1999:** Composites reinforced with cellulose based fibres, Prog. Polymer Science, 24, 221.
2. **Cerclé C., Sarazinb P., Basil D. Favis B.D. 2013:** High performance polyethylene/thermoplastic starch blends through controlled emulsification phenomena Carbohydrate Polymers 92, 138– 148
3. **Dyadychev V., Pugacheva H., Kildeychik A., 2010:** Co-injection molding as one of the most popular injection molding Technologies for manufacture of polymeric details from secondary raw materials, TEKA Commision of motorization and Power Industry in Agriculture, PAN, Volume Xc, 57-62.
4. **Gujral H.S., Sodhi N.S., 2002:** Back extrusion properties of wheat porridge *(Dalia)*. Journal of Food Engineering 52, 53-56.

5. **Janssen L.P.B.M., Moscicki L. (Eds) 2008:** Thermoplastic Starch, Wiley-VCH Verlag GmbH & Co. KGaA, Weinheim, 1-29.
6. **Labet, M., Thielemans, W., & Dufresne, A. 2007:** Polymer grafting onto starchnanocrystals. Biomacromolecules, 8, 2916–2927.
7. **Lee S-Y., Luna-Guzman I., Chang S., Barrett D.M., Guinard J-X., 1999:**Relating descriptive analysis and instrumental texture data of processed diced tomatoes. Food Quality and Preference. 10, 447-455
8. **Mitrus M., 2006:** Investigations of thermoplastic starch extrusion cooking process stability, TEKA Commission of motorization and Power Industry in Agriculture PAN, Volume VIa, 138-144.
9. **Mitrus M., Oniszczuk T., 2007:** Wpływ obróbki ciśnieniowo-termicznej na właściwości mechaniczne skrobi termoplastycznej, Właściwości geometryczne, mechaniczne i strukturalne surowców i produktów spożywczych, Wyd. Nauk. FRNA, Lublin, 149-150.
10. **Moscicki L. (Ed) 2011:** Extrusion-Cooking Techniques, Wiley-VCH Verlag GmbH & Co. KGaA, Weinheim, 177-188.
11. **Mościcki L., Mitrus M., Wójtowicz A., Oniszczuk T., Rejak A., Janssen L., 2012:** Application of extrusion-cooking for processing of thermoplastic starch (TPS), Food Research International, Vol. 47, , pp 291-299.
12. **Oniszczuk T., Pilawka R.,2013:** Wpływ dodatku włókien celulozowych na wytrzymałość termiczną skrobi termoplastycznej, Przemysł Chemiczny, 2, 265-269,
13. **Oniszczuk T., Pilawka R., Oniszczuk A., 2013:** Wpływ dodatku mielonej kory sosnowej na wytrzymałość termiczną skrobi termoplastycznej, Przemysł Chemiczny, 8, 1554-1557.
14. **Oniszczuk T., Wójtowicz A., Mitrus M., Mościcki L., Combrzyński M., Rejak A., Gładyszewska B., 2012:** Influence of proces conditions and fillers addition on extrusion-cooking efficiency and SME of thermoplastic potato starch, Teka Commision of Motorization and Energetics in Agriculture, Polish Academy of Sciences Branch in Lublin, vol. 123, No 1, pp. 181-184,
15. **Oniszczuk T., Wójtowicz A., Mitrus M., Mościcki L., Combrzyński M., Rejak A., Gładyszewska B., 2012:** Biodegradation of TPS mouldings enriched with natural fillers, Teka Commision of Motorization and Energetics in Agriculture, Polish Academy of Sciences Branch in Lublin, vol. 123, No 1, pp. 175-180,
16. **Sarazin P., Li G., Orts W. J., & Favis, B. D. 2008:** Binary and ternary blends of polylactide, polycaprolactone and thermoplastic starch. Polymer, 49(2), 599–609.
17. **Sobczak P., 2006:** Sorbitol addition on extrusion process, TEKA Commission of Motorization and Power Industry in Agriculture PAN, Volume VIa, 163-169.
18. **Talja R. A., Peura M., Serimaa R., & Jouppila K., 2008:** Effect of amylose content on physical and mechanical properties of potato-starch-based edible films. Biomacromolecules, 9(2), 658–663.
19. **Teixeira, E., Dá Róz, A., Carvalho, A., & Curvelo A., 2007:** The effect of glycerol/sugar/water and sugar/water mixtures on the plasticization of thermoplasticcassava starch. Carbohydrate Polymers, 69, 619–624.
20. **Thomas D.J., Atwell W.A., 1997:** Starch Analysis Methods. In: Starches. Eagan Press, St. Paul, Minnesota, 13-18.
21. **Xie, F., Halley, P. J., Ave´ rous, L., 2012:** Rheology to understand and optimize processibility, structures and properties of starch polymeric materials. Prog. Polym. Sci., 37, 595–623
22. **Żakowska H., 2003:** Opakowania biodegradowalne, Centralny Ośrodek Badawczo-Rozwojowy Opakowań, Warszawa, 20-65.
23. **Zhang Y.R., Wang X.L., Zhao G.M., Wang Y.Z., 2013:** Influence of oxidized starch on the properties of thermoplastic starch. Carbohydrate Polymers 96, 358– 364.
24. **Zhang, Y. R., Zhang, S. D., Wang, X. L., Chen, R. Y., & Wang, Y. Z.,2009:** Effect of carbonyl content on the properties of thermoplastic oxidized starch. Carbohydrate Polymers, 78, 157-161.

CHARAKTERYSTYKA WYBRANYCH CECH REOLOGICZNYCH WODNYCH ROZTWORÓW ZIEMNIACZANYCH BIOKOMPOZYTÓW TPS

Streszczenie. Badaniom poddano wodne roztwory granulatów ziemniaczanej skrobi termoplastycznej (TPS). Granulaty skrobi termoplastycznej zostały wyprodukowane w z mieszanek skrobi ziemniaczanej, gliceryny oraz dodatku wypełniaczy w postaci włókien naturalnych. W badaniach zastosowano dwie konfiguracje układu plastyfikującego (L/D=16 oraz L/D=18) zmodyfikowanego ekstrudera jednoślimakowego TS-45 z dodatkowym chłodzeniem końcowej części cylindra. Badano wpływ prędkości obrotowej ślimaka ekstrudera, ilości oraz rodzaju stosowanych wypełniaczy na lepkości rozdrobnionych granulatów skrobi termoplastycznej. Podczas pomiarów zaobserwowano, że na lepkość pozorną roztworów ekstrudowanej skrobi ziemniaczanej miał wpływ rodzaj zastosowanego układu plastyfikującego ekstrudera stosowanego do produkcji granulatów TPS. Najwyższą lepkością charakteryzowały się roztwory ziemniaczanej TPS z dodatkiem włókien lnianych.

Słowa kluczowe: ekstruder, włókna, lepkość, skrobia termoplastyczna, ekstruzja, biokompozyty.

This research work has been supported by the funds for science for the years 2010-2012 as a research project NN313275738.

TEKA. COMMISSION OF MOTORIZATION AND ENERGETICS IN AGRICULTURE – 2014, Vol. 14, No. 4, 131–136

Characteristics of Selected Rheological Properties of Water Suspensions of Wheat TPS Biocomposites

Tomasz Oniszczuk, Agnieszka Wójtowicz, Leszek Mościcki, Andrzej Rejak, Magdalena Klimek, Maciej Combrzyński

Department of Food Process Engineering, Lublin University of Life Sciences
Doświadczalna 44, 20-236 Lublin, Poland, e-mail: tomasz.oniszczuk@up.lublin.pl

Received December 07.2014; accepted December 18.2014

Summary. The research covered the aqueous solutions of thermoplastic wheat starch (TPS) granules. The thermoplastic starch granules were produced from mixtures of wheat starch, glycerol and an additive of fillers in the form of natural fibres. In the study, a modified single-screw extrusion-cooker TS-45 was used with L/D=16 and L/D=18 with an extra cooling of the end part of the cylinder. The research focused on the effect of the extruder screw rotation speed, the volume and the type of plasticizing system used and on the apparent viscosity of pulverized granules of wheat TPS. During measurements it was observed that higher apparent viscosity values were recorded in those solutions of TPS that were produced with the extended version of the plasticizing system of TS-45 extruder.

Key words: extruder, fibre, viscosity, thermoplastic starch, extrusion, biocomposites.

INTRODUCTION

The production of biodegradable and environmentally friendly materials has recently come into focus of researchers worldwide. Such a material is expected to replace petroleum-based polymers which are very durable, yet represent a major environmental issue [10, 13, 28].

One of the main natural compounds extensively researched for the use as a biodegradable material is starch. The first attempts to obtain materials based on this component focused on the use of starch granules as a filler for synthetic polymers such as polyethylene and polypropylene [3].

In order to be further processed as a biodegradable material, natural starch must be transformed into thermoplastic starch (TPS). In this case, the granular structure of starch is completely degraded by the use of plasticizers in a high temperature during extrusion [1, 6, 14]. Unfortunately, pure thermoplastic starch has several disadvantages. They include low mechanical strength (fragility) and high sensitivity to environmental factors, e.g. moisture [1, 9, 18]. In order to offset these disadvantages, TPS is mixed with other polymers, thus yielding, in a simple, fast and inexpensive manner, mixtures with such properties that are generally not achievable when using individual polymeric materials [11, 27]. In order to improve the processing and mechanical properties of TPS, it is combined with, e.g. polyethylene (PE) [20, 22], polypropylene (PP) [21], and polyamide (PA) [24, 25]. In addition, in an attempt to obtain completely biodegradable materials, numerous TPS mixtures have been developed with various polymers which undergo complete degradation in the natural environment [26]. Among the biodegradable polymers, butylene polysuccinate (PBS) deserves special attention, not only because of its excellent biodegradability quality but also sufficient mechanical strength. Therefore some research has been carried out on the combination of PBS and TPS [5, 31].

Generally speaking, thermoplastic starch is considered a promising material for the production of packaging materials due to its reasonable cost, availability, renewability and biodegradability. Recently, its use has spread to many sectors, e.g. oil refining (grease), metallurgy (extraction of impurities from iron), textile (rubber) and paper (enhancement of paper strength) [15].

The properties of TPS are very much dependent on the natural origin of the starch, more specifically, on the ratio of its main two components: linear amylose and branched amylopectin. The share of amylose chains in starch is determined genetically and generally the same within a particular plant species. In standard starch, the amylose content accounts for 15-30% of the total starch weight; in special, high-amylose species it reaches 35-70% [8]. There are numerous studies on the effect of amylose and amylopectin content on the final properties of starch-based materials [8, 10, 12, 31]. TPS obtained from high-amylose starch has been proven to have better thermal and mechanical properties, still their processing (extrusion, in particular) is much more demanding [16, 17, 29, 30]. In order to enhance the mechanical and physical properties of TPS, various types of fillers can be used such as natural fibre or wood waste [24, 25].

The effect of the type of starch and used additives (fillers, plasticizers) on the properties of TPS is crucial when selecting raw materials for the production of biodegradable plastics. It also allows the optimization of properties of TPS-based mixtures for the industrial application of TPS products [1, 2, 23].

The aim of the study was to examine the apparent viscosity of suspensions of pulverized granules of thermoplastic wheat starch granules with different natural fillers.

MATERIALS AND METHODS

Wheat starch used in the study was Merizet 100 from Segezha, Ireland; flax fibre from a Polish producer; cellulose fibre Vivapur type 102 JRS from a German producer and ground pine bark. Technical glycerol of 99% purity was used as a plasticizer.

Wheat starch, glycerol and fillers in the form of flax fibres and ground bark were mixed for 20 minutes in a laboratory ribbon mixer. The glycerol accounted for 20% of the mixture weight, and the proportion of fillers in the prepared mixtures was 10, 20 and 30%. After mixing, the samples were left in sealed plastic bags for 24 hours in order for the mixture to homogenize [19].

The baro-thermal treatment was carried out on a modified single-screw extrusion-cooker, TS-45, equipped with two kinds of plasticizing systems with the screw length/diameter ratio of L/D=16/1 and L/D=18/1. A steel die was used with a hole of 3 mm in diameter. Granules were produced at the three extruder screw speeds: 60, 80 and 100 rpm. Temperature values were in the range of 60-110ºC. The temperature was controlled by a purpose-made cooling system. The extruder was equipped with a material feeder, a plasticizing system made up of the screw linked to the drive and housing, and a preheating device. To measure the temperature of the thermal and pressure treatment, thermocouples were used installed in the extruder cylinder; the results were displayed on the machine control panel. The screw speed during extrusion was monitored using a wireless electronic tachometer, DM-223AR [18, 19, 32].

The viscosity of aqueous solutions of thermoplastic starch was measured on the test machine Zwick BDO-FBO0,5TH, equipped with a back extrusion chamber. The granules were ground using a laboratory mill to obtain particles with a diameter of less than 0.8 mm. 10% thermoplastic starch suspensions were prepared with distilled water at 20°C. The viscosity measurements were made after 10 minutes of mixing. During the test, the following parameters were set: total test length 60 mm and the head speed 50 mm•min$^{-1.}$ During the study, the resistance force of the suspension was recorded during the movement of the plunger in one bottom-up measurement cycle, which was next converted into the apparent viscosity coefficient. The measurements were made using the testXpert 10v11 program [4, 7]. There were five replications, the final result being the arithmetic mean of the measurements.

RESULTS

Fig. 1 shows the dependence of the viscosity of aqueous solutions of thermoplastic wheat starch upon the applied screw speed of the L/D=16 version extruder and upon the content of cellulose fibre in the mixture. It was observed that the viscosity of the solution increased significantly ($p<0.05$) along with the increasing extruder screw speed and a higher addition of cellulose fibre. A similar trend was observed for maize starch.

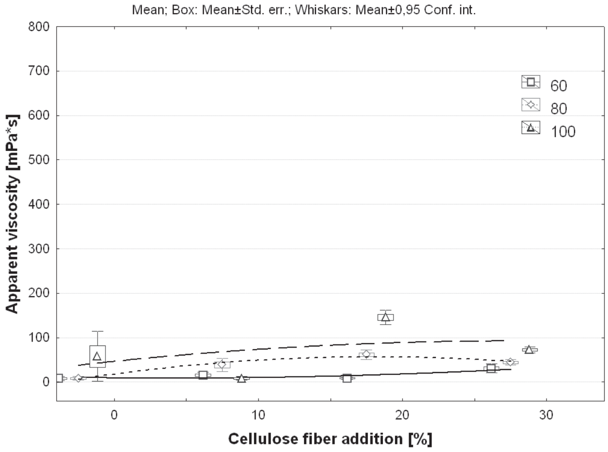

Fig. 1. The influence of cellulose fibres and the extruder screw speed on the apparent viscosity of wheat starch solutions (extruder plasticizing system of L/D=16).

The use of the L/D=18 plasticizing system (Fig. 2) resulted in an increase of apparent viscosity. The highest apparent viscosity values were reported for solutions with a 10% addition of cellulose fibre. It was also reported that with the increasing fibre content in the mixture, the viscosity of the solution decreased. This may be an indication that the addition of cellulose fibres had an adverse impact on their bond with the biopolymer matrix, which, in turn, had a negative bearing on the viscosity of the solution.

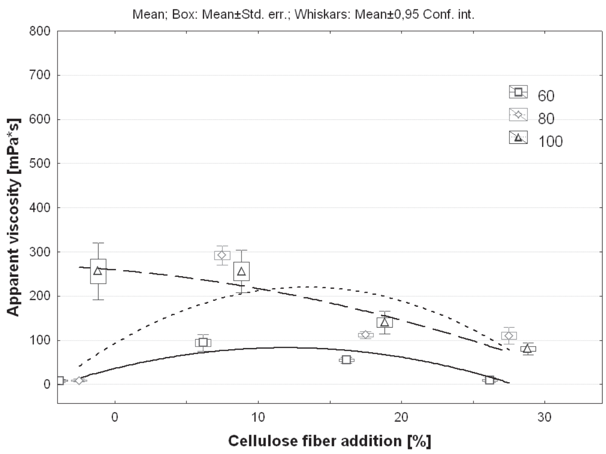

Fig. 2. The influence of cellulose fibres and the extruder screw speed on the apparent viscosity of wheat starch solutions (extruder plasticizing system of L/D=18).

Fig. 3 shows the effect of the addition of flax fibre on the value of apparent viscosity of the solutions of wheat thermoplastic starch. It was observed that with increasing extruder screw rotation speed, the viscosity of solutions rose, regardless of the plasticizing system used.

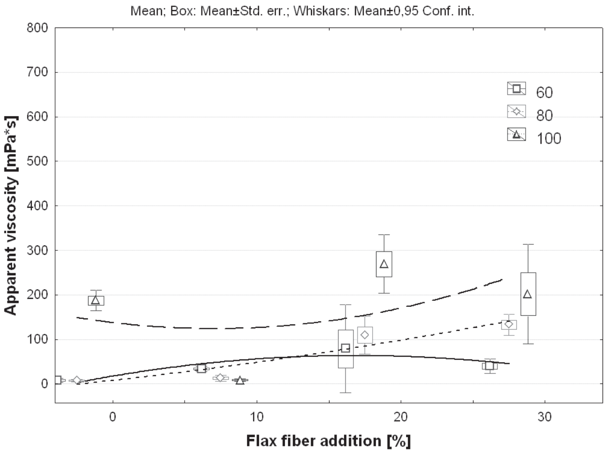

Fig. 3. The influence of flex fibres and the extruder screw speed on the apparent viscosity of wheat starch solutions (extruder plasticizing system of L/D=16).

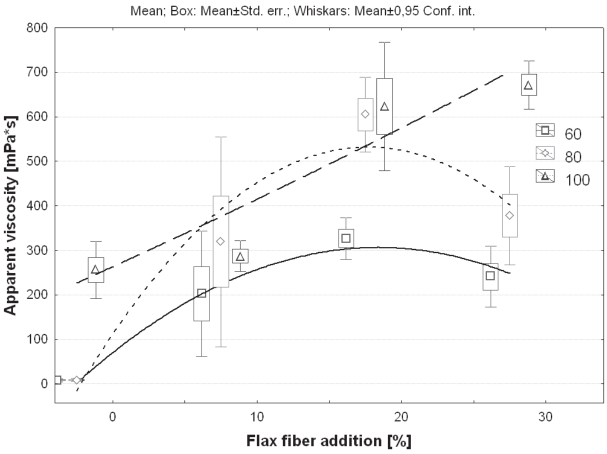

Fig. 4. The influence of flex fibres and the extruder screw speed on the apparent viscosity of wheat starch solutions (extruder plasticizing system of L/D=18).

Higher viscosity values were reported for the solutions of thermoplastic wheat starch with the addition of flax fibre at 100 rpm^{-1} of the extruder screw.

During tests, the TPS solutions delaminated, which testifies to a weak bond between flax fibre and wheat starch. In some cases, there was more resistance between the plunger and and the walls of the machine, which could have led to the high spread of apparent viscosity values (Fig. 4).

The apparent viscosity of solutions of wheat starch granules produced on the shorter version of the plasticizing system slightly increased along with the higher bark content in the granulated matter (Fig. 5). The top viscosity value was reported at a 10% content of ground bark and for the screw speed of 100 rpm^{-1}.

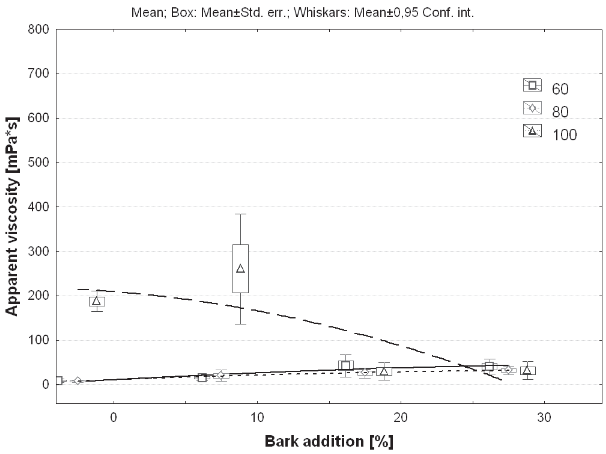

Fig. 5. The influence of ground bark addition and the extruder screw speed on the apparent viscosity of wheat starch solutions (extruder plasticizing system of L/D=16).

Table 1. The results of the statistical analysis of viscosity of aqueous solutions of thermoplastic wheat starch depending on the additives used.

Additive	L/D version	Screw rotation [rpm^{-1}]	Polynomial regression equation	F test values (3,23)	P value
Cellulose fibre	16	60	$y_{60} = 0.036x^2-0.288x+9.148$	12.839	0.00001
		80	$y_{80} = -0.119x^2+4.287x+17.918$	26.402	0.000000009
		100	$y_{100} = -0.059x^2+3.282x+46.435$	19.459	0.0000002
	18	60	$y_{60} = -0.327x^2+7.808x+36.158$	76.040	0.0000
		80	$y_{80} = -0.710x^2+18.989x+93.064$	319.028	0.00000
		100	$y_{100} = -0.147x^2-2.748x+258.953$	22.267	0.00000006
Flax fibre	16	60	$y_{60} = -0.162x^2+5.454x+17.425$	1.807	0.1658
		80	$y_{80} = 0.044x^2+3.631x+7.813$	36.962	0.0000
		100	$y_{100} = 0.276x^2-3.883x+137.562$	15.189	0.000003
	18	60	$y_{60} = -0.698x^2+25.679x+70.109$	14.351	0.000004
		80	$y_{80} = -1.343x^2+47.508x+111.830$	17.144	0.0000008
		100	$y_{100} = 0.044x^2+14.729x+263.149$	34.734	0.0000
Ground pine bark	16	60	$y_{60} = -0.021x^2+1.747x+10.515$	6.441	0.0015
		80	$y_{80} = -0.016x^2+1.206x+10.685$	5.895	0.0025
		100	$y_{100} = -0.178x^2-2.530x+208.945$	16.957	0.0000009
	18	60	$y_{60} = -0.011x^2+0.866x+12.580$	3.145	0.0385
		80	$y_{80} = 0.300x^2-1.175x+7.140$	13.101	0.000010
		100	$y_{100} = 0.633x^2-15.667x+199.430$	4.097	0.0144

No direct effect was noted of the screw speeds during extrusion on the value of the apparent viscosity of TPC wheat solutions with ground pine bark (Fig. 5).

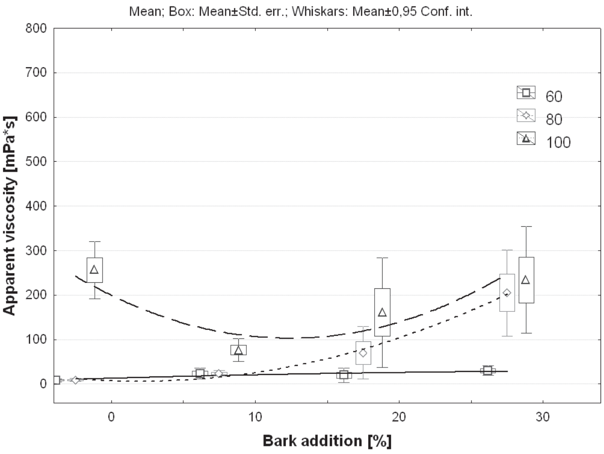

Fig. 6. The influence of ground bark addition and the extruder screw speed on the apparent viscosity of wheat starch solutions (extruder plasticizing system of L/D=18).

The use of the extended version of the plasticizing system of the extruder for the production of wheat TPS granules with the addition of bark had an impact on the increase in the value of apparent viscosity. The highest apparent viscosity values were reported for solutions with a 20 and 30% addition of ground bark. A similar trend was observed in that the rising extruder screw speed resulted in the increased viscosity of tested solutions.

CONCLUSIONS

- The aqueous solutions of thermoplastic wheat starch granules obtained with the extended L/D=18 extruder plasticizing system displayed higher apparent viscosity values.
- The addition of fillers such as natural fibres increased viscosity in the majority of examined aqueous solutions of TPS.
- The addition of flax fibre enhanced the viscosity of TPS solutions to the greatest extent.
- The rising extruder screw rotational speed resulted in a higher apparent viscosity value in the majority of examined solutions of TPS granules.

REFERENCES

1. **Carvalho A.J.F., Job A.E., N. Alves, A.A.S. Curvelo, A. Gandini., 2003:** Thermoplastic starch/natural rubber blends. Carbohydrate Polymers 53, 95–99.
2. **Dyadychev V., Pugacheva H., Kildeychik A., 2010:** Co-injection molding as one of the most popular injection molding Technologies for manufacture of polymeric details from secondary raw materials, TEKA Commision of motorization and Power Industry in Agriculture, PAN, Volume Xc, 57-62.
3. **Griffin, G. J. L. 1977**: US Patent, 4,021,388
4. **Gujral H.S., Sodhi N.S., 2002:** Back extrusion properties of wheat porridge *(Dalia).* Journal of Food Engineering 52, 53-56.
5. **He, Y.-S., Zeng, J.-B., Li, S.-L., Wang, Y.-Z., 2012:** Crystallization behavior of partially miscible biodegradable poly- (butylene succinate)/poly(ethylene succinate) blends.
 Thermochim. Acta, 529, 80–86.
6. **Janssen L.P.B.M., Moscicki L. (Eds) 2008:** Thermoplastic Starch, Wiley-VCH Verlag GmbH & Co. KGaA, Weinheim, 1-29.
7. **Lee S-Y., Luna-Guzman I., Chang S., Barrett D.M., Guinard J-X., 1999:**Relating descriptive analysis and instrumental texture data of processed diced tomatoes. Food Quality and Preference. 10, 447-455
8. **Li, M., Liu, P., Zou, W., Yu, L. et al., 2011:** Extrusion processing and characterization of edible starch films with different amylose contents. J. Food Eng., 106, 95–101.
9. **Li J., Luo X., Lin X., and Zhou Y., 2013:** Comparative study on the blends of PBS/thermoplastic starch prepared from waxy and normal corn starches. Starch, 65, 831–839
10. **Liu, H., Xie, F., Yu, L., Chen, L., Li, L., 2009:** Thermal processing of starch-based polymers. Prog. Polym. Sci., 34, 1348–1368.
11. **Liu, H., Yu, L., Simon, G., Dean, K., Chen, L., 2009:** Effects of annealing on gelatinization and microstructures of corn starches with different amylose/amylopectin ratios. Carbohydr. Polym., 77, 662–669.
12. **Liu, P., Xie, F., Li, M., Liu, X. et al., 2011:** Phase transitions of maize starches with different amylose contents in glycerol–water systems. Carbohydr. Polym., 85, 180–187.
13. **Mitrus M., 2006:** Investigations of thermoplastic starch extrusion cooking process stability, TEKA Commission of motorization and Power Industry in Agriculture PAN, Volume VIa, 138-144.
14. **Mościcki L., Mitrus M., Wójtowicz A., Oniszczuk T., Rejak A., Janssen L., 2012:** Application of extrusion-cooking for processing of thermoplastic starch (TPS), Food Research International, Vol. 47, , pp 291-299.
15. **Morais Teixeira E., Ro´z A. ,L., Carvalho A., J., F., Antonio Curvelo, A., A., S., 2005:** Preparation and Characterisation of Thermoplastic Starches from Cassava Starch, Cassava Root and Cassava Bagasse, Macromol. Symp., 229, 266–275
16. **Oniszczuk T., Pilawka R.,2013:** Wpływ dodatku włókien celulozowych na wytrzymałość termiczną skrobi termoplastycznej, Przemysł Chemiczny, 2, 265-269,
17. **Oniszczuk T., Pilawka R., Oniszczuk A., 2013:** Wpływ dodatku mielonej kory sosnowej na wytrzymałość termiczną skrobi termoplastycznej, Przemysł Chemiczny, 8, 1554-1557.
18. **Oniszczuk T., Wójtowicz A., Mitrus M., Mościcki L., Combrzyński M., Rejak A., Gładyszewska B., 2012:** Influence of proces conditions and fillers addition on

extrusion-cooking efficiency and SME of thermoplastic potato starch, Teka Commision of Motorization and Energetics in Agriculture, Polish Academy of Sciences Branch in Lublin, vol. 123, No 1, pp. 181-184,
19. **Oniszczuk T., Wójtowicz A., Mitrus M., Mościcki L., Combrzyński M., Rejak A., Gładyszewska B., 2012:** Biodegradation of TPS mouldings enriched with natural fillers, Teka Commision of Motorization and Energetics in Agriculture, Polish Academy of Sciences Branch in Lublin, vol. 123, No 1, pp. 175-180,
20. **Pedroso, A. G., Rosa, D. S., 2005:** Mechanical, thermal and morphological characterization of recycled LDPE/corn starch blends. Carbohydr. Polym., 59, 1–9.
21. **Ramis, X., Cadenato, A., Salla, J. M., Morancho, J. M. et al., 2004:** Thermal degradation of polypropylene/starchbased materials with enhanced biodegradability. Polym. Degrad. Stability, 86, 483–491.
22. **Shujun, W., Jiugao, Y., Jinglin, Y.,2005:** Preparation and characterization of compatible thermoplastic starch/ polyethylene blends. Polym. Degrad. Stability, 87, 395–401.
23. **Sobczak P., 2006:** Sorbitol addition on extrusion process, TEKA Commission of Motorization and Power Industry in Agriculture PAN, Volume VIa, 163-169.
24. **Teyssandier, F., Cassagnau, P., Ge´ rard, J. F., Mignard, N., Me´ Lis, F., 2012:** Morphology and mechanical properties of PA12/plasticized starch blends prepared by highshear extrusion. Mater. Chem. Phys. 133, 913– 923.
25. **Teyssandier, F., Cassagnau, P., Ge´ Rard, J. F., Mignard, N., 2011:** Reactive compatibilization of PA12/plasticized starch blends: towards improved mechanical properties. Eur. Polym. J. , 47, 2361–2371.
26. **Wang, N., Yu, J., Chang, P. R., Ma, X., 2013:** Influence of citric acid on the properties of glycerol-plasticized dry starch (DTPS) and DTPS/poly(lactic acid) blends. Starch, 2007, 59, 409–417. 838 J. Li et al. Starch,2013, 65, 831–839
27. **Xie F., Halley P. J., Ave´ Rous L., 2012:** Rheology to understand and optimize processibility, structures and properties of starch polymeric materials. Prog. Polym. Sci.,37,595–623.
28. **Yu, L., Dean, K., Li, L., 2006:** Polymer blends and composites from renewable resources. Prog. Polym. Sci., 31, 576–602.
29. **Zeng, J.-B., Jiao, L., Li, Y.-D., Srinivasan, M. et al., 2011:** Biobased blends of starch and poly(butylene succinate) with improved miscibility, mechanical properties, and reduced water absorption. Carbohydr. Polym. 83, 762–768.
30. **Zhang, Y. R., Zhang, S. D., Wang, X. L., Chen, R. Y., & Wang, Y. Z.,2009:** Effect of carbonyl content on the properties of thermoplastic oxidized starch. CarbohydratePolymers, 78, 157–161.
31. **Zou, W., Yu, L., Liu, X., Chen, L. et al., 2012:** Effects of amylose/ amylopectin ratio on starch-based superabsorbent polymers. Carbohydr. Polym. 87, 1583–1588.
32. **Zullo, R., Iannace, S., 2009:** The effects of different starch sources and plasticizers on film blowing of thermoplastic starch: correlation among process, elongational properties and macromolecular structure. Carbohydr. Polym., 77, 376–383.

CHARAKTERYSTYKA WYBRANYCH CECH REOLOGICZNYCH WODNYCH ROZTWORÓW PSZENNYCH BIOKOMPOZYTÓW TPS

Streszczenie. Badaniom poddano wodne roztwory granulatów pszennej skrobi termoplastycznej (TPS). Granulaty skrobi termoplastycznej zostały wyprodukowane z mieszanek skrobi pszennej, gliceryny oraz dodatku wypełniaczy w postaci włókien naturalnych. W badaniach zastosowano zmodyfikowany ekstruder jednoślimakowy TS-45 o L/D=16 i L/D=18 z dodatkowym chłodzeniem końcowej części cylindra urządzenia. Badano wpływ prędkości obrotowej ślimaka ekstrudera, ilości oraz rodzaju stosowanego wypełniacza na lepkość rozdrobnionych granulatów pszennej skrobi termoplastycznej. Podczas pomiarów zaobserwowano, że wyższymi wartościami lepkości pozornej charakteryzowały się roztwory TPS wytworzonej na dłuższej wersji układu plastyfikującego ekstrudera TS-45.
Słowa kluczowe: ekstruder, włókna, lepkość, skrobia termoplastyczna, ekstruzja, biokompozyty.

This research work has been supported by the funds for science for the years 2010-2012 as a research project NN313275738.

TEKA. COMMISSION OF MOTORIZATION AND ENERGETICS IN AGRICULTURE – 2014, Vol. 14, No. 4, 137–142

Vehicle Transport Organization of Food Requiring Refrigeration

Halina Pawlak, Piotr Maksym, Jacek Skwarcz

University of Life Sciences in Lublin, Department of Technology Fundamentals
Doświadczalna 44, 20-236 Lublin, Poland

Received December 09.2014; accepted December 19.2014

Summary. The paper presents a description of the legal requirements for car transport of foods that require refrigeration. Were also carried out a survey among drivers involved in this kind of transport, in order to assess the knowledge of drivers about the transport of perishable food that requires cooling.
Key words: perishable foodstuff, vehicle transport, legislation.

INTRODUCTION

Nowadays the demand is rapidly growing for food with high sensory quality, fresh and rich in nutrients. This phenomenon is not only the driving force for the development of agri-food industry, but also in the field of logistics and transport of refrigerated foods. This progress has resulted in the possibility of provision of even very distant markets for perishable foodstuff. [9, 12].

More and more often, the transport of food products has been using methods of preservation of these products involving the application of the cooling systems. This allows the short-term storage of fresh food at a temperature from 10 to 0 °C or long-term storage in a frozen state at a temperature from -12 to -22 °C [1, 2].

The advantage of the method of cooling is a complete stop or slowing down of microbial growth in both chilled and frozen foods. Furthermore, foods preserved by this method retain vitamins and organoleptic characteristics of the fresh food.The fulfillment of such conditions requires compliance with the principles of transport conditions of perishable foodstuffs and the selection of proper means of transport. Special means of transport for perishable food items are:
– (insulated equipment),
– (refrigerated equipment),
– (mechanically refrigerated equipment),
– (heated equipment).

Participation in road transport of perishable goods, as well as dangerous goods, has been systematically increasing, which requires strict compliance with the relevant provisions [4, 8, 14, 15].

Persistence and quality of transported, refrigerated food products depends mainly on micro-climatic conditions prevailing in the cargo area. The main parameter is the temperature, which depends on the product being transported. the variations of the temperature should be kept to the minimum [13, 16].

During the loading, transport and unloading, the highest temperature of frozen and deep-frozen foods should not exceed the temperatures given in Table 1

Table 1.Temperature required for the transport of frozen and deep-frozen foodstuff [1, 2, 5, 13].

Type of food article	The required transport temperature
Frozen or deep-frozen cream and fruit juice concentrates	-20ºC
Frozen and deep-frozen fishes	-18ºC
Any other deep-frozen foodstuffs	-18ºC
Frozen butter and other fats	-14ºC
Frozen offal, egg yolks, poultry and game	-12ºC
Frozen meat	-10ºC
Any other frozen foodstuffs	-10ºC

This temperature may increase, for example in the evaporator during the defrosting of the means of transport (mechanically refrigerated equipment). In such case, the temperature is allowed to increase no more than a 3° C with respect to the required temperatures.

Furthermore, the highest temperature anywhere in cargo during loading, transport and unloading of non-frozen foods should not exceed the temperatures given in Table 2.

Table 2. Temperature required for the transport of non-frozen and non-deep-frozen foodstuff [1, 2, 5, 13].

Type of food article	The required transport temperature
Poultry	+3ºC 1)
Butter	+6ºC
Game	+4ºC
Milk tanker (raw or pasteurised) intended for direct human consumption	+4ºC 1)
Industrial milk	+6ºC 1)
Milky products (yogurt, kefir, sour cream, cottage cheese)	+4ºC 1)
Fishes (should always be transported in ice) 2)	+2ºC
Prepared meat products	+6ºC
Meat (excluding poultry)	+7ºC
Poultry and rabbits	+4ºC

1) In principle, transport time should not exceed 48 hours.
2) With the exception of smoked fish, salted, dried or live.
3) With the exception of products in the stabilized state by salting, smoking, drying or sterilization.

Another important parameter of mechanically refrigerated equipment is humidity, which sets automatically and does not require control.

Moreover, the interior of transport should be clean in order not to lead to the development of microorganisms. Before loading, in accordance with the principles of good transport, refrigeration compartment of the vehicle should be cooled to a temperature appropriate for a given food product.

Carriers must be informed (need to know) about the fact that transport of frozen, deep-frozen and unfrozen food must be included as a component of the storage time. Therefore, the drivers carrying food should note that transportation of certain articles of food may be close to the optimum storage time and therefore often vehicles should be treated as a special kind of magazine [16].

Suitable conditions for the transport of food and sanitary safety, as in force in Poland since 1984 ATP (A-agreement, T-transportation, P-perishable) agreement of the "International Carriage of Perishable foodstuffs and the special equipment for such carriage"require appropriate identification of means of transport and the required documents [10].

Means of transport intended for the carriage of perishable food products, which meet the terms of the agreement ATP, should be marked by signs ATP (Fig. 1), which is mounted in a visible location on the wall of the building isothermal for the passenger side. The table contains the marking class of ATP, month, year and validity of the certificate.

Fig. 1. Certification plate of compliance of the equipment – *the particulars in square brackets are given by way of example [1, 2]

On the other hand the driver should have the original certificate of ATP in Polish and English. Sample guidelines for verification of the equipment in the transport of food are shown in Figure 2

The requirements related to the admission of vehicles to traffic must be consistent with the requirements contained in the ATP agreement (Agreement on the International Carriage of Perishable Foodstuffs and on the Special Equipment to be used for such Carriage).

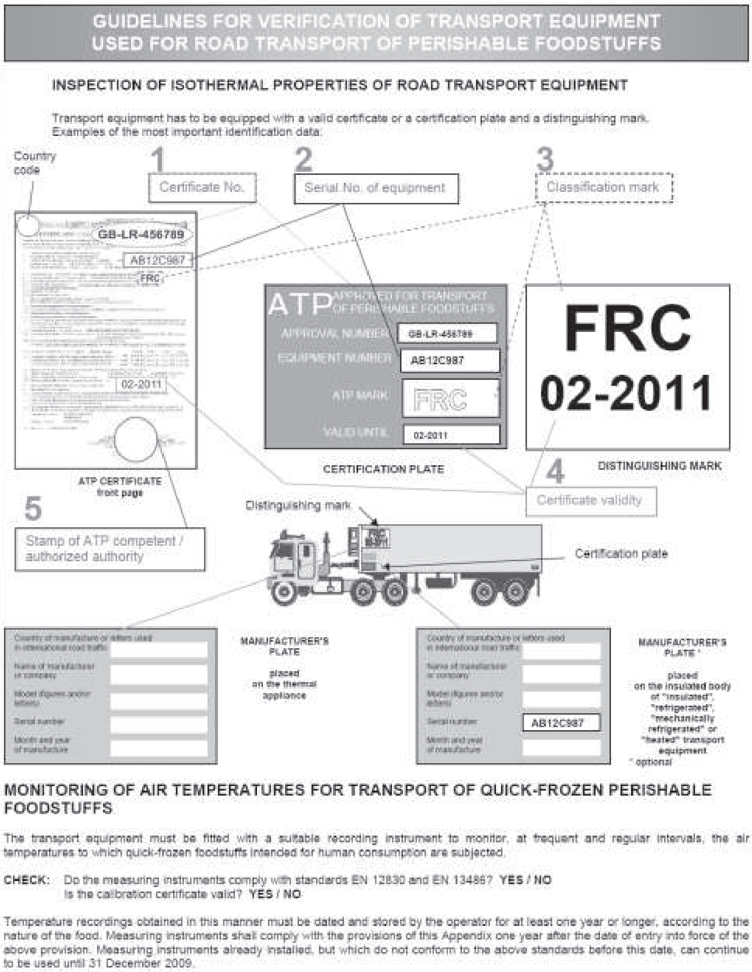

Fig. 2. ATP example of good practice [3].

The United Nation Economic Commission for Europe has information about the performing centers (Competent Authorities and Test Stations list) [3, 7]. COCH performs periodic checks of insulated body in order to extend the period of validity of the ATP certificate (FRC FNA).

For example, in the context of accreditation for the Polish Centre for Accreditation, COCH performs:

– inspections which are the basis for obtaining certification of ATP,
– measurements of the overall coefficient “k” of heat transfer for both the new means of refrigeration transport and the in-service one as the basis for obtaining certification of ATP,
– complete testing of mechanically refrigerated transport (air-conditioned semi-trailers, refrigerated trailers, refrigerated trucks, etc.) and not mechanically refrigerated transport (icehouse cars),
– research on the effective refrigerating capacity of the cooling unit,
– measurements of the overall coefficient “k” of heat transfer for liquid foodstuffs tank trucks [6].

The domestic and international provisions require the carrier to transport equipment with a measuring device recording the air temperature inside the vehicle. Waveforms obtained from the temperature changes registration, depending on the type of product being transported, must be kept for at least one year.Monitoring and recording of temperature also applies to loading of goods, which should be chilled to the optimum storage temperature (transport) refrigerant. It is also important to control the temperature of food products being unloaded [11].

The driver (employee) has to be competent and possess the knowledge of all the requirements contained in these regulations.

THE AIM AND THE RANGE OF WORK

Transportation of food requires from carriers the knowledge of road traffic regulations and specific regulations concerning the carriage of perishable foods.

The main aim of the study was to examine the drivers' knowledge of the requirements relating to the transport of frozen and perishable food. The study was conducted among drivers transporting food in the Lublin region.

METHODOLOGY

The study used an authorial questionnaire with basic information about the respondents (age, years of work in the profession as a driver, etc.) and other specific questions. An anonymous questionnaire sheet was prepared in the Department of Technology Fundamentals. The survey included the following questions:

QUESTIONNAIRE SHEET

Please kindly complete a survey, which will be used to check the drivers' knowledge about the knowledge requirements for the transport of food in special conditions.

Table 3. General information

1. Age		
2. The experience of work in the driver's profession (in years)		
3. The experience of work in perishable foodstuff vehicle transport (in years)		
4. The type of transport character	regular	
	casual	

Table 4. Information on the used type of isothermal transport vehicle

1. Insulated equipment	
2. Refrigerated equipment	
3. Mechanically refrigerated equipment	
4. Other	

Table 5. Information on time, temperature and kind of perishable foodstuff

1. Are you always informed on what kind of products you transport?	Yes	No	I don'tknow
2. Do you know what is the required temperature during transport of food?	Yes	No	I don'tknow
3. Do you know the time required for the transport of food?	Yes	No	I don'tknow
4. Do you know the required time associated with loading and unloading of transported food?	Yes	No	I don'tknow

Table 6. Information on vehicle designation, necessary transport documents and general rules of vehicle transport

1. Do you know how a car for the transporting of food should be marked?	Yes	No	I don'tknow
2. Do you know what document is necessary while transporting food?	Yes	No	I don'tknow
3. Do you know where the ATP rating plaque should be placed?	Yes	No	I don'tknow
4. Do you know what the first letters of the ATP rating plaque are?	Yes	No	I don'tknow
5. Do you know the rules of “good transport practice”?	Yes	No	I don'tknow

The survey was conducted in three service companies operating in the transport of food.

RESULTS

The survey was carried out among 23 drivers between the ages of 24 to 45, who have been working in the profession of driver from 2 to 22 years and have experience in the transport of food from 1 year to 5 years. Information concerning the type of transport used is shown in Figure 3, and the work experience in the transport of food in Figure 4.

Approximately 80% of the surveyed drivers have had a 5-year or longer work experience in the transport of food. 74 % respondents from all the means of transport of perishable foods used mechanically refrigerated equipment.

Twenty of all the tested drivers declared that they always have the information as to what kind of food is transported by them (Figure 5), but only 38% of drivers know the rules of “good transport practice” (Figure 6).

Over 90% of the drivers can tell what the required temperature for the transport of food is. Similarly, the drivers are aware of the time limit, depending on the types of transported food. Almost all of the respondents know where the ATP rating plaque should be placed and how a car should be properly marked for the transporting of food.

CONCLUSIONS

A food carrier should remember that he is also a consumer. On his knowledge of the procedures followed for the transport of perishable products, their quality depends. The conducted surveys have shown that the examined carriers are competent as to the requirements for the transport of deep-frozen and frozen food products.

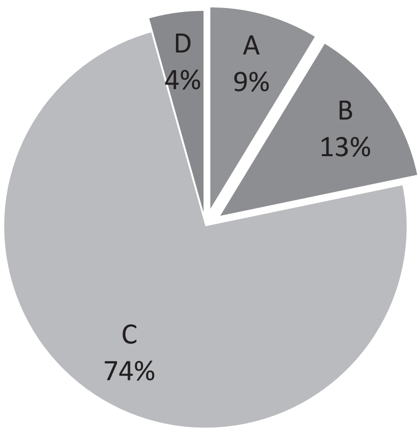

Fig. 3. Information about the vehicle kind used: A – insulated equipment, B – refrigerated equipment, C – mechanically refrigerated equipment, D – other.

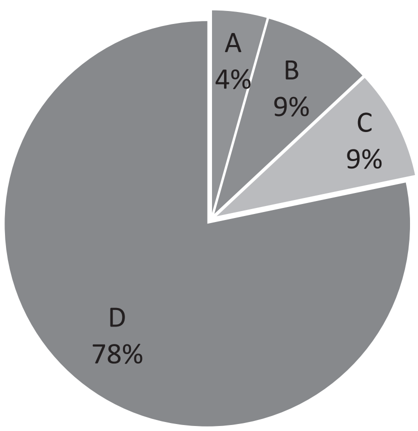

Fig. 4. The experience (in years) of work in perishable foodstuff vehicle transport: A – below 1 year, B – 1-3 years, C – 3-5 years, D – 5 years and more.

Among the surveyed drivers there were mainly the carriers of fish and frozen or deep-frozen products. Requirements related to the archiving of shipping documentation, registration and cyclic temperature control in vehicles were met. The problem to which the attention was drawn by the driver was associated with increases in the time of unloading of the goods. The consequence of that situation may be a raise of the temperature in the vehicle.This situation is usually caused by the lack of assistance from another person (assistant driver, handling assistant at the customer). Therefore, the unloading time may be longer due to self-unloading.

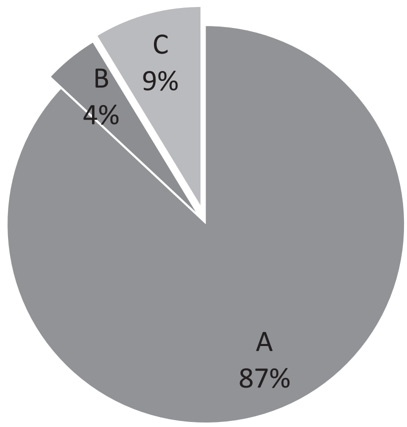

Fig. 5. Are you always informed on what kind of products you transport? A – Yes, B – No, C – I don’t know

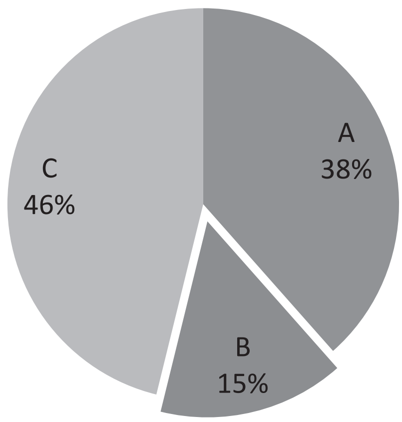

Fig. 6. Do you know the rules of “good transport practice”? A – Yes, B – No, C – I don’t know

REFRERENCES

1. ATP Agreement (valid from 23.09.2013) [online access] http://www.unece.org/fileadmin/DAM/trans/main/wp11/wp11doc/ATP-2013_e.pdf
2. ATP Agreement (valid from 23.11.2014) [online access] http://www.unece.org/fileadmin/DAM/trans/doc/2014/wp11/ATP-2014_e.pdf
3. ATP Handbook. [online access] http://www.unece.org/fileadmin/DAM/trans/doc/2014/wp11/Handbook-2014e.pdf
4. **Bęczkowska S., Grabarek I., Choromański W. 2012:** Modelowanie ryzyka w drogowym transporcie towarów

niebezpiecznych z uwzględnieniem czynnika ludzkiego. Ergonomia w warunkach gospodarki opartej na wiedzy. Redakcja: Złowodzki M., Ogińska H., Juliszewski T., Pawlak H. Komitet Ergonomii PAN, Kraków-Lublin.
5. **Bieńczak K., Zwierzycki W. 2006:** Samochody chłodnicze w transporcie żywności. Systherm. Poznań.
6. Centralny Ośrodek Chłodnictwa – zakres badań ATP [online access] http://www.coch.pl/Badania-ATP,15,b-en.
7. Competent Authorities and Test Stations List [online access] http://www.unece.org/fileadmin/DAM/trans/main/wp11/teststations.pdf
8. **Kwaśniowski S. 1997:** Zasady dobru urządzeń chłodniczych i grzewczych do nadwozi izotermicznych. w.: Pojazdy izotermiczne i chłodnicze. Oficyna Wydawnicza Politechniki Wrocławskiej. Wrocław.
9. **Łaski M., Paluch S. 2005:** Transport drogowy osób i rzeczy. Grupa IMAGE, Warszawa.
10. Oświadczenie o przystąpieniu do umowy o międzynarodowych przewozach szybko psujących się artykułów żywnościowych i o specjalnych środkach transportu przeznaczonych do tych przewozów (ATP). Dz. U. 1984 nr 49, poz. 254. 26 października 1984. [online access] http://isap.sejm.gov.pl/Download?id=WDU19840490254&type=2
11. **Prochowski L., Żuchowski A. 2006:** Samochody ciężarowe i autobusy. Wydawnictwa Komunikacji i Łączności, Warszawa.
12. **Rydzkowski W., Wojewódzka-Król K. 2005:** Transport. Wydawnictwo Naukowe PWN, Warszawa.
13. **Steindel M., Schnotale J. 2008:** Mrożona żywność i jej transport zgodnie z przepisami Unii Europejskiej. Samochodowy transport chłodniczy. Dodatek miesięcznika Chłodnictwo & Klimatyzacja. Euro-Media, Warszawa, 5-14.
14. Ustawa o transporcie drogowym, Dz. U. 2001 Nr 125 poz. 1371z dnia 6 września 2001 r.[online access]http://isap.sejm.gov.pl/Download?id=WDU20011251371&type=3
15. Ustawa o transporcie drogowym Dz.U. 2013 poz. 1414 z dnia 15 października 2013 r. [online access]http://isap.sejm.gov.pl/Download?id=WDU20130001414&type=1
16. **Zwierzycki W., Bieńczak K., Rochatka T., Stachowiak A., Tyczewski P. 2008:** Badania pojazdów chłodniczych oraz kontrola temperatury w ładowni. Samochodowy transport chłodniczy. Dodatek miesięcznika Chłodnictwo & Klimatyzacja. Euro-Media, Warszawa, 15-18.

ORGANIZACJA TRANSPORTU SAMOCHODOWEGO ŻYWNOŚCI WYMAGAJĄCEJ CHŁODZENIA

Streszczenie. W artykule zaprezentowano opis wymagań prawnych związanych z transportem żywności wymagającej chłodzenia. Przeprowadzono ankietę wśród kierowców związanych z takim rodzajem transport. Ankieta miała na celu sprawdzenie stanu wiedzy kierowców w zakresie przewozu żywności szybkopsującej się, która wymaga chłodzenia.

Słowa kluczowe: artykuły żywnościowe, transport samochodowy, regulacja prawna

The Dynamic Vibrations Hydraulic Quencher

Leonid Pelevin, Mykola Karpenko

Kyiv National University of Construction and Architecture
Povitroflotskyy Prosp., 31, Kyiv, Ukraine, 03680, e-mail: karpenko_knuba@ukr.net

Received December 01.2014; accepted December 17.2014

Summary. A review and analysis were carried out of the developed hydraulic system for quenching dynamic oscillations. The mathematical model was made for determining the time delay in operation of the hydraulic system for dynamic quenching of oscillations. A calculation was made of soil cleavage period and operation time delay of dynamic oscillations quencher, from which it is possible in theory to establish the ability of the hydraulic system for dynamic oscillations quenching to operate in time. The hydraulic system was developed for dynamic oscillations quenching inside the working unit to prevent the transmission of vibrations to the base of the machine. An analysis was performed of the damper's means and the method of dynamic damping on which the hydraulic system was developed for dynamic oscillations quenching. The mathematical sequence was built for the determination of operation time delay of the quencher. The parameters have allowed to construct the experimental model of hydraulic system for dynamic oscillations quenching.

Key words: quencher, dynamic oscillations, hydraulic system, time lag response, soil cleavage period.

INTRODUCTION

The construction often includes works that cannot be performed by conventional machines. In this case, using a special technique, which is equipped by active action engines and used for ground operations can be consider as a solution.

One of the disadvantages of this special technology is the transmission of vibrations from the working body to base machine, accompanied by the premature wearing down of the basic machine parts which do not participate in the ground destruction.

To solve the above-mentioned problem amortizable equipment can be used to isolate vibrations caused by the working body movement from the base machine.

Given that the current cushioning devices are not effective enough, there is demand for the construction of a new hydraulic system for dynamic oscillations quenching as well as mathematical model for the determination of the main characteristics of the new system, namely: determining the time delay in the operation of the hydraulic system for dynamic oscillations quenching, its evaluation, timeliness, triggering of specified dynamic fluctuations.

PURPOSE OF WORK

Based on the results of the dynamic analysis of the method and vibration cushioning devices the work aimed to develop:

– A mathematical model for determining the time delay in the operation of the hydraulic system for dynamic oscillations quenching;
– A hydraulic construction developed by the authors for extinguishing dynamic oscillations that arise inside the working part in order to make their transmission to the base machine impossible.

THE MAIN MATERIAL

In engineering it is often necessary to damp the vibration transmitted to the machine from its working equipment. Basically, it concerns machines with dynamic (active) working tools. As a result of work, the vibrations can be transmitted to the machine and cause destruction. To prevent transmitting the vibrations from the working body to the base machine the so-called springy elements are used, which try to put out the vibrations transmitted to the base machine. The main method of vibration damping is called – a method of dynamic vibration damping [3, 4, 5, 15, 19].

The method of dynamic vibration damping is based on the application of additional protective devices to change the vibration properties in a given object. The work of the dynamic quencher is based on putting out the force transmitted to the object. This dynamic quenching differs from another method of reducing vibration, characterized by imposition of the additional kinematic object linkages, such as fixing some of its points [2, 19].

Changing the vibrating condition of the base machine when joining a dynamic quencher can be achieved by the redistribution of vibrational energy from the object to the quencher and in the direction of the increasing energy dissipation fluctuations [13, 20]. The former is implemented by changing the system's settings of the object-quencher over the frequencies of the vibration excitation by correcting the elastic-inertial properties of the system. In this case, the devices attachable to the object are called inertial dynamic quenchers. An inertial quencher is used to suppress harmonic mono or narrowband random fluctuations.

During a vibration's load of the wider frequency range the second method is preferred. It is based on increasing dissipative properties of the system by attaching additional specific damping elements to the object. Dynamic quencher dissipative types are called vibration absorbers [3]. The combined ways of the dynamic quenching using both correction elastic-inertial and dissipative properties of the system are also possible. In such cases we talk about the dynamic quencher of friction [7, 16].

When implementing dynamic quencher counteraction fluctuations the object is affected by reactions that are passed to it from the attached bodies. For this reason, considerable effects with limited amplitudes of the masses adjusted can be achieved only by large mass (moment of inertia) of connected bodies, typically ≈ 5...20% of the reduced mass (moment of inertia) primary system with an appropriate form of vibrations within the frequency quenching which is performed, respectively [3].

Typically, a dynamic quencher is used to achieve a local effect: a reduction of the object's vibration in the parts where the quencher is fastened. Often it may be associated even with the deterioration of the object's vibration in the other less appropriate places.

a *b*

Fig. 1. The overall look of shock absorbing passive elements: *a* – spring (of vehicle), *b* – spring

Dynamic quencher can be constructively implemented based on the passive elements (Fig. 1) (masses, springs, shock absorbers, dampers) and the active ones, which have their own power sources.

In the last case we are talking about the use of automatic control units that use elements driven by an electric, hydraulic or pneumatic system. Their combination of passive devices is successful, an example of which is the shock absorber shown in Fig. 2.

Fig. 2. General view of the shock absorber

The utilization of the active elements expands the possibilities of dynamic vibration suppression, because it allows to conduct continuous adjustment of the parameters of dynamic quencher as a function of excitation acting, and thus to perform quenching in conditions of changing vibration loads. A similar result can be achieved sometimes by means of passive devices with nonlinear characteristics.

Shock absorber is the device which converts mechanical energy into thermal and is used for vibration damping and shock absorption. It bumps acting on the casing (frame). Shock absorbers are used in conjunction with elastic elements: springs (of a vehicle), pillows, etc.

Hydraulic shock absorbers have become the most commonly used. In a hydraulic shock absorber the resistance force depends on the speed of rod movement. Oil is the working medium. The principle of operation of the shock absorber is based on the reciprocating movement of the piston shock absorber, which through a small hole puts oil from one chamber to another, converting mechanical energy into the heat energy.

Today, the generally used solutions for vibration damping devices are those which utilize the hydraulic elements. Hydraulic dampers as opposed to friction ones, have the longer duration of work and can quench a small oscillation amplitude.

Fig. 3 shows the design of the damper, which contains an adjusting screw. This allows to increase the resistance value of the liquid flowing through the channel and thus control the damping, according to [9, 12, 13].

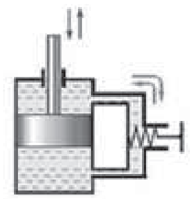

Fig. 3. Liquid damper's adjusting screw

Nowadays, the most promising system is the hydraulic vibration damping one, which is designed based on hydraulic shock absorbers and dampers.

In the design of hydraulic systems for blanking the oscillations the dynamic characteristics of systems must be considered, in particular, the transfer speed signals and the total system performance, pressure fluctuations in various points of the system (including hydraulic shocks), sustainability and quality of system transients [1, 11].

Movement of actuating mechanism always comes with some delay in relation to the input signal. The identification of the delay's amount allows to determine the system's dynamic, the total response time and the need to introduce appropriate units to compensate for the delay calculation, depending on the frequency control signal and set according to the corresponding pulses [8, 17, 9].

To perform the system's calculations it is necessary to know the basic system parameters, including the size of pipelines, hydraulic and mechanical resistance properties of the working fluid and hydraulic machines as well as hydraulic power source characteristics [6].

Total delay time of the system's response can be defined as a first approximation by the formula:

$$t_d = \frac{\Delta V + V_1}{Q_h + 0{,}5Q_b}, \tag{1}$$

where:
ΔV – reduces the volume of liquid in the system by increasing the pressure on the value of Δp, m^3, V_1 – volume of fluid required to fill additional volumes in the system, m^3, Q_b – leak in the system for working pressure, m^3/s, Q_h – the nominal flow rate in the system, m^3/s.

In this case Q_h and V_1 are determined from the formula:

$$Q_h = \frac{17{,}1N_h}{P_h}, \tag{2}$$

where:
N_h – hydraulic drive power, kW, P_h – nominal pressure of hydraulic system MPa.

The volume of the fluid required to fill the additional volume in the system V_1 is 5...10% of the total volume of fluid in the hydraulic system V, m^3. The total volume of fluid in the hydraulic system is calculated as follows:

$$V = V_c + V_e, \tag{3}$$

where:
V_e – the amount of hydraulic fluid that is equipped in hydraulic system, m^3, V_c – the amount of hydraulic fluid that is in the pipeline hydraulic system Eq. (3), which is calculated by the equation:

$$V_c = \frac{\pi D^2}{4} L, \tag{4}$$

where:
L – total length of pipelines, m, D – internal diameter hydraulic of the pipeline, m^2, calculated by the formula:

$$D = 4{,}5\sqrt{Q_h / W}, \tag{5}$$

where:
W – speed liquid in the hydraulic system at a prescribed pressure, m/s.

$$V_1 = (0{,}05 \ldots 0{,}1)V. \qquad (6)$$

At first approaching the delay operation of the system Eq. (1) we obtain the equation:

$$t_d = \frac{\Delta V + V_1}{Q_h} \cdot \frac{1}{1 - \dfrac{Q_b}{2Q_h}}. \qquad (7)$$

In the view of that:

$$Q_b = K_b P, \qquad (8)$$

where:
P – operating pressure in the system, MPa, K_b – the coefficient of leakage of liquid, received from the equation:

$$K_b = j\frac{61{,}2N_h}{P^2}, \qquad (9)$$

where:
j – coefficient of the changes in the units of measurement of l/min in m^3/s and 0.278 matter.

In this case, reduction in the volume of liquid in the system while increasing pressure by the value of Δp is calculated as follows:

$$\Delta V = \delta S_1 L, \qquad (10)$$

where:
δ – coefficient of decrease of the liquid, which depends on the operating pressure; S_1 – cross-section inner diameter hydraulic of the pipeline, m^2.

Moreover, S_1 is calculated as follows:

$$S_1 = \frac{\pi D^2}{4}. \qquad (11)$$

Finally, after determining equations will get simplified the delay triggering and performance will look like:

$$t_d = \frac{\delta S_1 L + V_1}{Q_h - 0{,}5K_b P}. \qquad (12)$$

From the dependence it is obvious that to reduce the time delay triggering it is necessary:

1. Working channels and pipelines should be as short and rigid as possible;
2. Volume losses should be lowered to a minimum;
3. Pump capacity should be significant.

In general, the performance of the dynamic oscillations quencher is determined for each particular system, provided that the signal can be transmitted with a specific delay, but performance must be such as not to violate the stability of the whole circuit [18].

To achieve the stated conditions, we need to find out the time of soil cleavage, i.e. the time at which the dynamic ripper makes one complete cycle of the movement T_c [14], which is inverse to the average oscillation frequency maxima of cutting the soil, and is given by:

$$T_c = \frac{1}{\bar{n}_m} \text{ s}, \qquad (13)$$

$$\bar{n}_m = \frac{\bar{n}_0}{0{,}63 \ldots 0{,}87} \text{ 1/s}, \qquad (14)$$

where:

$$\bar{n}_0 = (2{,}0 \ldots 2{,}8)\frac{W_w}{H} \text{ 1/s}$$

H – the average oscillation frequency of cutting soil,
m - loosening depth,
W_w – speed of the working body.

Let us etermine the dependence of the time of delay of triggering quencher dynamic fluctuations of hydraulic parameters [2, 19].

Suppose that a dynamic body is working in rocky soil at the depth of H = 0,3 m, in which case the rate of dynamic body is

W_w= 2 m/s.

First of all determine the time of soil cleavage:

$$T_c = \frac{1}{\bar{n}_m} = \frac{1}{15{,}3} = 0{,}09 \text{ s}. \qquad (15)$$

Determine the relationship Eq. (14) between the middle frequency oscillation cutting forces:

$$\bar{n}_m = \frac{\bar{n}_0}{0{,}63 \ldots 0{,}87} = \frac{13{,}3}{0{,}87} = 15{,}3 \text{ 1/s}, \qquad (16)$$

$$\bar{n}_0 = 2 \cdot \frac{2}{0{,}3} = 13{,}3 \text{ 1/s}. \qquad (17)$$

The initial data of the hydraulic system for blanking dynamic oscillations: N_h = 100 kW, P_h = 25 MPa, P = 30 MPa, L = 20 m, W = 4.25 m/s.

Let us carry out the calculation:

$$Q_h = \frac{17{,}1 \cdot 100}{25} = 68{,}1 \text{ m}^3\text{/s}, \quad (18)$$

$$D = 4{,}5 \cdot \sqrt{68{,}1/4{,}25} = 18 \text{ mm}, \quad (19)$$

$$V_{\text{con.}} = \frac{3{,}14 \cdot 0{,}018^2}{4} \cdot 20 = 0{,}0051 \text{ m}^3, \quad (20)$$

$$V_1 = (0{,}0051 + 0{,}0549) \cdot 0{,}1 = 0{,}006 \text{ m}^3, \quad (21)$$

$$S_1 = \frac{3{,}14 \cdot 0{,}018^2}{4} = 0{,}00026 \text{ m}^2, \quad (22)$$

$$K_b = 0{,}278 \frac{61{,}2 \cdot 100}{30^2} = 1{,}89 \text{ kW/MPa}^2, \quad (23)$$

$$t_\text{d} = \frac{30 \cdot 0{,}00026 \cdot 20 + 0{,}006}{68{,}1 - 0{,}5 \cdot 1{,}89 \cdot 30} = 0{,}004 \text{ s.} \quad (24)$$

From the resulting example we can conclude that the system performance satisfies oscillation quenching specified condition of this dynamic device's triggering delay is lower than 15 % of the soil cleavage time.

By changing the parameters of hydraulic system dynamic quenching fluctuations – namely the supply of hydraulic fluid in the system and reduction of fluid volume ratio, and substituting them in the present calculation, we obtain the dependence of the delay in the operation of the hydraulic system dynamic quenching oscillation (speed) on the hydraulic fluid supply system (Fig. 4) and on the coefficient reduction of fluid (Fig. 5).

The hydraulic quencher dynamic fluctuations were developed to improve the efficiency of dynamic quenching of oscillations, which is based on the use of the above-mentioned system.

The dynamic oscillations quencher (Fig. 6, 7) works as follows [10].

Vibrations that are transmitted from the working body to the base machine are blanked with the help of dynamic fluctuations quencher *1*. At active work, the oscillatory body rod *3* tries to

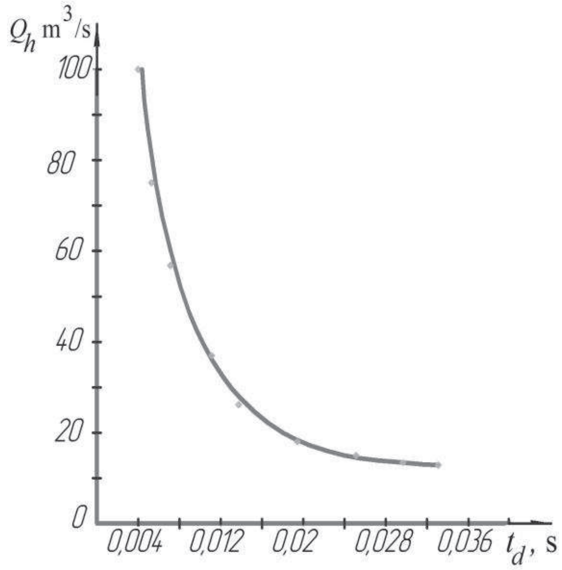

Fig. 4. Graph of the time delay dependence during the operation of hydraulic blanking dynamic fluctuations on hydraulic fluid supply.

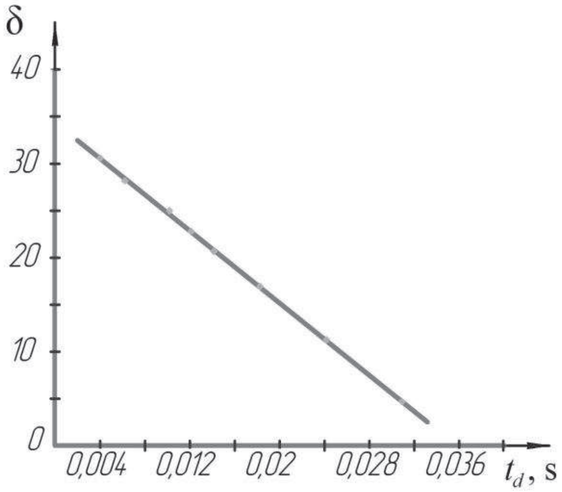

Fig. 5. Graph of the time delay dependence during the operation of hydraulic blanking dynamic fluctuations on the fluid amount reduction coefficient

reproduce vibrational motion in the housing *2*. However, when the direction of the vibrational motion is directed, for example, left by movement of fluid through the holes throttled *6* plunger *4*, *8* rods blocking valve and plunger valve *11* are moving blocking right. Thus blocking rods *8* press the valve rods washer *7*. Meanwhile, blocking plunger valve *11* presses the plunger *4*, blocking throttling holes *6*, so that the liquid begins to flow through passage the holes *12*, which extinguish the movement of the rod *3* left. Once the

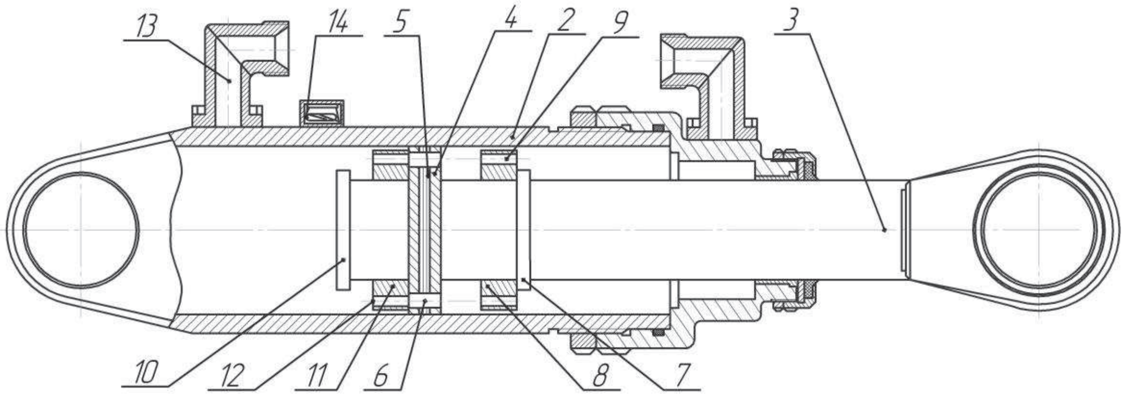

Fig. 6. Quencher of dynamic fluctuations

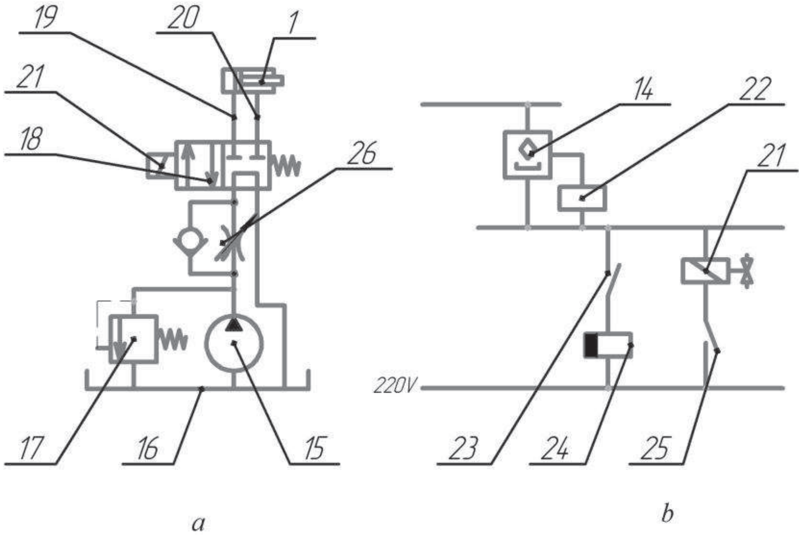

Fig. 7. The hydraulic circuit control in dynamic oscillations quencher *a* and electrical circuit control distributor *b*

plunger *4* reaches the reed switch *14*, the magnetic field of the magnet constant step *5* shut reed contacts *14* (Fig. 7, *b*). The signal will go to detention relay *22*, which shut normally open contact *23*. He, in turn, the delay relay exclusion 24 is turned on. After that, delay relay exclusion *24* shuts contact *25*, which starts the electromagnetic control 21. The electromagnetic control *21* toggles the distributor *18* in the left position. Hydraulic pump *15* works through the variable orifice with check valve *26*, which regulates the supply of hydraulic fluid distributor *18* and pressure line *19* takes an additional portion of the fluid in the plunger cavity quencher dynamic fluctuations *1*. Excess fluid flows out of rods quencher dynamic cavity oscillations *1* through the drain line *20* and distributor *18* to the tank of hydraulic fluid *16*. When plunger *3* moves to the right by moving the working fluid through the throttling holes *6*, *8,* rods blocking valve and plunger valve *11* move left. Valve blocking plunger *11* presses washer *10* and valve blocking rods *8* press plunger *4* blocking throttling hole *6*. As a result, the liquid begins to flow through passage *9* , putting the movement of the rod *3* right. Once the plunger *4* moves away from the reed switch *14* and the magnetic field of the magnet constant step *5* stops to influence the reed switch *14* (reed switch contacts open up *14*), the signal ceases to be submitted normally to open contact *23*. This, in turn, relays switching delay open up exclusion *24*. It will work for a while, allowing the hydraulic pump *15* to submit several additional portions of the liquid in the plunger cavity oscillations quencher *1*-for-*4* plunger removal of reed switch *14*. After exclusion of relay contact delay *24,* the *25*, *21* will control the electromagnetic switch distributor *18* in the far right position, then feed additional portion of the liquid to the quencher dynamic fluctuations *1* end. Hydraulic fluid is fed to the quencher through the pipe *13*.

Because of the dynamic fluctuations quencher *1* reduces dynamic fluctuations in the base machine, during the working bodies active action.

CONCLUSIONS

1. Based on the analysis of dynamic cushioning devices for vibration in the hydraulic system, the mathematical model of the process of determining the delay time of their operation is worked out, which allows to design these systems.
2. Based on the values, the dependency graphs are built of: time delay operation dependence of the hydraulic system dynamic oscillations on quenching coefficients of reduction of fluid and supply of hydraulic fluid. By changing these parameters the system was designed for adjusting the hydraulic damping system dynamic oscillations.
3. A new design was performed of hydraulic blanking of dynamic fluctuations with the ability to change the filling parameters.
4. The design provides adjustable vibration base machine for vibrations attachments.

REFERENCES

1. **Bud'ko V., 2003.** Dynamics and regulation hidropnevmosystem.: K.: NAU, 64 (in Ukraine).
2. **Cândea I., Popescu S., 2003.** Theoretical and experimental study on soil vibrators used for the germinal layer preparation. TEKA: kom. Mot. Energ. Roln., OL PAN, vol. 3. (6), 55-62.
3. **Chelomej V.N., 1981.** Vibrations in Technology: Handbook: in 6 volumes. Red. Sovet: (pred.).-M.: Mashinostroenie, T. 6, 456 (in Russian).
4. **Emtsev B., 1987.** Technical hydromechanics.: M.: Mashinostroenie, 439 (in Russian).
5. **Gavrilenko B. Minin V., 1958.** Hydraulic drive. : M.: Mashinostroenie, 240 (in Russian).
6. **Gijom M., 1964.** Investigation and calculation of hydraulic systems.-M.: Mashinostroenie, 387 (in Russian).
7. **Korobochkin B., 1976.** dynamics of hydraulic machines. M.: Mashinostroenie, 240 (in Russian).
8. **Lewis E., Sterh H., 1966.** Hydraulic control system. M.: Mashinostroenie, 407 (in Russian).
9. **Nagorniy V., Denisov A., 1991.** Devices of automation and hydro pneumatic. M.: Mashinostroenie, 367 (in Russian).
10. **Patent** Ukraine № 90197 from May 12.2014 (in Ukraine).
11. **Popov D., 1987.** Dynamics and regulation of hydraulic and pneumatic systems. M.: Mashinostroenie, 464 (in Russian).
12. **Schokdemper, 2014** Available at: http://nl.wikipedia.org/wiki/Schokdemper, accessed 20 Jul. 2014 (in Nederlands).
13. **Shorin V., 1980.** Elimination of fluctuations in air pipes. M.: Mashinostroenie, 156 (in Russian).
14. **Vetrov Ju., Vlasov V., 1995.** Machines for excavation. Sample calculation: Teach. user.. – K.:ISDO, 304 (in Russian).
15. **Vilde A., Cesnieks S., Rucins A., 2004.** Minimisation of Soil Tillage. TEKA: kom. Mot. Energ. Roln., OL PAN, vol. 4. (30), 237-243.
16. **Vilde A., Rucins A., 2004.** The Impact of Soil Physical and Mechanical Properties on Draft Resistance of Ploughs. TEKA: kom. Mot. Energ. Roln., OL PAN, vol. 4. (31), 243-249.
17. **Vilde A., Tanaś W., 2005.** Determination of the soilfriction coefficient and specific adhesion. TEKA: kom. Mot. Energ. Roln., OL PAN, vol. 5. (24), 212-217.
18. **Walusiak S., Dziubiński M., Pietrzyk W., 2005.** An analysis of hydraulic braking system reliability. TEKA: kom. Mot. Energ. Roln., OL PAN, vol. 5. (25), 217-226.
19. **Zakharchuk B., Telushkin V., 1987.** Bulldozer and rippers. M.: Mashinostroenie, 240 (in Russian).
20. **Zipkin Ya., 1977.** Foundations of the theory of automatic systems. M.: Mashinostroenie, 560 (in Russian).

ГИДРАВЛИЧЕСКИЙ ГАСИТЕЛЬ ДИНАМИЧЕСКИХ КОЛЕБАНИЯХ

Аннотация. Проведен обзор и анализ существующих амортизирующих устройств. Рассмотрен метод динамического гашения колебаний. Составлена математическая модель определения времени запаздывания срабатывания гидроавтоматической системы гашения динамических колебаний, значение которого позволяет создавать гидроавтома-тические системы гашения колебаний вовремя реагирующих на динамические внешние возмущения. Проведен расчет периода скалывания грунта при работе рыхлителя и времени запаздывания срабаты-вания гасителя динамических колебаний, на основе которых устанавливается способность гидроавтоматической системы гашения дина-мических колебаний вовремя срабатывать обеспечивая предотвращение передачи колебаний к базовой машине. Разработана гидроавтоматическая система гашения дина-мических колебаний, возникающих на рабо-чем органе, для предотвращения передачи этих колебаний к базовой машине.

Ключевые слова: гаситель, динамические колебания, гидроавтоматическая система, время запаздывания срабатывания, период скалывания грунта.

Correlation of Plastic Forming and Structure Formation Parameters in Powder Materials

Lyudmila Ryabicheva, Dmytro Usatyuk, Yuri Nikitin

Volodymyr Dahl East Ukrainian National University,
Department of Engineering Mechanics, Chair of Material Science
Molodizhny bl., 20a, Lugansk, 91034, Ukraine, e-mail: resource.saving@gmail.com

Received December 04.2014; accepted December 17.2014

Summary. A theoretical analysis of the kinetics of softening processes occurring in the powder porous body during deformation at high temperatures has been conducted. Constitutive equations relating the deformation parameters and structure formation parameters that are characterizing dynamic softening processes during deformation. The linear dependence of the axial stress logarithm and accumulated deformation of hard phase as a function of the reciprocal of the temperature. The activation energy of dynamic softening at uniaxial compression estimated. It has shown that at low deformation temperatures the softening mechanism is dynamic recovery and polygonization while dynamic recrystallization is taking place at elevated temperatures. Porosity decreases the activation energy of dynamic softening. The dynamic softening mechanism in powder material was confirmed by metallographic analysis.

Key words: mathematical model, recovery, polygonization, recrystallization, activation energy.

INTRODUCTION

A wide variety of working conditions of machine parts require the development of materials with special properties that ensure high wear resistance [1, 2]. This problem may be solved by implementation of new materials produced by a combination of heat treatment and plastic forming processes. The power and kinematic parameters of plastic deformation during hot and semi-hot deformation take an influence on structure of powder materials and changing of their operational properties. Consequently, investigation of the deformation of powder materials is important for solving problem of interrelation of deformation parameters and structure formation. This question has deeply studied for deformation of compact materials [3, 4]. It has shown clearly that temperature, strain rate and intensity of deformation take an influence on structure formation parameters that are determining the mechanism of softening process [5]. It has established theoretically and experimentally that increment of material's plasticity at small degrees of deformation and low temperatures is stipulated by dynamic recovery and polygonization, while it is connected with the kinetics of dynamic recrystallization at increasing of the temperature and degree of deformation [6, 7, 8]. Increasing of strain rate leads to growing resistance of deformation, decrease in plasticity due to intensification of hardening processes [9]. Obviously, the same dynamic softening processes may be observed into the solid phase of powder material [10]. However, the kinetics of softening processes is under the influence of pore phase presented in powder materials.

This paper is aimed in theoretical analysis of the kinetics of softening processes taking place in the powder material during plastic deformation at elevated temperatures and determination of dependences between deformation and structure formation parameters.

MATERIALS AND METHODS

Plastic forming at any conditions, on a basis of dislocation representations, may be characterized by changing of dislocation structure in hard phase of powder material, which causes the development of two mutually balanced processes - hardening and softening. The expression of changing the dislocations' density during plastic deformation may be written as [11]:

$$\dot{\rho} = \eta\dot{\varepsilon} - k\rho, \tag{1}$$

where: ρ – is the dislocation density; k – is the Boltzmann function; $\dot{\varepsilon}$ – is the strain rate; η – is the coefficient that characterises the ability of hard phase to accumulate dislocations at particular strain rate.

The first term on the right side of the equation (1) describes the hard phase hardening and increment of dislocation density per unit of time that is growing with the strain rate $\dot{\varepsilon}$. The second term describes decreasing of strength through decrementing of dislocation density due to thermally activated processes expressed by the Boltzmann function:

$$k = k_0 \exp(-E / kT), \tag{2}$$

where: k_0 – is the frequency factor that is independent of temperature; E – is the activation energy of softening processes; T – is the absolute temperature.

The equation (1) has a solution [12] at the constant strain rate $\dot{\varepsilon}(t) = \varsigma = const$ and boundary conditions $\rho(0) = \rho_0$:

$$\rho = \left(\rho_0 - \frac{\eta\varsigma}{k}\right) \exp\left(-k\frac{\omega}{\varsigma}\right) + \frac{\eta\varsigma}{k}, \tag{3}$$

where: ω – is the accumulated deformation with taking into account the influence of porosity.

The accumulated deformation of hard phase is determined by the following expression [13]:

$$\omega = \int_0^\tau W d\tau, \tag{4}$$

where: W – is the rate of changing the accumulated deformation of powder material; τ – is the period of time.

The rate of changing the accumulated deformation of powder material may be written in the following way [13]:

$$W = \frac{1}{\sqrt{1-\theta}}\sqrt{\psi e^2 + \varphi\gamma^2}, \tag{5}$$

where: ψ, φ – are porosity functions; e – is the volume changing rate; γ – is the shape changing rate.

Porosity functions may be calculated by expressions [13]:

$$\psi = \frac{2}{3}\frac{(1-\theta)^3}{\theta}, \quad \varphi = (1-\theta)^2, \tag{6}$$

and assuming of (Eq. 4) and (Eq. 5),

$$\omega = \int_0^\tau \frac{1}{\sqrt{1-\theta}}\sqrt{\varphi\gamma^2 + \psi e^2}\, d\tau. \tag{7}$$

The volume changing rate for uniaxial compression may be written as:

$$e = e_z + 2e_r, \tag{8}$$

a shape changing rate may be determined using the formula:

$$\gamma = \sqrt{\frac{2}{3}}\left|e_z - e_r\right|, \tag{9}$$

considering the equation:

$$\frac{e_r}{e_z} = \nu = \frac{r-1}{2+r}, \tag{10}$$

after substitution to (Eq. 8) the volume changing rate has transformed to the formula:

$$e = (1 + 2\nu)e_z. \tag{11}$$

A spherical component of the stress tensor:

$$p = \frac{1}{3}\sigma_z, \tag{12}$$

the intensity of shear stress is determined by the formula:

$$\tau = \sqrt{\frac{2}{3}}\left|\sigma_z\right|. \tag{13}$$

Loading surface of powder body with taking into account pore formation process may be implemented in the form of:

$$\alpha(p-a)^2+\beta\tau^2=c^2, \tag{14}$$

where: α, β, a, c – are coefficients that are dependent on the porosity [13].

The following equation that describes dimensional changes during uniaxial compression has obtained in [7] on the basis of the plasticity law (Eq. 14) while considering (Eq. 12) and (Eq. 13):

$$r=\frac{1}{3}\frac{\alpha}{\beta}\left(1-3\frac{\alpha}{\sigma_z}\right)= \\ =\frac{1}{3}\frac{\alpha}{\beta}\left[\frac{-6\alpha\beta-\sqrt{c^2(\alpha+6\beta)-6\alpha\beta a^2}}{\alpha a-\sqrt{c^2(\alpha+6\beta)-6\alpha\beta a^2}}\right]. \tag{15}$$

The equation of axial stress under uniaxial compression looks like:

$$\sigma_z=\frac{3\alpha a}{\alpha+6\beta}-\frac{\sqrt{6}\sqrt{c^2(\alpha+6\beta)-6\alpha\beta a^2}}{\alpha+6\beta}. \tag{16}$$

Therefore, changing of porosity and accumulated deformation during forming operation may be calculated from the expressions:

$$\frac{d\theta}{d\varepsilon_z}=(1-\theta)(1-2\nu), \\ \frac{d\omega}{d\varepsilon_z}=\frac{1}{\sqrt{1-\theta}}\sqrt{\frac{2}{3}\frac{1}{r^2}\varphi+\psi(1-2\nu)sign(e_z)}. \tag{17}$$

It is possible to determine the axial stress and accumulated deformation from (Eq. 16) and (Eq. 17). The right side of (Eq. 17) contains nonlinear functions of porosity, consequently, solution of differential equations' system was performed numerically by the Newton-Raphson method. The function (Eq. 3) describes a decrementing change of dislocations' density ρ [11]. The value of ρ asymptotically goes to the limiting value $\eta\varsigma/k$ at $\omega\to\infty$ and $\tau\to\infty$. The value of $\eta\varsigma/k$ depends on the deformation temperature and activation energy of thermally activated softening process according to (Eq. 2) at the condition $\eta\varsigma=const$.

The ultimate density of dislocations under the given conditions of deformation goes to the value of $\eta\varsigma/k$ based on the expression (3). The average dislocations' density for maximum stress reached for this stage of deformation defined similarly to [12]:

$$\rho_k=\chi\frac{\eta\varsigma}{k}, \tag{18}$$

where: χ - is the ratio that is within $0<\chi<1$.

The dependence of the maximum flow stress σ_z for the certain deformation stage from the dislocation density ρ_k may be assumed in the following way [8]:

$$\sigma_z=A(\rho_k)^n, \tag{19}$$

where: A and n - are constants.

The expression (Eq. 19) after the substitution of (Eq. 18) looks like:

$$\sigma_z=A\left(\chi\frac{\eta\varsigma}{k}\right)^n. \tag{20}$$

After taking the logarithm, substitution of (Eq. 2) and transformations obtained:

$$ln\,\sigma_z=ln\left[A\left(\chi\frac{\eta\varsigma}{k_0}\right)^n\right]+\frac{nE}{RT}. \tag{21}$$

Obviously, the maximum flow stress σ_z for certain forming stage is corresponding to the accumulated deformation ω_k. Then, substituting the expression (3) the value of accumulated strain and equating (3) and (8), after transformations we obtain:

$$\omega_k=\frac{\varsigma}{k}ln\left[\left(\rho_0\frac{k}{\eta\varsigma-1}\right)(\chi-1)^{-1}\right]. \tag{22}$$

It has assumed from (Eq. 22) that the factor $ln\left[(\rho_0 k/(\eta\varsigma-1))(\chi-1)^{-1}\right]$ in case of balance between hardening and softening processes tends to a constant value for a certain flow stress. In this case, the rate of changing the dislocation density goes to zero. The following equation obtained from (Eq. 1) at a constant strain rate:

$$\frac{1}{\rho_K} = \frac{k}{\eta \varsigma}. \tag{23}$$

Then:

$$ln\left[\left(\rho_0 \frac{k}{\eta\varsigma} - 1\right)(\chi - 1)^{-1}\right] = ln\left[\left(\frac{\rho_0}{\rho_{\hat{e}}} - 1\right)(\chi - 1)^{-1}\right] \tag{24}$$

It has accepted that the dislocation density of the hard phase before and after deformation are different by 10-100 times [14], and $\chi \approx 0,8 \div 0,9$, means that the value of (Eq. 24) may be approximately determined as $ln\,10 \approx 2,3$.

The equation (Eq. 22) was transformed to the form:

$$\omega_K \approx 2,3\frac{\varsigma}{k} \cong 2,3\frac{\varsigma}{k_0} exp\left(\frac{E}{RT}\right). \tag{25}$$

than, after taking the logarithm, obtained:

$$ln\,\omega_K = ln\frac{\varsigma}{k_0} - \frac{E}{RT}. \tag{26}$$

Equations (Eq. 21) and (Eq. 26) are relations connecting the main parameters of the deformation of the porous body flow stress, accumulated deformation of hard phase, strain rate, temperature and structural characteristics of the powder material (η, k, E, ρ_K), which characterizes softening process during deformation at the elevated temperatures. A linear character of dependences of the accumulated deformation and corresponding stress from the reciprocal temperature follows from these equations with a slope of the line equal to the activation energy of dynamic softening process flowing by one or another mechanism.

A slope of the function $ln\,\omega_K = f(1/T)$ is E/RT and corresponding to (Eq. 26). Consequently, the slope of the function $ln\,\sigma_z = f(1/T)$ is nE/RT according to (Eq. 21). Therefore, slopes of these functions different by the value n are characterizing a maximum possible density of dislocations.

RESULTS AND DISCUSSION

Verification of the mathematical model has performed for evaluation of the activation energy

performed for evaluation of the activation energy
of dynamic softening processes at uniaxial compression of copper-titanium powder material. Samples were prepared from charge consists of copper powder PMS–1 and titanium powder BT1–0 with a mass fraction of titanium 0.5% and a porosity of 5-10% after sintering at 900 – 920 ºC during 3 hours into a synthesis gas atmosphere. Samples were deformed on the testing machine ZD–4 at temperatures of 100, 300, 400 and 600 ºC with strain rate 0.01 s^{-1} while recording of the indicator diagram.

The accumulated deformation values were calculated using (Eq. 17), axial stress values - by (Eq. 16), dependences $ln\,\sigma_z - 1/T$ and $ln\,\omega_K - 1/T$ (Fig. 1) have drawn.

The obtained dependences are straight lines, except for the points at 400 °C, in which there are gaps of functions due to deformation aging. Straight lines consist of two branches - low temperature branch that is characterizing deformation process at 100 – 300 ºC and high temperature branch for deformation process at 400 – 600 ºC. Slopes of these functions define the activation energy of dynamic softening passing through a particular mechanism. The degree of deformation characterizes by the stage N.

The low-temperature branch possess the lowest activation energy (Fig. 2a) with values within 0.20-0.39 eV at 5 % porosity samples and 0.12-0.28 eV at 10 % porosity, which is the result of dynamic recovery and polygonisation [9].

The activation energy at high temperatures grows more than 10 times (Fig. 2b) that indicates more intensive softening. The greatest increment of activation energy 2.3-2.6 eV has observed at high temperatures during the third stage. In this case, the activation energy of softening comparable with the activation energy of self-diffusion of pure copper, equal to 2.79 eV [14], so we can assume that softening during the third step carries out by dynamic recrystallization.

It should be noted that the value of activation energy of softening process depends on the initial porosity of samples and takes higher values at 5% porosity (Fig. 2).

The presence of pores decelerates the dynamic softening that has confirmed by experimental studies [15]. For example, E = 2.6 eV at θ_0 = 5% and E = 2.3 eV at θ_0 = 10% for high temperature deformation when softening takes place by dynamic recrystallization.

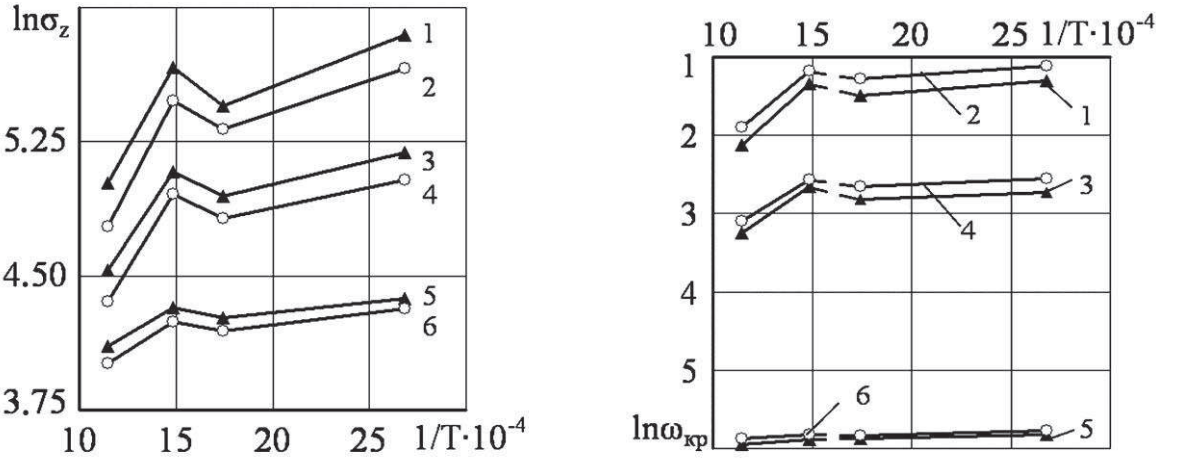

Fig. 1. The dependences $ln\,\sigma_z - 1/T$ – a, $|ln\,\omega_K| - 1/T$ – b: ▲ – θ_0 = 5 %; ○ – θ_0 = 10 %; 1, 2 – N = 1; 3, 4 – N = 2; 5, 6 – N = 3

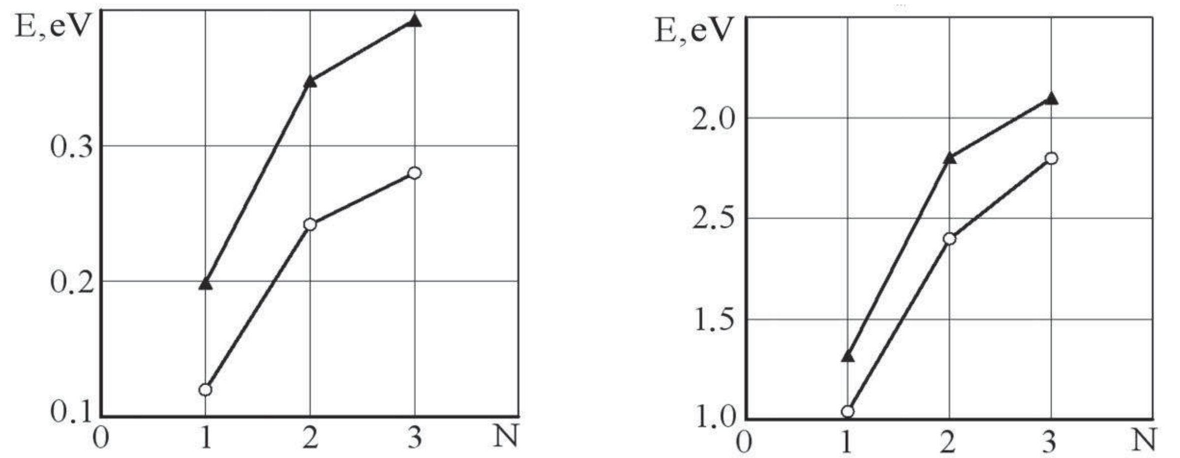

Fig. 2. Variation of activation energy during softening process: a – is the low-temperature branch; b – is the high-temperature branch; ▲ – θ_0 = 5 %; ○ – θ_0 = 10 %.

The existence of low-temperature and high-temperature branches on dependences $ln\,\sigma_z - 1/T$, that characterize softening mechanism has been verified by metallographic analysis. The character of structure changes in the powder material with 0.5 % Ti and 10 % porosity depends upon the temperature of deformation and observed at magnification ^{x}4000 (Fig. 3). Grain shape and condition of their boundaries characterize the processes occurring in the powder material during its deformation [16]. These experiments allowed to explain observed phenomena, establish the beginning of dynamic recrystallization and follow the kinetics of its development.

The starting structure after sintering of the powder material into a synthesis gas atmosphere at 900 – 920 ºC is characterized by the presence of copper grains, pores and titanium particles (Fig. 3, a). A considerable inequigranularity of microstructure has been observed. It has connected with inhomogeneous development of static recrystallization during sintering due to inhomogeneous stress state formed at compaction of charge from copper and titanium powders into a closed matrix [17].

Shapes of deformed copper grains observed on the photo of metallographic section of sample deformed by compression to the degree of deformation 0.69 at temperature 100 °C and strain rate 0.001 s^{-1} (Fig. 3, b) are different of equiaxed grains formed during sintering (Fig. 3, a). The dynamic recovery does not lead to rebuilding of structure, so distorted boundaries appeared as the consequence of severe deformation of hard phase. The refinement of grains has observed near titanium particles due to a local increase of internal stresses around the particles of alloying addition.

Deformation at 400 °C leads to formation of complex-shaped boundaries (Fig. 3, c) that indicates processes associated with the migration of grain boundaries and formation of new ones. New interfaces presented by coherent particles of precipitates have formed at 400 °C as the result of decomposition of a supersaturated solid solution during deformation of the copper-titanium materials [18, 19] that promotes the primary recrystallization [20]. However, the development of dynamic recrystallization inhibited due to blocking of grain boundaries by particles, thus preventing of their migration and resulting in assuming of serpentine shape (Fig. 3, c).

The microstructure of the sample after deformation at 600 ºC is characterized by the presence of equiaxial copper grains formed as the result of dynamic recrystallization (Fig. 3, d).

The recrystallized grains have a polygonal shape. Intragranular twins, appeared during dynamic recrystallization, have formed by separation of growing twins from double angle boundaries [21] as the result of recrystallized grain growth. It should be noted that equiaxial structure is formed by the volume of sample. It allows to suggest a uniform and complete flow of dynamic recrystallization at 600 ºC.

Increase of titanium content up to 2 % in the powder material of 5 % porosity at low temperature deformation leads to growing of the stress and ultimate degree of deformation that is corresponding to changing the activation energy and, consequently, the deformation mechanism. These processes provide grain refinement during compression to various degrees of deformation (Fig. 4). Different barriers like grain boundaries and pores, twin boundaries and titanium particles are places of defects concentration in copper-titanium powder materials, where the most fine- grained structure has been observed (Fig. 4, b). Grain refinement on boundaries of copper and titanium particles during plastic deformation is a consequence of differences in the plastic and elastic properties of copper and titanium.

Formation of finer grain size less than 2 μm has been observed near titanium particles (Fig. 5, a) as a result of compression of samples containing 2 % of titanium at 400 °C until the degree of deformation 0.081. High values of stresses and deformations in these places promotes to beginning of dynamic recrystallization leading to formation of new grains. However, intermediate phases, precipitated as a result of the strain aging [19], are inhibiting growth of dynamically recrystallized grains [22]. Consequently, anisomerous structure near titanium particles preserved up to degree of deformation 0.262 (Fig. 5, b). Further compaction to the degree of deformation 0.673 forms a homogeneous fine-grained structure

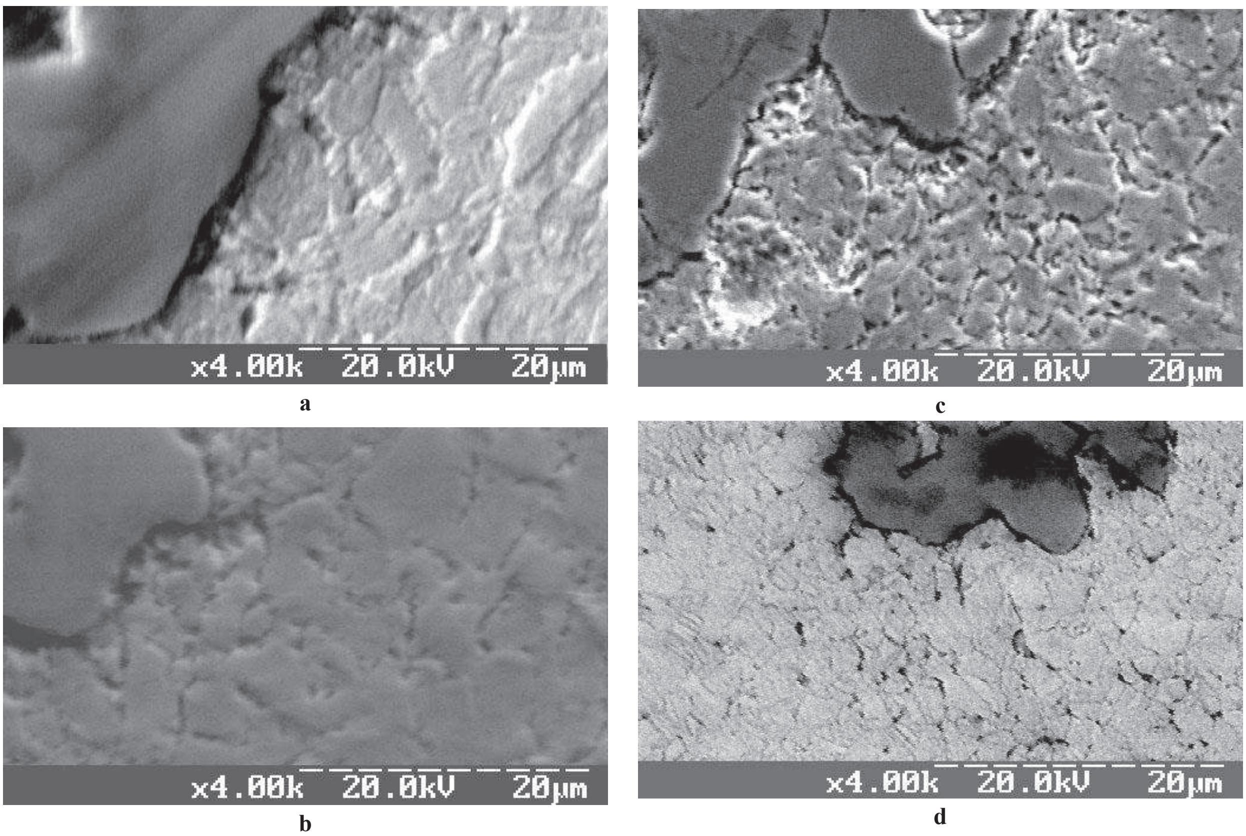

Fig. 3. Microstructures of samples with 0.5% Ti and 10 % porosity; a – after sintering; after deforming to degree of deformation 0.69 at strain rate 0.001 s^{-1}: b – t = 100 ºC; c – t = 400 ºC; d – t = 600 ºC.

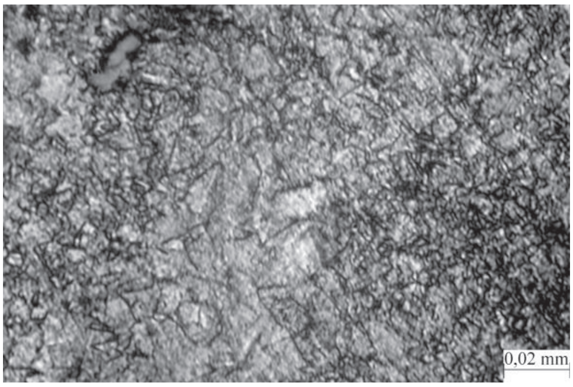

a

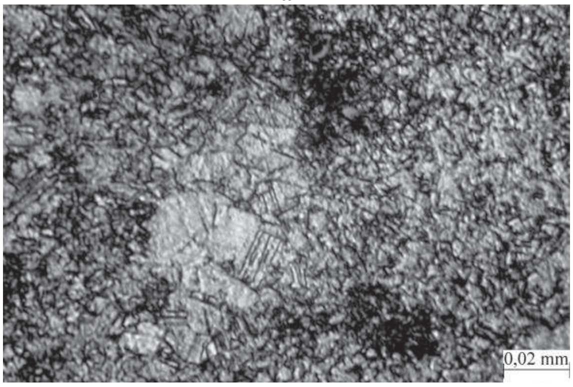

b

Fig. 4. Microstructure of samples: 2% Ti; 5% porosity; compression at 100 °C and strain rate of 0.001 s^{-1}: a - 0.079 the degree of deformation; b - the degree of deformation of 0.26

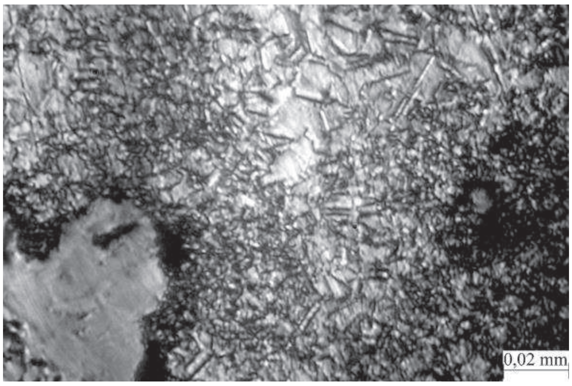

a

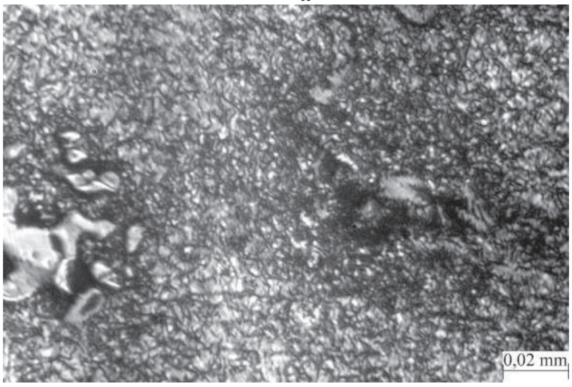

b

Fig. 5. Microstructure of samples: 2% Ti; 5% porosity; compression at 400 °C at a strain rate of 0.001 s^{-1}: a - 0.081 the degree of deformation; b - the degree of deformation of 0.262.

with the copper grain size 7.28 μm by improving of completeness of the dynamic recrystallization.

Deformation at 600 ºC follows by intensive decrease of copper grain size while increasing degree of deformation, which is typical for copper-titanium powder material with 0.5 % and 2 % of titanium (Fig. 6). Metallographic studies have shown that anisomerous structure observed at low deformation degrees of 0.040 – 0.046 and caused by inhomogeneous development of dynamic recrystallization. Formation of a homogeneous fine-grained structure due to increasing of dynamic recrystallization rate have occurred, while increasing of deformation degree to 0.118.

The microstructures of samples with 2 % and 0.5 % Ti after compression is characterized by copper grains with serrated boundaries (Fig. 6). The structure of samples with 0.5% Ti is less stable, grain boundaries are extremely tortuous and include a large number of "tips." The reason of serration is local heterogeneity of deformation in the border volumes and the consequent difference in the density of defects into local volumes on both sides of the original boundary that is stimulating migration of small areas to the volume with higher density of defects. Toothed shape of boundaries indicates the dynamic recrystallization [23]. Reduction of curvature of grain boundaries in

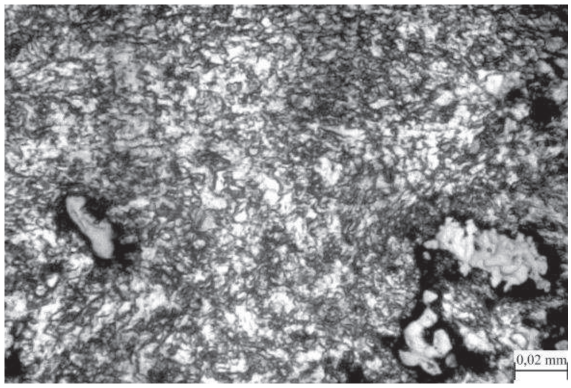

a

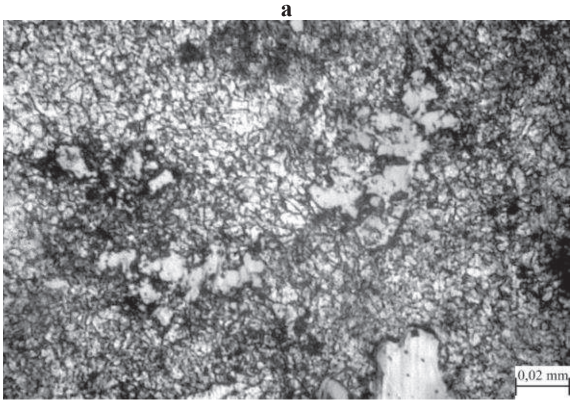

b

Fig. 6. The microstructure of samples of 10% porosity after compression strain rate of 0.001 s^{-1} at a temperature and deformation degree 600 ºC 0.916: and - 0.5% Ti, b - 2% Ti.

samples with 2 % Ti is associated with inhibition of grain boundaries' migration by pores, titanium particles and disperse precipitations (Fig. 6).

Increasing of the deformation temperature causes softening of hard phase and, as shown by metallographic analysis, softening of copper begins at 100 °C for the account of recovery and above 300 ºC – by the dynamic recrystallization.

Commercially pure titanium (BT1–0) recrystallizes at temperatures 750 – 800 ºC [24]. Therefore, we can assume that in the investigated temperature range (100 – 600 ºC) softening takes place for the account of the dynamic recovery.

Obviously, the dynamic recovery does not allow to complete internal release of stresses removal and titanium particles are crushed because of high intensity of plastic deformation.

CONCLUSIONS

1. Theoretical analysis of the kinetics of softening processes has been conducted for deformation at high temperatures and based on the dislocation concepts of plastic deformation and plasticity theory of porous powder bodies. Constitutive equations that are relating the main parameters of the deformation - flow stress, accumulated deformation of hard phase, strain rate, temperature and structural characteristics of the material - ability to accumulate dislocations, Boltzmann function, activation energy, density of dislocations, which may be used for evaluation the mechanism of dynamic softening during deformation of porous powder materials at the elevated temperatures.
2. The linear character of the dependencies $ln\,\sigma_z - 1/T$ and $ln\,\omega_K - 1/T$, which allows to determine the mechanism of dynamic softening of porous bodies has found. It has established by estimating of activation energy that at low temperatures the deformation mechanism is dynamic softening and recovery polygonization, at high temperatures - dynamic recrystallization. The presence of porosity phase reduces the activation energy of softening and makes its development less intensive.
3. The mechanism of dynamic softening was confirmed by metallographic examination of structure evolution in compression samples from copper-titanium powder materials of different titanium content.

REFERENCES

1. **Pirowski Z., Gościański M., 2013.:** Casting alloys for agricultural tools operating under the harsh conditions of abrasive wear, TEKA. Commission of Motorization and Energetics in Agriculture, Vol. 13, No. 1, pp. 119–126.
2. **Gromenko, V., Krivonosov, S. and Snizhko A., 2012.:** X-RAY Structural Research of Products of Cavitational Erosion of Metals, TEKA. Commission of Motorization and Energetics in Agriculture, – 2012, Vol. 12, No.3, pp. 41-45.
3. **Abbod M.F., Sellars C.M., Cizek P., Linkens D.A. and Mahfouf M., 2003.:** Modelling the Flow Behaviour, Recrystallization and Crystallographic Texture in Hot Deformed Fe-30 wt.% Ni Austenite, Acta Mater, No. 51, pp. 5051-5062.
4. **Luton M.J., Sellars C.M., 1969.:** Dynamic Recrystallization in Nickel and Nickel-Iron Alloys During High Temperature Deformation, Acta Matallurgica, Vol. 17, pp. 1033-1043.
5. **Elwazri A.M., Essadiqi E., Yue S.,** 2004.: Kinetics of Metadynamic Recrystallization in Microalloyed Hypereutectoid Steels, ISIJ International, Vol. 44, No 4, pp. 744-752.
6. **Poliak E.I., Jones J.J., 2003.** Initiation of Dynamic Recrystallization in Constant Strain Rate Hot Deformation, ISIJ International, Vol. 43, No. 5, pp. 684-691.
7. **Ryabicheva L.A., 1998.:** The Phenomenological Approach to Estimation of Structure by Macroscopic Parameters of the, Izvestija vuzov, Ferrous Metallurgy, No. 7, pp. 26-30. (in Russian)
8. **Meyers M.A., Lasalvia J.C., Nestorenko V.F., Chen Y.J. and Kad B.K., 1996.:** Dynamic Recrystallization in High Stain Rate Deformation Processing of ReX`96, the Third International Conference on Recrystallization and Related Phenomena, pp. 279–286.
9. **Ryabicheva L.A., 1996.:** The Bitmap control of structure formation processes at hot stamping, East-Ukrainian State University, Luhansk. (in Russian)
10. **Bardi F., Cabibbo M., Evangelista E., Sipgarelli S. and Vukcevic M., 2003.:** An analysis of hot deformation of an Al-Cu-Mg alloy produced by powder metallurgy, Materials Science and Engineering A, Vol. 339, No 1-2, pp. 43-52.
11. **Zouhar G., 1974.:** Beurteilung der Erholungs- und Rekristallisationsneigung der Stähle bei der Warmformgebung mit Hilfe des Warmtorsionsversuchs, Neue Hütte, No 7, pp. 418-423. (in German)
12. **Leshhinskij V.M., Ryabicheva L.A., 1997.:** Simulation of the dynamic recrystallization process, Metallovedenie i termoobrabotka, No. 1, pp. 9-11. (in Russian)
13. **Shtern M.B., 1989.:** A model of the processes of deformation of compressible materials with an allowance made for pore formation II. Uniaxial ten-

sion and compression of porous bodies, Powder Metallurgy and Metal Ceramics, Vol. 28, Issue 6, pp. 446-451.
14. **Frost H.J., Ashby M.F., 1982.:** Deformation-Mechanism Maps, Pergamon Press.
15. **Gaponova O., Ryabicheva L., 2008.** Deforming of the Copper-Titanium Powder Materials at Elevated Temperatures, International Conference Deformation and fracture in structural PM materials" DF PM 2008 Proceedings, Stará Lesná, High Tatras, Slovak Republic, pp. 202-206.
16. **Haessner F., 1978.:** Recrystallization of metallic materials, Shtuttgart, Dr Riederer Verlag GmbH.
17. **Kolerov O.K., 1973.:** Characteristics of primary recrystallization and its role in the sintering of metal powders, Powder Metallurgy and Metal Ceramics, Vol. 12, Issue 3, pp. 192-195.
18. **Lawson C.L., Hanson R.J., 1974:** Solving Least Squares Problems, Prentice–Hall.
19. **Soffa W.A., Laughlin D.E., 2004.:** High-strength age hardening copper–titanium alloys: redivivus, Progress in Materials Science, No. 49, pp. 347–366.
20. **McLean D., 1957.:** Grain Boundaries in Metals, Oxford University Press, London.
21. **Beljaev S.P., Lihachev V.A., Myshljaev M.M. and Sen'kov O.N., 1981.:** Dynamic recrystallization of aluminium, Physics of Metals and Metallography, Vol.52, No3, pp. 617-626. (in Russian)
22. **Gorelik S.S., 1978.:** Recrystallization of metals and alloys, Moscow, Metallurgy. (in Russian)
23. **McDonald D.T., Humphreys F.J., Bate P.S., 2007.:** Microstructure and texture of dynamically recrystallized copper and copper – tin alloys, Materials Science Forum, Vol. 550, pp. 393-398.
24. **Kapyrin G.I., 1977.:** Titanium alloys in machine building, Leningrad, Mashinostroenie. (in Russian)

ВЗАИМОСВЯЗЬ ПАРАМЕТРОВ ПЛАСТИЧЕСКОГО ДЕФОРМИРОВАНИЯ И СТРУКТУРООБРАЗОВАНИЯ В ПОРОШКОВЫХ МАТЕРИАЛАХ

Резюме. Проведен теоретический анализ кинетики разупрочняющих процессов, проходящих в порошковом пористом теле при деформировании в области повышенных температур. Получены определяющие уравнения, связывающие параметры деформации и параметры структурообразования, которые характеризуют процессы динамического разупрочнения при деформировании. Показана линейная зависимость логарифма осевого напряжения и накопленной деформации твердой фазы в функции обратной температуры. Выполнена оценка энергии активации динамического разупрочнения при одноосном сжатии. Показано, что при низких температурах деформации механизмом разупрочнения является динамический возврат и полигонизация, при повышенных температурах – динамическая рекристаллизация. Пористость снижает энергию активации динамического разупрочнения. Металлографический анализ подтверждает механизм динамического разупрочнения порошкового материала.

Ключевые слова: математическая модель, возврат, полигонизация, рекристаллизация, энергия активации.

Calculation of Deflection of One-Layer and Two-Layer Slabs Supported on Four Sides

Dmytro Smorkalov

Kyiv National University of Construction and Architecture
Povitroflotskyy Prosp., 31, Kyiv, Ukraine, 03680, e-mail: smorkalov@i.ua

Received December 04.2014; accepted December 17.2014

Summary. The article presents the method and results of experimental research of deflection of one-layer and two-layer slabs influenced by short-term lateral load. The proposed method of calculation is based on the limit equilibrium method, the calculation of slab deflections values by LIRA-CAD bundled software. The comparison is carried out of experimental and theoretical results of slabs deflection calculation.
Key words: slab, deflection, steel fiber concrete.

INTRODUCTION

Layered constructions have been increasingly applied in building recently. When appropriate composition of separate layers is selected, multi-layer constructions with perfect construction properties may be created [9]. Layers are mostly composed of heavy concrete and effective steel fiber concrete. Such constructive decisions have a widespread use in road and airfield pavements, logistics areas, heavy-weight industrial floors, etc. [13, 15, 16]. Among the most promising trends of reasonable usage of steel fiber concrete is its application in composite structures, as a rule, in combination with concrete or ferroconcrete, with distinct partition of functions of every material. In particular, the steel fiber concrete that is rather thriftily applied along the construction outline, in a thin layer, provides high crack resistance of constructions, as well as its high durability due to high indices of tensile strength, frost resistance, corrosion resistance and high rates of other types of resistance of the steel fiber concrete [14]. At the same time, this solution provides necessary preconditions for significant reduction of strength and value of the primary concrete and reduction of the number of reinforcement rod. Thus, there are preconditions for obtaining high indices created while their cost drops.

PURPOSE OF WORK

The main purpose of proposed work is the comparison of proposed method of deflection calculation for layered slabs under lateral load with the results of experimental research.

EXPERIMENTAL RESEARCH

According to the set purpose of research, slabs of 4 series were produced, two slabs for each series. The scope and outline of experimental studies is set in Table 1 [5].

The total size of single-layer slabs amounts to 800×800×60 mm; the thickness of each layer of reinforced concrete (concrete and steel fiber concrete) in two-layer slabs is 30 mm.

Series I (ПФ) represents a slab made of steel fiber concrete.

Series II (ПЗ) represents a single-layer reinforced concrete slab with single-layer reinforcement Ø4 Bp-I laid at the bottom of the slab with protective concrete layer 10 mm thick with 75 mm pitch

Series III (ПБФ) represents a two-layer concrete slab, the top layer of which is made of unreinforced heavy concrete and the below one – of the steel fiber concrete.

Series IV (ПЗФ) of the studied samples represents slabs consisting of an upper layer of steel fiber concrete and a heavy concrete layer reinforced with metal reinforcement mesh Ø4 Bp-I set with 75 mm pitch.

Slab concreting was carried out in two stages. Slabs of ПЗ grade and concrete layers of ПЗФ and ПБФ slabs were concreted at the first stage. Siliceous sand and giant gravel of 5…10 mm fraction; Portland cement of M400 grade was used as binding material; water-to-cement ratio amounted to W/C = 0,4. Plates of П3 and П3Ф grade were reinforced with binding wire mesh of Bp-I grade, 4 mm in diameter and 75 mm pitch in two directions. Concrete protective layer was 10 mm. The surface is bush-hammered while the concrete is immature.

At the second stage, after 4 days, slabs of ПФ grade were concreted and steel fiber concrete layer slabs of П3Ф grade were additionally concreted.

Steel fiber concrete contained steel fiber with diameter $d_f = 1.0$ mm and length $l_f = 36$ mm; volume percent of reinforcement was $\mu_f = 1\%$. Fine concrete without coarse aggregate was used as a concrete matrix; water-to-cement ratio equaled to W/C = 0,4.

Table 1. Scope of experimental studies

Series	Slab grade	Section	Composition
I	ПФ-1	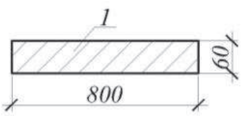	1–steel fiber concrete
	ПФ-2		
II	П3-1	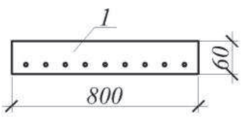	1–reinforced concrete
	П3-2		
III	ПБФ-1	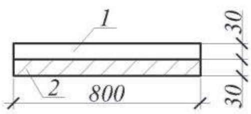	1–concrete; 2–steel fiber concrete
	ПБФ-2		
IV	П3Ф-1	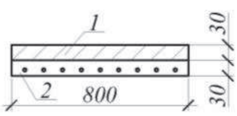	1–steel fiber concrete; 2–reinforced concrete
	П3Ф-2		

General appearance of testing bench is showed in Fig. 1.

The same calculation model was applied for both the one- and two-layer slabs exposed by lateral load: a slab is hinge-supported on four sides and influenced by evenly distributed load (Fig. 2)

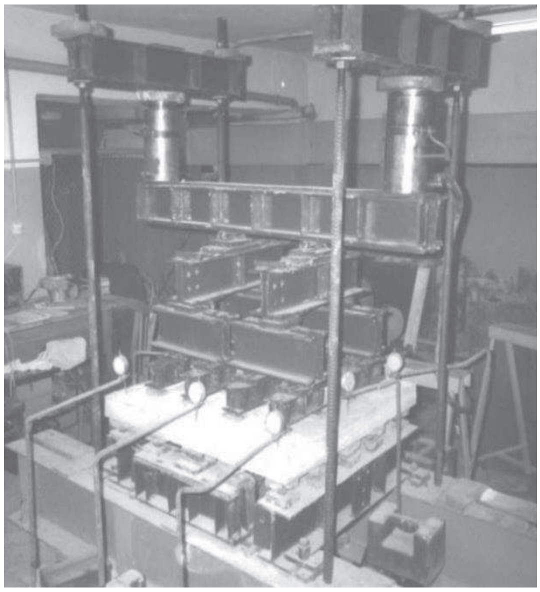

Fig. 1. General appearance of testing bench

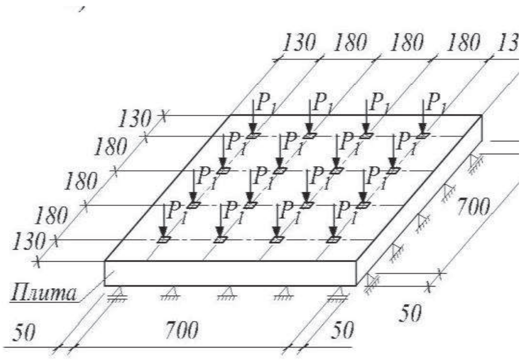

a

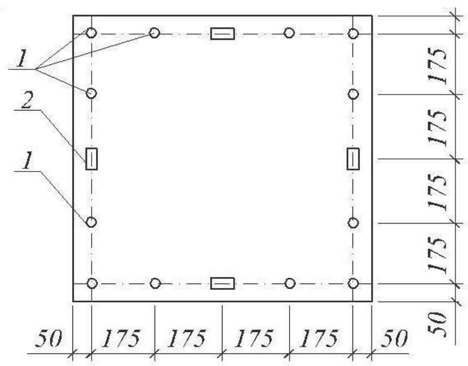

b

Fig. 2. Distribution of load (*a*), and support (*b*) upon slab: *1* – hinged support, *2* – cylinder support

It is suggested that 16 concentrated forces evenly allocated on the slabs surface show no significant difference during the operation, as compared to evenly distributed load, that is why in further theoretical study of strength, crack resistance, and deformation of studied slabs a design model was adopted for slabs supported by hinged bearings on four sides and influenced by evenly distributed load. The load was applied by degrees P_i=2,0 kN with 15-minute timing at each stage to take readings from devices. The value of load was fixed by indices of model forcemeter of hydraulic pumping station. Before testing the hydraulic system consisting of a pumping station, jacks, and model forcemeter was calibrated using model forcemeter of Tokarev system.

During the application of load in the center of the slab deflections and deformations over supports were recorded using time indicators with 0.01 mm scale graduation value.

The load was applied by two hydraulic jacks of 250 kN united by common oil circuit connected to a common pump station.

Before testing the slabs, physical and mechanical properties of used materials were determined: those of heavy concrete, steel fiber concrete and reinforcement (Table 2).

Table 2. Physical and mechanical properties of concretes and reinforcement

Type of concrete or fitting	Strength, MPa		Tensile strength, MPa	Starting elasticity factor, MPa
	cube	prism		
concrete	16,3	11,9	1,5	22500
Steel fiber concrete	19,8	14,5	1,63	24600
Reinforcement Bp-1	–	–	393	192000

According to results of experimental studies with regard to nature of destruction [10], all slabs collapsed according to normal sections.

CALCULATION OF DEFLECTION

The proposed method based on the limit equilibrium method, which may be represented – during the state of limit equilibrium – by the system of disks united along the lines of fracture with plastic hinges.

As proposed by A. A. Gvozdev [4], it is possible to make use of characteristic points 1 and 2 on the diagram (Fig. 3).

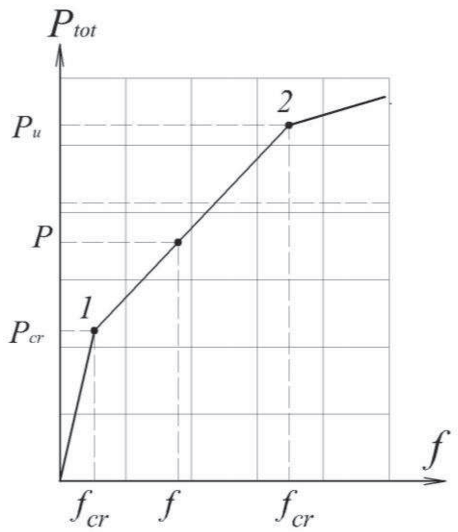

Fig. 3. Design diagram of slab deflection:
1 – cracking, *2* – appearance of the plastic hinge

Deflection values in the areas between f_{cr} and fu are determined by interpolation.

The general view of the formula f of slab deflection of slab supported on four sides and bearing a cracks, may be obtained from the following ratio:

$$\frac{q_u - q_{cr}}{q - q_{cr}} = \frac{f_u - f_{cr}}{f - f_{cr}}, \tag{1}$$

where:
q_u and q_{cr} – load at destruction and crack formation;
f_u and f_{cr} – slab deflection at the moment of destruction and crack formation correspondingly.

It should look as follows:

$$f = f_{cr} + \frac{q - q_{cr}}{q_u - q_{cr}}(f_u - f_{cr}). \tag{2}$$

The value f_{cr} is determined based on elastic system calculation according to load q_{cr}, which in turn may be obtained by bending factor, when first crack appeared in a slab area with the highest tension.

The deflections f at the moment of formation of plastic hinges may be determined as follows.

Until the conditional yield point of reinforcement achieved along all the lines of fracture, cracks are formed and significantly increased on a slab. At the same time, areas with cracks will be especially distorted that will mostly determine the maximum value of slab deflection.

If insignificant curvature of slab areas neglected bearing no cracks, but rigidity is high, the slab calculation model may be represented as stiff disks connected by yielding bracing with width Δ. Bending rigidity of all joints is calculated according to V.M. Murashov theory [7], though the coefficient ψ is taken as a one, as the reinforcements reaches instability the influence of stretched concrete between cracks disappears or becomes insignificant. This assumption substantially simplifies the calculation.

For further simplification the angle fracture between discs equal to $\frac{\Delta}{r}$ is assumed as if concentrated along the lines of fracture. The calculated deflection surface prior to exhaustion of the bearing capacity turns out to be similar to the surface used in calculating by limit equilibrium method for the calculation of works on possible movements. Though such likening is not accurate, it allows determining the maximum deflection at a rather decent level.

There is a calculation model of square slab presented on Fig. 3 and a diagram of angle rotation at slab center deflection that is equal to f_u. Owing to symmetry, the fracture diagram of value Δ for all plastic hinges is the same.

Rigid discs of the slab will turn in relation to supports by angle:

$$\frac{\varphi}{2} = \frac{2f_u}{l}. \tag{3}$$

Mutual angle adjacent discs

$$\varphi = \frac{2\sqrt{2}f_u}{l} = \Delta\frac{1}{r}, \tag{4}$$

whereof:

$$f_u = \frac{l\Delta f_{ym}}{2\sqrt{2}E_s(d-x)}. \tag{5}$$

where:

$\frac{1}{r}$ – curvature-multiplication of which by Δ equals to reciprocal angle of rotation of adjacent discs

$$\frac{1}{r} = \frac{f_{ym}}{E_s(d-x)}, \tag{6}$$

$\frac{1}{2\sqrt{2}}$ – factor derived from geometrical considerations, which is transition to the angle of rotation of the disk relative to the support,

For fiber reinforced structures (such as fiber concrete) the value f_y and E_s at the point of critical steel stress is replaced by the value f_{ctf} and elastic modulus E_f suitable to the material. For two-layer slabs the given geometric, strength, deformation properties of two materials are used.

By the combination of Eq. (2)-(6) we can define a final ratio for the calculation of current deflection of the slab supported by four sides influenced by evenly distributed load:

$$f = f_{cr} + \frac{q - q_{cr}}{q_u - q_{cr}}\left(\frac{1}{r}\Delta - f_{cr}\right), \tag{7}$$

where:

f_{cr} – slab deflection at the moment of of formation of the first cracks in stretched area of the element;

q_{cr} – load, when first cracks were created;

q_u – load corresponding to the limit of the slab bearing capacity;

Thus, the calculated width of deformed area Δ remains unknown in the Eq. (7); as a result it is not possible to calculate the value f.

In order to solve such problem the following method of finding the desired value of deflection f may be proposed. First of all, a boundary value of the slab deflection is set according to the standards for that class of structures $f_u=[f]$ apply it in the Eq. (7) $f=f_u=[f]$. The Eq. (7) is settled with respect to value Δ and then obtained result is applied to the Eq. (5), therefore obtaining the deflection at the time of formation of plastic hinges with regard to real-specified parameters. At the same time, the result of Eq. (7) shows the value of current deflection by introducing the calculated value of width of deformed area Δ.

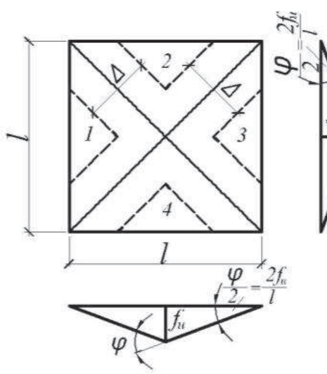

a

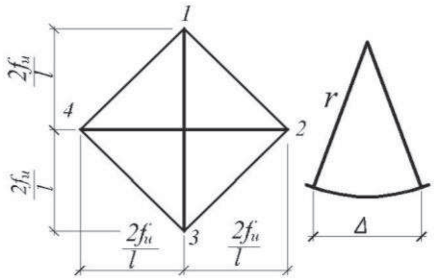

b

Fig. 4. Calculation diagram of square slab influenced by evenly distributed load:
a – fracture diagram; *b* – diagram of disc rotation angle rate

The value of fcr and qcr can be calculated if the combine Eq. (7) with the formula B.H.Galerkina [2] for square plates, supported on four sides, the deflection at the center of slabs:

$$f = 0{,}04706\frac{ql^4}{E_i h^3}\ . \qquad (8)$$

To determine the width of the deformed zone Δ slabs a series of isolated points on several research graphs deflections. Points are usually prescribed in the operational (working) load range: often – is 0,7...0,8 from destructive load. To find the value Δ using Eq. (6) and (7), taking into account the specific slabs construction.

Results of calculation of one- and two-layer slabs by the limit equilibrium method are shown in Fig. 7, 8.

Considering complexity of mathematical calculations for slab deflection due to analytical methods [6] and unsatisfactory precision of results, a decision was made to do calculations on computing machine with a help of LIRA-CAD bundled software [3, 8].

The basis of LIRA-CAD is represented by the calculation of components and structures by finite element method [3].

The calculation model of a slab (Fig. 5) is built out of tridimensional finite elements (type CE-36). The slab is separated into 1444 finite elements according to plan. The sectional area of the slab is composed of 12 layers 5 mm each. The load is applied in the form of 16 concentrated forces. The distribution of load and supports is accepted as in Fig. 2.

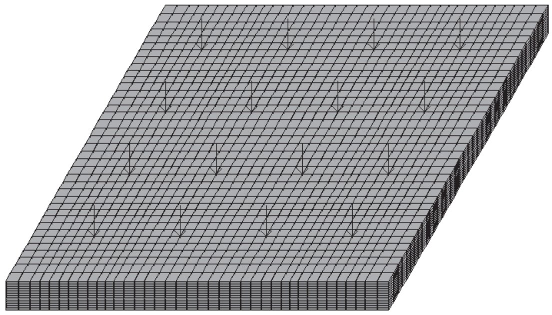

a

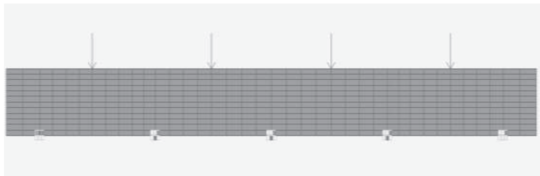

b

Fig. 5. Calculation model of slab in LIRA-CAD:
a – general view; *b* – side view

The CE-36 finite element is a universal tridimensional eight-node isoparametric finite element, designed for the calculation of tridimensional constructions. There is a diagram represented in Fig. 4. Each of finite element nodes has three degrees of variance *U, V, W* defined with regard to global coordinates *X, Y, Z* and are linear displacements according to axis, whose positive direction coincides with the direction of coordinate axis. As a result of modeling, there are 19,773 nodes and 17,328 elements

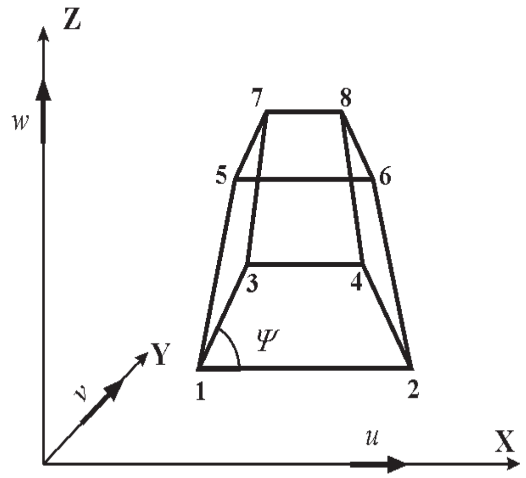

Fig. 6. Diagram of CE-36 finite element

The assumed calculation model makes it possible to change the rigidity of materials for both one-layer and two-layer slabs.

The slab calculation was performed in linear position for loads corresponding to loading pitches at testing. Non-linear physical-mechanical properties were taken into consideration by means of changing the elasticity modulus.

Initial values of elasticity modulus for concrete and steel fiber concrete were assumed according to [1], that is $E_c = 22{,}5 \cdot 10^3$ MPa, $E_{cf} = 23{,}8 \cdot 10^3$ MPa.

In accordance with recommendations [11] the nonlinear behavior of construction is recommended to consider by means of introducing decreasing coefficients: 0,2 – in case of any cracks, or 0,3 – in case no cracks revealed.

That is why during the calculations the decreasing coefficient was 0,3 before appearance of any cracks and 0,2 – after the first cracks appeared. Reduction of slab rigidity as a result of crack was also considered by means of introducing zero rigidity elements in the tensile area within height of the crack. The rigidity of slab supports was not reduced to avoid forcing through the slab thickness

As a result of calculation of one-layer slabs in LIRA bundled software, diagrams of deflection of the slab center f of the total pressure $P_{tot}=16P_i$ were obtained, which are presented in Fig. 7.

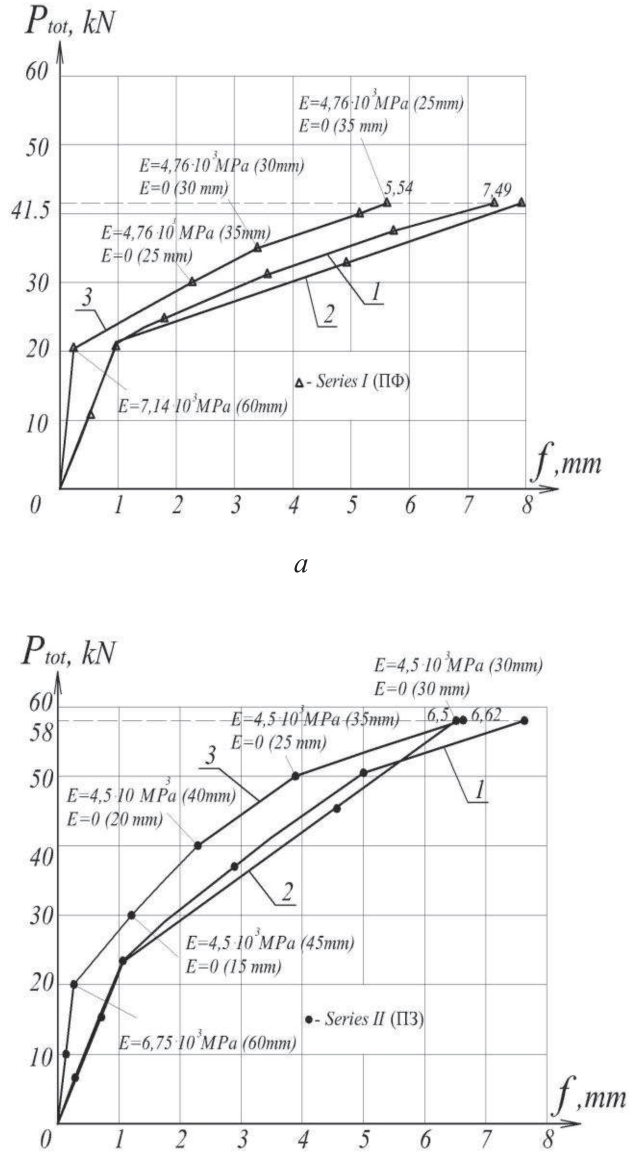

Fig. 7. Calculation results for deflection of one-layer slabs of series I grade ПФ (*a*) and slabs of series II grade ПЗ (*b*): *1* – experimental*; 2* – calculation by the limit equilibrium method; *3* – calculated in LIRA bundled software

When calculating the two-layer slabs, relevant elasticity modulus of material was applied for each slab layer. The value of decreasing coefficients and zero elasticity elements were applied similar to the calculation of one-layer slabs.

As a result of calculation of two-layer slabs by means of LIRA bundled software, diagrams of deflection of the slab center f of the total pressure $P_{tot}=16P_i$ were obtained, which are presented in Fig. 8.

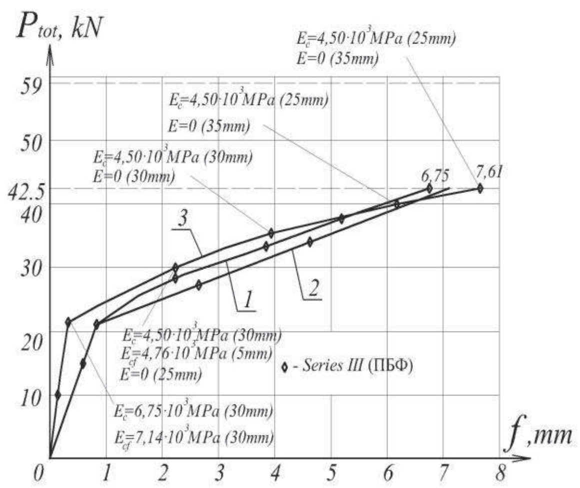

a

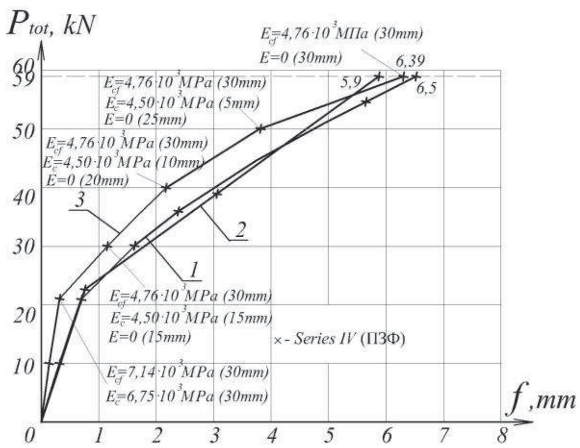

b

Fig. 8. Calculation results for deflection of two-layer slabs of series III grade ПБФ (*a*) and slabs of series IV grade ПЗФ (*b*): *1* – experimental; *2* – calculation by the limit equilibrium method; *3* – calculated in LIRA bundled software

CONCLUSIONS

1. Given that today's construction industry is represented by the vigorous process of increasing the strength of construction materials, particularly concrete and reinforcement, due to achievements in chemistry, there is a strengthening of quality indicators of buildings and constructions, in particular bearing construction arrangements. Thus, systems making it possible to work in a multi-axial load state (shell structures, slabs, wall-beams, etc.) are getting more popular. There is an opportunity to significantly reduce the cost by reduction of cross-section operational overcuts at the expense of increased strength of materials. The new technologies make it possible to perform the most complex design elements made of any materials. Considering the current trends, it should be noted that the issue of performance reliability for buildings and structures is not about the strength requirements, but the rigidity of elements and buildings in general. Therefore, the study of rigidity (most commonly the deflections) of examined slabs seems to be a topical issue.

2. Another question this work bears an answer to is the feasibility of using multi-layer slabs. From the point of view of rigidity (bending) of slabs, the two-layer slabs have an advantage: they show 10% less deflections, than the one-layer ones. Considering the higher level of crack resistance of tow-layer slabs, the use of two-layer slabs is absolutely justified.

3. Calculation by a computer using LIRA bundled software provides wide opportunities to determine rigidity (deflection) for both single-layer and multi-layer slabs owing to computing technologies. However, the obtained calculation results indicate a deficiency in accuracy, compared to the experimental data. The fact is that compliance with regulatory guidelines, implemented to consider nonlinear structure operation by introduction of decreasing coefficients, sometimes does not match the actual conditions of slab deformation. Furthermore, there are some doubts as to the correctness of defining the depth crack distribution along the slab height, which determines its actual rigidity.

4. The comparative analysis of experimental and theoretical diagrams of slab deflection evidences good matching of results. Deviations at maximum loads were as follows: for one-layer slabs of series I (ПФ) – 26%, for slabs of series II (ПЗ) – 13%; for two-layer slabs of series III (ПБФ) – 11%, for slabs of series IV (ПЗФ) – 2%. Such deviation in calculations may be explained by complexity of defining the real rigidity of slabs, i.e. the definition of deformation modulus and the height of crack creation to set the zero rigidity elements.

REFERENCES

1. **Barashykov A.Ya., Smorkalov D.V., 2014.** Calculation of solidity of one-layer and two-layer reinforced concrete slabs supported on four sides. Resource efficient materials, structures,

buildings, and constructions: Collected studies. Rivne, 2014, Issue 28, 127-134 (in Ukraine).

2. **Galerkin B.G., 1933.** The resilient thin plate. M, Gosstroiizdat, 1933, 458 (in Russian).
3. **Gorodetsky A.S., Schmukler V.S., Bondarev A.V., 2003**. Information Technology of calculation and design of building konstruktsiy: Proc. Manual. Kharkiv, NTU "KPI", 2003, 889 (in Russian).
4. **Gvozdev A.A., 1949**. Calculation of bearing capacity by limit equilibrium method. Moscow, Stroyizdat, 1949, 280 (in Russian).
5. **Zhuravskyi O.D., Smorkalov D.V., 2002.** Methodology and results of experimental studies of two-layer slabs. Steel reinforcement concrete constructions. Research, design, construction, operation: Collected research papers, Issue 5, Kryvyi Rig, KTU, 2002 (in Ukraine).
6. **Korolyov A.N.** Calculation methods for slab deflections supported on four sides at short-term load. Concrete and reinforced concrete Vol. 3, 1960, 9-11 (in Russian).
7. **Murashev V.I., 1950**. Crack resistance, stiffness and strength of concrete. M, Mashstroyizdat, 1950, 230 (in Russian).
8. **LIRA-CAD 2011.** Tutorial: Electronic Edition , 2011, 396 (in Russian).
9. **Rudenko N., 2010.** The development of conception of new generation concretes. TEKA: Kom. Mot. Energ. Roln, 2014, Vol. XB, 128-133.
10. **Smorkalov D.V., 2003**. Crack resistance and fracture modes for two-layer slabs. Resource efficient materials, structures, buildings, and constructions: Collected research papers. Rivne, 2003, Issue 9, 323-330 (in Ukraine).
11. **Snyder M. 1972.** Factors affecting the flexural strength of steel fibrous concrete. ACI Journal, 1972, Vol. 69, No. 2, 96-100.
12. **SP 52-103-2007, 2007.** Code of practice on design and construction. Reinforced concrete cast-in-place constructions of buildings. Moscow, 2007 (in Russian).
13. **Stages A., 1981**. Ring fiber reinforced concrete. ACI Journal. 1981, Vol. 78, No. 5, 369-373.
14. **ACI Journal. 1973**. State-of-the-art report on fiber reinforced concrete, 1973, Vol. 70, 729-744.
15. **Tarasov V.P., 1974.** The use of fiber-reinforced concrete in construction. Industrial construction. 1974, Vol. 7, 44-45 (in Russian).
16. **Tattersall G.H., 1974.** Bond strength in steel-fibre-reinforced concrete. Journal of Concrete Research. 1974, Vol. 26, No. 87, 105-113.

РАСЧЕТ ПРОГИБОВ ОДНО- И ДВУХСЛОЙНЫХ ПЛИТ, ОПЕРТЫХ ПО КОНТУРУ

Аннотация. Приведены методика и результаты экспериментальных исследований прогибов однослойных и двухслойных плит под действием поперечного кратковременного нагрузки. Рассчитаны прогибы плит способом, основанном на методе предельного равновесия, и методом конечных элементов, с помощью програмного комплекса ЛИРА. Выполнены сравнения экспериментальных и теоретических результатов расчета прогибов плит.

Ключевые слова: плита, прогиб, сталефибробетон

Working of Deep-Water Minerals with Sectored Way

Mykhailo Sukach

Kyiv National University of Construction and Architecture
Povitroflotskyy prosp., 31, Kyiv, Ukraine, 03680, e-mail: msukach@ua.fm

Received December 09.2014; accepted December 19.2014

Summary. The article presents the problems of obtaining the bottom minerals from the depth of water. The sectored way of working mine is suggested and schemes of movement of the bottom mining are proposed. The calculations are done of movement trajectory of the carriage and length of the hose-cable of the mining machine, taking into account the turn inside and outside the sector.

Key words: deep-water minerals, sectored way, movement trajectory, hose-cable, concretions.

INTRODUCTION

The geological investigations performed in the central areas of oceans during the last decades, allowed to made it possible to investigate the promising for industrial developments areas of poly-metal ore accumulations – concretions – primarily in the region of Clarion-Clipperton on the Pacific ocean [2, 12, 13]. On the regional stage of the geological survey the deposits with overall density of concretions occurrence are identified (up to 10...20 kg/м²), that contain the industrial concentration of manganese, nickel, copper and cobalt [7, 18, 19].

At the same way the technology and technical ways needed for the survey and experimental testing stages of works were developed: collection of concretions and lift to watercraft, pre-processing, storage and handling of the extracted mass to the ore-transporting ship [1, 3, 4, 11, 16].

The conditions of concretions occurrence are complex and unique – it is the depth of 4000...6000 м, low carrying capacity of sediments, big quantity of rocky exits and cavities, variable configuration of sedimentations. The above-specified factors significantly affected the operation of the survey, pilot-testing machines and machinery at the bottom [9, 14, 17]. In such conditions it is reasonable to perform the exploitation works using the fixed or inactive mountain reconnaissance complexes, that include the elevation system that interacts with base bottom module of collection aggregate and fast moving gathering working parts.

The latter are connected to base unit hose cable which provides transportation of the extracted rock mass and energy supply to drive the carriage of the gathering working body [5, 6, 10, 15].

PURPOSE OF THE ARTICLE

The research aimed at the grounding of the possibility of the technological scheme of clearing excavation by sector ways with any predetermined or regulated angle of disclosure of sector. At that, two options of carriage trajectories were offered – with a turn inside the sector or beyond its contours (Fig. 1, 2).

RESEARCH AND CALCULATIONS

The carriage can maneuver at some distance from base module, the maximum radius depends on the length of hose-cable that is reeled from the coil. To determine the amount of time needed for the processing, it is required to identify the area of sector and the length of the way travelled by the carriage, whereas for finding the volume of extraction – the amount of costs on the unprocessed areas of the sector.

During the work of carriage with turn inside the sector contours on each operation cycle of the part of circle with width B inside the sector with angle α is processed. At the end of the strip the carriage is turned 180°, moreover the hose-cable is reeled to the length B that equals the width of carriage and the next operation cycle (see Fig. 1).

The initial data for calculation: α – the angle of turn of sector; B – width of carriage: L_m – length of hose-cable or maximum radius, passed by the carriage; L_0 – radius of the base module of collecting aggregate. Needed parameters:

K – number of operation cycles; R_0 – minimal radius, starting from which the carriage maneuver is possible; S – processed (developed) area; S^* – full area of the sector; E – percentage of the developed area; L – way, passed by the carriage; D – specific area, i.e. the area, reduced to the unit of way, passed by the carriage.

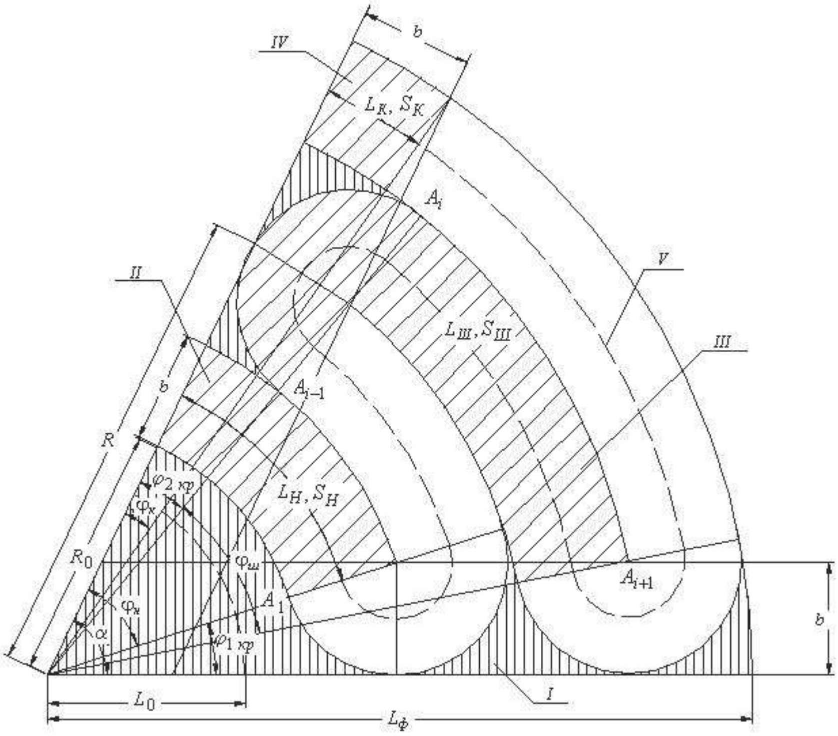

Fig. 1. Calculated scheme of carriage motion trajectory with turns into a sector:
I –not processed areas; *II* - *IV* – processed zones, from them *II* – in the first measure, *III* – on intermediate measures, *IV* – on the last measure; *V* –carriage motion trajectory

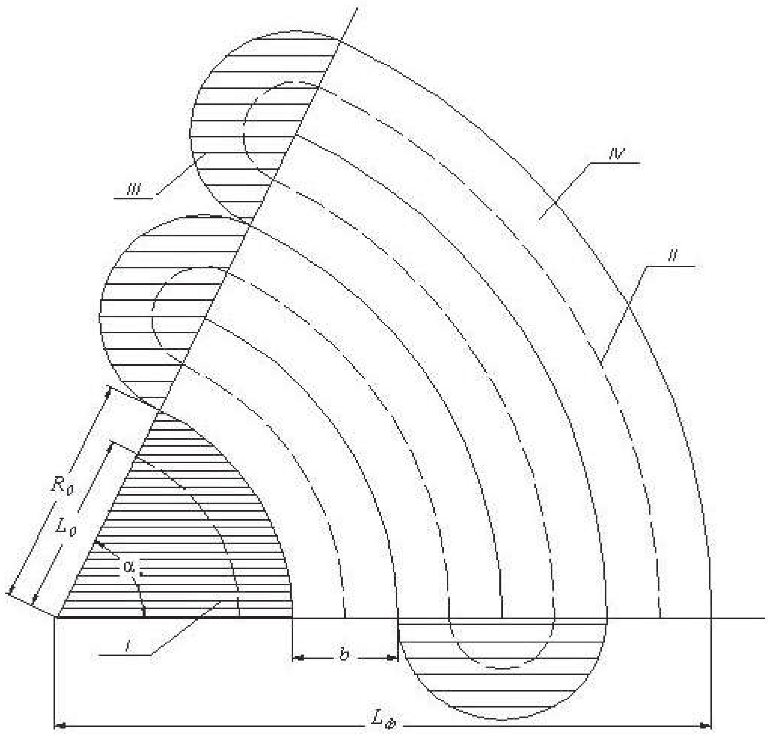

Fig. 2. Calculation scheme of carriage motion trajectory with turns out of sector:
I – not processed space; *II* –carriage motion trajectory; *III* – superfluous areas; *IV* – processed areas

Full area of sector:

$$S^* = \frac{1}{2}(\alpha L_m^2)\,. \tag{1}$$

Number of operation cycles of carriage:

$$K' = (L_m - L_0)/B\,. \tag{2}$$

Minimal radius of carriage turn:

$$R_0' = L_m - KB\,. \tag{3}$$

For the full turn of carriage inside the sector the following conditions are required:

$$\varphi_{1\,cr} + \varphi_{2\,cr} \le \alpha\,, \tag{4}$$

where:

$$\varphi_{1\,cr} = \arcsin B/(R_0 + B)\,, \tag{5}$$

$$\varphi_{2\,cr} = \arcsin B/(R_0 + 2BE)\,. \tag{6}$$

At that $R_0 = R_0' + B$ is used so that to satisfy the condition (4), in this case $K = K' - \xi$, where ξ – safety factor.

Note, that with $K' = 0$ processing is not possible, and with $K' = 1$ only one operation cycle is processed. In the latter case, K is considered equal K', and $R_0 = R_0'$.

In the first operation cycle the carriage is moved from position A_0 to position A_1;
Hose-cable is turned (rotated) at the angle:

$$\varphi_{in} = \alpha - \arcsin B/(R_0 + B)\,. \tag{7}$$

Center of carriage moves the way:

$$L_{in} = (R_0 + B/2)\varphi_{in}\,, \tag{8}$$

processed (developed) area:

$$S_{in} = \frac{1}{2}\left[(R_0 + B)^2 - R_0^2\right]\varphi_{in}\,. \tag{9}$$

At each interim operation cycle the carriage rotates 180° from point A_{i+1} to A, and the length of hose-cable increases by width of the carriage B; then the carriage moves from point A_1 to point A_{i+1}, in the result of which the hose-cable rotates at the angle:

$$\varphi_h = \alpha - \arcsin\frac{B}{R} - \arcsin\frac{B}{B+R}\,, \tag{10}$$

where: R – distance from the carriage to the point of mantling of hose-cable to base module of collecting aggregate.

On each operation cycle the center of carriage passes the way:

$$L_h = \pi B/2 + (R_0 + B/2)\,\varphi_h\,. \tag{11}$$

The processed area makes up:

$$S_h = \frac{1}{2\pi}B^2 + \frac{1}{2}\left[(R + BE^2 - R^2\right]\varphi_h\,. \tag{12}$$

At the last step of the operation cycle after the processing of the land, the area of which is determined by Eq. (10) – (12), the hose-cable rotates at the angle:

$$\varphi_c = \arcsin\frac{B}{L_m}\,. \tag{13}$$

At that the carriage passes the way:

$$L_c = (L_m + B/2)\,\varphi_c\,. \tag{14}$$

And the land is processed:

$$S_c = \frac{1}{2}\left[L_m^2 - (L_m - B)^2\right]\varphi_{\hat{e}}\,. \tag{15}$$

The total way and area (L i S) one calculates as sum of corresponding sizes of areas on the initial, all the intermediate ones and the final operation cycle.

The percentage of the processed area:

$$E = (S/S^*)100\,, \tag{16}$$

specific area:

$$D = S / L . \tag{17}$$

With work of carriage with turn outside the contours of sector with angle α on each operation cycle the carriage processes the part of the circle with width B (see Fig. 2). At that the part of the hose-cable that equals the width of the carriage operation cycle is reeled from the coil placed on the base module of collecting carriage.

When you save the similar to the above considered variant output data, you need to add to the desired (searched) parameters the following: S_1 – area, processed by the carriage outside the contours of the sectors (extra area); E – percentage of extra area; L_1 – extra way and E_1 – percentage of extra way.

In this case the full area of sector, the number of operation cycles and minimal radius are accordingly determined with Eq. (1) – (3).

Useful area, processed with aggregate:

$$S = \frac{1}{2\alpha}(L_m^2 - R_0^2) . \tag{18}$$

Extra space at that is:

$$S_1 = (K - 1)\frac{1}{2\pi}B^2 . \tag{19}$$

Since processing of K operation cycles one needs to perform (K – 1) of turns. The percentage of processed area in the sector is determined with expression (16).

The percentage of extra areas processed by the carriage (%):

$$E_1 = \frac{S_1}{S + S_1}100 . \tag{20}$$

The way passed by the carriage consists of segments of way with useful processing and ways passed for rotation. Useful way is calculated with the formula:

$$\begin{aligned} L &= (R_0 + B/2)\alpha + (R_0 + B/2 + B)\alpha + \\ &\ldots[R_0 + B/2 + (K-1)B]\alpha = \\ &= \frac{1}{2\alpha}K(2R_0 + KB) . \end{aligned} \tag{21}$$

Extra way, or way passed for the turn:

$$L_1 = (K - 1)\pi\frac{B}{2} . \tag{22}$$

Extra way, passed by carriage (%):

$$E_L = \frac{L}{L + L_1}100 , \tag{23}$$

specific area:

$$D = \frac{S}{L + L_1} . \tag{24}$$

Mathematical model is done for collecting aggregate that processes with sector scheme the ore deposits with complex configuration with big quantity of obstacles on the bottom like rocky exits and cavities, etc. By means of computer program the following values are calculated; K, R_0, S, S^*, S_1, E, E_1, L, L_1, E_L, D for angles α = 45°...315°, width of carriage seizing B = 1,5...6,5 м with length of hose-cable L_m = 100...200 м.

Hand productivity of mining company with 1 million of concretions can obtain minerals with minimal losses by using as part of the collection aggregate of lightweight high-speed carriage, that has to be characterized by coordinating connection with the base module.

CONCLUSIONS

1. In the depth of the open ocean there are big areas with concretions lying on the bottom surface with increased (up to 10...20 kg/м²) density. Mining conditions of these deposits are notably hard due to prominence of landforms and the presence of rocky exits.
2. Due to the necessity of choosing equipment and technology of sewage treatment works, the organization of excavation works with the scheme with sedentary collection unit (base module) and fast moving excavation unit (pickup) is suggested.
3. The determination of parameters of minerals extraction is given basing on the extraction of more than 1 mill of concretions per year with their minimal losses by means of usage of coordinating connection between the pickup and base module with sector scheme.
4. The mathematical model is given and key parameters of sector method of concretions pickup are calculated.

REFERENCES

1. **Bakurov G., 1988.** Ships for deep-water mountain geological researches. Moscow, Shipbuilding, № 3, 12-16.
2. **Ferromanganese** concretions of the central part of the Pacific ocean, **1986.** Under editing I.O. Murdmaa, N.C. Skorniakova. Moscow, Nauka, 344.
3. **Fouco I., 1982.** Modern state of technique of booty of deep-water ferrimanganese concretions. ВЦП, № E-41418, Moscow, 28.12.83, ist. Fusen, Vol. 29, 99-167.
4. **Nurok G., Brujakin Yu., Bubis Yu. and other**. Mining technology from the bottom of lakes, seas and oceans. Moscow, Nedra, 381.
5. **Ogorodnikov C.П., 1986.** Hydromechanization of development of soils. Moscow, Stroyizdat, 256.
6. **Paschkin V., Iakovlev P., Cokolov V., 1999**. Dredging, рефулерные and гидро the mechanized works: train aid. Odesa, Astroprint, 432.
7. **Schniukov E., Ziborov A., 2004.** Mineral riches of the Black sea. Kyiv, NANU, 279.
8. **Shkaryvsky G., 2014.** Estimation of influence structurally of layout charts of power facilities on completing of aggregates on their base. Motrol: kom. Mot. Energ. Roln., OL PAN, Vol. 16, No 3, 165-171.
9. **Sukach M., 2004**. Booty and portage of ocean metal of containing crusts. Industrial hydraulic and pneumatic, Vol. 3(9), 8-11.
10. **Sukach M., 2004.** Workflows of deep machines. Kyiv, Naukova dumka, 364.
11. **Sukach M., 2012**. Deep-water technique and technology for development of minerals of the World ocean. Labours VI ISTK "Energia-2012", Simferopol-Alupka, 9.
12. **Sukach M., 2012**. Problems of booty of hard minerals from the bottom of the World ocean. Motrol: kom. Mot. Energ. Roln., OL PAN, Vol. 14 (1), 116-122.
13. **Sukach M., 2013.** Prospects of разработки of marine deposits of mineral raw material. Innovations in science are innovations in education: collection of labours. JuRGPU (NPI), Novocherkassk, 285-291.
14. **Sukach M., 2013.** Research and development deep-water booty technique. Kyiv, GBDMM, Vol. 82, 57-65.
15. **Sukach M., Lysak S., Sosnowski S., 2010**. Kinematic analysis of the work – ing process of trencher. TEKA: kom. Mot. Energ. Roln., OL PAN, Vol. X, 425-431.
16. **Sukach M., Lytvynenko I., Bondar D., 2009**. System of the automated management and measuring of parameters of technological processes. Motrol: kom. Mot. Energ. Roln., OL PAN, Vol. 11B, 186-189.
17. **Technical** instructions on the production of the marine dredging, **1986**. РД 31.74.08-85.- Moscow, W/S Mortechinform reklama, 172.
18. **Ziborov A., 2006.** To obtain or not obtain the black Sea sapropels in Ukraine. Geology and minerals of the World ocean, Vol. 1, 92-99.
19. **Ziborov A., 2008**. Prospects and tasks of mastering of marine deposits of mineral raw material. Geology and minerals of the World ocean, Vol. 3, 5-18.

РАЗРАБОТКА ГЛУБОКОВОДНЫХ ПОЛЕЗНЫХ ИСКОПАЕМЫХ СЕКТОРНЫМ СПОСОБОМ

Аннотация. Показаны проблемы добычи донных полезных ископаемых из большой глубины. Предложен секторный способ разработки месторождения и приведены схемы движения донного добывающего агрегата. Выполнены расчеты траектории движения каретки и длины шлангокабеля добывающей машины с учетом разворота внутри сектора и вне его пределов.

Ключевые слова: глубоководные полезные ископаемые, секторный способ, траектория движения, шлангокабель, конкреции.

TEKA. COMMISSION OF MOTORIZATION AND ENERGETICS IN AGRICULTURE – 2014, Vol. 14, No. 4, 175–180

Comparison of the Usefulness of Cluster Analysis and Rough Set Theory in Estimating the Rate of Mass Accumulation of Waste in Rural Areas

Tomasz Szul, Krzysztof Nęcka

Department of Power Engineering and Agricultural Processes Automation, Agricultural University of Cracow
Balicka Str. 116B, 30-149 Kraków, Poland, e-mail: tomasz.szul@ur.krakow.pl

Received December 01.2014; accepted December 17.2014

Summary. The study shows the comparison between *k-means* and *EM* methods of clustering and the rough set theory as far as determining the rate of mass accumulation of waste in rural areas is concerned. Performed comparative analyses reveal that the average mean absolute percentage error – MAPE for *k-means* and *EM* algorithm ranged between 33 and 41% for the training set and between 20% and 40% for the test set. The rough set theory was characterised by a much better quality of prognosis, for which MAPE value established for the test set was 14%.
Key words: cluster analysis, households, waste, rough set theory.

INTRODUCTION

Amendments to the Act on Maintaining Cleanliness and Order in the Municipalities of 13 September 1996 entered into force in January 2012 and were again amended in January 2013 [consolidated text: Journal of Laws of 2012, item 391]. These changes revolutionised waste management system. According to the amendments, the municipalities became owners of waste and as such took control over waste management in their areas. Waste management requires considerable financial resources, which are estimated at PLN 650–890 million per year in Poland, which constitutes 8–10% of all the environmental expenditures [Konieczna, Kulczycka 2011]. Apart from economic criteria, the creation of waste management system has to encompass also the criteria of social acceptability and ecological effectiveness. The basis of rational waste management planning is the rate of waste accumulation, whose proper selection is the most important task of the planning stage [Kempa 1983]. The amount of generated waste is influenced by economic, social and infrastructural factors. Determining the groups of elements that affect the change in the amount of generated waste is not enough, as it is not known how strong their interactions are [Malinowski et al. 2009, Tałałaj 2011, Szul et al. 2014]. In the choice of a method allowing to develop a model that predicts the amount of generated waste and is the basis of management planning in a given area, a municipality, should take into account a number of features, which will expectedly have an essential effect on the final outcome. Due to defining a number of features, i.e. mutually correlated quantitative and qualitative variables, it is an interesting alternative to apply methods using cluster analysis and the rough set theory.

Methods of cluster analysis are often used in objects and features clustering. This concept was introduced by Tryon in 1939. Currently, this term includes many different algorithms of classification [Hartigan 1975; Hartigan, Wong 1978; Nęcka 2013; Sneat & Sokal 1973; Ward 1963; Witten & Frank 2000], among which the popular ones are *k-means* and *EM* algorithms. Generally, it can be said that cluster analysis is an exploratory analysis of data, aiming at extracting objects from a large set in such a way that elements belonging to one group are as homogenous as possible within particular groups and as different as possible from objects belonging to other groups. Cluster analysis methods allow to identify structures present in a set, but they do not explain the mechanism of their creation.

A classic *k-means* clustering algorithm was popularised by Hartigan [Hartigan 1975; Hartigan, Wong 1978]. During its implementation, as the first step, observations are randomly allocated to an established *k* number of clusters. Next, observations are transferred between the clusters in such a way that the means in the clusters (for all variables) are as different from one another as possible. As the optimal number of clusters is not known, it has to be determined by an expert or on the basis of the developed algorithms. Usually the number of clusters is selected with the use of *v-fold cross validation* algorithm. The idea of this method is to divide the whole sample into *v* subsets, and then, the same analysis is in turn performed on the observations of *v-1* subsets, i.e. on the so-called training sample. Next, the results of the analysis are applied to the data of the training sample, which had not been so far used in the analysis, and the measure of predictive power is determined on its basis. The results of *v* repetitions are aggregated and give one assessment of the model's stability, i.e. its ability to predict new observations.

Another popular procedure is *EM* method cluster analysis, whose detailed description was presented by Witten and Frank [2000]. This algorithm calculates the probability of cluster membership, with the assumption of one or many probability distributions. The aim of the algorithm is to maximise the general probability for a given division into clusters. The advantage of *EM* algorithm over *k-means* algorithm is the fact that it can be used both for quantitative and qualitative variables.

Another method is the rough set theory, which was introduced in the 1980s by professor Zdzisław Pawlak [1982]. It is a relatively new mathematical method of data analysis. It is used as a tool for the synthesis of advanced and effective analyses methods and for the reduction of data sets [Muruszkiewicz 2004]. Rough sets serve as a methodology in the process of discovering knowledge in databases. This process is usually both iterative and interactive (a lot of decisions are made by the user) [Sodłacki 2001]. The rough set theory is very significant in the process of data extraction due to the fact that it is one of the fastest developing areas of artificial intelligence. It is used to describe imprecise, uncertain knowledge, to model decision-making systems and approximate reasoning [Semeniuk-Polskowska 2001]. Methodology of deduction that uses rough set theory refers only to the qualitative nature of the objects' features. This causes limitations and difficulties when we deal with quantitative and not qualitative features. In such a case, the integration of valued tolerance relation proves useful [Stefanowski and Tsoukias 2000]. It allows to introduce more flexibility to the rough set theory when examining data and to analyse observations expressed in a quantitative form. This course of action is aimed at selecting the most important conditional attributes which are necessary to make the right decision in individual decision-making subgroups [Renigier 2008]. Standard assumption of the rough set theory is based on the indiscernibility relation concept as a precise equivalence relation, which means that the objects will be indiscernible only when they have similar attributes (0 – 1 system). Application of valued tolerance relation to the rough set theory allows determination of the upper and lower approximation of a set with different levels of indiscernibility relation [d'Amato 2006]. Owing to this solution, one can compare two sets of data and achieve a result in the 0...1 range, which constitutes the level of indiscernibility relation. This range is a membership function derived from the assumptions of the fuzzy set theory. The closer the result to 1, the more similar are the objects (indiscernible) with regard to the analysed attribute, and the closer the result to 0, the more discernible they are [Renigier-Biłozor 2008, 2008a, Renigier-Biłozor, Biłozor 2013, Stefanowski 2001].

The rough set theory is a certain theory of knowledge (theory of information systems) and serves as a tool for describing uncertain, imprecise knowledge, for modelling approximation reasonings and decision making systems as well as systems of feature and classification recognition. The results of theoretical study within RST involve logics, set theory, knowledge representation, data filtering, algorithmic problems connected with information systems [Nguyen 2013, Semeniuk-Polskowska 2001]. Although developed a short time ago, rough set theory is used in a number of new fields of study. Nowadays, it is used both in medicine, pharmacology, economics, banking, chemistry, sociology, acoustics, linguistics, general engineering, neuroengineering as well as in the diagnostics of machines, geography, land management and environmental engineering – the publications of results can be found, inter alia, in [Bondar-Nowakowska 2000, Deja 2000, Hachoł, Bondar-Nowakowska and Reinhard 2008, Komorowski et al. 1999, Mróżek and Płonka 1999, Pawlak 1997, Polkowski and Skowron 2001, Renigier 2006, Renigier-Biłozor 2011, Renigier-Biłozor and Biłozor 2007, 2013, Renigier-Biłozor and Wiśniewski 2012, Słowiński 1999, Szul et al. 2014].

METHODOLOGY

The research was limited to two commonly used methods of cluster analysis, i.e. *k-means* and *EM* methods. In both the methods, calculations began with dividing objects into the training and test set, then input variables were standardised and the number of clusters established. *V-fold cross validation* was performed in order to establish an optimal number of clusters. Next, "Generalised cluster analysis" module available in *Statistica 10.0* program was used. It transferred objects between these clusters in such a way as to minimise variability within the clusters and maximise variability between the clusters. The following distances were set while performing analyses with *k-means* method:

Euclidean distance – geometric distance within a multidimensional space:

$$\text{Euclidean distance } = \sqrt{\sum_{i=1}^{n}\left(X_i\text{-}Y_i\right)^2}\ , \tag{1}$$

Manhattan distance – sum of differences measured along dimensions:

$$\text{Manhattan distance} = \sum_{i=1}^{n}|X_i\text{-}Y_i|\ . \tag{2}$$

Chebyshev distance – it is used when we want to define two objects as „different", when they differ in one dimension:

$$\text{Chebyshev distance } (X, Y) = \max|X_i\text{-}Y_i|\ , \tag{3}$$

As the next step, these methods were compared with the calculations using the rough set theory, whose detailed methodology was presented inter alia in the following studies: [Pawlak 1997, Renigier-Biłozor 2008, Szul et al. 2014].

In this method, municipalities selected for analysis were divided in a way analogous to the analysis of clusters into two subsets: the training set and the test set. Objects within the training set were presented in the form of a decision table where the features characterising the municipalities were described with condition attributes. The decision attribute of the rate of mass accumulation of waste in households, kg·(person·year)$^{-1}$ was also established. Next, the matrix of „valued tolerance relation" was calculated for condition attributes:

$$R_j(x,p) = \max\left(\sum_{j=1}^{n} R_j(x,p)\right), \tag{4}$$

where:

R_j – valued tolerance relation,

x – attribute of the considered object,

p – attribute belonging to the conditional part of the considered decision rule,

where

$$R_j(x,y) = \frac{\max(0, \min(c_j(x)\ c\ (y)\ + k - \max((c_j(x)\ c\ (y)))}{k}, \tag{5}$$

where:

$R_j(x,y)$ – is the relation between two sets with a membership function [0,1],

$c_j(x), c_j(y)$ – variable of the analysed object,

k – coefficient taken as a standard deviation in the set of a given attribute of the analysed object.

After having determined indiscernibility classes for condition and decision attributes, quality and accuracy indicators of approximations within individual decisions sub-clusters were calculated:

$$\gamma_c(X) = \frac{card(POS_c(U))}{card(\underline{O}X_i)}, \tag{6}$$

where:

$\underline{O}X$ – the number of lower approximation objects (cardinality of the lower approximation of X set),

$\bar{O}X$ – the number of upper approximation objects (cardinality of the upper approximation of X set),

POS_c – the number of objects in the indiscernibility class of a decision attribute.

$$\beta_c(X) = \frac{card(\underline{O}X)}{card(\bar{O}X)}, \tag{7}$$

where:

$\underline{O}X$– the number of lower approximation objects (cardinality of the lower approximation of X set),

$\bar{O}X$– the number of upper approximation objects (cardinality of the upper approximation of X set).

Having distinguished representative decision rules the author determined the rate of mass accumulation of waste. For this purpose the municipalities from the test set were used. Applying valued tolerance relation (VTR), the author checked to which of the decision rules selected above the analysed municipality has the highest level of membership.

The quality of the match between the predicted rate of mass accumulation of waste in households and its real value was estimated by determining the value of error:

$$ME = \frac{1}{n} \cdot \sum_{i=1}^{n} d_i - d_i^p, \tag{8}$$

$$APE = \frac{|d_i - d_i^p|}{d_i} \cdot 100, \tag{9}$$

$$MAPE = \frac{1}{n} \cdot \sum_{i=1}^{n} \frac{|d_i - d_i^p|}{d_i} \cdot 100, \tag{10}$$

where:

d_i – the rate of mass accumulation of waste in the households, kg·(person·year)$^{-1}$'

d_i^p – predicted rate of mass accumulation of waste in the households, kg·(person·year)$^{-1}$.

RESULTS

Analyses presented in the study were performed on the basis of statistical data from Małopolska Voivodeship of 2012 [GUS 2013]. During this time in the analysed area 1001 thousand Mg of waste was generated, which constitutes 7,8% of the waste stream on a national scale. The indicator expressing the amount of waste produced per one inhabitant in 2012 was 300 kg·(person·year)$^{-1}$ for Małopolska Voyvodeship and it was only slightly lower than the national average, i.e. 314 kg·(person·year)$^{-1}$. An average household in Małopolska produces 118 kg·(person·year)$^{-1}$, while in the rural areas this value is lower by about 45%.

The comparative analysis of individual methods' effectiveness while determining the rate of waste accumulation for rural areas was done on the example of the set of 60 randomly chosen rural municipalities and rural areas of urban and rural municipalities of Małopolska Voivodeship. The number of objects within the set was chosen in a way to enable the level of confidence of 95%. Then, the municipalities chosen for the analysis were divided into two subsets: the training set containing 40 objects and the test set comprising 20 objects.

Objects within the training set were presented in the form of a decision table (Table 1) where the features characterising the municipalities were marked with symbols $c_1 \div c_7$, and the rate of mass accumulation of waste in households, which is a decision attribute was marked with *d* symbol.

Table 1. Information system (decision table)

Municipality/ object number	Condition attributes							Decision attribute
	c1	c2	c3	c4	c5	c6	c7	d

Source: own study on the basis of General Statistical Office's data

For the aforementioned attributes, domains were determined according to the following assumptions:

c_1 – population density, [people·km^{-2}],

c_2 – average area of agricultural land, [ha],

c_3 – building's age rate (established as a weighted arithmetic mean of the number of buildings from different periods of time i.e. before 1944, 1945-1970, 1971-1988, 1989-2002, 2003-2012),

c_4 – participation of buildings heated with natural gas,

c_5 – municipality type, (1 – suburban, 2 – tourist, 3 – agricultural),

c_6 – participation of households deriving income from agricultural activity,

c_7 – income rate (municipalities' own income – participation in taxes comprising national budget income personal income tax), [PLN·(person·year)$^{-1}$],

d – the rate of mass accumulation of waste in the households, [kg·(person·year)$^{-1}$].

The values of particular attributes were established on the basis of statistical data included in the Regional Data Bank of General Statistical Office for 2012 and 2010 General Agricultural Census available on the General Statistical Office's website [GUS 2013].

With the use of condition attributes ($c_1 – c_7$), the training set was divided by *Statistica 10.0* program into an optimal number of clusters on the basis of *v-fold cross validation*. Observations from the test set were assigned to different groups. Then, on the basis of the training set, mean values of the decision attribute ($d_{śr}$ [kg·(person·year)$^{-1}$]), its variability and the coefficient (V[%]) were determined for individual clusters. The results of achieved analyses are presented in Table 2.

Table 2. Decision attribute's variability for determined clusters

cluster:	Clustering algorithm:							
	k-means – distance between the objects:						EM	
	Euclidean		Manhattan		Chebyshev			
	$d_{śr}$	V	$d_{śr}$	V	$d_{śr}$	V	$d_{śr}$	V
1	50	47	52	36	53	33	60	40
2	55	26	56	35	93	31	84	34
3	86	32	85	33			97	38
4	107	26	107	26				

As the final step, individual clusters of the test set were attributed with decision algorithm values i.e. the rate of mass accumulation of waste from households, determined on the basis of the training set. The achieved values were compared with real data and the error level was established. The achieved results are presented in Table 3.

The performed analyses show that the mean value of the rest for all methods of cluster analysis determined for the training set was 0 [kg·(person·year)$^{-1}$]. For the training set it oscillated between – 3 [kg·(person·year)$^{-1}$] for the rough set theory and 22 [kg·(person·year)$^{-1}$] for *k-means* method, for which the Euclidean distance between objects was calculated. In case of the training set observations, *k-means* method of clustering generated underestimated prognoses independently of the type of distance calculated between objects, contrary to *EM* method and the rough set theory. The average MAPE for *k-means* and *EM* algorithm ranged between 33 and 41% for the training set and between 20% and 40% for the test set. The rough set theory was characterised by a much better quality of prognosis, for which MAPE value was 14%.

With the purpose of a better presentation of the changes in differences generated for individual methods, empirical distribution function for APE has been shown in Figure 1.

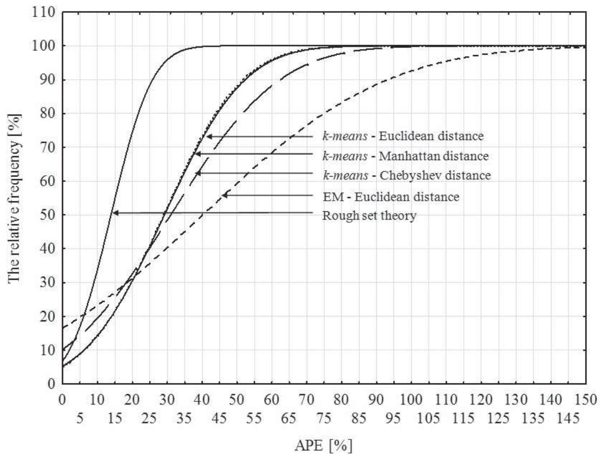

Fig. 1. Comparison of empirical distribution function for APE

On the empirical distribution function for APE diagram (Fig. 1) we can see that the rough set theory was characterised by the best quality of prognosis of the rate of mass accumulation of waste in households for the test set. Participation of error with the lowest value was similar to *k-means* clustering method and it was less than 10% of the observations. The advantage of rough set theory for such a small test was very much visible for bigger errors of the prognosis. Maximum APE value determined with this method did not go beyond 40% whereas for *k-means* method it was around 80-90%. The lowest quality of prognosis despite the highest percentage of low value errors was characteristic of *EM* method of clustering. Low value errors accounted for almost 20% of observations, but at the same time the maximum values of errors were as high as150%.

CONCLUSIONS

The performed comparative analyses show that the average mean error – ME for all methods of cluster analyses determined for the training set was 0 [kg·(person·year)$^{-1}$]. For the training set it varied from – 3 [kg·(person·year)$^{-1}$] for rough set theory to 22 [kg·(person·year)$^{-1}$] for *k-means* method, for which the Euclidean distance between objects was calculated. In case of the training set observations, *k-means* method of clustering generated underestimated prognoses independently of the type of distance calculated between objects, contrary to *EM* method and the rough set theory.

Table 3. Characteristic of the estimation error of the rate of mass accumulation of waste in households

Sample:	Error clustering algorithm:									
	k-means – distance between the objects:						EM		Rough set theory	
	Euclidean		Manhattan		Chebyshev					
	ME	MAPE	ME	MAPE	ME	MAPE	ME	MAPE	ME	MAPE
training	0	33	0	35	0	35	0	41	-	-
test	22	29	10	31	20	29	-6	40	-3	14

The average MAPE of prognosis for *k-means* and *EM* algorithm ranged between 33 and 41% for the training set and between 20% and 40% for the test set. The rough set theory was characterised by the best quality of prognosis, for which MAPE value was 14%.

The performed analyses have proved that rough set theory should be used for estimating the rate of mass accumulation of waste from rural areas especially when the number of objects within the cluster is low.

REFERENCES

1. **Bondar-Nowakowska E., 2000:** Oddziaływanie robót konserwacyjnych na florę i faunę koryt wybranych cieków nizinnych. Zesz. Nauk. AR Wrocław. Rozprawy CLXXIII, nr 391, 100.
2. **Deja R., 2000:** Zastosowanie teorii zbiorów przybliżonych w analizie konfliktów. Praca doktorska. Instytut Podstaw Informatyki Polskiej Akademii Nauk.
3. Główny Urząd Statystyczny. Bank Danych Lokalnych. http://stat.gov.pl/bdl/app/strona.html?p_name=indeks.
4. **Hachoł J., Bondar-Nowakowska E., Reinhard A., 2008:** Oddziaływanie wybranych elementów koryta cieku na zbiorowiska naczyniowych roślin wodnych. Infrastruktura i Ekologia Terenów Wiejskich. Nr 7/2008, Polska Akademia Nauk, Oddział w Krakowie, 255-266.
5. **Hartigan J. A., Wong M. A., 1978:** Algorithm 136. A k-means clustering algorithm. Applied Statistics. 28. 100.
6. **Hartigan, J. A., 1975:** Clustering algorithms. New York: Wiley.
7. **Kempa E.S., 1983:** Gospodarka odpadami miejskimi. Arkady. Warszawa.
8. **Komorowski, J. Pawlak, Z., Polkowski, L. & Skowron, A., 1999:** Rough sets: A tutorial." Rough fuzzy hybridization: A new trend in decision-making. 3-98.
9. **Konieczna R., Kulczycka J., 2011:** Analiza ekonomiczna systemów gospodarki odpadami. cz. II. IGSMiE PAN, Karków.
10. **Malinowski M., Krakowiak-Bal A., Sikora J., Woźniak A., 2009:** Ilości generowanych odpadów komunalnych w aspekcie typów gospodarczych gmin województwa małopolskiego.. Infrastruktura i Ekologia Terenów Wiejskich. Nr 9, Polska Akademia Nauk, Oddział w Krakowie, 181–191.
11. **Mróżek A., Płonka L. 1999.** Analiza danych metodą zbiorów przybliżonych. Akademicka Oficyna Wydawnicza PLJ, Warszawa.
12. **Nęcka K., 2013:** Selection of decisive variables for the construction of typical end user power demand profiles. TEKA Komisji Motoryzacji i Energetyki Rolnictwa Vol. 13 No 2. Lublin. 1 91-96.
13. Nutech Solution – Science for Businnes. 2005. http://www.nutechsolutions.com.pl/.
14. **Pawlak Z. 1997.** Rough set approach to knowledge-based decision support. European Journal of Operational Research , 99 (1), 48-57.
15. **Polkowski, L. Skowron, A., 2001:** Rough mereological calculi of granules: A rough set approach to computation. Computational Intelligence, 17 (3), 472-492.
16. **Renigier M., 2006:** Zastosowanie analizy danych metodą zbiorów przybliżonych do zarządzania zasobami nieruchomości. Studia i Materiały Towarzystwa Naukowego nieruchomości 14(1). 203-213.
17. **Renigier-Biłozor M, Biłozor A., 2013:** Opracowanie systemu wspomagania podejmowania decyzji z wykorzystaniem teorii zbiorów rozmytych oraz teorii zbiorów przybliżonych w procesie kształtowania bezpieczeństwa przestrzeni. Acta Scientiarum Polonorum. Administratio Locorum 12 (1). 38-47.
18. **Renigier-Biłozor M,. 2011:** Analiza rynków nieruchomości z wykorzystaniem teorii zbiorów przybliżonych. Studia i Materiały Towarzystwa Naukowego nieruchomości Vol 19 (1). 107-119.
19. **Renigier-Biłozor M. Wiśniewski R., 2012:** The Effectivencess of real estete market versus efficiency of its participants. European Spatial Research and Policy. Vo. 19 nr 1. 95-110.
20. **Renigier-Biłozor M., Biłozor A., 2007:** Application of the rough set theory and the fuzzy set theory in land management. Aplication 28 june 2007 r. Annual conference The European Real Estate Society – ERES. Londyn.
21. **Śleszyński P., 2009-2010:** a) Delimitacja obszarów wiejskich o najgorszych wskaźnikach rozwoju społeczno-gospodarczego; b) Delimitacja obszarów wiejskich o najgorszych wskaźnikach dostępności do usług publicznych; c) opracowania map i konsultacje kartograficzne, IGiPZ PAN, Warszawa, 7+5 + mapy, dla: Ministerstwo Rozwoju Regionalnego (Krajowa Strategia Rozwoju Regionalnego).
22. **Słowiński R., 1992:** Intelligent decision support. Applications and advances of the rough sets theory. Kluwer Academic Publshers., Dordrecht.
23. **Sneath, P. H. A., & Sokal, R. R., 1973:** Numerical taxonomy. San Francisco: W. H. Freeman & Co.
24. **Szul T., Knaga J., Nęcka K., 2014:** Application of rough set theory for establishing the rate of mass accumulation of waste in the households in rural areas. Ecological Chemistry and Engineering S. w druku.
25. **Tałałaj I.A., 2011:** Wpływ wybranych czynników społeczno-ekonomicznych na zmiany ilości odpadów komunalnych w województwie podlaskim. Inżynieria Ekologiczna. Nr 25.
26. **Tryon, R. C., 1939:** Cluster Analysis. Ann Arbor, MI: Edwards Brothers
27. **Ward, J. H. 1963.** Hierarchical grouping to optimize an objective function. Journal of the American Statistical Association, 58, 236.
28. **Witten, I., H., & Frank, E., 2000:** Data Mining: Practical Machine Learning Tools and Techniques. New York: Morgan Kaufmann.

PORÓWNANIE PRZYDATNOŚCI ANALIZY SKUPIEŃ ORAZ TEORII ZBIORÓW PRZYBLIŻONYCH DO SZACOWANIA WSKAŹNIKA MASOWEGO NAGROMADZENIA ODPADÓW NA OBSZARACH WIEJSKICH

Streszczenie. W pracy przedstawiono porównanie metod grupowania *k*-śednich i *EM* oraz Teorii Zbiorów Przybliżonych do wyznaczania wskaźnika masowego nagromadzenia odpadów odbiorców wiejskich. Z wykonanych analiz porównawczych wynika, że średnia wartość błędu MAPE dla algorytmu *k-średnich* i *EM* zawierała się w przedziale od 33 do 41% dla zbioru uczącego i w zakresie od 20% do 40% dla zbioru testowego. Dużo lepszą jakością prognozy wskaźnika charakteryzowała sie Teoria Zbiorów Przybliżonych, dla której wartość MAPE wyznaczona dla zbioru testowego kształtowała sie na poziomie 14%.

Słowa kluczowe: analiza skupień, gospodarstwa domowe, odpady, Teoria Zbiorów Przybliżonych.

TEKA. COMMISSION OF MOTORIZATION AND ENERGETICS IN AGRICULTURE – 2014, Vol. 14, No. 4, 181–184

An Analysis of Variability in Demand for Natural Gas at Rural Households

Małgorzata Trojanowska, Dorota Lipczyńska

Department of Power Engineering and Agricultural Processes Automation, Agricultural University of Cracow
Balicka Str. 116B, 30-149 Kraków, Poland, e-mail: malgorzata.trojanowska@ur.krakow.pl

Received December 11.2014; accepted December 19.2014

Summary. The variability in hourly demand for natural gas in rural households was analyzed at various time intervals. The results enabled the determination of typical daily courses of gas consumption by this group of consumers, separately for workdays and weekends, divided into two periods i.e. high and low gas demand. For the purpose of drawing typical curves of the loads of rural gas networks, the courses of gas consumption were classified with the use of variance analysis, cluster analysis, and based on the principal indicators describing the variability in gas consumption.

Key words: gas market, typical profiles of natural gas consumption.

INTRODUCTION

Despite great efforts being made to open up the natural gas market in Poland, it has not been fully liberalised yet. At the end of December 2012, the gas exchange was launched at the Polish Power Exchange, and a partial deregulation of gas prices for industry occurred in 2013, whilst on 1 August 2014, a new entity, PGNiG Retail LLC was spun-off from the existing structure of the Polish Oil and Gas Company Joint Stock Company (PGNiG SA). All the trade services in the area of natural gas sales to retail clients were spun off to this new company. At present there is no possibility to liberalise natural gas prices for retail consumers, but according to experts it will happen within the next couple of years.

For business entities involved in sales of natural gas, this near perspective of the liberalisation of gas market means the increasing importance of developed forecasts of demand for this fuel, particularly short-term forecasts [2, 6, 11, 14, 16, 17, 19, 20].

In the energy industry, the most demanding market in terms of the quality of forecasts is the electricity market. One of the ways to predict the demand in the electricity industry is to determine the demand for electricity on the basis of typical load profiles of customers [1, 7, 8, 15]. By analogy, this method can also be used to forecast the demand for natural gas [5].

The aim of the presented study was to analyse the variability of demand for natural gas in rural households at different time intervals for the purpose of determining the typical daily courses of gas consumption by this group of consumers. This study focused on the daily and weekly variability in gas consumption within the periods of high and low demand for this fuel.

MATERIALS AND METHODS

In this study, a statistical analysis of the consumption of natural gas by rural households, which are a specific customer group of natural gas distribution companies, was carried out. In order to obtain typical profiles of daily gas usage, the courses of gas consumption were categorised with the use of variance analysis, cluster analysis, particularly the agglomeration and k-means methods, as well as using principal indicators describing gas consumption.

Calculations were made on the basis of data of a gas company, pertaining to gas consumption by rural customers supplied via a low-pressure network from a selected grade I gas pressure reduction station located in the province of Lower Silesia.

In the study area, the density of the natural gas distribution network is 10.5 km per 100 km^2, and the consumption of gas per resident is ca. 42 m^3.

RESULTS

Individual consumers use natural gas for heating buildings, providing domestic hot water and cooking meals. The amount of consumption depends on a number of factors [3, 4, 12, 13, 15, 17, 18], among which air temperature is particularly important. The correlation coefficient between the mean daily demand for gas in a given month and the mean temperature is -0.97. Examples of the changes of the two correlated values are presented in Fig. 1.

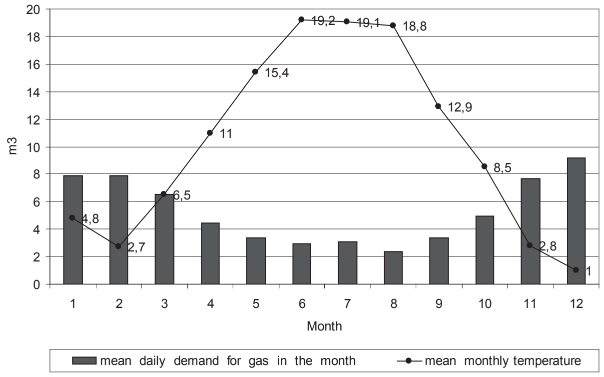

Fig. 1. The mean daily demand for natural gas in particular months of the year vis-à-vis mean monthly air temperature

The variance analysis completed in this study showed that the values of average daily gas consumption by rural households over a month-long period did not differ significantly from one another from November to March, and from April to October. These two periods are considered separately later in the paper and are referred to as periods of high and low consumption of natural gas, respectively.

When a large number of consumers are supplied at the same time, certain regularities can be seen in the timing of gas consumption. These changes are illustrated in Fig. 2 where the courses of demand for gas are presented in particular hours of July and December.

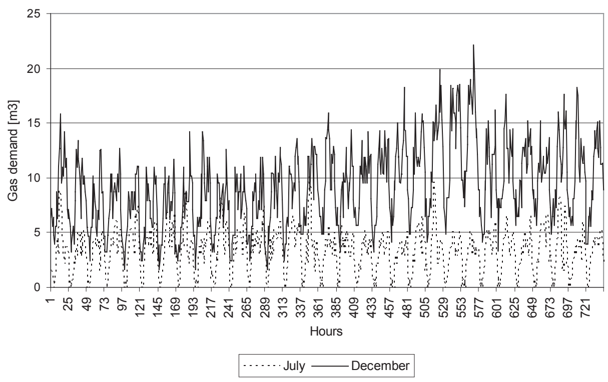

Fig. 2. The courses of demand for gas in particular hours of July and December

A similarity analysis of daily loads of gas networks was performed in order to identify the regularity in the courses of changes. For the purposes of the similarity analysis of gas consumption in particular days of the week, normalized vectors of daily courses, called normalized daily profiles, were determined and classified using the *Cluster analysis* module in the Statistica software package, in particular the agglomeration and k-means methods.

The normalized profiles of daily loads of gas networks containing information on the shape of the course were determined according to the following formula [9]:

$$g_i = \frac{G_i - G_{dsr}}{\sum_{j=1}^{24}\left(G_j - G_{dsr}\right)^2}, \qquad i = 1, 2, \ldots, 24 \tag{1}$$

where:
Gi, Gj – load in i[th] (j[th]) hour,
Gdsr – mean load in 24 hours.

Both methods produced the same results for the period of high and low consumption alike, which permitted two characteristic days of the week i.e.: workday and weekend day, with respect to the daily variability of demand for gas (Fig. 3).

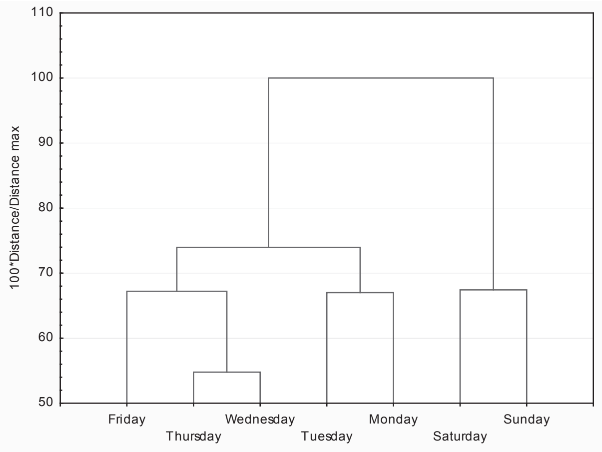

Fig. 3. Diagram of agglomeration of similarities of daily profiles of gas consumption on particular days of week

Sets of various indicators characterising the variability in loads are often used to classify the daily courses of demand [1, 10, 15]. Among the indicators most often used to describe the variability in demand for electricity are the medium and base level of load [1, 15]. These were defined for natural gas in the following way:

– medium level of gas load

$$m = \frac{G_{sr}}{G_{\max}}, \tag{2}$$

– base level of gas load

$$m_o = \frac{G_{\min}}{G_{\max}}, \tag{3}$$

where:
Gsr, Gmax, Gmin are medium, maximum, and minimum levels of gas consumption, respectively.

The values of these indicators for daily and weekly periods were compiled in Table 1.

Table 1 shows that the courses of demand for gas in the low-consumption-period are characterized by greater unevenness and lesser balanced than in the high-consumption period. The differences are so great that there was a need to develop standard daily load graphs separately for each of these periods.

Table 1. Indicators of daily and weekly load of gas network

Value	Period of low gas consumption				Period of high gas consumption			
	m_d	m_{do}	m_t	m_{to}	m_d	m_{do}	m_t	m_{to}
Mean	0.48	0.01	0.37	0.00	0.60	0.21	0.52	0.13
Minimum	0.31	0.00	0.28	0.00	0.41	0.07	0.43	0.05
Maximum	0.75	0.33	0.50	0.00	0.71	0.43	0.63	0.22

As a result of the analysis performed four typical reduced profiles of daily gas consumption by rural consumers i.e. for a workday and a weekend day during the low-consumption-period, and for a workday and a weekend day during the high-consumption-period, in the form of averaged courses, and corrected, at the same time. The reference value was the respective maximum hourly demand for gas in the low- or high-consumption-periods. The profiles are presented in Figs 4 and 5.

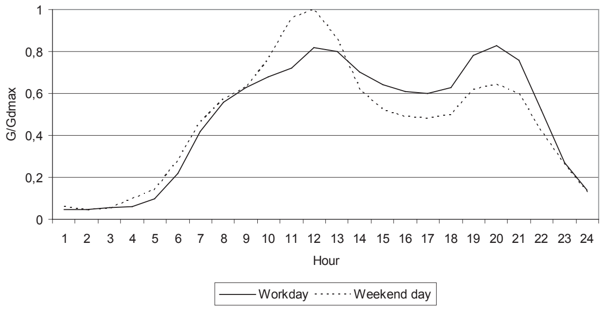

Fig. 4. Typical profiles of daily gas demand in low gas consumption period

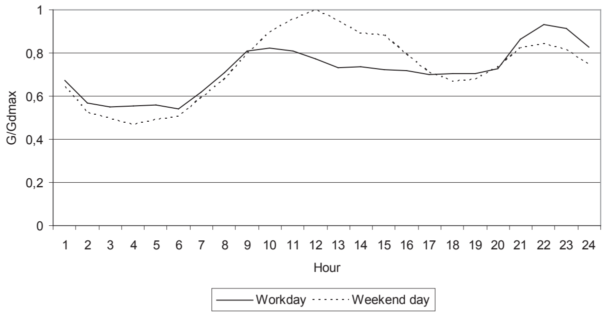

Fig. 5. Typical profiles of daily gas demand in high gas consumption period

The studies demonstrated that gas consumption by rural households on weekend days is slightly higher than on workdays (in the last two years – by ca. 1%), though it is much more uneven, with clearly marked peaks of consumption in the midday hours.

CONCLUSIONS

The demand for gas in rural households shows periodic daily, weekly, and monthly fluctuations.

Considering the shapes of gas usage curves, four standard profiles were distinguished representing the consumption, i.e. for a workday and a weekend day, respectively for periods of high and low demand for gas. These curves can be used both for the purpose of operating gas distribution networks and in short-term forecasts of gas demand by households in rural areas. At present, gas traders usually use the simplest, naive method to predict demand.

REFERENCES

1. Analiza i prognoza obciążeń elektroenergetycznych. Praca zbiorowa 1971: WN-T Warszawa.
2. **Azadeh A., Asadzadeh S.M., Ghanbari A. 2010:** An adaptive network-based fuzzy inference system for short-term natural gas demand estimation: Uncertain and complex environments. Energy Policy 38, 1529-1536.
3. **Bianco V., Scarpa F., Tagliafico L.A. 2014:** Analysis and future outlook of natural gas consumption in the Italian residential sector. Energy Conversion and Management 87, 754-764.
4. **Brabec M., Konar O., Pelikan E., Maly M. 2008:** A nonlinear mixed effects model for the prediction of natural gas consumption by individual customers. International Journal of Forecasting 24, 659–678.
5. **Brabec M., Konar O., Maly M., Pelikan E., Vondracek J. 2008:** A statistical model for natural gas standardized load profiles. J Roy Statist. Soc. Series C: Applied Statistics 58(1), 123–39.
6. **Chen Q., She Y., Xu X. 2013:** Combination model for short-term load forecasting. The Open Automation and Control Systems Journal 5, 124-132.
7. **Chicco G. 2012:** Overview and performance assessment of the clustering methods for electrical load pattern grouping. Energy 42, 68-80.
8. **Ferreira A.M.S., Cavalcante C.A., Fontes C.H., Marambio J. 2012:** A new proposal of typification of load profiles to support the decision-making in the sector of electric energy distribution. Internacional Industrial Conference on Engineering and Operations Management 9-12 July 2012 Guimarães Portugalia, ID 18.1-ID18.7.
9. **Dudek G. 2004:** Wybrane metody analizy szeregów czasowych obciążeń elektroenergetycznych. Materiały Konferencji Naukowej *Prognozowanie w elektroenergetyce PE ,04*. Częstochowa, 116 – 125.
10. **Góra S. 1975:** Gospodarka elektroenergetyczna w przemyśle. PWN Warszawa.
11. **Kelner J.M. 2003:** Prognozowanie krótkoterminowe poborów gazu z sieci przesyłowych metodą sztucznych sieci neuronowych. Gaz, Woda i Technika Sanitarna 6, 196-204.
12. **Melikoglu M. 2013: Vision 2023:** Forecasting Turkey's natural gas demand between 2013 and 2030. Renewable and Sustainable Energy Reviews 22, 393-400.

13. **Nai-ming X., Chao-qing Y., Ying-jie Y. 2015:** Forecasting China's energy demand and self-sufficiency rate by grey forecasting model and Markov model. Electrical Power and Energy Systems 66, 1-8.
14. **Potočnik P., Soldo B., Šimunović G., Šarić T., Jeromen A., Govekar E. 2014:** Comparison of static and adaptive models for short-term residential natural gas forecasting in Croatia. Applied Energy 129, 94-103.
15. Prognozowanie w elektroenergetyce. Zagadnienia wybrane (red. I. Dobrzańska). 2002: Wydawnictwo Politechniki Częstochowskiej, Częstochowa.
16. **Smith P., Husejn S. 1997:** Forecasting short term regional gas demand using an expert system. Expert Systems with Applications 10(2), 265-273.
17. **Soldo B. 2012:** Forecasting natural gas consumption. Applied Energy 92, 26-37.
18. **Taspınar F., Celebi N., Tutkun N. 2013:** Forecasting of daily natural gas consumption on regional basis in Turkey using various computational methods. Energy and Buildings 56, 23-31.
19. **Vondráček, J.; Pelikán, E.; Konár O.; Čermáková J.; Eben K.; Malý M., Brabec M. 2008:** A statistical model for the estimation of natural gas consumption. Applied Energy 85, 362-370.
20. **Yu F., Xul X. 2014:** A short-term load forecasting model of natural gas based on optimized genetic algorithm and improved BP neural network. Applied Energy 134, 102-113.

ANALIZA ZMIENNOŚCI ZAPOTRZEBOWANIA WIEJSKICH GOSPODARSTW NA GAZ ZIEMNY

Streszczenie. Przeanalizowano zmienność godzinowego poboru gazu ziemnego przez wiejskie gospodarstwa domowe w różnych interwałach czasowych i na tej podstawie opracowano typowe dobowe przebiegi zużycia gazu przez tę grupę odbiorców, oddzielnie dla dni roboczych i weekendowych, w rozbiciu na dwa okresy tj. dużego i małego zapotrzebowania na gaz. Dla potrzeb opracowania typowych krzywych obciążenia wiejskich sieci gazowych, przebiegi poboru gazu klasyfikowano z wykorzystaniem analizy wariancji, analizy skupień, a także w oparciu o podstawowe wskaźniki opisujące zmienność zużycia gazu.

Słowa kluczowe: rynek gazu, typowe profile zużycia gazu ziemnego.

Determination of the Rheological Properties of Biofuels Containing SBME Biocomponent

Grzegorz Wcisło

Faculty of Production Engineering and Power Technologies
University of Agriculture in Krakow, Poland
email: grzegorz.wcislo@ur.krakow.pl

Received December 08.2014; accepted December 19.2014

Summary. Similarly to diesel oil (B7), Biodiesla B100 SBME dynamic viscosity at positive temperatures in principle increases with decreasing temperature. Having exceeded -10°C, it begins to increase rapidly. The dynamic viscosity for B100 SBME at -20°C was 173 mPas, for B50 SBME – 67mPas and for B20 SBME – 67mPas. The study has shown that B100 SBME cannot be used in practice as a pure fuel without a package of viscosity-lowering additives. At the same time, the viscosity values for B5 and B20 biofuels, in particular at positive temperatures, are close to the viscosity of diesel fuel. Under such conditions one can safely use B7 and B20 biofuels in compression-ignition engines, even in those with a state-of-the-art injection apparatus.

Key words: diesel engine, Biodiesel, biofuel, SFME, dynamic viscosity, shearing rate.

INTRODUCTION

Quality standards PN-EN 590:2006 for diesel fuel and EN ISO3104 for FAME fuel determine only kinematic viscosity. No obligatory norm has been introduced so far for determining dynamic viscosity. Kinematic viscosity is a parameter describing the resistance of fluid flow due to gravity forces. In order to determine kinematic viscosity the time flow for constant fluid volume through a capillary tube of a standard viscosimeter under the influence of gravity forces is measured, under repeatable conditions and at known, strictly controlled temperature. The value of kinematic viscosity is computed by multiplying the flow time by viscosimeter standardization constant. However, the norm allows three groups of viscosimeters, so the methods of measurements may differ from the described above depending on the kind and range of the tested fluid viscosity [6, 17].

Analysis of the subject literature shows various values of RME kinematic viscosity, which according to some authors at the temperature of e.g. 20°C ranged from 6 [3] to 2000 [mPas] [4]. However, it seems that the scatter of results was not so wide but was rather due to a measurement error or application of little precise methods. Therefore even a small mistake during measurement may cause a considerable scatter of obtained kinematic viscosity values. Additionally such error may be multiplied at dynamic viscosity determination [13,14,15,16].

In recent years a rapid development of injection apparatus based on pump-injectors or common rail has been observed, where very high pressure occurs. In this situation it is most important to determine the fluid flow resistance under dynamic, not static conditions. It is the more important when type "B" fuels with biocomponent supplement of higher viscosity are used for ZS engine feeding. Therefore dynamic, not kinematic viscosity should be determined most precisely. So far dynamic viscosity has not been determined separately, only obtained from kinematic viscosity. It was due to a lack of proper tools which were relatively expensive. However, a dynamic development of rheometers in recent years, particularly dynamic types, allowed for a most precise determination of dynamic viscosity. Moreover, for a better assessment of fuel mechanical properties the influence of many rheological parameters on the behaviour of fuels or biofuels may be also tested.

The advantages of using rotational rheometers for viscosity determination comprise: small volume of fuel sample (about 50ml is enough), full automatic and computerized measurements, possibility of testing both viscous and elastic properties, possible investigation of tixotropy and antitixotropy phenomena.

Dynamic viscosity is a measure of fluid's resistance to flow or fluid deformation – Polish standard PN-EN ISO 3104. It also affects the injection course, stream range and fuel spraying in the engine combustion chamber. It influences lubrication properties, which is particularly important in the case of rotational injection pumps because in the pumps of this type the pump elements are lubricated with diesel oil. It may be the reason why one sometimes encounters the opinion that small viscosity and resulting good flow properties are more important for the engine start up than the cetane number [2,3,5,8]. There is also a strict relationship between viscosity, temperature and shearing rate.

There is a serious problem concerning an excessive viscosity of some biofuels, which in recent years has become one of the key issues. It is primarily connected with the use of injection apparatus, which supplies fuel to the engine at dynamic pressure reaching 2600bar. Therefore even a slight increase in this parameter may negatively affect the work of injection apparatus. The fact that biofuels would enter the fuel markets was known in 1997, so the manufacturers should adjust the injection systems also for the fuels with a 20 to 40% higher viscosity. Biodiesel quality also poses a problem. It turns out that usually FAME has more products of incomplete conversion to esters of oil obtained through transesterification process. EN-14214 standard for FAME Biodiesel fuel states the maximum allowable amount of monoacyloglycerols in fuels as 0.8%, whereas diacylglyceryl ethers only 0.2% (m/m). Another problem is wrong separation of ester from glycerine phase, since even trace amounts of glycerine phase left over lead to a considerable increase in viscosity. As results from he Author's own research, viscosity of properly separated glycerine phase obtained after rapeseed oil methanolysis at 20°C is about 940[mPas], whereas in diesel fuel about 8[mPas], RME esters about 13[mPas], whereas rapeseed oil about 70[mPas]. It results from the data given above that at 20°C oil viscosity is 5,5 times higher and viscosity of glycerine phase by over 72 times higher than RME viscosity [7].

METHODS OF RESEARCH

Measuring set with two coaxial cylinders was applied in the rheometer. Beside the cone/plate viscometer it is one of the most precise devices for measuring dynamic viscosity of fuels and biofuels. Figure 1 shows the schematic diagram of the measuring set with marked parameters which served to formulate the main relationships: for tangent force, oscillating torque, shearing force and dynamic viscosity.

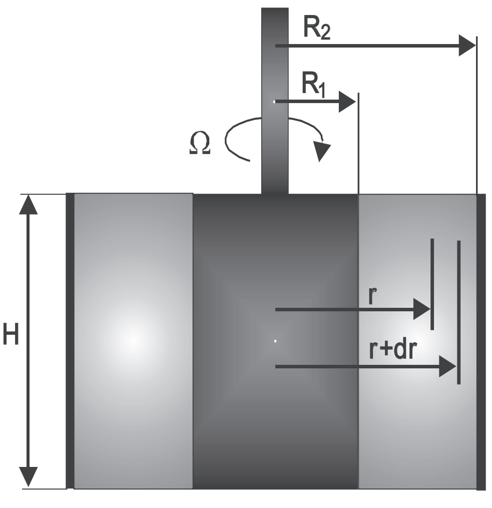

Fig. 1. Measuring set with coaxial cylinders

Assuming that the tested sample has the height *H*, tangent force in the fluid at the distance *r* from the rotation axis may be expressed by the formula 1. Considering rotating frequency of the spinning element and outer diameter of the spinning element R_1 and inner diameter of cylinder sleeve R_2 filled with the tested fluid, we may derive formula 2 describing the relationship for shearing force. If oscillating torque caused by tangent force is equal it may be generally written as $M=F \cdot r$. On the other hand for the set applied in the rheometer, i.e. measuring set with coaxial cylinders, the oscillating torque may be shown by formula 3. Tangent friction forces transferred by the fluid to the inner cylinder cause the described oscillating torque *M*. Considering the above mentioned assumptions the formula for dynamic viscosity using coaxial cylinder set may be described using formula 4.

$$F_r = 2\pi r H \tau_r , \tag{1}$$

$$\dot{\gamma} = \frac{2\Omega}{1-\frac{R_1^2}{R_2^2}} , \tag{2}$$

$$M = \frac{4\pi\eta H\Omega}{\frac{1}{R_1^2}-\frac{1}{R_2^2}} , \tag{3}$$

$$\eta = \frac{1}{4\pi H}\left(\frac{1}{R_1^2}-\frac{1}{R_2^2}\right)\frac{M}{\Omega} , \tag{4}$$

where:
Ω – rotating frequency of the spinning element
M – oscillating torque acting on spinning element axis
H – height of biofuel sample
r – distance from rotation axis
R_1 – outer radius
R_2 – inner radius of cylinder sleeve

AIM AND SCOPE OF RESEARCH

The research aimed at determining the effect of temperature on dynamic viscosity of Biodiesel SBME type biofuels. Three kinds of fuels were prepared: ON (B7), B20, B50 and B100. The value attached to "B" letter denotes volumetric proportion of SBME (methyl esters obtained from soya bean's oil) in the mixture with fuel oil.

These biofuels were selected because of the current attempts to create an alternative to Biodiesel obtained from SBME soya bean oil. Currently in Poland, it is possible to purchase sunflower oil at a price competitive to soya bean oil.

These biofuel types were selected because, currently passed act on biocomponents and biofuels allows to use up to 7% (v/v) of biocomponent supplements in fuels without the obligatory relevant information for the buyer about the supplement. In accordance with the National Index Target, in 2014 in Poland we needed to consume on average 7.1% of biofuels and/or bio-components in relation to the total fuel consumption, calculating in energy terms.

The second chosen biofuel was B20 since by 2020 a mean biocomponent share in the total balance of fuels consumed by the transport will reach at least 20%. The third biofuel selected for comapartive testing was B100, or pure SBME ester. In addition, for comparison purposes tests were performed on the commercial diesel and RME fuels from a service station being part of Bliska service station chain.

The basic fuel for type B50 and B20 biofeuls was the commercial VERVA ON fuel oil manufactured by PKN ORLEN S.A. company. The research determined the variability of dynamic viscosity within the temperature range from -20 to 50ºC. The range of temperatures was assumed because due to the applied thermostatic bath it was impossible to lower the sample temperature below -20ºC. On the other hand raising the upper temperature above 50ºC was considered unnecessary because it does not generally affect a change of dynamic viscosity. In the initial part of the test shearing rate of the rheometer spindle was constant 1050 [s^{-1}].

CHARACTERIZATION OF MEASURING STAND

The main device used at the measuring stand was ReolabQC rheometer manufactured by a German Anton Paar GmbH company (Fig. 2). The rheometer is a devise designed for determining mechanical and rheological parameters of fluids and fuels. The device measures among others dynamic viscosity, surface tension, shearing forces, shearing rate, shearing tension, etc. The rheometer is also equipped with a temperature sensor and integrated system of time measurement. In order to determine the effect of temperature on the above mentioned parameters, the rheometer used at the measuring stand was additionally equipped with thermostatic bath made by an Austrian Grant company. The results of research using measuring system of the viscosimeter were sent to a computer and saved there to be subsequently processed using RHEOPLUS/32 V3.0.

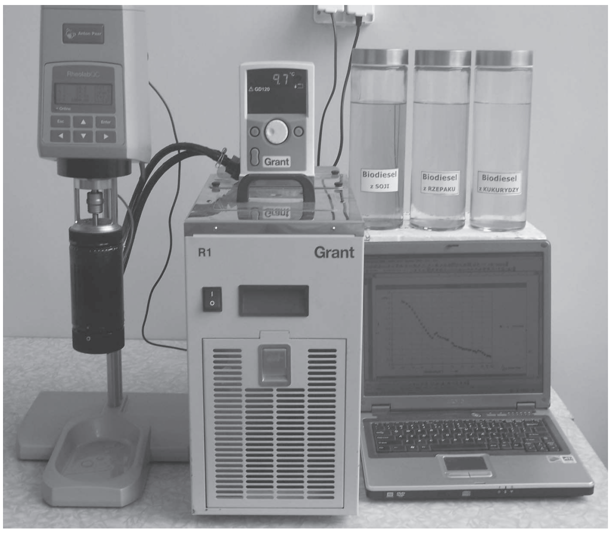

Fig. 2. The researchers post was furbished with a reometer and tub thermostats

The rheometer was equipped with internal memory and the system for research programme generation. Figure 3 presents the algorithm of the ReolabQC rheometer external control. The rheometer may be externally controlled by a computer which allows for creating and editing measuring programmes, which makes possible optional and multiple parameter setting and saving them without the necessity of deleting.

RESULTS AND DISCUSSION

Figures 4 through 5 show the results of research on determining the effect of temperature on dynamic viscosity.

CONCLUSIONS

Dynamic viscosity of B100 SBME Biodiesel in the temperature range from 50 to -20ºC assumes the values from c.a. 10 to 173 [mPas]. Dynamic viscosity of B50 SBME Biodiesel at 50ºC was 9[mPas]. When the temperature was decreasing its value was increasing and at -20ºC reached 67[mPas]. Dynamic viscosity for B20 SBME Biodiesel at 30ºC was 8,5[mPas], but with cooling fuel sample it was growing to reach 35[mPas] at -20ºC. Dynamic viscosity of diesel oil (B7), in the temperature range from 50 to -20ºC assumes the values from c.a. 7,8 to 17 [mPas]. Conducted research demnstrated that dynamic viscosity of "B" biofuels is considerably affected by the temperature. Therefore, for a better assessment of the effect of SE engine feeding with biofuels on the durability and reliability of the injection apparatus, not kinematic but dynamic viscosity should be considered. It is important because the changes of dynamic viscosity illustrate the actual changes of the flow resistance accompanying engine feeding with biofuels and biocomponents. Currently conducted research focuses on introduction of a proper standard for determining dynamic viscosity of fuels and biofuels. There are standards for rotation rheometers by means of which dynamic viscosity and other parameters, including surface tension, shearing forces, shearing rate or shearing tension may be highly precisely determined, which will make possible a better analysis of rheological properties of fuels and biofuels.

REFERENCES

1. **Cieślikowski B., Juliszewski T., Mazurkiewicz J., 2006:** Lepkość kinematyczna biopaliwa i fazy glicerynowej. Inżynieria Rolnicza, vol. 12, 59-65.
2. **Cisek J., Mruk A., Hlavňa V. 2011:** The properties of a HDV Diesel engine fuelled by crude rapeseed oil. Teka Komisji Motoryzacji i Energetyki Rolnictwa, Vol. XI, 29-39.

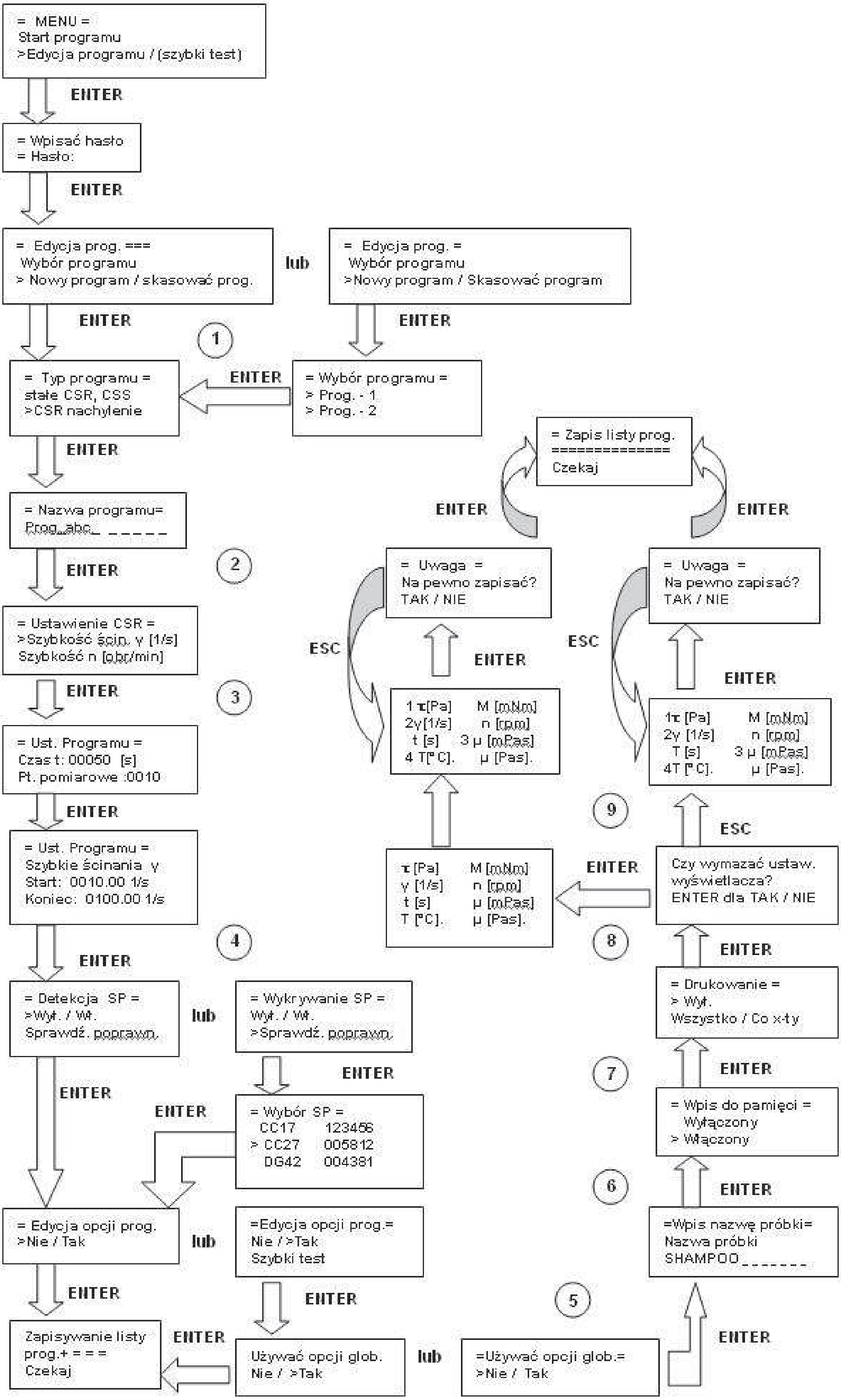

Fig. 3. The algorithmic work schemata is using the reometer ReolabQC

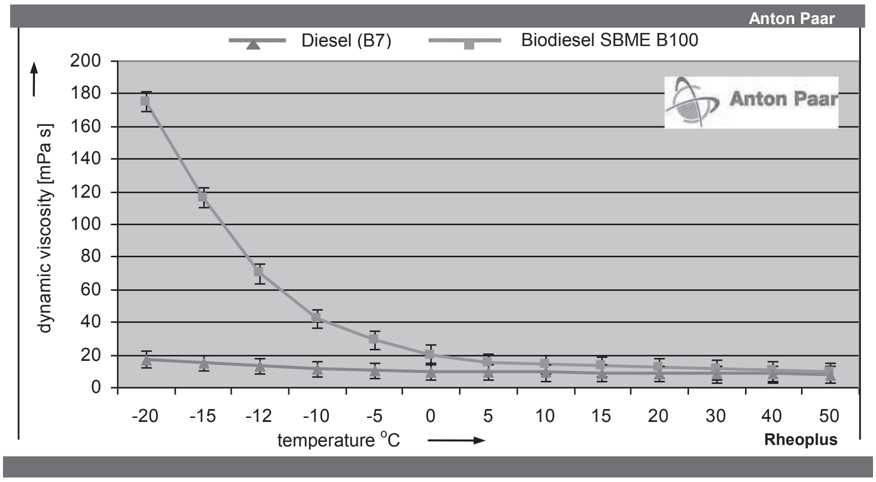

Fig. 4. Diagram of B100 SBME and Diesel (B7) dynamic viscosity dependence in the function of temperature

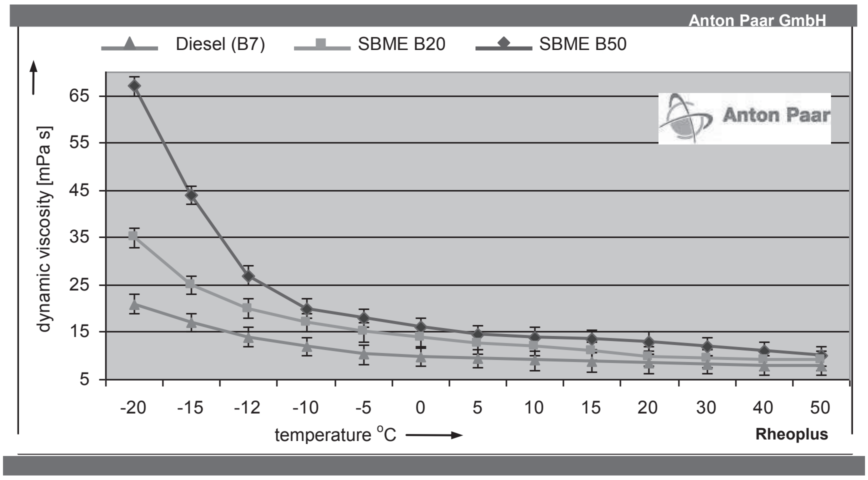

Fig. 5. Diagram of B50, B20 SBME and Diesel (B7) dynamic viscosity dependence in the function of temperature

3. **Cisek J., Mruk A. 2012:** Właściwości silnika ZS zasilanego naturalnym olejem rzepakowym. Zeszyty Naukowe Instytutu Pojazdów Politechniki Warszawskiej z serii Mechanika Ekologia Bezpieczeństwo Mechatronika, Vol. 1(87)/2012, 5-16.
4. Biodiesel 2006, Handling and Use Guidelines. U.S. Department of Energy, Third Edition, September 2006.
5. BRONIARZ-PRESS L., Różańska S., Kmiecik J., 2013: Analiza reologiczna paliw i biopaliw ciekłych. Ap. Chem. 52, 3, 159-16.
6. **Uzdowski M. 2006:** Możliwości wykorzystania mieszanin paliw tradycyjnych i alternatywnych do zasilania silników ZS. Motrol Vol. 8A. 280-285.
7. **Tys J. i in. 2003:** Technologiczne i ekonomiczne uwarunkowania produkcji biopaliwa z rzepaku. Instytut Agrofizyki im. Bohdana Dobrzańskiego PAN w Lublinie.
8. **Szlachta Z., 2002:** Zasilanie silników wysokoprężnych paliwami rzepakowymi. 2002, WKiŁ.
9. **Szlachta Z., Zabłocki M., Cisek J. Sowa. K., 1995:** Badania wpływu paliw z oleju rzepakowego na rozruch i pracę silników wysokoprężnych w niskich temperaturach otoczenia. Badania wykonane w ramach projektu KBN nr 9 S604 013 04. Kraków 1995. Sprawozdanie IPSiSS PK, nr 490/KBN/95 (mat. nie publikowane).
10. Standard DIN 53019 - Układ pomiarowy reometru o cylindrach współosiowych.
11. Polish Standard PN-EN 590:2011. Paliwa do pojazdów samochodowych - Oleje napędowe - Wymagania i metody badań. Polish
12. Standard PN-EN ISO 3104:2004. Przetwory naftowe. Ciecze przezroczyste i nieprzezroczyste. Oznaczanie lepkości kinematycznej i obliczanie lepkości dynamicznej.
13. **Wcisło G. 2008:** Wyznaczenie wpływu temperatury na lepkość dynamiczną biopaliw roślinnych. Inżynieria Rolnicza, vol. 10 (108), 277-282.
14. **Wcisło, G. 2013:** Analiza wpływu odmian rzepaku na własności biopaliw RME oraz parametry pracy silnika o zapłonie samoczynnym. Monografia habilitacyjna. Wydawnictwo FALL, Kraków.
15. **Wcisło, G. 2005:** Determining Energy Value of Biodiesel FAME. Materiały z konferencji PTNSS KONGRES – 2005, "Combustion Engines", 93.
16. **Wcisło G. 2009:** Determining Rheological Properties of CSME Biodiesel Type Biofuels, „Combustion Engines", Vol. 2009-SC1, 20-25.
17. Ustawa z dnia 25 sierpnia 2006 r. o biokomponentach i biopaliwach ciekłych (Dz. U. 2006 nr 169 poz. 1199 z późn. zm.)

OKREŚLENIE WŁASNOŚCI REOLOGICZNYCH BIOPALIW ZAWIERAJĄCYCH BIOKOMPONENT SBME

Streszczenie. Lepkość dynamiczna Biodiesla B100 SBME w zakresie dodatnich temperatur w zasadzie rośnie wraz z obniżaniem temperatury, podobnie jak oleju napędowego (B7). Natomiast po przekroczeniu -10oC zaczyna gwałtownie rosnąć. Lepkość dynamiczna w temperaturze -20oC B100 SBME wynosiła 173mPas, B50 SBME 67mPas, natomiast B50 SBME 35mPa. Przeprowadzone badania pokazały, że w praktyce B100 CSME nie może być stosowane jako samoistne paliwo, bez zastosowania pakietu dodatków obniżających lepkość.Natomiast dla biopaliw typu B5 i B20 wartości lepkości szczególnie w zakresie dodatnich temperatur są zbliżone do lepkości oleju napędowego. W takich warunkach bez obaw można używać B7 i B20 do zasilania silników z zapłonem samoczynnych nawet posiadających nowoczesną aparaturę wtryskową.

Słowa kluczowe: silnik wysokoprężny, Biodiesel, biopaliwo, SFME, lepkość dynamiczna, szybkość ścinania.

TEKA. COMMISSION OF MOTORIZATION AND ENERGETICS IN AGRICULTURE – 2014, Vol. 14, No. 4, 191–196

The Determination of Energetic Potential of Waste Wood Biomass Coming from Dębica Forestry Management Area as a Potential Basis for Ethanol Biofuels of II Generation

[1]Grzegorz Wcisło, [2]Natalia Labak

[1]Faculty of Production Engineering and Power Technologies
University of Agriculture in Krakow, Poland
[2]PhD student at the University of Agriculture in Krakow, Poland

Received December 08.2014; accepted December 19.2014

Summary. The goal of this study was to determine the heat of combustion (top calorific value) and the determination of fuel value (bottom calorific value) of waste wood biomass of potential raw material for the manufacture of ethanol biofuels of second generation. There determined the energy potential of waste wood biomass, which may be obtained for energy purposes from the territory of Dębica Forest Management Area. The highest heat of combustion and calorific value among the studied five species of forest wood: pine, birch, oak, ash and poplar featured pine – 21,3 MJ/kg (19.1 MJ/kg), and the lowest oak – 18.5 MJ/kg (16.58 MJ/kg). From the above results, that the calorific value (similarly to heat of combustion) of pine is approx. 15% The fuel value of wood obtained yearly by the Dębica Forest Management Area over 6 years (2005-2011) is 38, 6 PJ.

Key words: biomass, ethanol, biofuels of II generation, heat of combustion, top calorific value.

INTRODUCTION

The quick economic development, which took place in the second half of the twentieth century, brought about a modification in the use of energy raw materials. A new model of global economy was shaped, which is mainly based on oil and earth gas, with decreasing use of black coal. The energy industry has the biggest share in emission of greenhouse gases into the atmosphere. In Poland the manufacture of electric energy is based mainly on black coal (60.8%), lignite (34.9%), earth gas (1.6%) and renewable energy sources (in total 2.8%) [4,8,9,10]. Unfortunately the energy sector based on oil and coal causes excessive emissions of the so called greenhouse gases, mainly CO_2 [11,14]. For that reason in recent year more and more emphasis is put on efforts to limit the emission of undesirable gases. The European Union published several documents, that order a gradual replacement of mineral fuels with renewable ones. The 2001/77/CE directive states, that until 2020 the share of renewable energy in the total balance of consumed energy shall be 20%.

In Poland since 2007 it has been legal to manufacture fuels and introduce them into free circulation. Manufactured are biofuels of first generation, that is mainly biodiesel and bioethanol, and they are introduced as biofuels and fuel additives. In 2014 the average share of biofuels and fuel bioadditives of the total fuel consumption amounted to at least 7.1%, considering energy value in relation to Diesel fuel and petrols. Simultaneously with the manufacture of first generation biofuels works have been started on new generation biofuels, the so called second generation. One of the objectives of the new biofuels was to manufacture them from nonfood sources. Bioethanol may be manufactured of forestry and agricultural biomasses, which include cellulose and lignocellulose. A very interesting idea seems to be the use of forestry wood waste.

For Europe the main sources of biomass with cellulose and lignocellulose content are forests. For that reason it is today important to assess the energy potential of wood waste biomass. This is also of local importance, because at locations with large resources of cellulose biomass in future will be constructed manufacturing facilities of second generation biofuels for transport. The development of the above fuels will cause partial independence from oil supplies and generate new jobs, and what is most important, it shall favourably influence the environment. At present the area of forests in Poland is 9,048 thousand hectares, which corresponds a forestation rate of 28.9% [5,6]. In 2011 the area of forests in Poland was 9,143.6 thousand hectares (according to GUS (Polish national statistical agency) – the condition as of 31.12.2011), which was equivalent to 29.2% forestation rate [6].

THE CHARACTERISTICS OF THE STUDIED DĘBICA FOREST MANAGEMENT AREA

The Dębica Forest Management Area is located in Podkarpackie Province, Districts of Dębica and Sędziszów – Ropczyce. The Forest Management Area includes two forest circuits – Dębica and Żdżary and is divided into eleven forestries. The total Forest Management Area comprises 11,126 hectares (forest area 10,941 hectares). In addition the Dębica Forest Management Area supervises forests, which do not belong to the State Treasure, of total area of 7,617 hectares – Fig. 1. The main forest species are : pine 50.5%, beech 29.3 %, fir 7.9 %, oak 6.7%.

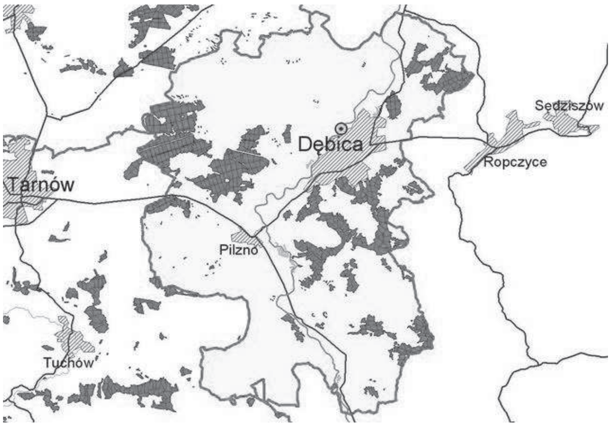

Fig. 1. The natural and geographic location of the Dębica Forest Management Area

CHARACTERISTICS OF WOOD WASTE BIOMASS WITH REFERENCE TO ITS ENERGY PROPERTIES

Wood waste biomass displays the most favourable parameters in relation to volume among the types of biomass used for energy purposes. The cost of energy obtained from wood waste biomass is decisively lower as compared with traditional sources. If we adopt the cost of energy obtained from wood at the level of 6.03 gr/KWh (gr =1/100 PLN) as 100% in particular conditions, then the cost of energy obtained from burning of coke is 169% of that value, from burning of liquid gas and earth gas 246 % and 170-195% of that value respectively, and from burning of black coal 94 % of that value, without the cost of transport [12,13,17].

The share of particular components with wood waste biomass differs depending on species (Table 1). Particularly worth noting is the difference when comparing wood of conifers and deciduous trees. This aspect is reflected both in the cost of transport, effectiveness of wood burning process as well as mineral content of ash remained after burning.

Table 1. Percentage share of wood, green mass and bark with particular wood waste biomass species [2]

Wood waste biomass	Wood [%]	Green mass [%]	Bark [%]
Deciduous trees	60-75	15-20	10-20
Conifers	70-80	10-15	10-15

By using the PER (Pure Energy Ratio) expressed as relations between obtained energy and consumed energy we are able to determine the economic value of a particular fuel. For coal the value of this ratio is included between 10 and 15, for oil it amounts to 20, and for phytomass and fuels manufactured from it is between 0.5 and 1.5 [1]. The low value of this coefficient results from high energy outlays related to use, forestation, transport and processing of these raw materials.

Wood waste biomass features in comparison with other traditional fuels two undoubted advantages:

– the unceasing reproducibility of wood in forests,
– its availability in our geographic conditions [2].

According to studies the calorific value of dry forest wood biomass is on the average lower with approx. 20% as compared with calorific value of black coal and with approx. 50% lower than calorific value of fuel oil (37.7 MJ/kg) and earth gas 36.8 MJ/m³) [3].

Average humidity of deciduous wood directly after clearing reaches 80 %.

Wood waste biomass burns easily and is a valuable fuel, if dried properly. Wood dried outdoors in a natural way contains 15-20% total humidity. When burning wood with excessive content of humidity problems can occur with igniting, that is its ignition time will be longer and it will be more difficult to reach proper boiler efficiency [15]. In Fig. 2 was presented the relation between wood calorific value and total humidity.

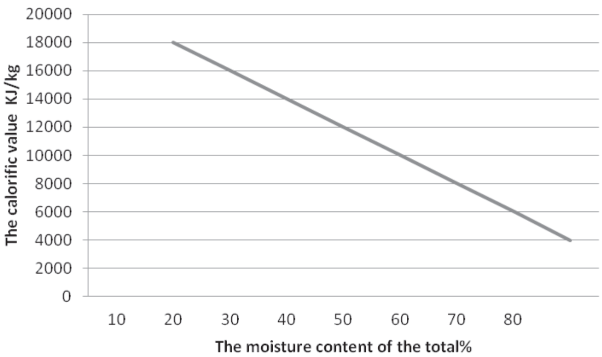

Fig. 2. Calorific value as function of total humidity content in wood (Voltz 1995)

CHEMICAL COMPOSITION OF WOOD WASTE BIOMASS

Generally the chemical composition of particular wood species is similar, and consists of (dry mass): coal (48-51%), oxygen (42-45%), hydrogen (6-7%), nitrogen (0.01-3%)

Besides wood, the wood waste biomass is composed of green mass (leaves, branches, needle cover) and bark. Ashes in bark constitute 1-1.5%, and in wood 0.4 -0.7%. Ashes include nutrients, which occur in the form of microelements and oxides, like: K_20, Na_2O, P_2O_5, CaO, MgO. The content of selected microelements is presented in Table 7. Besides the specified components the wood waste biomass includes: resins, tannins, waxes, fats, alkaloids and mineral salts [2].

Due to large content of volatile parts (80-85%) wood ignites easily. Most part of volatile components are emitted at temperatures 250-350°C, but the process of thermal decomposition of wood starts at approx. 210°C.

OBJECTIVE AND SCOPE OF THE WORK

The goal of this study was to determine the heat of combustion (top calorific value) and the determination of fuel value (bottom calorific value) of waste wood biomass of potential raw material for the manufacture of ethanol biofuels of second generation. There will be determined the energy potential of waste wood biomass, which may be obtained for energy purposes from the territory of Dębica Forest Management Area. The obtained results shall be used in the above Forest Management Area in order to develop a long term waste wood management strategy. The wood biomass studied in order to determine energy parameters was dried to reach the technical humidity of 8%.

APLLIED METHOD

The goal of the study was the determination of energy potential of waste wood biomass, which is a potential raw material for the manufacture of ethanol biofuels of II generation of cellulose biomass obtained from wood in the Dębica Forest Management Area. The basis for the determination of these parameters was the determination of heat of combustion when burning wood samples coming from the above Forest Management Area. The study included the following species of wood present in the Dębica Forest Management Area: Scots pine (Pinus sylvestris), warty birch (Betula pendula), English oak (Quercus rubra), ash (Fraxinus tremula), poplar (Populus tremula). The material was collected without bark from top part of bolt or log. Then the material was comminuted and dried using H SPT-200 Vacuum Drier to reach the technical humidity of 8%.

DETERMINATION OF HEAT OF COMBUSTION AND CALORIFIC VALUE OF FIVE FOREST WOOD SPECIES

The study was performed in compliance with Polish standards PN-86/C-04062 and PN-81/G-04513 Solid fuels, determination of heat of combustion and calorific value in force [16,17]. Heat of combustion was determined using automatic KL-10 calorimeter manufactured by „Precyzja Bit" company. The diagram of the calorimeter is presented in Fig 3.

DETERMINATION OF TOP HEAT OF COMBUSTION (CALORIFIC VALUE)

The determination of heat of combustion in the calorimeter is based on the simplified equation of thermal balance of the calorimeter presented below:

$$Q_c^a\, m_{pal} + Q_d m_d = (m_w c_w t + m_s c_s)\, \Delta t = K\Delta t$$

where:
Q^a_c – heat of wood combustion related to the analytical sample,
m_{pal} – weight of wood sample,
Q_d – heat of combustion of steel wire,
m_d – weight of wire,
m_w – weight of water in calorimetric vessel,
c_w – specific heat of water,
m_s – weight of solid bodies of calorimeter – bomb and vessel,
c_s – specific heat of solid bodies,
Dt – corrected temperature increase,
K – constant, thermal capacity of calorimeter.

Heat of combustion was determined by the calorimeter using the following relation:

$$Q_c^a = \frac{K\Delta t}{m_{pal}}$$

Calorific value was calculated on the basis of the previously determined heat of combustion. The calorific value was referred to the analytical condition and calculated using the formula below:

$$Q_w^a = Q_c^a - \frac{m_{H2O}}{m_{pal}} \cdot r\ ,$$

where:
Heat of evaporation r = 2500 kJ/kg. The sum of water weights related to fuel humidity and weight of water from burning of hydrogen included in fuel is the quantity of water after condensing, that is analytical humidity expressed in humidity kg/ wood kg.

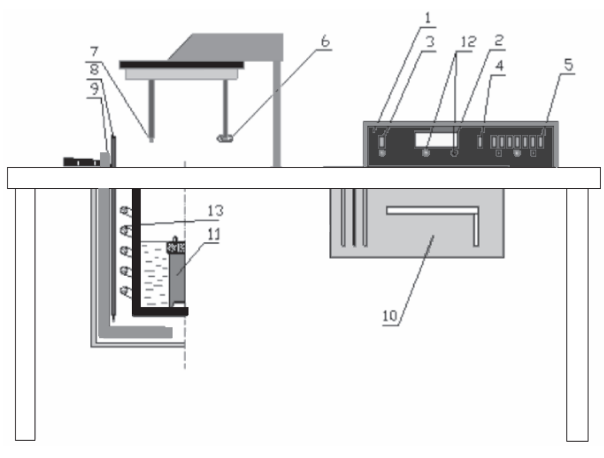

where:
1. control unit,
2. display of heat of combustion,
3. computer system computer system,
4. digital display,
5. agitator,
6. calorimetric bomb,
7. electric switch,
8. thermometer,
9. signalling diodes,
10. start of measurement,
11. water mantel thermometer,
12. agitator of water mantel,
13. coil.

Fig. 3. Schematic diagram of KL10 calorimeter.

Using stoichiometric equations we are able to calculate, that from 1 kg hydrogen we can obtain 9kg water, that is 9h, which can be presented using the formula below :

$$\frac{m_{H2O}}{m_{pal}} = 9h^a + W^a \frac{kgH_2O}{kgpaliwa}$$

As a result we obtained the relation for calculating calorific value, when we know the heat of combustion

$$Q_w^a = Q_c^a - r(9h^a + W^a)$$

From the above relations results, that in order to determine the calorific value it is necessary to know the content of hydrogen and analytical humidity in the studied fuel.

TEST RESULTS

In Fig. 4 we presented test results for the determination of calorific value and calculation of heat of combustion of studied forest wood species at absolute humidity of 8%.

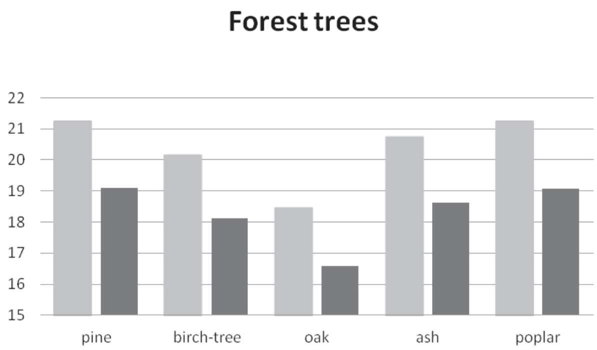

Fig. 4. Comparison of heat of combustion and calorific value of studied forest trees at humidity of 8%

The highest calorific value among the studied wood waste biomass shows pine (Pinus sylvestris) – 19.1 MJ/kg, and a lower one oak (Quercus rubra) – 16.58 MJ/kg. From the above results, that the calorific value of pine (as well as heat of combustion) is approx. 15% higher as compared with calorific value of oak. A probable cause, that pine wood gives more energy than oak wood is the fact, that it contains more volatile oils and resins, which considerably increase its calorific value [2].

The calorific value of wood depends on its type, humidity and processing form. Despite the fact, that wood transactions are settled almost exclusively in volume units – cubic meters, generally its calorific value is determined by its specific mass. For example a cut down pine has density of 700 kg/m³, but in totally dry condition its density falls to 480 kg/m³.

For energy purposes it is best to use dry wood, however sometimes the waste wood biomass stored for energy purposes features different humidity. A material, which has already been dried, for example in periods with heavy rains or in winter can become moist and will feature a lower calorific value. To illustrate, what the influence on calorific value of wood from forest trees humidity can have, taking into consideration the already obtained test results, theoretical calculations of calorific values of particular wood species at assumed humidity of 20, 30 and 40% respectively were performed. The results of calculation were presented in Table 2 and in the figure was presented the influence of humidity on calorific value of wood species at humidity of 8 %.

Table 2. Humidity impact on calorific value of particular wood species.

Type of wood	Bottom calorific value [MJ/kg]			
	at 8% humidity	at 20% humidity	at 30 % humidity	at 40 % humidity
Pine	19,10	16,805	14,895	12,985
Birch	18,11	15,938	14,127	12,316
Oak	16,59	14,595	12,936	11,278
Ash	18,63	16,393	14,530	12,667
Poplar	19,08	16,794	14,886	12,977

In compliance with statistical information made available by the Dębica Forest Management Area, knowing the percentage share of particular wood species in the whole waste wood biomass obtained yearly by the above management area was calculated the total calorific value for all species that constitute the forest stand of the above

Table 3. Energy potential of waste wood biomass obtained in subsequent years by the Dębica Forest Management Area .

Energy potential of wood obtained in subsequent years				
Year	Quantity of wood obtained in the subsequent years [m³]	Calorific value of wood [MJ]	Calorific value of wood [GJ]	Electric energy [MWh]
2005	40 737	3880570588	3880570.59	1077936.27
2006	52 838	5033301145	5033301.14	1398139.21
2007	58 405	5563608641	5563608.64	1545446.84
2008	70 102	6677854515	6677854.51	1854959.59
2009	62 266	5931404086	5931404.09	1647612.25
2010	59 806	5697066662	5697066.66	1582518.52
2011	60 890	5800327543	5800327.54	1611202.1
In total	405 044	38584133179	38584133.2	10717814.8
Average yearly result	**62 944**	**5995989766**	**5995989.77**	**1665552.7**

management area. The results are presented in Table 3 below.

From Table 3 results, that the calorific value of wood calculated in [GJ] from the total of wood obtained yearly by the Dębica Forest Management Area over the period of 6 years (2005-2011) is 38584133.2 [GJ], as a result of the assumption, that 1MWh = 3600MJ, the obtained in this period biomass is equal to electric energy of 10,717,814.8 MWh over a period of six years, and expressed as average yearly quantity it is 1,665,552.7 MWh, which converted into [GJ] yields yearly 5,995,989.7 energy.

In Table 4 were summarised test results, which show, what is the calorific value of the biomass from all sorts of waste wood at the example of year 2010.

Table 4. Energy potential of all sorts of waste wood obtained yearly by the Dębica Forest Management Area at the example of year 2010.

Energy potential of waste wood		
Type of obtained assortment from waste wood	Year 2010 [m³]	Calorific value [GJ]
Dead wood from standing trees	3,465	478,170
Dead wood from lying trees	4,398	606,924
Dead wood from twigs	23,265	3,210,570
Dead wood from stumps and roots	129,417	17,859,546
In total	160,545	22,155,210

The calorific value of all assortments of waste wood obtained by the Dębica Forest Management Area at the example of year 2010 was 22,155,210 GJ.

CONCLUSIONS

1. The state owned National Forests (Lasy Państwowe) enterprise is able to deliver wood waste biomass for energy purposes in the form of different assortments such as: small dimensioned wood, rests from clearings, windfall wood, fuel wood and low quality pulp wood in case of natural disasters (hurricanes, floods, insect pest infestations), wood of higher quality for protection reasons, in order to prevent their depreciation in the forest.
2. Forest wood waste biomass is a perfect raw material for the manufacture of ethanol biofuels of II generation, because it is possible to obtain large quantities of biomass with cellulose and lignocellulose content.
3. The highest heat of combustion and calorific value among the studied five species of forest wood: pine, birch, oak, ash and poplar featured pine – 21,3 MJ/kg (19.1 MJ/kg), and the lowest oak – 18.5 MJ/kg (16.58 MJ/kg). From the above results, that the calorific value (similarly to heat of combustion) of pine is approx. 15% higher than the calorific value of oak. The probable cause of the fact, that pine wood has higher energy value than oak wood, is because pine has more volatile oils and resins which considerably increase its calorific value.
4. The fuel value of wood obtained yearly by the Dębica Forest Management Area over 6 years (2005-2011) is 38,584,133.2 GJ. This amount of energy equals 10,717,814.8 MWh electric energy. An average based on medium yearly result of 1,665,552.7 MWh is equal to 5,995,989.7 GJ energy.
5. The fuel value of all assortments of waste wood obtained by the Dębica Forest Management Area at the example of year 2010 totalled 22,155,210 GJ.

REFERENCES

1. **Bučko, J., Osvald, A, 1997**: Rozklad dreva teplom a ohňom. TU vo Zvolene, 100
2. **Domański M., i inni, 2007**: Drewno jako materiał energetyczny. Wydawnictwo SGGW. Warszawa.
3. **Glijer L., 1999**: Procesy spalania i walory środowiskowe wykorzystania drewna do celów grzewczych. Post. Tech. Leś. nr 72, 8–22.
4. **Laurów Z., 2003**: Wykorzystanie surowca drzewnego do celów energetycznych. Biblioteczka leśniczego. Zeszyt nr. 183.
5. **GUS, 2004**: Ochrona Środowiska. Warszawa.
6. **GUS, 2008**: Ochrona Środowiska. Warszawa.
7. **GUS, 20011**: Ochrona Środowiska. Warszawa.
8. **Janowicz L., 2006**: Biomasa w Polsce. Energetyka i Ekologia.
9. **Łukasik A., 2008**: Szanse dla robinii w Polsce. Trybuna Leśnika nr. 12/2008
10. **RDLP w Katowicach**, 2012: Nadleśnictwo Kobiór Plan Urządzania Lasu na okres 01.01.2003- 31.12. 2012
11. **Romer E., 1999:** Regiony klimatyczne Polski. PWTN, ser. B, nr 20, Wrocław.
12. **Trampler T i in., 1990**: „Regionalizacje Przyrodniczo-Leśna na podstawach ekologiczno-fizjograficznych." PWRiL, Warszawa.
13. **Wisz J., Matwiejew A., 2005**: Biomasa- badania w laboratorium w aspekcie przydatności do energetycznego spalania. Energetyka 2005
14. **Zamorowski K., 2006**: Współspalanie biomasy w kotle rusztowym. Energetyka nr 01.
15. **Voltz K. R., 1995**: Holtz-Rohstoff der Zukunft. Holtz-Zentralblatt, Stutgart nr. 147: 2459-2460.
16. **PN-86/C-04062**: Paliwa ciekłe. Oznaczanie ciepła spalania i wartości opałowej.
17. **PN-81/G-04513**: Paliwa stałe. Oznaczanie ciepła spalania i wartości opałowej.

OKREŚLENIE POTENCJAŁU ENERGETYCZNEGO DENDROMASY ODPADOWEJ POCHODZĄCEJ Z NADLEŚNICTWA DĘBICA JAKO POTENCJALNEJ BAZY DLA BIOPALIW ETANOLOWYCH II GENERACJI

Streszczenie. Celem pracy było oznaczenie ciepła spalania (wartości opałowej górnej) oraz wyznaczenie wartości opałowej (wartości opałowej dolnej) biomasy z drewna odpadowego potencjalnego surowca do produkcji biopaliw etanolowych II generacji. Następnie zostanie określony potencjał energetyczny dendromasy jaki można pozyskać na cele energetyczne z terenu

Nadleśnictwa Dębica. Najwyższym ciepłem spalania i wartością opałową wśród przebadanych pięciu gatunków drzew leśnych: sosna, brzoza, dąb, jesion i topola charakteryzowała się sosna – 21,3 19,1 MJ/kg (19,1 MJ/kg), natomiast najmniejszą dąb – 18,5 MJ/kg (16,58 MJ/kg). Wartość opałowa drewna pozyskiwanego corocznie przez Nadleśnictwo Dębica na przestrzeni 6 lat (2005-2011) wynosi 38, 6 PJ.

Słowa kluczowe: biomasa, etanol, biopaliwa II generacji, ciepło spalania, wartość opałowa.

TEKA. COMMISSION OF MOTORIZATION AND ENERGETICS IN AGRICULTURE – 2014, Vol. 14, No. 4, 197–200

Determination of the Impact of the Type of Camelina Oil Used for Production of Biofuels on the Fractional Composition of CSME

[1,2]Grzegorz Wcisło, [2]Bolesław Pracuch

[1]Faculty of Production Engineering and Power Technologies, University of Agriculture in Krakow, Poland
[2]BioEnergia Małopolska Centre for Renewable Energy Sources, Poland
e-mail: Grzegorz.wcislo@ur.krakow.pl

Received December 08.2014; accepted December 19.2014

Summary. The aim of the study was to determine the impact of the frying process on the fractional composition of CSME Biodiesel in comparison to the CSME obtained from unused (fresh) camelina oil. The freshly pressed camelina oil was divided into two portions. One was used for frying chips at 190°C for a period of 10 hours. The study showed the CSME biodiesel produced from unused (pure) camelina oil generally has better distillation properties. The temperatures at the start of distillation were similar for both of the CSMEs. Within the 30-70% mid-range temperatures, the CSME produced from the used cooking camelina oil was characterized by higher distillation temperatures for the same volume of fuel. The largest differences were observed for the 90% and 95% distillation temperatures and the final temperature of the distillation process. This may testify to lower purity of the CSME produced from the used cooking oil. In such a biofuel there may be more less volatile mono- and diglycerides or other chemicals which e.g. remain in the oil after frying. It must be said, though, these are not solid particles, as those were separated from the oil through filtration.
Key words: Biodiesel, Biodiesel, diesel engine , fractional composition, temperature distillation.

INTRODUCTION

In accordance with the Act on bio-components and liquid fuels (adopted by the Polish Sejm on 25 August 2006), biofuels may be produced and marketed legally in Poland as of 1 January 2007. So far the country has launched 10 major installations intended for the production of FAME (RME) biofuels, whose total production capacity is estimated to be as high as 1 million tonnes of esters a year. On the other hand, the annual national demand for diesel fuel is around 7.5 million tonnes per year. The use of a fuel additive in the form of 6% (v/v) of bio-component necessitates production of approx. 450,000 tonnes of esters per year.

Recently, there has been a great interest among individuals, including farmers, as well as companies and institutions being in possession of vehicle fleets in the possibility of producing biofuels for their own purposes. Under the law currently applicable in Poland, one may legally produce biofuels for their own purposes. Among especially privileged groups are farmers, who are allowed to produce raw material for the production of biofuels for their purposes, which significantly reduces the production cost for this energy carrier.

FAME Biodiesel is obtained in the process of transesterification. Its parameters deviate slightly from those of the diesel fuel, however, if the transesterification process is carried out properly, the resulting biofuel can be used as an additive in the form of a diesel bio-component or used as a 100% pure fuel. B100 FAME biodiesel has better parameters compared to the diesel fuel: higher cetane number, better lubricating properties, higher ignition temperature and low sulfur content [3,4,6].

One of the principal parameters used for assessing the suitability of FAME biodiesels for compression-ignition engines is the fractional composition, which is the reason why this very subject was chosen for investigation by the authors of this paper. The aim of the research presented below was to determine and compare the fractional compositions of two CSME biofuels: one produced from pure camelina / canola oil and the other derived from the same oil but used in the process of frying chips in a restaurant for a period of one week. When used in frying, the oil was heated to the temperature of 190°C.

A growing demand for biofuels produced mainly from rape-seed oil makes producers search for new alternative plants, Gold of pleasure (Camelina Sativa), a dicotyledon belonging to brassicas (plants of the cabbage family) being one of them [10,11,12]. As far as soils are concerned Gold of pleasure is undemanding, compared with oilseed rape, and can be grown on soils of the 5th and 6th classes. Around 700dm^3 of oil can be obtained from 1 hectar of land while applying a one-step method of cold pressing [9]. Biofuel of the CSME Biodiesel type (Camelina Sativa Methyl Esters) was produced in a GW-10 reactor constructed by one of the authors (G.W).

PRODUCTION OF RME BIOFUELS IN THE PROCESS OF TRANSESTERIFICATION FROM PURE OIL AND USED OIL

Calculating the optimum (stoichiometric) amount of reactants needed to carry out the transesterification process usually involves the usage of simplified models [5]. However, in order to determine the appropriate amount of reactants needed to produce RME, the authors of this paper used a model developed by one of the co-authors, which makes it possible to optimally determine the quantities of methyl alcohol and the catalyst necessary for the process of transesterification – Fig. 1 [7]. The following ratio was used for the purpose of transesterification of canola oils: for each 1 dm^3 of oil, a mixture obtained from dissolution of 7.5g of KOH in 0.15 dm^3 of CH3OH was used. Transesterification was performed in a single step, with the temperature of the start of the process being 50ºC. P.a. purity CH_3OH methyl alcohol of a molecular weight of 32.04 g/mol was used for the transesterification process, along with p.a. purity KOH potassium hydroxide with a molecular weight of 56.11 g/mol as the catalyst.

Methyl alcohol (methanol) was used for transesterification of Gold of pleasure oil with alkaline potassium hydroxide (potassium hydroxide pure p.a.) as a catalyst in the reaction.

The process of transesterification was carried out in two stages and the obtained degree of oil transition into methyl esters was equal to 97.2% (m/m). The result has proved that the obtained CSME biofuel complies with EN 14214 standards of biofuel for a high pressure engine, as regards the ester content in FAME (Fatty Acid Methyl Esters).

DETERMINATION OF THE IMPACT OF THE TYPE OF CAMELINA OIL USED FOR BIOFUEL PRODUCTION ON THE FRACTIONAL COMPOSITION OF CSME BIODIESEL

A very important parameter used for the assessment of fuel/biofuel operating properties is their fractional composition. Said parameter is determined on the basis of the temperatures of distillation. The temperature of fuel ignition in an engine largely depends on the temperature of the start of distillation and the amount of fuel vaporised in the initial stage of distillation. The higher content of lightweight fractions is, the better self-igniting properties are, which translates directly into gentler way of starting the engine [8, 13, 14].

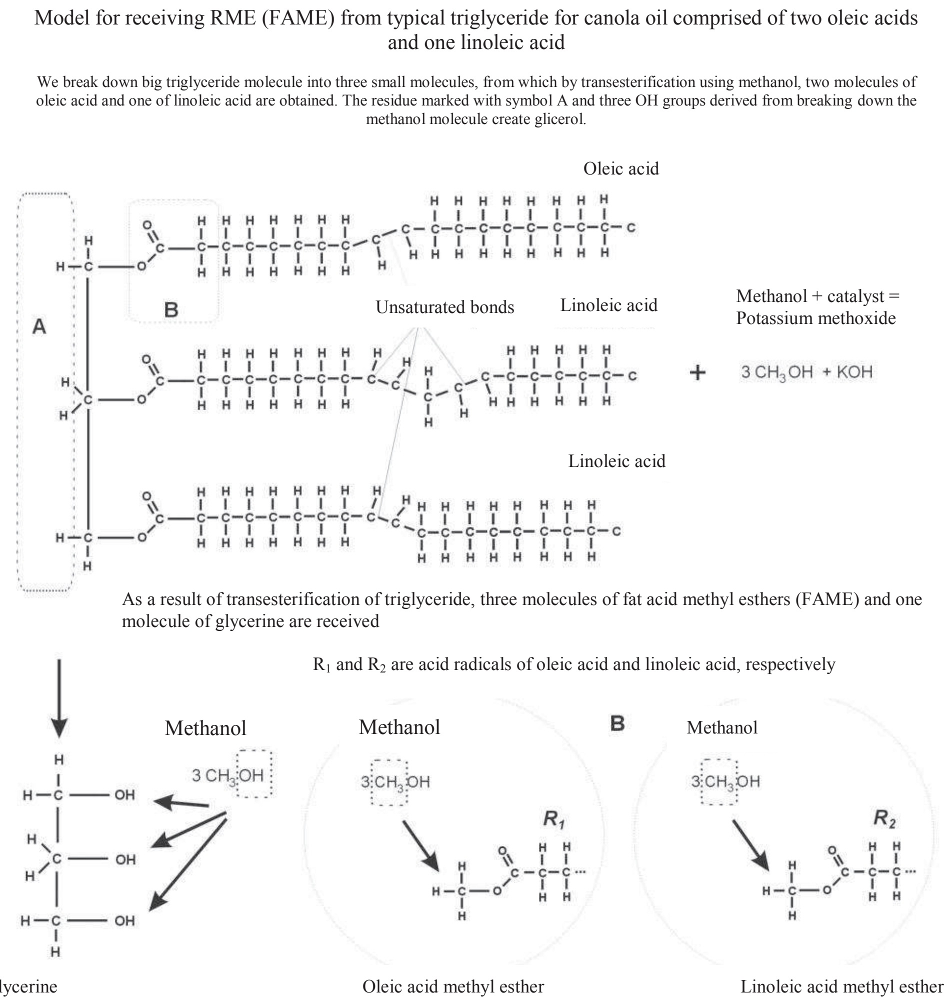

Fig. 1. Diagram of rapeseed oil transesterification

Vegetable oils have worse distillation properties, and thus worse engine-starting properties, compared to FAME [1, 2, 7].

In order to achieve proper starting and combustion properties, it is very important to establish five points. These are: the temperature at the start of distillation, the temperature for distillation of 10% (v/v) fuel, the temperature for evaporation of 65% (v/v) fuel, the temperature for distillation of 95% (v/v) fuel and the temperature at the end of the distillation process.

The research determining the fractional compositions of CSME biofuels obtained from pure and used canola oil was carried out in the biofuels laboratory of “BioEnergia” Malopolski Centre for Renewable Energy Sources at a workstation equipped with a camera for determining the composition of the fuels and biofuels with the method of normal distillation – Fig 2.

Fig. 2. Photo bench equipped with a distiller HAD 620/1 by Herzog

RESULTS

Table 1 summarizes the results of the research determining these distillation properties of CSME B100 Biodiesels. For comparison purposes, the table shows the results of the research on the distillation temperatures of RME B100 Biodiesel obtained from BLISKA service station chain owned by PKN ORLEN group and Ekodiesel fuel obtained from PKN ORLEN group service stations.

Table 2 summarizes the values of the most important points of the distillation curve for RME Biodiesels obtained from both of the canola oils, i.e. the temperatures at the start and end of the distillation process and the percentage (v/v) of distilled fuels at or below 250°C and 350°C.

Table 1. Comparison of distillation temperatures for two CSME Biodiesels and RME Biodiesel from BLISKA service stations and diesel fuel

% [v/v] of distillation	CSME Biodiesel from pure oil	CSME Biodiesel from used oil	RME Biodiesel BLISKA	ON
0	306	308	304	178
5	314	315	310	192
10	322	322	319	202
15	334	336	334	216
20	341	343	339	222
25	346	347	345	234
30	351	356	347	241
35	355	361	349	248
40	358	363	351	255
45	362	367	352	263
50	364	370	356	270
55	365	372	358	279
60	368	375	360	287
65	370	377	361	295
70	372	379	362	305
75	373	381	363	313
80	376	383	365	322
85	379	387	368	333
90	381	392	370	341
95	384	395	372	353
100	391	402	389	361

Table 2. Characteristic distillation curve points for diesel and CSME biofuels

Up to this temperature, % (v/v) was distilled				
fuel	Start of distillation [°C]	End of distillation [°C]	up to 250°C distils v/v [%]	up to 350°C distils v/v [%]
CSME Biodiesel from pure oil	306	391	0	29
CSME Biodiesel from used oil	308	402	0	27
RME Biodiesel BLISKA	304	389	0	37
ON	171	361	36	93

CONCLUSIONS

The study has shown that CSME Biodiesel produced from unused (fresh) camelina oil is characterized by better distillation properties. The initial stages of distillation and the quantity of middle distillates in said CSMEs are similar. The start of distillation for both the CSMEs occurred at approx. 305ºC. Approx. 35% (v/v) of RME was distilled up to 350ºC. Greater differences were observed for the 90% (v/v) distillation temperatures and at the end of the distillation process. 90% (v/v) CSME CSME vaporised up to the temperature of 270ºC, whearas for biufuel derived from used oil the temperature was 282ºC. CSME obtained from the fresh camelina oil was entirely distilled up to the temperature of 386ºC, while RME derived from the used camelina oil vaporised on reaching 392.0ºC. This may testify to lower purity of the CSME produced from used cooking oil. In such biofuel, there may be more less volatile mono- and diglycerides or other chemicals which result from the lower level of oil-to-biofuel conversion and/or are an effect of residues from the process of frying chips. It must be said, though, these were not solid particles, as those were separated from the oil through filtration.

After the comparison of the results for both the CSMEs with a commercial RME biofuel obtained from BLISKA service stations, it turned out that biofuels from camelina are characterized by slightly worse distillation properties. Notable is the difference in the quantity of RME distilled up to the temperature of 350°C, since BLISKA service station biofuels vaporized in greater amounts – 10% (v/v) more than the CSME produced from the pure oil and 14% more than the CSME from the used cooking camelina oil.

Both the CSMEs do not comply with the requirements set by EN 14214 for FAME plant biofuels due to the final distillation temperature. Under the above-mentioned standard, the temperature of 360° C needs to vaporise the entire amount of biofuel.

REFERENCES

1. **Cisek J., Mruk A., Hlavňa V. 2011:** The properties of a HDV Diesel engine fuelled by crude rapeseed oil. Teka Komisji Motoryzacji i Energetyki Rolnictwa, Vol. XI, 29-39.
2. **Cisek J., Mruk A. 2012:** Właściwości silnika ZS zasilanego naturalnym olejem rzepakowym. Zeszyty Naukowe Instytutu Pojazdów Politechniki Warszawskiej z serii Mechanika Ekologia Bezpieczeństwo Mechatronika, Vol. 1(87)/2012, 5-16.
3. **Jakóbiec J., Ambrozik A. 2009:** Procesy starzenia estrów metylowych kwasów tłuszczowych oleju rzepakowego. Inżynieria Rolnicza 5 (114), s. 85-90. 2009.
4. **Uzdowski M. 2006**: Możliwości wykorzystania mieszanin paliw tradycyjnych i alternatywnych do zasilania silników ZS. Motrol Vol. 8A. 280-285.
5. **Tys J. i in. 2003:** Technologiczne i ekonomiczne uwarunkowania produkcji biopaliwa z rzepaku. Instytut Agrofizyki im. Bohdana Dobrzańskiego PAN w Lublinie.
6. **Wcisło. G. 2011**: Testing AFME and RME biofuels for composition of fatty acids. Teka Komisji Motoryzacji i Energetyki Rolnictwa, 2011, Vol. XI C, 393-399.
7. **Wcisło. G. 2010**: Utilization of used oils and fat for manufacturing FAME biofuels. Teka Komisji Motoryzacji i Energetyki Rolnictwa, 2010, Vol. X, s. 509-516. 2010.
8. **Wcisło. G. 2010**: Przetwarzanie biomasy na cele energetyczne. Praca zbiorowa pod redakcją Frączek J. Uniwersytet Rolniczy im. H. Kołłątaja, Kraków. 85-146.
9. **Wcisło G. 2009** : Określenie składu frakcyjnego biopaliw rolniczych zawierających biokomponent CSME. Inżynieria Rolnicza Vol . 9 (118).
10. **Wojtkowiak R. and others. 2009**: Production Costs in a Novel Method of Manufacture of the Methyl Esters From False Flax (Camelina Sativa L.) Oil for Feed the Piston Compression-Ignition Engines. Journal of Research and Application in Agriculture Engineering. Vol. 54(4).
11. **Wojtkowiak R. and others. 2007**: Olej lniankowy jako paliwo do zasilania silników z zapłonem samoczynnym. Monografia pod redakcją Z. Zbytka. tom 4: Wybrane zagadnienia ekologiczne we współczesnym rolnictwie. Przemysłowy Instytut Maszyn Rolniczych, Poznań. 204-214.
12. **Wojtkowiak R. and others. 2007**: Koszt produkcji paliwa z oleju lniankowego do silników z zapłonem samoczynnym. Monografia pod redakcją Z. Zbytka, tom 4: Wybrane zagadnienia ekologiczne we współczesnym rolnictwie. Przemysłowy Instytut Maszyn Rolniczych, Poznań. 215-230.
13. **Szlachta Z. 2002**: Zasilanie silników wysokoprężnych paliwami rzepakowymi, Wydawnictwa Komunikacji i Łączności WKŁ – Warszawa.
14. **Biodiesel 2006**, Handling and Use Guidelines. U.S. Department of Energy, Third Edition, September 2006.
15. **Ustawa** z dnia 25 sierpnia 2006 r. o biokomponentach i biopaliwach ciekłych (Dz. U. 2006 nr 169 poz. 1199 z późn. zm.)

OKREŚLENIE WPŁYWU RODZAJU UŻYTEGO OLEJU RZEPAKOWEGO DO PRODUKCJI BIOPALIW NA SKŁAD FRAKCYJNY CSME

Streszczenie. Przeprowadzone badania pokazały, że niezależnie od rodzaju zastosowanego oleju lnianki do produkcji RME, czy będzie to olej nieużyty lub zużyty, zakresy temperatur destylacji były podobne. Niewielkie różnice zanotowano jedynie dla temperatur końca destylacji. CSME wyprodukowane z zużytego oleju lnianki potrzebowało wyższych temperatur do odparowania całej objętości FAME. Może to świadczyć o mniejszej czystości CSME uzyskanego ze zużytego oleju. W takim biopaliwie może znajdować się więcej mało lotnych mono i di-glicerydów lub innych związków, które np. pozostały w oleju po procesie smażenia frytek. Przy czym nie chodzi tu o cząstki stałe, ponieważ te zostały oddzielone od oleju podczas filtracji.

Słowa kluczowe: Biodiesel, biopaliwo, silnik wysokoprężny, skład frakcyjny, temperatury destylacji.

TEKA. COMMISSION OF MOTORIZATION AND ENERGETICS IN AGRICULTURE – 2014, Vol. 14, No. 4, 201–210

Effects of Pre-Sowing Magnetic Stimulation on the Growth, Development and Changes in Physicochemical Properties in Sugar Beet Seedlings

Miłosz Zardzewiały, Grzegorz Zaguła, Czesław Puchalski

Department of Bioenergy Technologies, University of Rzeszow
ul. Rejtana 16C, 35-959 Rzeszow, Poland

Received December 02.2014; accepted December 17.2014

Summary. The magnetic field is a physical factor to improve germination and development of plants. The laboratory experiment was conducted to determine the effect of pre-sowing magnetic field stimulation on the ability of growth and development and changes in the physicochemical properties of sugar beet seedlings. Used magnetic field of low frequency f=50 Hz, B = 10, 20, 40 mT, exposure time t = 60 seconds. Then identified the most favorable induction. In the rest of the experiment the results were compared with a control group, taking into account changes in the basic physical and chemical properties of beet seedlings. The observations carried out during the experiment focused on the growth of plants and determining the basic composition of micro- and macronutrients in the emerging plants.

Key words: magnetic fields; physicochemical composition; heavy metals; sugar beet germination.

INTRODUCTION

Sugar beet (Beta vulgaris subsp. vulgaris convar. crassaprovar. altissima) is an industrial plant with large contents of sucrose and, after sugarcane, it is the second most important source of sugar produced for consumption, accounting for approx. 30-40% of global production [45]. Sugar beet belongs to the Chenopodiaceae family. It originated from the coasts of the Mediterranean, Caspian and Black Seas. In Poland and 38 other countries globally sugar beet is the basic raw material used for production of sugar in the temperate climate zone [21]. Moreover sugar beet may be a valuable forage crop or raw material for various branches of industry [10].

Crop cultivation is indispensable for human existence, for production of food of both plant and animal origin. People must continuously increase food production due to the growing population. In order to provide sustenance for people, in adequate quantity and quality, it is necessary to significantly improve fruitfulness in plants. This can be achieved by using two groups of technologies: those necessary for enhancing genotypes of cultivars as well as more effective and environmentally friendly cultivation systems. Until the eighteenth century crops were increased by expanding area designated for cultivation. Starting from the nineteenth century application of scientific achievements became more and more important; these included theoretical basics of soil chemistry and agronomy, initiated production of superphosphate and import of nitrates from Chile to the USA and Europe, synthesis of ammonia and construction of the first ammonia factory. The first natural pesticide was tobacco extract, used from the early eighteenth century to destroy aphids, and the first synthetic agent was dinitroorthocresolate [44]. Contemporary agriculture utilizes large amounts of chemical agents which adversely impact the environment and the condition of soil. Therefore various endeavours are initiated in order to reduce application of chemical substances and restore biodiversity [20]. Yet, in order to enhance sowing material in the times of the disturbed natural environment it is necessary to look for new, safe methods for achieving this [32]. Recent years have seen a notable increase in the size of farming areas designated for cultivation of crops by means of ecological or integrated methods; there is alsogrowing interest in pro-ecological methods of improving the quality and health of seeds [20].

During the last decade more and more research has focused on effects of pre-sowing electromagnetic radiation on seed field performance. This type of stimulation is cost-effective, and does not adversely impact the plants. Hence, there is a great need for developing new methods of enhancing seeds [19, 36].

Quality of seeds used for sowing is a major factor impacting growth and development of plants, and ultimatelythe yield. By applying various methods of enhancing sowing material it is possible to considerably improve its germination rate [17].Physical factors such as infrared, ultraviolet, laser, or microwave radiation, ultrasounds or electric, magnetic and electromagnetic field are more and more frequently used to stimulate seeds before sowing. These methods are considered to be safe for the environment; hence they may prove useful for organic farming [30, 38].

Physical agents most definitely will not replace effective chemical methods, yet they may be a beneficial supplement for the latter. One of the factors which may prove useful for stimulating seed vigour and growth of plants is magnetic field, because its impact on seeds and growth of plants is noticeable even with low induction values [7, 14]. Impact of magnetic field on plants depends on its size and nature. Plants are exposed to different types of magnetic field – static (with constant magnetic induction), alternating [18], oscillating [34] and pulsed [6].

Numerous studies allow a conclusion that stimulation of seeds with magnetic field, before sowing, results in higher crops without the use of additional mineral fertilizers [42]. Previous research conducted in laboratories and at micro-fields show highly positive effect of stimulation by means of magnetic field on germination and growth as well as yield in selected cereals, pulses, root crops, vegetables and flowering plants [5, 8, 11, 13, 23, 26, 31, 37, 40].

Table 1. Magnetic field values in research. [1, 2, 8, 9, 22, 25, 31, 35].

Plant	Magnetic field value
Wheat	From a few mT to 1 T
Sugar snap peas	30 mT, 85 mT, 120 mT, 180 mT
Flowering plants	30 mT, 90 mT
Potato	20 mT, 40 mT, 80 mT
Maize	150 mT, 50 mT

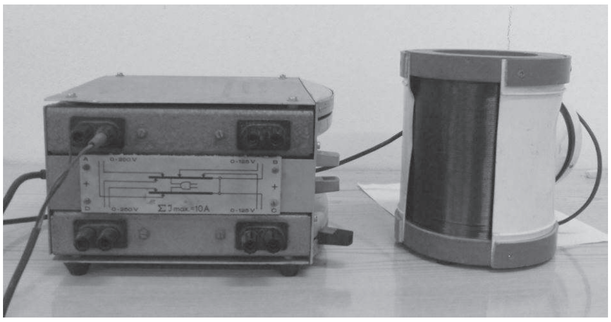

Fig. 1a. Multilayer air core inductor.

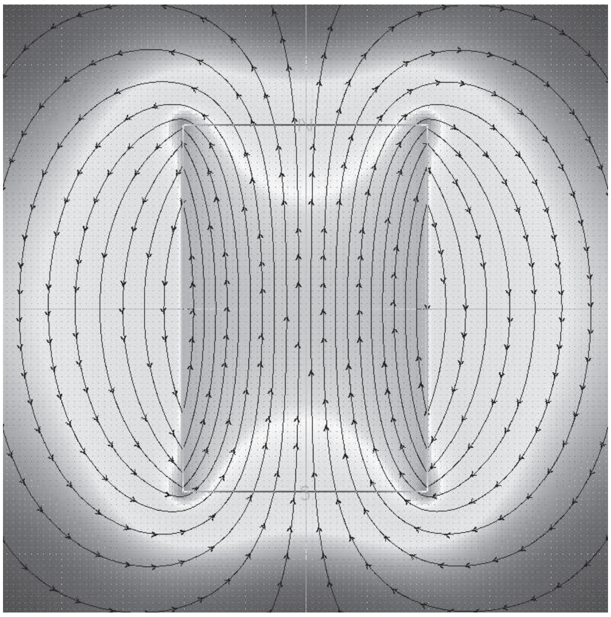

Fig. 1b. Simulated homogeneity of the surrounding field distribution.

The purpose of the present study was to define the impact of stimulation with slow-changing magnetic field with induction values of 10, 20 and 40 mT, at frequency of50Hz and duration of exposition 60 seconds on the emergence and growth of sugar beet seedlings; additionally after the most beneficial magnetic field was identified, changes in physicochemical properties of sugar beet seedlings were also investigated.

MATERIAL AND METHODS

Ten cultivars of sugar beet Beta vulgaris L were selected for the study. Seeds of each cultivar were divided into 4 groups (each comprising 36 seeds). Each cultivar was exposed to alternating magnetic field of 10, 20 and 40mT at frequency of 50Hz, in order to determine the field with the most beneficial impact on the speed of germination and growth of seeds. The pre-sowing 60-second magnetic stimulation was conducted by means of air core inductor – solenoid of copper wire 1 mm, 12 coils (figure 1a, 1b). Inductor parameters: Length – 0.15m, Diameter – 0.11m. Number of coils – 115 in 13 winding layers.

One group, i.e. control seeds, was not subjected to stimulation. The laboratory experiment was carried out in phytotron with constant conditions, i.e. temperature 25° C ± 1° C, humidity 85% and constant illumination. Seeds in groups of36 were planted in pots filled with soil. The total of 40 pots were placed in the phytotron (for each cultivar there were four variants: – 10mT, 20mT, 40mTat frequency of 50Hzand the control sample).

The experiment was continued for 10 days. Each day at the same time the seeds were watered with distilled water, 15 ml per each pot. The number of emerging shoots was recorded and the lengths of seedlings were compared during the consecutive days of the experiment. At the end of the experiment the results were entered into a summary table and, based on that, graphs were complied to show the effects of magnetic field on germination rate in the specific cultivars; finally the most beneficial magnetic field was identified for further physicochemical tests. Analytical measurements of the control sample and the sprouts from seeds stimulated with the optimum magnetic field were performed using the following equipment:

- TGA 701 Leco® thermogravimetricanalyzer, to determine the contents of water, ash, and volatile substances;
- True Spec CHNLeco® elemental determinator, to identify the contents of basic building elements;
- ICP OES iCAP Dual 6500 Thermo®, to determine concentrations of selected micro and macro elements, with the use of microwave mineralization.

RESULTS

Findings of the experiment allow a conclusion that pre-sowing stimulation of seeds with a magnetic field significantly impacted the ability of sugar beets to germinate, both during the initial seven days-(Figure2) (mean results for the 10 cultivars) and throughout the entire experiment-10 days. The speed of germination in the seeds stimulated with magnetic field was significantly higher.

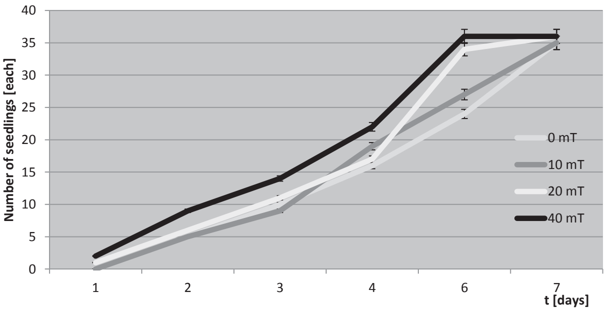

Fig. 2. Effects of pre-sowing stimulation with magnetic field on the speed of germination in the seeds of sugar beets during the initial seven days of the experiment–mean values for 10 cultivars.

The results of the study suggest that 40mT magnetic field had the most beneficial impact on the sprouting vigour in sugar beets of all the magnetic field values applied in the experiment, i.e. 10mT and 20mT and 40mT (Figure 3).

Therefore, sprouts which emerged from seeds stimulated with 40mT magnetic field were selected for further analytical tests. Presented below, the results provide comparative data for the contents of microelements, macroelements, heavy metals, water and ash in the control sample and the sample exposed to the optimum magnetic field before sowing.

During the 10-day process the most notable was the fourth day of the experiment, when the most pronounced difference was observed between the number of seedlings in the control sample and the sprouts emerging from magnetically stimulated seeds(Table 2). The difference of up to 20% was in favour of the magnetically induced seeds. The results for all the cultivars, presented in the following summary table, confirm the above statement.

Table 2. Number of shoots on the fourth day of the experiment in samples stimulated with magnetic field and in the control sample.

	Number of shoots [each]			
Sugar beet cultivar no.	**40 mT magnetic field**	**SD**	**Control sample – 0 mT**	**SD**
13 - Milton	15	0.7	9	1.9
8 - Primadonna	16	1.4	11	2.9
23 - Schubert	22	1.9	13	0.8
25 - Alegra	23	2.1	17	1.8
14 - Agent	24	0.9	17	1.4
2 - Janosik	28	2.5	21	1.6
5 - Danuśka	27	3.0	18	2.8
4 - Agnieszka	29	2.4	18	2.3
26 - Silvetta	31	1.9	23	2.9
27 - Tadeusz	36	2.8	23	1.7

Figure 3 presents concentrations of selected heavy metals in shoots of prestimulated plants in comparison to seedlings which had not been exposed to magnetic stimulation. The graph shows decreased tendency for accumulating harmful metals following magnetic prestimulation of the sowing material, in particular for such elements as zinc, nickel and lead. On average thedifference in the overall amount of accumulated harmful elements reaches 30% per a cultivar and the standard deviation between results for specific cultivars does not exceed 3%.

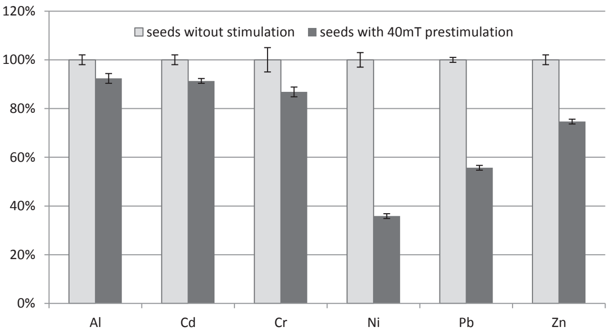

Fig. 3. Heavy metals concentration in seedlings subjected and not subjected to magnetic stimulation – mean results for the 10 cultivars.

Figure 4 shows the tendency ofplants emerging from seeds stimulated magnetically to accumulate greater quantities of macroelements. The tendency is visible for each element and does not depend on the cultivar, which can be seen in the small, maximum 2% standard deviation in measurements for various cultivars.

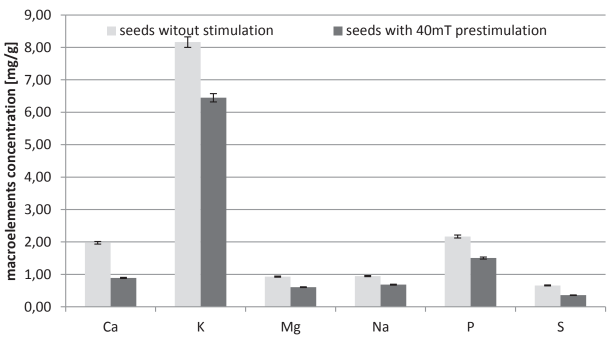

Fig. 4. Concentrations of selected macroelements-mean results for the investigated cultivars.

The tendency for shoots of plants prestimulated with alternating magnetic field to accumulate smaller quantities of mineral components is confirmed by results of thermogravimetric analysis. Figure 5 presents the consistent tendency in the measurements of total ash in incinerated plant material. Results of these analyses are statistically significant for each of the 10 cultivars under discussion.

These findings are further confirmed by measurements of water content in the emerging seedlings. As demonstrated by Figure 6, the results showed the seedlings subjected to stimulation before sowing tended to accumulate greater quantity of free water. In this stimulation group,in each case,

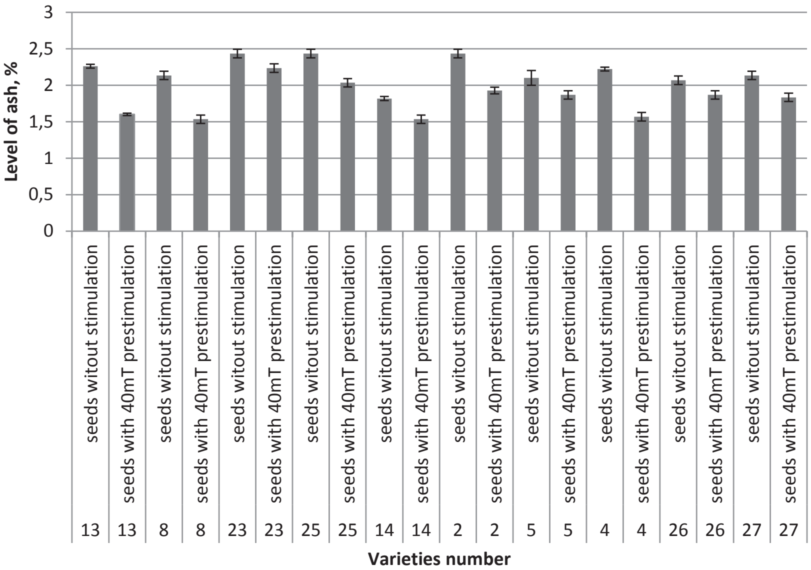

Fig. 5. Results of analyses investigatingash content in the examined beet root seedlings.

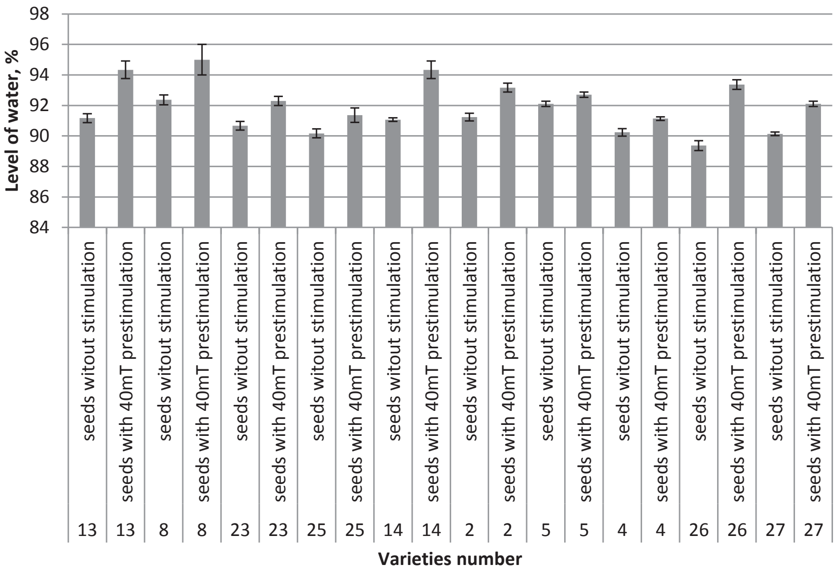

Fig. 6. Results of analyses investigating water content in the examined sugar beet seedlings after drying test at temperature of 105°C.

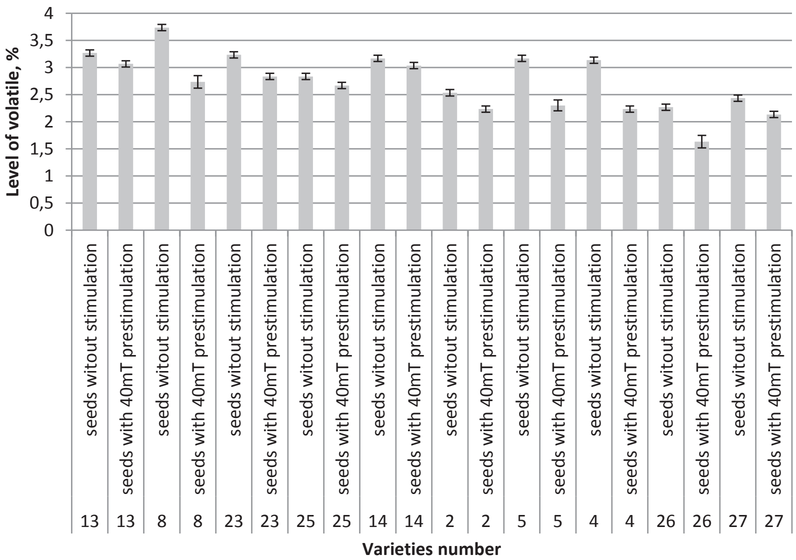

Fig. 7. Results of analyses investigating volatiles content in the examined sugar beet seedlings of the 10 selected cultivars.

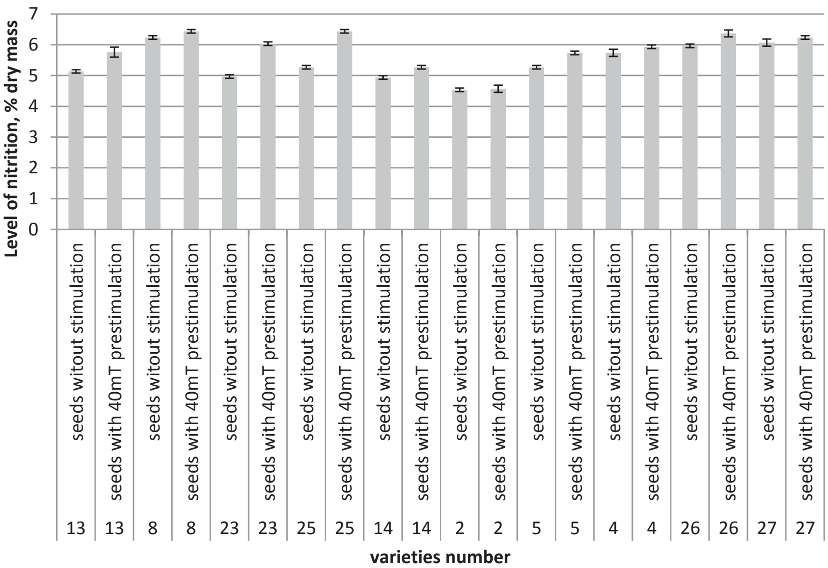

Fig. 8. Results of analyses investigating nitrogen content in the dry mass of seedlings.

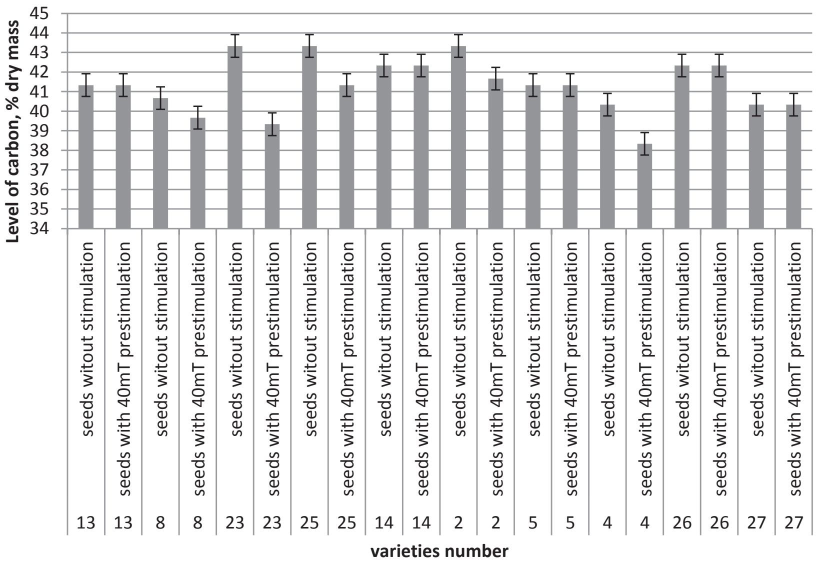

Fig. 9. Results of analyses investigating carbon content in the dry mass of seedlings.

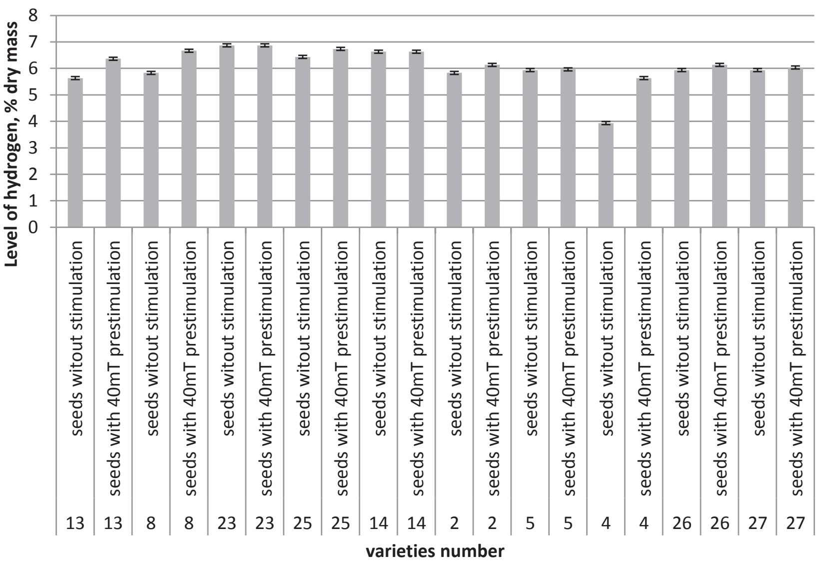

Fig. 10. Results of analyses investigating hydrogen content in the dry mass of seedlings.

water content was higher, on average by 2%, in comparison with the sample which had not been stimulated with magnetic field.

Another investigated parameter was the contents of volatiles which were determined in thermogravimetric analyzer by incinerating raw plant sample at the temperature of 900°C for the duration of 15 minutes, in covered containers. In this case the results were also unambiguous. As illustrated by Figure 7, each cultivar was found with statistically significant decrease in this parameter for sprouts emerging from seeds treated with 40mT stimulation before sowing.

Finally, the investigated parameters included the basic building elements impacting the stability of the plants' tissues and cells, i.e. carbon, hydrogen and nitrogen, which were examined by means of element determinator employing near infrared band to examine dry analytical sample exposed to carrier gases. The findings related to nitrogen content in dried samples of beet seedlings for each cultivar show the content of this element increases as a result of magnetic pre-stimulation (Figure 8). This tendency is particularly pronounced in cultivars 25 and 23 where the relevant increase reaches the value of 20% (nominally, increase from 5 to 6%).

Carbon content in dry mass tends to decrease in cultivars 2, 4, 23 and 25. In the remaining cultivars no statistically significant difference was found between samples stimulated before sowing and those planted without stimulation (Figure 9).Changes in hydrogen content in the seedling dry mass, associated with the quantity of water bounded in chemical compounds of fruit tissue, tended to increase as a result of the applied prestimulation procedure in half of the cultivars of sugar beets in question. In the remaining cultivars no significant changes were found for this parameter (Figure10).

DISCUSSION

Many available publications describe studies investing the effects of magnetic field on plants. Relevant reported findings show that in most cases short-term application of the physical factor involving pre-sowing magnetic stimulation of seeds impacts the parameters of seedlings in the investigated plants.

Wójcik [42] showed that stimulation with 75mT magnetic field for the duration of 30 seconds beneficially impacted capacity for germination, sugar content and overall yield in sugar beets. As a result of magnetic stimulation there was a slight decrease in the content of melassigenic substances. According to Rochalska [40] stimulation of sugar beet seeds with magnetic field of 5mT 16 Hz positively affected the vigour of these seeds, chlorophyll content during vegetation and, finally, resulted in increased yield and sugar content in the roots.

Kornarzyński [23] reported beneficial effects of the magnetic field of 30 and 90 mT on germination in flowering plants. Positive impact of magnetic field is particularly visible if seeds germinate in stressful conditions, such as low temperature and shortage of water. Pre-sowing stimulation of seeds improves sprouting capacity in sugarsnap peas, particularly if there is shortage of moisture in the soil. Such treatment seems to be more effective in these conditions than in a situation of optimal moisture [33].

A study carried out by Bilalis et al. [6] showed that magnetic field could replace hormones in vegetative propagation. The obtained results provided evidence for the fact that magnetic field stimulated the rooting process in oregano plants. On the other hand a combined use of magnetic field and hormones led to significantly lower percentage of correctly rooted plants than when magnetic field alone was applied. Magnetic stimulation methods ensuring better oregano seedlings may potentially be useful for producers of planting material, particularly in organic farming where chemical agents are not allowed.

Ahmet Esitken and Metin Turan [15] conducted a study investigating the effect of magnetic field on the yield and kation accumulation in strawberry leaves. The experiment was carried out in a greenhouse. The plants were exposed to magnetic field of 0.096 T, 0.192 T and 0.384 T. All inductions of the magnetic field increased the mean weight of fruit in comparison with the control sample. The best fruit yield was achieved by applying 0.096 T field. Magnetic field with induction increased to 0.384 T resulted in higher contents of N, K, Ca, Mg, Cu, Fe, Mn, Zn, Na and lower content of P and Sin strawberry leaves.

Masafumi Muraji et al. [27] investigated the impact of alternating magnetic field on the growth rate of primary roots in maize. Maize seedlings were growing in darkness, at a constant temperature (25°C) and humidity (100%). They were exposed to 5 mT alternating magnetic field at frequencies of 5, 10, 20 or 40 Hz. The rates of root growth in the plants subjected to each frequency of the magnetic field were measured and compared with the control sample. Root growth rate in seedlings developing in the presence of magnetic field of varied frequencies increased in relation to the control group. The highest pace of growth was observed in seedlings exposed to alternating magnetic field of 10 Hz frequency.

Moreover Alkassab A.T. and Albach D.C. [3] researched the response of Mexican aster Cosmos bipinnatus (Asteraceae) and field mustard Sinapisarvensis (Brassicaceae) to magnetically treated water (MTW) from germination to flowering. Used for treating water a magnetic treatment device in the range of 3.5–136 mT.

MTW affected growth and several biochemical parameters of treated plants depending on the number of passes of water. Irrigation water MTW resulted in increasing plant height, the amount of leaves and branches per plant and chlorophyll content compared to the control not irrigated water MTW.

The present study explicitly demonstrated the effects of pre-sowing stimulation applied to the planting material of 10 selected cultivars of sugar beet on physicochemical properties of the emerging seedlings. Most significantly, 40mT magnetic field of 50Hz frequency impacted the tendency of the examined seedlings to accumulate basic macro and micro elements; the results were also manifested in lower content of total ash. Importantly, the reduced accumulation of harmful elements such as: Al, Cd, Cr, Ni, Pb, Zn may be of particular importance in a situation when seeds are planted in soil contaminated by industry, fertilizers or crop protection agents. The previously known methods of preventing heavy metals accumulation, such as liming or soil ionization are very expensive and may lead to changes in the structure, pH and other starvation related soil conditions [4, 12, 16, 24, 28, 41, 43]. On the other hand pre-stimulation, without interfering with the soil structure and properties, prevents accumulation of heavy metals which are a major hazard for people and animals. Additionally, as demonstrated by these authors, the faster pace of seed germination following magnetic stimulation suggests another agritechnical advantage. The possibility to achieve faster germination rate allows for higher crops from such seeds.

CONCLUSIONS

1. Pre-sowing stimulation of sugar beet seeds was most effective with the applied magnetic field induction of 40mT and frequency of 50 Hz.
2. By using 40mT induction it was possible to improve sugar beet germination rate.
3. There was a nearly 20% increase in the number of sugar beet seedlings on the fourth day of the experiment, in comparison with the control sample, which was not pre-stimulated with magnetic field.
4. There was notable decrease in heavy metals accumulation in the seedlings of beets exposed to magnetic stimulation, which was particularly significant in the case of lead, nickel and zinc concentrations.

REFERENCES

1. **Aksenov S.I., Bulychew A.A., Grunina T. Yu. & Turovetsky V.B. 2001.:** Effect of elf-emf treatment on wheat seeds at different stages of germination and possible mechanisms of their origin. Electromagnetic Biology and Medicine, 20, 231-253.
2. **Aladjadjiyan A. 2003.:** Study of the influence of magnetic field on some biological characteristics of zea mays. Journal of Central European Agriculture, vol. 2, 3, 89-94.
3. **Alkassab A.T. & Albach D.C. 2014.:** Response of Mexican aster Cosmos bipinnatus and field mustard Sinapisarvensis to irrigation with magnetically treated water (MTW). Biological Agriculture & Horticulture: An International Journal for Sustainable Production Systems, vol. 30, 1, 62-72.
4. **Baran S., Martyn W. & Bojarski J. 1998.:** Wpływ wermikompostu z osadu ściekowego i węglanu wapnia na migrację metali ciężkich do łańcucha troficznego [Effect of vermicompost from sewage sludge and calcium carbonate on migration of heavy metals to trophic chain]. Zeszyty Problemowe Postępów Nauk Rolniczych, 461, 111–120. Polish.
5. **Belyavskaya N.A. 2004.:** Biological effects due to weak magnetic field on plants. Advances in Space Research, 34, 1566-1574.
6. **Bilalis D., Katsenios N., Efthimiadou A., Efthimiadis P. & Karkanis A. 2012.:** Pulsed electromagnetic fields effect in oregano rooting and vegetative propagation: A potential new organic method. Acta Agriculturae Scandinavica, Section B – Soil & Plant Science, vol. 62, 1, 94-99.
7. **Bovelli R. & Bennici A. 2000.:** Stimulation of germination callus growth and shoot regeneration of Nicotiana tabacum L. by Pulsing Electromagnetic Fields (PEMF). Horticultural Science, 14, 3-6.
8. **Bujak K. & Frant M.2009.:** Wpływ przedsiewnej stymulacji nasion zmiennym polem magnetycznym na plonowanie pszenicy jarej [Effect of pre-sowing stimulation of seeds with alternating magnetic field on the yields of spring wheat]. Acta Agrophysica, 14(1), 19-29. Polish.
9. **Bujak K. & Frant M. 2010.:** Wpływ przedsiewnej stymulacji nasion zmiennym polem magnetycznym na plonowanie i jakość technologiczną ziarna pszenicy ozimej [Effect of pre-sowing stimulation of seeds with alternatingmagnetic field on yield and technologicalquality of grains in winter wheat]. Acta Agrophysica, 15(2), 233-245. Polish.
10. **Byszewski W. 1979.** Biologia buraka cukrowego [Biology of sugarbeet]. PWN. Warszawa, Poland.
11. **Camps-Raga B., Gyawali S. & Islam N.E. 2009.:** Germination rate studies of soybean under static and low-frequently magnetic field. IEEE Transaction an Dielectrics and Electrical Insulaton, vol. 16, 5, 1317-1321.
12. **Chłopecka A., Bacon J.R., Wilson M.J. & Kay I. 1996.:** Forms of cadmium, lead and zinc in soils form Southwest Poland. Journal of Environment Quality, 25, 69–79.
13. **Cieśla A., Kraszewski W., Skowron M.& Syrek P. 2006.:** Wykorzystanie silnego pola magnetycznego wzbudzonego przez elektromagnes nadprzewodnikowy do biostymulacji przedsiewnej nasion [Application of strong magnetic field induced by super conducting electromagnet for pre-sowing biostimulation of seeds]. Materials of the Third International Conference "Effects of magnetic fields in agricultural environment". Lublin, p. 36-33. Polish.
14. **Dulbińska D.A. 1973.:** Wlianie postoiannovo magnitnovo pola na rost prorostkov kukuruzy [Effect of static magnetic field on the growth of maize seedlings]. Fiziol. Rast, vol. 20, 1, 183-186. Russian.
15. **Esitken A.& Turan M. 2004.:** Alternating magnetic field effects on yield and plant nutrient element composition of strawberry (Fragaria x ananassa cv. camarosa). Acta Agriculturae Scandinavica, Section B – Soil & Plant Science, vol. 54, 3, 135-139.
16. **Gorlach E. 1995.:** Metale ciężkie jako czynnik zagrażający żyzności gleby [Heavy metals as a factor impairing soil fertility]. Zeszyty Problemowe Postępów Nauk Rolniczych, 421a, 113–122. Polish.
17. **Górecki R. J. & Grzesiuk S. 1994.:** Światowe tendencje i kierunki uszlachetniania materiałów siewnych [Global trends for enhancing planting materials]. Proceedings of the conference "Planting material enhancements". Olsztyn – Kortowo. p. 9-24. Polish.
18. **Hernandez A. C., Dominguez-Pacheco A, Carballo C.A., Cruz-Orea A., Ivanov R., López Bonilla J. L. &**

Valcarcel Montañez J. P. 2009.: Alternating Magnetic Field Irradiation Effects on Three Genotype Maize Seed Field Performance. Acta Agrophysica, vol.14, 1, 7-17.
19. **Hernandez A.C., Dominguez P.A., Cruz O.A., Ivanov R., Carballo C.A. & Zepeda B.R. 2010.** Laser in agriculture. International Agrophysics, 24, 407-422.
20. **Janas R. & Grzesik M. 2006.:** Proekologiczne metody poprawy jakości nasion roślin ogrodniczych [Pro-ecological methods of improving quality of seeds for horticulture]. Zeszyty Naukowe Postępów Nauk Rolniczych, 510, 213-221. Polish.
21. **Jasińska Z., Kotecki A. 2003.:** Szczegółowa uprawa roślin [Plant growing in detail], vol. I, p. 395-403. Wrocław. Polish.
22. **Kordas L. 2002.:** The effect of magnetic field on growth, development and the yield of spring wheat. Polish Journal of Environmental Studies, vol. 11, 5, 527-530.
23. **Kornarzyński K. 2006.:** Wpływ pola magnetycznego i elektrycznego na kiełkowanie nasion wybranych roślin kwiatowych [Effects of magnetic and electric field on germination of selected flowering plants]. Inżynieria rolnicza, 5, 305-312. Polish.
24. **Kuziemska B. & Kalembasa S. 1997.:** Wpływ wapnowania, dawki i rodzaju osadów ściekowych oraz nawożenia NPK na plon, skład chemiczny roślin i gleby, część III. Zawartośćwybranych metallic ciężkich w material roślinnym [Effects of liming, dosage and type of sewage sludge and fertilizing on yield, chemical composition of plants and soil, part III. Selected heavy metals content in plant material]. Archiwum Ochrony Środowiska, 1–2, 127-138. Polish.
25. **Marks N. & Szecówka P.S. 2010.:** Impact of variable magnetic field stimulation on growth of aboveground parts of potato plants. International Agrophysics, 24, 165-170.
26. **Moon J. & Chung H. 2000.:** Acceleration of germination of potato seed by applying AC electric and magnetic fields. Journal of Electrostatics, 48, 103-114.
27. **Muraji M., Asai T.& Tatebe W. 1998.:** Primary root growth rate of zea mays seedlings grown in an alternating magnetic field of different frequencies. Bioelectrochemistry and Bioenergetics, 1, 271-273.
28. **Niemyska-Łukaszuk J. 1995.:** Wpływ składu granulometrycznego i odczynu gleby na zawartość przyswajalnych form metali ciężkich [Effect of granulometric composition and soil pH on the content of assimilable heavy metals]. Zeszyty Problemowe Postępów Nauk Rolniczych, 418, 459– 464.Polish.
29. **Pietruszewski S. 2000.:** Wpływ pola magnetycznego na plony buraka cukrowego odmian Kalwia i Polko [Effect of magnetic field on the yield of Kalwia and Polko cultivars of sugarbeet]. Inżynieria Rolnicza, 5, 207-210. Polish.
30. **Pietruszewski S., Muszyński S. & Dziewulska A. 2007.:** Electromagnetic fields and electromagnetic radiation as non invasive external stimulants for seeds (selected methods and responses). International Agrophysics, 21, 95-100.
31. **Pietruszewski S. 1999.:** Magnetyczna biostymulacja materiału siewnego pszenicy jarej [Magnetic biostimulation of spring wheat planting material]. Rozprawy naukowe 220. Akademia Rolnicza Lublin. Polish.
32. **Podleśny J. 1997.:** Wpływ przedsiewnego traktowania nasion światłem laserowym na kształtowanie cech morfologicznych i plonowanie bobiku [Effecs of pre-sowingtreatment of seeds with laser light on morphological properties and yield in viciafaba]. Zeszyty Problemowe. Postępów Nauk Rolniczych, 446, 435- 439. Polish.
33. **Podleśny J. & Pietruszewski S. 2007.:** Wpływ stymulacji magnetycznej nasion na wzrost i plonowanie grochu siewnego uprawianego przy różnej wilgotności gleby [Effects of magnetic stimulation of seeds on the growth and yield of sugarsnap peas cultivated in soils of varied moisture level]. Inżynieria rolnicza, 8, 207-212. Polish.
34. **Racuciu M. 2011.:** 50 Hz Frequency Magnetic Field Effects on Mitotic Activity in the Maize Root. Romanian Journal of Biophysics, vol. 21, 1, 53-62.
35. **Racuciu M., Creanga D. & Horga I. 2008.:** Plant growth under static magnetic field influence. Romanian Journal of Physics, 53, 331-336.
36. **Rochalska M., Grabowska-Topczewska K. & Mackiewicz A. 2011.:** Influence of alternating low frequency magnetic field on improvement of seed quality. International Agrophysics, 25, 265-269.
37. **Rochalska M. 2001.:** Poprawa jakości materiału siewnego za pomocą zmiennego pola magnetycznego-część I. Badania laboratoryjne [Enhancement of planting material with alternating magnetic field – part I. Laboratory experiment]. Biuletyn IHAR, 217, 61-75. Polish.
38. **Rochalska M. 2003.:** Wpływ pola magnetycznego na nasiona i rośliny [Effects of magnetic field on seeds and plant]. Postępy nauk rolniczych, 1, 92-99. Polish.
39. **Rochalska M. & Orzeszko-Rywka A. 2008.:** Influence of alternating magnetic field on respiration of sugar beet seeds. International Agrophysics, 22, 255-259.
40. **Rochalska M., Grabowska K. & Ziarnik A. 2008.:** Impact of low frequency magnetic fields on yield and quality of sugar beet. InternationalAgrophysics, 23, 163-174.
41. **Rosa R., Zaniewicz-Bajkowska A., Franczuk J.& Kosterna E. 2009.:** Wpływ wapnowania gleby na akumulację ołowiu w sześciu odmianach buraka ćwikłowego [Effect of liming on lead accumulation in six cultivars of red beet]. Ochrona Środowiska i Zasobów Naturalnych, 41, 462-469. Polish.
42. **Wójcik S. 2006.:** Plonowanie i jakość technologiczna korzeni buraka cukrowego w zależności od stymulacji nasion [Yields and technological quality of red beetroots depending on stimulation of seeds]. Inżynieria rolnicza, 6, 383-388. Polish.
43. **Zaniewicz-Bajkowska A., Rosa R., Franczuk J. & Kosterna E. 2009.:** Wapnowanie gleby, a akumulacja kadmu w buraku ćwikłowym [Soil liming and cadmium accumulation in red beet]. Ochrona Środowiska i Zasobów Naturalnych, 41, 377-384. Polish.
44. **Zimny J., Banaszak Z. & Marciniak K. 2011.:** Nowoczesne technologie w produkcji roślinnej – przyjazne dla człowieka i środowiska [Modern technologies in plant production – friendly for people and the environment]. Polish Journal of Agronomy, 7, 102–112.Polish.

45. **Żurawska M. 2008.:** Jaki siew taki zbiór [You will harvest what you sow]. Burak Cukrowy, 1, 21-24. Polish.

WPŁYW PRZEDSIEWNEJ STYMULACJI MAGNETYCZNEJ NA WZROST, ROZWÓJ I ZMIANY WŁAŚCIWOŚCI FIZYKOCHEMICZNYCH ROŚLIN BURAKA CUKROWEGO.

Streszczenie. Pole magnetyczne jest czynnikiem do fizycznej poprawy kiełkowania i rozwoju roślin. Doświadczenie laboratoryjne przeprowadzono w celu określenia wpływu stymulacji przedsiewnej nasion zmiennym polem magnetycznym na ich zdolność wzrostu i rozwoju oraz zmiany w fizykochemicznych właściwościach kiełków buraków cukrowych. Stosowano pole magnetyczne o niskiej częstotliwości f = 50 Hz, B = 10, 20, 40 mT, czas ekspozycji t = 60 sekund. Następnie najbardziej korzystną indukcję zidentyfikowano i w dalszej części doświadczenia jej efekty porównywano z grupą kontrolną, biorąc pod uwagę zmiany w podstawowych właściwościach fizykochemicznych siewek buraków. Prowadzone w czasie eksperymentu obserwacje koncentrują się na wzroście roślin i określeniu podstawowego składu mikro- i makroskładników w wschodzących roślinach.

Słowa kluczowe: pola magnetyczne; skład fizykochemiczny; metale ciężkie; kiełkowania buraków cukrowych.

TEKA. COMMISSION OF MOTORIZATION AND ENERGETICS IN AGRICULTURE – 2014, Vol. 14, No. 4, 211–216

Analysis of Oil Leaks in a Variable-Height Gap Between the Cylinder Block and the Valve Plate in a Piston Pump by Means of Author-Designed Software and CFD Fluent

Tadeusz Zloto, Damian Sochacki, Piotr Stryjewski

Institute of Mechanical Technologies, Czestochowa University of Technology
Al. Armii Krajowej 21, 42-201 Czestochowa, e-mail: zlotot@o2.pl

Received December 04.2014; accepted December 19.2014

Summary. The paper presents computational models for obtaining oil leaks intensity in a variable height gap between the cylinder block and the valve plate in an axial piton pump. The computations are based on numerical methods and commercially available software CFD Fluent. By means of the models developed analysis of leak flow intensity is performed for variable parameters and dimensions of the pump.
Key words: oil leaks, gap between the cylinder block and valve plate, piston pump.

INTRODUCTION

Piston pumps are applied in the drives of complex machines with high demands concerning efficiency and reliability. This provides an incentive for continuous development towards improving exploitation parameters of those machines by modernizing their construction [8, 9, 17] The range of applications of piston pumps is wide and still expanding. Examples of devices employing piston pumps are presented in Fig. 1 [7, 14, 15, 16].

The most important applications of hydraulic piston machines include:
- aviation industry (airplanes);
- automotive industry (presses, machining centres, injection molding machines);
- heavy industry (pressure foundries, rolling mills, cokeries);
- construction industry (excavators, loaders, extension arms);
- foresting and agriculture machines (cranes, elevators, drilling rigs, harvesters);
- military vehicles (multi-function vehicles, vehicles used for constructing bridges).

The biggest manufacturers include such companies as Parker and Bosch-Rexroth.

In piston pumps energy losses occur at the mating surfaces: piston-cylinder, slipper-swash plate and cylinder block-valve plate. The latter forms the valve system, an important part of every hydraulic pump, which deserves special attention in examining the characteristics of hydraulic machines.

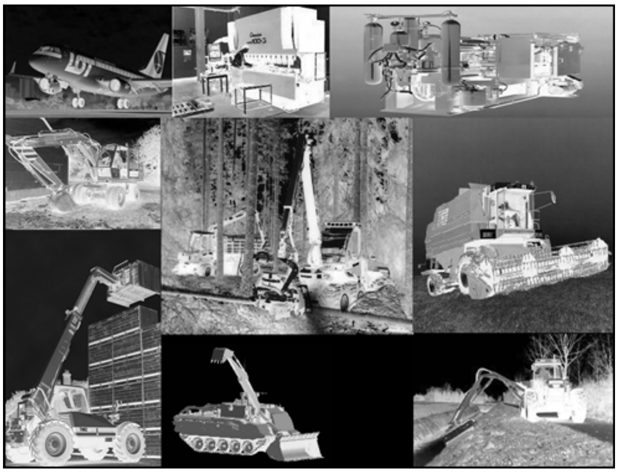

Fig. 1. Applications of piston pumps

In real conditions, the gap between the cylinder block and the valve plate is of variable height due to differences in torques coming from hydrostatic pressing and relieving forces which affect the position of the cylinder block [1, 2, 3, 4, 11, 12, 13, 18].

When a pump is operating, oil leaks to the outside and inside of the valve plate affecting the volumetric efficiency of the pump and its other parameters.

The paper employs numerical methods and a computational model developed within the software package CFD Fluent for determining oil leaks intensity in the valve system of an axial piston pump.

COMPUTATION MODEL OF OIL FLOW INTENSITY IN THE GAP BETWEEN THE CYLINDER BLOCK AND VALVE PLATE

To determine oil flow intensity in the gap between the cylinder block and valve plate, a numerical model was developed [18]. The following assumptions were adopted in the model [5, 10]:

– the flow is laminar;
– surfaces are infinitely rigid;
– the liquid completely fills the gap;
– tangent stress is Newtonian;
– the liquid is incompressible;
– inertia forces of the liquid are negligible.

Besides, cavitation and heat transfer phenomena were disregarded.

In the model developed, the valve plate was divided into four zones of oil leak flow, namely the discharge port, the inlet port, the upper transition zone and the lower transition zone. In all the four zones oil leaks occur to the inside and outside of the valve plate. In the transition zones, there are also leaks between the discharge and inlet zones.

In the transition zones, the oil leak intensity was obtained from the elementary product of the variable-height gap and the mean flow velocity as in the formula below:

$$Q = P\frac{1}{n}\sum_{i=0}^{n}\left(\upsilon_r\right)_{sr\,i} \tag{1}$$

where:
P – total cross-section area of the gap,
n – number of interpolation intervals,
$(\upsilon_r)_{sri}$ – mean flow velocity.

The flow cross-section was obtained on the basis of the numerical integration by trapezoidal rule, according to [6]:

$$P = l_n\left[\frac{h(r,\varphi_0)+h(r,\varphi_n)}{2}+\sum_{i=1}^{n-1}h(r,\varphi_i)\right] \tag{2}$$

where:
$h(r, \phi)$ – height of the variable-height gap at the radius and angle under consideration;
ϕ_0 – angle at the entry of the zone under consideration,
ϕ_n – angle at the exit of the zone under consideration,
n – number of intervals in the numerical integration by trapezoidal rule,
l_n – length of the interval in the numerical integration.

The gap height in a given interval was obtained from

$$h = -r\sin\varphi\cdot\cos\delta\cdot tg\varepsilon - r\cos\varphi\cdot\sin\delta\cdot tg\varepsilon + Rtg\varepsilon + h_1 \tag{3}$$

where
r – current radius of a given cross-section,
ϕ- angle of a given flow cross-section,
ε – inclination angle of the cylinder block,
δ – angle between the axis x and the smallest gap height h_1,
R – radius of the cylinder block.

The computation model of the oil leak intensity was implemented in the programming language C++ with the use of the VCL library. The software so developed makes it possible to analyse the leak flow intensity in a variable-height front gap in the valve system of different construction variants of a piston pump. The software also enables the user to set the accuracy of computations by prescribing the number n of interpolation intervals. Thanks to using the VCL library, it is possible to represent the results visually in the form of graphs and to save them as text files.

The total leak flow intensity in the valve system is obtained by adding the leaks from the particular flow zones.

COMPUTATION MODEL OF OIL LEAK FLOW INTENSITY EMPLOYING CFD FLUENT

An alternative method of examining oil leak flow intensity in the gap between the cylinder block and valve plate was developed on the basis of commercially available software CFD Fluent. The stages of building the model of the variable-height gap in the CFD Fluent package are presented in Fig. 2.

The geometrical model of the variable-height gap was constructed in the Auto-Cad programme for two construction types of the valve plate: with positive overlap and with relief grooves (Fig.3). In both cases, the same dimensions of the radius were applied r_1 = 0.0284 m, r_2 = 0.0304 m, r_3 = 0.0356 m and r_4 = 0.0376 m respectively, and the same length of the transition zones α_m, equal to 45[°].

A numerical grid generated automatically in the programme Gambit was then implemented on the geometrical model of the variable-height gap. The grid consists of volumetric cells of the Hex/Wedge type suitable for the gap shape. Besides, the regions of boundary conditions were specified in the programme Gambit (Fig.4).

The last stage of constructing the numerical model of the variable-height gap in the valve system is to enter the numerical grid with the boundary condition regions to the programme Fluent, in which the values of oil pressure in the boundary regions are determined and simulations of oil pressure distribution are performed. On the basis of the so obtained pressure area on the inside and outside of the valve plate, the oil leak flow intensity is determined.

Fig. 2. Stages of building the model of the variable-height gap in the CFD Fluent package

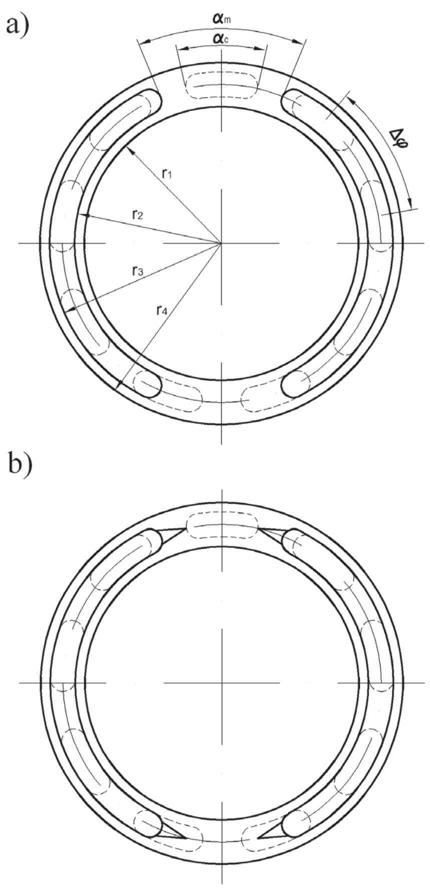

Fig. 3. Construction variants of the valve plate a) with positive overlap b) with relief grooves

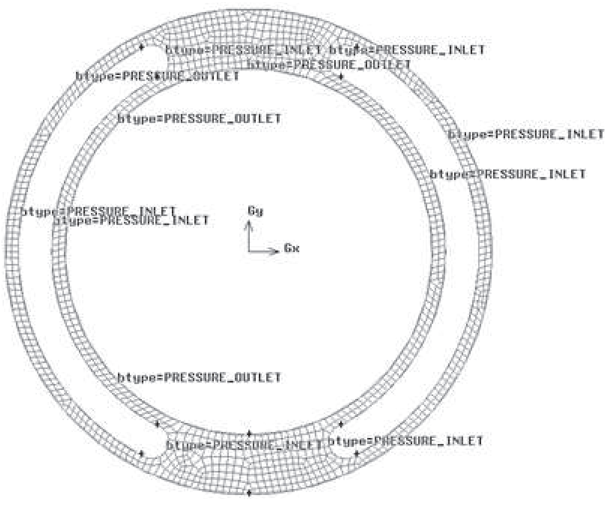

Fig. 4. Numerical grid consisting of volumetric cells of the Hex/Wedge type and boundary condition region

RESULTS OF COMPUTATIONS

The computational models developed and described above were applied for determining the total oil leak flow intensity in the gap between the cylinder block and valve plate in a hydraulic piston pump. The analysis was performed for variable dimensions and exploitation parameters such as the discharge pressure p_t, the angular velocity ω of the cylinder block, the dynamic viscosity η of oil and the angle ε of the cylinder block inclination for two constructional variants of the valve plate: the positive overlap variant and the relief groove variant.

The following input data were assumed in the computational model:

- in the pressure port the discharge pressure $p_t = 32$ MPa,
- in the suction port the inlet pressure $p_s = 0.1$ MPa,
- outside and inside the valve plate the pressure p_o = 0 MPa,
- angular velocity ω of the cylinder block ω = 157 rad/s,
- oil dynamic viscosity coefficient η = 0.0258 Pas,
- angle δ = 0.785 rad between the axis x and the smallest gap height h_1,
- angle between the cylinder block and valve plate ε = 0.000523 rad,
- minimal gap height $h_1 = 2\cdot10^{-6}$m,
- characteristic radiuses of the valve plate in a given pump are $r_1 = 0.0284$ m, $r_2 = 0.0304$ m, $r_3 = 0.0356$ m and $r_4 = 0.0376$ m.

Fig. 5 presents the variation of the oil leak flow intensity as a function of the discharge pressure p_t.

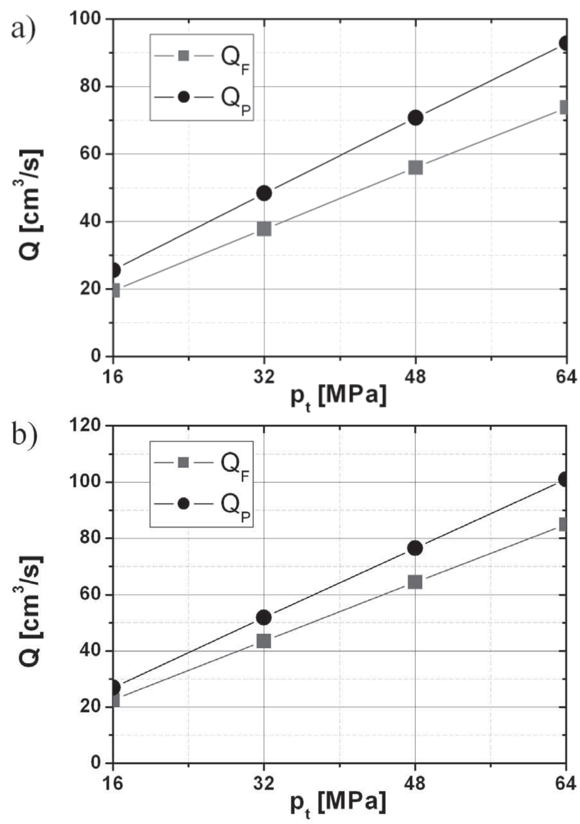

Fig. 5. Total oil leak flow intensity in the valve system as a function of the discharge pressure p_t obtained by means of the programme Q_P developed by the authors and CFD Fluent Q_F a) positive overlap valve plate, b) valve plate with relief grooves

Increase in the discharge pressure causes linear increase in the leak flow intensity.

Fig. 6 presents the variation of the oil leak flow intensity as a function of the angular velocity ω of the cylinder block.

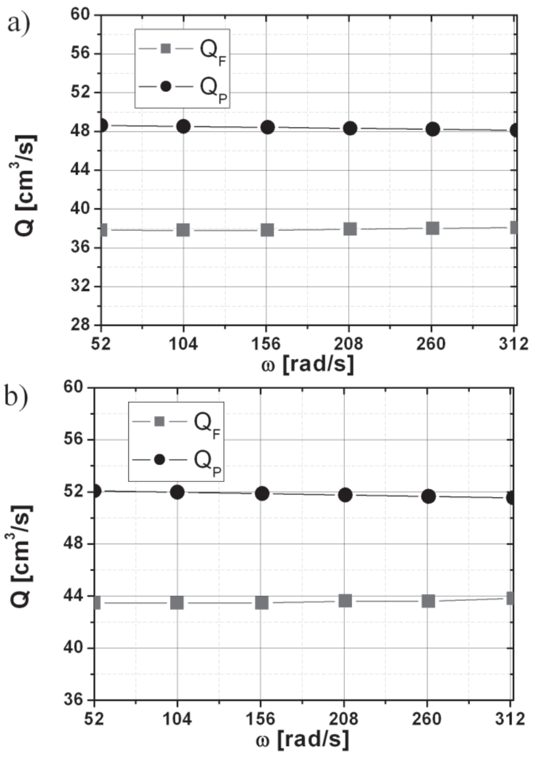

Fig. 6. Total oil leak flow intensity in the valve system as a function of the angular velocity ω of the cylinder block obtained by means of the programme Q_P developed by the authors and CFD Fluent Q_F a) positive overlap valve plate, b) valve plate with relief grooves

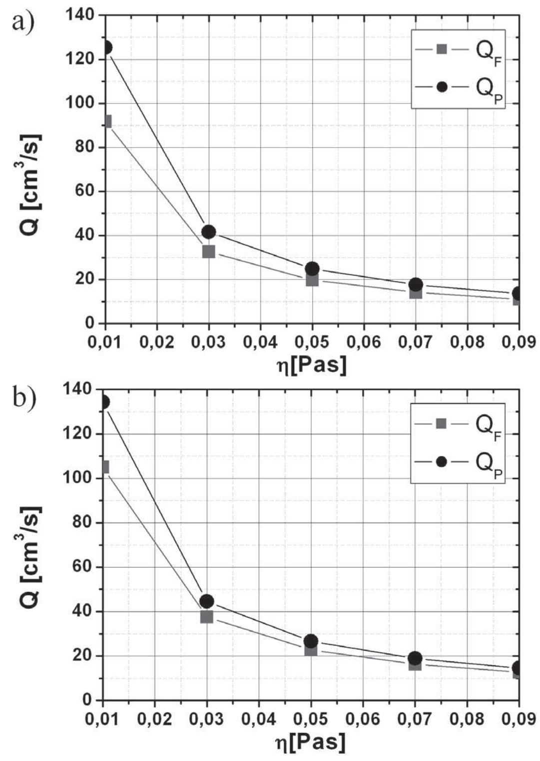

Fig. 7. Total oil leak flow intensity in the valve system as a function of the dynamic viscosity η of oil obtained by means of the programme Q_P developed by the authors and CFD Fluent Q_F a) positive overlap valve plate, b) valve plate with relief grooves

Increase in the angular velocity of the cylinder block does not significantly affect the leak flow intensity.

Fig.7 presents the variation of the oil leak flow intensity as a function of the dynamic viscosity coefficient η of oil.

Increase in the dynamic viscosity of oil causes decrease in the oil leak flow intensity in the valve system.

Fig. 8 presents the variation of the oil leak flow intensity as a function of the angle ε of the cylinder block inclination obtained by means of the programme developed by the authors and by means of CFD Fluent.

It can be observed that increase in the inclination angle of the cylinder block leads to a significant increase in the intensity of leak flow in the valve system.

Having obtained the results of oil leak flow intensity from the two sources, i.e. the programme developed by the authors and from CFD Fluent, we went on to compare them. The comparison was made by calculating relative differences (4) between the results of oil leak flow intensity obtained from Q_P and from CFD Fluent Q_F. The relative differences were calculated according to:

$$\delta_Q = \frac{|Q_P - Q_F|}{|Q_F|} \cdot 100\% \,, \tag{4}$$

Table 1 presents selected relative differences between the results obtained from the two sources, i.e. the authors' programme and CFD Fluent for the variable angle ε of the cylinder block inclination.

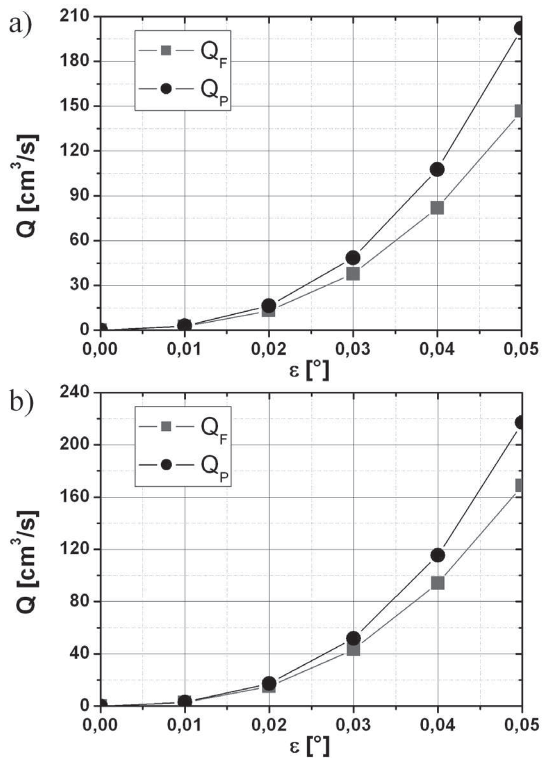

Fig. 8. Total oil leak flow intensity in the valve system as a function of the angle ε at which the cylinder block is inclined obtained by means of the programme Q_P developed by the authors and CFD Fluent Q_F a) positive overlap valve plate, b) valve plate with relief grooves

Table 1. Relative differences δ_Q between the values of total leak flow intensities obtained from the authors' programme and from CFD Fluent depending on the angle ε of the cylinder block inclination for the two variants of the valve plate

ε [°]	Positive overlap	Relief grooves
	δ_Q [%]	δ_Q [%]
0	6,43	3,83
0,01	17,53	10,4
0,0 2	24,25	15,68
0,03	28,1	19,31
0,04	31,52	22,69
0,05	37,88	28,68

As can be seen, the values of the relative differences between the results obtained from the authors' programme and from CFD Fluent increase with the increase in the angle ε of the cylinder block inclination. In the case of a positive overlap valve the increase is from 6% to about 38% and in the case of a valve with relief grooves the difference groes from about 4% to about 29%.

CONCLUSIONS

The study can be concluded by the following observations:

1. The models developed provide adequate tools for determining the flow intensity of oil leaks depending on the variable parameters and dimensions of the pump.
2. Increase in the cylinder block inclination angle and in the discharge pressure cause increase in the intensity of oil leak flow. Increase in the dynamic viscosity contributes to decrease in the intensity of leak flow and increase in the angular velocity of the cylinder block does not significantly affect it.
3. The intensity of oil leaks is greater for a valve plate with relief grooves than for a positive overlap valve plate.

REFERENCES

1. **Ivantysyn J., Ivantysynova M., 2001:** Hydrostatic Pumps and Motors. Akademia Books International. New Delhi.
2. **Jang D.S., 1997:** Verlustananalise an Axialkolbenheiten. Dissertation. RWTH, Aachen.
3. **Kaczmarek R., Rutański J., 1982:** Pompy wielotłoczkowe osiowe. Pomiar grubości szczeliny w rozdzielaczu z wykorzystaniem indukcyjnych czujników pomiarowych. Przegląd Mechaniczny nr 23-24.
4. **Kondakow L. A., 1975:** Uszczelnienia układów hydraulicznych. WNT, Warszawa.
5. **Nikitin G.A., 1982:** Szczielewyje i łabirintnyje uplotnienia gidroagregatow. Maszinostrojenie, Moskwa.
6. **Majchrzak E., Mochnacki B., 1994:** Metody numeryczne. Podstawy teoretyczne, aspekty praktyczne i algorytmy. Wydawnictwo Politechniki Śląskiej, Gliwice.
7. **Murrenhoff H., 2005:** Grundlagen der Fluidtechnik. Teil 1: Hydraulik, Shaker Verlag, Aachen.
8. **Osiecki A., 1998:** Hydrostatyczny napęd maszyn. WNT, Warszawa.
9. **Osiecki A., Osiecki L., 1998:** Prace rozwojowe nad nową konstrukcją pomp wielotłoczkowych osiowych. Hydraulika i Pneumatyka Nr 4, s. 4-9.
10. **Osipow A.F., 1966:** Objemnyje gidrowliczieskie maszi-ny. Maszinostrojenie, Moskwa.
11. **Pasynkov R.M., 1965:** K razczietu torcowych razpriedielitielei aksialno-porszniewych nasosow. Viestnik Maszinostrojenia Nr 1, 22-26.
12. **Pasynkov R.M.,1976:** Wlijanie pieriekosa cilindrowowo bloka na rabotu tarcowowo razpriedielitiela aksialno-porszniewoj gidromasziny. Viestnik Maszinostrojenia Nr 10, 49-50.
13. **Podolski M. E., 1981:** Upornyje podszipniki skolżenia, Leningrad.
14. **Ryzhakov A., Nikolenko I., Dreszer K., 2009:** Selection of discretely adjustable pump parameters for hydraulic drives of mobile equipment. Polska Akademia Nauk, Teka Komisji Motoryzacji i Energetyki Rolnictwa, Tom IX, s. 267-276, Lublin.
15. **Szydelski Z., Olechowicz J., 1986:** Elementy napędu i sterowania hydraulicznego i pneumatycznego. PWN, Warszawa.
16. **Stryczek S.,1995:** Napęd Hydrostatyczny, Tom 1. WNT, Warszawa.
17. **Zhang Y., 2000:** Verbesserung des Anlauf- und Langsamlaufverhaltens eines Axialkolbenmotors in Schrägscheibenbauweise durch konstruktive und materialtechnische Maβnahmen. Dissertation RWTH, Aachen.
18. **Zloto T., Sochacki D.,2011:** Oil Leakage in a Variable-Height Gap Between the Cylinder Block and the Valve Plate in a Piston Pump. Polska Akademia Nauk, Teka Komisji Motoryzacji i Energetyki, Vol. V, nr 11C, 353-360, Lublin.

ANALIZA PRZECIEKÓW OLEJU W SZCZELINIE ROZRZĄDU POMPY WIELOTŁOCZKOWEJ Z UWZGLĘDNIENIEM WŁASNEGO PROGRAMU I CFD FLUENT

Streszczenie. W pracy przedstawiono modele obliczeniowe do określania natężenia przepływu przecieków oleju w szczelinie o zmiennej wysokości pomiędzy blokiem cylindrowym i tarczą rozdzielacza pompy wielotłoczkowej. W obliczeniach wykorzystano metody numeryczne oraz komercyjny program CFD Fluent. Stosując opracowane modele przeprowadzono analizę natężenia przepływu przecieków dla zmiennych parametrów geometryczno-eksploatacyjnych pompy.

Słowa kluczowe: przecieki oleju, szczelina pomiędzy blokiem cylindrowym i tarczą rozdzielacza, pompa tłokowa.

Spis treści

List of the Reviewers

1. Leszek Mościcki
2. Janusz Laskowski
3. Ignacy Niedziółka
4. Dariusz Dziki
5. Stanisław Sosnowski
6. Tadeusz Złoto
7. Kazimierz Zawiślak
8. Marek Kuna-Broniowski
9. Andrzej Kornacki
10. V.O. Płoskyi
11. Petro Kulikov
12. A.M. Stankevich

Editors of the „TEKA" quarterly journal of the Commission of Motorization and Energetics in Agriculture would like to inform both the authors and readers that an agreement was signed with the Interdisciplinary Centre for Mathematical and Computational Modelling at the Warsaw University referred to as "ICM". Therefore, ICM is the owner and operator of the IT system needed to conduct and support a digital scientific library accessible to users via the Internet called the "ICM Internet Platform", which ensures the safety of development, storage and retrieval of published materials provided to users. ICM is obliged to put all the articles printed in the "Teka" on the ICM Internet Platform. ICM develops metadata, which are then indexed in the "Agro" database.

Impact Factor of the TEKA quarterly journal according to the Commission of Motorization and Energetics in Agriculture is 2,07 (June 2014).

GUIDELINES FOR AUTHORS (2014)

The journal publishes the original research papers. The papers (min. 8 pages) should not exceed 12 pages including tables and figures. Acceptance of papers for publication is based on two independent reviews commissioned by the Editor.

Authors are asked to transfer to the Publisher the copyright of their articles as well as written permissions for reproduction of figures and tables from unpublished or copyrighted materials.

Articles should be submitted electronically to the Editor and fulfill the following formal requirements:
- Clear and grammatically correct script in English,
- Format of popular Windows text editors (A4 size, 12 points Times New Roman font, single interline, left and right margin of 2,5 cm),
- Every page of the paper including the title page, text, references, tables and figures should be numbered,
- SI units should be used.

Please organize the script in the following order (without subtitles):
Title, Author(s) name (s), Affiliations, Full postal addresses, Corresponding author's e-mail
Abstract (up to 200 words), Keywords (up to 5 words), Introduction, Materials and Methods, Results, Discussion (a combined Results and Discussion section can also be appropriate), Conclusions (numbered), References, Tables, Figures and their captions

Note that the following should be observed:
An informative and concise title; Abstract without any undefined abbreviations or unspecified references; No nomenclature (all explanations placed in the text); References cited by the numbered system (max 5 items in one place); Tables and figures (without frames) placed out of the text (after References) and figures additionally prepared in the graphical file format jpg or cdr.

Make sure that the tables do not exceed the printed area of the page. Number them according to their sequence in the text. References to all the tables must be in the text. Do not use vertical lines to separate columns. Capitalize the word 'table' when used with a number, e.g. (Table1).

Number the figures according to their sequence in the text. Identify them at the bottom of line drawings by their number and the name of the author. Special attention should be paid to the lettering of figures – the size of lettering must be big enough to allow reduction (even 10 times). Begin the description of figures with a capital letter and observe the following order, e.g. Time(s), Moisture (%, vol), (%, $m^3m^{-3)}$ or (%, gg^{-1}), Thermal conductivity (W $m^{-1}K^{-1}$).

Type the captions to all figures on a separate sheet at the end of the manuscript.

Give all the explanations in the figure caption. Drawn text in the figures should be kept to a minimum. Capitalize and abbreviate 'figure' when it is used with a number, e.g. (Fig. 1).

Colour figures will not be printed.

Make sure that the reference list contains about 30 items. It should be numbered serially and arranged alphabetically by the name of the first author and then others, e.g.
7. Kasaja O., Azarevich G. and Bannel A.N. 2009. Econometric Analysis of Banking Financial Results in Poland. Journal of Academy of Business and Economics (JABE), Vol. IV. Nr 1, 202–210.

References cited in the text should be given in parentheses and include a number e.g. [7].

Any item in the References list that is not in English, French or German should be marked, e.g. (in Italian), (in Polish).

Leave ample space around equations. Subscripts and superscripts have to be clear. Equations should be numbered serially on the right-hand side in parentheses. Capitalize and abbreviate 'equation' when it is used with a number, e.g. Eq. (1). Spell out when it begins a sentence. Symbols for physical quantities in formulae and in the text must be in italics. Algebraic symbols are printed in upright type.

Acknowledgements will be printed after a written permission is sent (by the regular post, on paper) from persons or heads of institutions mentioned by name.